



# ADVANCES IN CHEMICAL ENGINEERING

Volume 6

Thomas B. Drew

## CONTRIBUTORS TO THIS VOLUME

ANDREAS ACRIVOS

R. ARIS

S. G. BANKOFF

JOHN C. BERG

MICHEL BOUDART

HOWARD BRENNER

A. G. FREDRICKSON

SAMUEL SIDEMAN

H. M. TSUCHIYA

# ADVANCES IN CHEMICAL ENGINEERING

*Edited by*

THOMAS B. DREW

*Department of Chemical Engineering  
Massachusetts Institute of Technology  
Cambridge, Massachusetts*

JOHN W. HOOPES, JR.

*Atlas Chemical Industries, Inc.  
Wilmington, Delaware*

THEODORE VERMEULEN

*Department of Chemical Engineering  
University of California  
Berkeley, California*

*Assistant Editor*

Giles R. Cokelet

*Division of Chemistry and Chemical Engineering  
California Institute of Technology  
Pasadena, California*

Volume 6



Academic Press • New York • London 1966

COPYRIGHT © 1966, BY ACADEMIC PRESS INC.

ALL RIGHTS RESERVED

NO PART OF THIS BOOK MAY BE REPRODUCED IN ANY FORM,  
BY PHOTOSTAT, MICROFILM, OR ANY OTHER MEANS,  
WITHOUT WRITTEN PERMISSION FROM THE PUBLISHERS.

ACADEMIC PRESS INC.  
111 FIFTH AVENUE  
New York, New York 10003

*United Kingdom Edition*  
Published by  
ACADEMIC PRESS INC. (LONDON) LTD.  
Berkeley Square House  
London W.1

*Library of Congress Catalog Card Number: 56-6600*

PRINTED IN THE UNITED STATES OF AMERICA



## CONTRIBUTORS TO VOLUME 6

Numbers in parentheses indicate the pages on which the authors' contributions begin.

ANDREAS ACRIVOS, *Stanford University, Stanford, California* (61)

R. ARIS, *Department of Chemical Engineering, University of Minnesota, Minneapolis, Minnesota* (125)

S. G. BANKOFF, *Department of Chemical Engineering, Northwestern University, Evanston, Illinois* (1)

JOHN C. BERG, *University of Washington, Seattle, Washington* (61)

MICHEL BOUDART, *Stanford University, Stanford, California* (61)

HOWARD BRENNER\*, *Department of Chemical Engineering, New York University, Bronx, New York* (287)

A. G. FREDRICKSON, *Department of Chemical Engineering, University of Minnesota, Minneapolis, Minnesota* (125)

SAMUEL SIDEMAN, *Department of Chemical Engineering, Technion, Israel Institute of Technology, Haifa, Israel* (207)

H. M. TSUCHIYA, *Department of Chemical Engineering, University of Minnesota, Minneapolis, Minnesota* (125)

\* Present address: Department of Chemical Engineering, Carnegie Institute of Technology, Pittsburgh, Pennsylvania.

## PREFACE

With Volume 6, "Advances in Chemical Engineering" enters its second decade. The favorable reception accorded the first five volumes (for which undoubtedly the authors of the several chapters, rather than the editors, are to be thanked and congratulated) has confirmed our belief that there is a place in the chemical engineering literature for periodic critical reviews which authoritatively bring old topics up to date or summarize new developments. Viewed in 1966, the need is clearly far greater than in 1956; the literature grows exponentially and, more and more, pressure for space is condensing original papers to unintelligibility for other than the narrow specialist. Our aim still is to provide a forum in which a qualified specialist in one area presents the advances in his field in terms intelligible and interesting to a specialist in a different area. Thus results the interchange that expedites major advances in all fields.

THOMAS B. DREW  
JOHN W. HOOPES, JR.  
THEODORE VERMEULEN  
GILES R. COKELET

*September, 1966*

# DIFFUSION-CONTROLLED BUBBLE GROWTH

S. G. Bankoff

Department of Chemical Engineering  
Northwestern University, Evanston, Illinois

|   |    |
|---|----|
| I. Introduction .....   | 1  |
| II. Spherically Symmetric Bubble Growth .....   | 3  |
| A. Formulation of the Problem .....   | 3  |
| B. Asymptotic Growth of a Vapor Bubble in an Initially Uniformly Superheated One-Component Liquid ..... | 7  |
| C. Bubble Growth under Nonuniform Initial Conditions .....  | 20 |
| D. Two-Component Liquids .....  | 33 |
| E. Gas Bubble Growth .....  | 34 |
| III. Experimental Bubble Growth Data .....  | 35 |
| A. Vapor Bubbles .....  | 35 |
| B. Gas Bubbles .....  | 37 |
| IV. Surface Boiling .....   | 42 |
| A. Subcooled Boiling .....  | 42 |
| B. Zuber's Model .....  | 47 |
| C. Forster's Model .....  | 49 |
| V. Miscellaneous Topics .....   | 49 |
| A. Nucleation .....   | 49 |
| B. Rapid Heating .....  | 51 |
| C. Microlayer Vaporization .....  | 52 |
| D. Other Bubble Properties .....  | 52 |
| VI. Concluding Remarks .....  | 53 |
| Nomenclature .....  | 54 |
| References .....  | 56 |

## I. Introduction

In a previous article (B8), the subject of diffusion-controlled phase change, subject to two provisos, was reviewed in some detail. These constraints were the following: (1) the motion must be induced solely by the phase change; and (2) the diffusion and pressure equations must be, within a negligible error, uncoupled. The latter restriction implies that forces and accelerations

need not be considered in formulating the differential equation or the boundary conditions for the diffusion problem. In theory, at least, this latter restriction is not applicable to rapid vaporization processes. In particular, the study of diffusive bubble growth processes, with which this article is concerned, adds an extra dimension of complexity over those situations studied heretofore. It is not only necessary to consider the convective motion, resulting from the large change in density upon vaporization, in the diffusion equation, but also separately to consider the equation of motion, since inertial, surface tension, and viscous effects may be appreciable. In practice, however, diffusion effects control in the late, or asymptotic, stage of bubble growth, and most theoretical effort to date has centered upon an understanding of this simpler case. Fortunately, the asymptotic solutions are applicable, with small error, during most of the lifetime of the visible bubble, so that principal interest for process application centers upon them. These theories will, therefore, be reviewed in some detail, since they represent important specializations of the general theory of diffusion-limited phase change.

Nevertheless, although bubble formation and growth play an important role in the mechanics of boiling heat transfer, solid-liquid reactions with gas evolution (including electrolysis), cavitation (with its associated degradation of propulsion and pumping characteristics), and effervescence (precipitation of gas bubbles from a supersaturated solution), present applications of bubble dynamics theory are quite limited. The theory deals with the spherically symmetric growth of a single bubble in a large body of liquid at rest at infinity. In actual practice, bubbles nearly always originate as microscopic bits of gas or vapor entrapped in small crevices on a solid surface. Often the solid surface is large in extent compared to the bubble diameter, so that departure from spherical (or hemispherical) flow symmetry is frequently significant. Turbulence, bubble interaction, bubble coalescence, and translational velocity of the fluid with respect to the bubble are other complicating factors. It is necessary, therefore, to consider phenomenological theories for various aspects of bubble behavior; since these are less well founded in experiment, while *a priori* error estimates cannot be obtained, these will be only briefly reviewed.

Not only is theoretical analysis in this field difficult, but also experimental measurements of the velocity and temperature fields surrounding a bubble are at the limit of present capabilities, because of the small length and time scales involved. This lack of information, together with the uncertainty introduced by the presence of the solid wall, make comparison of theory with experiment difficult. The status of experimental information on bubble growth rates is, therefore, briefly reviewed. Finally, a number of special topics, including bubble nucleation, are touched upon. Some general comments conclude the review.

Several recent applications hinge strongly on diffusion-controlled bubble dynamics. The self-regulating properties of water- or organic-moderated nuclear reactors depend upon a reduction in reactivity in the course of a power excursion. A portion of this reduction can be attributed to expansion of the moderator as a result of void formation. It is doubtful, however, that single-bubble growth theory can be meaningfully applied to the expulsion of moderator from heterogeneous reactors, since coalescence of bubbles to form a continuous vapor film on the hot fuel surfaces occurs rapidly. On the other hand, shutdown of the KEWB reactor, which is an experimental aqueous homogeneous reactor, during power transients is attributed to the formation of numerous radiolytic gas bubbles throughout the liquid (B26). An interesting recent application, connected with a dry photographic process, is the formation of minute gas bubbles in molten plastic as the result of decomposition of a diazo compound (B14). A major difficulty, even in these applications, is not so much an estimate of the growth rate of any particular bubble as it is an estimate of the rate of nucleation of new bubbles per unit volume. The theory of bubble nucleation is still not well understood, but it seems very likely that heterogeneous nucleation (from gas or vapor entrapped in crevices on solid surfaces) dominates over homogeneous nucleation (from statistical density fluctuations) (B2, B3, F2). This means that the nucleation characteristics, even in the absence of macroscopic solid surfaces, depend upon the suspended particle population; a systematic study of this relationship is not yet available.

The subject of diffusion-controlled bubble growth is, of course, a rather small part of the large subject of bubble dynamics, whose scope is too broad to be included in this review. Specifically excluded are cavitation bubbles, whose collapse is inertia rather than diffusion controlled, the formation and detachment of bubbles from orifices, oscillations of bubbles in a pressure field, and the challenging subject of the mechanism of nucleate boiling heat transfer, in which bubble formation and detachment must certainly play a dominant role.

## II. Spherically Symmetric Bubble Growth

### A. FORMULATION OF THE PROBLEM

Consider the growth of a small vapor or gas bubble, far from any other body, initially in equilibrium with a large volume of stationary liquid, as a result of a small displacement from equilibrium. The bubble maintains a spherical shape because of surface tension, and the liquid motion is purely radial. Note that this does not imply that the temperature or concentration field is likewise spherically symmetric. The governing equations and boundary

and initial conditions for bubble growth have been discussed by a number of authors (P6, P7, S3, S11, S13a).

Upon integrating the continuity equation for the laminar, purely radial flow of an incompressible fluid, the liquid velocity  $u$  is found to be

$$ur^2 = \mathcal{F}(t), \quad u = u(r, t), \quad r > R(t) \quad (1)$$

where  $\mathcal{F}(t)$  is a function of time to be determined in this case from the conditions at the bubble surface  $R = R(t)$ . A mass balance on the bubble requires that

$$\frac{d}{dt} (\frac{4}{3}\pi R^3 \rho') = 4\pi R^2 \rho [\dot{R} - u(R, t)] \quad (2)$$

where the dot denotes time differentiation and primed quantities refer to the vapor properties. The bracketed term on the right is the net velocity normal to the bubble surface, expressing the fact that the liquid at the bubble wall has a velocity slightly different from that of the wall. On the left-hand side the vapor density varies relatively slowly compared to the bubble volume, which usually increases by several orders of magnitude. Hence, it is satisfactory to consider a time-averaged vapor density  $\langle \rho' \rangle$  whereupon Eqs. (1) and (2) give

$$u(R, t) = \varepsilon \dot{R}, \quad \varepsilon = 1 - \frac{\langle \rho' \rangle}{\rho} \quad (3)$$

$$u(r, t) = \varepsilon \dot{R} R^2 r^{-2}$$

By integrating the stress equation for the radial motion of an incompressible Newtonian fluid from the bubble wall to infinity, the equation of motion for the bubble wall was obtained by Scriven (S3), upon using Eq. (3), in the form

$$R\ddot{R} + \left(2 - \frac{\varepsilon}{2}\right)\dot{R}^2 = \frac{p(R) - p_\infty}{\varepsilon\rho} - 4\nu \frac{\dot{R}}{R} \quad (4)$$

where  $p_\infty$  and  $p(R)$  are the pressures far from the bubble and at the bubble wall, and  $\nu$  is the liquid kinematic viscosity. The pressure  $p(R)$  is related to the pressure within the bubble  $p_b$  by<sup>1</sup>

$$p_b = p(R) + \frac{2\sigma}{R} \quad (5)$$

<sup>1</sup> In some cases the dynamic surface tension may exceed the equilibrium value. Scriven (S4) shows that for a Newtonian surface viscosity model an extra term equal to  $4\kappa\dot{R}/R^2$  should be added to the right-hand side of Eq. (5), where  $\kappa$  is the effective surface-dilational viscosity.

It is now assumed that the contents of the bubble are at all times in equilibrium with the liquid at the bubble wall.<sup>2</sup> Plesset and Zwick (P6) show that the average bubble wall velocity (of the order of 10 cm/sec for a steam bubble at atmospheric pressure with 10°C superheat) is much less than the acoustic velocity in either liquid or vapor, so that compressibility effects can be neglected. Also, the velocity of the bubble wall is considerably less than the average velocity with which evaporating molecules stream away from the surface, given in terms of the absolute evaporation rate as  $\gamma(R_g T/2\pi M)^{1/2}$ , where  $\gamma$  is an accommodation coefficient. The critical velocity for a water surface at 100°C is about 8 m/sec, which is appreciably higher than the mean bubble wall velocity, so that the departure from the equilibrium vapor pressure is negligibly small. For organic liquids, whose accommodation coefficients are thought to be higher than those of water (W4), this neglect is even better justified. Finally, because of the relatively large thermal diffusivity of the vapor, temperature gradients within the bubble may be neglected under most circumstances. In water vapor at atmospheric pressure the characteristic diffusion length  $(2\alpha't)^{1/2}$  is 0.24 cm for  $t = 0.01$  sec, at which time the bubble radius for 10°C superheat is about 0.1 cm. For all but the fastest-growing vapor bubbles, therefore, the assumption of thermodynamic equilibrium between the vapor and the bubble wall liquid is justified, and

$$p_b = p_g + p_v \quad (6)$$

where  $p_g$  is the inert gas partial pressure and  $p_v$  is the vapor pressure of the liquid at the bubble wall. The equations of motion finally become

$$\frac{p(R) - p_\infty}{\varepsilon\rho} = \frac{p_v + p_g - p_\infty - 2\sigma/R}{\varepsilon\rho} = R\ddot{R} + \left(2 - \frac{\varepsilon}{2}\right)\dot{R}^2 + 4v\frac{\dot{R}}{R} \quad (7)$$

Normally the viscous term is negligibly small (Z5), and  $\varepsilon \sim 1$ . In this case the equation reduces to the extension of the potential flow (Rayleigh) equation (L4), given by Plesset (P3), taking surface tension into account.

The energy equation, assuming spherical symmetry, constant thermal properties, and negligible viscous dissipation, becomes

$$\frac{\partial T}{\partial t} = \alpha \left( \frac{\partial^2 T}{\partial r^2} + \frac{2}{r} \frac{\partial T}{\partial r} \right) - \frac{\varepsilon \dot{R} R^2}{r^2} \frac{\partial T}{\partial r} + \frac{Q}{\rho c_p} \quad (8)$$

where  $Q$ , the volume rate of heat release, may be a function of both space and time. Similarly, in a multicomponent mixture, assuming constant mass density and diffusivity, a mass diffusion equation for one of the components (taken

<sup>2</sup> This is not true in the final stages of collapse of cavitation bubbles, which are not diffusion limited.

to be the more volatile component in a two-component mixture) is

$$\frac{\partial C_A}{\partial t} = \mathcal{D} \left( \frac{\partial^2 C_A}{\partial r^2} + \frac{2}{r} \frac{\partial C_A}{\partial r} \right) - \frac{\varepsilon \dot{R} R^2}{r^2} \frac{\partial C_A}{\partial r} + Q' \quad (9)$$

where  $Q'$  represents the instantaneous local rate of concentration increase due to the presence of distributed mass sources. For  $t < 0$ , the bubble is in equilibrium with the surrounding liquid, so that

$$R(0) = \frac{2\sigma}{p_{v0} + p_g - p_\infty} + \delta_1 \quad (10)$$

where  $\delta_1$  represents a small displacement from the equilibrium bubble radius (S3). Alternatively, the initial displacement from equilibrium may be considered to be caused by a weak volume heat source (P7). The asymptotic growth rate is not affected by the details of the initial displacement, providing that it is small. What is affected is the waiting time for the surface tension and inertial effects to be relaxed. The initial temperature and concentration are specified functions of position:

$$T(\mathbf{r}, 0) = g(\mathbf{r}) \quad (11)$$

$$C_A(\mathbf{r}, 0) = h(\mathbf{r}) \quad (12)$$

where  $\mathbf{r}$  is the radius vector. Equating the rate of increase of the mass of the more volatile component  $A$  in the bubble to the convective and diffusive flux across the bubble surface gives

$$\frac{d}{dt} (y_A \rho' R) = (1 - \varepsilon) \dot{R} C_A(R, t) + \mathcal{D} \frac{\partial C_A(R, t)}{\partial r} \quad (13)$$

where  $y_A$  is the mass fraction of  $A$  in the vapor. Similarly, the heat balance at the bubble wall, neglecting small terms, requires that

$$\frac{d}{dt} (\rho' R \bar{L}) = k \frac{\partial T(R, t)}{\partial r} \quad (14)$$

where  $\bar{L}$  represents the average heat of vaporization per unit mass of volatile material in the bubble, evaluated at the bubble wall temperature. Finally, the specification of a boundedness condition at infinity and the requirement that the bubble contents be at all times in equilibrium with the liquid at the bubble wall complete the statement of the problem. Note that the equilibrium requirement implies the absence of concentration and temperature gradients within the bubble at all times, and the uniformity of concentration and temperature, at any instant, over the entire bubble surface. This requirement applies even when the initial temperature and concentration fields in the liquid are not spherically symmetric.



When put into dimensionless form, the full problem involves eight or more dimensionless parameters, whose magnitude must be examined for any particular problem before deciding which terms can be safely neglected. This question is discussed in detail by Langlois (L5) with reference to isothermal gas bubble growth. For example, the effect of inert (nondiffusant) gas in the initial bubble is neglected hereafter; however, in the early stages of bubble growth it plays a significant role, as discussed by Dergarabedian (D2, D3), Ma and Wang (M1), and Lienhard (L7). The complete set of equations is obviously quite formidable, and it is instructive to consider first the simplest case. This involves a single diffusant from an initially uniform liquid.

## B. ASYMPTOTIC GROWTH OF A VAPOR BUBBLE IN AN INITIALLY UNIFORMLY SUPERHEATED ONE-COMPONENT LIQUID

### 1. *Self-Similar (Exact) Solutions*

During the asymptotic growth stage, viscous and inertial effects are negligible. Likewise, the partial pressure of the small inert gas residue becomes negligible compared to the vapor partial pressure within the bubble. Hence, the equation of motion (4) reduces to the statement that the bubble is in mechanical equilibrium with its surroundings, and, to an excellent degree of approximation, the internal bubble pressure is equal to the ambient pressure. The growth is then strictly diffusion controlled, so that the solution developed by Kirkaldy (K4) for spherically symmetric phase growth where a density change is involved is applicable.<sup>3</sup> The difficulty is that it is necessary to extend the asymptotic stage all the way back to zero radius, which does not agree with the physical facts. The bubble actually begins at some finite, nonzero radius; and the inertial and surface tension terms are appreciable during the early stage of bubble growth. The exact solution, therefore, deals with an associated problem, which it is hoped closely approximates asymptotically the solution of the complete problem. The approximation error can only be determined by other methods.

In 1958, Kirkaldy (K4) published a self-similar solution for the growth, limited by the diffusion of heat or mass, of slabs, cylinders, or spheres of initially negligible size from a large body of surrounding quiescent fluid of

<sup>3</sup> This paper has been generally overlooked by workers in the bubble dynamics field largely because Kirkaldy was concerned with exact solutions for the growth of ice particles, and was, in fact, principally concerned with establishing the validity of the quasi-steady approximation in this problem. However, his solution is correct for spherical symmetry in one, two, or three dimensions, with convection induced by the phase change, and hence would be applicable to the growth of plane or cylindrical bubbles, as well as spherical bubbles. A summary of this analysis is given in (B8).

initially uniform concentration or temperature, where the densities of the two phases are constant but not necessarily equal. Nearly simultaneously, Birkhoff, Margulies, and Horning (B19) published the same solution for a growing vapor or gas bubble, and explored in some detail the nature of the solution. In 1959, Scriven (S3, S4) rederived this solution and extended it to two-component systems. Specializing Kirkaldy's results (B8) to the case of a bubble growing from zero radius in an initially superheated liquid containing no heat sources, the temperature distribution in the liquid is

$$\theta = \frac{\Phi_3(\eta)}{\Phi_3(\beta)}, \quad \theta = \frac{T - T_\infty}{T_s - T_\infty} \quad (15)$$

where  $T_s$  and  $T_\infty$  are the saturation temperature and the temperature far from the bubble, and where the growth function for spherical symmetry in three dimensions is

$$\Phi_3(\eta) = \int_\eta^\infty z^{-2} \exp\left(\frac{-\beta^3 \varepsilon}{2z} - \frac{z^2}{4}\right) dz \quad (16)$$

Here  $\eta$  is the Boltzmann (B21) transformation variable  $r/(\alpha t)^{1/2}$ . To evaluate the growth constant  $\beta$ , where  $R = \beta(\alpha t)^{1/2}$ , use is made of the heat balance at the bubble wall, Eq. (14), where, from Eq. (15),

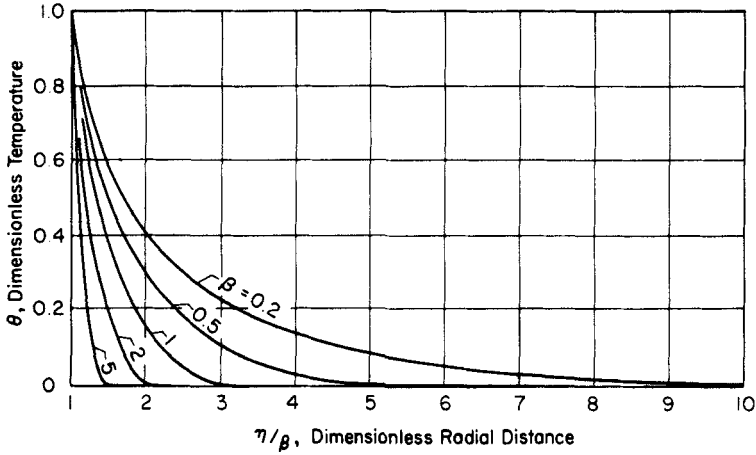
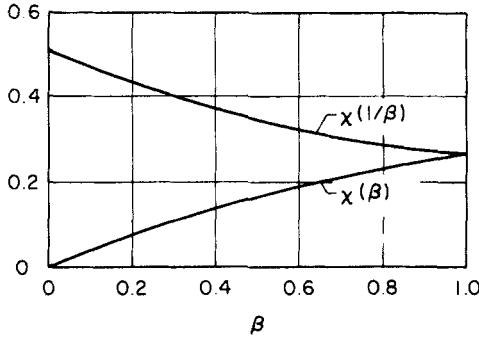
$$\frac{\partial T(R, t)}{\partial r} = \frac{(T_s - T_\infty)\Phi_3'(\beta)}{(\alpha t)^{1/2}\Phi_3(\beta)}, \quad \Phi_3'(\eta) = \frac{d\Phi_3}{d\eta} \quad (17)$$

Hence  $\beta$  is the real root of

$$\frac{N_J}{\beta} \equiv \frac{\rho c_p (T_\infty - T_s)}{\beta \rho' \bar{L}} = -\frac{\Phi_3(\beta)}{2\Phi_3'(\beta)} = \chi(\beta) \quad (18)$$

where  $N_J$ , termed by Savic (S1) the Jakob number, may be thought of as a dimensionless driving force for bubble growth. Birkhoff, Margulies, and Horning (B19) present plots of the temperature distribution [Eq. (15)] (Fig. 1), as well as the growth function  $\chi$  (Fig. 2). It is seen that  $\beta > 5$  corresponds approximately to  $N_J > 2.5$ , giving a rough criterion for the validity of the zero-order thin thermal boundary layer assumption, to be discussed in detail later. In particular, it is shown that (B19) for  $\varepsilon = 0$

$$\lim_{\beta \rightarrow \infty} \frac{N_J}{\beta} = \left(\frac{\pi}{12}\right)^{1/2} \quad (19)$$


 FIG. 1. Temperature profiles;  $\theta(\eta)$  vs  $(\eta/\beta)$  curves for different growth constants (B19).

 FIG. 2.  $\chi(\beta)$  and  $\chi(1/\beta)$  vs  $\beta$ , for  $0 \leq \beta \leq 1$  (B19).

which implies

$$R = \left(\frac{12}{\pi}\right)^{1/2} N_J(\alpha t)^{1/2} \quad (20)$$

a result identical with the leading term of the Plesset-Zwick (P7; also B7) solutions for the asymptotic growth phase. An analogous treatment is given for the isothermal growth of a gas bubble from a uniformly supersaturated solution, for which the parameter corresponding to the Jakob number is  $N_J' = (C_\infty - C_s)/C_g$ . For water saturated with  $N_2$  at  $20^\circ\text{C}$  and heated suddenly to just below the boiling point,  $N_J' = 0.021$ , so that the growth rate is slow (B19). For  $\beta$  small, Eq. (18) gives  $\beta \cong (2N_J')^{1/2}$ ,<sup>4</sup> as noted previously by Kirkaldy.

<sup>4</sup> There is a misprint in Eq. (26) of this reference at this point.

Birkhoff *et al.* then discuss the validity of neglecting the inertial terms in the equation of motion, Eq. (4), and conclude that it is justified if

$$R \gg \beta^2 \alpha \left[ \frac{\rho}{8p(R)} \right]^{1/2} \quad (21)$$

For water boiling at 1 atm with a superheat of 1°C, the right-hand side of Eq. (21) has the value  $10^{-5}$  cm, and for 10°C,  $10^{-3}$  cm. Hence, the inertial terms are generally negligible in the visible bubble range, which justifies focusing attention on the asymptotic phase of bubble growth.

## 2. Approximate Solutions

The requirements for a self-similar solution of the bubble growth problem to exist are quite restrictive. In particular, the bubble must begin its growth at zero radius; inertial, viscous, and surface tension terms must be neglected at all times; and the initial temperature and/or concentration distribution in the liquid must be uniform. Actually, the bubble begins its growth at a small nonzero radius. In the early growth phase, which determines the waiting time between bubbles, or in the growth of bubbles in highly viscous polymeric media, neglect of inertial, surface tension, and viscous effects is not allowable. Further, vapor bubbles originating at a hot surface, as in nucleate boiling, grow in an environment where the temperature gradients are initially quite large, so that the assumption of uniform initial temperature cannot, in general, be made. Exact solutions of the complete equations cannot be found, so that approximate solutions of greater generality than the self-similar solution are of considerable value.

One of the earliest simplifications to be applied to the problem of the growth of diffusion-controlled vapor bubbles was the notion of a thin thermal boundary layer. This arises from the fact that at moderate pressures the volume of liquid surrounding the bubble cooled by vaporization is small compared to the volume of the bubble, in view of the large liquid to vapor density ratio. Bosnjakovic (B22) defined an effective heat transfer coefficient to the bubble, which can be estimated from a plane approximation, ignoring the effects of curvature and of stretching on the heat transfer through the boundary layer. In 1954, two different improvements of the plane approximation were published simultaneously: (1) a perturbation procedure by Plesset and Zwick (P7), based upon a Lagrangian formulation of the equations of motion and of heat diffusion; and (2) a more intuitive, although somewhat simpler, approach by Forster and Zuber (F5), based upon the notion that the moving bubble wall is equivalent to a distributed spherical heat sink expanding through a stationary medium. We begin with the Plesset-Zwick solution and its subsequent extensions, and then treat the Forster-Zuber solution and its extensions.

*a. Plesset-Zwick Perturbation Solution.* Plesset and Zwick (P6), as a preliminary to a consideration of the vapor bubble growth problem, presented a solution in successive approximations for the heat diffusion across a spherical boundary with radial motion. The approximations were based upon the notion that a thin thermal boundary layer, in which essentially all the temperature variation occurs, surrounds the bubble wall. Taking  $\varepsilon = 1$ , Eq. (8) becomes

$$\frac{\partial T}{\partial t} + \frac{R^2 \dot{R}}{r^2} \frac{\partial T}{\partial r} = \alpha \left( \frac{\partial^2 T}{\partial r^2} + \frac{2}{r} \frac{\partial T}{\partial r} \right) \quad (22)$$

assuming the absence of volume heat sources.

A transformation is now introduced to the new variables

$$\zeta = \int_0^t R^4(t') dt' \quad (23)$$

$$U = \int_0^m T_e(m', t) dm' + K(t), \quad T_e = T - T_\infty \quad (24)$$

$$m = \frac{4}{3}[r^3 - R^3(t)] \quad (25)$$

Here  $m$  is proportional to the volume of a spherical shell of liquid between the bubble wall and the radial position coordinate  $r$ , and hence, represents a Lagrangian coordinate, providing that a negligible volume of liquid is vaporized.  $U$  is therefore a measure of the heat content of the spherical shell, to within an arbitrary additive function of time,  $K(t)$ ; alternatively, it may be viewed as a temperature potential function. In terms of the new coordinates the diffusion equation becomes

$$\frac{r^4}{R^4} \frac{\partial^2 U}{\partial m^2} - \frac{1}{\alpha} \frac{\partial U}{\partial \zeta} = 0 \quad (26)$$

where the arbitrary additive function of time has been chosen to make the right-hand side zero, and  $U(m, 0) = 0$ . The boundary condition at infinity is

$$\frac{\partial U(\infty, \zeta)}{\partial m} = 0 \quad (27)$$

At the bubble wall one has

$$\frac{\partial^2 U(0, \zeta)}{\partial m^2} = \frac{1}{R^2} \frac{\partial T(R)}{\partial r} = F(\zeta) \quad (28)$$

a function of time to be determined from a heat balance on the bubble.

Noting that

$$\frac{r^4}{R^4} = \left(1 + \frac{3m}{R^3}\right)^{4/3} = 1 + \frac{4m}{R^3} + 2\left(\frac{m}{R^3}\right)^2 - \dots \quad (29)$$

for  $(3m/R^3) < 1$ , and, letting  $U = U_0 + U_1 + \dots$ , Eq. (26) can be written

$$\left(1 + \frac{4m}{R^3} + \frac{2m^2}{R^6} - \dots\right) \frac{\partial^2(U_0 + U_1 + \dots)}{\partial m^2} - \frac{1}{\alpha} \frac{\partial(U_0 + U_1 + \dots)}{\partial \zeta} = 0 \quad (30)$$

The zero-order approximation is then given by

$$\frac{\partial^2 U_0}{\partial m^2} - \frac{1}{\alpha} \frac{\partial U_0}{\partial \zeta} = 0 \quad (31)$$

subject to the initial and boundary conditions

$$U_0(m, 0) = \frac{\partial U_0(\infty, 0)}{\partial m} = 0; \quad \frac{\partial^2 U_0(0, \zeta)}{\partial m^2} = F(\zeta) \quad (32)$$

The solution to this linear boundary value problem is obtained by Laplace transformation, yielding for the zero-order estimate of the bubble wall temperature

$$T_0(0, t) - T_\infty = - \left(\frac{\alpha}{\pi}\right)^{1/2} \int_0^t \frac{R^2(x)(\partial T / \partial r)_{r=R(x)}}{\left\{\int_x^t R^4(z) dz\right\}^{1/2}} dx \quad (33)$$

Note that the effect of a spatially uniform heat source can be added directly to this expression. If the variations in  $R(t)$  are sufficiently small, Eq. (33) simplifies to

$$T_0(0, t) - T_\infty = - \left(\frac{\alpha}{\pi}\right)^{1/2} \int_0^t \frac{(\partial T / \partial r)_{r=R(x)}}{(t-x)^{1/2}} dx \quad (34)$$

corresponding to the plane approximation obtained by neglecting the curvature of the boundary.

The first-order correction, from Eq. (30), satisfies

$$\frac{\partial^2 U_1}{\partial m^2} - \frac{1}{\alpha} \frac{\partial U_1}{\partial \zeta} = - \frac{4m}{R^3} \frac{\partial^2 U_0}{\partial m^2} \quad (35)$$

where the inhomogeneous term on the right-hand side may be treated as a known function. The initial and boundary conditions are homogeneous:

$$U_1(m, 0) = \frac{\partial U_1(\infty, \zeta)}{\partial m} = \frac{\partial^2 U_1(0, \zeta)}{\partial m^2} = 0 \quad (36)$$

This correction term is obtained as a convolution integral, and bounds obtained by the mean-value theorem.

Plesset and Zwick (P7) then substitute the zero-order temperature solution [Eq. (33)] into the equation of motion [Eq. (4)] to obtain the bubble radius and internal pressure as a function of time. In a sense theirs is still the only complete solution to the problem of a bubble growing from the critical (equilibrium) radius. The solution is obtained in several stages, by expansions for  $(R/R_0 - 1)$  small and large, and for intermediate values, where  $R_0$  is the initial bubble radius (Z6). These solutions are patched together by appropriate matching conditions to give a solution whose error can be shown to be small at every stage, provided that the thin thermal boundary layer assumption is valid. Our present concern, however, is only with the asymptotic stage, which encompasses the visible range of bubble radii for the usual liquids. The pressure of the vapor at the bubble wall may be approximated by a linear function of temperature,

$$\frac{p(R) - p_\infty}{\rho} = A(T - T_s) \quad (37)$$

Assuming negligible inert gas pressure in the bubble,  $\varepsilon = 1$ , and negligible viscous effects, Eq. (7) can be rewritten<sup>5</sup>

$$\frac{1}{2R^2\dot{R}} \frac{d}{dt} (R^3\dot{R}^2) = A(T - T_\infty) + \frac{2\sigma}{\rho R_0} \left(1 - \frac{R_0}{R}\right) \quad (38a)$$

where, from Eqs. (10) and (37),

$$2\sigma/\rho R_0 = A(T_\infty - T_s) \quad (38b)$$

In terms of the variables

$$R^* = R^3/R_0^3 \quad (39a)$$

$$\zeta^* = \frac{K_1}{R_0^4} \int_0^t R^4(t') dt' \quad (39b)$$

$$K_1 = (2\sigma/\rho R_0^3)^{1/2} \quad (39c)$$

this equation becomes

$$\frac{1}{6\dot{R}^*} \frac{d}{d\zeta^*} (R^{*7/3}\dot{R}^{*2}) = 1 - \frac{1}{R^{*1/3}} - K_2 \int_0^{\zeta^*} \frac{\dot{R}^*(z) dz}{(\zeta^* - z)^{1/2}}, \quad (40)$$

where

$$\dot{R}^* = \frac{dR^*}{d\zeta^*}, \quad K_2 = \frac{AL\rho'}{3kR_0K_1} \left(\frac{\alpha}{\pi K_1}\right)^{1/2} \quad (41)$$

<sup>5</sup> Eq. (15) of the reference has a misprint at this point.

For  $R \gg R_0$ , the solution is obtained by taking the solution to be of the form

$$R^*(\zeta^*) = 1, \quad 0 < \zeta^* \leq \zeta_1^* \quad (42a)$$

$$R^*(\zeta^*) \sim \frac{2}{\pi K_2} (\zeta^* - \zeta_0^*)^{1/2} \left\{ 1 + \frac{b_1}{(\zeta^* - \zeta_0^*)^{1/6}} + \cdots + \frac{b_5}{(\zeta^* - \zeta_0^*)^{5/6}} + \frac{b_6 \ln(\zeta^* - \zeta_0^*)}{(\zeta^* - \zeta_0^*)} \right\},$$

$$\zeta^* > \zeta_1^* \quad (42b)$$

where  $\zeta_1^*$  represents a delay time determined by the requirement from Eq. (42a) that  $R^*(\zeta_1^*) = 1$ , and  $\zeta_0^*$  is available for matching the asymptotic solution to the preceding phase of bubble growth.

Upon matching coefficients of corresponding powers of  $(\zeta^* - \zeta_0^*)$ , the leading terms in the asymptotic solutions are found to be of the form

$$R \sim R_0 \left( \frac{2}{\pi K_2} \right) \left( \frac{K_1 t}{3} \right)^{1/2} \{1 + O(t^{-1/2})\}$$

$$= \left( \frac{12}{\pi} \right)^{1/2} \frac{k(T_\infty - T_s)}{L\rho'} \left( \frac{t}{\alpha} \right)^{1/2} \{1 + O(t^{-1/2})\} \quad (43)$$

$$(T - T_\infty) \sim -\frac{\alpha^2 R_0^2}{A} \{1 + O(t^{-1/2})\} \quad (44)$$

The predicted radius-time curves agree well (Fig. 3) with the data of Dergarabedian (D2, D3) on the asymptotic growth of vapor bubbles in water and  $\text{CCl}_4$  superheated at atmospheric pressure by radiant energy. Note, in contrast to the self-similar solutions, that the bubble radius grows as the square root of time only to the order of the leading term of the asymptotic expansion. For the smallest measured radii ( $\sim 0.01$  cm), the error in neglecting the remaining terms in Eq. (42b) was less than 10%. To this error must be added the error due to neglecting the first-order temperature correction [Eq. (35)], estimated also to be less than 10%. Both of these errors decrease rapidly as the bubble continues to grow.

*b. Extensions of the Plesset-Zwick Method.* (1). *Iteration-perturbation method.* In the Plesset-Zwick analysis the boundary condition for the heat diffusion problem is obtained by equating the heat conducted from the liquid to the increase in enthalpy of the bubble contents, which depends upon the unknown bubble volume. This leads to an implicit nonlinear integrodiffer-



ential equation for the bubble radius, so that even the calculation of the first-order correction poses considerable difficulties. Bankoff and Mikesell (B10) noted that in the asymptotic stage the bubble wall temperature may be taken, with small error, to be equal to the saturation temperature at the ambient pressure. The replacement of the heat flux conditions by the temperature

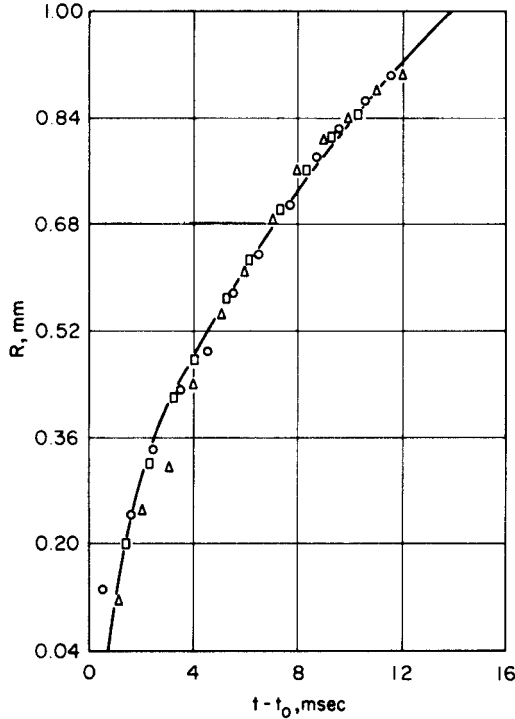


FIG. 3. Comparison of theoretical radius-time values with three sets of experimental values obtained (D2) in water superheated to 104.5°C at an external pressure of 1 atm (P7).

condition at the bubble wall was later made part of a consistent approximation scheme (B7) by introducing a second series of approximations (which was shown to converge very rapidly) to the bubble pressure, based upon the notion that the inertial and surface tension terms in the equation of motion [Eq. (7)] are small. As a preliminary, Eq. (7) can be written in terms of the variables given by Eqs. (23–25), neglecting the difference between  $\varepsilon$  and unity, and also the viscous term

$$g[R(\zeta)] \equiv p_b - p_\infty = \frac{2\sigma}{R} + \rho R^4 \frac{d}{d\zeta} \left( R^4 \frac{dR}{d\zeta} \right) + \frac{3}{2} \rho R^8 \left( \frac{dR}{d\zeta} \right)^2 \quad (45)$$

Hence, one may employ an iteration scheme which, for the zero-order perturbation, is

$$\frac{\partial^2 U_0^j}{\partial m^2} - \frac{1}{\alpha} \frac{\partial U_0^j}{\partial \zeta} = 0, \quad j = 0, 1, \dots; \quad \frac{\partial U_0^j(m, 0)}{\partial m} = \varphi(m) \quad (46)$$

$$\frac{\partial U_0^j(\infty, \zeta)}{\partial m} = 0; \quad \frac{\partial U_0^j(0, \zeta)}{\partial m} = T_v(p^j) - T_\infty; \quad p^0 = p_\infty \quad (47)$$

Here  $U_0^j$  refers to the  $j$ th approximation to  $U_0$ ; and  $T_v(p^j)$  is the saturation temperature corresponding to the  $j$ th approximation of the pressure within the bubble. The heat flux condition in Eq. (14) may be integrated to give

$$R^j(\zeta) = \left[ \frac{3k}{L\rho'} \int_0^\zeta \frac{\partial^2 U_0^j(0, z)}{\partial m^2} dz \right]^{1/3} \quad (48)$$

whence Eq. (45) yields

$$p^{j+1} = g[R^j(\zeta)] + p_\infty \quad (49)$$

The iteration then proceeds with this new estimate of the pressure within the bubble.

For water boiling at atmospheric pressure at a superheat of 4.5°C (D2, D3), for which inertial effects are relatively significant ( $N_J = 12.0$ ) the surface tension and inertial correction terms are 0.012 and 0.009 atm, respectively, at the first observable datum point ( $R = 0.004$  cm), and decrease very rapidly thereafter. In contrast, the ratio of the first- to the zero-order perturbation for this experiment was 3.7%. Hence, the replacement of the heat flux boundary condition by a temperature boundary condition is fully justified. In this way the zero- and first-order terms were obtained exactly, and the second-order perturbation estimated:

$$V_0 \equiv R_0^3 = 6N_J \left( \frac{\alpha_\zeta'}{\pi} \right)^{1/2} \quad (50)$$

$$V_1 = \frac{4V_0}{9N_J} \quad (51)$$

$$V_2 \doteq \frac{-5\pi V_1}{12(N_J + 4/9)} \quad (52)$$

where

$$V = R^3 = V_0 + V_1 + V_2 + \dots \quad (53)$$

and

$$V_i = O(N_J^{-i}), \quad i = 0, 1, 2, \dots \quad (54)$$

The zero-order solution can be readily shown to be identical with that given by Plesset and Zwick (P7). In accordance with the observations of Birkhoff, Margulies, and Horning (B19), the perturbation procedure converges rapidly for  $N_j > 2.5$ .<sup>6</sup> Some information concerning the variation of the Jakob number with system pressure can be obtained from the data of Cichelli and Bonilla (C2), who boiled a number of organic liquids from a chromium-plated horizontal surface. For these data the excess temperature of the heating surface at maximum flux (departure from nucleate boiling) has been related to the reduced pressure by an equation of the form (B6)

$$T_w - T_s = 45 \log_{10} p_r \quad (55)$$

where  $T_w$  and  $T_s$  are the wall and saturation temperatures, and  $p_r$  is the reduced pressure. The corresponding variation in the Jakob number with reduced pressure for two common liquids is shown in Fig. 4. As might be expected, the inertial correction term becomes entirely negligible at higher pressures, justifying the termination of the iteration scheme in Eqs. (46–49) at  $j = 0$ . At higher pressures, on the other hand, the perturbation series converges slowly, or possibly not at all. The application of this technique to bubble dynamics with non-isothermal initial conditions and in two-component liquids will be discussed later.

(2) *Barlow-Langlois solution of bubble growth in a viscous fluid.* Barlow and Langlois (B14) treat, in connection with a proposed dry photographic process based upon light sensitization of a diazo compound, the isothermal growth of nitrogen bubbles from a supersaturated, highly viscous, plastic melt. As a first approximation the fluid is assumed to be Newtonian in behavior. The equilibrium between the gas concentration within the bubble and the dissolved gas concentration at the bubble wall is expressed in terms of Henry's law:  $C_g = k_H C(R, t)$ . The diffusion equation is solved in the absence of sources of dissolved gas, which implies that the decomposition of

<sup>6</sup> Professor L. A. Skinner, in a private communication (S13b), makes some interesting comments, based upon Fig. 2, on the validity of the thin thermal boundary layer assumption. Approximating the curve by a straight line in the interval  $0.2 < 1/\beta < \infty$ , one obtains

$$\frac{\chi(1/\beta) - \chi(\infty)}{\beta} \cong -0.4$$

which, in view of Eqs. (18) and (19), can be written as

$$\beta = (12/\pi)^{1/2} N_j (1 + 0.4/N_j), \quad \beta > 5 \quad \text{or} \quad N_j > 2.5 \quad (19')$$

Hence, for  $N_j > 4$ , the error of the thin boundary layer approximation is less than 10 percent, while at  $N_j = 2.5$  the error is 16 percent. The first two terms of the above perturbation solution, Eqs. (50) and (51), yield, upon inverting to the real time domain,

$$R(t) = \beta' (\alpha t)^{1/2}; \quad \beta' = (12/\pi)^{1/2} N_j (1 + (4/9)/N_j)$$

Noting the close comparison with Eq. (19'), Skinner suggests that, in related problems which do not have exact solutions, the first-order correction will continue to be reasonably accurate.

the diazo compound upon heating the plastic is completed prior to the initiation of bubble growth. A transformation to the Lagrangian coordinates introduced by Plesset and Zwick gives, upon employing the thin boundary

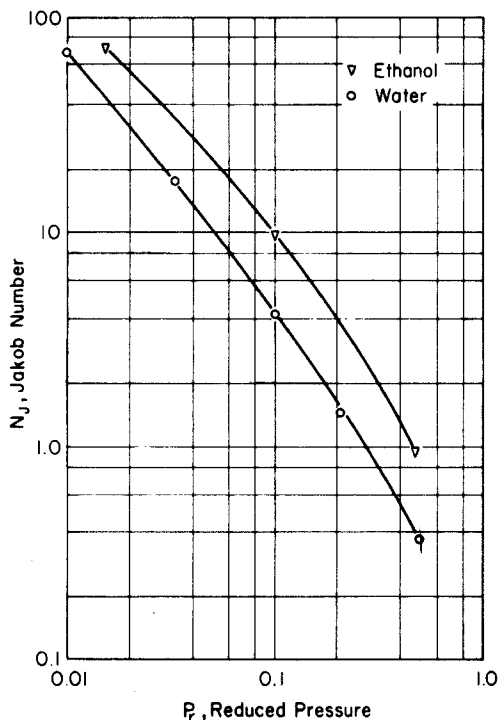


FIG. 4. Jakob number of maximum heat flux vs reduced pressure curves for ethanol and water (B7).

layer assumption (equivalent to truncating the perturbation expansion at the leading term), for the gas concentration (density) in the bubble

$$\frac{C_g}{k_H} = C_\infty - \frac{1}{3(\pi\mathcal{D})^{1/2}} \int_0^\zeta \frac{1}{(\zeta - \zeta')^{1/2}} \frac{d(R^3 C_g)}{d\zeta'} d\zeta' \quad (56)$$

which can be compared with the solution for the bubble wall temperature in the corresponding heat diffusion problem. From Eq. (7), assuming ideal gas behavior and  $\varepsilon = 1$ , one obtains

$$C_g = \frac{M}{R_g T} \left[ p_\infty + \rho R \ddot{R} + \frac{3}{2} \rho \dot{R}^2 + 4\mu \frac{\dot{R}}{R} + \frac{2\sigma}{R} \right] \quad (57)$$

Upon combining these equations the difficulty due to the singularity of the

integrand is avoided by taking the Cauchy principal value (H1, M8). Eventually, the integrodifferential equation

$$\begin{aligned} \frac{1}{C_\infty k_H} \int_0^t \left\{ 1 + \left[ \frac{R^3 k_H}{3} \left( \pi \mathcal{D} \int_{t'}^t R^4 dt'' \right)^{1/2} \right] \right\} C_g R^4 dt' \\ = \frac{2R_0^3 k_H}{3(\pi \mathcal{D})^{1/2}} \left[ \int_0^t R^4 dt' \right]^{1/2} + \int_0^t R^4 dt' \quad (58) \end{aligned}$$

is obtained, where  $C_g$  is given by Eq. (57). This is obviously a formidable equation, which illustrates the complications which arise when employing a flux boundary condition at the bubble wall in solving the diffusion problem. A simpler form would be expected if a concentration boundary condition were used, in a double (perturbation-iteration) approximation series similar to that given above for the heat diffusion problem. The relation to the functional equations discussed in (B8), derived by Kolodner (K5), Boley (B20), and others for the free boundary position should also be noted. In common with all integral representations, they have the advantage of representing all features of the solution, so that limiting cases (such as  $[(R/R_0) - 1]$  small or large) can be derived from the same expression. Barlow and Langlois find in this way that the bubble radius initially increases linearly with time in a viscous melt. For the asymptotic stage where the bubble pressure is essentially equal to the ambient pressure, the self-similar solution of Birkhoff *et al.* can be employed. However, since the bubbles are here much smaller ( $\sim 1-2 \mu$ ) than those measured in boiling and the liquid viscosity much higher ( $\sim 10^6$  dyn-sec/cm), a direct numerical solution of Eq. (58), neglecting inertial terms, is necessary over most of the range of interest. The simpler problem of the growth or collapse of a bubble where viscous and inertial effects control was previously considered by Poritsky (P8).

*c. Forster-Zuber Moving Source Solutions.* Forster and Zuber (F5) obtained an approximate solution for the heat diffusion problem by considering the moving bubble wall to be a spherical heat sink in a stationary medium. This gives the temperature at the bubble wall as

$$\begin{aligned} T_\infty - T_b = \frac{L\rho'}{\rho c_p (\pi \alpha)^{1/2}} \int_0^t \frac{R(t') \dot{R}(t')}{R(t)(t-t')^{1/2}} \\ \left\{ \exp \left[ -\frac{[R(t) - R(t')]^2}{4\alpha(t-t')} \right] - \exp \left[ -\frac{[R(t) + R(t')]^2}{4\alpha(t-t')} \right] \right\} dt' \quad (59) \end{aligned}$$

This is equivalent to replacing the actual problem by an approximating problem, in which the heat conduction takes place in a stationary liquid,

followed by a discontinuous motion of the bubble radius from  $R_0$  to an appropriate  $R(t)$ , where  $R(t)$  is determined by the heat conducted through the bubble wall. Forster (F4) later expands this notion to a sequence of discontinuous motions and stationary heat conduction periods as an approximating procedure to any moving-boundary diffusion problem. Since the complete analytical solution must be evaluated at each point in space at each time interval, this finite-difference procedure may be lengthier than direct numerical methods.

For the asymptotic stage of bubble growth, the inertial terms of the equations of motion are neglected, and the integral in Eq. (59) is simplified by physical arguments and application of the mean-value theorem to give

$$\frac{R}{R_0} + \log \left( \frac{R - R_0}{R_1 - R_0} \right) - \frac{N_J(\pi\alpha t)^{1/2}}{R_0}, \quad R > R_1 \quad (60)$$

$R_1$  may here be regarded as an arbitrary constant with which to match the solution to the solution for earlier times. For  $R \gg R_1$ , this becomes

$$\beta/N_J = (\pi)^{1/2}, \quad \beta = R/(\alpha t)^{1/2} \quad (61)$$

which is 9% higher than the constant,  $(12/\pi)^{1/2}$ , of the Plesset-Zwick asymptotic solution, Eq. (43). The latter constant is also the limit for large  $N_J$  of the exact solution given by Birkhoff *et al.* The Forster-Zuber theory is conceptually simpler than the Plesset-Zwick theory and may be perfectly adequate in many practical problems, although error estimates are difficult to obtain. The Plesset-Zwick theory has the advantage that the approximations are based directly upon the governing equations, so that a rigorous error estimate is available at every stage, and, in principle at least, higher-order corrections can be obtained.

Yang and Clark (Y1) have applied this source theory to two-component bubble growth problems, including the case where one of the components is a noncondensable, nonsoluble gas. An example is helium gas bubbles introduced into liquid oxygen to provide subcooling of the liquid, in order to prevent pump cavitation in liquid rocket engines. A comparison is made with the exact theory, showing reasonable agreement.

## C. BUBBLE GROWTH UNDER NONUNIFORM INITIAL CONDITIONS

### 1. Introduction

In actual practice vapor bubbles almost always originate at solid surfaces, rather than in the midst of a large body of uniformly superheated liquid. This introduces a number of additional complications, whose effect in most cases is still largely unknown. Even for isolated bubbles the spherical shape is

usually distorted by buoyancy and inertial effects. Nevertheless, for analytical purposes it is usually assumed that the bubble retains a spherical, hemispherical, or a spherical segmental shape, depending upon the contact angle between the bubble and the solid surface. Unless this is  $90^\circ$ , the center of mass of the bubble translates with respect to the liquid, introducing an additional complication which is normally ignored. Furthermore, a velocity boundary layer is established around the expanding bubble in the neighborhood of the solid wall, which violates the assumption of the spherical symmetry of motion. Exact analysis of these complications has not yet proved possible. Consequently, three alternatives have been explored: (1) numerical solutions of the equations of change subject to suitable boundary conditions; (2) analytical solutions for the growth of a single bubble surrounded by a liquid of initially nonuniform temperature (where the temperature distribution is chosen to approximate the as-yet unmeasured temperature distribution in the liquid surrounding a bubble originating at a heated surface); and (3) alternatively, more or less heuristic theories, based upon physical arguments, which attempt to explain the main features of the process. The present section deals with the first two approaches.

## 2. Numerical Solutions

Once purely radial motion has been assumed, the solution can be obtained either numerically or analytically. The numerical solution has the advantage of permitting the formulation of more realistic initial and boundary conditions (although what these should be has not yet been experimentally determined). Griffith (G7) considers the growth of a hemispherical bubble on a heating surface, with initial radius  $R_0 < l$ , the thickness of the thermal boundary layer near the heating surface. The initial temperature distribution in the liquid near the wall is assumed to be linear through the thermal boundary layer, even in the neighborhood of the bubble wall, and constant outside this boundary layer. A numerical integration of the dimensionless energy and continuity equations is performed for various values of the parameters  $N_j$  and  $\omega = (T_w - T_\infty)/(T_\infty - T_b)$ . Note that the thermal boundary layer next to the heated wall grows thicker as growth proceeds and that radial temperature symmetry does not exist. The temperature of the bubble wall  $T_b$  is assumed to be the saturation temperature. The calculations are performed for bubble growth only. For small Jakob numbers, corresponding to large thermal boundary layers, the plane approximation is found to be inadequate. Griffith finds that for  $N_j = 0.35$  a significant quantity of heat is transferred from the surface to the bubble through the liquid, while at higher values of the Jakob number, corresponding to low pressure, the bubble grows primarily as a result of vaporization of the initially superheated liquid. A further interesting result is that for small Jakob numbers the maximum size attained by the

bubble is proportional to the thickness of the layer of superheated liquid near the surface, and is independent of  $N_J$ .

### 3. Analytical Solutions

*a. Savic and Gosnell (S2).* Savic and Gosnell used an entirely different technique from any of those discussed above. Upon taking  $\varepsilon = 1$  and  $Q = 0$  (no heat source), Eq. (8) becomes

$$\frac{\partial T}{\partial t} + \frac{\dot{R}R^2}{r^2} \frac{\partial T}{\partial r} = \alpha \frac{\partial^2 T}{\partial r^2} \quad (62)$$

where it has been assumed that  $(1/r)(\partial T/\partial r) \ll (\partial^2 T/\partial r^2)$ . It is seen that this is tantamount to the thin thermal boundary layer assumption. Defining a new spatial variable by  $y = r - R$ , Eq. (62) becomes

$$\alpha \frac{\partial^2 T}{\partial y^2} + \dot{R} \frac{\partial T}{\partial y} \left[ 1 - \frac{1}{(1 + y/R)^2} \right] = \frac{\partial T}{\partial t} \quad (63)$$

Note that this is not a Lagrangian transformation, although the bubble wall is immobilized. The initial temperature function is taken to be a quadratic polynomial

$$t = 0: \quad T - T_s = T_{b0} - a_1 y + a_2 y^2 \quad (64)$$

The bubble wall is assumed to be at the saturation temperature corresponding to the ambient pressure:

$$t > 0, \quad y = 0: \quad T = T_s \quad (65)$$

The heat balance at the bubble wall, Eq. (14), may be written

$$y = 0: \quad \frac{\partial T}{\partial y} = \frac{T_{b0} - T_s}{\alpha N_J} \dot{R} \quad (66)$$

New independent variables are now introduced into Eq. (63):  $s = y/R$  as a position variable, and  $R(t)$  as a time variable, giving

$$\frac{\alpha}{R\dot{R}} \frac{\partial^2 T}{\partial s^2} + \frac{\partial T}{\partial s} \left[ 1 + s - \frac{1}{(1 + s)^2} \right] = R \frac{\partial T}{\partial R} \quad (67)$$

For uniform temperature fields,  $R\dot{R}$  is nearly constant, in which case the variables become separable. A perturbation solution is, therefore, attempted of the form

$$R\dot{R} = b_0 + b_1 R + b_2 R^2 + \dots \quad (68)$$

$$T - T_s = d_0(s) + b_1 R d_1(s) + b_2 R^2 d_2(s) + \dots \quad (69)$$



which, on substitution into Eq. (67) and noting that

$$1 + s - (1 + s)^{-2} \cong 3s \quad (70)$$

if  $s \ll 1$ , gives eventually a set of confluent hypergeometric equations for the temperature field close to the bubble wall. In order to make the equations consistent with the assumed form of the initial temperature distribution, Eq. (64), it is necessary to consider both "inner" and "outer" boundary layer solutions, which are patched together at a convenient intermediate point. For details the reader is referred to the original reference. A comparison is made (Fig. 5) with the numerical solution of Griffith (G7) for the growth of a hemi-

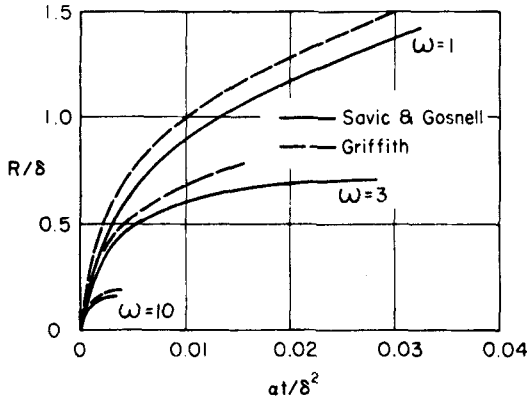


FIG. 5. Bubble growth curves for various  $\omega$  (S2).

spherical bubble on a heated plane surface, where the initial temperature decreases linearly through a wall boundary layer, outside of which it is uniform. In order to make a comparison, the inverse thickness of the superheated layer over the surface of the bubble is averaged to give an equivalent spherically symmetric problem. In general, the solutions are in agreement within 10 percent. The averaging procedure is justified by an extension of the analysis to axisymmetric temperature distributions. It is also verified, in agreement with Griffith's calculations (G7), by computation of the isotherms when the bubble projects a considerable distance beyond the heating surface boundary layer, that simultaneous vaporization near the bubble base and condensation at the crown occur, as postulated by Ellion (E2). Other arguments for the importance of this latent heat transport mechanism, especially in subcooled boiling, have been presented (B6, B9).

*b. Skinner and Bankoff (S12).* Bankoff and Mikesell (B10) employed, as noted, a variant of the Plesset-Zwick perturbation technique to obtain

bubble growth curves for initial temperatures which were exponential and ramp functions of the Lagrangian radial coordinate  $m$ . More recently, Skinner and Bankoff (S12) solved the problem for a spherically symmetric, but otherwise arbitrary, initial temperature distribution in the liquid,  $f(m)$ , and explored some features of the solution.

We define a dimensionless temperature by

$$g(m) \equiv [f(m) - T_s]/[f(0) - T_s] \quad (71)$$

and a dimensionless time by

$$\zeta_1 = \frac{\alpha}{l^2} \int_0^t \mathcal{R}^4(\tau) d\tau, \quad \mathcal{R} = \frac{R}{l} \quad (72)$$

where  $l$  is a characteristic length to be chosen later, and  $m$  is the position variable defined by Eq. (25). Frequently  $f(0) = T_{b0}$ , the initial bubble wall temperature, is identified, in the absence of other information, with the heater wall temperature  $T_w$ . The zero-order solution turns out, for zero initial radius, to be simply

$$\mathcal{R}_0^3(\zeta_1) = 3N_J \int_0^\infty g(m) \operatorname{erfc}\left(\frac{m}{2\zeta_1^{1/2}}\right) dm \quad (73)$$

This result, combined with the inverse of Eq. (72),

$$\frac{\alpha t}{l^2} = \int_0^{\zeta} \frac{d\zeta'}{\mathcal{R}_0^4(\zeta')} \quad (74)$$

gives a parametric representation for the bubble curve.

An important conclusion to be drawn from the form of Eq. (73) is that the nature of the initial temperature distribution some distance away from the bubble wall is of little consequence, so that no restriction need be made that the initial temperature variation occur entirely within a thin thermal boundary layer. For uniform initial superheat the effect of nonzero initial radius is next examined. Taking  $l = R(0)$ , a simple modification of the analysis leads to

$$\mathcal{R}_0^3(\zeta_1) = 1 + N_J (\zeta_1/\pi)^{1/2} \quad (75)$$

Substituting into Eq. (72), one obtains a cubic equation, whose solution is

$$R_0(t) = 2 \left( R^2(0) + \frac{4N_J^2 \alpha t}{\pi} \right)^{1/2} \cos \left[ \frac{\pi}{6} + \frac{1}{3} \sin^{-1} \left( 1 + \frac{4N_J^2 \alpha t}{\pi R^2(0)} \right)^{-3/2} \right] \quad (76)$$

This reduces to the leading term of the Plesset-Zwick asymptotic solution, Eq. (43), for large time, or for  $R(0)=0$ . The displacement between the two bubble radius expressions when the bubble radius has increased tenfold is

less than 2% of the bubble radius. The neglect of the initial radius in the self-similar solutions of Birkhoff *et al.* and Scriven is, therefore, justified, although it should be noted that the effect of neglecting the inertial and surface tension terms has not been considered.

The essential information concerning the behavior of the integral in Eq. (73) can be obtained from an examination of the solution for the initial temperature function  $g(m) = 1 - 2am/\pi^{1/2}$ , which may be looked upon as a truncated Maclaurin expansion of the temperature field. The first perturbation in the bubble volume was calculated exactly:

$$\frac{V_1}{V_0} = \frac{R_1^3}{R_0^3} = \frac{\frac{4}{9} - \frac{2}{3} \sum_{n=1}^{\infty} \frac{n+6}{(n+1)(n+3)} B\left(\frac{1}{2}, \frac{n}{2}\right) a^n \zeta_1^{n/2}}{N_J(1 - a(\zeta_1)^{1/2})} \quad (77)$$

where  $B(p, q)$  is the Beta function. For the uniform superheat case  $a = 0$ , and Eq. (51) is obtained; at the maximum radius it turns out, for  $a > 0$ , that

$$\frac{V_1}{V_0} \doteq -\frac{1.7}{N_J}; \quad \zeta_1 = \frac{1}{4a^2} \quad (78)$$

and when the bubble has collapsed to three-quarters its maximum size,

$$\frac{V_1}{V_0} \doteq -\frac{7.5}{N_J}; \quad \zeta_1 = \frac{9}{16a^2} \quad (79)$$

Clearly, as time proceeds, this ratio continues to grow, so that the region of applicability of the zero-order solution, based on the thin thermal boundary layer concept, cannot be extended very far into the collapse phase. This is in accord with the physical facts, since the thermal boundary layer thickness is monotonically increasing, while the bubble radius is shrinking.

Computations were carried out in detail for an exponential initial temperature distribution:

$$T(r, 0) = T_{\infty} + (T_w - T_{\infty}) \exp(-r^6/9l^6) \quad (80)$$

where  $l$  may be thought of as an initial thermal boundary layer thickness, and  $l/R \ll 1$  during most of the bubble life. In this case the bubble growing on a heated surface may tend to deform rather than pierce the thermal boundary in which it originates, implying that the temperature gradient near the bubble wall will be normal to it. On substituting into Eqs. (73) and (74), dimensionless radius-time curves were determined for various values of  $\omega \equiv (T_w - T_{\infty})/(T_w - T_s)$  (Figs. 6 and 7).

Finally, the restriction of spherically symmetric initial distributions can be removed, so that the solution for general initial temperature fields of the

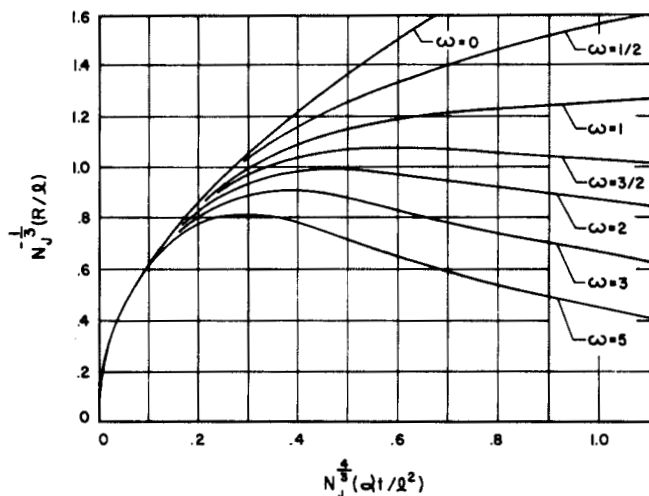


FIG. 6. Bubble growth curves for various  $\omega$  (S12);  $\omega > 1$  corresponds to subcooled boiling,  $\omega = 1$  to saturated boiling, and  $\omega = 0$  is the uniform initial superheat case.

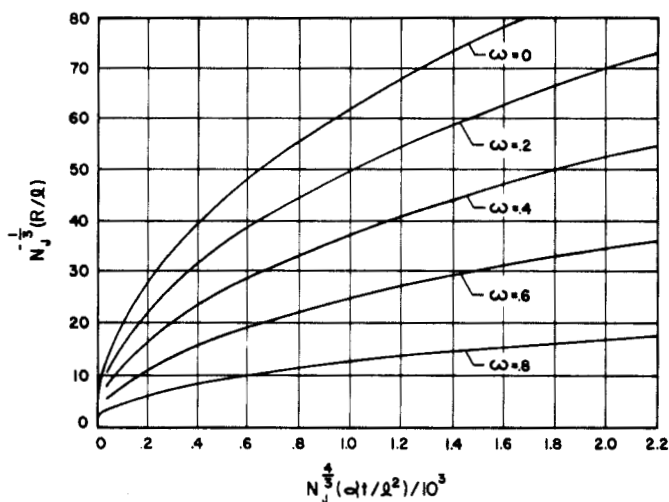


FIG. 7. Bubble growth curves for cases when the bulk liquid is superheated,  $0 \leq \omega < 1$  (S12).

form  $T(r, \theta, \varphi, 0) = f(r, \theta, \varphi)$  can be found (S11). For this problem the Laplacian operator on the right-hand side of Eq. (22) is given by

$$\nabla^2 = \frac{1}{r^2} \frac{\partial}{\partial r} \left( r^2 \frac{\partial}{\partial r} \right) + \frac{1}{r^2} \sin \theta \frac{\partial}{\partial \theta} \left( \sin \theta \frac{\partial}{\partial \theta} \right) + \frac{1}{r^2} \sin^2 \theta \frac{\partial^2}{\partial \varphi^2}$$

while the energy balance at the bubble wall now requires

$$\frac{dR}{dt} = \frac{k}{4\pi L\rho'} \int_0^{2\pi} \int_0^\pi \frac{\partial T(R, \theta, \varphi, t)}{\partial r} \sin \theta \, d\theta \, d\varphi \quad (81)$$

assuming constant vapor density and latent heat in the asymptotic bubble growth phase. With the introduction of the averaged temperature excess

$$\Theta(r, t) = \frac{1}{\Delta T} \int_0^{2\pi} \int_0^\pi [T(r, \theta, \varphi, t) - T_s] \sin \theta \, d\theta \, d\varphi \quad (82)$$

where

$$\Delta T = \int_0^{2\pi} \int_0^\pi [f(0, \theta, \varphi) - T_s] \sin \theta \, d\theta \, d\varphi \quad (83)$$

the differential equation, with associated initial and boundary conditions, then becomes

$$\frac{\partial \Theta}{\partial t} + \frac{dR^3/dt}{3r^2} \frac{\partial \Theta}{\partial r} = \frac{\alpha}{r^2} \frac{\partial}{\partial r} \left( r^2 \frac{\partial \Theta}{\partial r} \right) \quad (84)$$

$$\Theta(r, 0) = \frac{1}{\Delta T} \int_0^{2\pi} \int_0^\pi [f(r, \theta, \varphi) - T_s] \sin \theta \, d\theta \, d\varphi \triangleq g(r) \quad (85)$$

$$\frac{dR}{dt} = \alpha N_J'' \frac{\partial \Theta(R, t)}{\partial r} \quad (86)$$

$$\Theta(R, t) = 0 \quad (87)$$

The constant  $N_J''$  in Eq. (86) is a generalized Jakob number defined by

$$N_J'' = k \Delta T / \rho' L \alpha \quad (88)$$

In this form the parametric solutions, Eqs. (73) and (74), for the spherically symmetric problem can be applied immediately. Physically this implies that a bubble growing in an initially arbitrary temperature field grows at precisely the same rate as if the initial temperature were averaged in each thin spherical shell surrounding the bubble center. Two special cases are considered in detail: (1) the linear thermal boundary layer, of thickness  $l$ , next to the heating surface, outside of which the temperature is uniform; and (2) the exponential boundary layer, where the temperature is assumed to decay exponentially with distance from the wall. The latter distribution is of the form

$$f(r, \theta) = T_\infty + (T_w - T_\infty) \exp \left( -\frac{2r \cos \theta}{l} \right), \quad 0 < \theta \leq \pi/2 \quad (89)$$

It should be noted that in attempting to connect the temperature distributions given by Eqs. (80) and (89) to surface boiling, two separate limiting cases are being considered. Equation (80) implies that the thermal boundary layer associated with the hot surface becomes deformed around the bubble in a manner leading to the approximation of an initially spherically symmetric temperature distribution. This picture seems reasonable when the bubble radius at the start of asymptotic growth is somewhat larger than the thermal boundary layer thickness. On the other hand, Eq. (89) implies that the boundary layer thickness is large compared with the initial radius, so that the temperature field is essentially undisturbed as the bubble enters the asymptotic stage. The further assumptions are made that the bubble is hemispherical, thermal coupling between the vapor phase and the boiling surface is poor, and liquid heating across the surface is sufficiently low to be negligible over the bubble lifetime. Under these assumptions one has the equivalent problem of an entire vapor sphere growing in a liquid whose temperature field is symmetric about the equator plane.

The explicit solution for the exponential thermal boundary, Eq. (89), is conveniently expressed in parametric form

$$R^3(z) = \frac{6N_j'' z^3}{(\pi)^{1/2}} [1 - \omega\psi(z)] \quad (90)$$

$$\tau = \frac{\alpha t}{l^2} = \left( \frac{\pi^2}{6N_j''^4} \right)^{1/3} \int_0^z \frac{z \, dz}{[1 - \omega\psi(z)]^{4/3}} \quad (91)$$

where

$$\psi(z) = 3 \sum_{n=1}^{\infty} \frac{(-1)^{n+1} \Gamma(n/6 + 1)}{(n+3)(n+1)!} (48z^3)^{n/3} \quad (92)$$

These solutions are shown in Fig. 8, where  $\omega = 0$  represents uniform initial superheat. As the subcooling of the bulk liquid increases, a relatively long period of very slow change in radius is predicted. Similar behavior is frequently noted in boiling from surfaces.

For the linear case,

$$f(r, \theta) = \left\{ \begin{array}{ll} T_{\infty}, & 0 < \theta < \cos^{-1} l/r \\ T_{\infty} + (T_w - T_{\infty}) \frac{r \cos \theta}{l}, & \cos^{-1} l/r < \theta < \pi/2 \end{array} \right\}, \quad r/l > 1 \quad (93)$$

$$\left\{ T_{\infty} + (T_w - T_{\infty}) \left( 1 - \frac{r \cos \theta}{l} \right), \quad r/l < 1 \right.$$

The solution is somewhat more complicated (and is hence not given here), but leads to slightly larger bubble volumes (Fig. 9) than the exponential

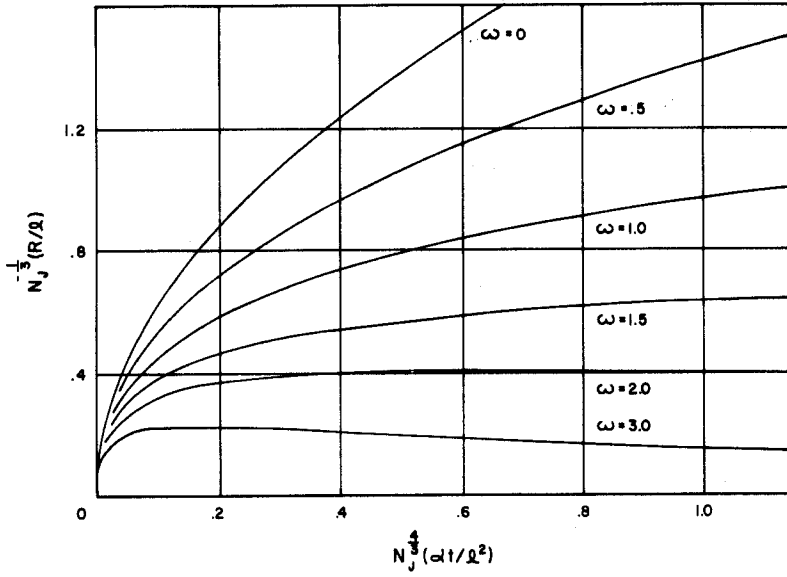


FIG. 8. Bubble growth curves for various  $\omega$  for the case of exponential thermal boundary (S11).

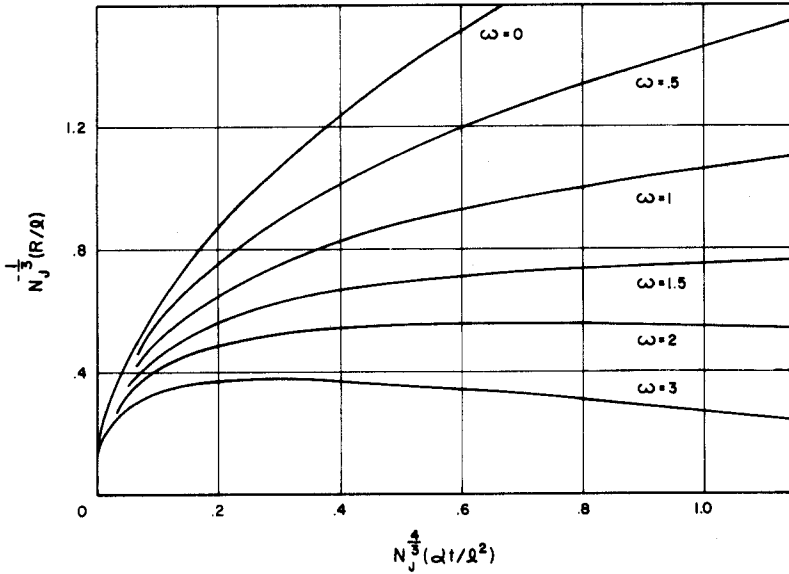


FIG. 9. Bubble growth curves for various  $\omega$  for the case of linear thermal boundary (S11).

boundary of equivalent superheat energy. This is to be expected, in view of the slightly greater thickness of the equivalent exponential layer. A comparison is made of the linear boundary solution at  $N_j = 5.3$  with Griffith's numerical solution of a similar problem (G7), in which the initial condition is given by Eq. (93), but a boundary condition is imposed of the form  $T = T_w$  at  $\theta = \pi/2$ . Griffith's growth rates are somewhat larger, since the wall now continues to transfer heat into the system after bubble growth has commenced (Fig. 10).

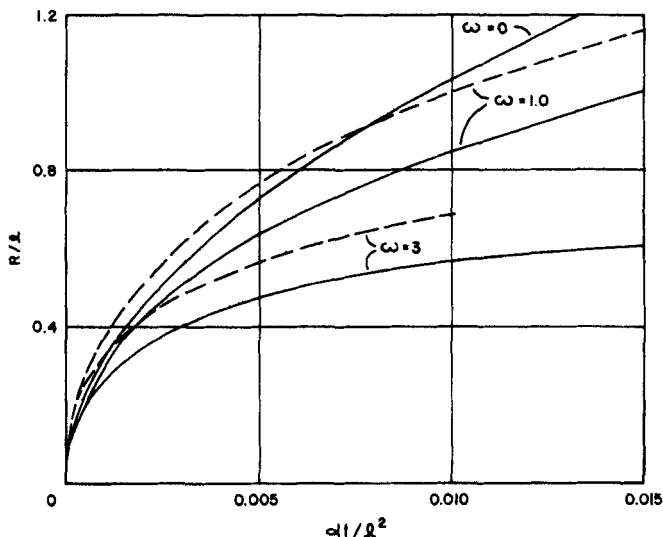


FIG. 10. Comparison between linear boundary solution and Griffith's numerical solution (dashed lines) at  $N_j = 5.3$  (S11).

*c. Dougherty and Rubin (D6).* Dougherty and Rubin consider the growth and collapse of vapor bubbles on a boiling surface by expanding the temperature field in terms of spherical harmonics, and retaining only the zero-order term. This is equivalent to averaging the temperature in the tangential direction. Although inertial terms are dropped, the small variation in vapor superheat with time, as well as the surface tension and viscous terms, are retained in arriving at a nonlinear integral equation for the radius of the vapor bubble. In the asymptotic stages this reduces to

$$R^2(t) \simeq R_1^2(t) + \int_{t_0}^t \{K(t-\tau)^{1/2}[R_i - (R - R_0)] - (t-\tau)\dot{R}^2(\tau)\} d\tau$$

$$K = \frac{4L^2\rho'}{keT_s} \left(\frac{\rho'}{\rho}\right) \left(\frac{\alpha}{\pi}\right)^{1/2} \quad (94)$$

where  $R_i$  is the radius of an isothermal vapor bubble whose vapor phase



remained at saturation temperature and pressure throughout the growth and collapse stages, and  $t_0$  is the time at which asymptotic growth commences.  $R_1$  is the bubble radius at the commencement of asymptotic growth and is given by a separate integral equation. At this point an argument is employed from the calculus of variations. Noting that the left-hand side of Eq. (94) is positive semidefinite, the collapse time is argued to correspond to a stationary point of the functional on the right-hand side. This is incorrectly stated to lead to a linear Euler equation for  $R(t)$ ,

$$t\ddot{R} + \dot{R} - \frac{1}{2}K(t)^{1/2} = 0 \quad (95)$$

whereas the correct Euler equation<sup>7</sup> is

$$(t_c - t)\ddot{R}(t) + \dot{R}(t) - \frac{1}{2}K(t_c - t)^{1/2} = 0 \quad (96)$$

Upon application of the boundary condition  $R(t_c) = 0$  the solution to this equation blows up.

*d. Han and Griffith (H2).* For the growth of a single bubble in a liquid of initially uniform superheat, all theories (including the simple plane approximation) predict that the radius asymptotically grows as the square root of time. Furthermore, the range of the predicted growth constants is relatively small. Noting this, Han and Griffith employ an empirical correction factor to take into account curvature and stretching of the thermal boundary layer, using the plane approximation. In addition, an empirical heat transfer coefficient, chosen to give best agreement with data, is defined for the heat transfer between the wall and the bubble base. The calculation is now very simple. A linear temperature profile is assumed initially in some thermal boundary layer next to the wall and a constant temperature outside of this region. A simplified model of bubble growth is taken, shown in Fig. 11, leading to the following equation for bubble growth:

$$\frac{dR}{dt} = \frac{\varphi_c \varphi_s}{\varphi_v} \frac{k}{\rho' L} \frac{\partial T(0, t)}{\partial x} + \frac{\varphi_b \tilde{h}(T_w - T_s)}{\varphi_v \rho' L} \quad (97)$$

where  $\varphi_c$  is the curvature factor to be discussed below;  $\varphi_s = (1 + \cos \varphi)/2$  is a surface factor which represents the ratio of the surface of the spherical segment to that of the complete sphere, and  $\varphi_b = (\sin^2 \varphi)/4$  and  $\varphi_v = [2 + \cos \varphi(2 + \sin^2 \varphi)]/4$  are similar base and volume ratios. Here  $\varphi$  is the contact angle, while  $\tilde{h}$  is the heat transfer coefficient from heating surface to steam bubble through its base area. It is important to note the assumption that the thermal boundary layer around the bubble is the same as that next to the wall. This implies physically that the bubble picks up the thermal boundary layer as it grows from a relatively small size, which is a plausible

<sup>7</sup> This was pointed out by Professor L. A. Skinner (S13b).

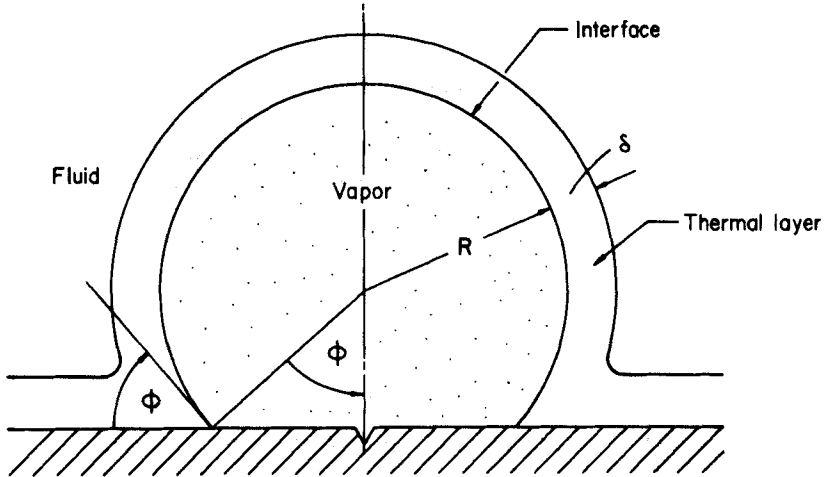


FIG. 11. Simplified model of bubble growth (H2).

limiting case for  $N_J \gg 1$ . However, one would expect, in this case, the boundary layer stretching error to be appreciable. On substituting the semi-infinite slab solution for the heat flux at the bubble wall one obtains

$$\frac{dR}{dt} = \frac{\varphi_c \varphi_s}{\varphi_v} \frac{k}{\rho' L} \frac{1}{(\pi \alpha t)^{1/2}} \left[ T_w - T_s - \frac{(T_w - T_\infty)}{\delta} (\pi \alpha t)^{1/2} \operatorname{erf} \left( \frac{\delta}{(4 \alpha t)^{1/2}} \right) \right] + \frac{\varphi_b \tilde{h} (T_w - T_s)}{\varphi_v \rho' L} \quad (98)$$

where  $\delta = (\pi \alpha t_w)^{1/2}$  is the computed thermal boundary layer thickness, and  $t_w$  is the waiting period between bubbles. For a bubble growing in an infinite fluid of uniform superheat this reduces to

$$\frac{dR}{dt} = \frac{\varphi_c k (T_w - T_s)}{\rho' L (\pi \alpha t)^{1/2}} = \frac{\varphi_c}{\pi^{1/2}} N_J \left( \frac{\alpha}{t} \right)^{1/2} \quad (99)$$

For the exact solution, Eq. (20), for a uniform initial superheat,  $\varphi_c = \sqrt{3}$ , while the plane approximation, treating the liquid surrounding the bubble as a semi-infinite slab, gives  $\varphi_c = 1$ . It is incorrectly stated then that, for  $\varphi = 0$  and  $\delta \ll R$ , the Plesset-Zwick thin thermal boundary layer solution leads to  $\varphi_c = \pi/2$ , whereas, as noted above, it agrees asymptotically with the exact solution. An empirical curvature factor is then manufactured to account for all three assumed cases,

$$\varphi_c = \left[ \sqrt{3} + \frac{\varphi}{\pi} (1 - \sqrt{3}) \right] \left[ \left( 1 - \frac{\varphi}{\pi} \right) \frac{[(\pi/(2\sqrt{3}))\bar{R} + \delta]}{\bar{R} + \delta} + \frac{\varphi}{\pi} \right] \quad (100)$$

where  $\bar{R}$  is the time-average bubble radius. Fairly good agreement is shown

with the measured  $R(t)$  of only three bubbles growing in distilled water at atmospheric pressure. It is evident that this theory, which may be useful for rough calculations, requires considerable additional experimental verification.

#### D. TWO-COMPONENT LIQUIDS

Van Wijk (V1) and Van Wijk, Vos, and Van Stralen (V3) pointed out that the temperature difference between a superheated binary liquid mixture and the dew point of the vapor bubbles which are formed shows a minimum at a certain low concentration of the more volatile component, and suggested that the bubble growth rate would also be least at this point. In the case of methyl ethyl ketone–water mixtures the minimum occurred at 4.1 wt. % ketone, which coincided with the experimentally observed maximum heat flux.

Scriven (S3), however, was the first to show that a self-similar solution could be found for a binary mixture of uniform initial temperature and composition. Detailed calculations were presented for the ethylene glycol–water system, shown in Fig. 12. In line with the observations of Van Wijk *et al.*, it

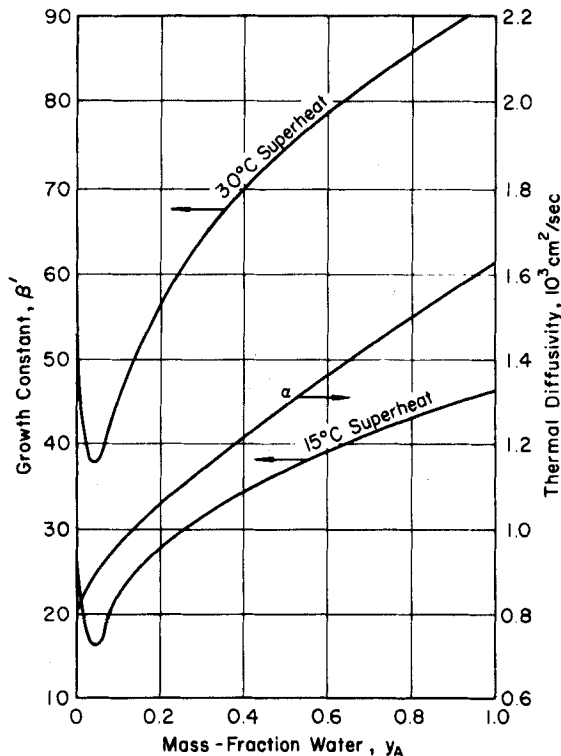


FIG. 12. Bubble growth in water–ethylene glycol solutions at 1 atm (S3).

is shown that the growth constant  $\beta$  goes through a minimum at about 0.05 wt fraction of water. This is attributable to the depletion of the volatile component near the bubble wall, while at the same time the temperature has been sufficiently depressed so that the volatility of the glycol is relatively low.

A more general two-component bubble growth solution (S13) permits both the initial temperature and concentration to be arbitrary functions of the radial distance. The same procedures used to solve the single-component problem are employed. A general solution is obtained and various limiting cases examined. For uniform initial conditions the solution is in agreement with the exact solution under conditions which assure rapid convergence of the perturbation procedure. An example problem is worked out for exponential temperature and concentration boundary layers initially surrounding the bubble. The process is somewhat more complicated than in single-component calculations since the time-average bubble temperature is not known *a priori*, so that an iterative scheme has to be established. By the space-averaging procedure discussed above it is thought that this technique can be extended to arbitrary initial temperature and concentration fields, so that this problem may be considered to be, in principle, solved.

#### E. GAS BUBBLE GROWTH

For isothermal gas bubble growth at atmospheric pressure,  $N_j'$  is usually small (Section II,B,1), so that  $\beta_3 \cong (2N_j')^{1/2}$ . This result is identical with that obtained by computing the concentration distribution at any instant from the Laplace equation (quasi-steady state approximation), and determining the bubble growth rate from the computed concentration gradient at the bubble wall. Kirkaldy (K4) discusses the conditions under which this simplification can be considered; a necessary condition is that the diffusion boundary layer thickness increase rapidly compared to the bubble radius, which is implied by small  $\beta$ . A less drastic simplification entails the neglect of the convective term, but not the time derivative, in the diffusion equation (quasi-stationary assumption). Fricke (F8) and Epstein and Plesset (E3) apply this approximation to the growth or dissolution of gas bubbles, and arrive at the result

$$\frac{dR}{dt} = \mathcal{D}N_j' \left[ \frac{1}{R} + \frac{1}{\delta} \right], \quad \delta = (\pi \mathcal{D}t)^{1/2} \quad (101)$$

This equation is solved exactly by Epstein and Plesset, and is also extended to include surface tension effects. Generally, for gas bubble growth,  $\delta/R \gg 1$ , corresponding to  $\beta \ll 1$ , and Eq. (101) reduces to the quasi-steady solution. This is in agreement with the limiting result obtained from the exact solution  $R \propto (2N_j' \mathcal{D}t)^{1/2}$ . On the other hand, when a gas bubble begins to dissolve,

$\delta/R \ll 1$ ; it is seen from Eq. (101) that, for this limiting case also,  $R \propto t^{-1/2}$ . However, eventually  $\delta/R \gg 1$  for a dissolving bubble, so that the steady-state solution prevails. For gas bubbles dissolving in water at atmospheric pressure with  $R(0) < 0.2$  mm, Houghton, Ritchie, and Thomson (H8) find that the transient term becomes negligible after about 100 sec. After this time the result reduces to the quasi-steady solution, governed by the Laplace equation, whose solutions have been extensively studied. For a bubble attached to a wall with zero contact angle, Liebermann (L6) thus shows that the rate of solution is reduced by a factor of  $\ln 2$ , leading to the result

$$\dot{R}^2(t) = R^2(0) - \frac{2\mathcal{D}N_J t}{\ln 2} \quad (102)$$

Manley (M3) extends this result to allow for nonzero contact angle.

Bruijn (B24) employs the quasi-stationary approximation, as discussed in Bankoff (B8), to the growth of vapor bubbles in superheated binary liquid mixtures. As noted previously, this neglect of the convective term in the diffusion equation is justified only when  $N_J \ll 1$ , which is usually not the case in atmospheric boiling. On the other hand, this technique would be applicable to isothermal gas bubble growth in three-component systems, where two of the components are dissolved gases.

Flatt (F3) computes bubble growth rates due to radiolytic gas formation in a power excursion in a homogeneous reactor. For very small bubbles the growth is assumed to be quasi-stationary so that the convective term can be dropped from the diffusion equation. A distributed exponential volume source is assumed. An integral equation for the radius is then obtained, from which upper and lower bounds for the radius of the bubble can be deduced.

For isothermal gas bubble growth in liquids of arbitrary initial concentration distribution, where the boundary layer volume is large compared to the bubble volume, it is recommended (S12) that a straightforward modification of the Epstein and Plesset (E3) quasi-stationary technique be employed.

### III. Experimental Bubble Growth Data

#### A. VAPOR BUBBLES

A classical set of experiments was performed by Dergarabedian (D2, D3) who irradiated water, carbon tetrachloride and other liquids, and photographed the asymptotic growth of minute bubbles originating within this uniformly superheated liquid. The superheat range was 2 to 10°C, and the pressure atmospheric, corresponding to  $N_J > 1$ . The initial and boundary conditions corresponded to the theory, so that the results are susceptible of

relatively unequivocal interpretation. As might be expected, the Plesset-Zwick theory gives good agreement with these results. The Forster-Zuber expression, Eq. (60), also gives good agreement with these data, despite the fact that the growth constant differs by 9%. This arises from the arbitrary choice of zero time for the asymptotic stage. For a more exact comparison of theory with experiment, microscopic bubble growth data would also have to be available. In most industrially important applications, however, bubbles grow while attached to solid surfaces, and most bubble growth data have been similarly obtained. Measurements of bubble growth in saturated or slightly subcooled pool boiling have been made by Patten (P1) of water at subatmospheric pressures from wires, and at atmospheric pressure by Vos and Van Stralen (V5) and Van Wijk and Van Stralen (V2) of water and water-methyl ethyl ketone mixtures from wires; by Bankoff and Mikesell (B11), based upon motion pictures taken by Zmola (Z3), of water from a horizontal strip; by Streng, Orell, and Westwater (S16) of pentane and ether from a flat vertical surface; and by Benjamin and Westwater (B17, B18) of water-ethylene glycol mixtures from a vertical copper surface with an artificial nucleation site. None of these experiments permits direct confirmation of the exact or of the boundary layer theories. The presence of the solid wall or wire, to an unknown degree, results in a distortion of the purely radial flow pattern postulated by the theory. More important, no measurements are available of the temperature (and/or concentration) fields in the liquid surrounding a bubble entering the asymptotic stage of growth. Without this information a discussion of the significance of the data and comparison with theory is necessarily of a heuristic nature. Nevertheless, some general observations can be made concerning all the data on saturated pool boiling:

1. Bubble growth from flat surfaces is almost always statistical in nature. This is apparently due to liquid turbulence induced by the wake of departing bubbles, coalescence with neighboring bubbles, momentary oscillating pressure fields within the fluid, and possible statistical variations in the nucleating surface. An exception is found in the experiments of Benjamin and Westwater (B17), who employed a 0.004-in. artificial cavity from which it was possible to produce a single stream of isolated bubbles. To some extent the same statistical behavior is observed in boiling from wires, although a greater degree of regularity seems to be present. For both horizontal surfaces and wires some bubbles were observed to vibrate, both before and after breaking away from the heating surface.

2. Even when photographed at framing speeds in excess of 5000 frames/sec, much of the total increment in bubble radius occurs in the first few frames. After this initial rapid growth period,  $t^{-1/2}R(t)$  usually decreases with time. The bubble is thus growing during most of its observable lifetime on the heating surface more slowly than predicted by the uniform superheat theory.

Perhaps the most extensive investigation is that of Streng, Orell, and Westwater (S16), who plotted  $R(t)$  on log-log paper for 86 pentane bubbles originating from a zinc surface with a superheat of 12°F. Upon fitting the best straight line to the late asymptotic data, a considerable statistical variation was observed, the mean exponent being 0.40, with a standard deviation of 0.04. A number of similar measurements were made at various heat fluxes and also in ether. Similar results were reported by Benjamin and Westwater for glycol-water mixtures. Although Scriven's theory is thus not applicable to these data, a qualitative confirmation was found of the theoretical prediction that the minimum growth coefficient occurs at about 5 wt-% in water-ethylene glycol mixtures.

Darby (D1) has recently made a photographic study of boiling of water and Freon 113 from a single nucleation site induced by external infrared irradiation. Surprisingly enough, the bubble radius was found to vary closely as  $t^{2/3}$  both before and after breakoff for all recorded runs. The data for both liquids were correlated by an expression of the form

$$R = 1.04 A_1^{2/3} (g\sigma)^{1/12} \left( \frac{c_p k}{L^2} \right)^{1/3} \left( \frac{\rho}{\rho'} \right)^{5/12} (T - T_s)^{2/3} t^{2/3} \quad (103)$$

where  $A_1$  is a constant obtained by comparison with the experimental data. It is not clear why the time exponent is so high, especially since the equipment is quite similar to that employed by Dergarabedian. One possibility is that the thermal boundary layer surrounding the bubble received an appreciable amount of irradiation after the initiation of growth, suggested by the fact that a continuous stream of bubbles was induced.

## B. GAS BUBBLES

Isothermal gas bubble growth, on the other hand, can be expected to conform more closely to the assumption of uniform initial conditions, since here the diffusion boundary layer is relatively thick. Westerheide and Westwater (W2, W3) measured the growth of hydrogen bubbles on a platinum cathode at constant emf (Fig. 13). The theoretical curves are obtained by calculating the growth constants in the exact solution which gives best fit with data. In the late asymptotic stage the faster-growing bubbles deviate significantly from this theoretical curve, presumably because the boundary layer thickness on the cathode is comparable to that of the bubble. It is found that the quasi-stationary solution, Eq. (101), gives a growth rate which is low by a factor of 14–21% when the theoretical supersaturation obtained by the above curve fitting is substituted. This is to be expected in view of the high modified Jakob numbers ( $N_j' \sim 0.4$ ), so that the quasi-stationary assumption would not be appropriate for such large supersaturations.

More extensive measurements of the growth of electrolytic bubbles were obtained by Glas and Westwater (G3), who made a number of interesting observations which will be reviewed here in some detail. The electrodes used

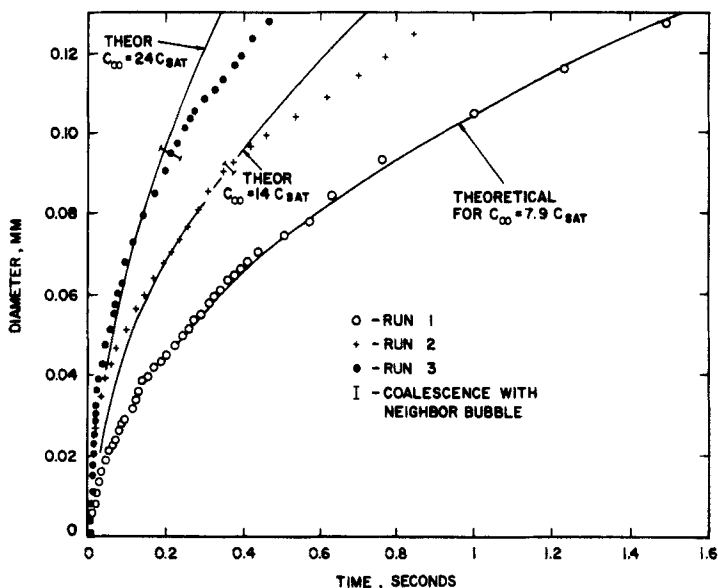


FIG. 13. Growth of hydrogen bubbles during electrolysis at constant emf. Run 1: 1N  $\text{H}_2\text{SO}_4$ , 1.24 v; Run 2: 0.1N  $\text{H}_2\text{SO}_4$ , 1.23 v; Run 3: 0.1N  $\text{H}_2\text{SO}_4$ , 1.47 v (W2).

were 0.127–0.508-mm wires of Pt, Ni, Fe, and Cu; the electrolytic gases were  $\text{H}_2$ ,  $\text{O}_2$ ,  $\text{Cl}_2$ , and  $\text{CO}_2$ . Most bubbles (Fig. 14) exhibited excellent straight-line plots of  $D$  vs  $t^{1/2}$ , from whose slope the effective supersaturation pressure can be calculated, based upon the self-similar solution for uniform initial conditions given by Birkhoff *et al.* (B19), and by Scriven (S3). Figure 15 shows a plot of the dimensionless driving force,  $N_j'/(1 - C_s/\rho) \equiv \Phi$ , vs the growth coefficient,  $\beta = 2\beta'$ , where  $\beta'$  is the growth coefficient defined by Scriven. It is seen that, except near the critical pressure,  $\Phi$  is very nearly equal to  $N_j'$ . In the same figure is shown the curve numerically computed by Buehl and Westwater (B25) for a bubble growing tangent to a wall which is not acting as a source of dissolved gas. At all  $N_j'$  the effect of the wall is to reduce the growth rate, but at  $N_j' \sim 1$ , the effect becomes negligible. On the other hand, for very slow growth  $\beta$  is about 30 percent smaller than in the absence at the wall.<sup>8</sup> The supersaturation ratios  $C_\infty/C_s$  computed in this

<sup>8</sup> As  $N_j' \rightarrow 0$ , corresponding to quasi-steady motion, the growth coefficient should be reduced by a factor of  $\ln 2$ , as in Eq. (102), in agreement with the numerical solution.



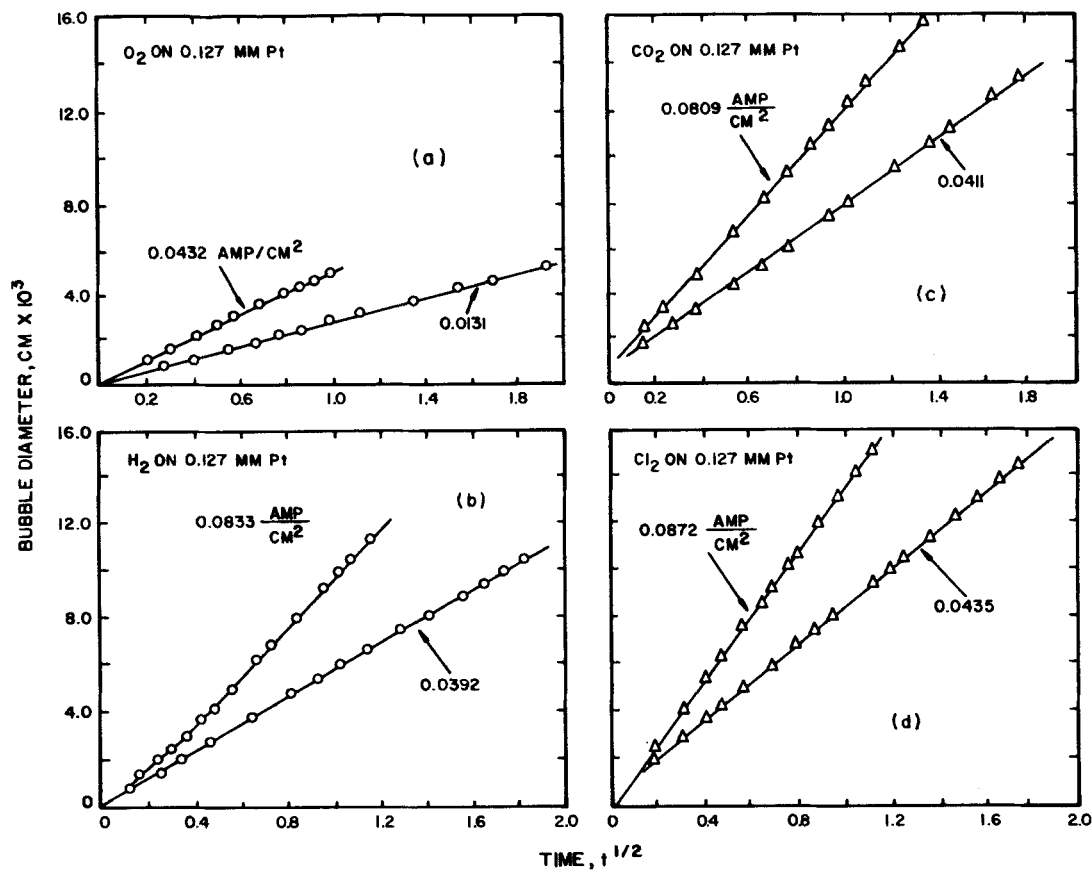


FIG. 14. Typical growth data for 8 bubbles at 1 atm: (a)  $O_2$  in 1.0N  $H_2SO_4$ , (b)  $H_2$  in 1.0N  $H_2SO_4$ , (c)  $CO_2$  in 1.0N  $Na_2C_2O_4$  plus 30%  $H_2SO_4$ , (d)  $Cl_2$  in 1.0N  $NaCl$  plus 0.01N  $NaOH$  (G3).

manner were 1.5/19.9 for  $H_2$ , 1.4/15.4 for  $O_2$ , 1.1/1.6 for  $CO_2$ , and 1.02/1.32 for  $Cl_2$ . Two separate models were proposed to correlate the effect of current density on  $\beta$ . A "steady-state" model considers the bubble volume (and hence  $\beta^3$ ) at any instant after growth initiates, to be proportional to the current density:  $\beta'I^{-1/3} = k_1$ , a constant. An "unsteady-state" model, patterned

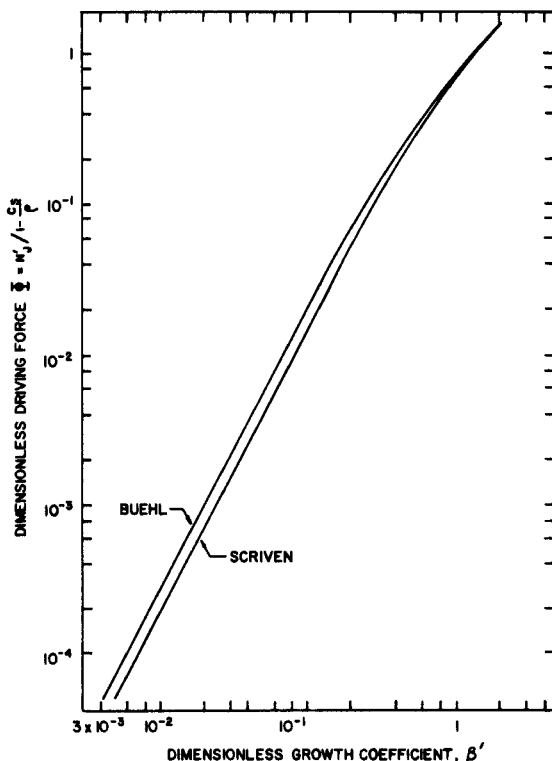


FIG. 15. Theoretical bubble growth constant at 1 atm: Scriven's values are for an isolated sphere; Buehl's values are for a sphere tangent to a plane (G3).

after a model proposed by Hsu (H10) for the analogous heat-transfer problem, computes the boundary layer thickness at the initiation of bubble growth from the observed waiting time  $t_w$  between bubbles. From the measured current density the average supersaturation  $C_\infty - C_s$  in the boundary layer can be computed. Assuming that the bubble grows in a uniform field of this average supersaturation, the dependence of  $\beta'$  on the current density  $I$  can be computed (Fig. 16). In this figure,  $k_1$  has been chosen for best fit of the data. Typical waiting times were 0.02–0.1 sec, and typical boundary layer thicknesses,  $\delta_w \cong (\pi D t_w)^{1/2}$ , were of the order of  $1 \times 10^{-3}$  cm. The difficulty in the latter approach now becomes apparent, in that  $D/\delta_w > 1$ , for nearly all

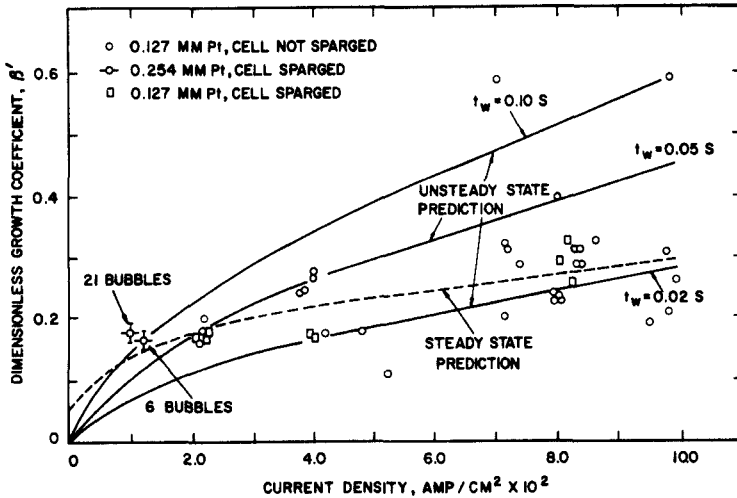


FIG. 16. Illustration of two theoretical models for effect of current density.  $\text{H}_2$  on Pt in  $1.0N \text{H}_2\text{SO}_4$  at 1 atm (G3).

the data points, so that the assumption that the bubble grows in a uniformly supersaturated fluid does not appear to be physically correct.

Another interesting result reported by Glas and Westwater was that hydrogen bubbles evolving from a polished nickel electrode (Fig. 17) showed an initially very rapid growth period,  $< 7 \times 10^{-4}$  sec, followed by a late asymptotic period during which  $(t^{1/2} \dot{R})$  was substantially constant. Note that

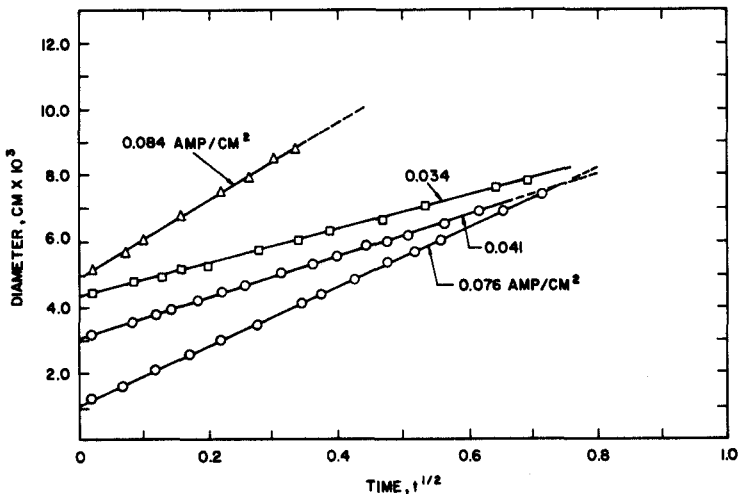


FIG. 17. Very rapid early growth in one movie frame followed by normal growth.  $\text{H}_2$  on four different sites on 0.127 mm Ni cathode in  $1.0N \text{H}_2\text{SO}_4$  at 1 atm (G3).

here  $[R(t) - R(t_0)]$  increases as the square root of time, where  $R(t_0)$  is the radius at the start of the late asymptotic growth, which is considerably different from the prediction of the self-similar solution,  $R(t) \sim t^{1/2}$ . It was observed that  $t_w$  was larger for this particular surface, resulting in higher supersaturations, possibly because of a higher degree of polish. All bubbles showed this initially very rapid growth, although usually the total growth in this period was sufficiently small that the extrapolated growth line (Fig. 14) passes close to the origin.<sup>9</sup>

The solution of gas bubbles is, in principle, a valuable means of measuring liquid-phase diffusivities. Mache (M2), Brandstaetter (B23), Liebermann (L6), and Manley (M3) measured the rate of solution of stationary air bubbles in partially saturated water. In general, the rate of diffusion at small bubble diameters is less than expected from theory; the probable explanation seems to be the accumulation of a film of organic material and/or dust particles at the bubble surface. Houghton, Ritchie, and Thomson (H8) extended the method to diffusivity measurements of a number of other gases. Doremus (D5) and Greene and Gaffney (G6) measured the solution rate of oxygen bubbles in molten glass.

#### IV. Surface Boiling

##### A. SUBCOOLED BOILING

As the bulk temperature of the liquid some distance away from the heating surface is decreased, the characteristics of the bubbles growing at the surface undergo a marked change. The bubbles become smaller and of higher fre-

<sup>9</sup> This behavior cannot be predicted by the self-similar theory. Indeed, it would be difficult to construct a physically reasonable nonuniform initial concentration distribution surrounding an isolated bubble which approximates this behavior. In order to do this, the supersaturation some distance from the bubble wall would be required to be uniform, but positive, while a thin layer of liquid at the bubble wall was initially very much more highly supersaturated. The measurements thus agree with the specific prediction of the uniform supersaturation theory that the bubble wall velocity decreases as the square root of time; but it seems quite likely that this is coincidental. In fact, the observed behavior more nearly coincides with the phenomenological viewpoints advanced by Zuber (Z4), Moore and Mesler (M7), and others (to be discussed briefly later) that the bubble initially grows within a thin, highly supersaturated layer, during which period growth is quite rapid. After its diameter becomes large compared to this layer, its growth slows down, and is controlled by the advance of the bubble wall into a fresh supply of supersaturated liquid. Throughout this process the possibility of gas evolution from a microlayer of liquid at the bubble base may be important. Obviously, these questions can be answered only by further experimental work. Incidentally, Glas and Westwater (G3) note that the contact angle, determined from the bubble radius and height, continuously decreases during bubble growth, assuming that the departure from sphericity was negligible. This decrease in apparent contact angle is not inconsistent with the notion that the advancing bubble leaves behind a thin tongue of liquid at the bubble base.

quency, and eventually cease entirely to detach. Coincidentally, the maximum heat flux which can be sustained at the wall increases. Gunther and Kreith (G10) reported a heat flux as high as 5 Btu/(sq in.)(sec) could be transferred to a pool of distilled water subcooled 145°F below saturation temperature, and Gunther (G9) reported that this limit could be increased by a factor of four by forced convection. Such enormous heat transfer rates have led to applications in cooling of rocket motors and other compact power devices. In a pool of water subcooled more than 100°F the surface boiling activity consists of a random distribution of very small vapor bubbles which never detach from the heating surface, but grow and collapse hemispherically with lifetimes less than one millisecond. In many respects these isolated hemispherical bubbles represent a simpler phenomenon than the loose, irregularly defined bubbles arising in saturated boiling. In Fig. 18 typical  $R(t)$  curves are shown for hemispherical bubbles originating on a stainless steel heater strip in distilled water at a temperature of 98°F. The camera framing rate was 14,000 frames per second, made possible by the use of a Kerr electro-optical shutter. It is of interest to note that the growth and collapse portions are nearly mirror images. At small subcoolings the collapse time is several times greater than the growth time. However, as the subcooling is increased, the asymmetry decreases and eventually disappears, for all practical purposes. Another interesting result shown in Fig. 18 is the temperature observed by a thermocouple traverse in the vicinity of the heating surface. In the two-phase region the observed temperature is a weighted average of the vapor and liquid temperatures. The fact that the saturation temperature corresponds to about half the maximum bubble radius away from the wall indicates that the liquid surrounding the top of the bubbles is substantially subcooled.

Symmetrical growth and collapse curves of the sort pictured herein are difficult to obtain by a laminar-flow heat-convection model. This is because the heat equation is not symmetric with respect to time reversal. On the other hand, such symmetry is observed in the growth and collapse of cavitation bubbles, and indeed, is implied by the extended Rayleigh equation (B11):

$$R \frac{d^2 R}{dt^2} + \frac{3}{2} \left( \frac{dR}{dt} \right)^2 + \frac{2\sigma}{\rho R} = \frac{\Delta p}{\rho}, \quad \Delta p = p(R) - p_\infty \quad (104)$$

If experimental growth and collapse bubble radius data are employed, this equation can be numerically integrated to obtain  $\Delta p$ , the difference between the pressure at the bubble wall and in the surroundings, as a function of time (P3). If  $\Delta p$  can be assumed to be nearly constant, the first integral of this equation is readily obtained,

$$\left( \frac{dR}{dt} \right)^2 \cong \frac{2\sigma}{\rho} \left[ \frac{R_m^2 - R^2}{R^3} \right] - \frac{2}{3} \frac{\Delta p}{\rho} \left[ \frac{R_m^3 - R^3}{R^3} \right] \quad (105)$$

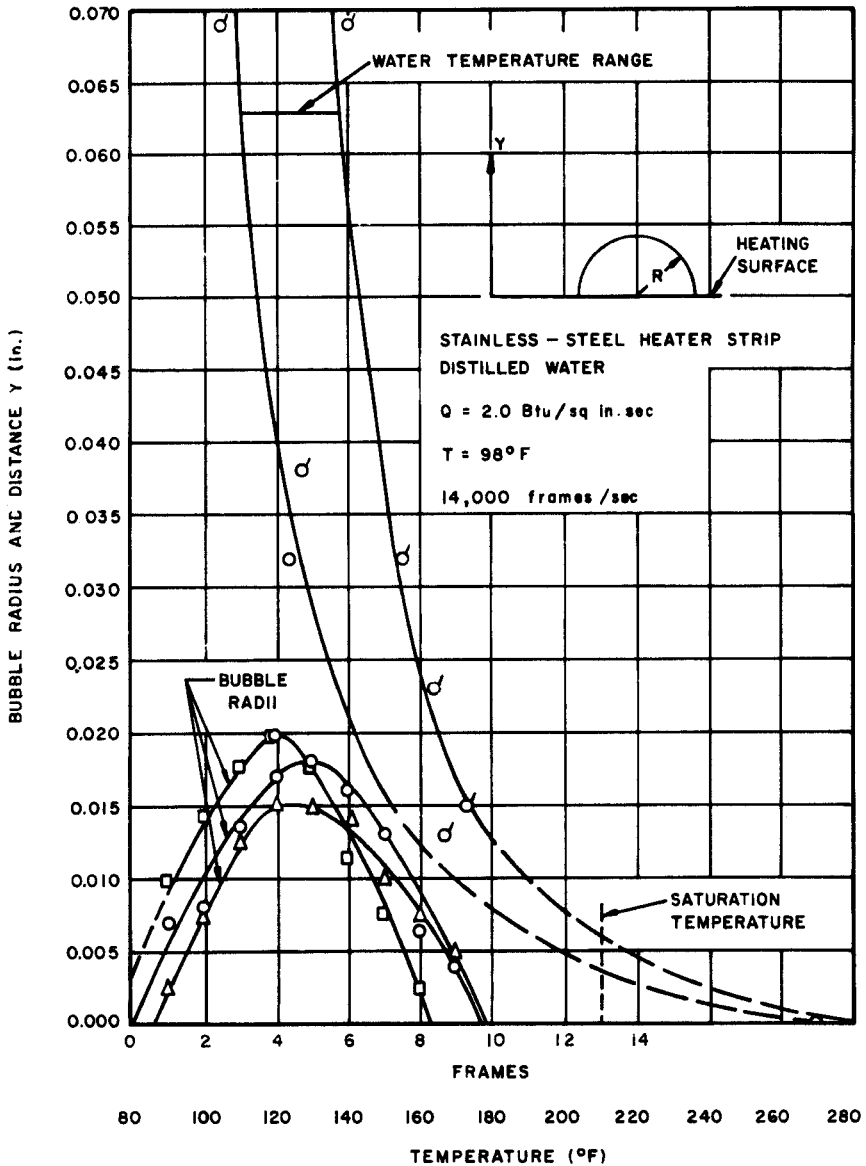


FIG. 18. Temperature distribution in water related to size of hemispherical bubbles (G10).

where the boundary condition  $\dot{R} = 0$  when  $R = R_m$  has been employed. It will be noted that, in fact, this equation has the desired symmetry, since the sign of  $\dot{R}$  does not affect the right-hand side. A further integration of this

equation can be performed numerically. A particularly simple result is obtained if the surface tension term can be neglected, resulting in (L4):

$$\frac{t_m}{R_m} = \left\{ \frac{\rho}{6(-\Delta p)} \right\}^{1/2} \frac{\Gamma(1/2) \Gamma(5/6)}{\Gamma(4/3)} \quad (106)$$

Bankoff and Mikesell (B11)<sup>10</sup> showed that this equation could be fairly well fitted to the bubble data of Gunther (G9) and of Ellion (E2) (Fig. 19), taken

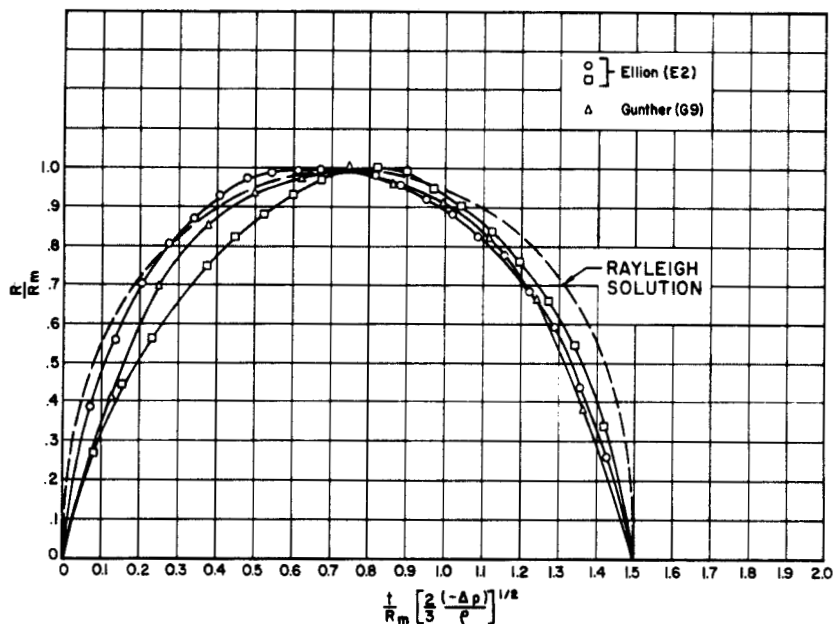


FIG. 19. Bubble growth curves from the data of Gunther (G9) and Ellion (E2) compared with Rayleigh solution, Eq. (106) (B11).

under highly subcooled boiling conditions. This shows that the pressure difference between the bubble interior and the surroundings was nonnegligible, and varied little during the visible lifetime of these bubbles.

Note that at this point no recourse need be made to any theory of energy transport, since the only equation necessary to describe the motion of the fluid is the pressure equation. The calculated pressure difference as a function of subcooling is shown in Fig. 20 from the data of Gunther and Kreith (G10) at a heat flux of 2.75 Btu/(sq in.)(sec) and a superficial liquid velocity of 10 ft/sec past the heating strip. One interpretation of these results is that the liquid surrounding the bubble has been given an initial supply of kinetic

<sup>10</sup> The reader is warned of several misprints in this reference.

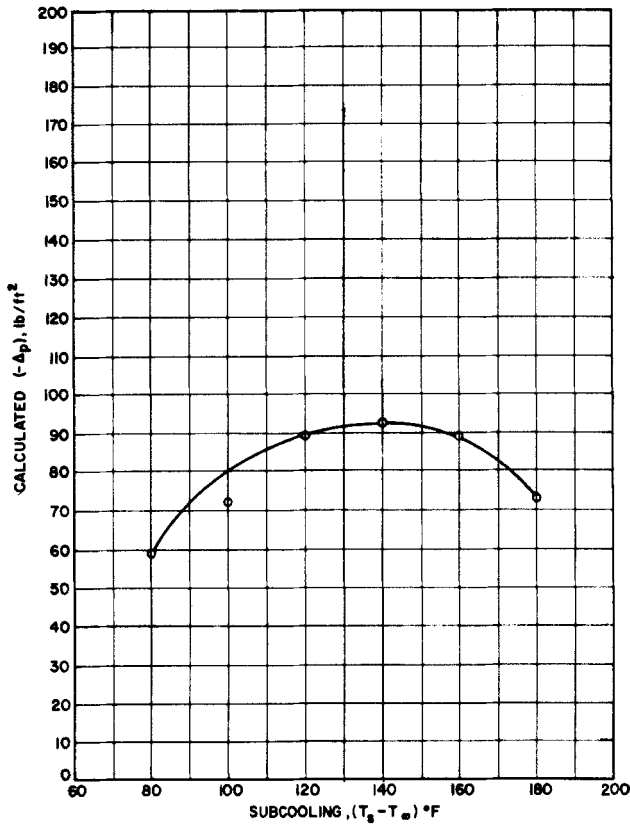


FIG. 20. Calculated pressure difference vs subcooling (B11).

energy, stemming from rapid vaporization of superheated liquid in the thermal boundary layer next to the heating surface. Thereafter, a negative pressure difference tends to slow up bubble growth, and eventually results in collapse. As might be expected, the initial kinetic energy decreases as the bulk temperature, and hence the superheat energy of the wall boundary layer, decreases. This is shown in Fig. 21, based on the same data. Since the pressure within the bubble is below saturation pressure, a good portion of the bubble wall must be below the saturation temperature. A nonequilibrium condition therefore exists, in which a portion of the bubble wall closest to the heating surface is at or above the saturation temperature, while other portions are substantially below this temperature. This implies that appreciable latent heat transport occurs by simultaneous vaporization from the hotter portions of the bubble surface and condensation on the colder regions. As pointed out by Gunther and Kreith (G10), small-scale turbulent diffusion must occur in the



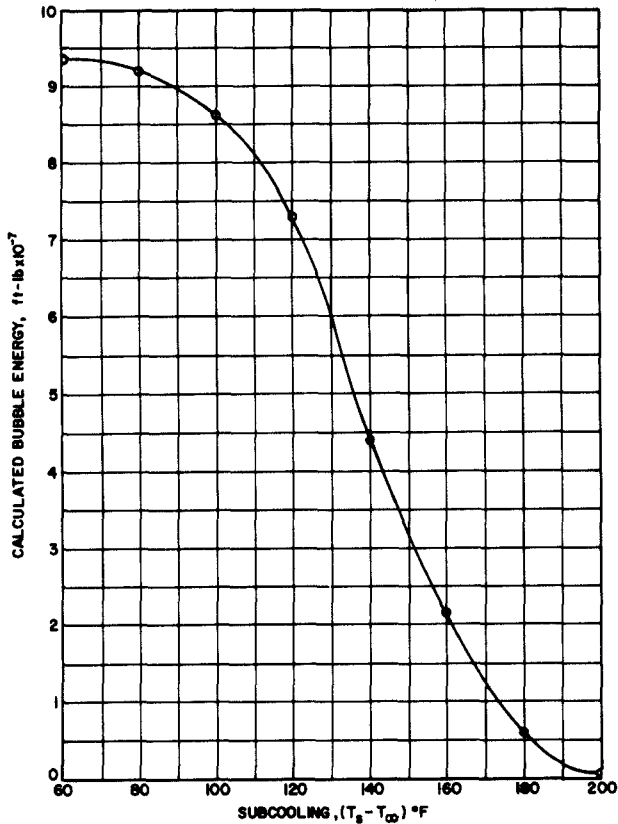


FIG. 21. Calculated initial bubble kinetic energy vs subcooling (B11).

thermal boundary layer at the upper portion of the bubble in order to maintain such temperature differences. That this is, in fact, the situation was demonstrated experimentally by Bankoff and Mason (B9), who measured heat transfer coefficients from an impinging water jet to bubbles formed by injection of steam through a pinhole in a flat surface. Exceptionally high heat transfer coefficients were recorded, the maximum being in excess of  $3 \times 10^5$  Btu/(hr)(sq ft)(°F). This is probably as high a heat transfer coefficient as one can find in the engineering literature, and must certainly be related to the striking efficiency of heat transfer in subcooled nucleate boiling.

#### B. ZUBER'S MODEL

The relevance of the theories for isolated bubble growth presented above to the problem of the growth of a bubble at a heating surface remains to be

established. In the meantime there is room for, and in fact a need for, phenomenological theories which focus on some hypothesized physical mechanism. By thus constructing a model for the bubble growth, relatively simple expressions can often be deduced from which comparisons with experimental data can be made. It is rare that a completely convincing argument can be made, since usually insufficient experimental evidence is available to verify that the proposed model actually represents all the physics of the problem; nevertheless, such theories can be extremely valuable.

Zuber (Z4) writes for the heat balance on the growing bubble

$$L\rho' \frac{dR}{dt} = b \left[ k \frac{T_w - T_s}{(\pi\alpha t)^{1/2}} - q_b \right] \quad (107)$$

where  $b$  is a curvature correction factor, and  $q_b$ , which represents a correction on the initially uniform temperature field heat flux, is identified with the steady-state heat flow from the heating surface to the liquid. Note that the effect of this correction term is to reduce the bubble growth rate compared to the uniform superheat case ( $R \propto t^{1/2}$ ), as noted above. Good agreement between theory and experiment is shown for three bubbles measured by Bankoff and Mikesell (B11), from unpublished film taken by Zmola (Z3), of saturated boiling from a horizontal strip, and also for several bubbles measured by Fritz and Ende (F9).

For subcooled boiling this equation predicts that the maximum radius  $R_m$  is reached when

$$(\pi\alpha t_m)^{1/2} = \frac{k \Delta T}{q_b}, \quad \Delta T = T_w - T_s \quad (108)$$

In dimensionless form this yields

$$R/R_m = (t/t_m)^{1/2} [2 - (t/t_m)^{1/2}] \quad (109)$$

where  $t_m$  is the time at which the maximum radius is reached. This growth expression is shown to agree with Ellion's data (E2) for subcooled pool boiling. However, it does not work well for the collapse phase. An explanation which is advanced is that in the collapse phase inertial terms dominate, so that the extended Rayleigh equation, Eq. (104), is appropriate. The physical justification is not clear, since the growth time for vapor bubbles from a heating surface is always less than or equal to the collapse time. The maximum bubble diameter is given by

$$\frac{D_m}{X_s} = \frac{\Delta T c_p \rho}{L\rho'} \quad (110)$$

where the thickness of the superheated liquid film is given by

$$X_s = \frac{k \Delta T}{Q} \quad (111)$$

This is an energy balance stating that the enthalpy of the superheated liquid film contributes, in some constant proportion, to the formation of a bubble which grows on the surface. The similarity to the discussions in the two preceding sections may be noted.

### C. FORSTER'S MODEL

Forster (F6) solves the same problem by a different approximate method. The temperature profile through the thermal boundary layer next to the heating surface is taken to be exponential. The rather strong assumption is then made that the heat flux through a surface element of the bubble can be equated to the one-dimensional heat flow through the surface of a semi-infinite strip initially at a uniform temperature equal to the local temperature of the thermal boundary layer of the wall before bubble growth began. This ignores the steep initial temperature gradients. Introducing this simplification into the integral heat balance equation for the bubble growth one finds that, for the early asymptotic stage,  $R(t) \propto t^{1/2}$ , while after the bubble has grown large compared to the thermal boundary layer,  $R(t) \propto t^{1/4}$ . Qualitatively, this trend is in the direction exhibited by the numerical and analytical solutions (G7, S2, S12).

## V. Miscellaneous Topics

A number of other topics, while highly germane to the general subject of bubble dynamics, are peripheral from the point of view of this review, and hence will be dealt with briefly below. Sufficient references are given in each case to enable the interested reader to pursue the subject further.

### A. NUCLEATION

In theory it is possible to nucleate bubbles either in the bulk phase or at solid surfaces as a result of statistical density fluctuations. In practice, the theoretical and measured fracture pressures of pure liquids are far in excess of those corresponding to the superheats or supersaturations for vapor or gas bubble nucleation experimentally observed in engineering systems (F2, F7, K1). On the other hand, conditions for homogeneous nucleation become favorable at extremely high superheats in the presence of ionizing radiation (G4, G5). The latter observation led to the introduction of the liquid-hydrogen bubble chamber. A simple explanation of this phenomenon is that the

electrical charges on the bubble surface repel each other, effectively reducing the surface tension. Also, high-energy particles, such as fission fragments, by vaporizing a minute volume of liquid, can induce nucleation under favorable circumstances (H5, N2, S5). More generally, however, the tensile stress at which nucleation is observed is of the order of 1–5 atm, which is far below the theoretical limits of  $10^2$ – $10^3$  atm. The reduction of this threshold level due to the presence of microscopic roughness elements in the container walls can be shown to be at most by a factor of two or so (B2), so that this possibility can also be ruled out. This means that nucleation in almost all systems of practical importance begins with pre-existing gas or vapor phase, usually trapped in microscopic cavities in the container walls or dust particles. Some theoretical conditions for microscopic grooves or cavities to be effective vapor traps have been deduced (B1, B3, B4), which are essentially of a geometrical nature, depending upon the liquid contact angle, and assuming quasi-static conditions. These give necessary, but not sufficient, conditions for nucleation. A dynamic theory for penetration of liquid into a potential nucleation site remains largely to be developed, although some preliminary work is available (B4). It has been shown that the superheat required to initiate boiling decreases with increasing surface roughness (C5), but the quantitative confirmation of theoretical superheats on the basis of measured surface properties is complicated by the difficulty in obtaining reproducible boiling from particular sites (B13). For this reason some attention has been paid to nucleation from artificial sites (G8, N1, W1). Statistical measurements have also been made of nucleation site densities (C3, G1, G2). Boiling from a liquid–liquid interface has been examined by Viskanta and Lottes (V4) and Otterman (O1), but the results are clouded by the difficulty in obtaining a dust-free interface. By assuming that the nucleation proceeds when the thermal boundary layer thickness at the heating surface reaches some critical fraction of the nucleus radius, the waiting time between bubbles can be calculated (H2, H10). There seems to be considerable evidence of the effects of diffusion of permanent gas into or out of the nucleation cavities, resulting in “aging” of a heating surface in the first few hours of boiling (B13)<sup>11</sup>, and the strong influence of

<sup>11</sup> There also appears to be a hysteresis, or time-lag effect, in cycling a heating surface around the nucleation temperature. Presumably this is due to some irreversibility in quenching of formerly active sites. This effect has generally not been taken into account in considering the effect of motion of boiling boundary in the response of boiling channels with subcooled inlet flows to power or flow oscillations. The delayed vaporization resulting from this effect is, in fact, probably the explanation for the sharp “bumping” at times observed in these systems. A dramatic illustration was reported by Zivi *et al.* (Z2), who found that the details of the internal channel construction had a marked effect on the smoothness of the exit void-fraction response to power modulation. A smooth welded channel had a considerably more peaked response than a soldered channel, in accordance with the observation that the solder contained numerous microscopic re-entrant cavities.

prepressurization or of prolonged immersion in promoting resistance to inception of cavitation (H3).

The prediction of the inception of cavitation is, of course, closely related to nucleation theory, but has generally been studied experimentally by modeling with reference to the hydrodynamic flow field (E1, L7, S15). The usual criterion is the Prandtl cavitation number (M6),

$$N_c = \frac{p_\infty - p_c}{\frac{1}{2}\rho u_\infty^2}, \quad (112)$$

which normalizes the critical underpressure at the surface with respect to the dynamic pressure of the free stream. Probably a more successful criterion would be the ratio of the critical underpressure to a characteristic capillary pressure, determined by the surface roughness distribution.

## B. RAPID HEATING

A situation of considerable practical concern is the growth of bubbles under rapid heating, such as occurs in fast power excursions in liquid-cooled nuclear reactors. Zwick (Z5) has considered bubble growth in liquids containing strong volume heat sources, by an extension of the perturbation analysis discussed above. It is assumed that the temperature far from the bubble increases linearly:  $T_\infty = T_s + bt$ , where  $t = 0$  corresponds to the instant when the surroundings reach the saturation temperature. The asymptotic phase is extrapolated backwards to zero initial radius, so that  $R(0) = 0$ . An implicit integral equation for  $R(t)$  is then obtained, which is manipulated to give "early" and "late" asymptotic solutions:

$$R \sim \begin{cases} 2 \left( \frac{3\alpha(t - t_w)}{\pi} \right)^{1/2} N_J, & t \rightarrow t_w \\ 6cbN_J \left( \frac{\alpha t^3}{7\pi} \right)^{1/2}, & t \rightarrow \infty \end{cases} \quad (113)$$

where  $t_w$  is a waiting time estimated from the early phase analysis, and  $c = 1 - (3/7)[1 - (1/3)B(3/2, 1/3)] = 0.932$ . Although the bubble begins to grow as the square root of time, it eventually increases as  $t^{3/2}$ . A similar result was obtained by Bankoff (B5) in an analysis of bubble dynamics from an exponentially heated plate.

Vapor formation rates in rapidly heated systems have been measured by Faneuff, McLean, and Scherrer (F1) and Cole (C4) for wires in a stationary liquid pool, and by Johnson *et al.* (J1, J2, T1) for a metal ribbon suspended in a channel flow. Void growth rates in a volume-heated boiling system were studied by Lipkis, Liu, and Zuber (L8). In practice the total vapor volume

depends upon the number of bubbles per cubic centimeter which begin to grow in every small time interval, which in turn depends upon a generally unknown nucleus distribution density function. Zwick (Z5) shows how one can infer this distribution function from measurements of the rate of vapor production in volume boiling through the application of linear transform theory.

### C. MICROLAYER VAPORIZATION

In 1936 Derjagin (D4) demonstrated the existence of thin liquid films at the base of bubbles attached to a solid surface, which was attributed to the variation of free interfacial energy of very thin films with their thickness. For stationary bubbles these films were of the order of  $10^{-5}$  cm thick. Bankoff (B12) called attention to the possibility of the existence of such films at the base of vapor bubbles in nucleate boiling, pointing out that such films would very rapidly evaporate. Moore and Mesler (M7), however, were the first to provide solid experimental confirmation that such microlayers do exist, by measuring the temperature depression of the solid surface directly beneath a number of growing bubbles. The thickness of the liquid film that had to evaporate in order to account for the observed temperature drop was computed to be of the order of  $2 \times 10^{-4}$  cm thick. This is of the right order of magnitude, considering the fact that films formed under dynamic conditions would be expected to be thicker than those existing under stationary bubbles. Similar measurements have been made by Hendricks and Sharp (H4).

### D. OTHER BUBBLE PROPERTIES

A number of other aspects of bubble behavior have received attention. Bubble growth under normal and reduced gravity conditions have been studied by Siegel and co-workers (K2, S9, S10, U1), and by Merte and Clark (M5) in an accelerating system. Bubble behavior in oscillating pressure fields has been analyzed by Houghton (H7) and Plesset and Hsieh (P5, H9). Plesset (P4), in a general review, discusses the stability of collapsing bubbles. Other characteristics of bubbles emanating at heating surfaces, such as mean bubble frequencies, break-off diameters, coalescence frequencies, and nucleation site densities, have been measured in various laboratories (B15, B16, K3, L1, L2, L3, M4, P2, S6, S7, S8). The effect of varying the surface tension in boiling heat transfer has been studied, among others by Myers and co-workers (K6, R2). Bubble parameters in the neighborhood of the critical heat flux have been studied by Cole (C4). Ruckenstein (R3), Chao (C1), and Zavoiskii (Z1) have studied bubble growth when the bubble center is translating with respect to the fluid.

## VI. Concluding Remarks

It is apparent from the preceding survey that, although much has been accomplished in this field, much remains to be done. The theory of isolated bubble growth in a liquid of arbitrary initial temperature and/or concentration distribution is now fairly well established, providing that the boundary layer volume is smaller than the bubble volume. Further research needs to be done on the matching of the quasi-stationary and the thin boundary layer solutions. The theory has to date focused on spherical or hemispherical bubbles, but more frequently bubbles in the shape of ellipsoids or spherical segments are observed growing on surfaces. A solution for these cases, based upon either ellipsoidal or bipolar coordinates, would be helpful. Horvay and Cahn (H6), employing a procedure due to Ivantsov (I1), showed that exact self-similar solutions exhibiting a square root of time dependency exist for a variety of shapes, including paraboloids and ellipsoids, providing that the quasi-stationary assumption is valid. A theoretical examination of the effect of heat transfer from the solid surface after the bubble has entered the asymptotic stage is also needed. Numerical solutions of the problem of two bubbles growing at a surface simultaneously would be helpful in understanding bubble interaction. An interesting and difficult numerical free-boundary problem is the computation of the velocity and temperature fields, and the bubble shape and position, during one complete cycle of bubble growth and departure.

The important advances, however, will be made in the experimental area. Thermocouples and hot wire anemometers of truly small dimensions and of time constants of the order of one microsecond are now becoming commercially available. In order to make a convincing comparison with theory it is necessary to have reasonably accurate measurements of the temperature and velocity fields surrounding the bubbles. Instantaneous as well as time-mean values are of interest. Steps have been taken in this direction in measuring the temperature depression in the solid underneath the bubble (H4, M7, R1). These measurements are quite difficult to make, and a good deal of deductive reasoning has to be employed in any case. It is important, when comparing radius-time curves for bubbles originating on a heating surface with theoretical predictions, that an attempt be made to determine the approximate thermal boundary layer thickness on the heating surface from the data. If, *a priori*, it is assumed that the bubble is initially in a uniform superheat field, much information is lost that could be obtained by finding the assumed nonuniform temperature field which gives the best fit to the data.

Much remains to be done experimentally and theoretically in other aspects of bubble behavior at solid surfaces, such as nucleation, coalescence,

departure, and interaction. These are not simple problems and they promise to tax the ingenuity of investigators for some time.

#### ACKNOWLEDGMENTS

This work was supported by a grant from the National Science Foundation. Once again, the valuable assistance of Dr. V. K. Pai in assembling and editing this manuscript is acknowledged with thanks. The comments of Professors L. A. Skinner and J. W. Westwater both of whom carefully reviewed the manuscript, were most helpful.

#### Nomenclature

|  |  |          |  |
|--|--|----------|--|
| $a$                                    | Constant, Eq. (77)   | $k_1$    | $= \beta'/I^{-1/3}$  |
| $a_1, a_2, \dots$                      | Constants, Eq. (64)  | $k_H$    | Henry's Law constant   |
| $A$                                    | $= A(T' - T_s)$ , linear function of temperature, Eq. (37)                           | $K$      | Constant, Eq. (94)   |
| $A_1$                                  | Constant, Eq. (102)  | $K_1$    | $= \left( \frac{2\sigma}{\rho R_0^3} \right)^{1/2}$ , Eq. (39c)            |
| $b$                                    | Constant, Eq. (113), or a curvature correction factor, Eq. (107)                     | $K_2$    | Constant, Eq. (41)   |
| $b_0, b_1, b_2$                        | Constants, Eq. (68)  | $l$      | Characteristic length or initial thermal boundary layer thickness          |
| $B(p, q)$                              | Beta function  | $L$      | Latent heat of vaporization  |
| $c$                                    | Constant, Eq. (113)  | $m$      | $= \frac{1}{3}[r^3 - R^3(t)]$ , position variable                          |
| $c_p$                                  | Specific heat at constant pressure   | $M$      | Molecular weight   |
| $C$                                    | Concentration  | $N_c$    | Prandtl cavitation number, Eq. (112)                                       |
| $d_0, d_1$                             | Functions of $s$ , Eq. (69)  | $N_J$    | $= \frac{\rho c_p (T_{bo} - T_s)}{\rho' L}$ , dimensionless (Jakob number) |
| $D$                                    | Bubble diameter  | $N_{J'}$ | $= \frac{C_\infty - C_s}{C_g}$ , dimensionless concentration               |
| $D_m$                                  | Maximum bubble diameter  | $N'J'$   | $= \frac{k \Delta T}{\rho' L \alpha}$ , generalized Jakob number, Eq. (88) |
| $D$                                    | Mass diffusivity   | $p$      | Pressure   |
| $f(m)$                                 | Initial temperature distribution in liquid, Eq. (71)                                 | $p_r$    | Reduced pressure   |
| $F(\zeta)$                             | $= \partial^2 U(0, \zeta) / \partial m^2$ , Eq. (28)                                 | $p_v$    | Vapor pressure of liquid   |
| $\mathcal{F}(t)$                       | Function of time, Eq. (1)  | $q_b$    | Correction term on the initial uniform temperature field, Eq. (107)        |
| $g(r)$                                 | Initial temperature distribution, Eq. (11)   | $Q$      | Heat flux density  |
| $g(m) = \frac{f(m) - T_s}{f(0) - T_s}$ | dimensionless initial temperature distribution, Eq. (71)                             | $Q'$     | Instantaneous local rate of concentration increase, Eq. (9)                |
| $g[R(\zeta)]$                          | Function defined in Eq. (45)   | $r$      | Radial position  |
| $h(r)$                                 | Initial concentration distribution in liquid, Eq. (12)                               | $R(t)$   | Bubble radius  |
| $\tilde{h}$                            | Heat transfer coefficient from heating surface to vapor bubble through its base area |          |  |
| $I$                                    | Current density  |          |  |
| $j$                                    | Iteration index  |          |  |
| $k$                                    | Thermal conductivity   |          |  |



|                   |   |                         |   |
|-------------------|---|-------------------------|---|
| $R_g$             | Universal gas constant  | $\beta'$                | $= \beta/2$   |
| $R_i$             | Radius of isothermal vapor bubble, Eq. (94)   | $\gamma$                | Accommodation coefficient   |
| $R_m$             | Maximum bubble radius   | $\Gamma$                | Gamma function  |
| $R_0$             | Initial bubble radius   | $\delta$                | Thickness of thermal boundary layer, Eq. (98)                                   |
| $R_1$             | Bubble radius at the commencement of asymptotic growth  | $\delta_1$              | Small displacement from equilibrium bubble radius, Eq. (10)                     |
| $R^*$             | $= R^3/R_0^3$ , dimensionless, Eq. (39a)  | $\Delta$                | Standard notation for difference  |
| $\mathcal{R}$     | $= R/l$ , dimensionless bubble radius, Eq. (73)   | $\varepsilon$           | $= [1 - \langle \rho' \rangle / \rho]$ , dimensionless term                     |
| $s$               | $= y/R$ , dimensionless radius  | $\zeta$                 | $= \int_0^t R^4(t') dt'$ , time variable, Eq. (23)                              |
| $t$               | Time  | $\zeta_1$               | $= \frac{\alpha}{l^2} \int_0^t \mathcal{R}^4(t') dt'$ , time variable, Eq. (73) |
| $t_c$             | Time at which bubble collapses to zero radius   | $\zeta^*$               | $= K_1 \zeta / R_0^*$ , time variable, Eq. (39b)                                |
| $t_m$             | Time at which maximum bubble radius is attained   | $\eta$                  | $= r/(\alpha t)^{1/2}$ , Boltzmann transformation variable                      |
| $t_w$             | Waiting period between bubbles  | $\theta$                | Spherical polar coordinate  |
| $T$               | Temperature   | $\theta(r, t)$          | $= (T - T_\infty)/(T_s - T_\infty)$ , dimensionless temperature, Eq. (15)       |
| $T_{b0}$          | $= f(0)$ , bubble wall temperature; for uniform superheat, $T_{b0} = T_\infty$ ; for bubbles originating at the heating surface, $T_{b0} \approx T_w$ | $\Theta(m, t)$          | Averaged temperature excess, defined in Eq. (82)                                |
| $T_e$             | Temperature excess, $(T - T_\infty)$ , Eq. (24)   | $\kappa$                | Effective surface dilational viscosity  |
| $u(r, t)$         | Liquid velocity, Eq. (1)  | $\mu$                   | Viscosity   |
| $U$               | $= \int_0^m T_e(m, t) dm$ , temperature potential function, Eq. (24)  | $\nu$                   | Kinematic viscosity   |
| $U_0, U_1, \dots$ | Perturbation functions of $U$   | $\rho$                  | Density   |
| $V$               | $= R^3(t)$ , Eq. (53)   | $\langle \rho' \rangle$ | Time-averaged vapor density   |
| $V_0, V_1, \dots$ | Perturbation functions of $V$   | $\sigma$                | Surface tension   |
| $x$               | Distance normal to the wall; or dummy variable in integration   | $\tau$                  | $= \frac{\alpha t}{l^2}$ , dimensionless time, Eq. (91)                         |
| $X_s$             | Thickness of superheated liquid film, Eq. (110)   | $\varphi$               | Contact angle; or spherical polar coordinate                                    |
| $y$               | $= (r - R)$ , position variable   | $\varphi(m)$            | $= \partial U_0^j(m, 0) / \partial m$ , Eq. (46)                                |
| $y_A$             | Mass fraction of volatile component A   | $\varphi_b$             | $= \frac{\sin^2 \varphi}{4}$ , base factor, Eq. (97)                            |
| $z$               | Dummy variable  | $\varphi_c$             | Curvature factor, Eq. (97)  |
|                   |   | $\varphi_s$             | $= \frac{1 + \cos \varphi}{2}$ , surface factor, Eq. (97)                       |

## GREEK LETTERS

- $\alpha$  Thermal diffusivity  
 $\beta = R/(\alpha t)^{1/2}$ , growth constant

|                                       |   |          |                             |
|---------------------------------------|---|----------|-----------------------------|
| $\varphi_v$                           | $= [2 + \cos \varphi(2 + \sin^2 \varphi)]/4$ ,<br>volume factor, Eq. (97) | $b$      | Condition within the bubble |
| $\Phi$                                | $= N_J/(1 - C_s/\rho)$ , constant,<br>Fig. (15)                           | $g$      | Gas                         |
| $\Phi_3(\eta)$                        | Function defined in Eq. (16)  | $m$      | Maximum                     |
| $\chi(\beta)$                         | Function defined in Eq. (18)  | $s$      | Saturated                   |
| $\psi(z)$                             | Function defined in Eq. (92)  | $v$      | Vapor                       |
| $\omega$                              | $= (T_w - T_\infty)/(T_w - T_s)$ , di-<br>mensionless temperature         | $w$      | Wall of the heating surface |
|                                       |   | $\infty$ | Condition at infinity       |
| SUBSCRIPTS (UNLESS OTHERWISE NOTED)   |   |          |                             |
| A Volatile component A                |   |          |                             |
| SUPERSCRIPTS (UNLESS OTHERWISE NOTED) |   |          |                             |
| ' Vapor phase                         |   |          |                             |
| — Average                             |   |          |                             |
| . Time derivative                     |   |          |                             |

## REFERENCES

- B1. Bankoff, S. G., *J. Phys. Chem.* **60**, 952 (1956).  
 B2. Bankoff, S. G., *J. Heat Transfer* **79**, 735 (1957).  
 B3. Bankoff, S. G., *A.I.Ch.E. (Am. Inst. Chem. Engrs.) J.* **4**, 24 (1958).  
 B4. Bankoff, S. G., *Chem. Eng. Progr., Symp. Ser.* **55**, No. 29, 87 (1959).  
 B5. Bankoff, S. G., *Ind. Eng. Chem., Fundamentals* **1**, 257 (1962).  
 B6. Bankoff, S. G., *A.I.Ch.E. (Am. Inst. Chem. Engrs.) J.* **8**, 63 (1962).  
 B7. Bankoff, S. G., *Appl. Sci. Res.* **A12**, 567 (1963).  
 B8. Bankoff, S. G., *Advan. Chem. Eng.* **5**, 75-150 (1964).  
 B9. Bankoff, S. G., and Mason, J. P., *A.I.Ch.E. (Am. Inst. Chem. Engrs.) J.* **8**, 30 (1962).  
 B10. Bankoff, S. G., and Mikesell, R. D., *Am. Soc. Mech. Engrs., Paper 58-A-105* (1958).  
 B11. Bankoff, S. G., and Mikesell, R. D., *Chem. Eng. Progr., Symp. Ser.* **55**, No. 29, 95 (1959).  
 B12. Bankoff, S. G., Colahan, W. J., Jr., and Bartz, D. R., "Summary on Conference on Bubble Dynamics and Boiling Heat Transfer." Jet Propulsion Lab., Cal. Inst. Tech., Pasadena, California, Memo. No. 20-137, 1956.  
 B13. Bankoff, S. G., Hajjar, A. J., and McGlothlin, B. B., Jr., *J. Appl. Phys.* **29**, 1739 (1958).  
 B14. Barlow, E. J., and Langlois, W. E., *IBM J. Res. Develop.* **6**, 329 (1962).  
 B15. Behar, M., *Houille Blanche* **18**, 692 (1963).  
 B16. Behar, M., and Semeria, R., *Compt. Rend.* **255**, 1331 (1962).  
 B17. Benjamin, J. E., and Westwater, J. W., "International Developments in Heat Transfer," Part II, p. 212. Am. Soc. Mech. Engrs., New York, 1961.  
 B18. Benjamin, J. E., and Westwater, J. W., *Proc. 5th Intern. Congr. High Speed Phot., Washington, 1960 D.C.*, Soc. Motion Picture and Television Engrs., New York, p. 290 (1962).  
 B19. Birkhoff, G., Margulies, R. S., and Horning, W. A., *Phys. Fluids* **1**, 201 (1958).  
 B20. Boley, B. A., *J. Math. Phys.* **40**, 300 (1961).  
 B21. Boltzmann, L., *Ann. Physik* [3] **53**, 959 (1894).  
 B22. Bosnjakovic, F., *Tech. Mech. Thermo-Dynam., Berlin* **1**, 358 (1930).  
 B23. Brandstaetter, F., *Österr. Akad. Wiss.* **161**, 107 (1952); cf. Houghton, G., Ritchie, P. D., and Thomson, J. A., *Chem. Eng. Sci.* **17**, 221 (1962).  
 B24. Bruijn, P. J., *Physica* **26**, 326 (1960).  
 B25. Buehl, W. M., and Westwater, J. W., *A.I.Ch.E. (Am. Inst. Chem. Engrs.) J.* (submitted for publication).  
 B26. Bumpus, C., Spiegler, P., and Norman, A., *Trans. Am. Nucl. Soc.* **4**, 70 (1961).  
 C1. Chao, B. T., *Phys. Fluids* **5**, 69 (1962).

- C2. Cichelli, M. T., and Bonilla, C. F., *Trans. Am. Inst. Chem. Engrs.* **41**, 755 (1945).
- C3. Clark, H. B., Streng, P. S., and Westwater, J. W., *Chem. Eng. Progr., Symp. Ser.* **55**, No. 29, 103 (1959).
- C4. Cole, R., *A.I.Ch.E. (Am. Inst. Chem. Engrs.) J.* **6**, 533 (1960).
- C5. Corty, C., and Foust, A. S., *Chem. Eng. Progr., Symp. Ser.* **51**, No. 17, 1 (1955).
- D1. Darby, R., *Chem. Eng. Sci.* **19**, 39 (1964).
- D2. Dergarabedian, P., *J. Appl. Mech.* **20**, 537 (1953).
- D3. Dergarabedian, P., *J. Fluid Mech.* **9**, 39 (1960).
- D4. Derjagin, B., *Acta Phys.-chim. URSS* **5**, 1 (1936); **10**, 333 (1937).
- D5. Doremus, R. H., *J. Am. Ceram. Soc.* **43**, 655 (1960).
- D6. Dougherty, D. E., and Rubin, H. H., *Proc. Heat Transfer Fluid Mech. Inst., 1963* p. 222. Stanford Univ. Press, Stanford, California, 1963.
- E1. Eisenberg, P., and Tulin, M. P., "Handbook of Fluid Dynamics" (V. L. Streeter, ed.), Section 12. McGraw-Hill, New York, 1961.
- E2. Ellion, M. E., "A Study of the Mechanism of Boiling Heat Transfer." Jet Propulsion Lab., Cal. Inst. Tech., Pasadena, California, Memo No. 20-88, 1954.
- E3. Epstein, P. E., and Plesset, M. S., *J. Chem. Phys.* **18**, 1505 (1950).
- F1. Faneuff, C. E., McLean, E. A., and Scherrer, V. E., *J. Appl. Phys.* **29**, 80 (1958).
- F2. Fisher, J. C., *J. Appl. Phys.* **19**, 1062 (1948).
- F3. Flatt, H. P., *Trans. Am. Nucl. Soc.* **1**, 48 (1958).
- F4. Forster, H. K., *A.I.Ch.E. (Am. Inst. Chem. Engrs.) J.* **3**, 535 (1957).
- F5. Forster, H. K., and Zuber, N., *J. Appl. Phys.* **25**, 474 (1954).
- F6. Forster, K. E., *Phys. Fluids* **4**, 448 (1961).
- F7. Frenkel, J., "Kinetic Theory of Liquids," Dover, New York, 1955.
- F8. Fricke, R., *Z. Physik. Chem. (Leipzig)* **104**, 363 (1923).
- F9. Fritz, W., and Ende, W., *Phys. Z.* **37**, 391 (1936).
- G1. Gaertner, R. F., *Chem. Eng. Progr., Symp. Ser.* **59**, No. 41, 52 (1963).
- G2. Gaertner, R. F., and Westwater, J. W., *Chem. Eng. Progr., Symp. Ser.* **55**, No. 30, 39 (1959).
- G3. Glas, J. P., and Westwater, J. W., *Intern. J. Heat Mass Transfer* **7**, 1427 (1964).
- G4. Glaser, D. A., *Phys. Rev.* **87**, 665 (1952).
- G5. Glaser, D. A., *Phys. Rev.* **91**, 762 (1953).
- G6. Greene, C. H., and Gaffney, R. F., *J. Am. Ceram. Soc.* **42**, 271 (1959).
- G7. Griffith, P., *J. Heat Transfer* **80**, 721 (1958).
- G8. Griffith, P., and Wallis, J. D., *Chem. Engr. Progr., Symp. Ser.* **55**, No. 30, 49 (1959).
- G9. Gunther, F. C., "Photographic Study of Surface Boiling Heat Transfer to Water with Forced Convection." Jet Propulsion Lab., Cal. Inst. Tech., Pasadena, California, Progr. Rept. No. 4-75, 1950.
- G10. Gunther, F. C., and Kreith, F., "Photographic Study of Bubble Formation in Heat Transfer to Subcooled Water." Jet Propulsion Lab., Cal. Inst. Tech., Pasadena, California, Progr. Rept. No. 4-120, 1950.
- H1. Hadamard, J., "Lectures on Cauchy's Problem in Linear Partial Differential Equations." Dover, New York, 1952.
- H2. Han, C. Y., and Griffith, P., "Mechanism of Heat Transfer in Nucleate Pool Boiling." Div. of Sponsored Res., Mass. Inst. Tech., Cambridge, Massachusetts, Rept. No. 7673-19, 1962.
- H3. Harvey, E. N., McElroy, W. D., and Whiteley, A. H., *J. Appl. Phys.* **18**, 162 (1947).
- H4. Hendricks, R. C., and Sharp, R. R., *NASA, Tech. Note TN D-2290* (1964).
- H5. Hetrick, D. L., and Gamble, D. P., *Trans. Am. Nucl. Soc.* **1**, 48 (1958).
- H6. Horvay, G., and Cahn, J. W., *Acta Met.* **9**, 695 (1961).

- H7. Houghton, G., *J. Acoust. Soc. Am.* **35**, 1387 (1963).
- H8. Houghton, G., Ritchie, P. D., and Thomson, J. A., *Chem. Eng. Sci.* **17**, 221 (1962).
- H9. Hsieh, D., and Plesset, M. S., *Phys. Fluids* **4**, 970 (1961).
- H10. Hsu, Y. Y., *J. Heat Transfer* **84**, 207 (1962).
- I1. Ivantsov, G. P., *Dokl. Akad. Nauk SSSR* **58**, 567 (1947); (Mathematical Physics) (transl. by G. Horvay), Rept. No. 60-RL-(2511M). G.E. Res. Lab., Schenectady, New York, 1960.
- J1. Johnson, H. A., Schrock, V. E., Fabric, S., and Selph, F. B., "Transient Boiling Heat Transfer and Void Volume Production in Channel Flow." Reactor Heat Transients Res., Univ. of Calif., Berkeley, California, SAN-1007, TID-4500, 1963.
- J2. Johnson, H. A., Schrock, V. E., Selph, F. B., Lienhard, J. H., and Rosztoczy, Z. R., "International Developments in Heat Transfer," Part II, p. 244. Am. Soc. Mech. Engrs., New York, 1961.
- K1. Kenrick, F. B., Gilbert, C. S., and Wismer, K. L., *J. Phys. Chem.* **28**, 1297 (1924).
- K2. Keshock, E. G., and Siegel, R., *NASA, Tech. Note TN- D-2299* (1964).
- K3. Kirby, D. B., and Westwater, J. W., *Chem. Eng. Sci.* **18**, 469 (1963).
- K4. Kirkaldy, J. J., *Can. J. Phys.* **36**, 446 (1958).
- K5. Kolodner, I., *Commun. Pure Appl. Math.* **9**, 1 (1956).
- K6. Kurihara, H. M., and Myers, J. E., *A.I.Ch.E. (Am. Inst. Chem. Engrs.) J.* **6**, 83 (1960).
- L1. Labuntsov, D. A., *Teplotnerg.* **12**, 19 (1959).
- L2. Labuntsov, D. A., *Inzh.-Fiz. Zh., Akad. Nauk Belorussk. SSR* **6**, 33 (1963); cf. *Chem. Abstr.* **59**, 8146g (1963).
- L3. Labuntsov, D. A., Kol'chugin, B. A., Golovin, V. S., Zakharova, E. A., and Vladimirova, L. N., *Tepl. Vysokih Temp. Akad. Nauk SSSR* **2**, 446 (1964); cf. *Chem. Abstr.* **61**, 12964b (1964).
- L4. Lamb, G., "Hydrodynamics." Dover, New York, 1949.
- L5. Langlois, W. E., *J. Fluid Mech.* **15**, 111 (1963).
- L6. Liebermann, L., *J. Appl. Phys.* **28**, 205 (1957).
- L7. Lienhard, J. H., "A Study of the Dynamics and Thermodynamics of Liquid-Gas-Vapor Bubbles." Washington State Inst. of Technology, Pullman, Washington, Bull. No. 266, 1964.
- L8. Lipkis, R. P., Liu, C., and Zuber, N., *Chem. Eng. Progr., Symp. Ser.* **52**, No. 18, 105 (1956).
- M1. Ma, J. T., and Wang, P. K., *IBM J. Res. Develop.* **6**, 472 (1962).
- M2. Mache, M., *Wien. Akad.* **138**, 529 (1929); cf. Houghton, G., Ritchie, P. D., and Thomson, J. A., *Chem. Eng. Sci.* **17**, 221 (1962).
- M3. Manley, D. M. J. P., *Brit. J. Appl. Phys.* **11**, 38 (1960).
- M4. McFadden, P. W., and Grassmann, P., *Intern. J. Heat Mass Transfer* **5**, 169 (1962).
- M5. Merte, H., Jr., and Clark, J. A., *J. Heat Transfer* **83**, 233 (1961).
- M6. Milne-Thomson, L. M., "Theoretical Hydrodynamics." Macmillan, New York, 1960.
- M7. Moore, F. D., and Mesler, R. B., *A.I.Ch.E. (Am. Inst. Chem. Engrs.) J.* **7**, 620 (1961).
- M8. Morse, P. M., and Feshbach, H., "Methods of Theoretical Physics," Vol. 1. McGraw-Hill, New York, 1953.
- N1. Nickelson, R. L., and Preckshot, G. W., *J. Chem. Eng. Data* **5**, 310 (1960).
- N2. Norman, A., and Spiegler, P., *Nucl. Sci. Eng.* **16**, 213 (1963).
- O1. Otterman, B., *Proc. Heat Transfer Fluid Mech. Inst.*, 1962 p. 185. Stanford Univ. Press, Stanford, California, 1962.
- P1. Patten, T. D., "Some Characteristics of Nucleate Boiling of Water at Sub-atmospheric Pressures." Thermodynamics and Fluid Mech. Convention, Inst. of Mech. Engrs., Cambridge, England, Paper No. 9, 1964.

- P2. Perkins, A. S., and Westwater, J. W., *A.I.Ch.E. (Am. Inst. Chem. Engrs.) J.* **2**, 471 (1956).
- P3. Plesset, M. S., *J. Appl. Mech.* **16**, 277 (1949).
- P4. Plesset, M. S., "Cavitation in Real Liquids" (R. Davies, ed.), pp. 1-17. Elsevier, Amsterdam, 1964.
- P5. Plesset, M. S., and Hsieh, D., *Phys. Fluids* **3**, 882 (1960).
- P6. Plesset, M. S., and Zwick, S. A., *J. Appl. Phys.* **23**, 95 (1952).
- P7. Plesset, M. S., and Zwick, S. A., *J. Appl. Phys.* **25**, 493 (1954).
- P8. Poritsky, H., *Proc. 1st U.S. Natl. Congr. Appl. Mech.* **1**, 813 (1951).
- R1. Rogers, T. F., and Mesler, R. B., *A.I.Ch.E. (Am. Inst. Chem. Engrs.) J.* **10**, 656 (1964).
- R2. Roll, J. B., and Myers, J. E., *A.I.Ch.E. (Am. Inst. Chem. Engrs.) J.* **10**, 530 (1964).
- R3. Ruckenstein, E., *Chem. Eng. Sci.* **10**, 22 (1959).
- S1. Savic, P., *Natl. Res. Council Can., Rept. MR-37* (1958).
- S2. Savic, P., and Gosnell, J. W., *Can. J. Chem. Eng.* **40**, 238 (1962).
- S3. Scriven, L. E., *Chem. Eng. Sci.* **10**, 1 (1959).
- S4. Scriven, L. E., *Chem. Eng. Sci.* **17**, 55 (1962).
- S5. Seitz, P., *Phys. Fluids* **1**, 2 (1958).
- S6. Semeria, R. L., "An Experimental Study of the Characteristics of Vapor Bubbles." Symp. on Two-Phase Fluid Flow, Inst. Mech. Engrs., London, Paper No. 7, 1962.
- S7. Semeria, R., *Houille Blanche* **18**, 679 (1963).
- S8. Semeria, R., *Compt. Rend.* **256**, 1227 (1963).
- S9. Siegel, R., and Keshock, E. G., *A.I.Ch.E. (Am. Inst. Chem. Engrs.) J.* **10**, 509 (1964).
- S10. Siegel, R., and Usiskin, C. M., *J. Heat Transfer* **81**, 230 (1959).
- S11. Skinner, L. A., Ph.D. Thesis, Northwestern Univ., Evanston, Illinois, 1963.
- S12. Skinner, L. A., and Bankoff, S. G., *Phys. Fluids* **7**, 1 (1964).
- S13. Skinner, L. A., and Bankoff, S. G., *Phys. Fluids* **7**, 643 (1964).
- S13a. Skinner, L. A., and Bankoff, S. G., *Phys. Fluids* **8**, 1417 (1965).
- S13b. Skinner, L. A., personal communication (1965).
- S14. Staniszewski, B. E., "Nucleate Boiling Bubble Growth and Departure." Div. of Sponsored Res., Mass. Inst. Tech., Cambridge, Massachusetts, Tech. Rept. No. 16, 1959.
- S15. Strasberg, M., "The Influence of Air-filled Nuclei on Cavitation Inception." David Taylor Model Basin, Navy Dept., Rept. No. 1078, 1957.
- S16. Streng, P. H., Orell, A., and Westwater, J. W., *A.I.Ch.E. (Am. Inst. Chem. Engrs.) J.* **7**, 578 (1961).
- T1. Tien, C. L., Schrock, V. E., and Johnson, H. A., "On the Prediction of Void Volume in Transient Satd. Pool Boiling." Reactor Heat Transients Res., Univ. of Calif., Berkeley, California, SAN-1004, TID-4500, 1962.
- U1. Usiskin, C. M., and Siegel, R., *J. Heat Transfer* **83**, 243 (1961).
- V1. Van Wijk, W. R., *Dechema Monograph.* **28**, 63 (1956).
- V2. Van Wijk, W. R., and Van Stralen, S. J. D., *Physica* **28**, 150 (1962).
- V3. Van Wijk, W. R., Vos, A. S., and Van Stralen, S. J. D., *Chem. Eng. Sci.* **5**, 68 (1956).
- V4. Viskanta, R., and Lottes, P. A., *Proc. Heat Transfer Fluid Mech. Inst.*, 1962 p. 171. Stanford Univ. Press, Stanford, California, 1962.
- V5. Vos, A. S., and Van Stralen, S. J. D., *Chem. Eng. Sci.* **5**, 50 (1956).
- W1. Wei, C. C., and Preckshot, G. W., *Chem. Eng. Sci.* **19**, 838 (1964).
- W2. Westerheide, D. E., and Westwater, J. W., *A.I.Ch.E. (Am. Inst. Chem. Engrs.) J.* **7**, 357 (1961).
- W3. Westwater, J. W., in "Cavitation in Real Liquids" (R. Davies, ed.), pp. 34-54 Elsevier, Amsterdam, 1964.

- W4. Wyllie, G., *Proc. Roy. Soc. (London)* **A197**, 383 (1949).
- Y1. Yang, W., and Clark, J. A., *J. Heat Transfer* **86**, 207 (1964).
- Z1. Zavoiskii, V. K., *Soviet J. At. Energy (English Transl.)* **10**, 272 (1961).
- Z2. Zivi, S. M., Wright, R. W., and Yeh, G. C. K., "Kinetic Studies of Heterogeneous Water Reactors." Space Tech. Labs., Redondo Beach, California, STL 6212, 1962.
- Z3. Zmola, P. C., Ph.D. Thesis, Purdue University, Lafayette, Indiana, 1950.
- Z4. Zuber, N., *Intern. J. Heat Mass Transfer* **2**, 83 (1961).
- Z5. Zwick, S. A., *Phys. Fluids* **3**, 685 (1960).
- Z6. Zwick, S. A., and Plesset, M. S., *J. Math. Phys.* **33**, 308 (1955).

# EVAPORATIVE CONVECTION

John C. Berg

University of Washington, Seattle, Washington

and

Andreas Acrivos and Michel Boudart

Stanford University, Stanford, California

Work done at Department of Chemical Engineering  
University of California, Berkeley, California

|   |     |
|---|-----|
| I. Introduction .....   | 61  |
| A. The Discovery of Evaporative Convection .....                          | 62  |
| B. The Two Mechanisms Which Drive Evaporative Convection .....            | 64  |
| C. Early Explorations .....   | 65  |
| II. Experimental Methods.....   | 71  |
| A. Suspended Particles .....  | 71  |
| B. Optical Methods.....   | 73  |
| C. Thermal and Other Methods .....  | 81  |
| III. Work of Lord Rayleigh; Hydrodynamic Stability Analysis .....         | 82  |
| A. Rayleigh's Approach .....  | 82  |
| B. Subsequent Development .....   | 94  |
| IV. The Morphology of Natural Convection in Horizontal Liquid Layers..... | 105 |
| A. Experimental Studies.....  | 107 |
| B. Surface Deformations .....   | 113 |
| C. Cell-Size Predictions from Linear Stability Theory .....               | 114 |
| D. Nonlinear Theory.....  | 118 |
| Nomenclature .....  | 120 |
| References .....  | 121 |

## I. Introduction

The convective flow which occurs spontaneously in evaporating liquids is one of the most spectacular performances that nature has hidden from our view. The show may be staged in a lake, in a bathtub, or in a teacup, but it

is rarely visible to the naked eye. Such flows also occur often in distillation, absorption, and extraction in which heat or mass transfer is occurring within or between fluid phases, and all such phenomena may come under the general heading of "natural," "free," or "spontaneous" convection.

The term "convection" was introduced in 1834 by William Prout "to denote a mode of propagation of heat" (by fluid motion), which had been discovered by Count Rumford 40 years earlier (B16). The notion of convection is actually more general, in that mass, or energy in some form other than heat, may be the object of transport. "Natural" and "free" are appended to "convection" to denote movement induced without the performance of external mechanical work on the fluid.

The object of the present review, a case study of evaporative convection, has the purpose of bringing together those aspects of the broader field of "free convection" which are of primary interest to chemical engineers. The specific problem of evaporative convection provides a particularly appropriate vehicle for such a study: first, because it typifies free convection occurring during and as a result of heat or mass transfer in a fluid layer; second, because it involves a fluid-fluid interface which gives rise to important surface phenomena in fluid mechanics; and third, because it provides a needed backdrop for the many experimental studies where spontaneous convection complicates any attempt to elucidate the molecular mechanism of the evaporation process *per se* (K1, P2).

While the specific subject of evaporative convection is at least implicit throughout this review, most of the development centers around simpler related problems, such as that of convection in a fluid layer confined between solid planes, or convection in a fluid layer with a free surface from which no evaporation takes place. Also the review is largely confined to convection in fluid layers sufficiently thin for the thickness itself to be a primary factor relative to the convection phenomena.

## A. THE DISCOVERY OF EVAPORATIVE CONVECTION

Cornelius Varley, an English microscope maker, appears to have been the first to notice, in 1836, "motions of extremely curious and wonderful characters in fluids undergoing evaporation" (V1). The motions were observed with the aid of a microscope by incorporating finely divided coal into the drops and films studied. It remained for James Thompson to give the first explanation of the phenomenon, which he provided in a letter to the Royal Society in 1855 "On Certain Curious Motions Observable at the Surfaces of Wine and Other Alcoholic Liquors" (T3). Thompson reported further observations of natural convection during evaporation in an 1882 note "On a Changing Tessellated Structure in Certain Liquids." He had noticed "in a tub of [soapy] water, in



the yard of a roadside inn, a structure showing itself, which appeared remarkable, and excited a good deal of curiosity. . . .” (T4). The superficial soap film, moved about by the underlying currents, had rendered the normally unseen convection visible. Though they are not the earliest record of such phenomena, Thompson’s observations are appropriate for introducing the subject of evaporative convection, because they illustrate the two mechanisms by which evaporation sustains natural convection, and because Thompson was apparently the first to give the correct explanation of each mechanism.

What Thompson had seen in his wine glass, and what others had noticed probably since the invention of the beverage, was evaporative convection driven by unbalanced surface tension. In a partially filled goblet of wine, a film of wine wetting the inside surface of the goblet will writhe, shrink into droplets, and run down. Thompson noted that “the tensile force [surface tension] is not the same in different liquids. Thus it is found to be much less in alcohol than in water.” He then explained the motions in the evaporating wine films in the following terms:

“The more watery portions of the entire surface, having more tension than those which are more alcoholic, drag the latter briskly away, sometimes even so as to form a horizontal ring of liquid high up round the interior of the vessel, and thicker than that by which the interior of the vessel was wet. Then the tendency is for the various parts of this ring or line to run together to those parts which happen to be most watery, and so there is no stable equilibrium, for the parts to which the various portions of the liquid aggregate themselves soon become too heavy to be sustained, and so they fall down. . . . The film adhering to the inside of the glass must very quickly become more watery than the rest, on account of the evaporation of the alcohol contained in it being more rapid than the evaporation of the water” (T3).

In contrast to the above mechanism, Thompson suggested a buoyancy mechanism to explain the tessellations in the tub of warm evaporating wash-water (T4).

“The phenomenon seems to be associated essentially with cooling of the liquid at its surface where exposed to the air, when the main body of the liquid is at a temperature somewhat above that assumed by a thin superficial film. A very slight excess of temperature in the body of the fluid above that of the surrounding air is sufficient to institute the tessellated changing structure.”

Figure 1 illustrates both phenomena described by Thompson. Actually both mechanisms are operative in both systems, but that of surface tension predominates in shallow layers while that of buoyancy dominates when the

layers are deep. Although this fact can now be demonstrated with certainty, it eluded researchers for over 100 years after Thompson's early observations.

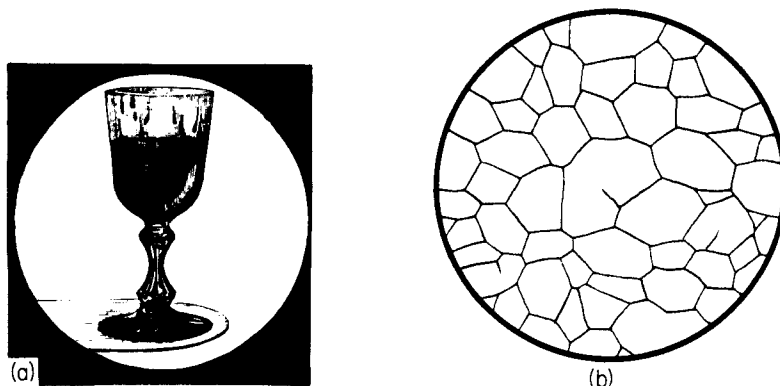


FIG. 1. Thompson's early observations of evaporative convection: (a) the wine-drop phenomenon as observed by Thompson in 1855 (B15) (© 1959 by Educational Services Inc. and reprinted by permission); (b) tessellations observed by Thompson at the surface of a tub of warm soapy water in 1882 (T4).

Just when an evaporating layer goes from "shallow" to "deep" in terms of the mechanism dominating its convection is treated later in this study.

## B. THE TWO MECHANISMS WHICH DRIVE EVAPORATIVE CONVECTION

Evaporation activates the *surface tension "engine"* when it causes the surface tension of the liquid right at the surface to exceed the value that would correspond to the bulk liquid beneath. It accomplishes this by removing heat from the surface region, thereby reducing the surface temperature below that of the bulk liquid. For virtually all liquids, surface tension rises as temperature falls (A1); evaporation, by reducing the surface temperature, thus raises the surface tension. Parenthetically this explains numerous reported values for surface tension which are too high (H5).

Any liquid whose surface layer has a tension higher than the equilibrium value corresponding to its bulk composition is potentially unstable, because the potential energy of the surface layer is not at a minimum. Surface tension is defined as the surface free energy per unit area (G1), so that the most stable arrangement for a liquid with a free surface would be the one in which the material of *least* surface tension is placed in the surface layer. Since this is the opposite of the situation encountered in an evaporating liquid, the latter is unstable with respect to surface forces, and tends to exhibit surface tension driven natural convection in seeking to rearrange itself into a more stable configuration.

In addition to the surface tension effect, evaporation activates the *buoyancy*

“engine” by causing the density of the liquid near the surface to become greater than that of the bulk liquid beneath when solutions evaporate, both by the depletion of the components of least density from the surface region and by surface cooling. It is possible, then, for evaporation to result in both an “adverse” temperature gradient and an “adverse” concentration gradient, the term “adverse” indicating that the arrangement is potentially unstable.

### C. EARLY EXPLORATIONS

Early work consisted chiefly of the reported chance observations and rough experiments concerning “spontaneous” fluid motions, which can now be attributed to surface tension, buoyancy, or to a combination of these effects. Evaporation was not the unique generator of spontaneous fluid motion, which was sometimes induced by heating the fluid from below, or by changing the composition in the surface region (by adding a foreign component or by contacting unequilibrated liquid phases with one another).

#### 1. *Surface Tension Driven Convection*

As early as 1686, Heyde observed spontaneous fluid motion when fragments of camphor were placed on olive oil (T6), while Romieu, in 1748, noted the same motion of camphor on the surface of water. Further observations were recorded and argued over until Tomlinson’s reviews in 1869 (T6). Tomlinson adopted the explanation first put forth by Carradori in 1794: reaction of camphor particles to the spreading force of a camphor film caused them to “dance,” whereas if the camphor were held still, the underlying fluid could be visibly set into motion. Other observations of surface tension convection recorded by 1869 included those of Varley (V1); Thompson (T3,1 T4); Matteuci, in 1833 (cf. T6), concerning the motion of ether laden bits of cork placed on water; Weber, in 1855, concerning evaporating drops of alcohol-water solutions; Tomlinson, in 1864 (T5), concerning the motion of particles of eugenic acid at the surface of water; Bois-Reymond, in 1858; and Lüttge, in 1869 (cf. T6).

During the 1870’s, Carlo Marangoni, who was apparently aware of Carradori’s work but not of Thompson’s, formulated a rather complete theory of surface tension driven flow (M2, M3). He noted that *flow* could result from surface tension variations as they are caused by differences in temperature and superficial concentration, and that, conversely, variations in temperature and concentration could be induced by an imposed surface flow. Marangoni ascribed several new rheological properties to the surface (notably surface viscosity, surface elasticity, and even surface plasticity), while remarking that perhaps some of these properties could be associated only with surface contamination. Most present-day authors ascribe the first explanation of surface tension driven flow to Marangoni, and term such flow a “Marangoni effect.”

## 2. *Buoyancy-Driven Convection*

Thermal convection, driven by gravity, seems to have been recorded first by Count Rumford in 1797 (R4). After accidentally observing the behavior of fluid in a thermometer he reported:

"I saw the whole mass of the liquid in the tube in a most rapid motion running swiftly in two opposite directions, up and down at the same time. . . . Some fine particles of dust had found their way into it and these particles which were intimately mixed with the spirits of wine, on their being illuminated by the sun's beam, became perfectly visible. On examining the motion of the spirits of wine with a lens, I found that the ascending current occupied the axis of the tube and that it descended by the sides of the tube. On inclining the tube a little, the rising current moved out of the axis and occupied the side of the tube which was uppermost, while the descending currents occupied the whole of the lower side of it" (R4).

Rumford went on to explain the phenomenon correctly in terms of the effect of heat on the fluid density: "[Heat] is transported by its particles, these particles being put in motion by the change which is produced in their specific gravity by the change of temperature. . . ."

Some scattered experiments followed those of Rumford but uncovered little new knowledge. Vettin, in 1857, reported convection currents resulting from a point heat source held in a chamber of smoky air (V4). Tyndall, in 1863, and von Bezold, in 1885 (A4), produced varied convection currents in cylinders of water by heating them in various ways. Czermak, in 1893, photographed trajectories obtained with a small heat source placed at the center of a cylindrical vessel of water containing suspended particles (V4). Finally, Guebhard, in 1897 (B6), noted regular patterns on an exposed photographic plate left in a developer bath, due to natural convection induced by evaporation.

## 3. *The Experiments of Henri Bénard*

At the turn of the century, Henri Bénard, a young French physicist, published the first truly systematic study of natural convection in a horizontal fluid layer (B4, B5, B6). In a horizontal liquid layer heated from below Bénard, sought to measure and to define the most stable steady-state convection currents prevailing under given conditions. He utilized liquid layers only a few millimeters in thickness, initially in an apparatus giving a free upper surface, and of considerable horizontal extent (about 20 cm) so that edge effects could not influence the form of the convection pattern. For these studies,

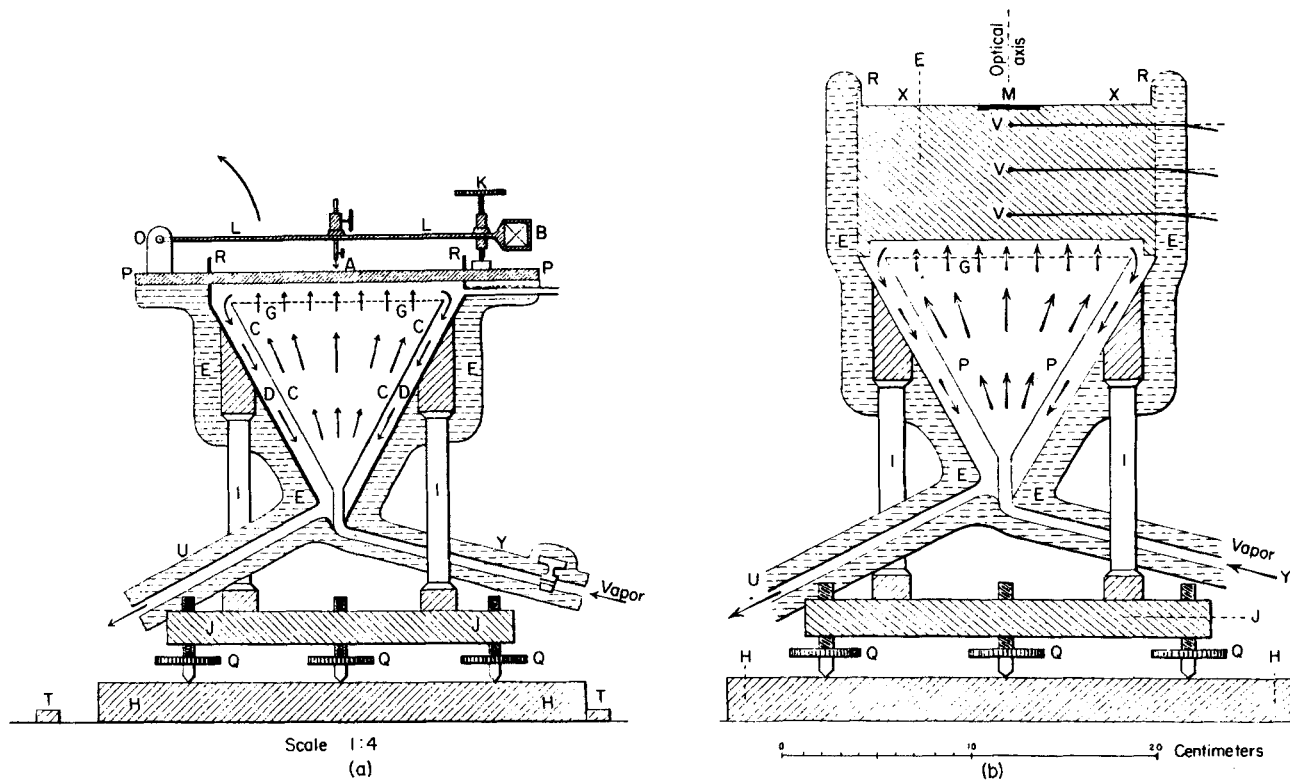


FIG. 2. Bénard's thermal apparatus (B6): (a) shows device for measurement of liquid depth; (b) used for heat flux measurements.

melted spermaceti<sup>1</sup> (cetyl palmitate) at or near 100°C proved to have a viscosity small enough to establish the steady-state regime within a short time and large enough so that this regime was stable toward minute unavoidable perturbations.

From a cylindrical block of iron, Bénard later fashioned a vessel, shown in Fig. 2, 20 cm in diameter and 8 cm thick, with thermocouples placed in the block for measuring vertical heat flux. The bottom of the vessel was an

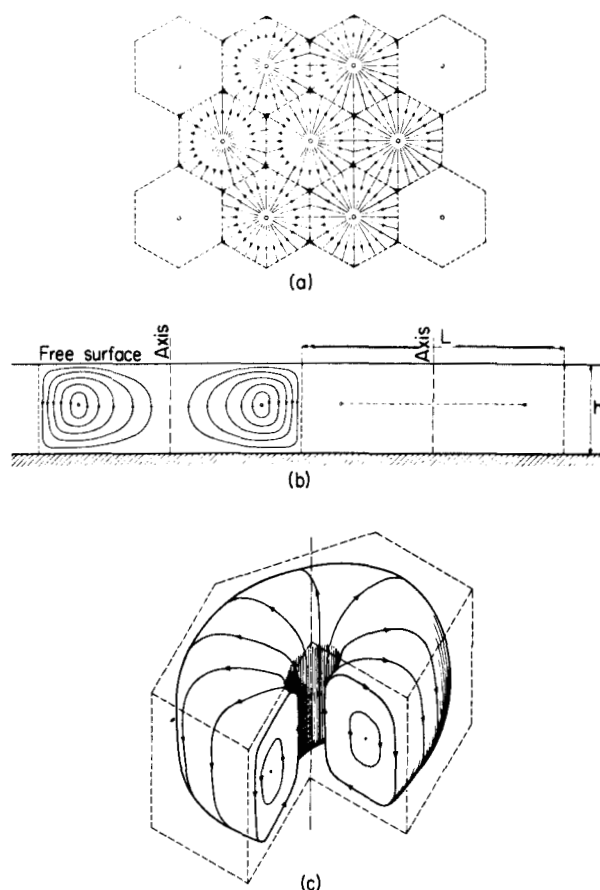


FIG. 3. Steady cellular convection as observed by Bénard (B8) (cf. A4) (courtesy of Ministry of Air, Paris): (a) top view; (b) side view; (c) perspective view.

<sup>1</sup> Bénard experimented with several different liquids and found that volatile liquids (ether at 15°C, alcohol at 50°C) produced rapid, chaotic, permanently unsteady motions. A qualitative description of the currents in evaporating ether was given by Bénard, but the bulk of his report concerns spermaceti.

excellent thermal conductor, and served to maintain the bottom surface (on which steam was condensing) at uniform temperature. The vessel was well insulated around the edges to prevent lateral dissipation of heat. Thermal conditions at the upper free surface were also kept as uniform as possible. The upper face of the metallic block forming the liquid container was dulled and blackened, except for a central area occupied by a flat circular steel mirror of 32 mm diam., cast into the iron "dish," which was used to view the convection.

Two types of procedures (discussed in detail below) were used to study the convection patterns, one employing the incorporation of solid particles into the fluid, and the other optical techniques. The circulation pattern revealed by these is best described with the aid of the drawings shown in Fig. 3 which pertain to the final steady-state convection pattern. The liquid rose in a series of vertical streams located at the centers of polygons, which, in this limiting stable state, constituted a network of regular hexagons. Upon reaching the surface, the liquid of the ascending streams spread radially from the centers toward the edges of the hexagons and then descended to the floor of the vessel where it flowed along the floor inward to the centers of ascension. Unsteady-state flow patterns which always preceded the steady patterns, were qualitatively similar to those of the final regime, and exhibited a polygonal structure (polygons had from four to seven sides) with liquid ascending at the center of the cells and descending along the partitions.

Bénard also showed that the character of the roughly cellular pattern which was initially established would depend upon any overall fluid motion that might have been present at the time of the inception of the cellular vortices. For example, if originally the fluid were in a slight translational motion, the

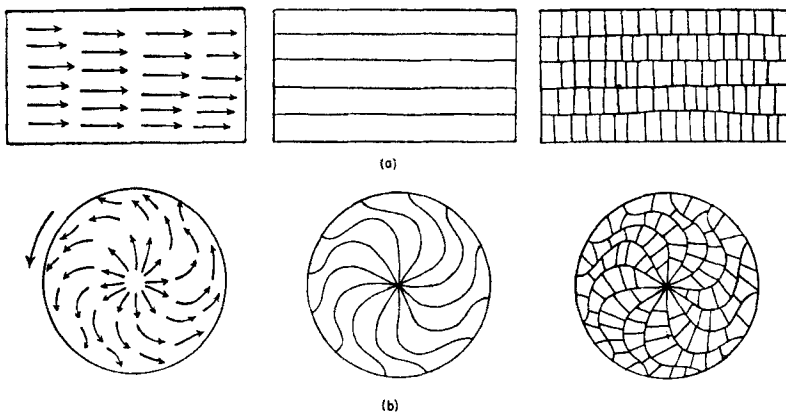


Fig. 4. The effect of fluid motion present at the inception of cellular convection (B4): (a) the effect of initial translational motion; (b) the effect of initial rotational motion.

cellular vortices would appear as shown in Fig. 4(a), whereas an initial rotational motion produced an unsteady pattern of the type shown in Fig. 4(b). In all cases, however, the final permanent regime was the same: a network of regular hexagons.

The chief results of Bénard's work are as follows:

(1) Melted spermaceti, and other nonvolatile liquids of like viscosity, exhibit a permanent convective regime. This regime is preceded first by a brief period in which no convection can be discerned, followed by a temporary flow structure comprising irregular polygons of varying size and number of sides. The permanent regime is established within a few minutes. If the liquid is volatile or has a very low viscosity, no stationary state is attained.

(2) Liquids of slight volatility can be made to exhibit a pseudopermanent regime, but the continually changing depth of the structure prevents the formation of a rigorously permanent regime. In a typical nonpermanent regime, evaporating ether, the "cells" seem to undergo a random translational motion, constantly growing and diminishing by exchange with their neighbors, and sometimes congregating in chains or colonies.

(3) Regardless of the thickness of the liquid layer (which was varied between 0.440 and 1.200 mm) the most stable convection pattern is a network of regular hexagons whose center-to-center distance is 3.2 times the thickness. In the nonpermanent regime, also, the cell size is proportional to the thickness.

(4) At constant temperatures, the ratio of cell size to layer thickness is unchanged by varying the heat flux as much as threefold.

(5) As the temperature is changed, the cell size reaches a minimum somewhere between 50 and 100°C; the temperature giving this minimum rises as the liquid-layer thickness is decreased.

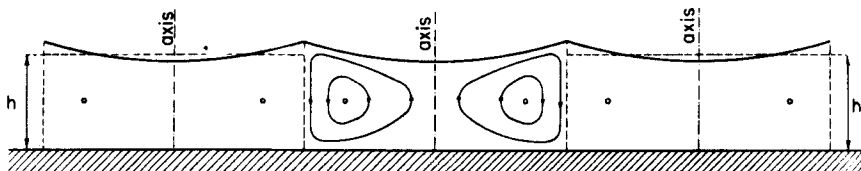


FIG. 5. Exaggerated elevation view of surface deformation caused by cellular convection (A4) (courtesy of Ministry of Air, Paris).

(6) The difference in surface elevation within the cellular vortices is of the order of  $1 \mu$ . Over the range of thicknesses studied, it varies inversely with layer thickness, and directly with temperature (see Fig. 5). Along the surface, the center of the cell was found to lie below the cell boundary.

(7) At a given temperature and heat flux, fluid velocity in the cells is independent of layer thickness, but directly proportional to the heat flux.

(8) Most important, but mentioned only casually by Bénard, there is



generally a minimum heat flux below which no convection seems to occur despite the "adverse" density profile. In terms of present knowledge, Bénard found that, during the preconvective period the viscosity and the thermal conductivity of the fluid are capable of damping and destroying small mechanical and thermal disturbances so that no convection results.

From these findings, Bénard established the two fundamental facts concerning natural convection (C2); "First, a certain critical temperature gradient has to be exceeded before instability can set in; second, the motions that ensue on surpassing the critical temperature gradient have a cellular pattern." His first conclusion opened the question as to when and under what conditions natural convection would occur, while the second provided new insight into a whole array of diverse phenomena: cellular cloud patterns (M4), the polygonal distribution of rocks in certain arctic regions (L8), lunar craters (B7), the cells of living tissue (B4), uneven drying of paint films (B3), regular patterns formed by photographic developer on films and plates (B10), cellular patterns formed during the solidification of glass (cf. S6), and sun spots (B11), to name but a few.

As will be shown below, Bénard's work also provided for many years ahead the experimental foundation for the study of cellular convection. His dramatic results inspired the work of many others, chief among them a group of French experimentalists, and a number of English theoretical physicists led by Lord Rayleigh.

In this review, we shall begin by discussing the experimental techniques which have been used to study either or both of the above two aspects of the problem. Stability criteria will be treated next. Finally, a thorough investigation of the cellular morphology will be given, with particular emphasis on evaporative convection.

## II. Experimental Methods

Many methods have been applied to the experimental investigation of convection in horizontal fluid layers, some best suited for determining the stability criterion, and others designed to study the fully developed convective flow patterns. Three principal types of experimental methods have been employed: (1) suspended particle methods; (2) optical methods; and (3) thermal methods. In addition, a few special techniques have been introduced which fall outside the above categories.

### A. SUSPENDED PARTICLES

Perhaps the most obvious technique for visualizing flow is to incorporate, into the fluid, small solid particles whose motion can be seen and photographed. It was the chance presence of such suspended solids that led to the

initial discovery of thermal convection. Later, Bénard employed the method to the fullest extent. Particles denser than the liquid medium were first deposited at the bottom of the layer and then swept by the centripetal cellular currents into small piles, whose regularity and spacing revealed both the dimensions of the cells and their geometry in the steady state. The unsteady convection patterns preceding the steady state could also be traced by following the movement of the small piles, which in this case were drawn into lines that moved about with the shifting, expanding, and contracting of the cellular vortices. Similarly, particles lighter than the fluid, such as lycopodium powder, were used by Bénard to visualize the cell boundaries, since the floating particles, swept radially outward from the cell centers, concentrated along the cell partitions and eventually at the ternary junctions of the hexagonal cells.

The behavior of fine particles having a density equal to that of the fluid, or of particles of colloidal size, is somewhat more complex. When a heated solid body is immersed in a fluid containing such particles, there is formed around the hot surface a thermal boundary layer which is completely free of such particles, and which customarily has a thickness of the order of 0.1 mm. The important fact for visualization purposes is that all the closed streamlines passing through this layer remain free of particles throughout their course; hence, the torus which forms the cell becomes enveloped in a particle-free envelope that renders it clearly visible. Bénard first photographed this pattern by directing light up through the heated glass bottom of the vessel, but since glass is a relatively poor thermal conductor, a completely steady convection was not achieved under these conditions. Bénard then replaced the glass with a metallic bottom, used highly reflective solid particles, and directed a beam of light onto the cellular layer. Flake-like particles, which aligned in the direction of the flow, were found best for this purpose; Bénard obtained good results using powdered aluminum, graphite, and the scales from butterflies' wings!

Subsequent investigators using the method of suspended particles have improved little upon Bénard's techniques. Volkovisky (V3) used aluminum particles to study the circulation in thin films of liquid, which was drawn up by surface tension forces onto a cold flat plate dipping into the liquid. Bell (B3) studied the flotation of pigment particles in drying paint films. Aluminum particles were used by Muller to study convection during the evaporation of thin layers of acetone (L2); and recently Linde (L4) employed them to study convection in thin *vertical* fluid layers, confined between parallel glass plates, undergoing gas absorption and desorption. Jarvis (J1) sprinkled talcum particles on a layer of evaporating water in order to trace convection patterns which were sometimes induced by blowing nitrogen gas against the surface. Also, many investigators used entrained smoke to follow convective movements in gaseous layers (A4, C1, S7, S13).

Suspended particles furnished a means both of viewing the developed flow patterns and of detecting the onset of convective instability, but the method is open to question regarding the extent to which the particles affect the phenomenon. Indeed, in certain experiments (C1, S13), the smoke-gas suspension had sufficiently different properties from those of the pure gases to produce anomalous stability results. Bénard, recognizing this inherent dilemma in the use of solid particles, devised optical techniques for following the fluid motion in detail without introducing any foreign objects.

## B. OPTICAL METHODS

A fluid layer undergoing thermal convection, or convection due to mass transfer, is optically nonuniform; its refractive index, being a function of temperature and of composition, varies from point to point. As a consequence, light rays passing through the fluid are deflected in a manner which depends on the refractive index variation, and therefore on the distribution of temperature, concentration, or both. Thus, optical techniques may be based on analyzing the behavior of light refracted by the medium. If the fluid layer undergoing convection has a free surface, there is also a free-surface relief that mirrors the convection going on beneath it, which may be studied by analyzing the deflections of light reflected from the surface. Both refracted and reflected light are thus used. They may be analyzed by three different experimental methods, each yielding somewhat different information concerning the convecting medium, and each subject to a great number of variations: (1) interferometry; (2) the schlieren method; and (3) the direct-shadow method.

### 1. *Interferometry*

The principles of the interferometric method are well known; the subject is generally discussed in beginning physics texts, to illustrate the wave character of light. When two beams of light originating from the same source are made to overlap, either by inclining or by lengthening one beam relative to the other in the region where they cross, their corresponding rays generally are no longer in phase with one another. Thus a plane surface that intercepts the beams in their region of crossing will be illuminated with a pattern of interference fringes.

Two types of interferometers, Fabry-Pérot and Mach-Zehnder, have been applied to the study of convection in horizontal fluid layers.

The Fabry-Pérot type used by Bénard, which produces "fringes of equal thickness," is shown schematically in Fig. 6. Monochromatic light from a source S is collimated by the lens L and is directed vertically onto the

flat horizontal glass plate G. Here some light is reflected.<sup>2</sup> The rest, transmitted by G, passes through the air film between the glass and the liquid layer, and is then partially reflected at the liquid surface F; the remaining part of the light passes through the liquid layer and is completely absorbed at the bottom surface which is dulled and blackened. If  $n_G$  and  $h$  denote,

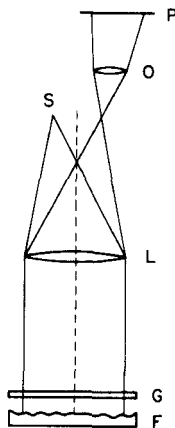


FIG. 6. Schematic drawing of the Fabry-Pérot interferometer of the type used by Bénard to obtain contour lines for the free surface of a liquid undergoing thermal convection.

respectively, the refractive index and the thickness of plate G, and if at a given horizontal position the separation between plate G and the liquid surface F is  $d$ , the two optical components of the ray differ in length by  $(2d + n_G h)$ . "Constructive interference," producing a bright fringe, occurs when this difference in path length is an integral number of wavelengths, both ray components having undergone a phase reversal upon reflection. In constructive interference, those points having fluid elevations such that the air film thickness is  $d$  will form bright contour lines. A sequence of contour lines is produced for a sequence of fluid elevations differing by one-half wavelength of light, i.e., a fraction of a micron. Figure 7 shows a schematic drawing of such contour lines as obtained by Bénard for the case of perfectly regular hexagonal convection cells. (The direction of the elevation changes, i.e., whether cell centers were relatively elevated or depressed, had to be determined by other means.)

The Mach-Zehnder interferometer, shown schematically in Fig. 8 and often used to study flow patterns in wind tunnels, has recently been employed

<sup>2</sup> Strictly, there is reflection at both surfaces of G; but since these surfaces are perfectly parallel, the components emerging from them have the same phase relationship for all rays, and contribute in no way to the formation of contour lines.

to determine temperature profiles in fluid layers heated from below (J6). Monochromatic light from the source  $S$  is collimated by the lens  $L$  and is directed toward the partially silvered mirror  $M$  which divides the incident light into two beams, 1 and 2. Plane mirrors  $M_2$  and  $M_3$  direct the two beams to the partially silvered mirror  $M_4$  where they are recombined, part of beam

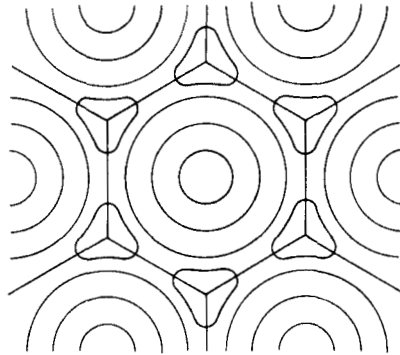


FIG. 7. Contour lines of the type obtained by Bénard for the free surface of a hexagonal convection cell using the Fabry-Pérot interferometer.

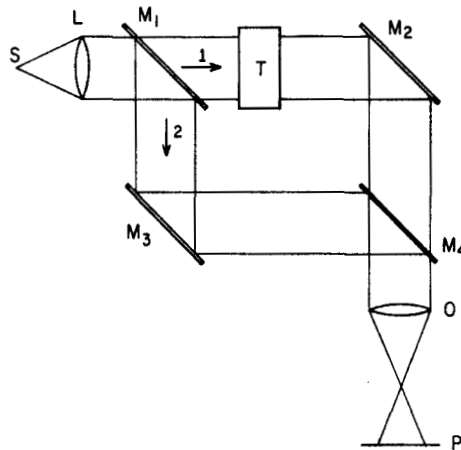


FIG. 8. Schematic drawing of the Mach-Zehnder interferometer.

2 being lost by reflection and part of beam 1 being lost by transmission at  $M_4$ . By proper adjustment of  $M_2$  and  $M_3$ , the beams emerging from  $M_4$  are inclined slightly to one another so that the objective lens  $O$  will project a uniform system of fringes on the photographic plate or viewing screen  $P$ . The light beams are widely spaced, so that a test section  $T$  may be inserted

in one beam without disturbing the other. Variations in refractive index within the test section will cause variations in the optical path length for the different rays of beam 1, resulting in a shift in the location of the interference fringes. The extent of fringe shift may then be related quantitatively to the refractive index distribution in the test section.

Two factors distinguish interferometry from the other optical methods to be discussed. Interferometry provides data related directly to the elevation or the refractive index of the liquid layer; and it yields data that are generally quantitative.

## 2. Schlieren Method

Schlieren methods provide the most commonly used procedure for investigating convective flow in a horizontal fluid layer. ("Schlieren," a German word, means "streaks.") In contrast to interferometry, this method often is only qualitative. The schlieren technique produces, on the photographic plate or viewing screen, light-intensity variations that are proportional to the *gradient* of refractive index of the medium (or, if the surface relief is under study, to the *slope* of the free surface). The basic principle of the method is that a ray of light passing through the medium in question (or reflected from the surface) undergoes an angular deflection directly proportional to the refractive index gradient (or to the slope of a reflecting surface) at each point along its path. The deviations of the ray are then monitored. The technique was invented by August Toepler in 1864, and the many variations to which it has been subjected are discussed extensively by Holder and North (H4), Schardin (S3), and others (B2).

The simple "two-mirror" arrangement, Fig. 9, serves to illustrate the

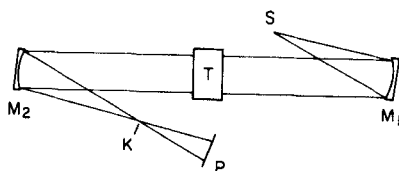


FIG. 9. Schematic drawing of a two-mirror schlieren system.

essential principles. Light from a small source  $S$  of well-defined shape is collimated by the parabolic mirror  $M_1$ , and is passed through the medium under study. Here some rays may undergo angular deflections, small enough to permit the rays to be gathered and refocused at  $K$  by the parabolic mirror  $M_2$ . Each of the light rays at  $T$  contains light from all points of the source  $S$ ; so that, upon leaving  $M_2$ , each of these independent rays is capable of producing an image of the source  $S$ .

If a ray experiences no deflection upon traversing this test section, the light-source image it forms will be located precisely at the point where the optical axis of the system intersects the focal plane K. It follows that, if none of the rays experience deflection, all of the source images will be superimposed in the same spot, forming a clear bright undistorted image of the light source. However, if a particular ray is deflected, its image of the light source in the focal plane K will lie away from the optical axis (see Fig. 10). Now,

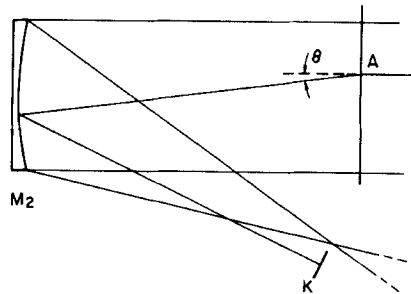


FIG. 10. Sketch showing the blockage of a light ray in a schlieren system. Deflected in the test section, the light ray emerging from A will never reach the viewing screen because it is blocked by the knife edge K.

beyond the focal plane of  $M_2$ , a viewing screen P is positioned so that an image of the test section is brought to focus upon it, regardless of the extent to which it is deflected. It is important to note that a ray piercing the test section will be brought to rest at the corresponding point in the *image* of the test section.

Thus there is a point-to-point correspondence between the test section and its image on the viewing screen, regardless of the deflections of the various rays. The ray deflections are rendered visible on the screen by blocking part of the light from reaching the screen with a diaphragm in the focal plane of  $M_2$ , so that points in the image corresponding to such rays appear dark. Often the diaphragm is a simple knife-edge K oriented to intercept a fraction of the light in the focal plane of the schlieren mirror,  $M_2$ , as shown in Fig. 10. If the knife edge is horizontal, rays deflected upward produce bright spots in the image, rays deflected downward produce dark spots, and rays deflected to the left or right remain unaffected. Correspondingly, the light intensity of the image varies in accordance with the sign and the magnitude of the vertical component of the refractive index gradient in the medium. Therefore, since these gradients are due to temperature or composition gradients, the schlieren patterns can be used to follow the flow in a system where the temperature or composition varies with position.

Bénard used the schlieren method (although not by this name) to obtain

photographs of the surface relief of thin liquid layers undergoing convection, where the light ray underwent deflections proportional to the slope of the surface at the point of incidence. Sellin (S8) has used a reflecting schlieren system to follow surface depressions due to turbulent vortices in forced convection. Linde (L4) has recently employed a schlieren technique (as well as suspended particles) to study spontaneous convection in a liquid confined between vertical glass plates, into which various gases were being absorbed. Orell and Westwater (O2, O3) have used a microscopic schlieren system to study convection during liquid-liquid mass transfer. Spangenberg and Rowland (S10) employed a two-mirror schlieren system to photograph convection in a deep tank of evaporating water. Berg (B12) used such a system to photograph evaporative convection in water, several organic liquids, and several binary solutions.

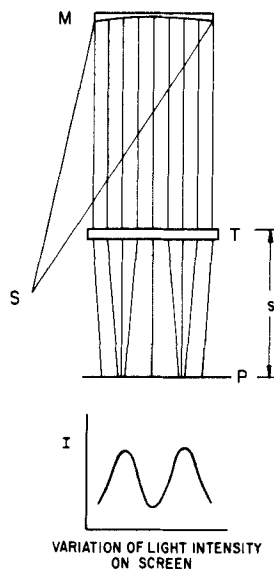


FIG. 11. A schematic drawing of the direct-shadow method showing formation of the shadow image of the liquid layer T on the screen P. It is evident that the nature of the distribution of the light intensity  $I$  depends to a large extent on the distances from the test section to the screen.

### 3. Direct-Shadow Method

The direct-shadow technique is probably the simplest in principle, but is subject to the greatest variation. As with the schlieren method, this technique when applied to the study of liquids generally yields only qualitative information. In contrast to the preceding methods, the direct-shadow technique detects differences from point to point in the *second* derivative of the surface



elevation with respect to the horizontal axis (i.e., the surface curvature) or, for a refracted light beam, differences in the divergence of the refractive index gradient.

Direct-shadow optics are much the same as for a schlieren system, but, as shown in Fig. 11, without the schlieren mirror or lens and the diaphragm knife edge. An image showing refractive index variations in the medium under study will result only if these variations produce beams that are either converging or diverging, i.e., if adjacent rays traversing the medium  $T$  are deflected by different amounts. It was noted above that a light ray is deflected through an angle directly proportional to the refractive index gradient. Hence, in the direct-shadow image, the light intensity at a certain point on the screen will be inversely proportional to the *divergence* of the refractive index gradient at the corresponding point in the test section. Figure 11 also shows that the intensity is inversely proportional to the distance of the viewing screen from the test section.

Bénard employed two variations of the direct-shadow method, using reflected light to obtain photographs of free-surface relief during convection. In particular because the free surfaces of his convection cells were essentially basins separated by ridges, from the optical standpoint they simulated concave mirrors separated by cylindrical convex mirrors. By adjusting the position of the viewing screen, as shown in Fig. 12, the cell centers could be

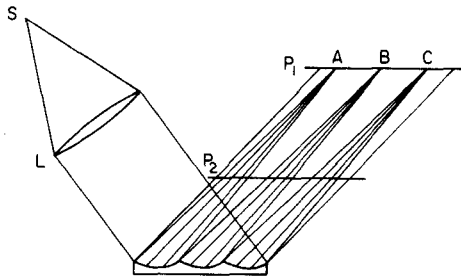


FIG. 12. Diagrammatic sketch of Bénard's direct-shadow system for locating the cell centers and cell partitions on the surface of the liquid. With the viewing screen at  $P_1$ , the cell centers appeared to be bright spots, A, B, and C on a dark background, whereas, when the screen was moved closer to the liquid, as at  $P_2$ , the image became one of dark lines on a bright background. Bénard's apparatus was actually somewhat different than shown, but the diagram illustrates its important features.

made to appear as bright spots A, B, and C on a dark background (at position  $P_1$ ); also, the cell partitions could be brought into focus as dark lines on a bright background by moving the screen closer to the liquid (as at  $P_2$ ). Bénard used these two focal distances to determine the radius of curvature of the concave cell surfaces. The second variation of the direct-shadow technique

involved projecting a rectangular grid onto a screen with light which was reflected from the free surface of the liquid, so that deformations in the grid image could be related to the curvature of the free surface.

The direct-shadow method has been employed in the study of free convection by many authors following Bénard, and unfortunately has often been mislabelled as a "schlieren" method. Levengood (L2) in a study of evaporative convection in pools of methyl alcohol, and Hickman (H2) in a study of surface behavior of boiling liquids, used modifications of Bénard's deformed grid technique.

Saunders, Fishenden, and Mansion (S2) developed a shadow technique in which the image of a long slit, or group of slits, illuminated by a carbon arc point source located several meters behind these slits was projected laterally through a liquid layer onto a screen. The deformations in the slit image were related, through the refractive index, to the temperature variations surrounding vertical and horizontal plates immersed in various fluids. Schmidt and Milverton (S4), Schmidt and Saunders (S5), and later Silveston (S9), used the technique for detecting the onset of convective instability in horizontal fluid layers heated from below.

A summary of the three optical techniques, listing the specific quantities to which each method is sensitive, is given in Table I.

TABLE I  
OPTICAL METHODS FOR THE INVESTIGATION OF FREE CONVECTION

| Method         | Sensitive to what property                        |   | Remarks   |
|----------------|---|---|---|
|                | Reflected beam                                    | Refracted beam  |   |
| Interferometry | Free surface elevation,<br>i.e., $h$              | Refractive index, $n$   | Best method for obtaining quantitative profiles of temperature or concentration |
| Schlieren      | Free surface slope,<br>i.e., $\text{grad } h^a$ , | Refractive index gradient, $\text{grad } n^a$                 | Best method for qualitative observations of convective flow patterns            |
| Shadow         | Free surface curvature, $\text{div grad } h$      | Divergence of refractive index gradient, $\text{div grad } n$ | Simple to construct; sometimes yields quantitative results                      |

<sup>a</sup> This, of course, refers to that component of the gradient which is perpendicular to the edge of the diaphragm.

A good review of all three optical methods, although oriented to wind tunnel work, is given by Holder and North (H4).

### C. THERMAL AND OTHER METHODS

Although the optical methods are clearly superior to use of solid particles in studying free convection, neither technique proves adequate for determining quantitatively the threshold conditions for convective instability. This is so because the precise point at which convection is first detected is always somewhat arbitrary when based on human observations. To remedy this situation, Schmidt and Milverton (S4) assumed that the onset of convection would be indicated by a sudden change in the overall heat transfer coefficient to the fluid; by measuring the heat transfer across a fluid layer confined between parallel horizontal plates, the lower of which was always maintained at the higher temperature, they were able to observe a striking increase in the slope of the heat-transfer rate plotted against temperature difference whenever the latter reached a particular value. This criterion for the onset of convection was both clear-cut and reproducible, and they interpreted it as indicating that the mechanism of pure heat conduction had given way to a combination of conduction with convection. Subsequently, the Schmidt-Milverton thermal technique was used successfully by others (S5, S9).

Other thermal methods for the study of natural convection have employed temperature probes placed at various positions within the fluid layer. Such methods provide a means of studying three-dimensional effects and are thus particularly appropriate for investigating deep fluid layers. Jarvis (J1, J2) measured liquid temperatures in and about the surface of evaporating water by means of a thermistor probe and detected the presence or absence of evaporative convection by the presence or absence of rapid temperature fluctuations at given points near the surface. Spangenberg and Rowland (S10) measured temperature profiles during evaporative convection with a thermopile. Ewing and McAllister (E1) and later Jarvis (J1) used an infrared radiometer to determine the surface temperature of water during evaporation, but no direct measure of the convection phenomena was obtained in this way.

In addition to the foregoing methods, other highly specialized techniques have also been used occasionally to investigate the cellular structure of free convection. For example, Mysels (M5) has employed the color change produced in a filter paper impregnated with cobaltous chloride and held just above the surface of evaporating water, to detect differences in the evaporation rate from different areas of the surface. Earlier, Dauzère (D1) had

quickly solidified a liquid layer undergoing cellular convection, so as to measure the surface deformations at leisure.

### III. Work of Lord Rayleigh; Hydrodynamic Stability Analysis

#### A. RAYLEIGH'S APPROACH

##### 1. *The Problem of Buoyancy-Driven Convection*

In 1916, when more than 70 years old, Lord Rayleigh (John William Strutt) published his famous paper "On Convection Currents in a Horizontal Layer of Fluid, When the Higher Temperature Is on the Under Side," which he presented as "an attempt to examine how far the interesting results obtained by Bénard in his careful and skilful experiments can be explained theoretically" (R1). Recalling the theoretical predictions he had made earlier regarding the disintegration of liquid jets into droplets, Rayleigh sought to predict by means of small-disturbance analysis the "disintegration" of a quiet layer of liquid when heated from below into cellular vortices.

It was known that jets about to disintegrate first become wavy or "varicose," then break up into a string of equal-sized detached masses that form droplets. Similarly, the experimentally observed regular cellular pattern in free convection suggested that the displacements (or velocities, etc.) resulting from the introduction and growth of disturbances would be spatially periodic, and that the different modes by which a system would fall away from an unstable equilibrium could be characterized in terms of one, two, or three time-independent wavelengths.

In the case of a liquid jet, a growing disturbance could be expressed in terms of a single wavelength which ultimately manifested itself as the wavelength of the observed varicosity preceding the disintegration of the jet. The problem of the unstably heated infinite layer of fluid was similar, except that the disturbance components, distributed over the horizontal plane, required *two* wavelengths for their description. Rayleigh sought to predict the dimensions of the Bénard cells by formulating his problem first in terms of an inviscid fluid analysis which was then extended to include viscosity.

The expected result, instability whenever the fluid density increased upward, proved true when the viscosity was neglected. But when viscous effects were taken into account Rayleigh discovered a thoroughly stable regime in which the density was *greater* at the top, as had been observed by Bénard. Although the problem of locating the threshold of convective instability eventually eclipsed the original problem of finding the preferred wavelengths, both pieces of information emerged from Rayleigh's solution which thus

constitutes one of the few completely solved problems of hydrodynamic stability.

## 2. Basic Concepts of Hydrodynamic Stability Analysis

Although hydrodynamic stability has been thoroughly reviewed by Lin (L3) and by Chandrasekhar (C3), some general comments on the subject are appropriate at this point. Rayleigh's problem, merely one in this general class, is concerned with the stability of an initial "flow regime" in which there is no flow.

To determine the stability of a given steady-state flow to infinitesimal disturbances, we examine first the fate of such disturbances after they first arise. If they decay with time, the regime is said to be *stable*; if they grow with time, the regime is said to be *unstable*.

The mathematical formulation of such a problem begins with the statement of the appropriate equations of change. In Rayleigh's problem, these were the equations of motion, the equation of continuity, and the equation of thermal-energy conservation, together with an appropriate equation of state. In their most general form, these equations are

$$\partial \rho / \partial t + \text{div}(\rho \mathbf{u}) = 0 \quad (\text{continuity equation}) \quad (1)$$

$$\rho D\mathbf{u}/Dt = \rho \mathbf{f} - \text{grad } p - (\frac{2}{3}) \text{grad}(\mu \text{div } \mathbf{u}) + \text{div}(\mu \text{def } \mathbf{u}) \quad (\text{equation of motion}) \quad (2)$$

$$\rho D(c_v T)/Dt = \text{div}(k \text{grad } T) - p \text{div } \mathbf{u} + (\mu/2)(\text{def } \mathbf{u}) \cdot (\text{def } \mathbf{u}) - (\frac{2}{3})\mu(\text{div } \mathbf{u})^2 \quad (\text{energy equation}) \quad (3)$$

$$\rho = \rho_0[1 - \alpha(T - T_0)] \quad (\text{equation of state}) \quad (4)$$

where

$c_v$  = heat capacity at constant volume,

$\mathbf{f}$  = body force, per unit mass of fluid,

$k$  = thermal conductivity,

$T$  = temperature,

$T_0$  = reference temperature,

$t$  = time,

$\mathbf{u}$  = fluid velocity,

$\text{def } \mathbf{u} = \text{grad } \mathbf{u} + (\text{grad } \mathbf{u}) \text{ transpose}$

$D/Dt$  = substantial derivative,

$\alpha$  = volumetric coefficient of thermal expansion,

$\rho$  = density,

$\rho_0$  = fluid density at  $T = T_0$ , and

$\mu$  = viscosity.

We now set

$$\mathbf{u} \equiv \hat{\mathbf{u}} + \hat{\mathbf{u}}; \quad T \equiv \hat{T} + \hat{T}, \text{ etc.} \quad (5)$$

where  $\hat{\phantom{x}}$  denotes the initial steady-state value of the variable and  $\hat{\phantom{x}}$  denotes its perturbation. In Rayleigh's problem, the vertical axis is generally designated as  $z$ , the origin is located in the bottom surface of the fluid layer, and the unperturbed temperature profile is assumed to be linear, so that

$$\hat{T} = \hat{T}_0 - \beta z \quad (6)$$

where  $\beta \equiv -d\hat{T}/dz$  is minus the steady-state linear temperature gradient and  $\hat{T}_0$  is the temperature at the bottom surface.

Gravity is considered to be the only body force, and therefore

$$\mathbf{f} = -g\mathbf{e}_z \quad (7)$$

where  $\mathbf{e}_x$ ,  $\mathbf{e}_y$ ,  $\mathbf{e}_z$  are unit vectors in the  $x$ ,  $y$ , and  $z$  directions, respectively.

These expressions are now substituted into Eqs. (1)–(4) which are then linearized by supposing the perturbations to be very small. Thus, in terms of the perturbed quantities  $\hat{\mathbf{u}}$ ,  $\hat{T}$ , etc. (but dropping the superscript  $\hat{\phantom{x}}$ ), we obtain

$$\text{div } \mathbf{u} = 0 \quad (8)$$

$$\partial \mathbf{u} / \partial t = g\alpha T \mathbf{e}_z - \text{grad } p + \nu \text{ div } (\text{grad } \mathbf{u}) \quad (9)$$

$$\partial T / \partial t - \beta \mathbf{u} \cdot \mathbf{e}_z = \kappa \text{ div } (\text{grad } T) \quad (10)$$

where  $\kappa \equiv k_0/\rho_0 c_{v0}$  is the thermal diffusivity, and  $\nu = \mu_0/\rho_0$  the kinematic viscosity. The derivation of the above linearized perturbation equations from the set of general equations (1)–(4) is carried out in detail by Chandrasekhar (C3).

### 3. The Solution of Rayleigh's Problem

In Rayleigh's words, "We now assume in the usual manner that the small quantities are proportional to  $e^{ilx} e^{imy} e^{qt}$ ," where the "small quantities" are of course the disturbance variables or perturbation quantities in Eqs. (8)–(10). In view of the linearity of the governing equations, we can express any one of these, say  $T$ , in terms of its Fourier transform

$$T(x, y, z, t) = \iint_{-\infty}^{\infty} T_{l,m}^*(z) e^{ilx} e^{imy} e^{q(l,m)t} dl dm \quad (11)$$

(where an asterisk denotes dependence on  $z$  only) provided that the system is infinite in extent in both the  $x$  and the  $y$  directions. For finite systems a somewhat different formulation is required (P3).

The different modes of the disturbance can then be thought of as giving rise to the various terms in Eq. (11), and refer to the different horizontal

patterns by which the unstable equilibrium may disintegrate. We note that “ $l$ ” and “ $m$ ” are wave numbers referred to some one pair of mutually perpendicular axes in the horizontal plane, so that use of Eq. (11) restricts the theoretical treatment to rectangular cells with two-dimensional roll cells being included as a limiting case. As we shall see presently, the stability analysis yields a “critical” value for the quantity  $a^2 \equiv l^2 + m^2$ , but not for the ratio  $l/m$ .

The particular boundary conditions to be satisfied at the top and bottom surfaces of the fluid layer determine the form of the  $z$  dependence of the solution, i.e., the functions  $T^*(z)$ ,  $u^*(z)$ , etc. These are then used to locate the “marginal state” and thereby the “critical” point of the system, by recalling that the parametric space (defined by the parameters of the differential equations) contains both stable and unstable regions and hence a boundary between these two domains which is termed the “marginal state” or the “state of neutral stability.” Furthermore, in most stability problems, all the parameters of the system are fixed *a priori* except for one which is allowed to vary continuously over some range; this one parameter then possesses some “critical” value that separates the stable from the unstable portions of the range.

Strictly speaking, then, the stability analysis is limited to locating the marginal state, that is, the region in parameter space where the real part of the growth constant  $q$  is zero. The state of marginal stability can be, of course, one of two kinds, depending on whether or not  $q^{(i)}$  (the imaginary part of the growth constant) is zero.

Thus, if  $q^{(i)}$  is zero, the marginal state is *stationary* in that the amplitudes of the disturbance variables exhibit no time dependence; whereas if  $q^{(i)}$  is not zero<sup>3</sup>, the amplitudes of the disturbances in the marginal state are periodic in time.

To locate the marginal state, expressions such as Eq. (11) are substituted into Eqs. (8–10). The real part of  $q$  is then set equal to zero, and the resulting set of linear homogeneous ordinary differential equations is solved, subject to the appropriate boundary conditions which are also generally homogeneous.

As a rule, a great deal of simplification in the equations results if  $q^{(i)}$  is assumed equal to zero at the marginal state, an assumption termed “the principle of exchange of stabilities,” which is frequently invoked in stability analyses without any attempt to justify it rigorously. Rayleigh himself showed that this step was correct for his problem, for the one set of boundary conditions that he considered; Pellew and Southwell (P3) extended the proof to other boundary conditions as well. Of course, the failure to account for oscillatory marginal states when these are indeed possible, amounts actually

<sup>3</sup> Actually, nonzero values of  $q^{(i)}$  will appear as conjugate pairs.

to solving an incorrect set of governing equations, thereby computing an incorrect set of conditions for the state of neutral stability.

When the viscosity is neglected, Eqs. (8–10) reduce to

$$\frac{\partial u_x}{\partial \tilde{x}} + \frac{\partial u_y}{\partial \tilde{y}} + \frac{\partial u_z}{\partial \tilde{z}} = 0 \quad (12)$$

$$\left. \begin{aligned} \frac{\partial u_x}{\partial \tilde{t}} &= -\frac{h}{\rho\kappa} \frac{\partial p}{\partial \tilde{x}} \\ \frac{\partial u_y}{\partial \tilde{t}} &= -\frac{h}{\rho\kappa} \frac{\partial p}{\partial \tilde{y}} \\ \frac{\partial u_z}{\partial \tilde{t}} &= -\frac{h}{\rho\kappa} \frac{\partial p}{\partial \tilde{z}} + \frac{g\alpha h^2}{\kappa} T \end{aligned} \right\} \quad (13)$$

$$\frac{\partial T}{\partial \tilde{t}} - \frac{h^2\beta}{\kappa} u_z = \frac{\partial^2 T}{\partial \tilde{x}^2} + \frac{\partial^2 T}{\partial \tilde{y}^2} + \frac{\partial^2 T}{\partial \tilde{z}^2} \quad (14)$$

where, as is common practice, the nondimensional coordinates  $(\tilde{x}, \tilde{y}, \tilde{z}) = (x/h, y/h, z/h)$  and  $\tilde{t} = tk/h^2$  have been introduced,  $h$  being the depth of the liquid layer. In what follows, the symbol “ $\sim$ ” will always refer to a dimensionless quantity. Also, the Cartesian coordinate system with respect to the fluid is that shown in Fig. 13.

When the disturbance variables of the type of Eq. (11) are substituted into the expressions shown above, there results

$$i\tilde{l}u_x^* + i\tilde{m}u_y^* + Du_z^* = 0 \quad (15)$$

$$\left. \begin{aligned} \tilde{q}u_x^* &= -\frac{i\tilde{l}h}{\kappa\rho} p^* \\ \tilde{q}u_y^* &= -\frac{i\tilde{m}h}{\kappa\rho} p^* \\ \tilde{q}u_z^* &= -\frac{h}{\rho\kappa} Dp^* + \frac{g\alpha h^2}{\kappa} T^* \end{aligned} \right\} \quad (16)$$

$$\tilde{q}T^* - \frac{h^2\beta}{\kappa} u_z^* = (D^2 - \tilde{l}^2 - \tilde{m}^2)T^* \quad (17)$$

where  $D$  is the operator  $d/d\tilde{z}$ ,  $\tilde{q} = q\kappa/h^2$ ,  $\tilde{l} = lh$ , and  $\tilde{m} = mh$ . Again, an asterisk denotes the portion of the given variable that depends on  $\tilde{z}$  only.

Next, by combining Eqs. (15) and (16) to eliminate  $u_x^*$ ,  $u_y^*$ , and  $p^*$ , we obtain

$$\tilde{q}(D^2 - \tilde{l}^2 - \tilde{m}^2)u_z^* = -(\tilde{l}^2 + \tilde{m}^2)\frac{g\alpha h^2}{\kappa} T^* \quad (18)$$



which may be combined with Eq. (17) to yield a single equation in terms of either  $T^*$  or  $u_z^*$ ,

$$\tilde{q}(D^2 - \tilde{a}^2)^2 T^* - \tilde{q}^2(D^2 - \tilde{a}^2) T^* - \frac{\tilde{a}^2 g \alpha \beta T^* h^4}{\kappa^2} = 0 \quad (19)$$

$$\tilde{q}(D^2 - \tilde{a}^2)^2 u_z^* - \tilde{q}^2(D^2 - \tilde{a}^2) u_z^* + \left( \tilde{a}^4 \tilde{q} - \tilde{a}^2 \frac{g \alpha \beta h^4}{\kappa^2} \right) u_z^* = 0 \quad (20)$$

where  $\tilde{a}^2$  has replaced  $\tilde{l}^2 + \tilde{m}^2$ .

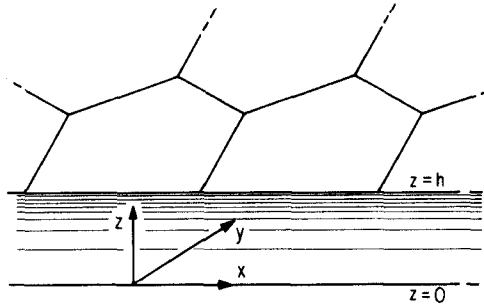


FIG. 13. Orientation of Cartesian coordinates in horizontal fluid layer.

Either equation may be considered. To locate now the marginal state, we set both the real part and the imaginary part of  $\tilde{q}$  equal to zero, thus obtaining, respectively, for Eqs. (19) and (20),

$$\tilde{a}^2 \left( \frac{g \alpha \beta h^4}{\kappa^2} \right) T^* = 0 \quad (21)$$

$$\tilde{a}^2 \left( \frac{g \alpha \beta h^4}{\kappa^2} \right) u_z^* = 0 \quad (22)$$

It follows in this simple case that the marginal state is specified by the condition

$$\tilde{a}^2 \frac{g \alpha \beta h^4}{\kappa^2} = 0 \quad (23)$$

The system is therefore stable whenever

$$\tilde{a}^2 \frac{g \alpha \beta h^4}{\kappa^2} < 0 \quad (24a)$$

but unstable if

$$\tilde{a}^2 \frac{g \alpha \beta h^4}{\kappa^2} > 0 \quad (24b)$$

Since all quantities on the left of Eq. (23), except for the temperature gradient  $\beta$ , are always positive, the sign of the expression depends on the sign of  $\beta$ . The conclusion which is reached on the basis of such an inviscid analysis is that a layer of fluid is always unstable when the temperature *decreases* upward ( $\beta > 0$ ) and always stable when the temperature *increases* upward ( $\beta < 0$ ).<sup>4</sup>

The stability analysis will now be extended to the more realistic case which includes the effect of viscosity. The pertinent equations are Eqs. (8)–(11); or, in nondimensional form, Eqs. (12), (14), and

$$\left. \begin{aligned} \frac{\partial u_x}{\partial \tilde{t}} &= -\frac{h}{\rho\kappa} \frac{\partial p}{\partial \tilde{x}} + N_{Pr} \operatorname{div}(\operatorname{grad} u_x) \\ \frac{\partial u_y}{\partial \tilde{t}} &= -\frac{h}{\rho\kappa} \frac{\partial p}{\partial \tilde{y}} + N_{Pr} \operatorname{div}(\operatorname{grad} u_y) \\ \frac{\partial u_z}{\partial \tilde{t}} &= -\frac{h}{\rho\kappa} \frac{\partial p}{\partial \tilde{z}} + \frac{g\alpha h^2}{\kappa} T + N_{Pr} \operatorname{div}(\operatorname{grad} u_z) \end{aligned} \right\} \quad (25)$$

where  $N_{Pr} = \nu/\kappa$  is the Prandtl number. These are now solved formally by assuming that

$$(u_x, u_y, u_z, p, T) = [u_x^*(\tilde{z}), u_y^*(\tilde{z}), u_z^*(\tilde{z}), p^*(\tilde{z}), T^*(\tilde{z})] \times e^{i\tilde{l}\tilde{x}} e^{i\tilde{m}\tilde{y}} e^{\tilde{q}\tilde{t}} \quad (26)$$

for which Eqs. (12), (14) and (25) become (15), (17), and

$$\left. \begin{aligned} \tilde{q}u_x^* &= -\frac{i\tilde{l}h}{\kappa\rho} p^* + N_{Pr}(D^2 - \tilde{a}^2)u_x^* \\ \tilde{q}u_y^* &= -\frac{i}{\rho\kappa} h p^* + N_{Pr}(D^2 - \tilde{a}^2)u_y^* \\ \tilde{q}u_z^* &= -\frac{h}{\rho\kappa} Dp^* + \frac{g\alpha h^2}{\kappa} T^* + N_{Pr}(D^2 - \tilde{a}^2)u_z^* \end{aligned} \right\} \quad (27)$$

Eqs. (27) are next combined with Eq. (15) to yield an expression analogous to Eq. (18):

$$(D^2 - \tilde{a}^2)[N_{Pr}(D^2 - \tilde{a}^2) - \tilde{q}]u_z^* - \tilde{a}^2 \frac{g\alpha h^2}{\kappa} T^* = 0 \quad (28)$$

<sup>4</sup> In certain rare instances, such as for water between 0 and 4°C,  $\alpha$ , the coefficient of thermal expansion of the fluid, is negative. In such instances, the converse of the stated conclusion would be true.

which, because of Eq. (17), becomes

$$(D^2 - \tilde{a}^2 - \tilde{q})(D^2 - \tilde{a}^2 - \tilde{q}/N_{Pr})(D^2 - \tilde{a}^2)T^* + \tilde{a}^2 RT^* = 0 \quad (29)$$

or

$$(D^2 - \tilde{a}^2 - \tilde{q})(D^2 - \tilde{a}^2 - \tilde{q}/N_{Pr})(D^2 - \tilde{a}^2)u_z^* + \tilde{a}^2 Ru_z^* = 0 \quad (30)$$

where  $R \equiv g\alpha\beta h^4/\kappa\nu$  is the Rayleigh number.<sup>5</sup>

Either Eq. (29) or Eq. (30) may be considered as the governing equation, subject to the appropriate boundary conditions of which six are required, three at the bottom surface ( $\tilde{z} = 0$ ) and three at the top ( $\tilde{z} = 1$ ). These boundary conditions may be expressed in terms of either  $T^*$  or  $u_z^*$ . Rayleigh considered the case in which both surfaces were isothermal, rigid, and "free,"

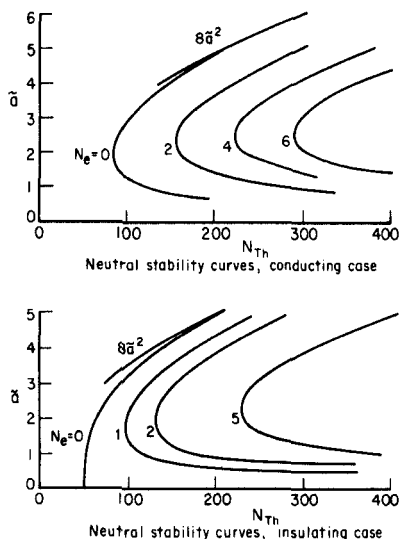


FIG. 14. Neutral stability curves as computed by Pearson.

and although the latter was an unrealistic condition, it simplified the problem to the point of allowing an analytic solution.

Invoking now the principle of exchange of stabilities, we seek to locate the stationary marginal state by setting both the real and the imaginary parts of  $\tilde{q}$  equal to zero, so that Eqs. (29) and (30) become

$$(D^2 - \tilde{a}^2)^3 T^* + \tilde{a}^2 R T^* = 0 \quad (31)$$

$$(D^2 - \tilde{a}^2)^3 u_z^* + \tilde{a}^2 R u_z^* = 0 \quad (32)$$

<sup>5</sup> The Rayleigh number is seen to be the product of the Grashof and Prandtl numbers used in empirical studies of free-convection systems.

which must be solved subject to the boundary conditions shown in Table II. In particular, we seek to determine the smallest characteristic value for  $R$  in terms of the wave number  $\tilde{a}$ .

TABLE II  
BOUNDARY CONDITIONS FOR RAYLEIGH'S PROBLEM

|                 |       | In terms of<br>temperature | In terms of<br>velocity | Physical meaning   |
|-----------------|-------|----------------------------|-------------------------|--------------------|
| $\tilde{z} = 1$ | (i)   | $T^* = 0$                  | $D^4 u_z^* = 0$         | Isothermal surface |
|                 | (ii)  | $D^2 T^* = 0$              | $u_z^* = 0$             | Rigid surface      |
|                 | (iii) | $D^4 T^* = 0$              | $D^2 u_z^* = 0$         | Free slip          |
| $\tilde{z} = 0$ | (iv)  | $T^* = 0$                  | $D^4 u_z^* = 0$         | Isothermal surface |
|                 | (v)   | $D^2 T^* = 0$              | $u_z^* = 0$             | Rigid surface      |
|                 | (vi)  | $D^4 T^* = 0$              | $D^2 u_z^* = 0$         | Free slip          |

It can easily be shown that the general solution to Eq. (31) [or (32)] may be expressed as

$$T^* = \sum_{i=1}^6 A_i e^{s_i \tilde{z}} \quad (33)$$

where the  $s_i$ 's are the roots of the indicial equation

$$(s^2 - \tilde{a}^2)^3 + \tilde{a}^2 R = 0 \quad (34)$$

These are

$$\begin{aligned} s_1, s_2 &= \pm i\tilde{a}(\lambda - 1)^{1/2} \\ s_3, s_4 &= \pm \frac{\tilde{a}}{(2)^{1/2}} [(1 + \lambda + \lambda^2)^{1/2} + (1 + \frac{1}{2}\lambda)]^{1/2} \\ &\quad + i[(1 + \lambda + \lambda^2)^{1/2} - (1 + \frac{1}{2}\lambda)]^{1/2} \\ s_5, s_6 &= \pm \frac{\tilde{a}}{(2)^{1/2}} [(1 + \lambda + \lambda^2)^{1/2} + (1 + \frac{1}{2}\lambda)]^{1/2} \\ &\quad - i[(1 + \lambda + \lambda^2)^{1/2} - (1 + \frac{1}{2}\lambda)]^{1/2} \end{aligned}$$

where  $\lambda = (R/\tilde{a}^4)^{1/3}$ .

In addition we require the determinant

$$\begin{vmatrix} e^{s_1} & e^{s_2} & e^{s_3} & e^{s_4} & e^{s_5} & e^{s_6} \\ s_1^2 e^{s_1} & s_2^2 e^{s_2} & s_3^2 e^{s_3} & s_4^2 e^{s_4} & s_5^2 e^{s_5} & s_6^2 e^{s_6} \\ s_1^4 e^{s_1} & s_2^4 e^{s_2} & s_3^4 e^{s_3} & s_4^4 e^{s_4} & s_5^4 e^{s_5} & s_6^4 e^{s_6} \\ 1 & 1 & 1 & 1 & 1 & 1 \\ s_1^2 & s_2^2 & s_3^2 & s_4^2 & s_5^2 & s_6^2 \\ s_1^4 & s_2^4 & s_3^4 & s_4^4 & s_5^4 & s_6^4 \end{vmatrix} = 0 \quad (35)$$

if Eq. (31) is to possess a nontrivial solution.

Rayleigh did not proceed exactly in this general way. Rather, because of the particular boundary conditions that he selected (summarized in Table II), he was able to set  $T^*$  proportional to  $\sin(j\pi\tilde{z})$ , where  $j$  is an integer. Then, on account of Eq. (31),

$$(j^2\pi^2 + \tilde{a}^2)^3 - \tilde{a}^2 R = 0 \quad (36)$$

and therefore,

$$R = (j^2\pi^2 + \tilde{a}^2)^3 / \tilde{a}^2$$

From this it follows that the critical Rayleigh number (or  $g\alpha\beta h^4/\kappa\nu$ ) is  $27\pi^4/4 = 657.5$ , corresponding to  $j = 1$  and to  $\tilde{a} = \pi/2^{1/2} = 2.22$ . Thus, as Bénard had observed, it is indeed possible that a layer of viscous fluid can be thoroughly stable to all infinitesimal perturbations, even when the "higher temperature is on the under side," and that convection can result only when a certain critical density gradient (temperature gradient) is exceeded.

To summarize then, Rayleigh, motivated by Bénard's experiments, deduced the conditions for the existence of stability (preconvective equilibrium) in viscous fluid layers heated from below, and laid the framework for the hydrodynamic stability analysis of such phenomena. However, as Rayleigh himself pointed out, the boundary conditions he employed corresponded neither to the experiments of Bénard, nor perhaps to any physically realizable system, and it became necessary therefore to extend Rayleigh's problem to other sets of boundary conditions.

#### 4. Refinements and Extensions of Rayleigh's Analysis

Rayleigh's approach to the thermal convection problem has been extended to include other boundary conditions, the more important of which are shown in Table III. Such a refinement can be accomplished either by solving a complicated characteristic equation of the type of Eq. (35), or by resorting to a "short cut."

On purely qualitative grounds Low and Brunt (L8), in 1925, proposed that the presence of a solid wall in place of a free surface should double Rayleigh's criterion for instability and that solid walls at both top and bottom should quadruple the critical Rayleigh number.

TABLE III  
SUMMARY OF BOUNDARY CONDITIONS USED IN THE RAYLEIGH PROBLEM

|       | Type of surface   | In terms of temperature | In terms of velocity          |
|-------|-------------------|-------------------------|-------------------------------|
| (i)   | Rigid             | $(D^2 - a^2)T^* = 0$    | $u_z^* = 0$                   |
| (ii)  | (a) Free slip     | $D^2(D^2 - a^2)T^* = 0$ | $D^2u_z^* = 0$                |
|       | (b) No slip       | $D(D^2 - a^2)T^* = 0$   | $Du_z^* = 0$                  |
| (iii) | (a) Conducting    | $T^* = 0$               | $(D^2 - a^2)u_z^* = 0$        |
|       | (b) Constant flux | $DT^* = 0$              | $D(D^2 - a^2)u_z^* = 0$       |
|       | (c) Radiating     | $(D + K)T^* = 0$        | $(D + K)(D^2 - a^2)u_z^* = 0$ |

In 1926–27, Jeffreys (J3, J4) attempted to extend Rayleigh's result to a more realistic set of boundary conditions, first using finite differences to obtain successive approximations to the solution of Eq. (31) and later using a method of undetermined coefficients for the case corresponding to two solid conducting boundaries. In the latter manner, he computed a critical Rayleigh number of 1709.5.

On the other hand, an earlier article of G. I. Taylor (T1) had already dealt with the stability of a viscous fluid in the annular region between a pair of coaxial cylinders rotating at different speeds, for which Taylor had shown that the initial Couette flow will break down into a series of toroidal vortices (now known as Taylor's vortices) if the relative speed of the two cylinders exceeded a certain critical value. As noted by Low (L8), this case was completely analogous to the Rayleigh problem involving two solid conducting boundaries, since the governing equations and boundary conditions for both problems are formally the same when the radii of the cylinders are nearly equal and when the cylinders are rotating at nearly the same speed. In Taylor's analysis, the "Taylor" number

$$\text{Ta} = 4(\Omega h^4/\nu^2) > 0 \quad (37)$$

where  $\Omega$  is the angular velocity of the cylinders, took the place of the Rayleigh number and its value at the critical point was found to equal 1706, corresponding to  $\tilde{a} = \pi$ . In addition Taylor accompanied his theory with a set of careful experiments, which dramatically verified his numerical predictions with respect to both the critical Taylor number and the vortex size and

thus provided the first unquestionable success for the linear stability analysis of a viscous fluid. Expecting to find a critical  $R$  around 1706, Low undertook to solve, the Rayleigh problem for solid boundaries (L6), and arrived at a critical  $R$  of 1704.4 for the case of two solid conducting boundaries. More important, he also obtained a critical  $R$  of 1108 for the case of a solid conducting boundary below and a rigid but free surface above. This, together with many other results arrived at subsequently, is shown in Table IV.

TABLE IV  
THE CRITICAL RAYLEIGH NUMBER AS CALCULATED BY VARIOUS  
INVESTIGATORS FOR DIFFERENT BOUNDARY CONDITIONS

| Type of boundary conditions <sup>a</sup>    | Solved by                         | Critical $R$ |
|---|-----------------------------------|--------------|
| Free-free                                   | Rayleigh (R4), 1916               | 657.5        |
| Solid-solid                                 | Jeffreys (J1), 1928               | 1709.5       |
|   | Low (L6), 1929                    | 1704.4       |
|   | Pellew and Southwell (P3), 1940   | 1707.8       |
| Solid-free                                  | Low (L6), 1929                    | 1108         |
|   | Pellew and Southwell (P3), 1940   | 1100.65      |
| Solid-solid (constant flux; top)            | Sparrow <i>et al.</i> (S11), 1964 | 1295.781     |
| Solid-solid (constant flux; top and bottom) | Sparrow <i>et al.</i> (S11), 1964 | 720.000      |
| Solid-free (constant flux; top)             | Sparrow <i>et al.</i> (S11), 1964 | 669.001      |
| Solid-free (constant flux; top and bottom)  | Sparrow <i>et al.</i> (S11), 1964 | 320.000      |

<sup>a</sup> All surfaces assumed rigid and isothermal unless otherwise stated.

Low also set forth the boundary conditions which would correspond to other physically real systems, noting that, in general, the bounding surfaces would not be perfect conductors and would require a thermal boundary condition of the form

$$\pm DT^* = KT^* \quad (38)$$

where  $K$  is a "radiation constant." It is worth remarking here that Eq. (38) properly describes the thermal condition at the upper surface in Bénard's experiments, and of any experiments in which the liquid layer is undergoing evaporation.

In 1940, Pellew and Southwell (P3) resolved the Rayleigh problem for "free-free," "solid-free," and "solid-solid" boundaries and obtained good

agreement with Rayleigh, Jeffreys, and Low (see Table IV). Moreover, with regard to cell shape, they freed themselves of the restriction to the rectangular configurations which had been imposed by Rayleigh and Jeffreys, writing:

“Within the assumptions of the approximate theory . . . a particular size is associated with every shape of cell (such that  $\tilde{a}^2$  takes a preferred value), but no particular shape is more likely than another to occur in a layer of indefinite extent. The explanation of the apparent preference for a hexagonal cell pattern must presumably be sought in a theory which takes account of second-order terms. This conjecture if correct goes some way towards explaining the rather indefinite nature of observed cell-formations” (P3).

As noted above, these authors also proved the general validity, for the Rayleigh problem, of the principle of exchange of stabilities. Further, by formulating the problem in terms of a variational principle, Pellew and Southwell devised a technique which led to a very rapid and accurate approximation for the critical Rayleigh number. Later, a second variational principle was presented by Chandrasekhar (C3). A review by Reid and Harris (R2) also includes other approximate methods for handling the “Bénard problem” with solid boundaries.

In a recent paper, Sparrow, Goldstein, and Jonsson (S11) presented the solution to the Rayleigh problem with a “radiation” boundary condition of the type of Eq. (38) at the upper free surface. Some of their results, for both a constant flux and a constant temperature bottom, are shown in Table IV. Of special interest is their solution for the limiting case of a constant-flux upper surface and a constant-flux bottom, for which the critical Rayleigh number was found to be only 320.

## B. SUBSEQUENT DEVELOPMENT

### 1. *Comparison of Experiment and Theory*

For historical reasons, we now compare the theory, as outlined above, with experimental observations. It was just such a comparison that led to much better understanding of the phenomenon under discussion and thus to substantial improvement in the general theoretical approach. This section will concern itself only with the *criterion of instability*; discussion of the morphology of the convection pattern will be deferred to a later point. It is advantageous now to subdivide the stability experiments into two categories: (1) fluid layers confined between solid plates, and (2) liquid layers having a single free surface. Obviously, evaporative convection belongs to this second category.



So far, all the experiments falling in the first category have been performed with both solid surfaces being maintained at constant uniform temperatures, this being in accord with boundary conditions (i)a, (ii)b, and (iii)a of Table III.

For such systems bounded by solid surfaces there has been good agreement between experiment and theory. A striking confirmation was achieved in 1935 by Schmidt and Milverton (S4), who studied the stability of a water layer confined between horizontal metal plates spaced from 4 to 5.5 mm apart, measuring the rate of heat transfer across the liquid layer as a function of temperature difference between the two plates. As described earlier, these authors noted an abrupt change in the heat-transfer coefficient at a Rayleigh number of  $1770 \pm 140$ , which compares favorably with the theoretical value of 1709. These results were further confirmed using a direct-shadow optical technique.

In 1936, Avsec (A2) confirmed Rayleigh's theory in a rough way for air layers confined between metal plates spaced from 1.1 to 6.3 cm apart. The onset of convection was detected visually by means of smoke within the chamber. In 1938, Schmidt and Saunders (S5) repeated the experiments of Schmidt and Milverton, using air as well as water, and obtained an average critical  $R$  of 1750. In 1958, an extensive study by Silveston (S9) using the Schmidt-Milverton technique confirmed the Rayleigh theory for four liquids in addition to water, for depths from 1.45 to 13 mm. Silveston's results yielded a critical Rayleigh number of  $1700 \pm 51$ .

In 1938, Chandra (C1) performed experiments with smoky air which confirmed the Rayleigh theory for depths above 1.0 cm (he employed depths from 4 mm to 1.6 cm), but for depths below this he observed a "columnar convection" for Rayleigh numbers well below the predicted critical value. In 1950, Sutton (S13) repeated the experiments of Chandra with both air and carbon dioxide and confirmed, for both gases, the occurrence of a subcritical columnar convection for depths less than 8 mm. These results appear to be due merely to the anomalous flow properties of smoke-air suspensions.

In contrast, for experiments with liquid layers having a free surface, the boundary conditions have been somewhat less definite. In most of them, the solid surface could be described accurately in terms of boundary conditions (i)a, (ii)b, and (iii)a of Table III, while the upper surface could perhaps be described fairly well by means of (i)a and (ii)a; however, experimental evidence may be cited which casts doubt on the appropriateness of both of these. The general thermal boundary condition, (iii)c, of which (iii)a and b are merely limiting cases, is usually required to complete the description of the free surface.

Experiments with free surfaces have not led to such success. Thus, although Bénard did not report the specific conditions for the onset of instability in pools of liquids, sufficient data were available to indicate a serious discrepancy

with Rayleigh's theory. In particular, Low and Brunt (L10) stated in 1925 that Bénard's convection "sets in with less than one-tenth of the gradient required by theory." They blamed the disagreement partly on the unrealistic boundary conditions used by Rayleigh, but primarily on the lack of knowledge concerning the viscosity and the thermal conductivity of spermaceti. Bénard himself (in Low, L7) acknowledged the discrepancy in 1930 as being a factor of  $10^{-4}$  or  $10^{-5}$ , while Vernotte (V2) in 1936 estimated the ratio at roughly  $10^{-2}$ .

Of the numerous convective experiments in horizontal liquids with free surfaces subsequent to Bénard's, only a few have yielded data that permit the calculation of a stability criterion; all these, however, show a grave discrepancy with the Rayleigh theory. In 1939, Volkovisky (V4) presented a study of convection in horizontal layers of various liquids, in which measurements of thermal conditions and layer thicknesses at the onset of instability were recorded for comparison with the Rayleigh theory. In Volkovisky's experiments, water, ethyl alcohol, and several hydrocarbon oils, were made to flow with a translational velocity of the order of a few millimeters per second, and the temperature gradients giving rise to instability were produced by heating the liquids from below. Gradients of the order of  $10\text{--}500^\circ\text{C/cm}$  were established. Critical Rayleigh numbers were computed from Volkovisky's data for three different liquids at depths of 1 and 2 mm, as follows:

| h(cm) | Water | Ethyl alcohol | Shell B14 oil <sup>6</sup> |
|-------|-------|---------------|----------------------------|
| 0.1   | 32.0  | 38.3          | 5.3                        |
| 0.2   | 131.5 | 194.6         | 34.3                       |

These results indicate a discrepancy ranging from  $1/2$  to  $1/200$  with predictions based on the Rayleigh theory using the most nearly appropriate boundary conditions, those of Sparrow *et al.* In addition the lack of consistency in the discrepancy suggested that in these experiments the propensity of the system to exhibit convective instability was not characterized by the Rayleigh number, but rather by other parameters indicative of a new mechanism.

In 1956, Block (B14) briefly described further experimental work on convective stability criteria in liquid pools down to thicknesses as small as  $50\ \mu$ , and noted that "at that thickness there was no indication that the limiting thickness, below which there would be stability, had been reached." Block continued: "This thickness is at least an order of magnitude smaller than the predicted critical depth for convective instability." Presumably Block established the temperature gradients by heating the liquid from below, but he gave no indication of the size of these gradients.

<sup>6</sup> A refined, heavy, viscous hydrocarbon oil. Volkovisky reports viscosity data but no other physical properties. The critical Rayleigh number, however, is reported.

Observations of Bénard patterns in drying paint films by Bell in 1952 [(B3); cf. Fig. 18b, p. 106] as well as by others (L7) indicated that convection could occur even when the Rayleigh number was negative, since these patterns occurred even when the free surface was made the under side.

Experimental information concerning the criteria for the onset of *evaporative* convection was reported in 1961 by Spangenberg and Rowland (S10), by Jarvis (J2), and more recently by Berg (unpublished). Spangenberg and Rowland studied evaporative convection in "deep" pools of evaporating water. No convection was observed for thicknesses less than 1 cm; for greater thicknesses evaporation times of approximately 70 sec were required to establish temperature gradients sufficient to cause instability. The Rayleigh number corresponding to the onset of convection was 1193, computed by "summing the R derived for each of several elementary strips, using the local temperature gradient indicated by the data." Temperature differences within the fluids were measured with a thermopile.

Jarvis' experiments (J1), in which he measured the surface temperature of evaporating water with a thermistor probe, suggested that the critical *depth* for the onset of evaporative convection in water at room temperature was 4 mm, but temperature profiles corresponding to conditions at the onset of evaporative convection were not reported. As described earlier, the presence or absence of evaporative convection was determined by the presence or absence of rapid temperature fluctuations near the surface.

Recently, Berg (B12a) obtained order-of-magnitude Rayleigh numbers for the onset of evaporative convection in 1-mm deep layers of six pure liquids, as shown in Table A. In these runs the onset of convection was detected with

TABLE A

| Liquid               | $R_c$ |
|----------------------|-------|
| Acetone              | 300   |
| Benzene              | 75    |
| Carbon tetrachloride | 100   |
| <i>n</i> -Heptane    | 60    |
| Isopropyl alcohol    | 30    |
| Methyl alcohol       | 60    |

a schlieren system, and the corresponding temperature profiles (which were nearly linear) were determined from cross plots of temperature-time curves obtained with a thermocouple probe.

A new type of discrepancy was uncovered by Jeffreys (J5) who showed in 1951 that, in contrast to the observations of Bénard, buoyancy-driven convection must lead to a free liquid surface that is *convex* over centers of ascending warm liquid.

The failure to obtain experimental confirmation of the Rayleigh theory when a free liquid surface is involved suggests that the Rayleigh theory based on the buoyancy mechanism is not adequate for such liquid systems. This is indeed the case; for, as had been known since the initial observations of Thompson in 1855, the liquid surface itself is the seat of the potential energy required to set the bulk fluid into motion. That the gradient of surface potential energy (i.e., of surface tension) established by temperature differences along the surface provides sufficient force to set a liquid layer in motion was confirmed quantitatively by Volkovisky (V3) in 1935, and by Luntz (L9) who in 1937 studied the flow of a liquid film ("festoon vortices") up a solid surface cooler above than below. Loewenthal (L5) had confirmed this effect as it is produced by concentration differences in 1931. Finally, Bénard himself had regarded surface tension as responsible for the free surface being concave above the centers of ascension of warm liquid when he remarked, "Surface tension, acting alone, produces a depression in the center of the cells, and an excess of static pressure along the boundary lines separating the concave depressions." In a sense, he also considered the possibility that the surface tension gradients could provide the driving force for the cellular convection itself.

## 2. *Pearson's Theory; the Surface Tension Mechanism*

The work of Bell, Block, and others motivated J. R. A. Pearson (P2) to propose in 1958 a radically different theoretical model for the thermal convection problem: a constant density layer with temperature-dependent surface tension.

In Pearson's analysis, the fluid is assumed to be supporting an adverse linear<sup>7</sup> temperature gradient  $\beta$ , and all the fluid properties except for the surface tension  $\sigma$  are taken to be independent of temperature. Thus, the governing equations for the present system are identical to those of the Rayleigh problem, except for the absence of the gravitational term, so that, in place of Eq. (29), there results

$$(D^2 - \tilde{a}^2)(D^2 - \tilde{a}^2 - \tilde{q})[\text{Pr}(D^2 - \tilde{a}^2) - \tilde{q}]T^* = 0 \quad (39a)$$

which simplifies to

$$(D^2 - \tilde{a}^2)^3 T^* = 0 \quad (39b)$$

if, as was verified recently (V5), the principle of exchange of stabilities is assumed to hold.

<sup>7</sup> The use of a linear profile, even for systems where the profiles are not linear, has been justified somewhat by Batchelor (B1), who showed that the most unstable case for any given temperature drop across the layer occurs when the gradient  $\beta$  is replaced by its maximum value.

Pearson's boundary conditions are shown in Table V. Equation (i) represents a heat balance at the upper surface where heat lost at a rate proportional to the surface temperature (such as by evaporation) is balanced by heat conducted to the surface from the liquid beneath. For the thermal conditions at the lower surface, two cases are considered as shown in Eqs. (iv): the surface is assumed either to be isothermal ( $T^* = 0$ ) or to support a constant heat flux ( $DT^* = 0$ ). Equations (ii) and (v) follow from the assumed nondeformability

TABLE V  
BOUNDARY CONDITIONS FOR PEARSON'S PROBLEM

|                                     | In terms of<br>temperature   | In terms of<br>velocity  | Physical meaning   |
|-------------------------------------|--|--|--|
| Top surface<br>( $\bar{z} = 1$ )    | (i) $(D + N_e)T^* = 0$<br>(ii) $(D^2 - \bar{a}^2)T^* = 0$<br>(iii) $D^2(D^2 - \bar{a}^2)T^*$<br>$= \bar{a}^2 N_{Th} T^*$ | $(D + N_e)(D^2 - \bar{a}^2)u_z^* = 0$<br>$u_z^* = 0 = 0$                                     | Radiating or<br>evaporating<br>Rigid balance<br>tangential force |
| Bottom surface<br>( $\bar{z} = 0$ ) | (iv) (a) $T^* = 0$<br>(b) $DT^* = 0$<br>(v) $(D^2 - \bar{a}^2)T^* = 0$<br>(vi) $D(D^2 - \bar{a}^2)T^* = 0$               | $(D^2 - \bar{a}^2)u_z^* = 0$<br>$D(D^2 - \bar{a}^2)u_z^* = 0$<br>$u_z^* = 0$<br>$Du_z^* = 0$ | Conducting<br>Constant flux<br>Rigid<br>No slip                  |

(rigid flatness) of both surfaces. Equation (iii) balances the surface forces due to the temperature-induced variation in surface tension against the shear stress of the underlying fluid, while Eq. (vi) expresses the condition of no slip at the lower surface.

The heart of Pearson's analysis lies in Eq. (iii), in which he accounts for the temperature variation in the surface tension:

$$\sigma = \sigma_0 + (\partial\sigma/\partial T_0)\hat{T}_s \quad (40)$$

Here  $\sigma$  is the surface tension,  $\sigma_0$  is its value in the undisturbed state, and  $\hat{T}_s$  is the disturbance temperature at the surface. The net surface tension force at a given point on the surface (equal to  $\text{grad } \sigma$ ) then becomes  $(\partial\sigma/\partial T_0) \text{grad } \hat{T}_s$ , where  $\text{grad}$  refers to the surface gradient.

The viscous traction of the underlying fluid is given by

$$\tau_z = e_x \mu \left( \frac{\partial u}{\partial y} + \frac{\partial v}{\partial x} \right) + e_y \mu \left( \frac{\partial w}{\partial x} + \frac{\partial u}{\partial z} \right) \quad (41)$$

where  $u$ ,  $v$ , and  $w$  are the velocity components in the  $x$ ,  $y$ , and  $z$  directions, respectively, and  $e_x$  and  $e_y$  are unit vectors in the  $x$  and  $y$  directions.

Equating now the surface divergences of the above two forces and dropping the superscript  $\wedge$  yields

$$\mu \left[ \frac{\partial}{\partial x} \left( \frac{\partial u}{\partial y} + \frac{\partial v}{\partial x} \right) + \frac{\partial}{\partial y} \left( \frac{\partial w}{\partial x} + \frac{\partial u}{\partial z} \right) \right] = \left( \frac{\partial \sigma}{\partial T_0} \right) \nabla_1^2 T_s \quad (42)$$

where  $\nabla_1^2 = \partial^2/\partial x^2 + \partial^2/\partial y^2$ . Upon substitution of the continuity equation and introduction of Eq. (17), Eq. (42) reduces to Eq. (iii), where we have chosen to term the dimensionless group

$$\left[ \frac{-\beta h^2 (d\sigma/dT)}{\mu \kappa} \right] \equiv N_{Th}$$

the Thompson number,<sup>8</sup> after James Thompson who was the first to explain surface tension driven flow. Note that, since  $d\sigma/dT$  is negative,  $N_{Th}$  is always positive when the liquid supports an adverse temperature gradient.

The solution to Pearson's problem may be expressed as

$$N_{Th} = \frac{8\tilde{a}(\tilde{a} \cosh \tilde{a} + N_e \sinh \tilde{a})(\tilde{a} - \sinh \tilde{a} \cosh \tilde{a})}{\tilde{a}^3 \cosh \tilde{a} - \sinh^3 \tilde{a}} \quad (43)$$

for the conducting case, and

$$N_{Th} = \frac{8\tilde{a}(\tilde{a} \cosh \tilde{a} + N_e \sinh \tilde{a})(\tilde{a} - \sinh \tilde{a} \cosh \tilde{a})}{(\tilde{a}^3 \sinh \tilde{a} - \tilde{a}^2 \cosh \tilde{a} + 2\tilde{a} \sinh \tilde{a} - \sinh^2 \tilde{a} \cosh \tilde{a})} \quad (44)$$

for the constant flux case.

These results are plotted in Fig. 14 (see p. 89). For  $N_e = 0$ , the critical Thompson number becomes 80 for the conducting case and 48 for the insulating case, which correspond to values of  $\tilde{a}$  equal to 2.0 and 0, respectively.

Following Pearson, we compare now the "critical thickness" of the fluid layer as computed from the theory based on the surface tension mechanism, with that based on Rayleigh's analysis of buoyancy-driven flows. One easily obtains that, for the conducting case,<sup>9</sup>

$$h_c (\text{surface tension}) = \left[ \frac{80\rho\nu\kappa}{-(d\sigma/dT)\beta} \right]^{1/2}$$

and

$$h_c (\text{buoyancy}) = \left[ \frac{1108\nu\kappa}{g\alpha\beta} \right]^{1/4}$$

<sup>8</sup> This group has also been termed the Marangoni number.

<sup>9</sup> Actually, in Pearson's calculation, the critical Rayleigh number was taken equal to 571, the value obtained by Jeffreys using incorrect boundary conditions. The correct value, 1108, was arrived at by Low.

which will be equal for a fluid depth of

$$\bar{h}_c = \left[ \frac{-(d\sigma/dT)}{\rho g \alpha} \cdot \frac{1108}{80} \right]^{1/2}$$

This led Pearson to remark:

“For most liquids at laboratory temperatures this relation leads to values for  $\bar{h}_c$  of the order of 1 cm. For thicknesses less than  $\bar{h}_c$ , then, we expect surface tension forces to be more effective than buoyancy forces in producing instability, and, for values of ( $h$ ) as small as 1 mm, the onset of cellular motion could confidently be attributed to surface tension rather than to buoyancy” (P2).

Pearson went on to conclude that all of Bénard’s experiments involved surface tension driven convection. Thus, in the case of spermaceti at 100°C, reasonable estimates for  $\kappa$  ( $5 \times 10^{-4}$ ) and  $\nu$  ( $5 \times 10^{-2}$ ) and Bénard’s reported values<sup>10</sup> for  $-(d\sigma/dT)$  ( $5 \times 10^{-2}$ ),  $\rho$  (0.806) and  $\alpha$  ( $7.7 \times 10^{-4}$ ), yield, for a 1-mm layer supporting a 1° temperature drop,

$$N_{Th} = \frac{(0.05)(10)(0.1)^2}{(0.806)(0.05)(5 \times 10^{-4})} = 248 > 89 \quad (\text{unstable})$$

$$R = \frac{(980)(7.7 \times 10^{-4})(10)(0.1)^4}{(0.05)(5 \times 10^{-4})} = 30 < 1108 \quad (\text{stable})$$

Also, Volkovisky’s stability data (see p. 96) can now be checked against the predictions based on Pearson’s work, with the results shown in Table B.

TABLE B

| h(cm) | Water |          | Ethyl alcohol |          | Shell B14 |          |
|-------|-------|----------|---------------|----------|-----------|----------|
|       | R     | $N_{Th}$ | R             | $N_{Th}$ | R         | $N_{Th}$ |
| 0.1   | 32.0  | 4000     | 40            | 540      | 5         | 320      |
| 0.2   | 130   | 4000     | 200           | 920      | 35        | 510      |

The values for Thompson number clearly indicate instability, although there is still a considerable spread between theory and experiment. The same was also true in Berg’s (B12a) experiments for which approximate critical Thompson numbers are shown in Table C. Likewise, in the experiments of Spangenberg and Rowland (with evaporative convection in water) the Thompson

<sup>10</sup> All these numerical quantities are reported in cgs units.

number was computed to be around 1500, also well into the unstable range.

Thus, even though it appears that the Pearson analysis is indeed the appropriate one for describing convection within thin liquid layers with a free surface, indications are that refinements in both the theory and the experiments will be required before a quantitative agreement can be achieved.

TABLE C  
APPROXIMATE EXPERIMENTAL CRITICAL THOMPSON  
NUMBERS FOR EVAPORATION CONVECTION IN 1-MM  
DEEP LAYERS OF EVAPORATING LIQUIDS (B12a)

| Liquid               | Th   |
|----------------------|------|
| Acetone              | 3400 |
| Benzene              | 950  |
| Carbon tetrachloride | 1400 |
| <i>n</i> -Heptane    | 700  |
| Isopropyl alcohol    | 200  |
| Methyl alcohol       | 650  |

Pearson's assumption of free surface nondeformability has been relaxed in a recent paper by Scriven and Sternling (S7) in which the model used was that of a Newtonian fluid surface subject to infinitesimal displacements from its mean plane. It was found that, for liquid layers of the order of 1 mm deep, the neutral stability curve was affected only at very small values of  $\tilde{a}$  (corresponding to disturbance wavelengths in excess of approximately 30 times the liquid depth); here  $N_{Th}$  approached minus infinity, thus implying that the system would always be unstable with respect to disturbances of very large wavelengths. Furthermore, these authors showed, in accord with the observations of Bénard, that the surface would be depressed at the cell centers where warm fluid ascends, and be elevated along the cell partitions. Since this effect is opposite to that in buoyancy-driven convection (J5), it appears that one should be able to determine experimentally whether buoyancy or surface tension dominates convection in any given situation by measuring the surface relief with any of the techniques outlined earlier.

It should be noted carefully that Pearson's analysis still contains the *assumption* that instability sets in only by a stationary marginal state, which of course excludes the actual possibility of an oscillatory marginal regime.

### 3. *The Combined Effect of Buoyancy and Surface Tension*

In the usual case, evaporation from the free surface of a horizontal liquid layer produces a situation favorable to both the buoyancy and the surface



tension mechanisms for evaporative convection. The distinction between them actually belongs as much to history as it does to nature, and, in a recent paper by Nield (N1), the rival mechanisms have been combined into a single analysis. The principle of exchange of stabilities was once again invoked, so that the governing equation became Eq. (31) or Eq. (32) (from the Rayleigh problem), while the boundary conditions were those of Pearson.

The numerical results for this combined problem indicate "that the two agencies causing instability reinforce one another and are tightly coupled." Nield attributes the tightness of the coupling, which can be seen in Fig. 15,

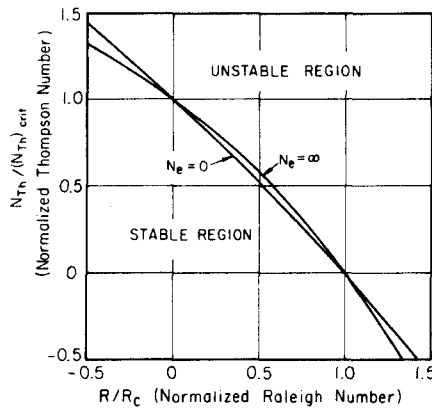


FIG. 15. Nield's stability diagram showing the combined effect of buoyancy and surface tension (N1) (courtesy of Cambridge University Press).

to the fact that cells formed by buoyancy and by surface tension are approximately of the same size.

#### 4. The Effect of Surface Active Agents

As the experimental evidence concerning the stability and convective behavior of a liquid layer with a free surface was being accumulated, there arose evidence pointing to the importance of an additional factor: the presence of surface contamination. As early as 1912, Dauzère (D3) showed that a monolayer of stearic acid was capable of inhibiting the onset of convection in thin layers of melted wax. Low (L7), and later Bell (B3), demonstrated that certain silicone monolayers prevented the occurrence of Bénard cells in drying paint films, while Langmuir and Langmuir (L1) noted that monolayers of several surfactants (oleic acid, cetyl alcohol, and others) eliminated the convection normally accompanying evaporation of aqueous ether solutions. Finally, Block (B14) noted the dramatic stabilizing effect of surface films on thin layers of several organic liquids, as well as on water:

"...Wherever and as soon as the layer [of spreading silicone] passed over the Bénard cell, the surface deformation disappeared and the flow stopped. . . Then the thickness of the liquid (covered by a monofilm) was increased until cellular surface deformations and circulation could again be seen. The thickness at which this occurred was 2 mm, which is, in this case, about the critical depth for the onset of convective instability."

The observed stabilizing effect of surfactants toward convection induced by surface tension has been confirmed theoretically in a recent paper by Berg and Acrivos (B13), in which the stability analysis technique and the physical model were the same as Pearson's except that the free-surface boundary condition [(iii) of Table III] took into account the presence of surface active agents. Critical values for the Thompson number were computed as functions of two dimensionless parameters, one embodying the "surface viscosity" and the other the "surface elasticity."

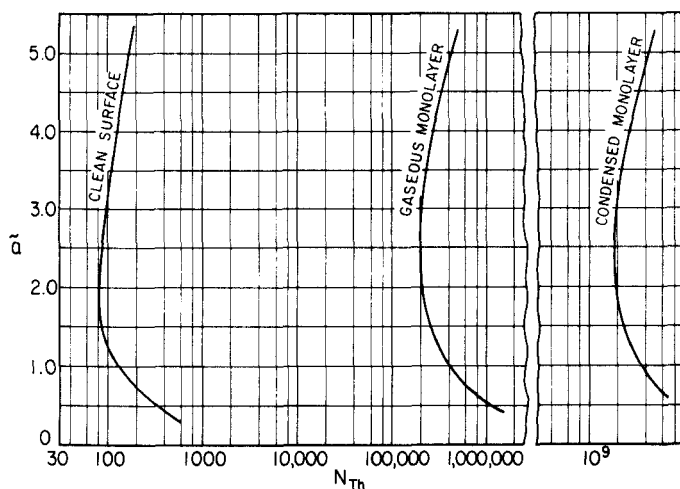


FIG. 16. Neutral stability curves showing the effect of surfactants.

The stabilizing influence of the surface viscosity of a typical monolayer was found to be negligible, in contrast to that of the "surface elasticity," which (even for a so-called "gaseous" monolayer) was sufficient to cause a dramatic stabilization. The shift in the Pearson neutral-stability curves brought about by the presence of a "gaseous" monolayer and also by a close-packed monolayer on a 1-mm deep water substrate is shown in Fig. 16. For this example, the gaseous monolayer having a surface pressure of 0.2 dyn/cm effected a 500-fold increase in the stability criterion, whereas, in

the presence of the close-packed monolayer, of stearic acid the theory predicted virtually complete elimination of the surface tension mechanism for instability.

Surface elasticity is not a structural property of the monolayer, but arises from the dependence of surface tension on the superficial concentration of the surfactant. Figure 17 depicts a small disturbance in which fluid is swept

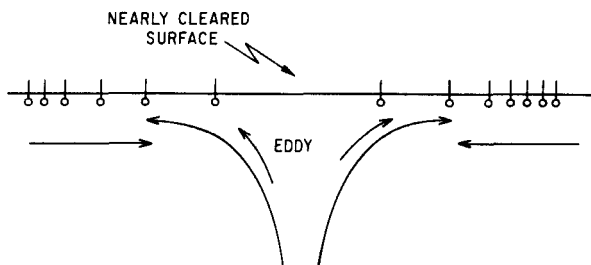


FIG. 17. Eddy bringing fresh liquid to the surface opposed by back-spreading pressure of surfactant film.

radially outward from a particular location on the surface, a disturbance which may be self-amplifying. If surfactant molecules are present, they will be swept outward with the movement of the substrate; since a local drop in surfactant concentration *increases* the surface tension, this will cause surface forces to develop which oppose the outward flow of the liquid. Such behavior simulates "elasticity."

One might have hoped that, following the modifications to the stability analyses for liquids with free surfaces, quantitative comparisons between experiment and theory could have been made, but such is not the case. Further refinement in both theory and experiment is still required. Nevertheless it is indeed encouraging that all of the experimentally observed *qualitative* effects regarding convective stability appear to be in agreement with the predictions of hydrodynamic stability theory.

#### IV. The Morphology of Natural Convection in Horizontal Liquid Layers

Up until this point, with the exception of the description of Bénard's results, we have concerned ourselves only with the stability criteria. Linear stability theory provided the theoretical tools, while optical and thermal methods were employed to detect experimentally the onset of instability. Quantitative agreement between experiment and theory has thus been achieved for gases and for liquids confined between solid plates, and qualitative agreement for liquids with free surfaces.

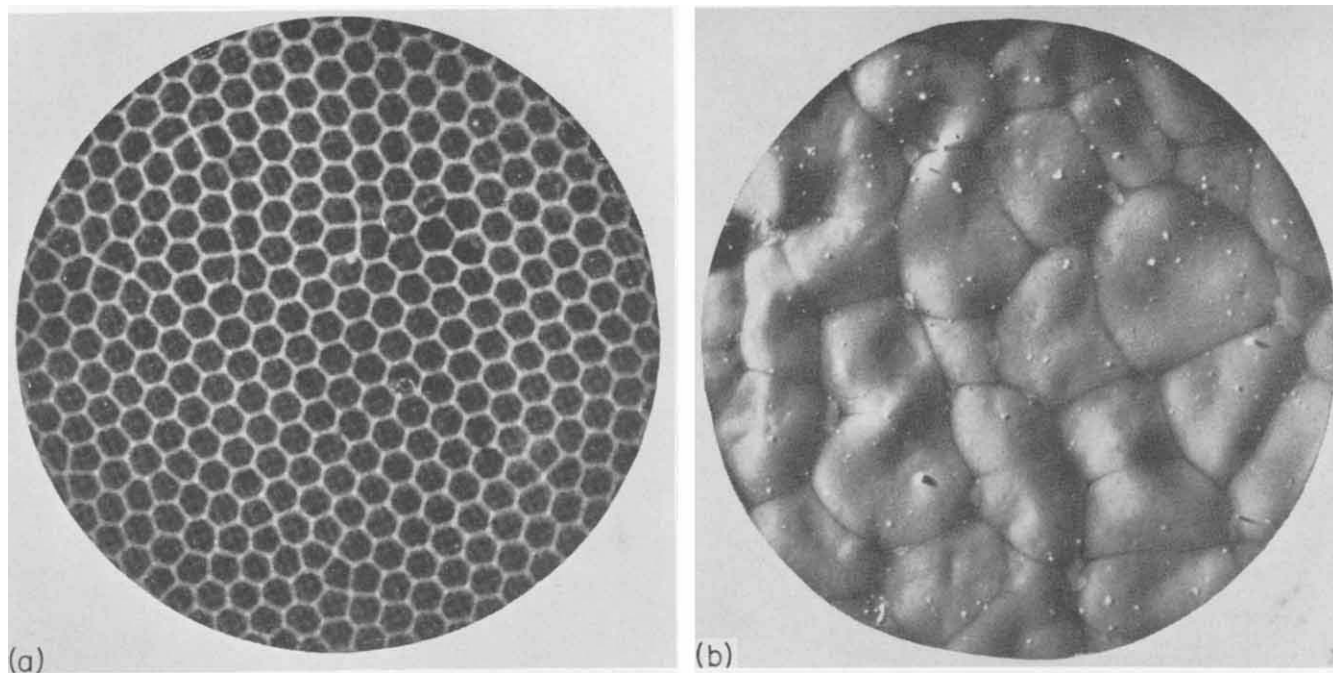


FIG. 18. (a) Bénard cells visualized by the direct-shadow method in which cell partitions act as cylindrical mirrors (A4) (see Fig. 12). Magnification  $2\times$ . (Courtesy of Ministry of Air, Paris.) (b) Bénard cells in a drying paint film (B3). Magnification about  $5\times$ . (Courtesy Oil and Colour Chemical Association, London.)

But what is known concerning the morphology of the convection? Most of the effort in this area has been experimental, and Bénard's work furnishes the foundation. He established that when a shallow liquid layer is freed of the influence of lateral walls, is subjected to no external shear, and is uniformly heated below, a regularized cellular convection pattern sets in, in which the cell divisions bear a definite relation to the thickness of the fluid layer. A photograph from Bénard's work is shown in Fig. 18, together with a photograph by Bell (B3) showing Bénard cells in a drying paint film.

We now review the more important experimental investigations following Bénard's, paying particular attention to studies of convection in liquid layers.

#### A. EXPERIMENTAL STUDIES

Dauzère (D1) produced solidified Bénard cells in 1907 by quickly cooling a thin layer of melted beeswax undergoing convection. Performing similar experiments in 1912 (D3, D4), he noticed that if the beeswax was boiled with water beforehand, or better still with an alkaline solution, the entire character of the cells would change. The cells isolated themselves into colonies separated by relatively quiet areas, and these colonies were eventually reduced to single isolated vortices (tourbillons isolés) (see Fig. 19) which, after 30 to 45 min,

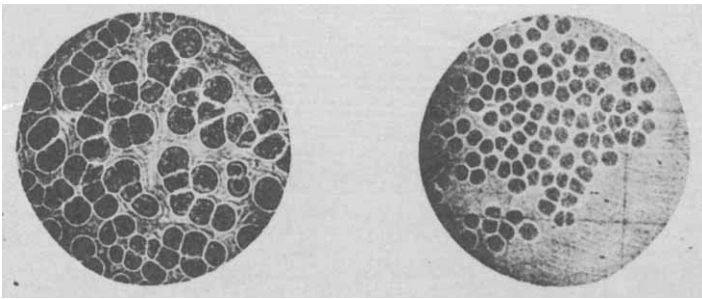


FIG. 19. Isolated Bénard cells in melted wax covered with a film of stearic acid (D5). Actual size. (Courtesy of Ministry of Air, Paris.)

would die out altogether. Dauzère first attributed the new cell species to the effect of superficial contaminants on the surface tension, but later (D5) thought that the reduced (or eliminated) circulation in the area separating the isolated vortices was due to a cohesive membrane of contaminants which tended to thermally isolate the liquid beneath it from the air above, thus reducing the heat flux and hence the convection. Unaware that the effect might be hydrodynamic instead of thermal, Dauzère cited as proof the fact that glass placed over the surface would also alter or stop the convection. Actually, in either case he had altered the "free slip" character of the liquid surface.

Dauzère later noted (D6) that if a film-covered surface was heated with sufficient intensity, yet another species of "cell" was born, often coexisting with the "isolated vortices." The pattern is worm-like in appearance (Fig. 20)

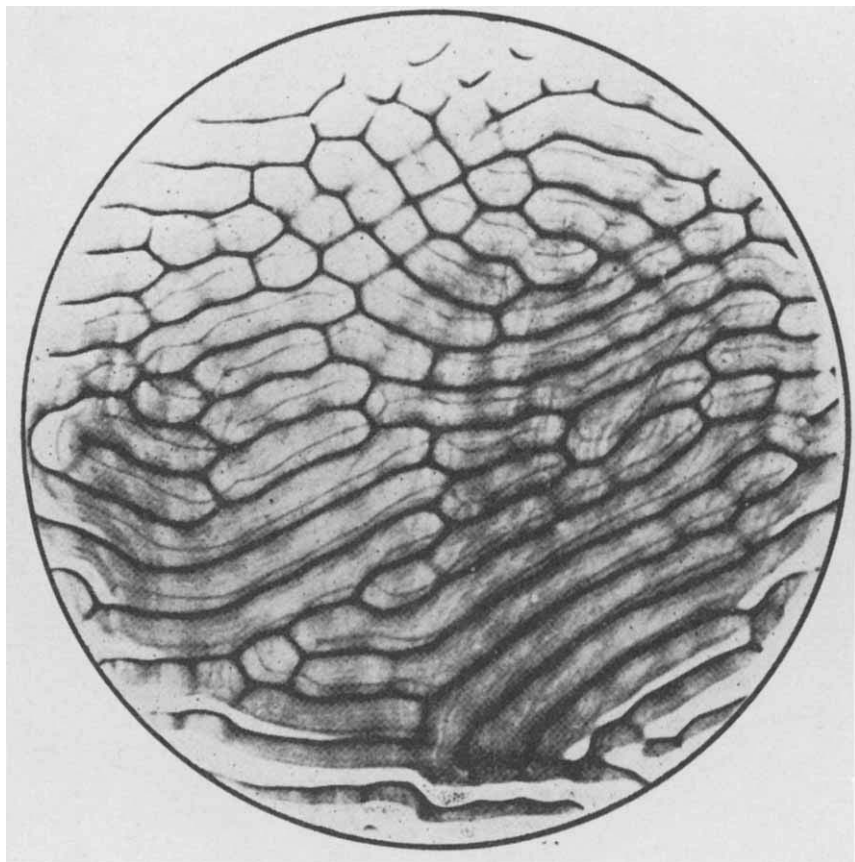


FIG. 20. Vermiculated rolls in melted wax covered with a film of stearic acid (A4). Magnification about  $2\times$ . (Courtesy of Ministry of Air, Paris.)

and Avsec (A4) later termed it one of "vermiculated rolls." This pattern bore resemblance to those produced earlier by Guebhard (cf. B6) and later by Bénard (B10) on exposed photographic plates acting as the top to a layer of photographic developer solution. Avsec (A4) observed this pattern in smoky air layers bounded on top by a glass plate. He attributed the pattern to the presence of a no-slip surface under conditions of insufficient heat flux to produce fully developed polygonal cells. Vermiculated rolls have also been observed by other investigators under other conditions, but in accord with Avsec, they have apparently always been formed at a no-slip surface.

Another type of cell pattern is formed when thin layers of some very volatile liquids evaporate. Bénard (B9) photographed an evaporating layer of ethyl ether (b.p., 35°C) and produced a permanently unsteady, roughly cellular structure. Thompson (T4), in 1882, had observed still another convective structure, which he termed "tesselations," in a deep layer of evaporating water (Fig. 1b) rendered visible by a soap scum at the surface. Thompson's "tesselations" differed from the cellular structure in a thin layer of evaporating ether in that the "cells" (i.e., the tessellations) were not closed nor did they appear to have any centers. Rather, these tessellations formed a permanently unsteady pattern as did the evaporating ether, but the motion was much more sluggish. In 1961, Spangenberg and Rowland (S10) photographed these tessellations in evaporating water by means of schlieren photography.

In 1927, the Langmuirs (L1) observed still another type of convection when they studied the evaporation of aqueous ether solutions. The convection was so violent and chaotic that the liquid surface "twitched" visibly during the evaporation.

All the experiments mentioned above seem to indicate that the size of the isolated vortices, the vermiculated rolls, and the unsteady cells (as in evaporating ether) are generally roughly proportional to the liquid depth, but no quantitative studies have ever been made on this point. In contrast, the size of the tessellations in deep water layers seems to bear no relation to depth, thus suggesting that once a given depth is exceeded the depth itself is no longer a significant parameter of the convection.

When the liquid heated below is subjected to an external shear, as in the case of a liquid flowing over a flat plate, the convection pattern usually orients itself in the direction of the shear. This was demonstrated first by Bénard (B8) (see Fig. 4) but was actually studied first by Idrac (cf. A4) in air. Later Terada (T2) investigated the phenomenon in liquids which were caused to flow down a heated flat plate. Bénard (B8, B9) compared the width of such rolls with the width predicted from Rayleigh's theory<sup>11</sup> obtaining a remarkable agreement which we now know was illusory. Longitudinal rolls in liquids were studied extensively by Volkovisky (V4) in 1939. He determined that at moderate flow velocities ( $< 3$  or  $4$  mm/sec) and high viscosities ( $> 20$  centistokes) the ratio of the roll width to the liquid depth was constant, between 1.90 and 2.10 for depths between 0.5 and 3.5 mm, while, for higher velocities and lower viscosities, the roll width became larger in relation to the liquid depth. When the velocity  $V$  (the overall flow velocity) was increased to 5.0 cm/sec for alcohol ( $\nu^{50} = 0.9$  centistokes) and to 3.5 cm/sec for a viscous oil ( $\nu^{75} = 45$  centistokes) the bands became crosshatched, forming a network of rectangular cells. Volkovisky also demonstrated the coexistence of cellular and roll vortices.

<sup>11</sup> This agreement was also achieved between the experimental hexagonal cell size and the size predicted by Rayleigh.

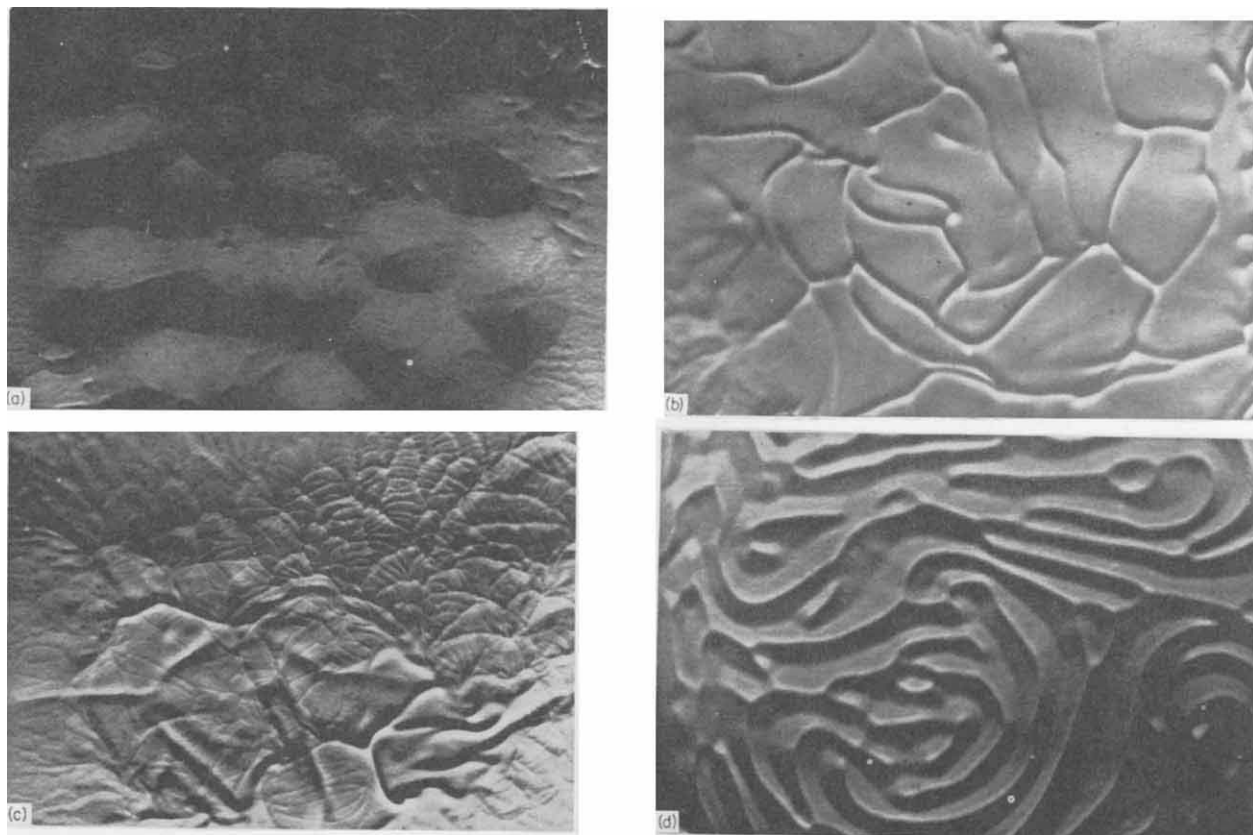


FIG. 21. Schlieren photographs of flow patterns of evaporative convection (top views, magnification  $1.8\times$ ): (a) cells: methanol,  $h = 2$  mm; (b) streamers: benzene,  $h = 10$  mm; (c) ribs: benzene,  $h = 10$  mm; (d) vermiculated rolls: carbon tetrachloride,  $h = 3$  mm.



In 1938, Avsec (A3) discovered yet another vortex structure due to shear velocity, a structure showing rolls *perpendicular* to  $V$ . Avsec demonstrated the existence of these “bandes transversales” in air with smoke, and their discovery suggested the thermoconvective origin of cloud formations which often show bands of clouds perpendicular to the wind velocity. Avsec later published (A4) an exhaustive study of the morphology of convection in air layers and of its application to meteorology.

Using schlieren optics, Berg (B12) obtained a variety of patterns of evaporative convection in pure liquids. Studies were made with acetone, benzene, carbon tetrachloride, *n*-heptane, isopropyl alcohol, and methyl alcohol, and experiments were performed to obtain information concerning the structure of the evaporative convection pattern as it was affected by the fluid properties, the thickness of the fluid layer, the vapor phase resistance to evaporation, and the presence of surfactants.

Four principal patterns of convection were distinguished when pure liquids were employed: cells, streamers, ribs, and vermiculated rolls. These names were chosen in an attempt to describe the actual appearance of the convection patterns and in accordance with historical designations. Examples are shown in Fig. 21. The patterns depicted there were exhibited in all of the liquids under various conditions. In particular, cells appeared to be the dominant patterns in all liquids for depths of 2 mm or less, and the cell size for the various liquids at the 1-mm and 2-mm depths is shown in Table VI. For a thin ( $< 2$  mm) layer of given liquid evaporating into still air, the cell size increased with the depth of the liquid layer, and the flow which the cellular schlieren pattern represented was the same as that observed by Bénard (see Fig. 3). These cells were quite immobile and generally neither grew nor decayed in size with time. A direct stream of dry nitrogen onto the surface of the liquid “sharpened” the cell peripheries and tended to reduce the cell size.

The second type of flow, generally observable when the liquid depth exceeded 7 or 8 mm, was that of streamers. These were “cold lines” in which cooled liquid would plunge in sheets into the interior of the fluid, as illustrated in Fig. 22. These streamers moved sluggishly about the fluid and resembled closely the networks described by Thompson, and photographed by Spangenberg and Rowland.

The third pattern, ribs, often coexisted with that of streamers when the liquid was *completely devoid* of surface contamination. These ribs moved rapidly about among the streamers, traveled perpendicular to themselves, and could be either perpendicular or parallel to the streamers. As the depth of the fluid layer was increased, ribs often began to appear even if the principal pattern was still cellular. These ribs then persisted while the depth was increased still further, with the pattern evolving into one of the streamers interspersed with these fast-moving ribs.

TABLE VI  
CELL SIZE IN EVAPORATIVE CONVECTION (B12)

| Material             | Depth of layer (mm) | Cell width (mm) | Cell width/layer depth |
|----------------------|---------------------|-----------------|------------------------|
| Acetone              | 1                   | 8.5             | 8.5                    |
|                      | 2                   | 14.0            | 7.0                    |
| Benzene              | 1                   | 2.8             | 2.8                    |
|                      | 2                   | 6.2             | 3.1                    |
|                      | 3                   | 15.0            | 5.0                    |
|                      | 4                   | 25.0            | 6.2                    |
| Carbon tetrachloride | 0.25                | 0.8             | 3.2                    |
|                      | 0.5                 | 1.6             | 3.2                    |
|                      | 1.0                 | 5.4             | 5.4                    |
|                      | 2.0                 | 14.0            | 7.0                    |
|                      | 3.0                 | 24.0            | 8.0                    |
| <i>n</i> -Heptane    | 1.0                 | 3.0             | 3.0                    |
|                      | 2.0                 | 11.0            | 5.5                    |
|                      | 3.0                 | 17.0            | 5.7                    |
| Isopropyl alcohol    | 1.0                 | 1.7             | 1.7                    |
|                      | 2.0                 | 3.8             | 1.9                    |
| Methyl alcohol       | 1.0                 | 4.5             | 4.5                    |
|                      | 2.0                 | 12.0            | 6.0                    |
|                      | 3.0                 | 17.0            | 5.6                    |

The fourth basic convection pattern, vermiculated rolls, was associated with the *presence* of a nonvolatile material of large molecular size in the surface region. For liquids containing such a material, a vermiculated roll pattern was found to prevail at intermediate depths (3–6 mm). At depths

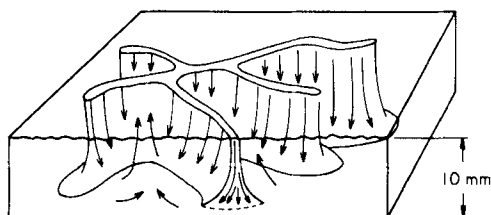


FIG. 22. Evaporative convection in cold streamers: cold fluid plunges along distinct lines in the surface and warm fluid rises slowly in the area between the streamers (B12).

of 2 and 3 mm, film-covered layers of acetone, benzene, and carbon tetrachloride all showed a pattern of vermiculated rolls while their clean-surfaced counterparts exhibited cellular convection. Figure 21(d) shows hot and cold lines side by side and wrapped around one another to give the appearance of worms, and the flow is shown diagrammatically in Fig. 23. This structure was

stable to a stream of dry nitrogen directed over the surface. Moreover, as the depth of the liquid was increased, the rolls became wider and the cold lines more distinct, while the hot lines, which originally alternated with the cold lines, became less and less well defined until they faded away altogether leaving a random network of cold lines which have been called streamers.

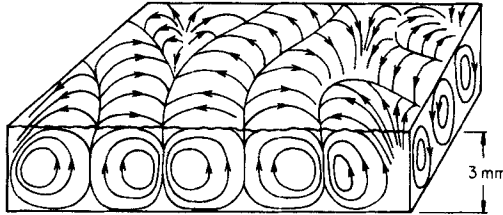


FIG. 23. Evaporative convection in vermiculated rolls: Cold fluid flows down in a relatively narrow region near the roll partition while warm fluid rises over a wider, less distinct region. As fluid depth is increased the warm partitions will lose their identity, and the cold partitions will become streamers (B12).

In summary, it has been demonstrated experimentally that during evaporation several types of convection patterns can exist in quiet shallow pools of liquids, in addition to the regular hexagons observed by Bénard; the appearance of these flow patterns can be altered drastically by the addition of surface-contaminating molecules.

## B. SURFACE DEFORMATIONS

As described earlier, Bénard performed a number of careful interferometric measurements of the deformation of the liquid surface during convection, and correctly attributed the observed relief to the forces of surface tension. Bénard's hexagonal cells were concave and were divided by ridges, whose level was  $1.7 \mu$  above the cell center when the layer of spermaceti was 1.20 mm thick and at a temperature of  $100^\circ\text{C}$ . Smaller thicknesses and lower temperatures yielded less pronounced ridges. Bénard's thermal measurements placed the lateral temperature difference between the cell center and the cell partitions at approximately  $1^\circ\text{C}$ . In 1939, Hershey (H1) obtained an expression for the steady-state surface elevation due to surface tension differences caused by temperature differences on the surface. This expression reduces to

$$\Delta h = \frac{3 \Delta \sigma}{\rho g h} = \frac{3(d\sigma/dT) \Delta T_{\text{lat}}}{\rho g h} \quad (45)$$

where  $\Delta h$  is the difference in surface elevation and  $\Delta T_{\text{lat}}$  the corresponding difference in surface temperature. Equation (45) yields a surface elevation of  $1.58 \mu$  for a 1.2-mm layer of spermaceti at  $100^\circ\text{C}$  with a lateral temperature

difference of  $1^{\circ}\text{C}$ . This result is in good accord with Bénard's measurements, but the dependence of the elevation on layer depth is the reverse of that indicated by Bénard. Hershey observed the surface deformations which he described by holding a glass rod, cooled in liquid air, to the bottom surface of a glass plate covered with a thin layer of liquid. While no actual measurements were taken, Hershey made the interesting observation that small amounts of surface-active agents (on water) caused the surface to flatten out completely.

It has already been mentioned that, if the surface deformation is due to buoyancy-driven thermal convection alone, the surface must be convex at the cell centers. Such behavior was observed by Spangenberg and Rowland (S10) for deep layers of evaporating water. Furthermore, in a repetition of one of Bénard's experiments, i.e., using approximately 1-mm-thick layers of melted wax, these authors obtained the puzzling result that in these systems the elevation also occurred above the cell centers.

By neglecting inertia terms, Orchard (O1) analyzed recently the two-dimensional flow of thin layers of viscous liquids and gels and obtained an expression for the rate of decay of surface irregularities. In Orchard's work, surface-tension forces varied from point to point as a result of the non-uniformity of the surface curvature.

### C. CELL-SIZE PREDICTIONS FROM LINEAR STABILITY THEORY

Theoretical work on the morphology of convection has been concerned chiefly with the prediction of the type and dimensions of the observed "cells" in terms of the liquid depth, the fluid properties, and the temperature difference between the top and bottom (or alternatively, the heat flux or the rate of evaporation). Information on convection morphology is obtainable from linear stability theory, as has already been shown by Rayleigh. Thus, if we *assume* a type of horizontal pattern (i.e., rolls, rectangles, triangles, hexagons, etc.) and if we *assume* that the final structure is simply the amplification of the fastest-growing mode of the initial infinitesimal disturbance (without change in wavelength), then the horizontal size of the structural unit or "cell" (roll, rectangle, hexagon, etc.) can be determined from the results of the pertinent linear stability theory.

For example, Rayleigh first assumed the horizontal structure to be rectangular (including two-dimensional rolls as a limiting case), and his final governing equations included the parameter  $\tilde{a}^2$  which, under the assumption of a rectangular pattern, became the sum of the squares of the dimensionless wave numbers of the disturbance mode along each of a pair of mutually perpendicular axes oriented arbitrarily in the horizontal plane. The critical value of  $R$ , i.e., the smallest eigenvalue, was found for each given  $\tilde{a}$ , and the  $\tilde{a}$  yielding the smallest value of  $R$  was taken as the parameter describing the

wavelength of the final convection pattern. In particular, if the structure is one of squares, then

$$\tilde{a} = 2\sqrt{2}\pi h/\lambda$$

where  $\lambda$  is the length of a diagonal (A4). If the structure is one of rolls,

$$\tilde{a} = \frac{2\pi h}{\lambda}$$

where  $\lambda$  is the width of a roll. The parameter “ $\tilde{a}$ ” is therefore a by-product of any calculation yielding the critical Rayleigh or Thompson number, and values of  $\tilde{a}$  thus determined are tabulated in Table VII for various sets of boundary conditions.

TABLE VII  
DIMENSIONLESS CRITICAL WAVE NUMBER FOR THE RAYLEIGH PROBLEM

| Type of boundary conditions | Solved by                       | $\tilde{a}$ |
|-----------------------------|---------------------------------|-------------|
| Free-free                   | Rayleigh (R1), 1916             | 2.22        |
| Solid-solid                 | Jeffreys (J4), 1928             | $\pi$       |
|                             | Pellew and Southwell (P3), 1940 | 3.13        |
| Solid-free                  | Pellew and Southwell (P3), 1940 | 2.68        |

For other types of patterns, we recall that the complete governing equation (or set of equations) is (are) reduced to an ordinary differential equation involving  $\tilde{z}$  only, by means of separation of variables. However, the equation in  $\tilde{x}$  and  $\tilde{y}$ , which was set aside since we considered only the equation in  $\tilde{z}$  for determining the critical stability parameter, also involved  $\tilde{a}$  and became

$$\frac{\partial^2 u_z^\dagger(\tilde{x}, \tilde{y})}{\partial \tilde{x}^2} + \frac{\partial^2 u_z^\dagger(\tilde{x}, \tilde{y})}{\partial \tilde{y}^2} = -\tilde{a}^2 u_z^\dagger(\tilde{x}, \tilde{y}) \quad (46)$$

where “ $\dagger$ ” denoted a function of  $\tilde{x}$  and  $\tilde{y}$  only.

Equation (46) is to be solved subject to the requirement that the cylindrical cell walls, i.e., the partitions separating the contiguous cells, be surfaces of symmetry, which in turn requires that on the cell wall the normal component of  $\text{grad}(u_z)$  [or equivalently of  $\text{grad}(T)$ , as shown by Pellew and Southwell (P3)] should vanish. Therefore

$$\mathbf{n} \cdot \text{grad}(u_z) = 0 \quad (47)$$

$\mathbf{n}$  being the outward unit normal to the cell wall. Equation (46) has a solution

for every possible periodic structure. However, if the resulting pattern is to be one of regular polygons, we must limit our consideration to squares, triangles, and hexagons. For squares, the solution to Eq. (46) subject to (47) is

$$u_z^*(\tilde{x}, \tilde{y}) = \cos\left(\frac{2\pi h}{\lambda} \tilde{x}\right) \cos\left(\frac{2\pi h}{\lambda} \tilde{y}\right) \quad (48)$$

where  $\lambda$  is the wavelength of the disturbance in both the  $x$  and  $y$  directions, so that

$$\tilde{a}^2 = 4\pi^2 \left[ 2 \left( \frac{h}{\lambda} \right)^2 \right] \quad \text{or} \quad \lambda = \frac{2\sqrt{2\pi h}}{\tilde{a}} \quad (49)$$

A plot of Eq. (48) will show  $\lambda$  to be the diagonal of the squares.

The entire flow for the marginal state may now be constructed. The  $z$  component of the velocity is given by

$$u_z = u_z^* \cos\left(\frac{2\pi h}{\lambda} \tilde{x}\right) \cos\left(\frac{2\pi h}{\lambda} \tilde{y}\right) \quad (50)$$

and the velocity components  $u_x$  and  $u_y$  may be recovered as follows: By eliminating  $p$  between the first and second of (25) and by dropping the term  $\partial/\partial \tilde{t}$ , there results

$$\text{div grad} \left( \frac{\partial u_y}{\partial \tilde{x}} - \frac{\partial u_x}{\partial \tilde{y}} \right) = 0 \quad (51)$$

while, because of the continuity equation,

$$-\left( \frac{\partial u_x}{\partial \tilde{x}} + \frac{\partial u_y}{\partial \tilde{y}} \right) = \frac{\partial u_z}{\partial \tilde{z}} \quad (52)$$

Eqs. (51) and (52) may be uncoupled next by letting

$$u_x \equiv -\frac{\partial \varphi}{\partial \tilde{x}} - \frac{\partial \psi}{\partial \tilde{y}}; \quad u_y \equiv -\frac{\partial \varphi}{\partial \tilde{y}} + \frac{\partial \psi}{\partial \tilde{x}} \quad (53)$$

so that

$$\text{div grad} \left( \frac{\partial^2 \psi}{\partial \tilde{x}^2} + \frac{\partial^2 \psi}{\partial \tilde{y}^2} \right) = 0 \quad (54)$$

$$\frac{\partial^2 \varphi}{\partial \tilde{x}^2} + \frac{\partial^2 \varphi}{\partial \tilde{y}^2} = \frac{\partial u_z}{\partial \tilde{z}} \quad (55)$$

which may be solved separately for  $\varphi$  and  $\psi$ .  $u_x$  and  $u_y$  are then recovered from Eq. (53). In this way streamlines and potential lines may be drawn as is shown in Fig. 24 for hexagons.

The flow characterizing hexagons is of greater interest because this seems experimentally to be the preferred form. Christopherson (C4), motivated by the work of Pellew and Southwell, was the first to obtain an exact solution to Eq. (46) for hexagons, which is

$$u_z^\dagger = \frac{1}{3}[u_z^\dagger]^0 \left\{ 2 \cos \frac{2\pi h}{\lambda\sqrt{3}} \tilde{x} \cos \frac{2\pi h}{3\lambda} \tilde{y} + \cos \frac{4\pi h}{3\lambda} \tilde{y} \right\} \quad (56)$$

where  $[u_z^\dagger]^0$  is the undetermined value of  $u_z$  at the origin, i.e., the center of the cell. This result clearly points out the fact that this linearized treatment

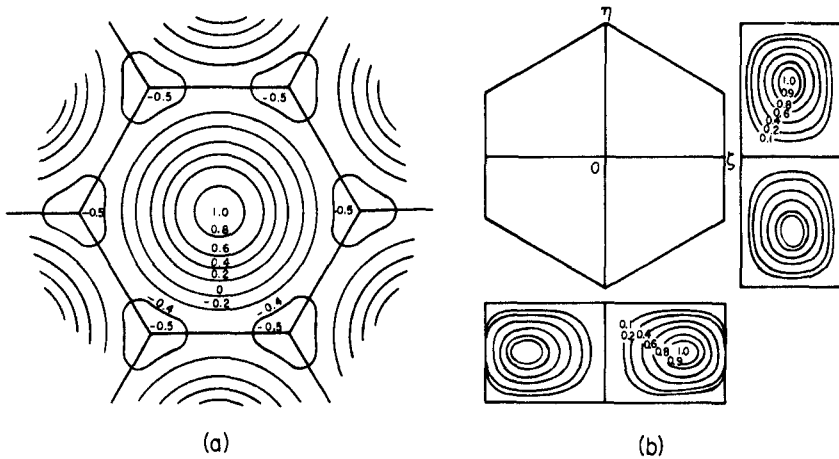


FIG. 24. Streamlines for the stationary marginal state in hexagonal cells: (a) lines of constant  $u_z^*$  (P3) (courtesy of the Royal Society); (b) side views of streamlines (R3) (courtesy of American Institute of Physics).

cannot tell us anything about the amplitudes or even the direction (sign) of the flow.

Christopherson's solution was generalized in 1960 by Bisshop (cf. C3), who obtained an expression which presumably includes all solutions to Eq. (46) with the required periodicity. The details of the integration to obtain streamlines for hexagonal cells are given by Reid and Harris (R3) and by Chandrasekhar (C3).

It must be remembered, however, that the above methods for calculating cellular flow patterns are valid only for infinitesimal amplitudes, because linear theory (which requires that disturbance flows grow exponentially without limit) cannot by itself predict the final steady flows which are established. On the other hand, flows of macroscopic amplitudes would require consideration of the nonlinear terms in the equations of motion and perhaps the variation of fluid properties with temperature. Still, researchers have persisted in

comparing their experimental cell sizes with the values obtained from linear stability theory, and in some cases have obtained striking, but meaningless, agreement as in Bénard's case (B8, B9). Once again, the assumption which is implicit in using linear theory to predict cell sizes is that, whatever other effects nonlinearity may have on the disturbance flow as it grows, the wavelength will remain unchanged. This assumption appears to be as difficult to correct as it is easy to criticize.

#### D. NONLINEAR THEORY

It is in the discussion of the morphology of the convection that the need for consideration of the nonlinear aspects of the theory becomes apparent. The occurrence of instability in a fluid layer which is isolated (to a degree readily attainable in the laboratory) from all but very small disturbances has been successfully predicted by the linear theory, so that the nonlinear aspects of the *stability problem* (i.e., the stability of the system toward *finite* rather than infinitesimal disturbances) have received little attention. But, unless we are willing to make the "constant wavelength" assumption stated above, linear theory reveals nothing at all about the morphology; while if we do make this assumption, all that we can calculate is the cell size for some assumed structure, and the corresponding streamlines for the marginal flow. Thus it is the purpose of nonlinear theory to provide answers to questions such as those listed below.

(1) What *structure* (squares, triangles, hexagons, etc.) will be established at steady state?

(2) What *direction* will the flow assume (up in the cell centers and down at the sides or vice versa?)

(3) What will be the *cell size of the final steady-state* configuration for Rayleigh (or Thompson) numbers in excess of the critical?

(4) What will be the *amplitude* of the final steady-state velocity and temperature disturbance for Rayleigh (or Thompson) numbers in excess of the critical?

(5) How are *heat and mass transfer rates* related to the Rayleigh (or Thompson) numbers in excess of the critical?

So far, the general point of departure for the nonlinear analyses attempted has been not the set of equations of motion in their complete form, but rather the set that results by neglecting the temperature dependence of all fluid properties except density, and also the dissipation of kinetic energy. This is known as the Boussinesq approximation. Using the Boussinesq equations, Woronetz (W1) was able in 1934 to obtain expressions for the velocity perturbations in a fluid confined between coaxial rotating cylinders or spheres which were maintained at different temperatures. Volkovisky (V3) used the



Boussinesq equations in 1939 to obtain an expression for the velocity along a filament of fluid rising above a point or line heat source placed at the bottom of a fluid layer.

Cellular convection was not treated until 1952 when Pillow (P4) formulated the nonlinear problem for two-dimensional flow between two horizontal plates. He obtained steady velocity profiles for the two-dimensional rolls by neglecting the effects of viscosity and heat conduction except in the region very near the boundaries. Using an approximate theory, he predicted a 5/4-power dependence of heat transfer rate on the temperature difference, which is the proportionality found experimentally.

Gor'kov (G2), in 1957, and Malkus and Veronis (M1), in 1958, succeeded in calculating the steady-state amplitude, as a function of the Rayleigh number, for a given cellular pattern and wavelength using the time-independent Boussinesq equations. A perturbation technique was employed in which the variables were expanded in terms of an amplitude parameter,  $\varepsilon$ , such as

$$u_z = \hat{u}_z + \varepsilon(\hat{u}_{z1} + \varepsilon\hat{u}_{z2} + \varepsilon^2\hat{u}_{z3} + \dots) \quad (57)$$

The Rayleigh number was also increased (holding  $\tilde{a}$  constant) from its critical value according to

$$R = R_c + \varepsilon R_1 + \varepsilon^2 R_2 + \dots \quad (58)$$

and a solution was obtained for the case of two free boundaries by retaining terms at least as far as  $\varepsilon^2$ .

In 1960, Stuart and Watson (cf. S12) examined the same problem using the time-dependent Boussinesq equations and obtained a solution which converged to that of Malkus and Veronis as time approached infinity, thus demonstrating that under unstable conditions a differential disturbance can indeed lead to finite amplitude steady convection.

For the case of two-dimensional roll cells, Malkus and Veronis also performed calculations on the heat transfer rate by using an approximate technique that they considered as being within 2 percent of the exact value, for Rayleigh numbers up to three times the critical. In accordance with experiment, their results show a 5/4-power dependence of heat transfer rate on temperature difference (or a 1/4-power dependence of Nusselt number on the Rayleigh number).

Kuo (K2) has recently obtained a solution to the nonlinear equations of cellular convection by expanding the dependent variables in series of orthogonal functions and by expanding the coefficients of these functions in a power series of an amplitude parameter. His solution also predicts a heat transfer rate proportional to the 5/4 power of the temperature difference.

The problem of cell shape was also treated by Malkus and Veronis, who suggested a criterion based on maximum vertical heat transport. For the case



|            |                    |               |                                 |
|------------|--------------------|---------------|---------------------------------|
| $\rho$     | Density            | $o$           | Refers to initial state         |
| $\sigma$   | Surface Tension    | $s$           | Surface                         |
| $\tau$     | Stress vector      | $x, y, z$     | Refers to Cartesian coordinates |
| $\varphi$  | Potential function |               |                                 |
| $\psi$     | Stream function    |               |                                 |
| $\Omega$   | Angular velocity   |               |                                 |
| SUBSCRIPTS |                    | SUPERSSCRIPTS |                                 |
| $b$        | Bottom             | $\sim$        | Dimensionless quantity          |
| $c$        | Critical           | $*$           | Refers to initial state         |
|            |                    | $\wedge$      | Perturbation                    |
|            |                    | $*$           | $z$ Dependence                  |
|            |                    | $\dagger$     | $x, y$ Dependence               |

## REFERENCES

- A1. Adamson, A. W., "Physical Chemistry of Surfaces," Vol. I. Reinhold, New York, 1963.
- A2. Avsec, D., *Compt. Rend.* **203**, 556 (1936).
- A3. Avsec, D., *Compt. Rend.* **206**, 40 (1938).
- A4. Avsec, D., *Publ. Sci. Tech. Min. Air (France)* **155** (1939).
- B1. Batchelor, G. K., *Quart. J. Roy. Meteorol. Soc.* **80**, 335 (1954).
- B2. "Schlieren Techniques for the Quantitative Study of Gas Mixing." Battelle Mem. Inst., Columbus, Ohio, Project Rand, R-164, 1949.
- B3. Bell, S. H., *J. Oil Colour Chemists Assoc.* **35**, 373 (1952).
- B4. Bénard, H., *Rev. Gen. Sci. Pures Appl. Bull. Assoc. Franc. Avan. Sci.* **11**, 1261 (1900).
- B5. Bénard, H., *Rev. Gen. Sci. Pures Appl. Bull. Assoc. Franc. Avan. Sci.*, **11**, 1309 (1900).
- B6. Bénard, H., *Ann. Chim. Phys.* [7] **23**, 62 (1901).
- B7. Bénard, H., *Compt. Rend.* **154**, 260 (1912).
- B8. Bénard, H., *Compt. Rend.* **185**, 1109 (1927).
- B9. Bénard, H., *Compt. Rend.* **185**, 1257 (1927).
- B10. Bénard, H., *Bull. Soc. Franc. Phys.* **266**, 1125 (1928).
- B11. Bénard, H., *Compt. Rend.* **201**, 1328, (1935).
- B12. Berg, J. C., Ph.D. Dissertation, University of California, Berkeley, California, 1964.
- B12a. Berg, J. C., unpublished experiments (1964).
- B13. Berg, J. C., and Acrivos, A., *Chem. Eng. Sci.* **20**, 737 (1965).
- B14. Block, M. J., *Nature* **178**, 650 (1956).
- B15. Boys, C. B., "Soap Bubbles and the Forces which Mould Them." Doubleday, New York, 1959.
- B16. Brown, S. C., *Daedalus* **86**, 340 (1957).
- B17. Brunt, D., *Proc. Roy. Soc.* **A124**, 201 (1929).
- C1. Chandra, K., *Proc. Roy. Soc.* **A164**, 231 (1938).
- C2. Chandrasekhar, S., *Daedalus* **86**, 323 (1957).
- C3. Chandrasekhar, S., "Hydrodynamic and Hydromagnetic Stability." Oxford Univ. Press, London and New York, 1962.
- C4. Christopherson, D. G., *Quart. J. Math.* **11**, 63 (1940).
- D1. Dauzère, C., *J. Phys.* [4] **6**, 892 (1907).
- D2. Dauzère, C., *J. Phys.* [4] **7**, 930 (1907).
- D3. Dauzère, C., *Compt. Rend.* **154**, 974 (1912).
- D4. Dauzère, C., *Compt. Rend.* **155**, 394 (1912).
- D5. Dauzère, C., *Compt. Rend.* **156**, 218 (1913).
- D6. Dauzère, C., *Compt. Rend.* **156**, 1228 (1913).
- E1. Ewing, G., and McAllister, E. D., *Science* **131**, 1374 (1960).
- G1. Gibbs, J. W., "Scientific Papers," Vol. I. Dover, New York, 1961.

- G2. Gor'kov, L. P., *Soviet Phys. JETP (English Transl.)* **6**, 311 (1958).
- G3. Graham, A., *Phil. Trans. Roy. Soc.* **A232** 285, (1933).
- H1. Hershey, A. V., *Phys. Rev.* **56**, 204 (1939).
- H2. Hickman, K. C. D., *Ind. Eng. Chem.* **44**, 1892 (1952).
- H3. "High Speed Aerodynamics and Jet Propulsion," Vol. IX, Princeton Univ. Press, Princeton, New Jersey, 1954, pp. 26-46.
- H4. Holder, D. W., and North, R. J., *AGARD Rept.* (1956).
- H5. Hommelen, J., *J. Colloid Sci.* **14**, 385 (1959).
- J1. Jarvis, N. L., *J. Colloid Sci.* **17**, 512 (1962).
- J2. Jarvis, N. L., Timmons, C. O., and Zisman, W. A., in "Retardation of Evaporation, by Monolayers" (V. K. La Mer, ed.), pp. 41-58. Academic Press, New York, 1962.
- J3. Jeffreys, H., *Phil. Mag.* [7] **2**, 833 (1926).
- J4. Jeffreys, H., *Proc. Roy. Soc.* **A118**, 195 (1928).
- J5. Jeffreys, H., *Quart. J. Mech.* [3] **4**, 283 (1951).
- J6. Jenkins, F. A., and White, H. E., "Fundamentals of Optics," 3rd. ed. McGraw-Hill, New York, 1957.
- K1. Knacke, O., and Stranski, I. N., *Prog. Metal Phys.* **5**, 181.
- K2. Kuo, H. L., *J. Fluid Mech.* **10**, 611 (1961).
- L1. Langmuir, I., and Langmuir, D. B., *J. Phys. Chem.* **31**, 1719 (1927).
- L2. Levengood, W. C., *Astrophys. J.* **129**, 483 (1959).
- L3. Lin, C. C., "The Theory of Hydrodynamic Stability." Cambridge Univ. Press, London and New York, 1955.
- L4. Linde, H., Pfaff, S., and C. Firkel, *Z. Physik. Chem. (Leipzig)* **224**, 72 (1964).
- L5. Loewenthal, M., *Phil. Mag.* [7] **12**, 462 (1931).
- L6. Low, A. R., *Proc. Roy. Soc.* **A125**, 180 (1929).
- L7. Low, A. R., *Proc. 3rd Intern. Congr. Appl. Mech.*, 1929, Vol. I, pp. 109-120. Norsted & Söner, Stockholm, 1930.
- L8. Low, A. R., and Brunt, D., *Nature* **115**, 299 (1925).
- L9. Luntz, M., *Compt. Rend.* **204**, 547 (1937).
- M1. Malkus, W. V. R., and Veronis, G., *J. Fluid Mech.* **4**, 225 (1958).
- M2. Marangoni, C., *Nuovo Cimento* [2] **16**, 239 (1871).
- M3. Marangoni, C., *Nuovo Cimento* [3] **3**, 97 (1878).
- M4. Miner, R. W., *Ann. N.Y. Acad. Sci.* **48**, (1947).
- M5. Mysels, K. J., *Science* **129**, 96 (1959).
- N1. Nield, D. A., *J. Fluid Mech.* **19**, 341 (1964).
- O1. Orchard, S. E., *Appl. Sci. Res.* **A11**, 451 (1963).
- O2. Orell, A., and Westwater, J. W., *Chem. Eng. Sci.* **16**, 127 (1961).
- O3. Orell, A., and Westwater, W. J., *A.I.Ch.E. (Am. Inst. Chem. Engrs.)* **8**, 350 (1962).
- P1. Palm, E., *J. Fluid Mech.* **8**, 183 (1960).
- P2. Pearson, J. R. A., *J. Fluid Mech.* **4**, 489 (1958).
- P3. Pellew, A., and Southwell, R. V., *Proc. Roy. Soc.* **A176**, 312 (1940).
- P4. Pillow, A. F., *Aeronaut. Res. Rept. Australia* **A79**, 1 (1952).
- R1. Rayleigh, Lord, *Phil. Mag.* [6] **32**, 529 (1916).
- R2. Reid, W. H., and Harris, D. L., *Phys. Fluids* **1**, 102 (1958).
- R3. Reid, W. H., and Harris, D. L., *Phys. Fluids* **2**, 716 (1959).
- R4. Rumford, Count, "Complete Works," Vol. 2, pp. 239 ff. Am. Acad. Arts Sci., Boston, Massachusetts, 1870.
- S1. Sartory, G., *Compt. Rend.* **208**, 327 (1939).
- S2. Saunders, D. A., Fishenden, M., and H. D. Mansion, *Engineering, London* **139**, 483 (1935).

- S3. Schardin, H., "Toepler's Schlieren Method: Basic Principles for Its Use and Quantitative Evaluation." David Taylor Model Basin, U.S. Navy Transl. No. 156, 1947.
- S4. Schmidt, R. J., and Milverton, S. W., *Proc. Roy. Soc. A* **152**, 586 (1935).
- S5. Schmidt, R. J., and Saunders, D. A., *Proc. Roy. Soc. A* **165**, 216 (1938).
- S6. Scriven, L. E., and Sternling, C. V., *Nature* **187**, 186 (1960).
- S7. Scriven, L. E., and Sternling, C. V., *J. Fluid Mech.* **19**, 321 (1964).
- S8. Sellin, R. H. J., *J. Sci. Instr.* **40**, 355 (1963).
- S9. Silveston, P. L., *Forsch. Ing. Wes.* **24**, 29 and 59 (1958).
- S10. Spangenberg, W. B., and Rowland, W. R., *Phys. Fluids* **4**, 743 (1961).
- S11. Sparrow, E. M., Goldstein, R. J., and Jonsson, V. K., *J. Fluid Mech.* **18**, 513 (1964).
- S12. Stuart, J. T., *Proc. 10th Intern. Congr. Appl. Mech.*, Stresa, Italy, 1960, p. 63, Elsevier, Amsterdam, 1962.
- S13. Sutton, O. G., *Proc. Roy. Soc. A* **204**, 297 (1950).
- T1. Taylor, G. I., *Phil. Trans. Roy. Soc. A* **223**, 289 (1923).
- T2. Terada, T., *Rept. Aeronaut. Res. Inst. Tokyo* **3**, 3(1928); **4**, 448 (1929).
- T3. Thompson, J. J., *Phil. Mag.* [4] **10**, 330 (1855).
- T4. Thompson J. J., *Proc. Roy. Phil. Soc. Glasgow.* **13**, 464 (1882).
- T5. Tomlinson, C., *Phil. Mag.* [4] **27**, 528 (1864).
- T6. Tomlinson, C., *Phil. Mag.* [4] **38**, 409 (1869).
- V1. Varley, C., *Trans. Roy. Soc. Arts Sci. Mauritius* **50**, 190 (1836).
- V2. Vernotte, P., *Compt. Rend.* **202**, 119 (1936).
- V3. Volkovisky, V., *Compt. Rend.* **200**, 1285 (1935).
- V4. Volkovisky, V., *Publ. Sci. Tech. Min. Air (France)* **151**, 1 (1939).
- V5. Vidal, A., and Acrivos, A., *Phys. Fluids* **9**, 615 (1966).
- W1. Woronetz, C., *Publ. Sci. Tech. Min. Air (France), Notes Tech.* **60**, 1 (1934).

# DYNAMICS OF MICROBIAL CELL POPULATIONS

H. M. Tsuchiya, A. G. Fredrickson, and R. Aris

Department of Chemical Engineering  
University of Minnesota

|  |     |
|--|-----|
| I. Introduction .....                                    | 125 |
| II. Possible Approaches to the Problem .....             | 126 |
| III. Unstructured Models.....                            | 127 |
| A. Segregated, Stochastic Models.....                    | 127 |
| B. Deterministic Models: Segregated or Distributed ..... | 131 |
| IV. Structured Models: Distributed.....                  | 140 |
| A. First Model.....                                      | 140 |
| B. The Bottleneck Model of the Lag Phase .....           | 142 |
| V. Models and Experimental Results.....                  | 164 |
| VI. Structured Models: Segregated .....                  | 175 |
| A. Steady-State Propagation: the Age Model .....         | 176 |
| B. General Equations for the Age Model.....              | 182 |
| C. A More General Model and Its Possible Extension.....  | 190 |
| VII. Growth of Single Microbial Cells .....              | 195 |
| VIII. Concluding Remarks.....                            | 198 |
| Appendix: Results from Probability Theory .....          | 199 |
| Nomenclature .....                                       | 202 |
| References .....   | 203 |

## I. Introduction

Biological systems in general, and their interaction with their environment, abound with an overwhelming complexity of detail through which general concepts and relationships cannot readily be perceived. Because of this complexity, many biologists are concerned with details, and have tended to neglect problems associated with integrated systems. On the other hand, engineers who have not yet encountered such complexity in manufacturing facilities are concerned with integrated systems which are just beginning to approach the complexity of biological systems. The limited work discussed below offers quantitative analyses of some simpler biological phenomena, and suggests experimental work that may profitably be carried out.

Standard biology texts list the related phenomena of growth and reproduction as minimal criteria for all biological systems. Hence this review is principally a summary of attempts to apply engineering analysis to elucidate growth and replication phenomena in very simple systems: cultures of unicellular organisms reproducing by binary fission. Parenthetically we suggest that other biological phenomena may also be examined with profit by chemical engineers, in particular the field of intracellular transport and transformation. If we assume that biological systems and processes have been optimized during the course of their evolution, such studies may lead to improved methods of treating industrial systems. The study of biological systems so as to apply the knowledge gained ("bionics") to nonbiological systems is familiar to electrical engineers.

Numerous investigations are being made of continuous propagation of microorganisms with a view to potential industrial applications, without much attention to the relations between batch and continuous processing. *All* the aspects observed in batch propagation must somehow manifest themselves in continuous propagation. Moreover, the dynamics of nonassociated cell populations warrants closer scrutiny *per se* because of basic scientific interest in the growth and reproduction of any organism with associated cells, including man. For instance, study of "aging" in microbial cultures may yield information useful to the medical subbranch of geriatrics. Again, the dynamics of microbial growth and reproduction may be of interest to demographers in today's study of the "population explosion."

## II. Possible Approaches to the Problem

A fundamental generalization of modern biology is the cell theory: that life is segregated into structural and functional units—cells—and that new cells arise only from pre-existing cells, at least on earth at the present time (see O1). In any complete theory of cellular population dynamics, the *number* of cells occupying a given region will be the fundamental variable. However, in many practical cases the model that one constructs omits certain variables, or admits them in a modified form. Thus the experimental number of microbial organisms may be replaced by the volume or dry weight of cells, the optical density of a cell suspension, or another measure.<sup>1</sup> A model for correlating such data would use the empirical measure of "concentration" of living substance, and would treat "life" as something distributed throughout the whole physical region in which cells occur. Hence one can classify a model of population dynamics as representing either a *distributed* or a *segregated* population. The "distributed" model is the simpler, since the

<sup>1</sup> Methods for counting cell numbers or measuring cell volume, etc., are discussed by Buchanan and Fulmer (B10).

process of *reproduction* is not (and cannot be) treated in this model. The process of *growth* can, of course, be treated in both models.

Another basis for classification of models of population dynamics is provided by the observation that cells may be assumed to be either *structured* or *unstructured*. In a segregated model, we assume a cell to be structured if we specify some means of *distinguishing* it from its fellows. This means may be visual, by comparison of morphology and size under the microscope, or it may be indirect, by comparison of the mass and chemical composition of cells. When we deal with a distributed model, the population will be "structured" if the composition of the population varies with the conditions of propagation. In other words, specification of the *state* of the population requires more than specification of a single quantity.

Finally, one may use either *stochastic* (probabilistic) or deterministic models. In fact, a population of microbial cells is always segregated and structured, and its growth and reproduction should be treated stochastically. On the other hand, the biological knowledge and mathematical tools necessary for the formulation and study of a completely general model do not exist, and a less general approach gives useful results.

### III. Unstructured Models

#### A. SEGREGATED, STOCHASTIC MODELS

We consider a population of indistinguishable individuals contained in some region  $V$  of space, that is, indistinguishable by any technique available to us. The number of individuals present at time  $t$  is a random variable  $X(t)$ , the "population size," that can assume only the discrete values  $0, 1, 2, \dots, x_m$ ; here  $x_m$  is some positive integer (which may be very large, depending on the size of  $V$ , the availability of nutrients in  $V$ , etc.). At this point, the extensive random variable  $X(t)$  is to be sharply distinguished from the intensive population density (the number of organisms per unit volume of  $V$ ); the population density need not be an integer.

The question to answer is: given an initial population size  $X(0) = x_0$ , and certain information about the probability of cell fission, what is the probability,  $P_x(t)$ , that  $X(t) = x$  for  $t > 0$ ? Clearly, the question can be answered by experiment, using the frequency interpretation of probability. One measures the population sizes in a large number (ensemble) of "identical" systems  $V$  as functions of time; the fraction of systems in which  $X(t) = x$  is then an approximation to the required probability.

We desire a *model* that will reproduce and/or predict the experimental observations. Such models have been constructed by statisticians and mathematicians. The model selected here is "the pure birth process," discussed in detail in many places [cf. Bharucha-Reid (B7) or Bailey (B1)].



Consider the following propositions:

$$A: X(t + \Delta t) = x$$

$$B_k: X(t) = x - k; \quad k = 0, 1, \dots, x - x_0$$

$C: X(0) = x_0$ ; cells reproduce by binary fission, cells are indistinguishable, etc.

That is,  $A$  is a proposition concerning the *state* ( $x$ ) of the system at time  $t + \Delta t$ , whereas the  $B_k$  are propositions concerning the state of the system at time  $t$ .

By definition of  $P_x(t)$ , we have<sup>2</sup>

$$P_x(t + \Delta t) = P(AB_0 + AB_1 + \dots + AB_{x-x_0} | C)$$

Hence, by Rule 2 of the theory of probability,

$$P_x(t + \Delta t) = P(AB_0 | C) + P(AB_1 | C) + \dots + P(AB_{x-x_0} | C) \quad (1)$$

since terms such as  $P(AB_0AB_1 | C)$  must vanish (propositions  $B_0$  and  $B_1$  are mutually exclusive). By Rule 1 of the theory of probability,

$$\begin{aligned} P(AB_k | C) &= P(B_k | C) P(A | B_k C) \\ &= P_{x-k}(t) P(A | B_k C) \end{aligned} \quad (2)$$

This is as far as the theory of probability can carry us. We must now introduce a model from which the conditional probabilities  $P(A | B_k C)$  can be calculated.

We assume that proliferation of cells is a *Markov process* (B7). With this assumption, the probabilities of transitions  $X(t) = x - k$  to  $X(t + \Delta t) = x$  will depend only on the state of the system at the beginning of the time interval  $t$  to  $t + \Delta t$ . In particular, the probabilities of transition will be independent of the history of the system prior to time  $t$ . Hence the model is the set of equations

$$\begin{aligned} P(A | B_0 C) &= 1 - f(x) \Delta t - O[(\Delta t)^2] \\ P(A | B_1 C) &= f(x - 1) \Delta t + O[(\Delta t)^2] \\ P(A | B_2 C) &= O[(\Delta t)^2] \end{aligned} \quad (3)$$

etc., where  $O$  means "of the order of," and  $f$  is an arbitrary but nonnegative function of its argument. Equations (3) say that the probability of one fission in a very short time interval is very much less than the probability of no fissions in that time interval, and similarly for two fissions, etc. The transitions for which probabilities are assumed in Eqs. (3) refer to increases in population size; this is tantamount to specifying the number of fissions, since in binary fission, each fission increases the population size by one unit.

<sup>2</sup> The appendix gives a brief review of probability theory, applicable here.

From Eqs. (1-3) we get

$$P_x(t + \Delta t) = P_x(t) \cdot \{1 - f(x) \Delta t - O[(\Delta t)^2]\} \\ + P_{x-1}(t) \cdot \{f(x-1) \Delta t + O[(\Delta t)^2]\} + O[(\Delta t)^2]$$

or, if this is rearranged and  $\Delta t$  allowed to approach zero, then

$$dP_x(t)/dt = -f(x) P_x(t) + f(x-1) P_{x-1}(t) \quad (4)$$

which is the difference-differential equation describing the model. Equation (4) describes only the *probability* of occurrence of various states ( $x$ ) as a function of time and a property ( $f(x)$ ) of the system and its surroundings; we make no attempt to derive a functional equation for the state itself.

A set of initial conditions is needed for the solution of the above problem. If the initial state is  $X(0) = x_0$  ( $x_0 = 1, 2, \dots, x_m$ ), then the required initial conditions are

$$P_x(0) = \begin{cases} 1, & x = x_0 \\ 0, & x \neq x_0 \end{cases} \quad (5)$$

As an example of a stochastic growth process we consider the special case where

$$f(x) = \lambda x \quad (6)^3$$

where  $\lambda$  is a constant. Since the probability of a single fission in the time interval  $\Delta t$  is directly proportional to the population size, the population size should increase without limit as  $t \rightarrow \infty$ , and we must let  $x_m$  be infinite.

The problem to be solved is now

$$dP_x(t)/dt = -\lambda x P_x(t) + \lambda(x-1) P_{x-1}(t) \quad (4a)$$

subject to the initial conditions given by Eq. (5). The solution is easily found by Laplace transform methods and the process of induction; it is

$$P_x(t) = \binom{x-1}{x-x_0} e^{-x_0 \lambda t} (1 - e^{-\lambda t})^{x-x_0} \quad (7)$$

where the  $\binom{n}{m}$  are the binomial coefficients. The moments  $M_i(t)$  of the distribution could in principle be calculated from Eq. (7), but it is simpler to use the method of generating functions (cf. F1).

<sup>3</sup> If we had taken  $f(x) = \gamma$  (constant),  $x_0 = 0$ , the problem would describe the *Poisson process*, for which

$$P_x(t) = e^{-\gamma t} \frac{(\gamma t)^x}{x!}$$

This cannot be the model of a growth process, of course, since it violates the basic principle that cells arise only from pre-existing cells.

The generating function  $G(s, t)$  is defined by

$$G(s, t) = \sum_{x=x_0}^{\infty} P_x(t) s^x \quad (8)$$

The  $r$ th moment of the distribution is of course

$$M_r(t) = E[X^r(t)] = \sum_{x=x_0}^{\infty} x^r P_x(t) \quad (9)$$

Hence one sees that the moments can be found from the generating function by the formulas

$$M_1(t) = \frac{\partial G(1, t)}{\partial s} \quad (10)$$

$$M_2(t) = \frac{\partial G(1, t)}{\partial s} + \frac{\partial^2 G(1, t)}{\partial s^2} \quad (11)$$

etc. In addition, since  $X(t)$  must have *some* value equal to or greater than  $x_0$ , we require

$$\sum_{x=x_0}^{\infty} P_x(t) = 1 \quad (12)$$

whence  $G(1, t)$  must equal unity.

From Eq. (4a) and the definition of the generating function, we find that  $G$  must satisfy

$$\frac{\partial G(s, t)}{\partial t} = \lambda s(s-1) \frac{\partial G(s, t)}{\partial s} \quad (13)$$

To obtain this result, we must remember that  $P_x(t) = 0$  if  $x < x_0$ . The general solution of Eq. (13) may be found; the required special solution is obtained by using the initial condition, Eq. (5), which shows that

$$G(s, 0) = s^{x_0} \quad (14)$$

The generating function is then

$$G(s, t) = \left[ 1 - \left( \frac{s-1}{s} \right) e^{\lambda t} \right]^{-x_0} \quad (15)$$

Equation (15) is seen to satisfy the condition required by Eq. (12).

From Eqs. (10) and (11), we find the mean and the variance of the distribution to be

$$E[X(t)] = M_1(t) = x_0 e^{\lambda t} \quad (16)$$

$$V[X(t)] = M_2(t) - M_1^2(t) = x_0 e^{\lambda t} (e^{\lambda t} - 1) \quad (17)$$

Equation (16) shows that the expected rate of increase of population size is

exponential. Thus, the problem just solved is the stochastic analog of the *Malthusian* growth process developed in the next section.

We note that

$$dM_i/dt = \lambda M_i \quad (18)$$

That is, the expected multiplication rate depends explicitly only on the expected state, and not on time. In other words, Eq. (18) is the differential equation of an *autonomous* system. Most of the models that have been proposed have the property of being autonomous.

One further conclusion of importance can be gleaned from these results. Consider the "spread" of observed population sizes about the mean value. A measure of the spread is the standard deviation or square root of the variance. The relative spread of observations is then the ratio of the standard deviation to the mean (often called the coefficient of variation), which for this case is

$$\left( \frac{1 - e^{-\lambda t}}{x_0} \right)^{1/2}$$

Hence, if  $x_0$  is small, we see that the degree of unpredictability in the results is large; that is, if many identical systems are observed, their population sizes will be widely scattered about the mean.

On the other hand, chemical engineers and most microbiologists rarely deal with growth situations in which  $x_0$  is small.<sup>4</sup> A lower bound for the size of systems used in these disciplines is something like one cubic centimeter. Ordinarily, there will be  $10^4$ – $10^{12}$  organisms in this volume, and the relative spread will range from 0.0001 up to 1%. By the central limit theorem, this means that only about 31% of identical systems observed would have population sizes differing from the expected size by more than the relative spread calculated above. Since an uncertainty of even 1 percent is usually well within the precision of conventional methods for determining population size, we can regard the growth process as deterministic for the practical purposes of engineering or microbiology. This re-expresses the well-known fact that we *can* predict with fair precision what a population size undergoing logarithmic growth will be at subsequent times.

Note, however, that if we choose to include cellular structure in our model we must then consider the *distribution* of structures in the cells of the population, and elements of randomness again enter the picture.

## B. DETERMINISTIC MODELS: SEGREGATED OR DISTRIBUTED

We now define with some precision the physical arrangement of systems of concern. Let the population of cells be contained in a vessel ("reactor" or

<sup>4</sup> A notable exception occurs in counting experiments [cf. Halvorson and Ziegler (H2) and Ziegler and Halvorson (Z2)].

“propagator”) of effective volume  $V$ . Cells are suspended in a liquid phase that contains nutrients including gases essential for their growth. Byproducts of cellular metabolism accumulate in the liquid. The contents of the propagation vessel are so well stirred that the distribution of cells and of chemical species is uniform throughout.

In biological parlance, the liquid phase is called the *medium*; the liquid phase with suspended cells is called the *culture*. The word *growth* refers to the totality of metabolic processes (physical and chemical) that results in production of protoplasmic material, production of metabolic byproducts, consumption of *substrates* (reactants, nutrients), etc. Later we shall refer to the growth of a single cell; here growth refers to the culture as a whole.

The case where the propagation vessel is charged with a growth medium and *inoculated* (seeded) with cells at some datum of time, and the culture is left to grow without subsequent addition or removal of material from the vessel (with the possible exception of gases), is called *batch growth*. This is the most common mode of propagation in current practice; the scale of batch propagation varies from test tube size in laboratories to 100,000-gallon fermentors or larger industrial installations. Batch growth was the case just treated in the last section on stochastic growth models. It is in connection with batch growth that the terms “lag phase,” “log growth phase,”<sup>5</sup> “stationary phase,” and “phase of decline” have arisen.

An alternate mode of propagation is provided by the so-called *chemostat* or continuous propagator.<sup>6</sup> In the continuous propagator, fresh medium containing no cells is fed to the vessel at a constant rate of  $Q$  volumes per unit time. Culture is removed from the vessel at the same rate, so that the effective volume of the vessel is constant. Variations on this scheme are possible; one might feed fresh medium intermittently, or one might place the feed rate under control of some output variable (such as the pH or optical density of the culture). In other cases a cascade of vessels might be used. For simplicity, we consider here only a single vessel where the feed rate is constant.

Evidently a steady-state situation may be possible in the continuous propagator. In this situation, cells grow in an unchanging physical and chemical environment (hence the name “chemostat”). This is one of the reasons that continuous propagation has excited the interest of microbiologists [cf. the proceedings of the Czech symposium (M2) and the S. C. I. symposium (S4)].

The mathematics of continuous propagation, for populations of unstructured cells, is easily written down: Let  $N$  be the population density of cells in the propagator, and let  $C$  be the concentration of “protoplasm”

<sup>5</sup> This is a misnomer; the kind of growth referred to is exponential, rather than logarithmic. In this review, the term “exponential growth” will be used.

<sup>6</sup> In engineering practice, such a system is often called a continuous stirred-tank reactor (C\*).

therein. The latter term is used roughly; it may refer to volume of wet cells per unit volume of culture (determined, e.g., by centrifugation), to the concentration of cellular nitrogen (as determined by chemical analysis), etc. *These two methods of expressing cell quantity are not always proportional.* The population density is not used in distributed models.

The *growth rate* may be expressed as either

$$R_c = \text{rate of production of cells (number) per unit volume of culture (strictly, this is a multiplication rate)}$$

or

$$R_p = \text{rate of production of "protoplasm" per unit volume of culture}$$

There is not necessarily a linear relation between  $R_c$  and  $R_p$ .

Number or material balance on  $V$  then yields

$$dN/dt = -(1/\theta)N + R_c \quad (19)$$

$$dC/dt = -(1/\theta)C + R_p \quad (20)$$

where  $\theta = V/Q$  is the nominal holding time.<sup>7</sup> In batch propagation,  $1/\theta = 0$  (infinite holding time), so that the growth rate becomes the time derivative of population density or concentration of protoplasm.

If a steady state is obtained in a continuous propagator, then clearly

$$r_c \equiv R_c/N = 1/\theta \quad (21)$$

$$r_p \equiv R_p/C = 1/\theta \quad (22)$$

that is, the specific growth rates ( $r_c$  or  $r_p$ ) must equal the reciprocal holding time. Cells and protoplasm are washed out as rapidly as they are formed.

*Expressions for Growth Rate.* At this stage, a model must be introduced if further progress is to be made, and we choose a deterministic model. All deterministic models which have been introduced (with two exceptions) have been autonomous; they assume that the growth rates are explicit functions only of the *state* of the system, and not of time. But state in an unstructured model can only refer to population density or to concentration of protoplasm, since, by definition, a model is unstructured if only one state variable appears. Thus, the model is

$$R_c = R_c(N) \quad (23)$$

$$R_p = R_p(C) \quad (24)$$

<sup>7</sup> Microbiologists prefer to use the reciprocal of  $\theta$ , which they call the "dilution rate." Herein, we adhere to the usual chemical engineering practice of using the holding time. Both usages have their advantages, of course.

By a Maclaurin series expansion of Eq. (23), for instance, we get

$$R_c = R_c(0) + \frac{dR_c(0)}{dN} N + \frac{d^2R_c(0)}{dN^2} \frac{N^2}{2!} + \dots \quad (25)$$

But  $R_c(0)$  must be zero, since cells arise only from pre-existing cells.

If we neglect all but the second term of Eq. (25), we have Malthus' law<sup>8</sup>:

$$R_c = \mu N \quad (26)$$

where  $\mu$  is a constant. Thus, for a batch system with  $N = N_0$  when  $t = 0$ , Eqs. (19) and (26) show that growth is exponential. On the other hand, we have for a continuous propagator

$$dN/dt = -(1/\theta)N + \mu N$$

whence the condition for steady state is

$$\mu = 1/\theta \quad (27)$$

The population density at steady state is indeterminate, and no steady state is possible unless Eq. (27) is fulfilled exactly. As a matter of fact Eq. (27) grossly contradicts experience, since in continuous propagation there is a *range* of holding times in which steady state can be achieved. Hence something is wrong with the Malthus model.

If all but the second and third terms in Eq. (25) are neglected, we get the law of Verhulst and Pearl (W2, P1), also called the "logistic law":

$$R_c = \mu N(1 - \beta N) \quad (28)$$

where  $\mu$  and  $\beta$  are positive constants. In batch growth Eq. (28) yields the *logistic curve*:

$$N = \frac{N_0 e^{\mu t}}{1 - \beta N_0(1 - e^{\mu t})} \quad (29)$$

One sees that  $N$  approaches  $1/\beta$  as  $t \rightarrow \infty$ . Equation (29) is a more realistic form than Malthus' law, since there is now a stationary phase following exponential growth.

Application of Eq. (28) to continuous propagation yields the steady-state condition

$$1/\theta = \mu(1 - \beta N) \quad (30)$$

According to this equation, all holding times greater than  $1/\mu$  will yield steady states with nonzero population density. If  $\theta = 1/\mu$ , a steady state will also

<sup>8</sup> According to Malthus, populations tend to increase exponentially, unless checked by some factor, such as a shortage of nutrients. A survey of some of the early literature on population growth is given by Whittaker (W2) and by Pearl (P1).

be obtained, but  $N$  will be zero therein. In contrast to Eq. (27), Eq. (30) yields the steady-state population density uniquely.

Clearly the foregoing result is "better" than that obtained from Malthus' law. However, any model such as Eq. (23) or (24) is suspect because it does not account for the effect of environment on growth, or the reciprocal effect of growth on environment; this will be considered shortly. Also experimental data exist which cannot be reconciled with such models. Finn and Wilson (F2), in a study of the continuous propagation of yeast, found that under certain conditions there did not appear to be any steady state; rather, the population density oscillated about some mean value, with a well-defined frequency. This brings the question of *stability* into the discussion; we will show that Eq. (23) is incompatible with the existence of the phenomenon observed by Finn and Wilson.

The question of stable operation of ordinary chemical reactors apparently originated with van Heerden (H6). Analyses of the stability question for such systems were given by Bilous and Amundson (B8) and Aris and Amundson (A2). Analysis depends on a purely mathematical result obtained by Liapunov (L3). This result is known as Liapunov's theorem, or the stability theorem, and a proof may be found in Davis' book (D1). A more advanced treatment of the stability problem is given by Hahn (H1). The analysis given below is essentially that of Spicer (S5).

If we do not specialize Eq. (23), the equation describing the dynamics of the continuous propagator is

$$dN/dt = -(1/\theta)N + R_c(N) \quad (31)$$

We denote possible steady-state population densities by  $\tilde{N}$ ; these are given by

$$R_c(\tilde{N})/\tilde{N} = 1/\theta \quad (32)$$

There may be multiple steady states if Eq. (32) has more than one real positive root.

Application of the stability theorem shows that the steady-state  $\tilde{N}$  will be a *stable node* if

$$R_c(\tilde{N})/\tilde{N} > dR_c(\tilde{N})/dN \quad (33)$$

The steady state  $\tilde{N}$  is an *unstable node* if the inequality is reversed. As shown by Spicer (S5), the inequality (33) will be fulfilled if and only if the derivative of the *specific* growth rate [Eq. (21)] is negative:  $dr_c(\tilde{N})/dN < 0$ .

On biological grounds, we have to assume that  $dr_c(N)/dN$  is *never* positive. This derivative is zero in the Malthusian case; in other cases, if the derivative were positive, growth in batch cultures would be faster than exponential (a circumstance which is never observed). It was for this reason that  $\beta$  was restricted to positive values in the Verhulst-Pearl law.



It is easy to show that the restriction  $dr_c(N)/dN < 0$  allows only one real positive root for Eq. (32). Thus there are not multiple steady states. The one steady state must be a node rather than a focus, so that no oscillations will be observed in approach to the steady state, and Eq. (23) cannot accommodate the Finn and Wilson phenomenon.

Finn and Wilson tried to circumvent this difficulty by introducing the *ad hoc* hypothesis that  $R_c$  was also an explicit function of time; this does away with the autonomous nature of the model. By so doing, they were able to make use of earlier work by Baron (B2) to obtain predictions of oscillation in population density.

Volterra (V2) postulated an unstructured growth model involving a "hereditary factor."<sup>9</sup> His equation for batch growth is

$$dN/dt = \mu N \left[ 1 - \beta N - \int_0^t N(t') K(t - t') dt' \right] \quad (34)$$

It is difficult even to obtain numerical solutions of this equation, in the general case. However, if the kernel  $K$  is a constant (say  $K_0$ ), the equation may be solved numerically. Plots of the solution may be found in Davis' book (D1) on p. 418. If  $K_0 = 0$ , one has the logistic equation. For  $K_0 > 0$ , a set of curves exhibiting exponential growth, a stationary phase, and a phase of decline are predicted for batch growth.

Volterra's equation and the modification of Eq. (23) proposed by Finn and Wilson are the only unstructured growth models that are not autonomous. As we have seen, the justification for models in which growth rates are explicit functions of time lies in the failure of simple autonomous growth models to predict certain observed phenomena. There are, however, other ways in which one can accommodate the phenomena without doing away with the convenient character of autonomous models.

One method was first suggested by M'Kendrick and Pai (M11), and completed by Monod (M12). Applications of it have been made by Monod (M13), Novick and Szilard (N2), Novick (N1), Maxon (M7), Herbert *et al.* (H10), and others. M'Kendrick and Pai assumed that growth would proceed at maximum rate (exponential growth in batch cultures) only if an "unlimited supply of nutriment" were available. When substrates for growth have been consumed, growth must stop. Hence they postulated that the growth rate is

$$R_c = vNC_s \quad (35)$$

where  $C_s$  is the concentration of the substance in the medium limiting growth (it is tacitly assumed that there is only one such substance). This in turn is influenced by the amount of growth which has occurred; i.e., M'Kendrick

<sup>9</sup> "Heredity" in Volterra's sense is not to be confused with the geneticist's use of the word.

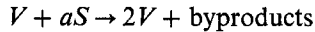
and Pai assume a *stoichiometric relation* of the form

$$-R_s = aR_c \quad (36)$$

where  $-R_s$  is the rate of consumption of substrate, and  $a$  is a stoichiometric coefficient.

In batch growth, Eqs. (35) and (36) lead to Eq. (29), the logistic equation with  $\mu = v(C_{s0} + aN_0)$  and  $\beta = a/(C_{s0} + aN_0)$ , where  $C_{s0}$  is the initial substrate concentration. The constants  $\mu$  and  $\beta$  are not now things simply to be determined by experiment, but must depend on initial conditions ( $C_{s0}$  and  $N_0$ ) in a specific manner.

Monod (M12) made two improvements on the theory of M'Kendrick and Pai. In the view of the latter authors, the essential process involved in growth may be represented as a chemical reaction



Here,  $V$  represents organisms and  $S$  is substrate. M'Kendrick and Pai took the measure of  $V$  to be the population density  $N$ . Inasmuch as a stoichiometric relation is assumed, however, the measure of  $V$  ought not to be population density, since the amount of substrate necessary to form one organism does not remain constant under different circumstances of propagation. Monod recommended instead that one use "*la masse de la substance vivante*," which fits the description of the quantity we called  $C$  earlier. In other words, a distributed model, rather than a segregated model, is to be used if stoichiometric relations appear. Monod's stoichiometric postulate is then

$$R_s = -aR_p \quad (37)$$

where  $a$  has different units than the  $a$  in Eq. (36).

Next, Monod recognized that the growth rate could have a maximum value,<sup>10</sup> and he postulated that the substrate dependence of growth rate followed the Michaelis-Menten (M8) form:

$$R_p = \frac{\mu C C_s}{K + C_s} \quad (38)$$

where  $\mu$  is now the maximum specific growth rate obtained when  $C_s$  is much greater than the Michaelis constant  $K$ . Equations (37) and (38) together are a complete statement of Monod's model, and they may now be applied to various special cases.

For instance, in *batch* growth with

$$\left. \begin{array}{l} C = C_0 \\ C_s = C_{s0} \end{array} \right\} \text{at } t = 0$$

<sup>10</sup> M'Kendrick and Pai (M11) saw this also, but did not incorporate it into their theory.

we find

$$\frac{dC}{dt} = -\frac{1}{a} \frac{dC_s}{dt} = \frac{\mu C C_s}{K + C_s} \quad (39)$$

The first equation of the foregoing gives

$$C_{s0} - C_s = a(C - C_0)$$

whence the second equation may be integrated to yield

$$\frac{K}{aC_0 + C_{s0}} \ln \frac{C_{s0}}{C_{s0} - a(C - C_0)} + \frac{K + aC_0 + C_{s0}}{aC_0 - C_{s0}} \ln \frac{C}{C_0} = \mu t \quad (40)$$

Provided that  $C_{s0} \gg K$  and  $C_{s0} \gg aC_0$ ,  $C$  will increase exponentially at first; however, growth will eventually stop, and the maximum concentration of protoplasm reached will be

$$\lim_{t \rightarrow \infty} C = C_0 + \frac{C_{s0}}{a} \approx \frac{C_{s0}}{a}$$

No phase of decline is predicted.

The postulated cause of the stationary phase is that all substrate is consumed. The existence of exponential growth in the initial stages of the batch is a consequence of the hyperbolic rate equation, Eq. (38). Thus, for  $C_s \gg K$ , it becomes approximately

$$R_p \approx \mu C \quad (38a)$$

and the rate is zero order in substrate.

For the continuous propagator, Monod's model requires

$$\frac{dC}{dt} = -\frac{1}{\theta} C + \frac{\mu C C_s}{K + C_s} \quad (41)$$

$$\frac{dC_s}{dt} = \frac{1}{\theta} (C_{sf} - C_s) - \frac{a\mu C C_s}{K + C_s} \quad (42)$$

where  $C_{sf}$  is the concentration of limiting substrate in the feed. There are two possible steady states:

$$(A) \begin{cases} C = 0 \\ C_s = C_{sf} \end{cases}$$

or

$$(B) \begin{cases} C = \frac{1}{a} \left[ C_{sf} - \frac{K}{\mu\theta - 1} \right] \\ C_s = \frac{K}{\mu\theta - 1}, \quad (\mu\theta > 1) \end{cases}$$

Stability analysis by Liapunov's theorem shows that<sup>11</sup>:

(i) Steady-state (*A*) is stable if

$$\frac{\mu C_{sf}}{K + C_{sf}} < \frac{1}{\theta}$$

Steady-state (*A*) is unstable if the inequality is reversed.

(ii) Steady-state (*B*) is stable if

$$\frac{\mu C_{sf}}{K + C_{sf}} > \frac{1}{\theta}$$

Steady-state (*B*) is unstable if the inequality is reversed. Moreover, if steady-state (*B*) is stable, it must be a node; it cannot be a vortex point or a focus.

Steady-state (*B*) is the interesting one, of course, since steady-state (*A*) corresponds to complete washout of cells. Stability analysis has shown that the two cannot coexist at the same holding time; either (*A*) is stable and (*B*) is unstable, or (*B*) is stable and (*A*) is unstable. Moreover, since (*B*) is a node if it is stable, we see that Monod's model will not predict oscillations—even damped ones—about a steady state of nonzero cell concentration. Hence, in this sense, there has been no improvement over the Verhulst–Pearl model.

However, the ideas involved in Monod's model can be extended somewhat so that predictions of oscillations can be obtained under certain conditions. This idea has been developed by Ramkrishna (R3). He recognized that several processes may be involved in growth, and that combinations of these processes may lead to oscillations of the type found by Finn and Wilson. In his simplest extension of the Monod model, Ramkrishna proposed that growth produces a *staling factor* which inhibits growth. This model, in which structure has not yet been introduced, is an improvement over Monod's model, since it predicts a phase of decline in batch growth, and damped oscillations in certain cases of continuous propagation. Since a generalization of this model to include structure is treated in the next section, we make no further mention of it here.

The problem of growth of mixed cultures (two or more interacting species occupying the same living space) has generated interest among biologists and mathematicians ever since the time of Volterra (V2) and Lotka (L4). Whitaker (W2) states that oscillations in the number of fish of various species present in the Adriatic Sea have been found to be in agreement with some of Volterra's equations; other cases of population interactions are discussed from a purely mathematical point of view by Davis (D1).

Moser (M14) applied extensions of Monod's model to growth of mixed

<sup>11</sup> For details, see Ramkrishna (R3).

cultures in the chemostat. Principal interest here was in the emergence of mutant populations. Very few experimental data exist with which to check the models.

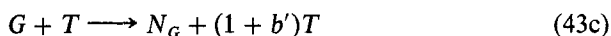
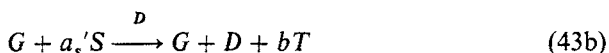
#### IV. Structured Models: Distributed

##### A. FIRST MODEL

The models just discussed have a number of serious deficiencies, despite their being able to provide reasonable descriptions of certain phenomena in a limited number of cases. A most notable deficiency is their inability to predict a lag phase in batch growth. Consideration of this led Ramkrishna (R3) to develop new models in which microbial cultures are endowed with a certain amount of biochemical structure; although these models are distributed rather than segregated, so that phenomena associated with reproduction cannot be treated, the models do predict qualitatively a number of phenomena that cannot be touched by unstructured models.

The basic supposition is that protoplasm is composed of two structural components, whose interaction with each other and with the surrounding medium produces growth. This idea arose in a paper of Weiss and Kavanau (W1). For convenience, we call the two structural components of protoplasm the *G* mass and the *D* mass. (In fact, protoplasm is composed of a large number of structural components, whose *geometrical* arrangement is also highly important to life processes.) Tentatively the *G* mass may be thought of as nucleic acids, and the *D* mass may be thought of as proteins.

In one of Ramkrishna's models, the processes of growth are assumed to be represented by the following set of "chemical reactions"<sup>12</sup>:



where *T* represents an inhibitor produced by growth, and *N<sub>G</sub>* and *N<sub>D</sub>* are "dead" forms of *G* and *D*, respectively. The rates of the first two (growth) reactions are assumed to be given by double substrate Michaelis-Menten kinetics (see, e.g., L1); thus, both *G* mass and *D* mass must be present for

<sup>12</sup> Ramkrishna's other models are modifications of the scheme proposed above. For instance, inhibitor might be produced by reactions (43a) and (43d), rather than by (43b) and (43c), as above.

growth to occur. The deactivating reactions are assumed to be second order, as written.

For batch growth, the kinetic equations are

$$dC_G/dt = R_G - KC_G C_T \quad (44a)$$

$$dC_D/dt = R_D - K' C_D C_T \quad (44b)$$

$$dC_S/dt = -a_s R_G - a'_s R_D \quad (44c)$$

$$dC_T/dt = b R_D + b' K C_G C_T \quad (44d)$$

in which the  $C$ 's denote the concentrations of the substances identified by the subscripts. In these equations, we have put

$$R_D = \frac{\mu C_S C_G C_D}{(K_s + C_S)(K_g + C_G)} \quad (45a)$$

$$R_D = \frac{\mu' C_S C_G C_D}{(K'_s + C_S)(K'_g + C_G)} \quad (45b)$$

Although these equations are coupled and nonlinear, numerical solutions can be obtained on the digital computer. Figure 1 shows the results of such a numerical integration procedure applied to the set of Eqs. (44). We see that all phases of the batch growth curve, including a lag phase, are exhibited by

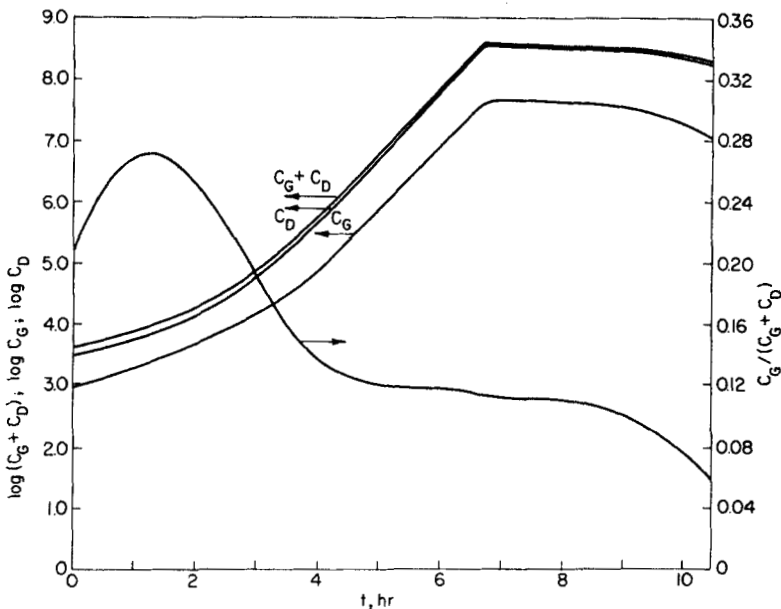


FIG. 1. Computer solution of Eqs. (44) and (45) for batch growth.

the curve of  $(C_G + C_D)$ —that is, the total concentration of viable protoplasm in the culture—vs time. Moreover, the plot of the fraction of biomass present as  $G$  follows the course of fraction of nucleic acids present found experimentally by Malmgren and Hedén in batch growth of *E. coli* (M3).

Other phenomena found in batch growth are predicted by the foregoing model. For instance, the model yields batch growth curves dependent on (i) the relative proportion of  $G$  and  $D$  in the inoculum, with its principal effect the length of the lag phase; and (ii) the size of the inoculum, with increases in size generally reducing the lag-phase duration. The model shows that the duration of the lag phase is increased for decreased initial amounts of  $G$  mass; a culture inoculated with cells from the phase of decline would have a longer lag phase than one from the exponential growth phase (cf. B10). The time course of growth is affected by the “physiological state” or “biological age” of the inoculum, for which a quantitative definition is the fraction of  $D$  present.

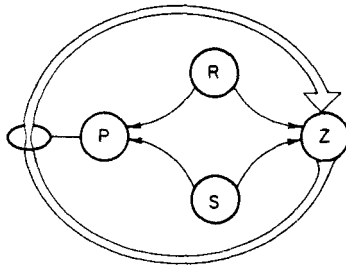
For point (ii) the predictions given above agree with the results of Henrici (H7) on growth of *E. coli*, and with those of Rabotnova and Mineeva (R1) on growth of *Torulopsis utilis* and *Pseudomonas fluorescens*. The maximum concentration of organism attained becomes roughly independent of inoculum size and dependent on initial substrate concentration, as known since Henrici’s experiments (H7).

Ramkrishna (R3) has applied this and similar models to continuous propagation, where these structured models display rather complicated stability characteristics; numerical computations indicate multiple steady states, steady states which are foci, and perhaps the existence of limit cycles. Thus the Finn and Wilson phenomenon can be accommodated in principle by a structured model.

## B. THE BOTTLENECK MODEL OF THE LAG PHASE

A distinctive feature of biological growth is that the period of exponential growth (growth phase) is preceded by an induction period (lag phase) during which no growth is observed. In the simpler growth models, in which the growth rate is initially proportional to the population size, the origin of time must be taken at the end of the lag phase. The object of this section is to explore a model which will include both the lag phase and the growth phase. This analysis is related to that of certain production processes in economic theory, known as bottleneck problems (B5), and since it may be a little unfamiliar we give first a verbal description of the method and results of the analysis, which we hope will enable the reader to see what it is all about. Even though this should give a useful overview, it scarcely needs to be added that the detailed mathematical analysis is needed if this approach is to be understood.

A simple model of a biological system that will exhibit a natural lag phase is the following. An organism  $Z$  lives on two nutrients  $R$  and  $S$ . Without loss of generality we can take  $R$  to be the nutrient that would be exhausted first, but both are required to maintain the viability of  $Z$ ; they might, for example, be a "nitrogen" source and an energy source. The growth or reproduction of  $Z$  is controlled by a critical product  $P$  (such as ATP or a polymerase) and  $R$  and  $S$  are also required for the formation of  $P$ . Schema A shows the system.



In the bottleneck problems of economic theory there is a critical intermediate product and the policy that maximizes the total production starts with a lag phase in which the stock of this critical product is built up; in the metaphor of the problem the "bottleneck" is enlarged. Similarly in our present formulation an objective function must be set up and must be justified in two ways: firstly, by showing that it is biologically meaningful, and secondly, by showing that it gives a behavior that corresponds, at least qualitatively, with observation. In the above model we will assume that the system behaves in such a way as to maximize the population of  $Z$  at the time of exhaustion of  $R$ . To justify this on the first count we may suppose that a large population of  $Z$  confers some advantage on the system in its environment. A larger project is to study both the system and its environment and this would require us to assume some larger objective. On the second count we have to show that the model exhibits a lag phase as an essential part of its optimal policy. We should also like it to show the following features: (a) the duration of the lag phase decreases with the decrease of available nutrient, and (b) this duration should also decrease with increase in the level of  $P$ , so that if growth has started and the organism is transferred into fresh nutrient the lag phase will be shorter. Ultimately we would like to show quantitative agreement between the relations of lag duration and growth rate to nutrient and critical product levels in the model and in a specific biological system or class of systems. This last must await a more detailed confrontation with experiment, but the correct qualitative features are shown. We will now give a verbal description of the equations and solution, referring, where necessary, to the equations of Sections IV, B, 1-6 by their number and to Figs. 6, 10, 11(a), 11(b), and 14 to give some impression of the results.



The rate of production of  $P$  is assumed to be proportional to the concentration of  $Z$ , with a proportionality (or rate) constant  $k_5$  which is the control variable of the system [Eq. (46)]. Thus if  $k_5 = 0$ , the concentration level of  $P$  remains constant.  $Z$  reproduces itself at a rate proportional to its own concentration, the rate constant being  $(k_1 - k_5)$  [Eq. (47)]. Thus, if  $k_5 = 0$ , no  $P$  is being produced and the growth rate of  $Z$  is the greatest that it can be, while if  $k_5 = k_1$ ,  $P$  is being produced but the population of  $Z$  is constant. We do not allow the production of  $P$  at the expense of  $Z$  so that  $k_5$  is never greater than  $k_1$  (Eq. 48). The nutrients are used at a rate proportional to the amount of  $Z$  present to maintain the viability of the organism and also at an additional rate proportional to the rate of production of  $P$  [Eqs. (49) and (50)].

Since the organism cannot be expected to have an innate sense of time, but could have a control mechanism based on concentration levels, we take the concentration of  $R$  as the independent variable in place of time by dividing each of the differential equations by the equation for the concentration  $c_r$ . The independent variable thus decreases from its value  $\rho$  at the beginning of the process to zero at the end. It does indeed turn out that the policy that gives the maximum final concentration of  $Z$  involves first a lag phase, during which the concentration of  $P$  increases but not that of  $Z$ , and then a growth phase, in which the concentration of  $P$  remains constant and growth of  $Z$  takes place. This only happens if the concentration of  $R$  is sufficiently large; if it is small, there is no lag phase and very little growth, but as  $\rho$  increases so does the duration of the lag phase and the subsequent rate of growth. There is a definite relation between the concentrations of  $P$ ,  $R$ , and  $S$  at the transition from the lag to the growth phase.

To get any further we have to give a definite form to the maximum rate of growth of  $Z$ , the constant  $k_1$ . In the dimensionless form into which these constants are put [Eq. (51)], this growth rate is  $\gamma$  and is taken to be  $a\pi^b\rho\sigma$ , where  $a$  and  $b$  are constants and  $\pi$ ,  $\rho$ , and  $\sigma$  the concentrations of  $P$ ,  $R$ , and  $S$ . By varying  $a$  and  $b$  we can simulate a number of conditions. If  $b = 1$ , the effect of the concentration of critical product  $P$  on the growth rate is linear. If  $b > 1$ , it is less than linear at low concentrations of  $P$  but rather more than linear at high concentrations: the reverse is true if  $b < 1$ . This switching surface, as it is called, between the lag and the growth phases has a form such as is shown in Fig. 6.  $\xi$  and  $\eta$  are dimensionless forms of the concentrations of  $R$  and  $S$  [Eq. (86)] and the figure shows the intersection of the switching surface with various planes of constant  $\pi$ . The region below the line  $\xi = \eta$  is not of interest since it is not consistent with the assumption that  $R$  is the nutrient first exhausted. If, for any level of concentration of  $P$ ,  $\pi$ , the available nutrient concentrations put the point  $(\xi, \eta)$  to the right of the curve corresponding to the value of  $\pi$ , then the system is in the lag phase and  $P$  is produced but  $Z$  remains constant. As  $P$  is produced the nutrients are exhausted and the point  $(\xi, \eta, \pi)$  representing the state of the system moves downwards and to the left in Fig. 6. If we think of the axis of  $\pi$  as coming vertically out

of the paper, then this point is moving upwards as well and will soon intersect the switching surface. Suppose that it intersects at such a point as "a" on the curve  $\pi = 1.9$  of Fig. 6. In Fig. 11(a) the attempt is made to represent this lag phase in three dimensions. The curve "abcde" is the curve  $\pi = 1.9$  of Fig. 6 and now lies in the horizontal plane  $\pi_s = 1.9$  (the suffix "s" refers to the value at the moment of switching). If switching from the lag to the growth phase takes place at "a," the value of  $\pi$  must have earlier been less than 1.9; the curve representing the state of the system therefore comes up from behind the switching surface as shown. In Fig. 11(b) the growth phase is shown, the vertical axis now being the dimensionless concentration of Z, namely,  $\chi$ . Since  $\chi$  has been constant during the lag phase, it has the same value  $\chi_s$  that it has at the switching surface. Thus  $\chi - \chi_s$  is the increase and it is convenient to put the zero of this at the point such as "a" where the switch between phases occurs; this means that the vertical ordinate is really  $\chi - \chi_s + \pi_s$ . Thus the curve through the point "a" in Fig. 11(b) represents the continuation of the history of the system in which the concentration of Z increases as the nutrients become used up.  $\chi_f$  is the final value of  $\chi$  and hence gives the level of Z when R is exhausted. Figure 10 shows the growth of Z as a function of the dimensionless time after switching,  $\tau - \tau_s$ . This depends on  $\chi_s$ , the size of the inoculum, for with a larger initial concentration the nutrient is more rapidly exhausted.

Finally, Fig. 14 shows the effect of taking the system in the growth phase and reinoculating it into fresh nutrient. Thus in the first lag phase, which is rather long, the concentration of Z,  $\chi$  is constant while the concentration of P,  $\pi$  rises. This passes naturally into a growth phase with  $\pi$  remaining constant and  $\chi$  increasing. The nutrient concentrations  $\xi$  and  $\eta$  fall continuously during this period, but before they have been exhausted they are restored to their initial levels. The second lag phase that ensues is very much shorter and is followed by a growth period during which the growth rate is much greater. Thus some of the principal features of biological growth processes are reproduced and the model merits further investigation and incorporation into a larger structure.

### 1. Equations for the Simplest Model

The following equations are the simplest that embody the features of the model we have just described.  $C$  will denote concentration with the subscript indicating the species in question.

*Production of P.* We assume the rate of production of P is proportional to  $C_z$  and that the constant of proportionality is the control variable of the system,

$$\frac{dC_P}{dt} = k_5 C_z \quad (46)$$

To say that  $k_5$  is the control variable of the system is to imply that it is some function of the state ( $C_r$ ,  $C_s$ ,  $C_p$ ,  $C_z$ ), and in looking for the optimal growth policy we are asking just what function  $k_5$  should be to achieve the maximum increase in  $Z$ .

*Reproduction of Z.* We assume that  $Z$  is either engaged in reproduction or in formation of  $P$  and that the total rate  $d(C_z + C_p)/dt$  is proportional to  $C_z$ . The constant of proportionality  $k_1$  may be a function of  $C_r$ ,  $C_s$ , and  $C_p$ . Thus

$$\frac{dC_z}{dt} = k_1 C_z - \frac{dC_p}{dt} = (k_1 - k_5) C_z \quad (47)$$

We do not allow  $Z$  to cannibalize; i.e.,  $P$  cannot be formed at the expense of  $Z$ , so that

$$0 \leq k_5 \leq k_1 \quad (48)$$

If  $k_5 = 0$ , then no  $P$  is being formed and the growth rate of  $Z$  is maximal. If  $k_5 = k_1$ ,  $Z$  is not growing but  $P$  is increasing.

*Use of Nutrients.* We assume that the rate of consumption of the two nutrients  $R$  and  $S$  is proportional to the amount of  $Z$  present and that when  $P$  is being formed they are consumed at an additional rate proportional to  $dC_p/dt$ . Thus

$$\frac{dC_s}{dt} = -k_2 C_z - k_3 \frac{dC_p}{dt} = -(k_2 + k_3 k_5) C_z \quad (49)$$

$$\frac{dC_r}{dt} = -k_4 C_z - k_6 \frac{dC_p}{dt} = -(k_4 + k_5 k_6) C_z \quad (50)$$

Before going further in setting up the problem let us introduce a change of variables. It is unlikely that the organism will have an innate sense of time and know at what future instant the nutrient  $R$  will be exhausted. However, it may well be able to detect the level of remaining nutrient and be controlled accordingly. Thus  $C_r$ , the concentration of the least-abundant nutrient, is the natural independent variable, rather than the time  $t$ . We can obtain equations with  $C_r$  as independent variable by dividing each equation by Eq. (50). Let us also introduce the abbreviations

$$\alpha = k_3, \quad \beta = k_6, \quad \gamma = k_1/k_4, \quad \lambda = k_5/k_4, \quad \omega = k_2/k_4 \quad (51)$$

Then Eqs. (46)–(49) become

$$\frac{dC_p}{dC_r} = \frac{-\lambda}{1 + \beta\lambda} \quad (52)$$

$$\frac{dC_z}{dC_r} = \frac{-\gamma + \lambda}{1 + \beta\lambda} \quad (53)$$

$$0 \leq \lambda \leq \gamma \quad (54)$$

and

$$\frac{dC_s}{dC_r} = \frac{\omega + \alpha\lambda}{1 + \beta\lambda} \quad (55)$$

At the beginning of the growth process,  $t = 0$ , we have

$$C_r = \rho, \quad C_s(\rho) = \sigma, \quad C_p(\rho) = \pi, \quad C_z(\rho) = \zeta \quad (56)$$

Thus  $C_z(0) - \zeta(\rho)$  is the increase in the amount of  $Z$  and is the quantity to be maximized. The optimal policy is the choice of  $\lambda(C_r)$ ,  $\rho \geq C_r \geq 0$ , that achieves this maximum and satisfies the restriction of Eq. (54).

## 2. Equations for the Optional Growth Policy

If the optimal choice of  $\lambda(C_r)$  were known it could be inserted in Eqs. (51)–(55), and these could be integrated to give the maximum increase

$$C_z(0) - \zeta = \int_0^\rho \frac{dC_z}{dC_r} dC_r = \int_0^\rho \frac{\gamma - \lambda}{1 + \beta\lambda} dC_r \quad (57)$$

The resulting maximum would of course depend on the initial values used for the integration of the equations, namely,  $\rho$ ,  $\sigma$ ,  $\pi$ , and  $\zeta$ . Let us therefore write

$$f(\rho, \sigma, \pi, \zeta) = \max \int_0^\rho \frac{\gamma - \lambda}{1 + \beta\lambda} dC_r \quad (58)$$

where the maximum is by the optimal choice of  $\lambda(C_r)$ ,  $0 \leq \lambda \leq \gamma$ , for the whole interval  $0 \leq C_r \leq \rho$ . We thus have a problem in the calculus of variations which may be tackled in a variety of ways. We choose here to make use of the notions of dynamic programming, though the methods of classical calculus of variations or the maximum principle of Pontryagin will lead to the same result.

Let us break the interval  $(0, \rho)$  into two parts,  $(\rho - \delta, \rho)$  and  $(0, \rho - \delta)$ , where  $0 \leq \delta \leq \rho$ . Then

$$f(\rho, \sigma, \pi, \zeta) \equiv \max \left[ \int_{\rho-\delta}^\rho \frac{\gamma - \lambda}{1 + \beta\lambda} dC_r + \int_0^{\rho-\delta} \frac{\gamma - \lambda}{1 + \beta\lambda} dC_r \right] \quad (59)$$

The maximization still requires the choice of  $\lambda$  over both intervals, but we should pause to see what the second integral really means. It is just such an integral as in Eq. (58), save that it is over the interval  $(0, \rho - \delta)$ . It will have a maximum value which is the same function  $f$  of the state  $(\rho - \delta)$ ,  $C_s(\rho - \delta)$ ,  $C_p(\rho - \delta)$ ,  $C_z(\rho - \delta)$  as the maximum of the integral over the whole interval  $(0, \rho)$  is of the state  $\rho$ ,  $C_s(\rho) = \sigma$ ,  $C_p(\rho) = \pi$ ,  $C_z(\rho) = \zeta$ . Moreover we shall clearly not get the maximum for the integral over the whole interval if we do

not have the maximum over the subinterval  $(0, \rho - \delta)$ , for we should have thrown away some advantage we might have had by using a suboptimal policy over the latter part of the interval. Thus

$$f(\rho, \sigma, \pi, \zeta) = \max \left[ \int_{\rho-\delta}^{\rho} \frac{\gamma - \lambda}{1 + \beta\lambda} dC_r, \right. \\ \left. + f(\rho - \delta, C_s(\rho - \delta), C_p(\rho - \delta), C_z(\rho - \delta)) \right] \quad (60)$$

and now the maximization requires only the optimal choice of  $\lambda(C_r)$  on the subinterval  $\rho \geq C_r \geq \rho - \delta$ , for the optimal choice on  $\rho - \delta \geq C_r \geq 0$  is implied by our using  $f$  for the second integral in Eq. (59). Equation (60) is true for all  $\delta$ ,  $0 \leq \delta \leq \rho$ , and is an application of Bellman's principle of optimality which states that "an optimal policy has the property that whatever the initial state and decision may be, the remaining decisions constitute an optimal policy with respect to the state resulting from the initial decision."

However, to get a useful equation out of (60) we need to let  $\delta$  become small and later tend to zero. From Taylor expansions, with the use of Eqs. (52), (53), and (55), we have

$$\begin{aligned} C_s(\rho - \delta) &= C_s(\rho) - \delta C'_s(\rho) + O(\delta^2) \\ &= \sigma - \delta \left( \frac{\omega + \alpha\lambda}{1 + \beta\lambda} \right) + O(\delta^2) \\ C_p(\rho - \delta) &= \pi + \delta \left( \frac{\lambda}{1 + \beta\lambda} \right) + O(\delta^2) \\ C_z(\rho - \delta) &= \zeta + \delta \left( \frac{\gamma - \lambda}{1 + \beta\lambda} \right) + O(\delta^2) \end{aligned}$$

Combining these with a Taylor expansion of  $f$  about the point  $\rho, \sigma, \pi, \zeta$ , we have

$$f(\rho - \delta, C_s(\rho - \delta), C_p(\rho - \delta), C_z(\rho - \delta)) = f(\rho, \sigma, \pi, \zeta) \\ - \delta \left[ f_\rho + f_\sigma \frac{\omega + \alpha\lambda}{1 + \beta\lambda} - f_\pi \frac{\lambda}{1 + \beta\lambda} - f_\zeta \frac{\gamma - \lambda}{1 + \beta\lambda} \right] + O(\delta^2) \quad (61)$$

where  $f_\rho$ , etc., denote the partial derivatives  $\partial f / \partial \rho$ , etc., evaluated at  $(\rho, \sigma, \pi, \zeta)$ , and  $O(\delta^2)$  denotes terms of order  $\delta^2$  and smaller. Moreover if  $\delta$  is small

$$\int_{\rho-\delta}^{\rho} \frac{\gamma - \lambda}{1 + \beta\lambda} dC_r = \delta \frac{\gamma - \lambda}{1 + \beta\lambda} + O(\delta^2) \quad (62)$$

and substituting Eqs. (61) and (62) in (60) we have

$$(\rho, \sigma, \pi, \zeta) = \max \left[ f(\rho, \sigma, \pi, \zeta) + \frac{\delta}{1 + \beta\lambda} \{ (1 + f_\zeta)(\gamma - \lambda) \right. \\ \left. + \lambda f_\pi - (\omega + \alpha\lambda)f_\sigma - (1 + \beta\lambda)f_\rho \} + O(\delta^2) \right]$$

This maximization is by choice of  $\lambda$  over a very short interval,  $\rho \geq C_r \geq \rho - \delta$ , and this choice does not affect the first term since no  $\lambda$  appears in it. We may therefore take  $f(\rho, \sigma, \pi, \zeta)$  outside the maximization sign and subtract it from both sides. If we then divide through by  $\delta$  and let  $\delta \rightarrow 0$  the remainder terms will vanish, leaving

$$\max \frac{1}{1 + \beta\lambda} \{ (1 + f_\zeta)(\gamma - \lambda) + \lambda f_\pi - (\omega + \alpha\lambda)f_\sigma - (1 + \beta\lambda)f_\rho \} = 0$$

We notice immediately that  $(1 + \beta\lambda)$  is always positive and that when the maximum of  $A(\lambda)/B(\lambda)$ ,  $B(\lambda) > 0$ , is zero then  $\max A(\lambda) = 0$ . Thus the equation could be rearranged and written

$$\max [ \{ (1 + f_\zeta)\gamma - \omega f_\sigma - f_\rho \} + \lambda \{ f_\pi - \beta f_\rho - \alpha f_\sigma - (1 + f_\zeta) \} ] = 0 \quad (63)$$

The choice to be made to find the maximum is of  $\lambda$ , the value of the control variable when  $C_r = \rho$ . We have thus reduced a variational problem requiring the choice of a whole function  $\lambda(C_r)$ ,  $\rho \geq C_r \geq 0$ , to the choice of one value,  $\lambda(\rho)$ .

Furthermore the choice of the optimal  $\lambda(\rho)$  is particularly simple. Let us write

$$\Gamma \equiv \gamma(1 + f_\zeta) - \omega f_\sigma - f_\rho \quad (64)$$

$$\Delta \equiv f_\pi - \beta f_\rho - \alpha f_\sigma - (1 + f_\zeta)$$

then

$$\max(\Gamma + \lambda\Delta) = 0 \quad (65)$$

Thus if  $\Delta > 0$ ,  $\lambda$  should have its maximum value, namely,  $\gamma$ ; whereas if  $\Delta < 0$ ,  $\lambda$  should have its minimum value, namely, zero. In fine,

$$\lambda = 0 \quad \text{if } \Delta < 0 \quad (66)$$

$$\lambda = \gamma \quad \text{if } \Delta > 0$$

This policy is good common sense, for the condition  $\Delta > 0$  could be written

$$f_\pi > \beta f_\rho + \alpha f_\sigma + f_\zeta + 1$$

Now  $f_\pi$  is  $\partial f / \partial \pi$ , i.e., the advantage to be gained by increasing  $\pi$ , whereas the left-hand side is a sum of partial derivatives with respect to  $\rho$ ,  $\sigma$ , and  $\zeta$ , i.e.,

the advantages to be gained from increasing  $\rho$ ,  $\sigma$ , and  $\zeta$ . Since the formation of  $P$  is at the expense of growth of  $Z$  and involves the consumption of  $R$  and  $S$ , the optimal policy will only demand the formation of  $P$  if the advantage  $f_\pi$  sufficiently dominates the other alternative of growth ( $\lambda = 0$ ). Thus the criterion  $\Delta > 0$  defines the lag phase, whereas  $\Delta < 0$  is the growth phase.

### 3. Boundary Conditions and Solution

When there is no nutrient  $R$  to begin with, the growth process cannot take place whatever the levels of  $P$ ,  $S$ , and  $Z$  may be. Thus

$$f(0, \sigma, \pi, \zeta) \equiv 0 \quad (67)$$

and so  $f_\sigma = f_\pi = f_\zeta = 0$  when  $\rho = 0$ . Also  $f_\rho > 0$ , for if a little  $R$  is present some growth is possible. Hence, at  $\rho = 0$ ,

$$\Delta = -\beta f_\rho - 1 < 0$$

and at the last the optimal policy is certainly to grow. This again is common (if somewhat Epicurean) sense, for when very little nutrient is left there is no point in expending it to enhance capacity for a growth that cannot take place—"let us eat, drink, and be merry, for tomorrow we die." Since  $\lambda = 0$  the partial differential equation (65) reduces to

$$\Gamma \equiv \gamma(1 + f_\zeta) - \omega f_\sigma - f_\rho = 0 \quad (68)$$

This is a conventional partial differential equation and may be integrated by the method of characteristics. The characteristic equations are

$$\frac{d\zeta}{ds} = \gamma, \quad \frac{d\rho}{ds} = -1, \quad \frac{d\sigma}{ds} = -\omega, \quad \frac{d\pi}{ds} = 0 \quad (69)$$

$$\frac{df}{ds} = -\gamma \quad (70)$$

$$\begin{aligned} \frac{df_\zeta}{ds} &= 0, & \frac{df_\rho}{ds} &= -\left(\frac{\partial\gamma}{\partial\rho}\right)(1 + f_\zeta), & \frac{df_\sigma}{ds} &= -\left(\frac{\partial\gamma}{\partial\sigma}\right)(1 + f_\zeta), \\ & & \frac{df_\pi}{ds} &= -\left(\frac{\partial\gamma}{\partial\pi}\right)(1 + f_\zeta) \end{aligned} \quad (71)$$

We observe that Eqs. (69) are just the growth equations (52), (53), and (55), with  $\lambda = 0$ . The characteristic equations (71) give

$$\frac{d\Delta}{ds} = \alpha\left(\frac{\partial\gamma}{\partial\sigma}\right) + \beta\left(\frac{\partial\gamma}{\partial\rho}\right) - \left(\frac{\partial\gamma}{\partial\pi}\right) \quad (72)$$

since by Eqs. (67) and (71)  $f_\zeta \equiv 0$ . From Eq. (68), when  $\rho = 0$ ,  $f_\rho = \gamma$ ; so the

equation for  $\Delta$  may be integrated with the condition  $\Delta = -1$  when

$$s = \rho = 0 \quad (73)$$

$\Delta$  will increase as  $\rho$  increases if

$$\frac{\partial \gamma}{\partial \pi} > \alpha \frac{\partial \gamma}{\partial \sigma} + \beta \frac{\partial \gamma}{\partial \rho} \quad (74)$$

When  $\Delta$  changes sign, the growth phase ends, and we move into the lag phase. (It should be remembered that increasing  $\rho$  takes us *back* from the end of the process.) The equation for  $f$  is then  $\Gamma + \gamma\Delta = 0$ ; i.e.,

$$\gamma f_{\pi} - (\alpha\gamma + \omega)f_{\sigma} - (1 + \beta\gamma)f_{\rho} = 0 \quad (75)$$

The characteristic equations of this are

$$\frac{d\zeta}{ds} = 0, \quad \frac{d\rho}{ds} = -(1 + \beta\gamma), \quad \frac{d\sigma}{ds} = -(\omega + \alpha\gamma), \quad \frac{d\pi}{ds} = \gamma \quad (76)$$

$$\frac{df}{ds} = 0 \quad (77)$$

$$\begin{aligned} \frac{df_{\zeta}}{ds} &= 0, & \frac{df_{\rho}}{ds} &= (\beta f_{\rho} + \alpha f_{\sigma} - f_{\pi}) \left( \frac{\partial \gamma}{\partial \rho} \right) \\ \frac{df_{\sigma}}{ds} &= (\beta f_{\rho} + \alpha f_{\sigma} - f_{\pi}) \left( \frac{\partial \gamma}{\partial \sigma} \right), & \frac{df_{\pi}}{ds} &= (\beta f_{\rho} + \alpha f_{\sigma} - f_{\pi}) \left( \frac{\partial \gamma}{\partial \pi} \right) \end{aligned} \quad (78)$$

Hence

$$\begin{aligned} \frac{d\Delta}{ds} &= (\beta f_{\rho} + \alpha f_{\sigma} - f_{\pi}) \left\{ \left( \frac{\partial \gamma}{\partial \pi} \right) - \alpha \left( \frac{\partial \gamma}{\partial \sigma} \right) - \beta \left( \frac{\partial \gamma}{\partial \rho} \right) \right\} \\ &= \left\{ \alpha \left( \frac{\partial \gamma}{\partial \sigma} \right) + \beta \left( \frac{\partial \gamma}{\partial \rho} \right) - \left( \frac{\partial \gamma}{\partial \pi} \right) \right\} (\Delta + 1) \end{aligned} \quad (79)$$

This shows that both  $\Delta$  and its derivative are continuous at the transition from the growth to the lag phases and  $\Delta$  will continue to increase so long as the criterion (74) obtains. This lays out the whole solution in terms of ordinary differential equations.

#### 4. A Specific Form for the Growth Rate

We now take a specific form for  $\gamma(\rho, \sigma, \pi)$  in order to obtain definite equations and results.  $\gamma$  must certainly vanish if either of the nutrients is absent, and by our hypotheses it must increase with increasing  $\pi$ . Let us set

$$\gamma = a\pi^b\rho\sigma \quad (80)$$



so that with choice of  $a$  and  $b$  we can simulate a variety of conditions. If  $b = 1$ , the growth depends linearly on the critical product; for  $b < 1$  the increase of  $\pi$  is ultimately less than linear suggesting an inhibition;  $b > 1$  implies a small effect for low values of  $\pi$  but a greatly enhanced effect for  $\pi \gg 1$ . The constant  $a$  puts an absolute magnitude on the growth rate; if we think of it as  $a'(\pi_c)^{-b}$ , it ascribes a critical value  $\pi_c$  to  $\pi$  above which inhibition ( $b < 1$ ) or enhancement ( $b > 1$ ) begins to take effect. Now Eq. (69) shows that  $\pi$  remains constant during the growth phase. Let  $\rho_f$  be its final value (and hence its value throughout growth) and let  $\rho_f = 0$ ,  $\sigma_f > 0$ , and  $\zeta_f$  be the final values of  $\rho$ ,  $\sigma$ , and  $\zeta$ . Then Eqs. (69) and (70) give

$$\rho = -s, \quad \sigma = \sigma_f - \omega s = \sigma_f + \omega \rho, \quad \pi = \pi_f \quad (81)$$

and

$$f = \zeta_f - \zeta = -a\pi_f^b \left\{ \frac{1}{3}\omega s^3 - \frac{1}{2}\sigma_f s^2 \right\} \quad (82)$$

$$= \frac{1}{2}a\pi_f^b \rho^2 \left\{ \sigma - \frac{1}{3}\omega \rho \right\} \quad (83)$$

The form of Eq. (83) is obtained from Eq. (82) by substituting for  $s$  from Eq. (81) so as to eliminate final values of everything except  $\zeta$ . By direct substitution it can be seen to satisfy the partial differential equation  $\Gamma = 0$ , Eq. (68). Substituting in  $\Delta$  gives

$$\Delta = -1 + \frac{1}{2}ab\pi^{b-1}\rho^2(\sigma - \frac{1}{3}\omega\rho) - \frac{1}{2}a\pi^b\rho\{(\alpha - \omega\beta)\rho + 2\beta\sigma\} \quad (84)$$

and the vanishing of  $\Delta$  gives a surface in  $\rho$ ,  $\sigma$ ,  $\pi$  space that corresponds to the transition from the lag to the growth phase. Let us explore this surface a little.

The equation  $\Delta = 0$  can be solved for  $\sigma$  in terms of  $\pi$  and  $\rho$  which will allow us to plot contours of the surface for constant  $\pi$  in the  $\rho$ ,  $\sigma$  plane. In fact,

$$\sigma = \frac{1 + \frac{1}{2}a\pi^b(\alpha - \omega\beta)\rho^2 + \frac{1}{6}ab\pi^{b-1}\omega\rho^3}{a\pi^{b-1}\rho(\frac{1}{2}b\rho - \beta\pi)} \quad (85)$$

so that  $\sigma$  is positive if  $\rho > 2\beta\pi/b$  and this is an asymptote for the contour of constant  $\pi$ . Since we have assumed that the nutrient  $S$  is not exhausted first, we have  $\sigma_f \geq 0$ ; we are only interested in the region  $\sigma > \omega\rho$ . For plotting these contours it is convenient to make a scale change through the definitions

$$\xi = b\rho/2\beta, \quad \eta = b\sigma/2\beta\omega, \quad V = b^2/4a\beta^3\omega, \quad W = 1 - \alpha/\beta\omega \quad (86)$$

Then

$$\eta = \frac{V\pi^{1-b} - \frac{1}{2}W\pi\xi^2 + \frac{1}{3}\xi^3}{\xi(\xi - \pi)} \quad (87)$$

reduces the equation to the form with fewest disposable parameters. In the  $\xi$ ,  $\eta$  plane we are only interested in the region  $\eta \geq \xi$ .

We note that  $\omega$  is the ratio of the rates of usage of the two nutrients  $S$  and  $R$  during growth phase; and  $\alpha/\beta$  is this ratio during the lag phase, with small  $C_x$ . Figures 2, 3, 4, and 5 show sets of contours for  $V = 0.125$  [cf.

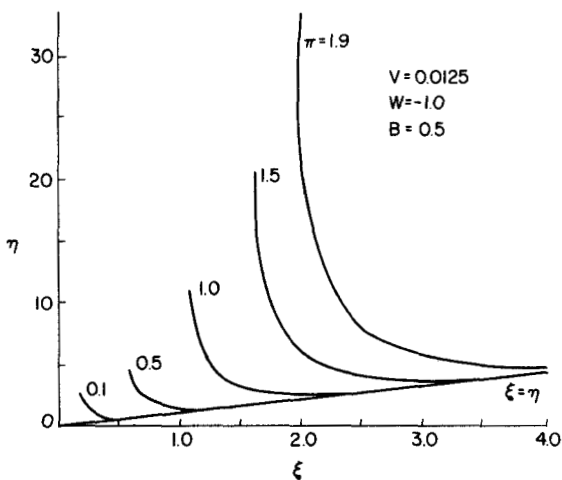


FIG. 2. Contours of the switching surface.

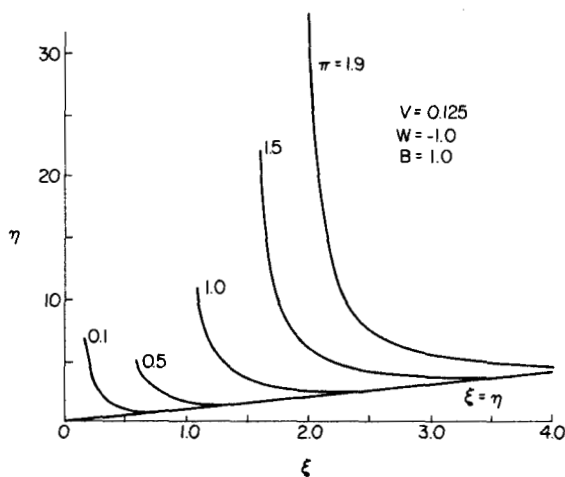


FIG. 3. Contours of the switching surface.

Eq. (86)],  $\alpha = \beta$ , and  $\omega = 0.5$  (i.e.,  $W = -1$ ), with an increasing sequence of the exponent  $b$  [cf. Eq. (80)]. For  $b = 0.5$  and  $1.0$  the surface is a smooth and fairly uniform ramp. For  $b > 1$  the first term dominates when  $\pi$  is small; so

the surface curves back and under, near the plane  $\pi = 0$ . The sequence of Figs. 6, 3, and 7 shows the effect of increasing  $V$  at constant  $W$  and  $b$ , i.e., of decreasing  $a$  or decreasing  $\beta$  (or  $\omega$ ) with  $\alpha = \beta$  (or  $\alpha = 2\beta\omega$ ). This evidently

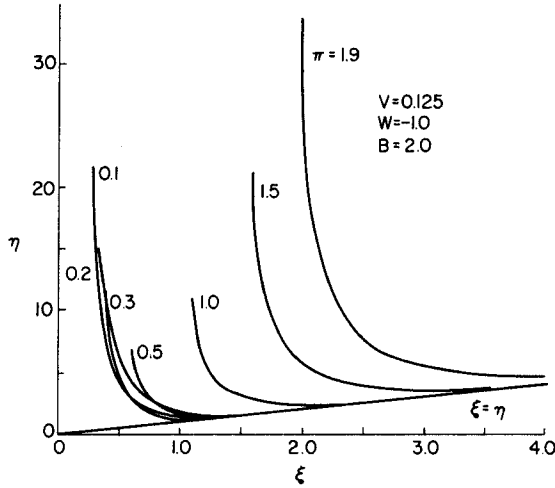


FIG. 4. Contours of the switching surface.

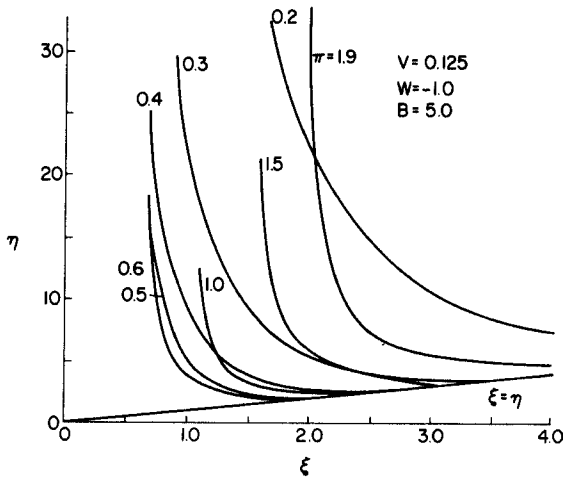


FIG. 5. Contours of the switching surface.

moves the surface away from the  $\eta$  axis but does not change its shape. A comparison of Figs. 3 and 8 shows a much more pronounced effect from an increase of  $\alpha$  from  $\alpha = 2\beta\omega$  to  $\alpha = 8\beta\omega$ . Hence the effect of increasing the

ratio  $\alpha/\beta$  is to bring back the switching surface and to give a longer growth period.

We notice that, except for  $b > 1$  with small  $\pi$ , the effect of increasing  $\pi$  for given  $\rho$ ,  $\sigma$  (or  $\xi$ ,  $\eta$ ) is to bring a point beneath the surface nearer to it.

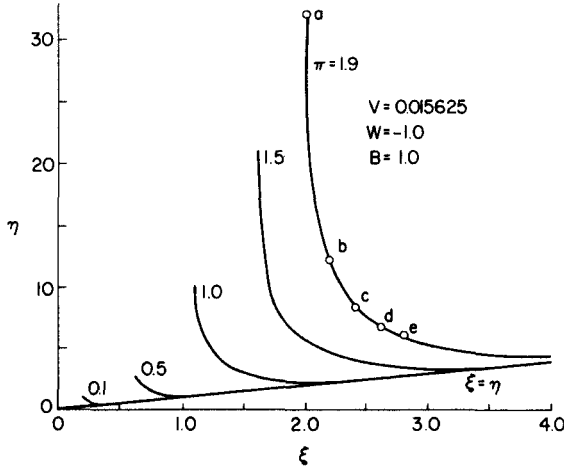


FIG. 6. Contours of the switching surface (see Fig. 3 for  $V = \frac{1}{8}$ ).

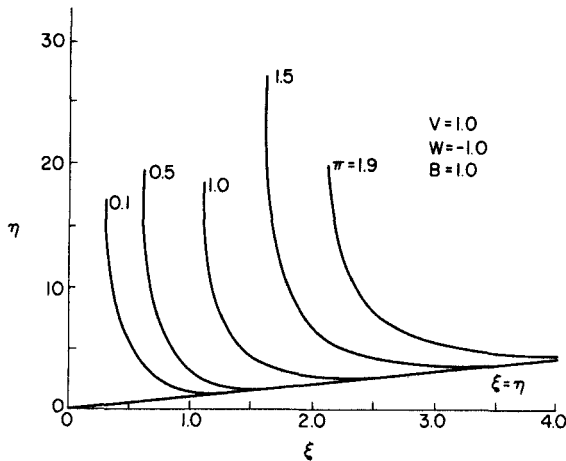


FIG. 7. Contours of the switching surface (see Fig. 3 for  $V = \frac{1}{8}$ ).

In fact, the value of  $\pi$  on the contour passing through a given nutrient point  $(\xi, \eta)$  is the level of critical product for which growth starts immediately. This again is in accordance with a biologically sensible picture.

### 5. The Solutions in the Lag and Growth Phases

With this understanding of the transition from lag to growth, we can set down the equations for the two phases. Let a suffix "s" denote a value at the switching point so that  $\eta_s$ ,  $\xi_s$ , and  $\pi_s$  satisfy Eq. (87). The value of  $\zeta_s$  depends actively on the initial value  $\zeta$  since it has been constant during the

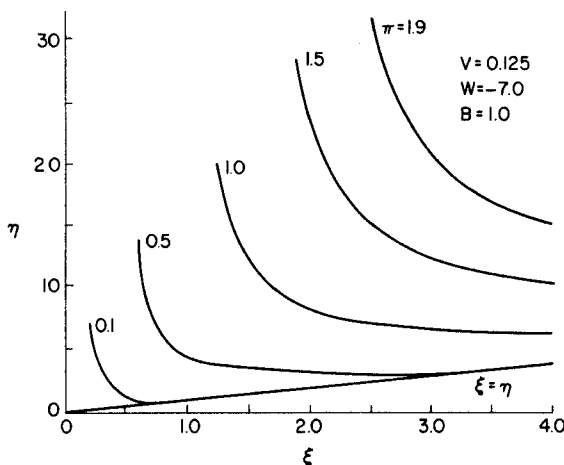


FIG. 8. Contours of the switching surface for  $W = -7.0$  (see Fig. 3 for  $W = -1.0$ ).

lag phase; we could normalize it to 1, except that the usage of the two nutrients during the lag phase does depend upon it. Since the change of variables given in Eq. (86) has proven useful for the switching surface when  $\gamma$  is given by (80), we will use it also for the growth equations. In addition, let us set

$$\chi = \frac{1}{2}bV\zeta \quad \text{and} \quad \tau = k_4 t / \beta V \quad (88)$$

Then during the growth phase

$$\frac{d\eta}{d\xi} = 1, \quad \frac{d\pi}{d\xi} = 0, \quad \frac{d\chi}{d\xi} = -\pi^b \xi \eta, \quad \frac{d\zeta}{d\xi} = \frac{-1}{\chi} \quad (89)$$

These equations may be integrated by quadratures from the switching surface, and give

$$\eta = (\eta_s - \xi_s) + \xi, \quad \pi = \pi_s \quad (90)$$

$$\chi = \chi_s + \pi_s^b \left\{ \frac{1}{2}(\eta_s - \xi_s)(\xi_s^2 - \xi^2) + \frac{1}{3}(\xi_s^3 - \xi^3) \right\} \quad (91)$$

$$\tau = \tau_s + \int_{\xi_s}^{\xi} \frac{d\xi}{\chi(\xi)} \quad (92)$$

Thus  $\chi_f$  (the final value of  $\chi$ , the amount of the organism present) is given by

$$\begin{aligned}\chi_f - \chi_s &= \frac{1}{6}\pi_s b \xi_s^2 (3\eta_s - \xi_s) \\ &= \frac{1}{12}\pi_s b \xi_s \frac{6V + \pi_s \xi_s^2 (2 - 3W)}{(\xi_s - \pi_s)}\end{aligned}\quad (93)$$

and the switching surface might itself be marked with contours of  $(\chi_f - \chi_s)$ .

Figure 9(a) shows  $(\chi - \chi_s)$  as a function of  $\xi$  during growth for five switching points,  $a, \dots, e$ , located on the contour  $\pi = 1.9$  in Fig. 6. These curves can be brought closer together if  $(\chi - \chi_s)/\xi_s \eta_s$  is plotted against  $\xi/\xi_s$  as shown in Fig. 9(b). From Eqs. (91) and (92) we can determine the actual

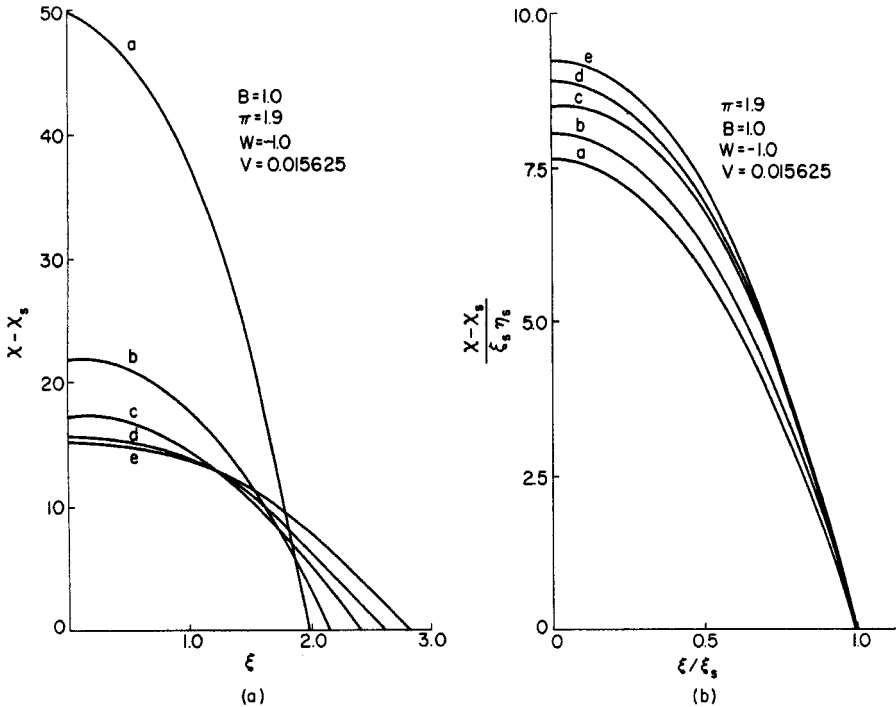


FIG. 9(a, b). Amount of growth as a function of substrate concentration for different initial substrate concentrations.

course of growth  $\chi(\tau)$ . This will depend on the value of  $\chi_s$  as the equations clearly show. Figure 10 shows  $\chi(\tau)$  for the trajectories from points  $a, \dots, e$  and for  $\chi_s = 10/128, 1/128, 1/1280$ . As  $\chi_s \rightarrow 0$ , the time to achieve the final value  $\chi_f$  tends to increase without bound. In fact for small  $\chi_s$

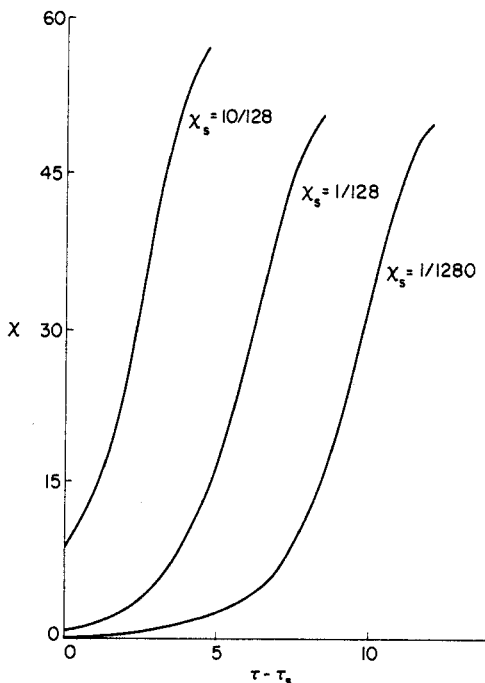


FIG. 10. Time course of growth for different initial inoculum sizes.

$$\tau - \tau_s \sim \frac{1}{\pi_s^b \xi_s \eta_s} \ln \left\{ 1 + \frac{\pi_s^b \xi_s \eta_s}{\chi_s} (\xi_s - \xi) \right\} + O(1) \quad (94)$$

where  $O(1)$  denotes a term that remains bounded as  $\chi_s \rightarrow 0$ . For large  $\chi_s$

$$\begin{aligned} \tau - \tau_s \sim \frac{\xi_s - \xi}{\chi_s} \left[ 1 - \frac{\pi_s^b}{12\chi_s} \{ (4\eta_s - \xi_s) \xi_s^2 \right. \\ \left. - 2(\xi_s + \eta_s) \xi (\xi_s + \xi) - \xi^3 \} \right] + O(\chi_s^{-3}) \end{aligned} \quad (95)$$

The switching surface and growth phase are shown in Fig. 11(b), where from the contour of constant  $\pi_s$  on the switching surface several trajectories with ordinate  $\chi - \chi_s$  above the  $\pi_s$  plane (i.e.,  $\chi - \chi_s + \pi_s$  above the base plane) are shown. This may be called a growth surface generated by this particular section of the switching surface.

During the lag phase Eqs. (76) and (77) apply, which in the current notation give

$$\frac{d\chi}{d\xi} = \frac{df}{d\xi} = 0, \quad \frac{d\eta}{d\xi} = 1 - W \frac{\beta\gamma}{1 + \beta\gamma}, \quad \frac{d\pi}{d\xi} = -\frac{2}{b} \frac{\beta\gamma}{1 + \beta\gamma} \quad (96)$$

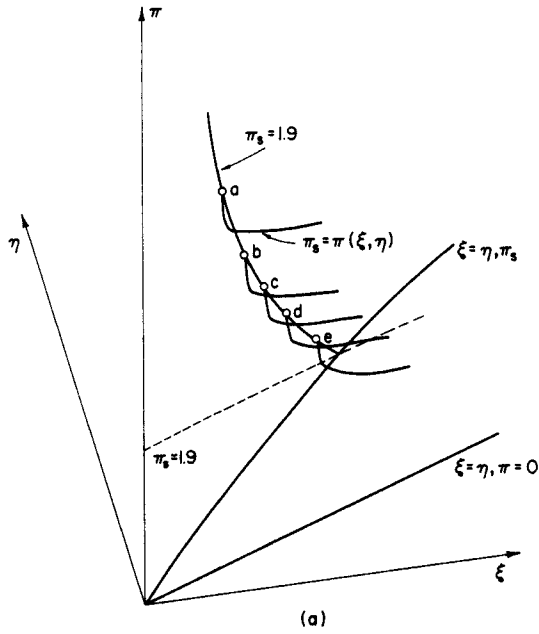


FIG. 11(a). Switching surface and the lag phase as calculated from the model. Three-dimensional plot.

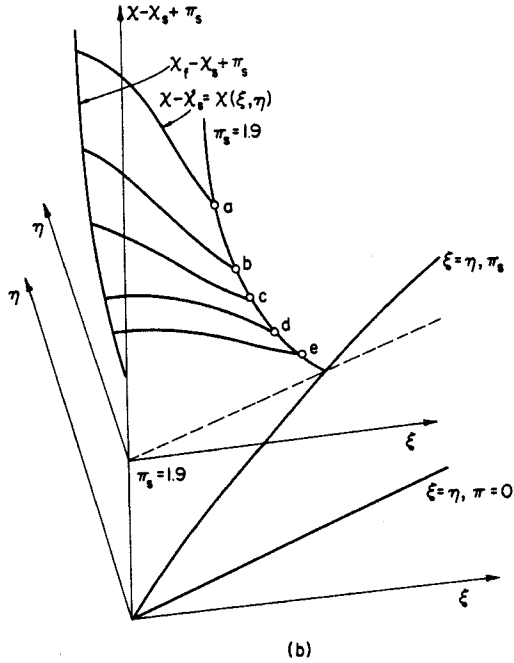


FIG. 11(b). Switching surface and growth phase as calculated from the model. Three-dimensional plot.



where

$$\beta\gamma = \beta a \eta^b \rho \sigma = \pi^b \xi \eta / V \quad (97)$$

These equations are less easy to integrate, apart from the first two which give  $\chi = \chi_s, f = f_s$  trivially. We do however notice that

$$\frac{d\pi}{d\xi} = \frac{2}{bW} \left( \frac{d\eta}{d\xi} - 1 \right)$$

Hence the trajectory reaching the switching surface at  $\xi_s, \eta_s, \pi_s$  must lie in the plane

$$\pi = \pi_s + \frac{2}{bW} \{(\eta - \eta_s) - (\xi - \xi_s)\} \quad (98)$$

If  $W < 0$  (i.e.,  $\alpha > \beta\omega$ ) the projection of the trajectory in the  $\xi, \eta$  plane climbs the plane of Eq. (98) from above the line  $\eta = \xi + \eta_s - \xi_s$ ; if  $W > 0$ , the trajectory again climbs the plane of Eq. (98), but this time from below the line  $\eta = \xi + \eta_s - \xi_s$ . In the special case  $W = 0$  the projection of the trajectory is the line of unit slope through  $(\xi_s, \eta_s)$ . It would be possible to use Eq. (98) to obtain an equation entirely in terms of  $\xi$  and  $\eta$ , but it is better to integrate these equations numerically from the point of attachment to the switching surface.

In any event we can learn a lot about the general shape of the solutions of these equations. We observe first that, as we go back in time and  $\xi$  increases,  $\pi$  will decrease for  $d\pi/d\xi$  is certainly negative. Hence either it will vanish for some  $\xi$  or will go asymptotically to zero. By Eq. (98) it must vanish on or be asymptotic to the line

$$\eta = \eta_0 + \xi = (\eta_s - \xi_s + \frac{1}{2}bW\pi_s) + \xi \quad (99)$$

This is possible for  $b > 1$ , for then

$$\pi^{1-b} \sim \left( \frac{b-1}{bV} \right) (\eta_0 + \frac{2}{3}\xi) \xi^2 \quad (100)$$

and

$$\beta\gamma \sim \left( \frac{3}{2} \frac{b}{b-1} \right)^{b/(b-1)} V^{1/(b-1)} \xi^{-(b+2)/(b-1)} \quad (101)$$

or for  $b = 1$ , when

$$\pi \sim \exp[-(1/V)(\eta_\infty + \frac{2}{3}\xi)\xi^2] \quad (102)$$

and

$$\beta\gamma \sim V\xi(\eta_\infty + \xi) \exp[-(1/V)(\eta_\infty + \frac{2}{3}\xi)\xi^2] \quad (103)$$

However, if  $b < 1$ , it is possible to reach the plane  $\pi = 0$  in a finite time. This

again is reasonable, for  $b < 1$  represents an enhancement of the rate at low values of  $\pi$ ; hence, it is possible to start from a zero value of  $\pi$ , and reach the switching surface in a finite time. The time is given by the integral

$$\tau_s - \tau = \frac{bV}{2\chi_s} \int_{\pi}^{\pi_s} \frac{d\pi}{\pi^b \xi \eta} \quad (104)$$

where  $\xi$  and  $\eta$  have to be evaluated along the path. Again this is dependent on  $\chi_s = \chi_0$ , the concentration of  $Z$  at the start, and it would be possible to get asymptotic expressions for large times.

The curves of Fig. 11(a) for which the ordinate is  $\pi$  show the development of the critical product. Figures 12 and 13 show variation of  $(\pi_s - \pi)$  with

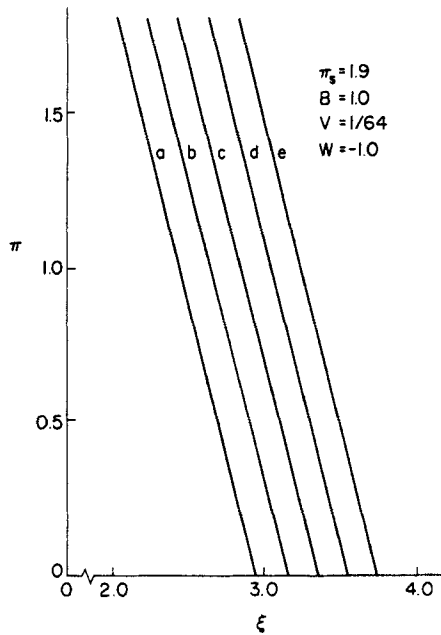


FIG. 12. Concentration of critical product during the lag phase as a function of limiting nutrient concentration.

$(\xi - \xi_s)$  and  $(\tau_s - \tau)$ , respectively, for the trajectories which join to those of Figs. 9 and 10. Figures 12 and 13 show the lag phase paths  $\pi$  vs  $\xi$  and  $\pi$  vs  $\tau$ .

It may also be shown at the expense of algebraic labor that, when  $b > 1$ , the path during the lag phase goes asymptotically to the upper side of the underfolded switching surface. Here the lag phase is never preceded by a growth phase; also, growth is not possible if the initial concentration of  $P$  puts the point  $(\xi, \eta, \pi)$  below the switching surface. This also would seem to

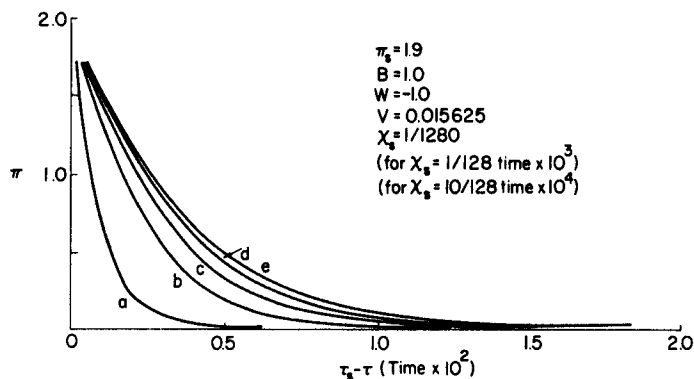


FIG. 13. Concentration of critical product during the lag phase as a function of time, for various initial limiting substrate concentrations.

accord with the fact that  $b > 1$  makes the effect of small  $\pi$  most unfavorable.

#### 6. Transfer into Fresh Nutrient

As an example of a known bacteriological phenomenon which this model exhibits we may consider a culture during its growth phase transferred into fresh medium; Fig. 14 shows a typical result taken from the calculations with

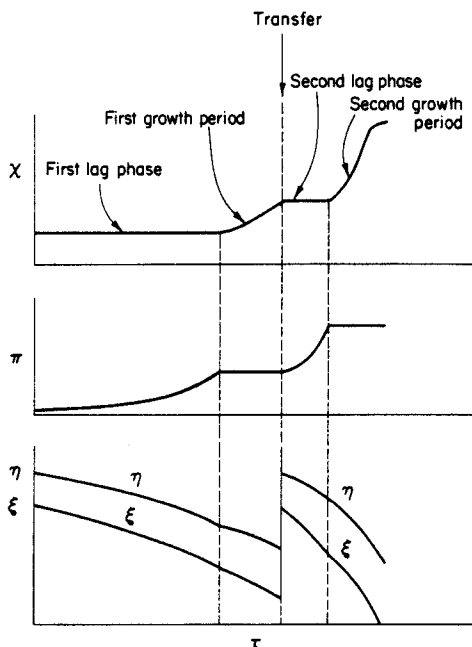


FIG. 14. Lag and growth phenomena upon transfer of cells as predicted from the model.

parameter values  $V = 1/64$ ,  $W = -1$ ,  $b = 1$ . The first growth phase is preceded by a long lag phase during which the critical product rises to the switching value. After the growth period has started, but before the nutrient has been exhausted, the nutrient concentrations are restored to their original values. There follows a shorter lag phase and a subsequent period of much more rapid growth.

This indeed suggests one of the tests of this model, for if the switching surface has the form we have supposed then there should be values of  $R$  and  $S$  for which the second lag phase just becomes zero. This would allow the experimental determination of the switching surface and hence of the function  $\gamma(\rho, \sigma, \pi)$ .

### 7. An Improved Model

The first model has been examined in sufficient detail to show that it has some promise at least, but it is useful to exhibit a slight extension that will embrace the whole life cycle of a culture. The same basic picture is retained, save that the usage of the nutrients is now divided into three parts:

- (i) to preserve the viability of  $Z$  at rates proportional to  $C_z$ ;
- (ii) in the reproduction of  $Z$  at rates proportional to  $dC_z/dt$ , provided that  $dC_z/dt > 0$  (if  $Z$  is actually decreasing we do not allow it to reform the nutrients);
- (iii) to form  $P$  at rates proportional to  $dC_p/dt$ .

Thus we would have

$$\frac{dC_r}{dt} = -k_1 C_z - k_2 \frac{dC_z}{dt} - k_3 \frac{dC_p}{dt} \quad (105)$$

$$\frac{dC_s}{dt} = -k_4 C_z - k_5 \frac{dC_z}{dt} - k_6 \frac{dC_p}{dt} \quad (106)$$

For the growth of  $Z$  we have a similar law to that of the previous model with

$$\frac{dC_z}{dt} = K(C_r, C_s, C_p)C_z - k_7 \frac{dC_p}{dt} \quad (107)$$

where this time the form of  $K$  is  $aC_p^b C_r C_s - \Theta$ . The new constant  $\Theta$  that has been introduced here is a constant death rate. If the rate of formation of  $P$  is proportional to  $C_z$  and is again the biological control variable, we may write

$$\frac{dC_p}{dt} = \frac{k}{k_7} C_z \quad (108)$$

and then

$$\frac{dC_z}{dt} = (K - k)C_z \quad \text{and} \quad 0 \leq k \leq K \quad (109)$$

We shall not treat this model further, but it is clear that it can also include a phase of decline when, the nutrients being exhausted, the population decreases exponentially.

## V. Models and Experimental Results

Establishment of the validity of a model of any natural phenomenon rests on the agreement of observations with predictions. Although the term "agreement" is somewhat subjective, we may say that a model is valid when: (i) it correctly predicts trends *in a number of cases*; and (ii) discrepancies between predictions and observations are within the latitude allowed by uncertainties of measurement and uncontrollable experimental variables.

It is important to note that the model should be applied to more than one case; if this is not done, the model is really a "curve fit" and does not command much respect or confidence. A model first becomes plausible if it reproduces observations for two cases quite different from each other. One ought not to rule out a model if it does not yield correct predictions for *all* imaginable experimental situations; the model may be valid for a few special sets of conditions, and it is then the task of inductive research to expand the scope of the model to new conditions.

Consider Monod's model of growth. It is often possible to arrange experimental conditions so that a single substrate does in fact limit growth. One can then proceed to test the more quantitative aspects of the model. Monod's model has been applied to two cases: batch growth and continuous propagation. To fulfill the first requirement for a valid model, it should predict the results of (say) continuous propagation from batch data, if the model is to be accepted.

Figure 15, in terms of dimensionless quantities, shows expected results of Monod's model for continuous propagation; productivity  $P$  is the amount of biomass formed per unit time per unit volume of culture:

$$P = QC/V = C/\theta \quad (110)$$

Herbert *et al.* (H10) studied the growth of *Aerobacter cloacae* in both continuous and batch propagators. The limiting substrate was glycerol. Constants  $\mu$  and  $a$  were determined from batch data; the constant  $K$  was determined from the holding time at which productivity was a maximum in continuous propagation—not highly accurate, but the best that could be done under the experimental circumstances.

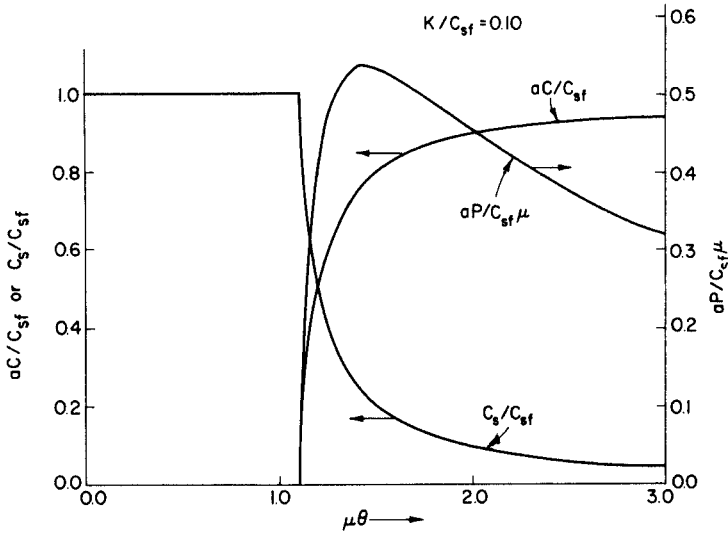


FIG. 15. Continuous propagation—predictions of Monod's model for steady-state values of various quantities as functions of holding time.

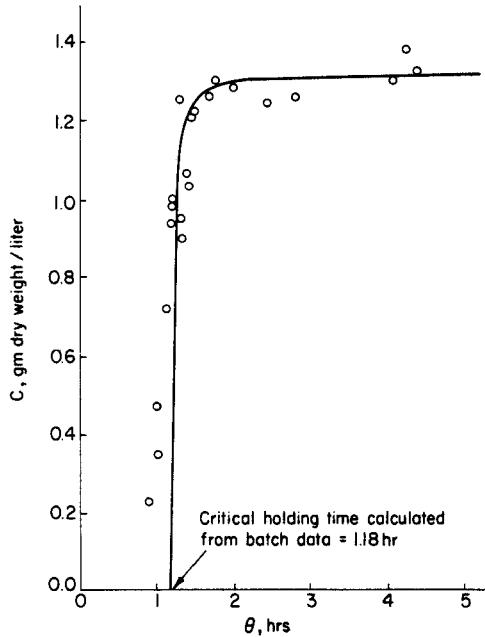


FIG. 16. Comparison of Monod's model with data of Herbert *et al.* (H10) on growth of *Aerobacter cloacae*. Solid line calculated from Monod's model with  $\mu = 0.85 \text{ hr}^{-1}$ ,  $K = 0.0123 \text{ g/liter}$ ,  $C_{sf} = 2.5 \text{ g/liter}$ , and  $a = 1.89 \text{ g/g}$ . Replotted from *J. Gen. Microbiol.* 14, 601-622 (1956), by permission of Cambridge University Press.

Experimental results of Herbert *et al.* are compared with predictions of Monod's model in Fig. 16. At long holding times, agreement of the model with experiment is good; this is not the case at holding times near the critical, where there is a definite trend not predicted by the model. Thus, it appears that the maximum specific growth rate ( $\mu$ ) is faster than that determined from batch experiments; also the stoichiometric coefficient  $a$  changes as  $\theta$  approaches the critical.

The authors remark that part of the discrepancy may be due to imperfect mixing in the culture vessel. They also imply that the discrepancies may point to inadequacies of the biological side of the model.

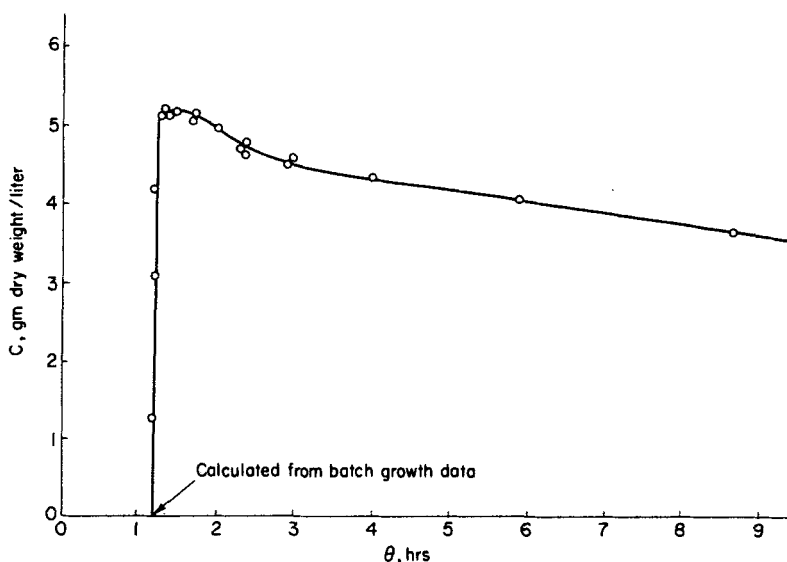


FIG. 17. Herbert's data (H8) on growth in continuous culture: *Aerobacter aerogenes* in glycerol medium. Replotted from p. 48 of "Continuous Culture of Microorganisms: A Symposium," by permission of the Publishing House of the Czechoslovak Academy of Sciences.

Figures 17 and 18 show the results of Herbert (H8) on continuous propagation of *Aerobacter aerogenes* and the yeast *Torula utilis*. Herbert states that, in both cases, the critical holding times agree well with values computed from results of batch experiments. At long holding times, however, there is considerable discrepancy from theory in the declining steady-state cell concentration.

Herbert attributes part of the discrepancy to the occurrence of endogenous metabolism, not accounted for in Monod's model. In other words, cells not only convert substrate into protoplasm, but they also carry on reactions

which consume cell substance. This effect can be incorporated into the model by writing

$$R_p = \frac{\mu C C_s}{K + C_s} - \mu_c C \quad (111)$$

in place of Eq. (38). Here  $\mu_c$  represents a rate constant for such reactions. Herbert states that incorporation of this term yields a curve having the trend shown in Figs. 17 and 18.

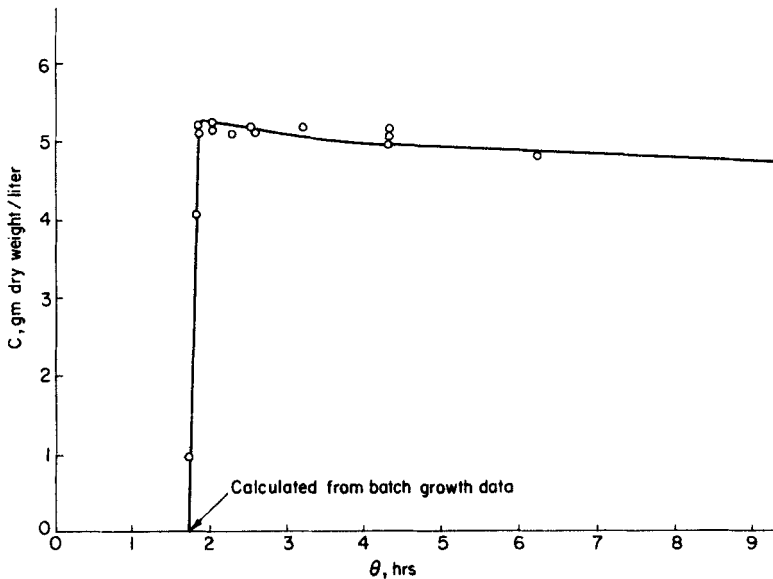


FIG. 18. Herbert's data (H8) on growth in continuous culture: *Torula utilis* in glucose medium. Replotted from p. 48 of "Continuous Culture of Microorganisms: A Symposium," by permission of the Publishing House of the Czechoslovak Academy of Sciences.

In a growing culture the rate of respiration may be assumed proportional to the rate of synthesis; that is,<sup>13</sup>

$$R_{\text{resp}} = \frac{\beta \mu C C_s}{K + C_s} \quad (112)$$

where  $\beta$  is a stoichiometric coefficient. From Eq. (22), the condition for steady

<sup>13</sup>  $R_{\text{resp}}$  is measured in terms of moles of oxygen consumed per unit volume of culture per unit time. Strictly speaking, a term for endogenous metabolism should also be added to the right-hand side of Eq. (112). In growing cultures, however, this term is usually small; moreover, its inclusion would not alter the conclusions drawn below.



state in the continuous propagator is

$$R_p/C = 1/\theta$$

Hence, from Eqs. (111) and (112), we find that the specific respiration rate should be a linear function of  $1/\theta$ :

$$\frac{R_{\text{resp}}}{C} = \frac{\beta \mu C_s}{K + C_s} = \beta \left( \frac{1}{\theta} + \mu_c \right)$$

Figure 19 shows Herbert's data on the respiration of *Aerobacter aerogenes*.

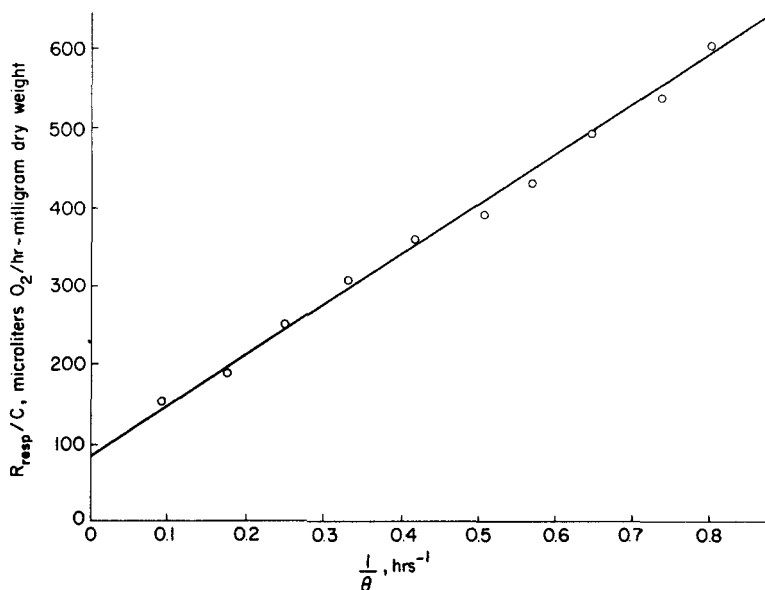


FIG. 19. Herbert's data (H8) on the specific rate of respiration of *Aerobacter aerogenes* in continuous culture. Replotted from p. 49 of "Continuous Culture of Microorganisms: A Symposium," by permission of the Publishing House of the Czechoslovak Academy of Sciences.

These data are in agreement with the foregoing equation, and serve as further confirmation of Herbert's hypothesis.

More recently, Marr and Harvey (M4) have pointed out that occurrence of endogenous metabolism will cause the yield of microbial mass obtained from unit mass of limiting substrate to change with holding time in continuous culture. Thus, if the apparent yield coefficient  $Y$  is defined as

$$Y \equiv \frac{R_p}{-R_s}$$

then Eq. (111) and the equation

$$-R_s = a \frac{\mu C C_s}{K + C_s} \quad (37a)$$

yield

$$1/Y = a(1 + \mu_c \theta)$$

where  $a$  is the true stoichiometric coefficient. Marr and Harvey were able to verify experimentally the foregoing linear relation between  $1/Y$  and  $\theta$  for a number of organisms.

Growth models of the Monod type have been applied to the microscopic, unicellular algae. Algae are plants (photosynthetic organisms) and as such show some interesting variations from heterotrophic organisms. The driving force for synthetic reactions in algae is not the energy stored in chemical substrates, but is in part, and sometimes exclusively, the energy of light absorbed by the pigment systems of algal cells. Hence, the growth rate of an alga is strongly dependent on the light intensity  $I$  seen by the cell.

A new circumstance arises here because the "concentration" of "limiting substrate" is the light intensity, and this can never be uniform in a propagator with an optical path of finite length. In other words, algal propagators cannot be assumed to be "perfectly stirred,"<sup>14</sup> and the macroscopic growth rate must be obtained by some sort of averaging procedure.

Tamiya *et al.* (T1) postulated that the *local* (microscopic) growth rate of an alga follows a kinetic expression similar to that of Michaelis and Menten:

$$R_p = \frac{\mu \nu C I}{\mu + \nu I} \quad (113a)$$

At high light intensities, this yields

$$R_p \approx \mu C \quad (113b)$$

and the growth process is said to be *light saturated*. The parameter  $\mu$  should be strongly temperature dependent. At low light intensities,

$$R_p \approx \nu C I \quad (113c)$$

The parameter  $\nu$  should be nearly temperature independent.

In an algal culture contained in a rectangular vessel of thickness  $L$  and irradiated from one side ( $I = I_0$  at  $x = 0$ ), the light intensity may be assumed

<sup>14</sup> However, Rieske *et al.* (R4) found that the rate of the so-called Hill reaction in chloroplast fragments depends on the *average* light intensity in a well-stirred suspension. This finding is consistent with the occurrence of "flashing light effects" (B9, E2, K4), and has been analyzed by Fredrickson *et al.* (F5). Miller *et al.* (M9) report a scheme to utilize the flashing light effect to improve the efficiency of light utilization by algal cultures.

to fall off according to Beer's law:

$$I = I_0 e^{-\varepsilon Cx} \quad (114)$$

Hence, the average growth rate is expected to depend on the absolute scale of the growth vessel.

The macroscopic rate of growth, assuming a uniform distribution of cells, is then

$$\begin{aligned} R_p &= \frac{1}{L} \int_0^L R_p(x) dx \\ &= \left[ \frac{\mu}{\varepsilon CL} \ln \frac{\mu + \nu I_0}{\mu + \nu I_0 e^{-\varepsilon CL}} \right] C \end{aligned} \quad (115)^{15}$$

Tamiya *et al.* (T1) found that Eq. (115) gave a good fit of their data for batch growth of *Chlorella ellipsoidea* in flat glass vessels. The expected temperature dependence of  $\mu$  and  $\nu$  was found, and the effect of incident light intensity was as predicted, though there was some inhibition of growth at very high incident intensities.

Equation (115) does not predict a limiting value of  $C$  in batch cultures. It must therefore be modified by inclusion of some sort of term for catabolism. The simplest assumption is

$$R_p = \left[ \frac{\mu}{\varepsilon CL} \ln \frac{\mu + \nu I_0}{\mu + \nu I_0 e^{-\varepsilon CL}} - \mu_c \right] C \quad (116)$$

where  $\mu_c$  is a constant.

Equation (116) may be substituted into Eq. (20) to yield an equation for continuous culture. The minimum holding time required to maintain a non-zero cell concentration is then given by

$$\frac{1}{\theta} + \mu_c = \frac{\mu \nu \bar{I}_0}{\mu + \nu I_0} \quad (117)$$

whereas in general

$$\frac{1}{\theta} = \frac{R_p}{C} \quad (22)$$

for steady state. Figure 20 shows a plot of steady-state concentration and productivity ( $C/\theta$ ) as a function of holding time for a particular choice of parameters in Eq. (116). The curve of productivity resembles that predicted by Monod's model for growth of nonphotosynthetic organisms. The shape of the concentration-holding time curve is typical of algal propagators (H3).

<sup>15</sup> Equation (115) shows that, at large values of  $C$ ,  $R_p$  becomes independent of  $C$ , so that batch growth should be *linear*. This is observed [see, e.g., Myers (M15)].

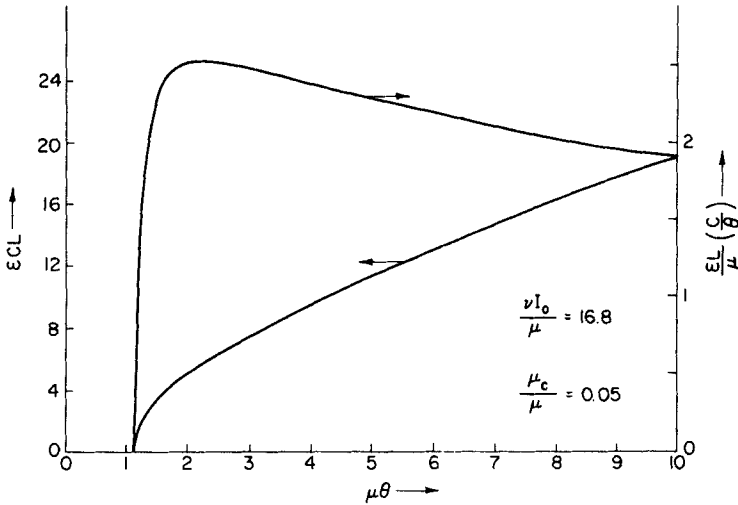


FIG. 20. Continuous propagation of algae as calculated from Eq. (116). Dimensionless cell concentration and productivity as a function of dimensionless holding time. The minimum holding time is a strong function of incident intensity,  $I_0$ .

Figure 21 is a plot of productivity vs steady-state cell concentration, calculated from the model with the same parameters as for Fig. 20.

The net rate of production of oxygen by growing algae may be postulated to be proportional to the growth rate  $R_p$ . Consumption of oxygen by respiration has already been accounted for in Eq. (116); this is the term involving

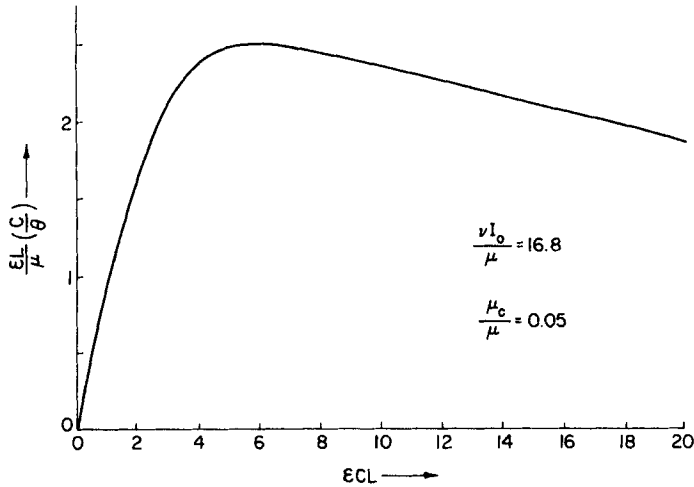


FIG. 21. Continuous propagation of algae as calculated from Eq. (116). Steady-state productivity as a function of steady-state cell concentration.

$\mu_c$ . Then  $R_{\text{photo}}$ , the net rate of oxygen production per unit volume of culture, is

$$R_{\text{photo}} = \beta R_p \quad (118)$$

where  $\beta$  is a stoichiometric coefficient. Hence, from Eq. (22),

$$\frac{R_{\text{photo}}}{C} = \beta \frac{R_p}{C} = \frac{\beta}{\theta} \quad (119)$$

That is, the specific net rate of photosynthesis should be proportional to the reciprocal holding time. Figure 22 shows data collected by Hanson *et al.* (H3) for photosynthesis in continuously propagated cultures of a *Chlorella* species. Equation (119) is seen to give a good "fit" of the experimental data; further corroboration of the theory is the fact that the stoichiometric coefficient  $\beta$  calculated from the overall stoichiometry of the photosynthetic reaction and cell compositions of *Chlorella* taken from the literature (M10) is in rough agreement with the value calculated from the data of Fig. 22.

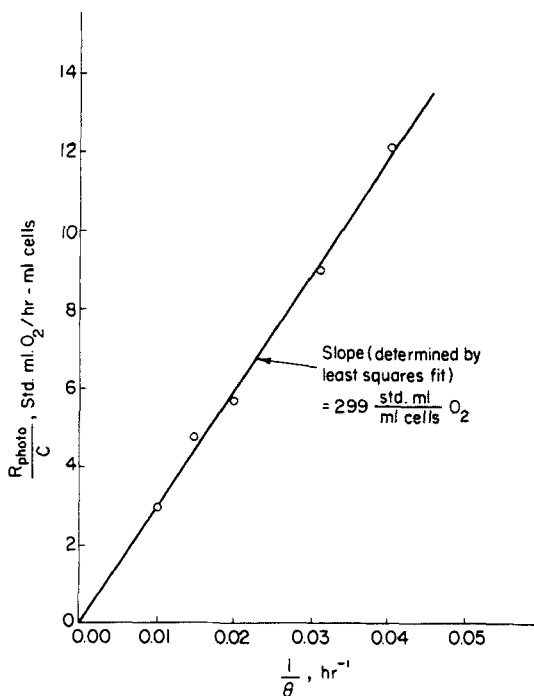


FIG. 22. Data of Hanson *et al.* (H3) on net specific rate of photosynthesis in continuous propagation of algae. This establishes the stoichiometric relation between growth and photosynthesis.

Myers and Graham (M16) studied the growth of *Chlorella ellipsoidea* in continuous culture. Their results are not given in such a way that direct comparison with the batch growth data of Tamiya *et al.* (T1) is possible; however, Myers and Graham found that the productivity at low cell concentrations seemed to be predictable from batch data which they obtained.

Trends of the experimental results of Myers and Graham can be compared with those predicted by Eq. (116). Figure 23 shows the experimental data of

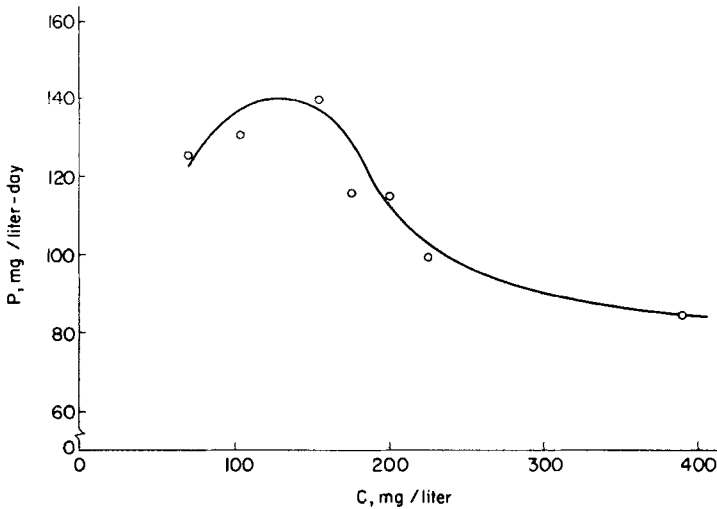


FIG. 23. Productivity of continuous *Chlorella* cultures as determined by Myers and Graham (M16). This should be compared with Fig. 21. Replotted from *Plant Physiol.* **34**, 345-352 (1959), by permission of the American Society of Plant Physiologists.

Myers and Graham. Qualitative agreement of the model with experimental results is indicated in the region of maximal productivity; at high algal concentrations, however, the productivity predicted by the model falls off incorrectly. Hence, the simple model outlined is somewhat inadequate.

Myers and Graham give three additional sets of experimental data which might account for some of the discrepancy. First, they noted that Beer's law is not strictly followed by the algal populations used. Deviations from Beer's law might have been apparent, rather than real, and might be attributed to edge effects. This is a practical, rather than a conceptual difficulty, of course.

Second, manometric experiments on cells taken from steady-state cultures at different holding times showed that the respiration rate of cells per unit mass was not constant; instead, respiration rate fell off with increasing holding time of the steady-state culture.

This result is reminiscent of Herbert's data (H8) on the respiration of

bacteria in continuous culture and of the data of Hanson *et al.* (H3) on photosynthesis in continuous culture. This effect is not necessarily the same, however, and may be indicative of a general slowing down of metabolism in slowly growing cultures.

Finally, Myers and Graham determined irradiance curves<sup>16</sup> for algal cells suspended in buffer solutions; cells were taken from steady-state cultures at different holding times again. At low light intensities, irradiance curves for cells were nearly independent of steady-state holding time. At saturating intensities, however, it was found that photosynthetic rate fell off with increasing holding time. This occurred in spite of the fact that chlorophyll content was highest in cells taken from high population density cultures.

The examples given show that there are marked variations in physiological characteristics of cells taken from continuous cultures at different steady-state conditions. This is also true of cells taken from different phases of batch cultures [see, e.g., Malmgren and Hedén [M3]]. Again, one observes considerable changes in morphology of cells at different conditions in both

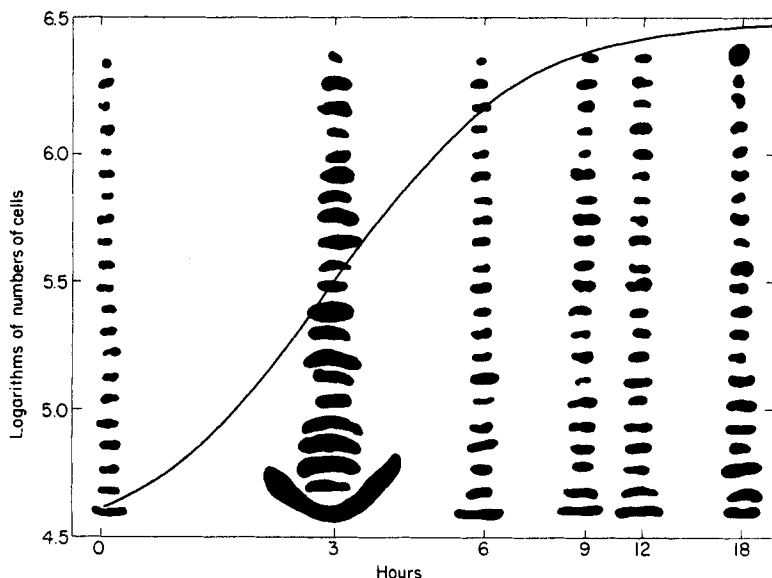


FIG. 24. Henrici's results (H7) showing morphologic variation during batch growth of *Bacillus coli* (*E. coli*). The shapes and sizes of cells selected at random were as suggested by the drawing. Redrawn from "Morphologic Variation and the Rate of Growth of Bacteria," by permission of Charles C. Thomas, Publishers.

<sup>16</sup> An irradiance curve is a plot of photosynthetic rate, as measured by oxygen production per unit cell mass, vs light intensity. Conditions are arranged so that little light is absorbed in passing through the suspension; averaging of rates is thus not necessary.

batch and continuous cultures [see Henrici (H7) and Herbert (H9)]. Figure 24, taken from Henrici's classic work, suggests this.<sup>17</sup>

Clearly, morphologic changes and physiologic changes are correlated in some fashion; Monod's model or extensions of it give no clue as to what this correlation might be. Hence, the basic reason for discrepancies between the model and experiment is probably due to failure of the model to account for cellular *structure*. Models such as those of Ramkrishna (R3) will probably account for some physiologic changes. However, we are also interested in morphologic changes and in reproduction of cells, so that it becomes necessary to consider structured, *segregated* models.

## VI. Structured Models: Segregated

The concept of a structured but distributed model can be carried further than in Section IV. However, we turn instead to the more complicated case of structured and segregated models. In other words, we now acknowledge that the culture is made up of *individuals*. [It should be remembered that we are speaking about a culture of cells, not about a population of cells forming a multicellular organism or a tissue; in the latter case there may be "communication" between the cells such that intercellular events achieve a degree of synchrony (cf. G1).]

Cells are continually being formed by fission while others are growing, being washed out, etc., in a continuous culture. Hence, it follows that cells in a culture exhibit a *distribution* of structures. Therefore, the gross metabolic rates of the culture represent averages over the distribution of cell structures. One of the principal problems is then to establish the factors which determine the distribution.

A sophisticated model of the dynamics of cell populations would have to take the distribution of cell structures into account. This presupposes that one has a quantitative *measure* of cell structure. Such a measure is not a single, scalar quantity. Rather, one would have to specify, for instance, how many enzymes of each kind a cell had, the geometrical arrangement of the enzyme molecules, the number and location of RNA and DNA molecules, etc. Undoubtedly the measure for this kind of information would be a matrix (higher order tensor). No one has formulated such a measure, however; probably this is due to lack of basic knowledge concerning the dynamics of subcellular processes.

As a slight digression, we can deduce from the foregoing a principle of

<sup>17</sup> Consideration of varying transport properties of cell walls and membranes may be important in the explanation of why sizes and shapes of microorganisms vary during the different phases of growth.



importance long recognized by those concerned with cultivation of microbial forms. Since structure is described by a set of quantities, rather than by a single quantity, the rate of change of structure—that is, the *growth rate of a cell*—is also described by a set of quantities. Moreover the set of quantities describing the structure follows different paths of development under different circumstances of propagation, so that the set of quantities in the growth-rate measure will bear different relations to one another. Hence a correlation between two simple measures of growth rate, say rate of increase of cell mass and rate of increase of cell numbers, may not be expected to hold when one alters the circumstances of propagation. To put it more precisely, it is not possible to predict the results of continuous propagation from the results of batch propagation when only single measures of growth rate are used. This was, of course, the point of Ramkrishna's work (R3).

#### A. STEADY-STATE PROPAGATION: THE AGE MODEL

To return to the principal line of development, one wonders if there is not some simplified semiempirical way of introducing cell structure (i.e., accounting for differences between cells) which can serve as a basis for a model. Several possibilities exist. The arguments for the first one, at least, are most easily developed by considering the steady state of a continuously propagated culture.

In such a culture, the environmental conditions “seen” by a cell are constant, on the average. By average, we mean the average over periods of time long in comparison to the reciprocal frequencies of random fluctuations of conditions on the molecular scale.<sup>18</sup> Moreover, the distribution of cell structures in this situation is constant.

Hence, if at one time (say,  $t$ ) we could pick out all cells of a given structure and “follow” this group of cells through its subsequent history, we could establish the distribution of structures in the culture. As a matter of fact, we can do this, in principle, by equating structure with *cell age* (which we herein-after denote by the symbol  $\tau$ ). We could also equate structure with cell *mass*, and this is done in Part C of this section.

We *define* the age of a cell as the length of time which has elapsed since the cell was formed by fission of its parent. We are arbitrary here, of course, since a definition of the instant of fission is required.<sup>19</sup> Nevertheless, the definition of age for our purpose must be quantitative and operational; it is to be distinguished sharply from qualitative and nonoperational terms such as “biological age,” etc., used in the literature.

<sup>18</sup> From the point of view of, say, a bacterial cell, these fluctuations may be rather important.

<sup>19</sup> We are aware that a septum in a potential daughter cell may begin to form before the septum in the parental cell is complete.

In general, the equation of cell age with cell structure can hold rigorously only in the steady state, and then only in the statistical sense. In the unsteady state, environmental conditions are changing with time so that the average pattern of development changes with time. The necessity for a statistical interpretation of our equation is due to two causes: first, random fluctuations of environmental and intracellular conditions on the molecular level mean that two cells having initially the same structure and exposed to the same environment (in the average sense) will develop at the same rate<sup>20</sup> only in the statistical sense; second, two cells just formed by fission (age  $\tau = 0$ ) will have identical structures only in the statistical sense. These factors require a model of populations of structured cells to be statistical in nature. This contrasts with models of populations of unstructured cells, where it was shown that the statistical approach was an unnecessary luxury.

Consider the following propositions concerning the fate of a cell in a steady-state, continuously propagated population:

- A. The cell is not washed out nor does it divide in the time interval  $\tau$  to  $\tau + \Delta\tau$ .
- B. The cell is present in the culture at time  $\tau$ .
- C. The cell was formed by fission of its parent at time zero (so that it has age  $\tau$  at time  $\tau$ ).

We seek the probability of  $(B | C)$ , of course; let this be

$$P(B | C) \equiv P(\tau) \quad (120)$$

so that

$$P(AB | C) = P(\tau + \Delta\tau)$$

Hence, by Rule 1 of the theory of probability,

$$P(AB | C) = P(A | BC) P(B | C)$$

or

$$P(\tau + \Delta\tau) = P(\tau) P(A | BC) \quad (121)$$

To get  $P(A | BC)$ , consider the propositions

- D. The cell divides in time  $\tau$  to  $\tau + \Delta\tau$ .
- E. The cell is washed out in time  $\tau$  to  $\tau + \Delta\tau$ .

By Rule 2 of the theory of probability,

$$P(A + D + E | BC) = 1 = P(A | BC) + P(D | BC) + P(E | BC)$$

or

$$P(A | BC) = 1 - P(D | BC) - P(E | BC) \quad (122)$$

<sup>20</sup> But as Schrödinger (S2) points out, the *results* achieved are deterministic, even though rates are subject to probability considerations.

This follows since A, D, and E are mutually exclusive and exhaustive events.

At this point, models must be introduced for the fission and washout processes. If we assume that the vessel is perfectly mixed, then washout probability ( $P(E | BC)$ ) is independent of cell age, and moreover

$$P(E | BC) = 1/\theta \Delta\tau + O[(\Delta\tau)^2] \quad (123)$$

where  $\theta = V/Q$  is the nominal holding time of a particle in the vessel. For the fission probability  $P(D | BC)$ , consider the most general assumption possible, namely,

$$P(D | BC) = \Gamma(\tau) \Delta\tau + O[(\Delta\tau)^2] \quad (124)$$

where  $\Gamma$  is an arbitrary (but nonnegative and at least piecewise continuous) function of cell age. By postulating the existence of the function  $\Gamma(\tau)$ , we are saying that the probability of fission of a cell changes with its age; viz., there is not much chance that a young cell will divide but there is a considerable chance that a somewhat older cell will divide in the given time interval when both are in identical environments. For the present, we need not specify the form of  $\Gamma(\tau)$ ; instead, we regard it as a quantity to be determined by experiment. Of course  $\Gamma(\tau)$  depends on environmental conditions, but since these are constant in steady-state culture, we need not express the dependence explicitly.

Equation (122) can now be written as

$$P(A | BC) = 1 - (1/\theta + \Gamma(\tau)) \Delta\tau - O[(\Delta\tau)^2] \quad (125)$$

so that Eq. (121) yields

$$P(\tau + \Delta\tau) = P(\tau)[1 - (1/\theta + \Gamma(\tau)) \Delta\tau - O[(\Delta\tau)^2]]$$

whence

$$\frac{dP(\tau)}{d\tau} = -(1/\theta + \Gamma(\tau)) P(\tau) \quad (126)$$

The initial condition for Eq. (126) is

$$P(0) = 1$$

so that

$$P(\tau) = \exp\left\{-\left(\frac{\tau}{\theta} + \int_0^\tau \Gamma(\tau') d\tau'\right)\right\} \quad (127)$$

We may give this result a frequency interpretation. Let  $U(\tau) d\tau$  be the number of cells, per unit volume of culture, having ages between  $\tau$  and  $\tau + d\tau$ . Then

$$U(\tau)/U(0) = P(\tau) \quad (128)$$

since in *steady-state* culture,  $U(\tau)/U(0)$  is the fraction of organisms formed at time zero which are still present, undivided, in the vessel at time  $\tau$ . Then by Eq. (127)

$$U(\tau) = U(0) \exp\left\{-\left(\frac{\tau}{\theta} + \int_0^\tau \Gamma(\tau') d\tau'\right)\right\} \quad (129)$$

which is the (nonnormalized) density of the age distribution function. This equation was also derived by Fredrickson and Tsuchiya (F4) by very different methods. Equivalent equations are given by Powell (P4) and Harris (H4).

The function  $\Gamma(\tau)$  could be determined indirectly if the ratio  $U(\tau)/U(0)$  could be determined. This is not possible, however, and a different but equivalent procedure must be used. In principle, it is possible to determine the distribution of division times in a population by microscopic examination. Let  $h(\tau)$  be the density of the distribution of division times; i.e.,  $h(\tau) d\tau$  is the probability that a cell has age between  $\tau$  and  $\tau + d\tau$  when it divides. Then, by Bayes' theorem [Eq. (A.6)], we easily find<sup>21</sup>

$$\Gamma(\tau) = h(\tau) \left(1 - \int_0^\tau h(\tau') d\tau'\right)^{-1} \quad (130)$$

Thus,  $\Gamma(\tau)$  can be calculated once  $h(\tau)$  has been measured experimentally, and the ratio  $U(\tau)/U(0)$  can then be calculated from Eq. (129).

The question now arises as to where subcellular kinetics and transport processes enter this picture. A partial answer is that these processes (along with the genetic capabilities of the organism) determine the function  $\Gamma(\tau)$ . We shall explore below a model of the reproduction process which leads to an explicit equation for  $\Gamma(\tau)$ .

Beyond the immediate problem of reproduction we are interested in the consumption of substrates by cells, the formation of new cellular material, and the release of metabolic by-products to the environment. One cannot ignore these questions; it is the growth of single cells that determines what the environmental conditions will be (apart from external controls applied), and the environmental conditions determine in turn what the growth and reproductive characteristics of the culture will be.

Suppose that we had either experimental or theoretical evidence concerning the growth rate of single cells in steady-state culture. In the most elementary approach, this information might be given as rate of increase of cell mass. In general, growth rate is not expressible as a single quantity, as stated earlier, but let us ignore this fact here. That is, we assume that the development of cells is independent of the particular circumstances of propagation.

<sup>21</sup> Harris (H4) also gives this equation (Section II, Part 1 of his paper).

Put  $r(\tau)$  equal to the average growth rate of a single cell of age  $\tau$ . The rate is expressed in terms of increase of cell mass and is taken to be an explicit function of cell age. Then the concentration  $C$  of biomass present may be established by material balance on the propagation vessel, the result for the steady state is

$$-\frac{C}{\theta} + \int_0^\infty r(\tau) U(\tau) d\tau = 0 \quad (131)$$

Again, if the addition of one unit of mass to a cell by growth consumes (on the average)  $\alpha_i$  mass units of the  $i$ th chemical species in the surrounding medium, material balance for the steady state yields

$$\frac{C_{if} - C_i}{\theta} - \int_0^\infty \alpha_i(\tau) r(\tau) U(\tau) d\tau = 0 \quad (132)$$

where  $C_i$  is the concentration of  $i$ th chemical species in the propagator effluent, and subscript  $f$  denotes feed conditions. If the  $i$ th species is a product of growth, then  $\alpha_i$  is negative, of course. Again, we assume that the stoichiometric coefficients  $\alpha_i$  depend on cell age.

The growth rate  $R_p$  and the stoichiometric coefficients  $a_i$  used in Monod's model represent averages over the distribution of cell ages. Thus, from Eq. (131) and the definition of  $R_p$ , we find

$$R_p = \int_0^\infty r(\tau) U(\tau) d\tau \quad (133)$$

and, from Eqs. (37) and (132),

$$a_i = \int_0^\infty \alpha_i(\tau) r(\tau) U(\tau) d\tau \bigg/ \int_0^\infty r(\tau) U(\tau) d\tau \quad (134)$$

In continuous, steady-state culture,  $R_p$  and  $a_i$  will in general depend on the holding time, since  $U(\tau)$  varies with holding time. Hence the model is able to account for dependence of stoichiometric coefficients and growth rates on the steady-state holding time; in Monod's model, there is no dependence of these quantities on holding time. It is possible, then, for the newer model to rationalize data such as those shown in Fig. 16.

Clearly the procedure just outlined is sufficient to establish a rather flexible model of continuous steady-state propagation. The information necessary for computational purposes is contained in the functions  $\Gamma(\tau)$ ,  $r(\tau)$ ,  $\alpha_1(\tau)$ ,  $\alpha_2(\tau)$ , ..., and it is these functions that describe intracellular dynamics. Present lack of understanding of these processes indicates that the functions  $\Gamma(\tau)$ , etc., must be determined experimentally. If, however, we had a model, we could write down what these functions should be.

One such model was proposed by Rahn (R2). In his model, growth of a cell involves replication of a fixed number  $N$  of entities (Rahn called these "genes" but we need not do so) within the cell. When all  $N$  entities have been replicated, the cell divides, and the process repeats itself.

The rate of replication is random, of course, since we are dealing with very small scale processes. Rahn suggested that his postulated entities were identical, in the sense that the order in which they are replicated is immaterial; indeed, simultaneous replication is not forbidden. Other hypotheses of the same general nature are possible, and have been reported in the literature [see, e.g., Kendall (K2) and Powell (P3)].

Let  $X(\tau)$  be the number of entities which have been replicated in a cell of age  $\tau$ . Of course,  $X(\tau)$  is a discrete random variable, which assumes values  $0, 1, 2, \dots, N$ . If we put  $P_x(\tau)$  equal to  $P(X(\tau) = x)$ , then it can be shown by a method essentially the same as used for the pure birth process (Section III, A), that  $P_x(\tau)$  satisfies the difference-differential equation

$$dP_x(\tau)/d\tau = -\gamma \cdot (N - x) P_x(\tau) + \gamma \cdot (N - x + 1) P_{x-1}(\tau) \quad (135)$$

The model from which this is obtained is that the probabilities of the transitions  $X(\tau) = x - k$  to  $X(\tau + \Delta\tau) = x$  are

$$\begin{aligned} \{1 - \gamma \cdot (N - x) \Delta\tau - O[(\Delta\tau)^2]\} & \quad \text{for } k = 0 \\ \{\gamma \cdot (N - x + 1) \Delta\tau + O[(\Delta\tau)^2]\} & \quad \text{for } k = 1 \end{aligned}$$

etc. Here the parameter  $\gamma$  must be assumed to be dependent on environmental conditions; in steady-state culture, these are constant, so  $\gamma$  is also constant.

Initial conditions for Eq. (135) are

$$P_x(0) = \begin{cases} 1, & x = 0 \\ 0, & x > 0 \end{cases} \quad (136)$$

whence it is easily shown that <sup>22</sup>

$$P_N(\tau) = (1 - e^{-\gamma\tau})^N \quad (137)$$

<sup>22</sup> The solution of Rahn's problem is

$$P_x(\tau) = (-1)^x \binom{N}{x} e^{-N\gamma\tau} (1 - e^{\gamma\tau})^x$$

whence one can easily show that

$$\sum_{x=0}^N P_x(\tau) = 1$$

and

$$E[X(\tau)] = N(1 - e^{-\gamma\tau})$$

The latter expression is the result obtained for product accumulation in a first-order batch chemical reaction (deterministic).

Since it is assumed that division follows as soon as  $N$  entities are replicated, it follows that  $dP_N/d\tau$  must be the density of the distribution of division times. Hence,

$$h(\tau) \equiv \frac{dP_N(\tau)}{d\tau} = \gamma N e^{-\gamma\tau} (1 - e^{-\gamma\tau})^{N-1} \quad (138)$$

so that by Eq. (130)

$$\Gamma(\tau) = \frac{\gamma N e^{-\gamma\tau} (1 - e^{-\gamma\tau})^{N-1}}{1 - (1 - e^{-\gamma\tau})^N} \quad (139)$$

In this view, the dependence of  $\Gamma$  on environmental conditions results from the dependence of  $\gamma$  on those conditions.

Experimentally, it has been found by Powell (P3), Kubitschek (K5), and others that the function  $h(\tau)$  derived from Rahn's hypotheses does reproduce the form of the observed density of division times; values of  $N$  reported vary from 25 (F3) to 400 (K5). It so happens, however, that other hypotheses can be made to fit the data as well, and there are observations (such as the correlation of division times of sister cells) which apparently contradict the model.

However, the important point here is the appearance of intracellular dynamics in the functions  $\Gamma(\tau)$ , etc. In principle these functions can be determined by experiments on *populations* of cells, so that it is not necessary to work with *single cells* to study the mechanism of cellular processes.

## B. GENERAL EQUATIONS FOR THE AGE MODEL

In the preceding section a probabilistic approach was taken to the problem of cell age distribution in continuous steady-state cultures. The density of the age distribution function

$$U(\tau) / \int_0^\infty U(\tau') d\tau'$$

was thereby determined [Eq. (129)], and the effect of environmental conditions on growth was incorporated by letting functions  $\Gamma$ ,  $r$ , and  $\alpha_i$  depend on those conditions, as well as on cell age. The set of equations given is not complete, since it does not determine the steady-state population density at a given holding time. Moreover, one would like to be able to make some statements about the *transient* behavior of populations; this cannot be done from the previous analysis.

We begin this section by developing a differential equation for  $U(t, \tau)$ , the nonnormalized density of the distribution of cell ages at time  $t$ . The population density itself is, of course,

$$N(t) = \int_0^\infty U(t, \tau) d\tau \quad (140)$$

In accord with the results of Section III,A, we regard the population density as an ordinary (i.e., nonrandom) variable. On the other hand, the age of randomly selected cells in the culture is a random variable, and we seek the law by which the distribution of ages changes with time.

Consider a cell which at time  $t$  has an age between  $\tau$  and  $\tau + d\tau$ ; for convenience, such a cell is said to be of group  $\tau$ . The number of cells of group  $\tau - d\tau$  at time  $t$ , per unit volume, is  $U(t, \tau - d\tau) d\tau$ . If we choose an increment of time  $dt = d\tau$ , then the fate of cells of group  $\tau - d\tau$  during time interval  $t$  to  $t + dt$  must be one of the following:

- A. the cell divides;
- B. the cell is washed out;
- C. the cell "ages" by an amount  $d\tau = dt$ .

If (C|D) is true, then the cell will be of group  $\tau$  at time  $t + dt$ . In the foregoing, "D" refers to our prior knowledge of the cell; that is, that it was of group  $\tau - d\tau$  at time  $t$ , etc.

By Rule 2 of the theory of probability

$$P(A + B + C | D) = P(A | D) + P(B | D) + P(C | D) = 1 \quad (141)$$

since A, B, and C are mutually exclusive and exhaustive events. But by definition of  $\Gamma(\tau)$  and the hypothesis of perfect mixing

$$P(A | D) = \Gamma(\tau - d\tau) dt$$

$$P(B | D) = 1/\theta dt$$

so that

$$P(C | D) = 1 - \{1/\theta + \Gamma(\tau - d\tau)\} dt \quad (142)$$

Thus Eq. (142) gives the probability  $P(C | D)$  that a cell of group  $\tau - d\tau$  at time  $t$  will be a cell of group  $\tau$  at time  $t + dt$  ( $d\tau = dt$ ).

We now adopt the frequency interpretation of probability. The number of cells of group  $\tau - d\tau$  at time  $t$  which become cells of group  $\tau$  at time  $t + dt$  is

$$U(t, \tau - d\tau) d\tau \cdot \left[ 1 - \left\{ \frac{1}{\theta} + \Gamma(\tau - d\tau) \right\} dt \right]$$

As a matter of fact, this must also be the number of cells (per unit volume) of group  $\tau$  present at time  $t + dt$ , since *all* cells of group  $\tau$  at time  $t$  will be washed out, divided, or aged to cells of group  $\tau + d\tau$  in time interval  $t$  to  $t + dt$ . The number of such cells, per unit volume, which are "lost" to group  $\tau$  in  $t$  to  $t + dt$  is  $U(t, \tau) d\tau$ . Hence, the *increase* in number of cells, per unit volume, of group  $\tau$  in time  $t$  to  $t + dt$  is

$$U(t, \tau - d\tau) d\tau \left[ 1 - \left\{ \frac{1}{\theta} + \Gamma(\tau - d\tau) \right\} dt \right] - U(t, \tau) d\tau$$



This must be equated to the accumulation of cells of group  $\tau$  in time  $t$  to  $t + dt$ ,

$$\frac{\partial}{\partial t} [U(t, \tau) d\tau] dt$$

Hence,

$$U(t, \tau - d\tau) d\tau \left[ 1 - \left( \frac{1}{\theta} + \Gamma(\tau - d\tau) \right) dt \right] - U(t, \tau) d\tau = \frac{\partial U(t, \tau)}{\partial t} d\tau dt$$

This may be rearranged to yield the partial differential equation

$$\left( \frac{\partial}{\partial t} + \frac{\partial}{\partial \tau} + \frac{1}{\theta} + \Gamma(\tau) \right) U(t, \tau) = 0 \quad (143)$$

This equation was derived by Fredrickson and Tsuchiya (F4) by a rather obscure method; a similar equation was found by Behnken *et al.* (B4) in their study of particle growth processes. Note that Eq. (143) for the steady-state case ( $\partial U / \partial t = 0$ ) reduces to that derived earlier, Eq. (126).

Equation (143) as it stands is valid for  $\tau > 0$ ; it does not hold for  $\tau = 0$  since there is no term for generation of cells of age zero. A boundary condition for Eq. (143) may be derived by making a number balance on cells of age 0 to  $d\tau$ .

The number of new cells per unit volume, which are formed in time  $t$  to  $t + dt$ , is

$$2 dt \int_0^{\infty} U(t, \tau) \Gamma(\tau) d\tau$$

The factor 2 arises since each fission produces two new cells. On the other hand, all cells of group 0 at time  $t$  will be "lost" to this particular age interval in time  $t$  to  $t + dt$  ( $d\tau = dt$ ) by fission, washout, or aging. The number so lost is  $U(t, 0) d\tau$ . There is no gain of cells of group 0 by aging of younger cells, since no cells are younger than  $\tau = 0$ . Hence, the inventory reads

$$2 dt \int_0^{\infty} U(t, \tau) \Gamma(\tau) d\tau - U(t, 0) d\tau = \frac{\partial U(t, 0)}{\partial t} d\tau dt$$

Since the right-hand side is a higher order differential, the required boundary condition is

$$U(t, 0) = 2 \int_0^{\infty} U(t, \tau) \Gamma(\tau) d\tau \quad (144)$$

This equation, which must be satisfied in the steady state as well as in the unsteady state, provides the missing piece of information necessary for the complete solution of the steady-state case treated earlier.

In Eqs. (143) and (144), we must take the function  $\Gamma$  to be at least an implicit function of time. Recall that  $\Gamma$  depends on environmental conditions,

and these in turn change with time in the transient case. Hence, if we define the vector  $\mathbf{C}$  by

$$\mathbf{C} = [C_1, C_2, \dots, C_M]$$

( $M$  = number of chemical species in the environment), then we must write

$$\Gamma = \Gamma(\tau, \mathbf{C})$$

Similar statements may be made about the growth rate per cell  $r$  and the stoichiometric coefficients  $\alpha_i$ .

The complete set of equations describing the continuous culture in the unsteady state is then

$$\left( \frac{\partial}{\partial t} + \frac{\partial}{\partial \tau} + \frac{1}{\theta} + \Gamma(\tau, \mathbf{C}) \right) U(t, \tau) = 0 \quad (145)$$

$$\frac{dC_i}{dt} = \frac{1}{\theta} (C_{if} - C_i) - \int_0^\infty \alpha_i(\tau, \mathbf{C}) r(\tau, \mathbf{C}) U(t, \tau) d\tau \quad (i = 1, 2, \dots, M) \quad (146)$$

together with the boundary condition

$$U(t, 0) = 2 \int_0^\infty \Gamma(\tau, \mathbf{C}) U(t, \tau) d\tau \quad (147)$$

Of course, a sufficient number of initial conditions must also be specified.

Equation (145) is the number balance (accounting) on cells of group  $\tau$ ; Eq. (147) is the number balance on cells of group 0. Equation (146) is a material balance on the  $i$ th chemical species in the medium; Eq. (132) is its steady-state form. In addition a balance on biomass yields the generalization of Eq. (131):

$$\frac{dC}{dt} = -\frac{1}{\theta} C + \int_0^\infty r(\tau, \mathbf{C}) U(t, \tau) d\tau \quad (148)$$

where  $C$  is the concentration of biomass. This equation is not independent, since the amount of biomass formed must equal the net amount of mass extracted from the environment.

At this point, a difficulty not present in the steady-state case arises. In the steady state, it seems sufficient to assume that  $\Gamma$  (and also  $r$  and the  $\alpha_i$ ) depends only on cell age  $\tau$  and environmental conditions  $\mathbf{C}$ . The treatment of Rahn's model given earlier, for example, makes this clear. But in the transient case, it appears that  $\Gamma$  should depend not only on  $\tau$  and  $\mathbf{C}$ , but also on (laboratory or absolute) time  $t$ .

Inspection of Rahn's model can also clarify this point. Consider a cell formed by fission at time  $t_0$ . At time  $t_0 + \tau$ , this cell will have age  $\tau$ . By Rahn's hypotheses, the probability of replication of one "gene" in time interval  $t_0 + \tau$  to  $t_0 + \tau + \Delta\tau$ , given that  $x$  "genes" have been replicated at time  $t_0 + \tau$ , is

$$\gamma(t_0 + \tau)(N - x + 1) \Delta\tau + O[(\Delta\tau)^2]$$

where the parameter  $\gamma$  must now depend on  $t_0 + \tau$ , since environmental conditions are changing in the transient state. In the steady-state case,  $\gamma$  could be regarded as constant.

Explicit introduction of time ( $t$  or  $t_0$ ) in the function  $\Gamma$  creates a much more difficult problem than that expressed by Eqs. (145)–(147), since the equations are no longer autonomous. Hence, in what follows, we ignore the dependence of  $\Gamma$  on  $t$ ; assume that  $\Gamma$  has the same form in the unsteady state as in the steady state, and work with the approximate equations already given. This procedure should be adequate, provided that environmental conditions are not changing too fast; that is, not changing much in the mean lifetime of a cell. Of course, if we had an adequate measure of cell structure, we should not have to resort to this kind of subterfuge.

As an example, consider the batchwise growth of a synchronized population of cells. A culture is said to be synchronized when all cells divide at the same time; for our purposes, we say that a culture is synchronized when all cells have the same age.

Various methods of synchronizing cultures have been discovered [see, e.g., Burns (B11) and Maaløe (M1)]. Some of these involve application of stress—such as sudden temperature changes—but we do not consider these here [since in shock, environmental conditions change rapidly and Eqs. (145)–(147) are not expected to hold]. Rather, we consider that the culture has been synchronized by the filtration technique developed by Maruyama and Yanagita (M6), Abbo and Pardee (A1), and others. Presumably this method does not alter the composition or physical conditions of the growth medium, and the synchronizing action is the selection of cells having narrow ranges of sizes and surface characteristics.

For example, assume that synchronization is perfect, and that it is effected at time  $t = 0$  when all cells selected have age  $\tau = 0$ . The requisite initial condition is then

$$U(0, \tau) = N_0 \delta(\tau) \quad (149)$$

where  $N_0$  is the initial population density of the synchronized culture, and  $\delta(\tau)$  is Dirac's delta function (see E4).

Let us also assume that density of the culture upon synchronization is quite low, so that subsequent growth, at least for some time, does not alter

the medium enough to alter the rates of subcellular processes.<sup>23</sup> If this is the case,  $\Gamma$  will depend only on  $\tau$ , and will be independent of  $C$ .

Assume that  $\Gamma$  has the form

$$\Gamma(\tau) = \gamma S(\tau - \tau_0) \quad (150)$$

where

$$S(\tau) = \begin{cases} 0, & \tau < 0 \\ 1, & \tau > 0 \end{cases}$$

is the "unit step function," and  $\gamma$  is the parameter appearing in Rahn's model of cell fission. The form of Eq. (150) is the limit of Rahn's model as the number of entities to be replicated ( $N$ ) becomes indefinitely large. In actuality,  $\Gamma$  would not be a sharp step as indicated by Eq. (150), but rather would be a smoothly rising step.

The pertinent equation is then

$$\left( \frac{\partial}{\partial t} + \frac{\partial}{\partial \tau} + \gamma S(\tau - \tau_0) \right) U(t, \tau) = 0 \quad (151)$$

and this is to be solved with initial condition Eq. (149) and boundary condition

$$U(t, 0) = 2\gamma \int_{\tau_0}^{\infty} U(t, \tau) d\tau \quad (152)$$

The solution may be found by Laplace transform methods; these lead to

$$\begin{aligned} \bar{N}(p) &= \int_0^{\infty} \bar{U}(p, \tau) d\tau \\ &= \frac{N_0}{1 - \frac{2\gamma}{p + \gamma} e^{-p\tau_0}} \left[ \frac{1}{p} (1 - e^{-p\tau_0}) + \frac{e^{-p\tau_0}}{p + \gamma} \right] \end{aligned} \quad (153)$$

where  $p$  is the Laplace transform variable, and the bar indicates a transformed quantity. The population density is found by inverting the expression (153) and is

$$\frac{N(t)}{N_0} = 1 + \sum_{m=1}^{P(t)} 2^{m-1} f[\gamma(t - m\tau_0), m] \quad (154)$$

<sup>23</sup> This is not an unreasonable assumption. For instance, growth rate is zero order in substrate concentration as long as that concentration is large enough. Indeed, the very occurrence of exponential growth in batch cultures indicates that metabolic rates are zero order in substrate concentrations therein.

Here  $P(t)$  is the largest integer such that  $t > P(t)\tau_0$ , and  $f$  is the function

$$f(y, m) = \frac{1}{(m-1)!} \int_0^y e^{-x} x^{m-1} dx \quad (155)$$

The time course of increase of  $N(t)$  predicted by Eq. (154) is shown in Fig. 25

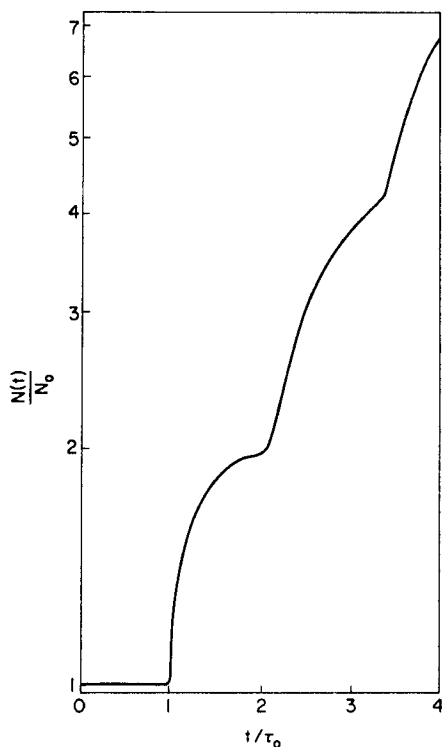


FIG. 25. Time course of population increase in an initially synchronous culture as calculated from Eq. (154).

for  $\gamma = 3.91 \text{ h}^{-1}$  and  $\tau_0 = 1 \text{ h}$ . This is to be compared, for instance, with the experimental data shown by Abbo and Pardee (A1; their Fig. 1).

Figure 25 shows that synchronization is gradually lost, and growth approximates to exponential increase, as time proceeds.<sup>24</sup> This is not apparent in the data of Abbo and Pardee; perhaps the desynchronization in any one generation of their culture was less than that assumed in the foregoing calculations. The spread in division times shown by their data is then

<sup>24</sup> Asymptotic formulas for the growth-rate constant and the age distribution in exponential growth are given in the example following.

explained by the probability that synchronization was not initially perfect. Of course the form assumed for  $\Gamma$  may be too simple.

Equation (154) does not predict a stationary phase or a phase of decline as time increases. This is so because we neglected the effect of the changing environment on  $\Gamma$ . If we solved the full set of equations<sup>25</sup> (145)–(147), a stationary phase would be predicted.

To close this section, we derive Powell's (P4) asymptotic formula for the density of the age distribution of a batch culture in exponential growth. As before, we assume that the culture is dilute enough so that  $\Gamma$  is not altered by growth,<sup>26</sup> at least for a number of generations. Then the requisite equations are

$$\left( \frac{\partial}{\partial t} + \frac{\partial}{\partial \tau} + \Gamma(\tau) \right) U(t, \tau) = 0 \quad (156)$$

with

$$U(t, 0) = 2 \int_0^\infty \Gamma(\tau) U(t, \tau) d\tau \quad (157)$$

No initial condition is specified as in the previous example since we seek the asymptotic solution valid after exponential growth has started.

A trial solution is therefore

$$U(t, \tau) = N_0 e^{\mu t} f(\tau) \quad (158)$$

where  $f(\tau)$ —the density of the age distribution—must be chosen so that

$$\int_0^\infty f(\tau) d\tau = 1 \quad (159)$$

Hence, the population density is

$$N(t) = \int_0^\infty U(t, \tau) d\tau = N_0 e^{\mu t} \quad (160)$$

so that  $\mu$  is the exponential growth rate constant.

Substitution of (158) into (156) yields

$$df(\tau)/d\tau + (\mu + \Gamma(\tau))f(\tau) = 0 \quad (161)$$

which by (157) must satisfy

$$f(0) = 2 \int_0^\infty \Gamma(\tau) f(\tau) d\tau \quad (162)$$

and also the normalizing condition, Eq. (159).

<sup>25</sup> This can be done numerically on the digital computer [for details, see Eakman (E1)].

<sup>26</sup> Indeed, it appears that exponential growth is possible only if there exists a range of environmental conditions in which  $\Gamma$  is constant.

The solution of (161) is

$$f(\tau) = f(0) \exp \left\{ - \left( \mu \tau + \int_0^\tau \Gamma(\tau') d\tau' \right) \right\} \quad (163)$$

so that Eq. (162) requires

$$\frac{1}{2} = \int_0^\infty \Gamma(\tau) \exp \left\{ - \left( \mu \tau + \int_0^\tau \Gamma(\tau') d\tau' \right) \right\} d\tau \quad (164)$$

Equation (164) gives the growth rate constant  $\mu$  as a function of  $\Gamma$ . The constant  $f(0)$  is determined from

$$f(0) = \left\{ \int_0^\infty e^{-\mu\tau} \exp \left( - \int_0^\tau \Gamma(\tau') d\tau' \right) d\tau \right\}^{-1} \quad (165)$$

which is derived from Eq. (159), of course.

Equations (163)–(165) are equivalent to Powell's solution for batch cultures. The analysis here shows that this solution is only valid asymptotically. For a batch culture which has just emerged from the lag phase, there is no reason to expect that the age distribution has the density given by Eq. (163). Therefore, there must be a transient period during which the density changes with time until the form (163) is approached asymptotically. The previous example on a synchronous culture shows that this transient period might last for two or more generations, depending on the initial departure of the age distribution from that given by Eq. (163). Of course the solution given will cease to be valid after sufficient growth has occurred to alter the value of  $\Gamma$  appreciably.

### C. A MORE GENERAL MODEL AND ITS POSSIBLE EXTENSION

Koch and Schaechter (K3) have pointed out a number of unsatisfactory features in use of cell age as an index or measure of cell structure. In particular they note that the model based on this predicts no correlation between the life spans of sister cells, whereas in fact these life spans are found to be correlated. Again, they note that the *mass* of cells at division (bacterial cells, at any rate) shows less "spread" about a mean value than does the age of cells at division. They also report that they have found that the mean size of bacteria, at division, changes in a regular fashion when cells are transferred to a medium in which growth rate and bacterial size are different.

On the basis of these observations and other arguments which we review, a different model for the growth of a population of structured cells was proposed by Koch and Schaechter. The postulates of the model are discussed below.

First: Growth at the cellular level is deterministic. This is essentially the same assumption as made in Parts A and B of this section, where only

the mean or expected growth rate of a cell,  $r$ , was found to be necessary for the model. There  $r$  was taken to be a function of cell age; in the model of Koch and Schaechter, however, the index of cell structure must be the cell mass  $m$ . As mentioned earlier, growth rate depends on environmental conditions, too, so that

$$r = r(m, C) \quad (166)$$

As a subpostulate, Koch and Schaechter assume that the growth of individual cells of a culture in exponential growth is also exponential, with the same growth rate constant as that of the culture. That is

$$r = \mu(C)m \quad (166a)$$

where  $(C)$  is the growth rate "constant" (in terms of cell mass) for the culture as a whole. This postulate is certainly not general,<sup>27</sup> but according to Koch and Schaechter, it is in accord with experimental findings for certain bacteria.

Second: The size (mass) of a cell at division is under genetic and environmental control, but the critical mass for fission shows small random variations about the mean value. The concept that cell division results when cells have attained a critical mass is not new; its history is reviewed by Koch and Schaechter. Random variations of cell size at division may be due to (i) the critical mass varying slightly from cell to cell; or (ii) appearance of visible evidence of fission in individual cells may be premature or delayed. In either case the observed variation is supposed to be due to the accumulation of small effects of a large number of random influences. Hence, as a subpostulate, Koch and Schaechter assume that the distribution of sizes at fission<sup>28</sup> is nearly Gaussian.

Third: Cell division results in an equal or nearly equal division of cytoplasmic mass between the daughter cells. Thus we define a function  $g(m', m, C)$  such that  $g(m', m, C) dm$  is the probability that a daughter cell, formed from a mother of mass  $m'$  in a medium of conditions  $C$ , will have mass  $m$  to  $m + dm$ . Clearly then,  $g$  must satisfy the following conditions:

$$g(m', m, C) = 0 \quad \text{if } m \geq m' \quad (167a)$$

$$\int_0^{m'} g(m', m, C) dm = 1 \quad (167b)$$

$$g(m', m, C) = g(m', m' - m, C) \quad (167c)$$

<sup>27</sup> This will be discussed in Section VII.

<sup>28</sup> That is, in batch cultures in exponential ("balanced") growth, or in continuous steady-state cultures.



Equation (167c) states that mass is conserved upon division of a cell. Koch and Schaechter assume that fission results in daughter cells of precisely equivalent masses; for this to be true, we must have

$$g(m', m, C) = \delta(\frac{1}{2}m' - m) \quad (168)$$

where  $\delta$  is Dirac's delta function.

Clearly these postulates suggest why cultures, even though initiated by single cells, do not grow synchronously through many generations.

Koch and Schaechter use these postulates to devise a formula for the distribution of cell masses in a batch culture growing exponentially (they obtained an approximate, asymptotic expression for this case). However, the model is more generally expressed as a set of integrodifferential equations. Let  $W(m, t) dm$  be the number of cells per unit volume, at time  $t$ , having mass between  $m$  and  $m + dm$ . The concentration of biomass  $C$  is then

$$C(t) = \int_0^\infty m W(m, t) dm \quad (169)$$

then one can show [see, e.g., (E1)] that in a continuous propagator, the pertinent equations for the model just described are

$$\begin{aligned} \frac{\partial}{\partial t} W(m, t) + \frac{\partial}{\partial m} \left\{ r(m, C) W(m, t) \right\} + \left\{ \frac{1}{\theta} + \Gamma'(m, C) \right\} W(m, t) \\ = 2 \int_m^\infty W(m', t) \Gamma'(m', C) g(m', m, C) dm' \end{aligned} \quad (170)$$

$$\frac{dC_i}{dt} = \frac{1}{\theta} (C_{if} - C_i) - \int_0^\infty \alpha_i(m, C) r(m, C) W(m, t) dm \quad (171)$$

subject to

$$\int_0^\infty \frac{\partial}{\partial m} \{ r(m, C) W(m, t) \} dm = 0 \quad (172)$$

and appropriate initial conditions for  $W(m, t)$  and the  $C_i$ . Here, the  $\alpha_i$  are the stoichiometric coefficients as before, and  $\Gamma'(m, C) dt$  is the probability that a cell of mass  $m$  in environment of conditions  $C$  at time  $t$  will divide in time  $t$  to  $t + dt$ . The meaning of  $\Gamma'$  is quite similar to that of the function  $\Gamma$  used in the two previous sections.

Equation (170) may be derived by the method used by Behnken *et al.* (B4) in their study of particle growth processes. The primary difference is that one must account for fission of cells, a possibility not considered in the work cited. Similar equations, but not containing the growth terms, have been considered by Valentas (V1) in his study of droplet breakup and coalescence phenomena in agitated, two-phase systems. Note that if fission always results

in sister cells of exactly the same mass, then the right-hand side of Eq. (170) becomes

$$2\Gamma'(2m, C) W(2m, t)$$

Hence, instead of an integrodifferential equation, we now have a functional equation (also a differential equation).

The boundary condition which solutions of Eq. (170) must satisfy could be obtained by making a "number balance" on cells of all sizes present. However, this can be reduced to the boundary condition given, Eq. (172). This is done by integrating Eq. (170) over all  $m$  and comparing the result with the number balance on cells of all sizes. In this process, Eq. (167b) must be used.

Equation (172) can also be written as

$$r(0, C) W(0, t) = \lim_{m \rightarrow \infty} r(m, C) W(m, t) \quad (173)$$

and this limit should be zero, since  $r(0, C) = 0$  (cells cannot originate from nothing) and  $W(0, t)$  is assumed finite. Equation (173) is the "regularity condition" postulated by Behnken *et al.* (B4) for their equations of the particle growth process.

It is of interest to note that Eqs. (170–172) reduce to Monod's model [Eqs. (41–42)] under certain conditions. These can be established by multiplying Eq. (170) by  $m$  and integrating the resulting equation over all  $m$ . One finds that Monod's equations are obtained if:

- (i) there is a single limiting substrate  $S$  so that  $C$  may be replaced by  $C_s$ ;
- (ii) the stoichiometric coefficient  $\alpha_i$  (for  $i = S$ ) is constant;
- (iii) the function  $g(m', m, C)$  is such that

$$\frac{1}{2}m' = \int_0^{m'} mg(m', m, C_s) dm \quad (174)$$

- (iv) the function  $r(m, C)$  is such that

$$r(m, C_s) = \frac{\mu C_s}{K + C_s^m} \quad (175)$$

where  $\mu$  and  $K$  are constants.

Equation (174) is always true, as can be shown from Eqs. (167b) and (167c). Equation (175) is seen to be a special case of the postulate of Koch and Schaechter [Eq. (166a)]. The conditions under which Eq. (175) *might* be valid are discussed in Section VII.

As mentioned previously, an important feature of this model is its ability to account for a correlation between the life spans of sister cells. The model which used age as an index of cell structure cannot do this.

With regard to the correlations, there are two extreme cases to be considered:

(1) If the function  $g(m', m, C)$  is such that there is a large probability that the daughter cells resulting from a fission will be of nearly the same size whereas the function  $\Gamma'(m, C)$  is such that the size of a cell at fission is rather variable, then the life spans of sister cells will have a positive coefficient of correlation.<sup>29</sup> The coefficient of correlation of the life spans of a mother cell and either of its daughters will be slightly negative in this case. Thus the progeny of a cell which was smaller than the average at fission are both likely to have life spans longer than the average, whereas the progeny of a cell which was larger than the average at fission are both likely to have life spans shorter than the average. The negative coefficient of correlation between the life spans of mother and daughter cells obviously follows from the same observations.

(2) If the function  $g(m', m, C)$  is such that there is a large probability that the daughter cells resulting from a fission will have quite different sizes whereas the function  $\Gamma'(m, C)$  is such that most fissions occur when cell sizes are very close to a certain value, then the life spans of sister cells will have a negative coefficient of correlation. In this case, the coefficient of correlation of the life spans of a mother cell and either of its daughters should be nearly zero. Thus, one daughter cell resulting from a fission is likely to have a life span longer than the average while the other is likely to have a life span shorter than the average. The life span of a daughter is more or less independent of the life span of its mother.

Positive coefficients of correlation between the life spans of sister cells have been observed in the bacteria by Koch and Schaechter (K3) and by Kubitschek (K5). A negative coefficient of correlation between the life spans of mother and daughter cells is reported by Koch and Schaechter (K3). They also find that in the organisms they studied, cells divided into nearly equal parts on fission. Hence, the experimental observations indicate that the first extreme mentioned above is more nearly correct. It is important to note that the theory predicts the correlations described without having to postulate any genetic inhomogeneity of the population; i.e., all cells may be of the same genotype.

It might be possible to extend the model discussed in the foregoing by positing that the mass of cells is of several different kinds; that is, the concept developed by Ramkrishna (R3) might be extended to segregated models. Use of this concept of structure to generalize Eq. (170) would certainly lead to a more flexible model, but the mathematical difficulties inherent in solving the equations of the model are very formidable.

<sup>29</sup> The coefficient of correlation for two discrete random variables is discussed, e.g., by Feller (F1), Section IX,8. For continuous random variables, see pp. 48–53 in Laning and Battin (L2). Estimation of the coefficient of correlation from sampling experiments may be accomplished by the method described, e.g., by Crow *et al.* (C4), p. 158.

### VII. Growth of Single Microbial Cells

In the model of growth discussed in Section VI,C, it is necessary to have an expression for the growth rate of a single cell. In this section, we discuss certain papers on growth of single cells which have appeared in the literature.

Von Bertalanffy (B6) hypothesized that growth of a single cell represents the results of competition between two opposing processes: *Aufbau* or assimilation and *Abbau* or endogenous metabolism. He assumed that the rate of *Abbau* is simply proportional to the mass of protoplasm in the cell. On the other hand, *Aufbau* must be assumed to be dependent on environmental conditions (e.g., on concentration of limiting substrate, in particular). Von Bertalanffy also postulated that the rate of assimilation is proportional to the *surface area* of the cell. The intuitive basis for these postulates is given on pp. 240–241 of his book.

The suggestion that the rate of assimilation of substrates by a cell might be proportional to the cell's surface area opens up a new field—biological transport—which this review has not previously considered. Thus, if the assimilation rate is assumed proportional to surface area, this rate could be controlled by the rate of transport of nutrilites from the cell's environment to the cell's interior.

In a steady-state situation, von Bertalanffy writes the growth rate of a single cell as

$$r(m, C) \equiv dm/d\tau = V_0(C)\sigma - \mu_c m \quad (176)$$

Here  $\sigma$  is the surface area of the cell of mass  $m$  and age  $\tau$ . Some important consequences of Eq. (176) can now be deduced.

Consider the growth of a rod-shaped cell (bacillus). Such a cell grows by elongation along its axis; there is essentially no change in the radius of the rod. Hence, if  $r$  is the radius of the cell and  $l$  its effective length, then  $\sigma = 2\pi r l$  and  $m = \pi r^2 l \rho$ , where  $\rho$  is the mean cell density. Substitution of these equations into Eq. (176) then shows that the length grows as

$$\frac{dl}{d\tau} = \left( \frac{2V_0}{r\rho} - \mu_c \right) l \quad (177)$$

The mass follows the same law for this case of *linear, intercalary* growth:

$$\frac{dm}{d\tau} = \left( \frac{2V_0}{r\rho} - \mu_c \right) m \quad (178)$$

Hence, in steady-state propagation, the mass of a bacillus should increase exponentially, up to the time the cell divides.

Equation (178) is exactly the form postulated by Koch and Schaechter (K3) [see Eq. (166a)]. Moreover, Eq. (178) shows that if

$$(i) \quad (2V_0/r\rho) \gg \mu_c$$

$$(ii) \quad V_0 \propto \frac{C_s}{K + C_s}$$

( $C_s$  = concentration of limiting substrate), then growth of a culture of rod-shaped cells should follow Monod's equations. On the other hand, if Condition (ii) above is valid but Condition (i) is not, then one can show that substitution of Eq. (178) into Eq. (170) leads to Herbert's generalization [Eq. (111)] of Monod's equations.

From this, we conclude that if Monod's equations (or Herbert's generalization thereof) and von Bertalanffy's equation [Eq. (176)] are valid, then the rate of transport of limiting substrate from environment to cell interior is proportional to  $C_s/(K + C_s)$ . However, if this transport were *Fickian*, the rate should be a linear function of  $C_s$ . Hence the simultaneous validity of Eq. (176) and Monod's equations for rod-shaped bacteria would appear to rule out ordinary transport and point instead to some more complicated mechanism.

Cohen and Monod (C2) have summarized experimental evidence which shows indeed that special mechanisms of transport of organic nutrients occur in bacteria. They call such transport systems *permeases*. This term ending in *-ase* implies that the system involves enzymes—an implication not yet proved by available data. At any rate, it is found that permease systems can lead to transport *against* an apparent rise in concentration, as well as other effects not possible with Fickian diffusion. Various hypothetical mechanisms for operation of permease systems yield rates of permeation which exhibit the Michaelis-Menten type of dependence on substrate (including water) concentration. Perhaps it is in the occurrence of one of these mechanisms that the rate equation [Eq. (38)] assumed by Monod and almost all subsequent workers finds its justification. [For further information on biological transport, see, e.g., Christensen (C1).]

For a spherical cell (coccus), one has

$$\sigma = 4\pi r^2$$

$$m = \frac{4}{3}\pi r^3 \rho$$

So that according to von Bertalanffy's equation, cell growth should follow the law

$$\frac{dr}{d\tau} = \frac{V_0}{\rho} - \frac{\mu_c}{3} r \quad (179)$$

When integrated, this equation yields a sigmoidal curve. The mass follows

$$\frac{dm}{d\tau} = V_0 \left[ (4\pi)^{1/3} \left( \frac{3}{\rho} \right)^{2/3} \right] m^{2/3} - \mu_c m \quad (180)$$

which also yields a sigmoidal curve on integration. In this case, there is a maximum possible cell size, given by

$$\lim_{\tau \rightarrow \infty} m = \frac{36\pi V_0^3}{\rho^2 \mu_c^3}$$

Thus, one sees from Eq. (180) that cultures of spherical bacteria should not follow Monod's equations.

Von Bertalanffy cites experimental data in support of his theory. For instance, he shows that the data of Bayne-Jones and Adolph (B3) on growth of single cells of *Bacillus megaterium* (rod-shaped) follow Eqs. (177) and (178), whereas their data (B3) on growth of the yeast *Saccharomyces cerevisiae* (roughly spherical) follow Eqs. (179) and (180). Other data cited are also in agreement with the model, as are more recent data, such as those of Schaechter *et al.* (S1) on growth of three rod-shaped bacteria (strains of *Escherichia coli*, *Proteus vulgaris*, and *Salmonella typhimurium*) and of Prescott (P5) on growth of an organism (*Amoeba proteus*) of irregular but more or less spherical shape. Prescott (P6) states that, with the exception of *Paramecium*, growth of single cells of protozoa is never "autocatalytic" (exponential). His view seems to be that this is a general conclusion, valid for all cells, since he suggests that speculations concerning "autocatalytic" growth of single cells should be stopped.

It must be mentioned that the foregoing treatment of linear growth of rod-shaped cells has assumed growth to be *intercalary*. That is, if we were to observe two points on the axis of the rod, we should observe that the distance between the points increases with time as growth lays down new material between them. (The relatively few experimental observations that have been made do not necessarily support that growth is completely intercalary.)

But a rod-shaped cell or a linear chain of rod-shaped cells can also exhibit another kind of linear growth—*apical*. In this mode of linear growth, cells or filaments of cells increase in length only at their apex; the distance between two adjacent points on the filament axis remains constant.

The experiments of Smith (S3), Stadler (S6), Zalokar (Z1), and Plomley (P2) have shown that the hyphae of various genera of fungi, both septate and nonseptate, exhibit apical linear growth rather than intercalary linear growth.

From these considerations, Emerson (E3) concluded that growth of a fungal culture in liquid medium ought to follow a different law than does growth of bacteria. In particular, he concluded that, for batch growth,

biomass concentration should rise as the cube of the time elapsed, rather than exponentially. Emerson's experimental data show that the third power law fits a larger portion of the growth curve than does the exponential law. The data of Marshall and Alexander (M5) on oxygen consumption by fungal cultures is also better fitted by a cubic law for growth. Neither set of experimental data is convincing, however.

Emerson's prediction of a third power growth law is based on the implicit assumption that the number density of fungal hyphae is spatially uniform and time invariant. Plomley's data (P2) for growth of *Chaetomium globosum* on agar plates are not in agreement with this assumption; they show that the number density of fungal hyphae is neither spatially uniform nor time invariant. Indeed, the *local* situation revealed by Plomley's experiments is strongly suggestive of the usual batch (exponential) growth situation. One still has to explain the data of Emerson (E3) and of Marshall and Alexander (M5), of course. The better "fit" of the third power law as contrasted with the exponential law might be due to oxygen limitation, a possibility supported by scrutiny of Emerson's data.

Again, mycologists have postulated (cf. H5) that the nongrowing central portions of fungal hyphae serve, in part at any rate, as food collectors for the growing apex. Zalokar's observations (Z1) on *cytoplasmic streaming*<sup>30</sup> indicate the essential correctness of this postulate. We suggest that studies of these transport phenomena might yield remarkable results to suitably talented chemical engineers.

### VIII. Concluding Remarks

The foregoing review has started from the simplest considerations and proceeded to the analysis of more complex cases in its attempt to describe the dynamics of microbial cell populations. Some of the models discussed in the review are new; others have appeared in the literature but are not generally known by chemical or biochemical engineers. At any rate, treatment of these models is not to be found in any available treatise on biochemical engineering or elsewhere in the chemical engineering literature. Possibly the most important reason for this apparent lack of concern is the feeling that the models advanced are unrealistic and not useful.

The validity of the limited number of models discussed (i.e., whether or not they are realistic) must be tested by experimental work. Hopefully these mathematical descriptions will suggest experiments specifically designed to test their predictions. It is in this process that the principal *present* utility of

<sup>30</sup> Cytoplasmic streaming is the biologists' term for intracellular convection. Its mechanism is not understood. A literature survey is given by Kamiya (K1); see especially pp. 11-13 for *streaming* in fungal hyphae.

models resides; the experimentalist so engaged will be called upon to display considerable ingenuity and skill.

### Appendix. Results from Probability Theory

We give here a résumé of the principal ideas of probability theory. The purpose is not to be comprehensive, but to summarize in a few paragraphs the concepts necessary for following the developments in the text, and to mention a few books in which extensive treatments of the theory are given.

In probability theory, we are concerned with propositions, or assertions about the occurrence of events. Generally speaking, these assertions will be conditional; that is, we assert that such and such is true if this and that are true. Some formal scheme of writing propositions is required, and we adopt the following:  $(A|B)$  means that "A is true if B is true." (Another way of putting this is to say that "A is true given B," or "A is true on data B.")

In many cases, we are interested in propositions concerning the occurrence of two or more events. Thus, let  $(AB|C)$  mean "both A and B are true, given that C is true," and let  $(A + B|C)$  mean "at least one of the events A or B is true if C is true." Finally, we denote the negation of a proposition by a small letter; e.g.,  $(a|B)$  means "A is not true if B is true."

The probability of propositions is denoted by a capital  $P$ ; viz.,  $P(A|B)$  means "the probability that A is true if B is true," with similar meanings for  $P(AB|C)$ , etc.

Probabilities of several propositions are related by the two fundamental rules given below. These rules may be treated as axioms (J2) or they may be derived from other axioms (C3), (J1). The rules are:

Rule 1:

$$\begin{aligned} P(AB|C) &= P(A|BC) P(B|C) \\ &= P(A|C) P(B|AC) \end{aligned} \quad (\text{A.1})$$

Rule 2:

$$P(A + B|C) = P(A|C) + P(B|C) - P(AB|C) \quad (\text{A.2})$$

In addition, we have the *conventions*

Rule 3: Certainty is represented by a unit probability.

Rule 4: Impossibility is represented by a zero probability.

Propositions A and B are said to be *independent* on data C if

Rule 5:

$$P(AB|C) = P(A|C) P(B|C) \quad (\text{A.3})$$



or, by Rule 1, if

$$P(A | BC) = P(A | C) \quad \text{and} \quad P(B | AC) = P(B | C)$$

Thus, if A and B are independent on data C, B is irrelevant to A given C, and A is irrelevant to B given C. Rule 5 is not generally true; a *reductio ad absurdum* of Rule 5 when improperly applied is given by Jeffreys (J2).

Two propositions A and B are said to be *mutually exclusive* on data C if

$$P(AB | C) = 0$$

whence, from Rule 2,

$$P(A + B | C) = P(A | C) + P(B | C) \quad (\text{A.4})$$

In particular,

$$P(A + a | C) = 1 = P(A | C) + P(a | C) \quad (\text{A.5})$$

so that a proposition and its negation are mutually exclusive. Mutually exclusive propositions A and B are said to be *exhaustive* if  $P(A + B | C) = 1$ ; thus, A and a are exhaustive.

*Bayes' theorem or the principle of inverse probability* is deducible from Rule 1 and is

$$P(A | BC) = P(A | C) \frac{P(B | AC)}{P(B | C)} \quad (\text{A.6})$$

According to Jeffreys (J2), Bayes' theorem is the principal rule used in learning from experience. Thus, suppose our belief in the plausibility of A is  $P(A | C)$ ; this is called the *prior probability*. If we are given new evidence, B, then Bayes' theorem provides the rule whereby we reassess the plausibility of A; this leads to the *posterior probability*,  $P(A | BC)$ .

Of course, somewhere along the line we have got to assign numerical values to probabilities such as  $P(A | C)$ ,  $P(B | C)$ , etc. For this purpose, we need a *model* of the process of interest.

In certain cases, probabilities can be assigned by the so-called "principle of insufficient reason." Thus, suppose we are involved in the vice of coin tossing. Consider the two mutually exclusive propositions

(A | C): A head turns up

(B | C): A tail turns up

Here, C represents our model of the coin-tossing process; namely, that the coin has two faces only, so that we can get only a head or a tail. These are

mutually exclusive, and we have no reason to choose one over the other. By Rule 2,

$$P(A + B | C) = P(A | C) + P(B | C) = 1$$

since  $P(AB | C) = 0$  (impossibility is represented by a probability of zero). But we have insufficient reason to choose  $(A | C)$  over  $(B | C)$  or vice versa; therefore,  $P(A | C) = P(B | C)$ , and both probabilities must equal  $\frac{1}{2}$ , by Rule 2. The same sort of reasoning can be employed for the assignment of probabilities in dice throwing, picking multicolored balls from urns, or in allotting energy levels to systems composed of one mole of an ideal gas. Notice that our model is not necessarily "right"; in the case of coin tossing, the coin might have two heads, or it might be biased in some manner of which we are not aware.

Many cases occur, however, in which the principle of insufficient reason is insufficient for the assignment of probabilities. That is, we are not able to reduce the problem to a statement of mutually exclusive, exhaustive, and equally likely propositions. As an example, consider the disintegration of a radioactive nucleus. We choose this example since it is similar to the processes mentioned in the text.<sup>31</sup>

Suppose we consider the proposition: "The nucleus will undergo fission in the time interval  $t$  to  $t + \Delta t$ ." This is conditional, of course, since it presupposes that the nucleus has not undergone fission in earlier time intervals. As a model for calculating the probability of the proposition, adopt the following. The conditional probability will certainly depend on the duration of the time interval,  $\Delta t$ ; it should be zero if  $\Delta t$  is zero. The probability should be continuous in  $\Delta t$ , so that the probability does not change by a finite amount in an infinitesimal interval of time. Moreover, the probability should be independent of absolute time  $t$ , since we have no reason to expect fission in one time interval to be more likely than fission in any other time interval. Hence, the required probability will be of the form  $f(\Delta t)$ , and Taylor series expansion about  $\Delta t = 0$  subject to hypotheses stated gives

$$f(\Delta t) = k \Delta t + O[(\Delta t)^2]$$

where  $k$  is a positive constant, and  $O$  means "of the order of." The model does not tell us the numerical value of  $k$ ; that could be estimated by experiment (if the model is "right") or calculated if we understood the processes involved in fission.

<sup>31</sup> As a matter of fact, the problem of radioactive decay is exactly the same as the problem of "washout" of particles from a perfectly mixed, continuous flow vessel. Thus, Eq. (124) of the text can be applied to yield the well-known law of radioactive decay.

## ACKNOWLEDGMENTS

It will be evident that we have relied on our students for much of the new work reported herein. They have also aided in many other ways. Special thanks are due to Doraiswami Ramkrishna, Charles Swanson, James Eakman, Howard Wick, and Daniel T. Hanson.

We must also acknowledge the contributions of the National Aeronautics and Space Administration, which supported our students' research under grant NsG 79-60.

## Nomenclature

|                       |   |             |  |
|-----------------------|---|-------------|--|
| $a, a_s, a_s',$       | Stoichiometric coefficients                               | $R_{resp}$  | Rate of respiration per unit volume  |
| $a_t, \dots$          |   | $R_{photo}$ | Rate of photosynthesis per unit volume                                       |
| $b, b'$               | Stoichiometric coefficients                               | $r$         | Growth rate of a single cell; radius of a cell                               |
| $C$                   | Concentration of biomass                                  | $r_c$       | Specific multiplication rate   |
| $C$                   | Concentration of chemical species in environment (vector) | $r_p$       | Specific growth rate   |
| $C_G, C_D, C_s,$      | Concentration of species                                  | $S$         | Substrate  |
| $C_z, C_l, \dots$     | denoted by subscript                                      | $T$         | Inhibitor  |
| $D$                   | $D$ mass  | $t$         | Time   |
| $E$                   | Expected value  | $U$         | Nonnormalized density of age distribution                                    |
| $G$                   | Generating function; $G$ mass                             | $V$         | Volume of propagator; variance; viable biomass; quantity defined by Eq. (86) |
| $h$                   | Density of distribution of division times                 | $V_0$       | Growth rate of a single cell, per unit area                                  |
| $I, I_0$              | Light intensity; incident light intensity                 | $W$         | Quantity defined by Eq. (86); nonnormalized density of mass distribution     |
| $K$                   | Kernel in Volterra's equation [Eq. (34)]                  | $X$         | Population size; random variable   |
| $K, K_s, K_s',$       | Michaelis constants                                       | $x$         | Particular value of population size  |
| $K_\theta, K_\theta'$ |   | $Y$         | Apparent yield coefficient   |
| $k_1, k_2, \dots$     | Rate constants in bottle-neck model                       | $Z$         | Organism   |
| $l$                   | Length of cell  |             |  |
| $M_r$                 | $r$ th moment of probability distribution                 |             |  |
| $m$                   | Mass of a cell  |             |  |
| $N$                   | Population density; number of "genes" in Rahn's model     |             |  |
| $P$                   | Probability; critical product; productivity [Eq. (110)]   |             |  |
| $Q$                   | Volumetric flow rate                                      |             |  |
| $R$                   | Substrate   |             |  |
| $R_c$                 | Multiplication rate of a culture per unit volume          |             |  |
| $R_p$                 | Growth rate of a culture per unit volume                  |             |  |
| $R_s$                 | Rate of production of substrate per unit volume           |             |  |

## GREEK LETTERS

|            |   |
|------------|---|
| $\alpha$   | Defined by Eq. (51)   |
| $\alpha_i$ | Stoichiometric coefficient for $i$ th chemical species                              |
| $\beta$    | Constant in Verhulst-Pearl law; defined by Eq. (51); stoichiometric coefficient     |
| $\Gamma$   | Defined by Eq. (64); probability of fission (per unit time) of a cell of age $\tau$ |

|             |  |            |   |
|-------------|--|------------|---|
| $\Gamma'$   | Probability of fission (per unit time) of a cell of mass $m$             | $\mu_c$    | Specific rate of endogenous metabolism                                  |
| $\gamma$    | Defined by Eq. (51); specific rate of "gene" replication in Rahn's model | $\nu$      | Constant in Eq. (35); specific rate of light reaction in photosynthesis |
| $\Delta$    | Defined by Eq. (64)  | $\pi$      | Initial value of $C_p$  |
| $\delta$    | Dirac's delta function   | $\xi$      | Defined by Eq. (86)   |
| $\epsilon$  | Extinction coefficient in Beer's law                                     | $\rho$     | Initial value of $C_R$ ; density of cell                                |
| $\zeta$     | Initial value of $C_z$   | $\sigma$   | Initial value of $C_s$ ; surface area of cell                           |
| $\eta$      | Defined by Eq. (86)  | $\tau$     | Defined by Eq. (88); age  |
| $\theta$    | Holding time   | $\chi$     | Defined by Eq. (88)   |
| $\lambda$   | Constant; defined by Eq. (51)  |            |   |
| $\mu, \mu'$ | Maximum specific growth rates  |            |   |
|             |  | SUBSCRIPTS |   |
|             |  | $f$        | Feed condition  |
|             |  | 0          | Initial condition   |

## REFERENCES

- A1. Abbo, F. E., and Pardee, A. B., *Biochim. Biophys. Acta* **39**, 478-485 (1960).  
A2. Aris, R., and Amundson, N. R., *Chem. Eng. Sci.* **7**, 121-131, 132-147, and 148-155 (1958).  
B1. Bailey, N. T. J., "The Elements of Stochastic Processes, with Applications to the Natural Sciences." Wiley, New York, 1964.  
B2. Baron, T., *Proc. 1st Midwestern Conf. Fluid Mech.*, pp. 216-225 (1951).  
B3. Bayne-Jones, S., and Adolph, E. F., *J. Cellular Comp. Physiol.* **1**, 387-407 (1932); see also Adolph, E. F., and Bayne-Jones, S. *ibid.* **1**, 409-427.  
B4. Behnken, D. W., Horowitz, J., and Katz, S., *Ind. Eng. Chem., Fundamentals* **2**, 212-216 (1963).  
B5. Bellman, R. E., "Dynamic Programming." Princeton Univ. Press, Princeton, New Jersey, 1957.  
B6. von Bertalanffy, L., "Theoretische Biologie," Vol. 2. Gebrüder Borntraeger, Berlin-Zehlendorf, 1942.  
B7. Bharucha-Reid, A. T., "Elements of the Theory of Markov Processes and Their Applications." McGraw-Hill, New York, 1960.  
B8. Bilous, O., and Amundson, N. R., *A.I.Ch.E. Journal* **1**, 513-521 (1955).  
B9. Brown, H. T., and Escombe, F., *Proc. Roy. Soc.* **B76**, 29-111 (1905).  
B10. Buchanan, R. E., and Fulmer, E. I., "Physiology and Biochemistry of Bacteria," Vol. I, Chapter II, pp. 4-62. Williams & Wilkins, Baltimore, Maryland, 1928.  
B11. Burns, V. W., *Progr. Biophys. Biophys. Chem.* **12**, 2-23 (1962).  
C1. Christensen, H. N., "Biological Transport." Benjamin, New York, 1962.  
C2. Cohen, G. N., and Monod, J., *Bacteriol. Rev.* **21**, 169-194 (1957).  
C3. Cox, R. T., "The Algebra of Probable Inference." Johns Hopkins Press, Baltimore, Maryland, 1961.  
C4. Crow, E. L., Davis, F. A., and Maxfield, M. W., "Statistics Manual." Dover, New York, 1960.  
D1. Davis, H. T., "Introduction to Nonlinear Differential and Integral Equations." Dover, New York, 1962.

- E1. Eakman, J. M., Ph.D. Thesis, University of Minnesota, Minneapolis, Minnesota, 1966.
- E2. Emerson, R., and Arnold, W., *J. Gen. Physiol.* **15**, 391–420 (1932); **16**, 191–205 (1933).
- E3. Emerson, S., *J. Bacteriol.* **60**, 221–223 (1950).
- E4. Erdélyi, A., in “Modern Mathematics for the Engineer” (E. F. Beckenbach, ed.), 2nd Series, Chapter 1, pp. 5–50. McGraw-Hill, New York, 1961.
- F1. Feller, W., “An Introduction to Probability Theory and its Applications,” 2nd ed., Vol. 1, Chapter XI, pp. 248–267. Wiley, New York, 1957.
- F2. Finn, R. K., and Wilson, R. E., *Agr. Food Chem.* **2**, 66–69 (1954).
- F3. Finney, D. J., and Martin, L., *Biometrics* **7**, 133–144 (1951).
- F4. Fredrickson, A. G., and Tsuchiya, H. M., *A.I.Ch.E. Journal* **9**, 459–468 (1963).
- F5. Fredrickson, A. G., Brown, A. H., Miller, R. L., and Tsuchiya, H. M., *J. Am. Rocket Soc.* **31**, 1429–1435 (1961).
- G1. Giese, A. C., “Cell Physiology,” 2nd. ed., Chapter 26, pp. 540–562. Saunders, Philadelphia, Pennsylvania, 1962.
- H1. Hahn, W., “Theory and Application of Liapunov’s Direct Method.” Prentice-Hall, Englewood Cliffs, New Jersey, 1963.
- H2. Halvorson, H. O., and Ziegler, N. R., *J. Bacteriol.* **25**, 101–121 (1933); **26**, 331–339 and 559–567 (1933).
- H3. Hanson, D. T. S., Tsuchiya, H. M., and Fredrickson, A. G., in press.
- H4. Harris, T. E., in “The Kinetics of Cellular Proliferation” (F. Stohlman, ed.), pp. 368–381. Grune & Stratton, New York, 1959.
- H5. Hawker, L. E., “Physiology of Fungi,” pp. 5–8 and 23–32. Univ. London Press, London, 1950.
- H6. van Heerden, C., *Ind. Eng. Chem.* **45**, 1242–1247 (1953).
- H7. Henrici, A. T., “Morphologic Variation and the Rate of Growth of Bacteria.” Thomas, Springfield, Illinois, 1928.
- H8. Herbert, D., in “Continuous Cultivation of Microorganisms. A Symposium” (I. Málek, ed.), pp. 44–52. Czech. Acad. Sci., Prague, 1958.
- H9. Herbert, D., *Symp. Soc. Gen. Microbiol.* **11**, 391–461 (1961).
- H10. Herbert, D., Elsworth, R., and Telling, R. C., *J. Gen. Microbiol.* **14**, 601–622 (1956)
- J1. Jaynes, E. T., “Probability Theory in Science and Engineering.” Socony-Mobil Oil Co., Dallas, Texas, 1958.
- J2. Jeffreys, H., “Theory of Probability,” 3rd. ed. Oxford Univ. Press, London and New York, 1961.
- K1. Kamiya, N., *Protoplasmatologia* **8**, Part 3, 1–199 (1959).
- K2. Kendall, D. G., *Biometrika* **35**, 316–330 (1948).
- K3. Koch, A. L., and Schaechter, M., *J. Gen. Microbiol.* **29**, 435–454 (1962).
- K4. Kok, B., *Biochim. Biophys. Acta* **21**, 245–258 (1956).
- K5. Kubitschek, H. E., *Exptl. Cell Res.* **26**, 439–450 (1962).
- L1. Laidler, K. J., “Chemical Kinetics,” pp. 304–308. McGraw-Hill, New York, 1950.
- L2. Laning, J. H., Jr., and Battin, R. H., “Random Processes in Automatic Control,” pp. 45–56. McGraw-Hill, New York, 1956.
- L3. Liapunov, A., *Ann. Toulouse* **9**, 203–474 (1907) (originally published in Russian in 1892).
- L4. Lotka, A. J., “Elements of Mathematical Biology.” Dover, New York, 1956.
- M1. Maaløe, O., in “The Bacteria” (I. C. Gunsalus and R. Y. Stanier, eds.), Vol. 4, Chapter 1, pp. 1–32. Academic Press, New York, 1962.
- M2. Málek, I., ed., “Continuous Cultivation of Microorganisms. A Symposium.” Czech. Acad. Sci., Prague, 1958.
- M3. Malmgren, B., and Hedén, C., *Acta Pathol. Microbiol. Scand.* **24**, 417–436, 437–447, 448–471, 472–495, and 496–504 (1947).

- M4. Marr, A. G., and Harvey, R. T., "The Maintenance Requirement of Bacteria in Continuous Culture." Paper presented to Chicago Meeting of American Chemical Society, Sept., 1964 (paper available from Division of Microbial Chemistry and Technology).
- M5. Marshall, K. C., and Alexander, M., *J. Bacteriol.* **80**, 412-416 (1960).
- M6. Maruyama, Y., and Yanagita, T., *J. Bacteriol.* **71**, 542-546 (1956).
- M7. Maxon, W. D., *Appl. Microbiol.* **3**, 110-122 (1955).
- M8. Michaelis, L., and Menten, M. L., *Biochem. Z.* **49**, 333-369 (1913).
- M9. Miller, R. L., Fredrickson, A. G., Brown, A. H., and Tsuchiya, H. M., *Ind. Eng. Chem., Proc. Design Develop.* **3**, 134-143 (1964).
- M10. Milner, H. W., in "Algal Culture from Laboratory to Pilot Plant" (J. S. Burlew, ed.), Chapter 19, pp. 285-302. Carnegie Inst. Washington, Washington, D.C., 1953.
- M11. M'Kendrick, A. G., and Pai, M. K., *Proc. Roy. Soc. Edinburgh* **31**, 649-655 (1910-11).
- M12. Monod, J., "Recherches sur la croissance des cultures bactériennes." Hermann et Cie, Paris, 1942.
- M13. Monod, J., *Ann. Rev. Microbiol.* **3**, 371-394 (1949); *Ann. Inst. Pasteur* **79**, 390-410 (1950).
- M14. Moser, H., "The Dynamics of Bacterial Populations Maintained in the Chemostat." Carnegie Inst. Washington, Washington, D.C., 1958.
- M15. Myers, J., in "Algal Culture from Laboratory to Pilot Plant" (J. S. Burlew, ed.), Chapter 4, pp. 37-54. Carnegie Inst. Washington, Washington, D.C., 1953.
- M16. Myers, J., and Graham, J. R., *Plant Physiol.* **34**, 345-352 (1959).
- N1. Novick, A., *Ann. Rev. Microbiol.* **9**, 97-110 (1955).
- N2. Novick, A., and Szilard, L., *Science* **112**, 715-716 (1950); *Proc. Natl. Acad. Sci. U.S.* **36**, 7087-19 (1950).
- O1. Oparin, A. I., "The Origin of Life on the Earth" (transl. by A. Syngé), 3rd ed. Academic Press, New York, 1957.
- P1. Pearl, R., "Introduction to Medical Biometry and Statistics," 3rd ed., pp. 459-470. Saunders, Philadelphia, Pennsylvania, 1940.
- P2. Plomley, N. J. B., *Australian J. Biol. Sci.* **12**, 53-64 (1959).
- P3. Powell, E. O., *Biometrika* **42**, 16-44 (1955).
- P4. Powell, E. O., *J. Gen. Microbiol.* **15**, 492-511 (1956).
- P5. Prescott, D. M., *Exptl. Cell. Res.*, **9**, 328-337 (1955).
- P6. Prescott, D. M., in "Synchrony in Cell Division and Growth" (E. Zeuthen, ed.), Chapter 3, pp. 71-97. Wiley (Interscience), New York, 1964.
- R1. Rabotnova, I. L., and Mineeva, L. A., *Microbiology (USSR) (English Transl.)* **28**, 331-335 (1959).
- R2. Rahn, O., *J. Gen. Physiol.* **15**, 257-277 (1932).
- R3. Ramkrishna, D., Ph.D. Thesis, University of Minnesota, Minneapolis, Minnesota, 1965.
- R4. Rieske, J. S., Lumry, R., and Spikes, J. D., *Plant Physiol.* **34**, 293-300 (1959).
- S1. Schaechter, M., Williamson, J. P., Hood, J. R., Jr., and Koch, A. L., *J. Gen. Microbiol.* **29**, 421-434 (1962).
- S2. Schrödinger, E., "What is Life?" Cambridge Univ. Press, London and New York, 1944.
- S3. Smith, J. H., *Ann. Botany (London)* **37**, 341-343 (1923); *New Phytologist* **23**, 65-78 (1924).
- S4. *Soc. Chem. Ind. (London), Monograph* 1961. **12**.
- S5. Spieker, C. C., *Biometrics*, **11**, 225-230 (1955).
- S6. Stadler, D. R., *J. Cellular Comp. Physiol.* **39**, 449-474 (1952).

- T1. Tamiya, H., Hase, E., Shibata, K., Mituya, A., Iwamura, T., Nihei, T., and Sasa, T., in "Algal Culture from Laboratory to Pilot Plant" (J. S. Burlew, ed.), Chapter 16, pp. 204–232. Carnegie Inst. Washington, Washington, D.C., 1953.
- V1. Valentas, K. J., Ph.D. Thesis, University of Minnesota, Minneapolis, Minnesota, 1964.
- V2. Volterra, V., "Theory of Functionals and of Integral and Integro-Differential Equations." Dover, New York, 1959.
- W1. Weiss, P., and Kavanau, J. L., *J. Gen. Physiol.* **41**, 1–47 (1957).
- W2. Whittaker, E. T., in "Theory of Functionals and of Integral and Integro-Differential Equations" (V. Volterra), pp. 5–28. Dover, New York, 1959.
- Z1. Zalokar, M., *Am. J. Botany* **46**, 602–610 (1959).
- Z2. Ziegler, N. R., and Halverson, H. O., *J. Bacteriol.* **29**, 609–634 (1935).

# DIRECT CONTACT HEAT TRANSFER BETWEEN IMMISCIBLE LIQUIDS

Samuel Sideman

Department of Chemical Engineering  
Technion, Israel Institute of Technology, Haifa, Israel

|  |     |
|--|-----|
| I. Introduction .....  | 207 |
| II. Equations Based on Dimensionless Similarity .....                            | 209 |
| III. Heat Transfer to Drops Moving in a Constant-Temperature Field .....         | 211 |
| A. Assumed Physical Models .....   | 211 |
| B. Rigid-Drop Model .....  | 211 |
| C. Completely Mixed-Drop Model .....   | 221 |
| D. Drops with Internal Circulation .....   | 222 |
| IV. Heat Transfer to Drops Moving in a Continuously Varying Temperature Field .. | 236 |
| A. Single-Drop Studies .....   | 236 |
| B. Countercurrent Spray-Column Heat Exchangers .....                             | 238 |
| C. Cocurrent Heat Exchangers .....   | 246 |
| V. Heat Transfer to Drops and Bubbles with Simultaneous Change of Phase .....    | 248 |
| A. Evaporation of Drops in Immiscible Liquid Media .....                         | 252 |
| B. Condensation of Bubbles in Immiscible Liquid Media .....                      | 262 |
| VI. Miscellaneous Effects on Heat Transfer .....                                 | 267 |
| A. Drop and Column End Effects .....   | 267 |
| B. Temperature and Temperature-Gradient Effects .....                            | 270 |
| C. Effect of Drop Diameter on Heat-Transfer Coefficient .....                    | 273 |
| VII. Related Works .....   | 277 |
| Nomenclature .....   | 278 |
| References .....   | 280 |

## 1. Introduction

Direct heat and mass transfer between dispersed and continuous liquid phases is utilized over a wide range of industrial applications. The advantages of direct-contact heat transfer over the conventional processes using metallic transfer surfaces have lately stimulated research on its utilization for water



desalination projects. These advantages, predominant factors in determining the feasibility of the various suggested projects, are

- (1) Simple design and relatively inexpensive equipment;
- (2) Low maintenance due to absence, or reduction, of scale formation on solid surfaces;
- (3) The obtainable close temperature approaches.

The larger volumes of fluids required in liquid-liquid heat transfer can sometimes be reduced by having the dispersed phase evaporate (or condense) within the continuous liquid medium. Latent, rather than sensible, heat transfer takes place in these "three-phase" exchangers, thus permitting a more effective heat-transfer process. Though this method is promising, relatively little is known about direct-contact heat transfer between immiscible liquids. The basic characteristics of heat transfer between dispersed and continuous media are thus of both scientific and practical interest.

Although most of the literature dealing with single drops is confined to mass transfer, the pertinent information is reported here in heat-transfer terms, using the classical analogies. However, interfacial agitation, regarded as concentration-dependent rather than temperature-dependent, may have affected some of the empirical equations in question. Hence care must be exercised when applying the latter to actual liquid-liquid heat-transfer operations.

The passage of a drop through a column of another liquid is characterized by three regimes: (a) drop formation and acceleration; (b) constant velocity; and (c) coalescence. In the present work the constant-velocity region is treated in detail in Sections II and III, whereas reference to the other two regions is made in Section VI. Section III deals with the fundamental case of a freely moving drop in a constant-temperature liquid. Section IV is mainly devoted to the interesting and highly important case of spray columns, where the drops move in a liquid under continuous temperature change. In Section V, the relatively new "three-phase" direct-contact heat transfer with change of phase is discussed. The various aspects of column end effects, drop temperature, and drop diameter are treated in Section VI.

The basic "classical" theories, such as the film, boundary layer, transient film, and penetration hypotheses are obviously outside the scope of this chapter, but the reader is assumed to be familiar with their basic concepts. Harriott's (H8) recent review on mass transfer to interfaces is recommended in this connection. An excellent treatise on the motion of drops and bubbles in fluid media is found in Levich's "Physicochemical Hydrodynamics" (L8, Ch. 8).

The two-film concept is convenient in describing transfer phenomena. However, use of this general concept, applicable even to agitated fluids near the interface, should not be taken as support for the classical stagnant film

hypothesis, better known as the "two-film theory." Instead, the general concepts of Toor's (T5) combined film penetration theory should preferably be borne in mind.

To adopt a common procedure here, the external film coefficient is expressed in terms of the Nusselt number. The internal coefficients, however, are given indirectly by the transfer efficiency,  $E_m$ , representing the fractional approach to the maximum possible heat transfer. Thus, by definition,

$$E_m \equiv \left( \frac{T_0 - T_i}{T_c - T_i} \right)$$

where  $T_0$  and  $T_i$  are the outlet and inlet mixing-cup average temperatures of the drop, and  $T_c$  is the constant temperature of the continuous medium. With heat capacities assumed to be constants,  $E_m$  is the ratio of the heat actually absorbed by the drop to the maximum transferable heat. The internal heat-transfer coefficients (defined as the actual amount of heat transferred per unit area, time, and temperature gradient), can conveniently be expressed in terms of  $E_m$  and drop area. Plots are available for this conversion (B15). It should be noted that  $E_m$  as defined here is confined to the constant-velocity region and is only identical with the over-all transfer efficiency,  $E_T$ , provided end effects are disregarded.

Despite intensive efforts towards better understanding of transfer phenomena between drops and continuous media, accurate prediction of the transfer coefficients for a given system can as yet only be hoped for. Nevertheless, accumulated experience may provide an indication of the transfer mechanism to be encountered and the relevant coefficients may be estimated accordingly. Conversely, given experimental data, the controlling mechanism may be defined. It is therefore of theoretical as well as of practical interest to survey, in as much detail as space allows, the commonly postulated models and suggested mechanisms of transfer to single drops (S8). Since most of the analyses are reported in terms of dimensionless groups, attempts to obtain general equations by dimensional analysis, as well as their inherent limitations, will be dealt with first.

## II. Equations Based on Dimensionless Similarity

Similarity criteria are ratios of the various forces or fluxes controlling the rate of the process involved. These are the momentum, viscous, gravity, and surface-tension forces and the conduction and convection terms, determined by the geometry of the system and the physical properties of the fluids. Density, viscosity, surface tension, heat capacity, and thermal conductivity are the physical properties to be considered.

The dimensionless equation describing the transfer phenomena may be obtained either by direct reference to the ratios of the physical quantities or by recourse to the classical techniques of dimensional analysis, i.e., the Buckingham II Theorem or Rayleigh's method of indices. In addition, the basic differential equations governing the process may be reduced to dimensionless form and the coefficients identified. In general, the dimensionless equation for heat transfer through the combined film is

$$N_{Nu} = f\left(N_{Re}, N_{Pr}, N_{We}, \frac{\rho_d}{\rho_c}, \frac{\mu_d}{\mu_c}, \frac{\alpha_d}{\alpha_c}\right) \quad (1)$$

However, if each of the films is considered separately, two equations similar to Eq. (1), but excluding the diffusivity-ratio term, are obtained (H5). Determination of the functional relationship between the various dimensionless groups is quite difficult, and many of the correlations reported (see Tables I-III) are abbreviated forms of Eq. (1). Obviously these introduce the assumption that effects of interfacial tension, phase viscosities, and density difference on the transfer coefficient are constant over the usual range of these properties. Since the range is normally narrow, the assumption is quite reasonable, though one may expect a fairly wide scatter of measured values for unusual systems.

An attempt to combine in a single dimensionless equation the numerous variables involved in extraction from a drop was reported recently. Lileeva and Smirnov (L14) derived the dimensionless groups from the four basic differential equations (motion, continuity, kinetic diffusion, and convection) and the initial and boundary conditions. The eleven groups derived were then reduced to the following equation:

$$\begin{aligned} (N_{Nu})_c &= 2.44 \times 10^{-12} (N_{Re})_d^{0.9} (N_{Re})_c^{0.2} (N_{Pr})_d^{0.5} (N_{Pr})_c^{0.5} (N_{Fo})^{-0.14} (N_{Gr})^{1.2} K^{-0.5} L^{-1.5} \end{aligned} \quad (2)$$

where  $N_{Fo}$  is the Fourier number,  $N_{Gr}$  the Grashof number,  $K$  the log-mean average of the distribution coefficients, and  $L$  a geometrical factor relating the drop and column diameters.

A large number of independent experiments is required to determine the functional relationship between the various dimensionless groups. Moreover, some of the groups are interrelated. The exponents of the relationship proposed in Eq. (2) were determined by assigning values to the exponents of the standard groups ( $N_{Re}$ ,  $N_{Pr}$ ) and, by trial and error, the numerical values of the other exponents were adjusted to fit the experimental data. Thus, though this relationship is applicable to extraction of acids from benzene drops into water, it cannot, by nature of its derivation, be considered as general.

### III. Heat Transfer to Drops Moving in a Constant-Temperature Field

#### A. ASSUMED PHYSICAL MODELS

A common, and more rigorous, procedure is based on deriving an equation from an assumed physical model, susceptible to mathematical analysis, and evaluating the assumptions of the model by means of experimental data. The three models to be discussed here are

- (a) Rigid drop;
- (b) Completely mixed drop;
- (c) Drop with internal circulation.

As already stated, it is not uncommon to determine the transfer mechanism for a given system by comparing the experimental data with theoretical values calculated from the corresponding models (M3). A method for testing experimental data with a view to determining the applicable transfer mechanism was suggested by Licht and Pansing (L13). The method, based on plotting  $\log(1 - E_T)$  vs time, is especially suitable for cases with long contact time. In the present chapter the mechanisms based on the above-mentioned models are studied with special emphasis on model (c). The various theoretical and empirical equations obtained by means of these models are summarized in Tables I-IV.

#### B. RIGID-DROP MODEL

This model is obviously an extension of the well-known theory of heat transferred by radial conduction. Solution of the basic differential equations depends on the boundary conditions stipulated, the boundary layer and velocity profiles of the continuous phase.

##### 1. *Transfer Coefficients outside a Rigid Drop*

Numerous workers (B16, F2, F4, H17, J4, K4, K7, L8, M2, S5, and others) estimated the external heat-transfer coefficient in the continuous phase by assuming a velocity profile in the boundary layer and ambient fluid. Except for very low Reynolds numbers, the exact boundary layer solutions only apply to the front part of the drop, up to the separation point. Fortunately, simple assumptions sometimes suffice for extending the derivation to the entire drop, and the relationships obtained are in agreement with experimental data. The limitations of the analytical solutions, as well as their application to nonspherical drops, is concisely demonstrated in Lochiel and Calderbank's (L18) recent study on mass transfer around axisymmetric bodies of revolutions.

TABLE I  
EQUATIONS FOR OUTSIDE NUSSELT NUMBER [ $(N_{Re})_c < 1$ ]: RIGID-DROP MODEL

| Equation no. | Source        | $(N_{Nu})_c$  | $(N_{Re})_c$ | $(N_{Pr})_c$ | $(N_{Pe})_c$ | Physical description                               | Derivation                                       |
|--------------|---------------|---|--------------|--------------|--------------|--|--|
| I-1          | (F2)          | $2 + \frac{(N_{Pe})_c}{2} + \frac{(N_{Pe})_c^2}{6} + \dots$                 | $< 1$        | —            | $< 1$        | Laminar flow<br>Thick concentration boundary layer | Boundary layer theory<br>Stokes stream function  |
| I-2          | (W3)          | $2 + \frac{9}{16}(N_{Pe})_c + \frac{9}{64}(N_{Pe})_c^2 + \dots$             | $< 1$        | —            | $< 1$        | Laminar flow<br>Thick concentration boundary layer | Boundary layer theory<br>approximated from (B12) |
| I-3          | (F3)          | $2 + 0.32(N_{Pe})_c^2$  | $< 1$        | —            | $< 1$        | Laminar flow                                       | Perturbation method                              |
| I-4          | (K6)          | $2 + 0.5(N_{Pe})_c + 0.3(N_{Pe})_c^2$                                       | $< 1$        | —            | $< 1$        | Laminar flow                                       | Perturbation method                              |
| I-5          | (B14)         | $2 + \frac{1}{2}(N_{Pe})_c + \frac{1}{4}(N_{Pe})_c^2 \ln(N_{Pe})_c + \dots$ | $< 1$        | —            | $< 10$       | Laminar flow                                       | Perturbation method                              |
| I-6          | (F2)          | $0.89(N_{Pe})_c^{1/3}$  | $< 1$        | —            | $> 10^3$     | Laminar flow<br>Thin concentration boundary layer  | Boundary layer theory<br>Stokes stream function  |
| I-7          | (B12, F2, W3) | $0.98(N_{Pe})_c^{1/3}$  | $< 1$        | —            | $> 10^3$     | Laminar flow<br>Thin concentration boundary layer  | Boundary layer theory<br>Stokes stream function  |
| I-8          | (A1)          | $1.075(N_{Pe})_c^{1/3}$   | $< 1$        | $\geq 1$     | —            | Liquid-solid mass transfer                         | Boundary layer theory<br>and empiricism          |

In general, correlations for  $N_{Pe} < 1$ ,  $N_{Re} < 1$  have the following form:

$$(N_{Nu})_c = \text{Polynomial}(N_{Pe}) \quad (3)$$

where  $N_{Pe} = N_{Re} \cdot N_{Pr}$ . Some of these relations are presented in Table I and compared in Fig. 1.

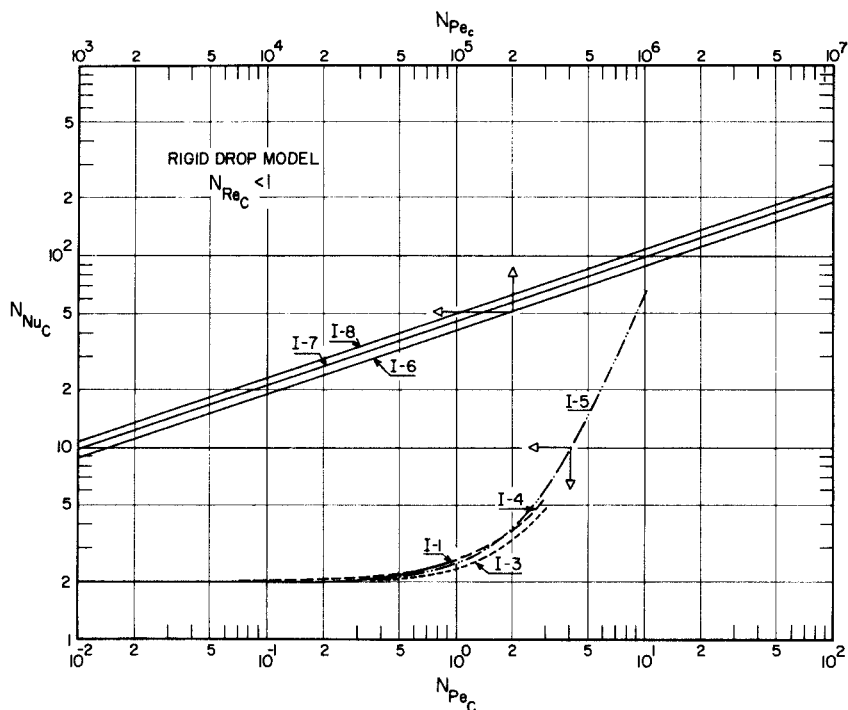


FIG. 1. Comparison of equations for outside Nusselt number (cf. Table I).

For the more common and practical operating range of  $N_{Pe} > 1$ , Eq. (1) reduces to

$$(N_{Nu})_c = a + b(N_{Re})_c^m (N_{Pr})_c^n \quad (4)$$

where

$$m = n = \frac{1}{3} \quad \text{for } N_{Pe} \gg 1; \quad N_{Re} < 1$$

and

$$m = \frac{1}{2} \quad n = \frac{1}{3} \quad \text{for } 1 < (N_{Re})_c < 10^4$$

The constants  $a$ ,  $b$ ,  $m$ , and  $n$ , as determined by various workers in the field, are seen in Table II. Some of the proposed equations for  $(N_{Re})_c > 1$  are

TABLE II  
EQUATIONS FOR OUTSIDE NUSSELT NUMBER  $[(N_{Re})_c > 1]$ : RIGID-DROP MODEL

| Equation no. | Source     | $(N_{Nu})_c$  | $(N_{Re})_c$      | $(N_{Pr})_c$ | Physical description                   | Derivation                           |
|--------------|------------|---|-------------------|--------------|--|--------------------------------------|
| II-1         | (A1)       | $0.8 (N_{Re})_c^{1/2} (N_{Pr})_c^{1/3}$   | $1 \ll - < 10^4$  | $> 1$        | Dissolving of solids                   | Boundary layer theory and empiricism |
| II-2         | (F4, G12)  | $2 + 0.55 (N_{Re})_c^{1/2} (N_{Pr})_c^{1/3}$  | 2–1000            | $< 1$        | Evaporation and sublimation            | Empirical                            |
|              |            |   | 20–160            | $> 1$        | Mass transfer, liquid–liquid           | Empirical                            |
| II-3         | (R3, R2)   | $2 + 0.60 (N_{Re})_c^{1/2} (N_{Pr})_c^{1/3}$  | 0–200             | $< 1$        | Evaporation                            | Empirical                            |
|              |            |   | $1-7 \times 10^4$ |              |  |                                      |
| II-4         | (H18)      | $2 + 0.54 (N_{Re})_c^{1/2} (N_{Pr})_c^{1/3}$  | 50–350            | 1–2          | Evaporation                            | Empirical                            |
| II-5         | (T1, G21)  | $2.1 + 0.42 (N_{Re})_c^{1/2} (N_{Pr})_c^{1/3}$  | 50–1000           | 1            | Evaporation                            | Empirical                            |
| II-6         | (R1)       | $2.83 + 0.60 (N_{Re})_c^{1/2} (N_{Pr})_c^{1/3}$   | 50–1000           | 1            | Evaporation                            | Empirical                            |
| II-7         | (G21)      | $2 + 0.57 (N_{Re})_c^{1/2} (N_{Pr})_c^{0.35}$   | $> 1$             | $> 1$        | Mass transfer, gas–liquid              | Empirical                            |
| II-8         | (K2)       | $2 + 0.57 f (N_{Re})_c^{1/2} (N_{Pr})_c^{1/2}$  | 0–2500            | 1            | Mass transfer                          | Empirical                            |
| II-9         | (G11)      | $2 + 0.95 (N_{Re})_c^{1/2} (N_{Pr})_c^{1/3}$  | 60–600            | $> 1$        | Mass transfer, liquid–solid            | Empirical                            |
| II-10        | (G4)       | $44 + 0.48 (N_{Re})_c^{1/2} (N_{Pr})_c^{1/3}$   | 20–835            | $> 1$        | Mass transfer, liquid–solid            | Empirical                            |
| II-11        | (W11, G4)  | $1.45 (N_{Re})_c^{0.35} (N_{Pr})_c^{1/3}$   | 4–400             | $\geq 1$     | Mass transfer, evaporation             | Empirical                            |
| II-12        | (W11, L16) | $0.43 (N_{Re})_c^{0.56} (N_{Pr})_c^{1/3}$   | 400– $10^5$       | 1            | Mass transfer, gas–liquid solid–liquid | Empirical                            |
| II-13        | (K4)       | $2 + 1.3 (N_{Pr})_c^{0.15} + 0.66 (N_{Re})_c^{1/2} (N_{Pr})_c^{0.31}$                       | $0.4-10^5$        | 0.7–400      | Heat transfer                          | Empirical                            |
| II-14        | (V2)       | $[1.2 + 0.53 (N_{Re})_c^{0.54}] (N_{Pr})_c^{0.3} \left( \frac{\mu_c}{\mu_d} \right)^{0.25}$ | $1-3 \times 10^5$ | 2–380        | Heat transfer                          | Empirical                            |
| II-15        | (M2, C1)   | $[0.97 + 0.68 (N_{Re})_c^{1/2}] (N_{Pr})_c^{0.3}$   | $< 10^3$          | $< 400$      | Heat transfer                          | Empirical                            |
| II-16        | (S20)      | $(N_{Nu})_0 + 0.347 (N_{Re})_c^{0.62} (N_{Pr})_c^{0.31}{}^b$                                | $< 10^4$          | 0.7–380      | Heat transfer                          | Empirical                            |

<sup>a</sup>  $f$  rises to about 2 as  $(N_{Re})_c$  goes from 0 to 10, then falls slowly to 1;  $f = 1$  for  $(N_{Re})_c > 80$ .

<sup>b</sup>  $(N_{Nu})_0 = 2 + 0.569 [(N_{Gr})_c (N_{Pr})_c]^{0.25}$ .

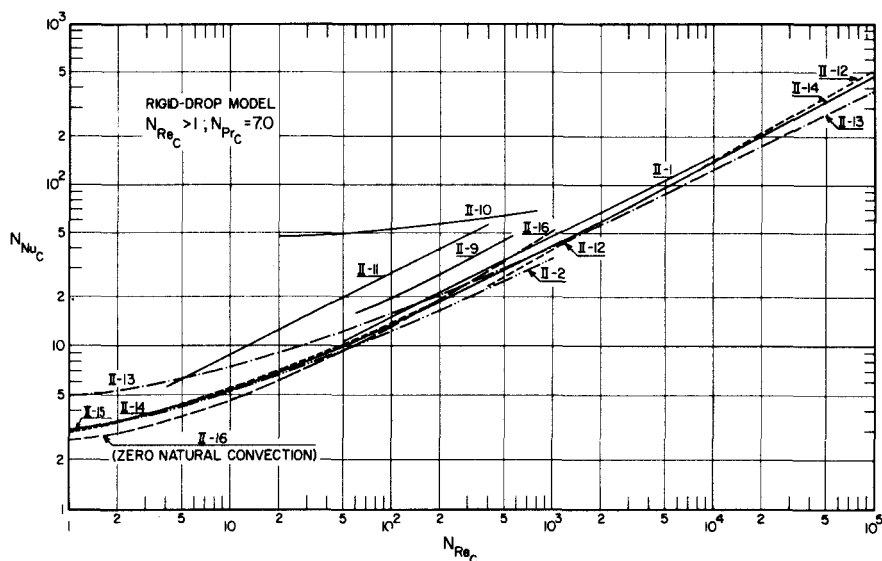


FIG. 2. Comparison of equations for outside Nusselt number (Table II).

compared in Fig. 2. The continuous phase was taken as water, with  $(N_{Pr})_c = 7$ . Some other references, dealing with boundary layer solutions for solid spheres and not included here, are given in (G21, H17, S20). As seen from Table II, most transfer data for solid spheres and stagnant drops up to Reynolds numbers of 1000 fit Eq. (4), with  $b$  varying between 0.43 and 0.95, the higher value most probably suitable for liquid-liquid systems. In general,  $b = 0.57$  is recommended (G21) and

$$(N_{Nu})_c = 2 + 0.57(N_{Re})_c^{1/2}(N_{Pr})_c^{1/3} \quad (5)$$

$(N_{Nu})_c = a = 2$  is the limiting value for diffusion into infinite stagnant medium, originally calculated by Langmuir (L3) in 1918 and confirmed since by numerous workers. However, as natural convection may be pronounced in liquid systems, higher limiting values may be obtained, especially with large spherical drops moving in liquids with low kinematic viscosities  $\nu$ , since for natural convection the Grashof number varies inversely as  $\nu^2$  and directly as cube of the diameter. Good agreement was obtained with  $b = 0.95$  for liquid-liquid and liquid-solid systems. However, a more general equation, suggested by Steinberger and Treybal (S20), based on the additivity of natural and forced convection and valid for all systems (including gas-liquid), is shown in Fig. 3:

$$(N_{Nu})_c = (N_{Nu})_0 + 0.347(N_{Re})_c^{0.62}(N_{Pr})_c^{0.31} \quad (6)$$



TABLE III EQUATIONS FOR OUTSIDE

| Equation no. | Source        | $(N_{\text{Nu}})_c$  | $(N_{\text{Re}})_c$ |
|--------------|---------------|--|---------------------|
| III-1        | (L8)          | $0.65(N_{\text{Pe}})_c^{1/2} \left( \frac{\mu_c}{\mu_c + \mu_d} \right)^{1/2}$   | $< 1$               |
| III-2        | (G21)         | $0.67(N_{\text{Pe}})_c^{1/2} \left( \frac{\mu_c}{\mu_d + \mu_c} \right)^{1/2}$   | $< 1$               |
| III-3        | (W3)          | $0.61(N_{\text{Pe}})_c^{1/2} \left( \frac{\mu_c}{\mu_d + \mu_c} \right)^{1/2}$   | $< 10$              |
| III-4        | (G21)         | $0.89(N_{\text{Pe}})_c^{1/3} \left( \frac{\mu_d + 1.33\mu_c}{\mu_d + \mu_c} \right)^{1/3}$   | $< 1$               |
| III-5        | (W3)          | $0.98(N_{\text{Pe}})_c^{1/3} \left( \frac{\mu_d + 1.58\mu_c}{\mu_d + \mu_c} \right)^{1/3}$   | $< 10$              |
| III-6        | (W3)          | $2 + \frac{9}{16}(N_{\text{Pe}})_c + \frac{9}{64}(N_{\text{Pe}})_c^2 + \dots$  | $< 10$              |
| III-7        | (B14)         | $2 + \frac{1}{2}(N_{\text{Pe}})_c + \frac{1}{4} \left( \frac{2\mu_c + 3\mu_d}{3\mu_c + 3\mu_d} \right) (N_{\text{Pe}})_c^2 \ln(N_{\text{Pe}})_c + \dots$ | $< 1$               |
| III-8        | (B6)          | $1.25(N_{\text{Pe}})_c^{1/2}$  | —                   |
| III-9        | (B10)         | $1.13(N_{\text{Pe}})_c^{1/2}$  | —                   |
| III-10       | (G21)         | $2 + 1.13(N_{\text{Pe}})_c^{1/2} K_v^{1/2}$  | $> 1$               |
| III-11       | (G21)<br>(C5) | $(N_{\text{Nu}})_{\text{rigid}}(1 - K_v)^{-1/2}$   | $> 1$               |
| III-12       | (E2)          | $\left( \frac{12}{\pi} \right)^{1/2} (N_{\text{Pe}})_c^{1/2}$  | $> 1$               |
| III-13       | (H13)         | $g(N_{\text{Pe}})_c^{1/2}$   | $> 1$               |
| III-14       | (G12)         | $0.6(N_{\text{Pe}})_c^{1/2}$   | $> 1$               |
| III-15       | (E2)          | $5.52 \left( \frac{\mu_c + \mu_d}{2\mu_c + 3\mu_d} \right)^{3.47} \left( \frac{D\sigma_c}{\mu_c^2} \right) (N_{\text{Pe}})_c^{1/2}$                      | $< 1500$            |
| III-16       | (G3)          | $-126 + 1.8(N_{\text{Re}})_c^{1/2}(N_{\text{Pr}})_c^{0.42}$  | 18–800              |
| III-17       | (T3)          | $-178 + 3.62(N_{\text{Re}})_c^{1/2}(N_{\text{Pr}})_c^{1/3}$  | 50–800              |
| III-18       | (G12)         | $50 + 8.5 \times 10^{-3}(N_{\text{Re}})_c(N_{\text{Pr}})_c^{0.7}$  | 100–700             |

# NUSSELT NUMBER: CIRCULATING-DROP MODEL

| $(N_{Pr})_c$ | $(N_{Pe})_c$  | Physical description              | Derivation  |
|--------------|---|-----------------------------------|---|
| —            | $\gg 1$   | Drop circulation                  | Hadamard steam function                             |
| —            | $\gg 2.4 \left( 3 \frac{\mu_d}{\mu_c} + 4 \right)^2 \left( \frac{\mu_d}{\mu_c} + 1 \right) \gg 1$     | Drop circulation                  | “Potential theory” plus Hadamard’s velocity         |
| —            | $\gg 2.8 \left( \frac{\mu_d + \mu_c}{\mu_c} \right) \left( \frac{12\mu_d + 19\mu_c}{\mu_c} \right)^2$ | Drop circulation                  | Hadamard stream function, approximation from (B12)  |
| —            | $\gg 1$   |                                   |   |
| —            | $\ll 2.4 \left( 3 \frac{\mu_d}{\mu_c} + 4 \right)^2 \left( \frac{\mu_d}{\mu_c} + 1 \right)$           | Drop circulation                  | Hadamard stream function                            |
| —            | $\ll 2.8 \left( \frac{\mu_d + \mu_c}{\mu_c} \right) \left( \frac{12\mu_d + 19\mu_c}{\mu_c} \right)^2$ | Drop circulation                  | Hadamard stream function, approximation from (B12)  |
| —            | $> 1000$  |                                   |   |
| —            | $< 1$   | Drop circulation                  | Hadamard stream function, approximation from (B12)  |
| —            | $< 10$  | Drop circulation                  | Perturbation technique                              |
| —            | 2–100   | Drop circulation                  | Potential flow                                      |
| —            | Large   | Drop circulation                  | Potential flow                                      |
| $> 1$        | —   | Drop circulation                  | Potential, modified                                 |
| $> 1$        | —   | Drop circulation                  | Reynolds analogy                                    |
| —            | Large   | Drop circulation                  | Simplified boundary-layer theory                    |
| $> 1$        | —   | Drop circulation                  | Empirical, mass transfer: gas-liquid; liquid-liquid |
| $> 1$        | —   | Drop circulation                  | Empirical, mass transfer: liquid-liquid             |
| $> 1$        | —   | Drop circulation                  | Empirical, heat transfer: liquid-liquid             |
| $\gg 1$      | —   | Drop circulation                  | Empirical, mass transfer: liquid-liquid             |
| $\gg 1$      | —   | With and without circulation      | Empirical, mass transfer: liquid-liquid             |
| $> 1$        | —   | Drop circulation plus oscillation | Empirical, mass transfer: liquid-liquid             |

TABLE IV INSIDE TRANSFER-EFFICIENCY EQUATIONS: RIGID- AND CIRCULATING-DROP MODELS (S8)

| Eq. no. | Source | $E_m$   | Eigenvalue         | Description  | Derivation                |
|---------|--------|---|--------------------|--|---------------------------|
| IV-1    | (N3)   | $1 - \frac{6}{\pi^2} \sum_{n=1}^{\infty} \frac{1}{n^2} \exp\left[\frac{-\pi^2 n^2 \alpha \theta}{R^2}\right]$ |                    | Rigid sphere: $h_c = \infty, T_c = \text{const}$   | Conduction equation       |
| IV-2    | (V1)   | $\left[1 - \exp\left(\frac{-\pi^2 \alpha \theta}{R^2}\right)\right]^{1/2}$                                    |                    | Rigid sphere: $h_c = \infty, T_c = \text{const}$   | Empirical, Eq. (IV-1)     |
| IV-3    | (G22)  | $1 - 6 \sum_{n=1}^{\infty} A_n \exp\left[\frac{-\lambda_n^2 \alpha \theta}{R^2}\right]$                       | Table A-1          | Rigid sphere: $h_c \neq \infty, T_c = \text{const}$  | Conduction equation       |
| IV-4    | (K5)   | $1 - \frac{3}{8} \sum_{n=1}^{\infty} A_n^2 \exp\left[\frac{-\lambda_n^2 16 \alpha \theta}{R^2}\right]$        | Table A-2          | Drop circulation: $h_c = \infty, T_c = \text{const}, \sigma = 0, N_{Re} < 1$                     | Hadamard stream function  |
| IV-5    | (E2)   | $1 - \frac{3}{8} \sum_{n=1}^{\infty} A_n^2 \exp\left[\frac{-\lambda_n^2 16 \alpha \theta}{R^2}\right]$        | Table A-3          | Drop circulation: $h_c \neq \infty, T_c = \text{const}, \sigma = 0, N_{Re} < 1$                  | Hadamard stream function  |
| IV-6    | (C1)   | $\left[1 - \exp\left(\frac{-2.25 \pi^2 \alpha \theta}{R^2}\right)\right]^{1/2}$                               |                    | Drop circulation: $h_c = \infty, T_c = \text{const}, 10 < N_{Re} < 200, 6 < N_{Pr} < 3000$       | Empirical, Eq. (IV-4)     |
| IV-7    | (H5)   | $1 - 2 \sum_{n=1}^{\infty} A_n^2 \exp\left[\frac{-\lambda_n \alpha \theta (N_{Pr})_d}{512 R^2}\right]$        | $\lambda_1 = 2.88$ | Drop circulation allowed with a radial motion: $N_{Re} = 1000, h_c = \infty, T_c = \text{const}$ | Einstein equation         |
| IV-8    | (J2)   | $1 - 6 \sum_{n=1}^{\infty} A_n \exp\left[\frac{-\lambda_n^2 R \alpha \theta}{R^2}\right]$                     | Table A-1          | Drop circulation or oscillation: $10 < N_{Re} < 120, 315 < N_{Re} < 620$                         | Empirical, Eq. (IV-3)     |
| IV-9    | (J2)   | $0.905 \left(\frac{R \pi^2 \alpha \theta}{R^2}\right)^{1/2} + 0.0189$   |                    | Drop circulation or oscillation: $E_m < 0.5$   | Curve fitting, Eq. (IV-8) |
| IV-10   | (J2)   | $1 - 6 A_1 \exp[-\lambda_1^2 R \alpha \theta / R^2]$  | Table A-1          | Drop circulation or oscillation: $E_m > 0.5$   | Eq. (IV-8)                |

where

$$(N_{Nu})_0 = 2 + 0.569[(N_{Gr})_c(N_{Pr})_c]^{0.25} \quad (7)$$

is the natural-convection contribution to transfer, when  $(N_{Gr})_c \cdot (N_{Pr})_c < 10^8$ .

Oscillation of the wake, already setting in at Reynolds numbers of about 200 for stagnant drops and 500 for solid spheres (G12), as well as of the drops, increases the transfer rate. Direct proportionality between the transfer coefficient and  $(N_{Re})_c$  may be approached (G12). This is probably why Steinberger and Treybal (S20) found that the exponent  $m = 0.62$  for Reynolds

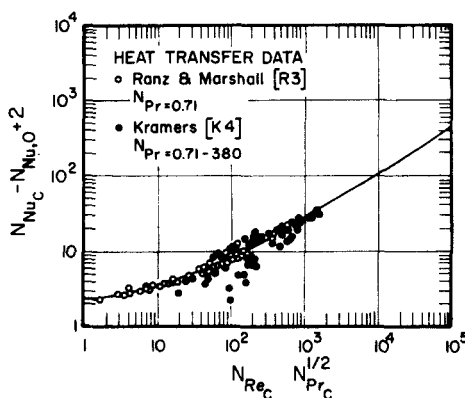


FIG. 3. Comparison of Eq. (6) with literature data (S20). (Courtesy of American Institute of Chemical Engineers.)

number gave the best fit in their general correlation, in the extended range of  $1 < (N_{Re})_c < 30000$ . If transfer in the wake region is assumed to obey the transient film mechanism postulated by the penetration theories of Higbie (H15) or Danckwerts (D2), an exponent higher than  $n = \frac{1}{2}$  would be expected for the Prandtl number. However, Eqs. (5) or (6) should be satisfactory for most dispersed-phase problems, where fluid spheres would not exceed  $(N_{Re})_c = 1000$ .

It is of interest to note that, by judicious definition of the characteristic diameter of nonspherical bodies, good agreement with the equations for spherical solids was obtained. A diameter defined by the total surface area of the body, divided by the perimeter normal to flow, was successfully used for spheres, hemispheres, cubes, prisms, and cylinders (P1), yielding  $a = 0$ ;  $b = 0.692$ ;  $m = 0.514$ ; and  $n = \frac{1}{2}$  [Eq. (4)]. Similar results were obtained for spheroids (S14), namely  $a = 0$ ;  $b = 0.74$ ;  $m = 0.5$ ; and  $n = \frac{1}{2}$ . The commonly used equivalent diameter of a sphere of the same volume as the body yields transfer coefficients increasing with eccentricity (S14).

## 2. Transfer Coefficients inside a Rigid Drop

Newman (N3), Geddes (G16), and others obtained the internal transfer efficiency, for the special case of zero resistance of the external film. By solving the unsteady-state diffusion equation, they obtained the following expression for the transfer efficiency:

$$E_m = 1 - \frac{6}{\pi^2} \sum_{n=1}^{\infty} \frac{1}{n^2} \exp \left[ -\frac{\pi^2 n^2 \alpha_d \Theta}{R^2} \right] \quad (8)$$

where  $\alpha$  is the thermal diffusivity,  $\Theta$  the time, and  $R$  the radius of the drop.

Evidently Eq. (8) yields the highest transfer coefficient for small drops (less than 1–2 mm. diam.), mainly encountered in agitating systems where the rigid-drop model should apply.

The transfer efficiency, calculated by Brown (B15) as a function of time for various water-drop diameters, is presented in Fig. 4, indicating the minimum residence time required for a given transfer efficiency.

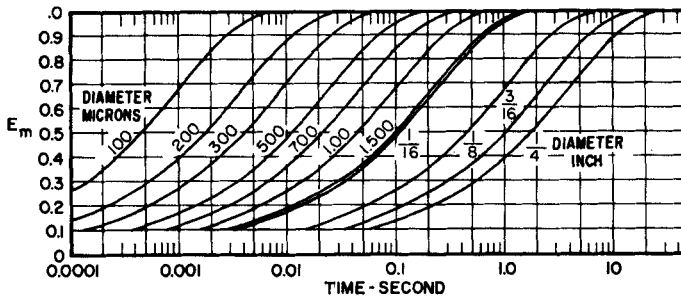


FIG. 4. Time of heating, by conduction, a sphere of water: Eq. (8), zero initial temperature, thermal diffusivity  $0.0065 \text{ ft}^2/\text{hr}$  (B15). (Courtesy of American Society of Mechanical Engineers.)

A simplified solution based on experimental data was suggested by Vermeulen (V1):

$$E_m = \left[ 1 - \exp \left( -\frac{\pi^2 \alpha_d \Theta}{R^2} \right) \right]^{1/2} \quad (9)$$

An approximate solution applicable for  $\alpha\Theta/R^2 < 10^{-2}$  can be obtained (H13) by using the solution for diffusion from a plane surface into an infinitely thick layer, which gives

$$E_m \simeq \frac{6}{\pi^{1/2}} \left( \frac{\alpha_d \Theta}{R^2} \right)^{1/2} \quad (10)$$

However, comparison of Eqs. (8), (9), and (10) (Fig. 10) shows Eq. (10) to yield somewhat higher values of  $E_m$  even in the limited range indicated here.

Grober (G22) and Jakob (J1) included the external film resistance, and obtained

$$E_m = 1 - 6 \sum_{n=1}^{\infty} A_n \exp \left[ -\frac{\lambda_n^2 \alpha \Theta}{R^2} \right] \quad (11)$$

A graphical solution of Eq. (11) is given by McAdams (M2). A modified form of this graph, suggested by Calderbank (C1), is presented in Fig. 5. The constants  $A_n$  and eigenvalues  $\lambda_n$  are given in the Appendix, Table A-I.

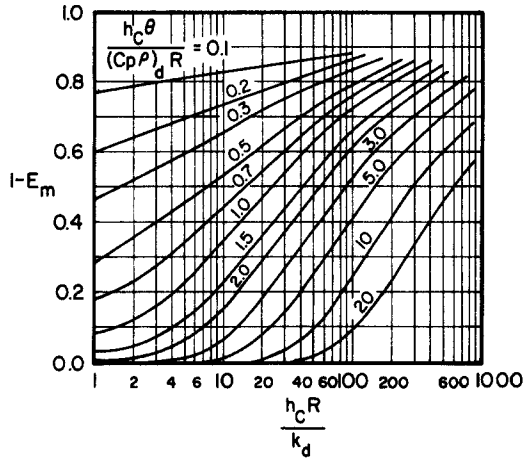


FIG. 5. Transfer efficiency by diffusion into spheres with finite continuous-phase resistance (C1). (Courtesy of *Chemical Engineering Science*.)

### C. COMPLETELY MIXED-DROP MODEL

In accordance with the two-film theory, the two phases are considered to have uniform, though different, bulk temperatures. The over-all heat-transfer coefficient through the combined films  $U$  is defined by

$$dQ/d\Theta = AU(T_c - T_d) \quad (12)$$

where  $dQ = (VC_p \rho T)_d$  is the heat transferred to the drop, and  $A$  and  $V$  are the surface area and volume of the drop, respectively. Integration over the duration of contact between the phases yields

$$E_m = 1 - \exp \left[ -\left( \frac{A}{V \rho C_p} \right)_d U \Theta \right] \quad (13)$$

For the classical case of a completely mixed drop, where the internal film resistance is negligible compared with that of the external film, we have  $U = h_c$ ; i.e., the external resistance governs the transfer rate.

Similarly, adaptation of the Higbie penetration theory for a completely mixed drop, with the contact time assumed to be identical with that required for the drop to traverse a distance equal to its diameter, yields [see also Eq. (29)]

$$E_m \simeq 1 - \exp \left[ -3.39 \left( \frac{\alpha_c \Theta}{R^2} \right)^{0.5} \right] \quad (14)$$

## D. DROPS WITH INTERNAL CIRCULATION

### 1. General Characteristics of the Model

Drop circulation is by far the most important and stimulating model and numerous workers have treated its momentum-, heat-, and mass-transfer aspects both theoretically<sup>1</sup> and experimentally.<sup>2</sup>

A drop (or bubble) moving in a viscous fluid tends to circulate internally (Fig. 6) due to the shear stress applied at its interface by the ambient fluid.

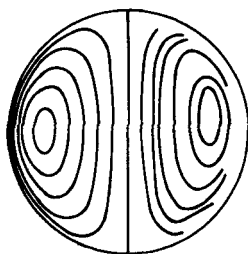


FIG. 6. Comparison of theoretical and experimental circulation patterns: glycerine drop in castor oil (S18).

As a result of the motion of the interface, the viscous friction is lower and the drop velocity higher. Hence the transfer rate is increased by a factor approximately equal to  $1.9(N_{Pr})^{1/6}$  compared with the rigid drop. One may expect circulation to increase with drop size and the viscosity ratio  $\mu_c/\mu_d$  of the two fluids.

According to the classical theories of Hadamard (H2), Rybczynski (R9), and Boussinesq (B10), circulation sets in whenever a drop moves in a viscous fluid. Figure 6 shows Hadamard streamlines compared with the experimental ones obtained by Spelles (S18). Experiments (G8) indicated that circulation takes place readily, though not exclusively (G5), in the presence of a suitable driving force (temperature or concentration gradients) and only above a

<sup>1</sup> B4, B10, B12, D6, D7, F5, H2, H5, H15, K5, K6, L6, L7, L8, R8, R9, S3, and others.

<sup>2</sup> B13, C1, D8, E2, G3, G5, G6, G8, G12, G20, H4, H5, L15, L17, M3, R6, R8, S8, S18, T3, T4, and others.

certain level of the Reynolds number; i.e., whenever the drag force exceeds a certain minimum discussed below. The Reynolds number at which circulation sets in within the drop decreases with increasing viscosity of the continuous phase (G10).

Garner and Skelland (G9) suggested an equation for the critical Reynolds number determining the onset of circulation, but it is rather inaccurate since circulation is highly dependent on fluid purity and on the presence of surface active impurities (G5, G21, L17). The lower the interfacial tension, the lower the transitional Reynolds number (G8), and the higher the over-all transfer coefficient (L11, S6). For a drop with high surface tension, minute amounts of impurities suffice to produce an appreciable surface-tension gradient at the interface, thus greatly retarding circulation. Bond (B8, B9) included surface tension in his criterion for the onset of circulation, inferring that the latter was restricted by the interfacial tension when the radius was small enough. However, this criterion was derived from experimental data in the streamline region and is rather inadequate in the practical ranges of the Reynolds numbers, especially since circulation is known to be strongly affected by immeasurably small changes in surface tension due to surface active agents (D6, L17). Thus retardation of circulation is associated with surface-tension gradients along the interface, rather than a simple reduction in surface tension. For a given system, the effect of a surface-tension gradient increases with decreasing drop diameter, and below a certain size (as shown later) circulation is reduced or arrested with the transfer coefficients approaching the "rigid-drop" values.

It is now generally agreed that an adsorbed film of a surface active agent, which sets up tangential forces on the surface of the drop, is responsible for reducing or arresting drop circulation. The motion of the drop's interface causes a concentration gradient of the surface active agent, resulting in a gradient in the interfacial tension. [Polar oils are less susceptible, having lower energies of adsorption and higher rates of desorption of surface active material compared with nonpolar oils (D6).] The ensuing tangential forces are codirectional with the decreasing interfacial tension; they affect the flow characteristics at the interface by counterbalancing part of the shearing stress exerted by the continuous phase on the drop surface, and thereby reduce circulation. For a given system the resistance to circulation in the drop depends on its diameter; the smaller the drop, the larger will be the surface pressure gradient between its front and rear, and the smaller will be the tangential friction stress (D6). A force equilibrium at any point on the interface (G21, S4) gives

$$\frac{\partial \sigma}{\partial x} = \mu_c \frac{du_c}{dy} - \mu_d \frac{du_d}{dy} \quad (15)$$



where the  $x$  and  $y$  directions, respectively, are parallel and normal to the drop interface. Thus circulation within the drop will be retarded appreciably, or even arrested, if the interfacial tension gradient and external viscous drag are of the same order of magnitude. If the rear of the drop is covered beyond  $\phi > 135^\circ$ , drag coefficients will correspond to the experimental values for solid spheres.

According to Savic (S3), Levich (L8), and others (D6, H3, L17), an immobile "cap" may be formed at the bottom of the drop, confining circulation to its front part only. This is due to the relatively small velocities at the vicinity of the rear stagnation point, and to accumulation of the surface active material near the point of flow separation (H3), if present. The resulting interfacial-tension gradient should prevent transmission of tangential stress to the interior fluid, thus creating a stagnant region in the rear part of the drop. This may explain why the second vortex ring inside the drop, predicted by Hamielec and Johnson (H3) for the intermediate range of Reynolds numbers, has never been observed.

If the rate of desorption of surfactants is very much greater than the rate at which the drop traverses through a distance equivalent to its diameter (about 0.02 sec), one may expect (D6) no accumulation of surfactants at the rear end. A quantitative semiempirical expression for the degree of drop circulation as a function of the viscous forces, drop diameter, densities and the compressional modulus of the surface film (surface-tension gradient), as well as the empirical fraction of liquid circulating, has been suggested by Davies (D6).

Levich (L8) and others (S4) have suggested a criterion for the critical drop diameter, incorporating the difference between the limiting interfacial tension  $\sigma_s$  (determined for large concentrations of surface active impurities) and that of the pure system  $\sigma$ . The proposed critical transition radius is given by Eq. 58 (Section VI,C). The dependence of circulation on the difference in interfacial tension has been experimentally verified (D6, G21), but no proof of the validity of this criterion has been reported. However, application of this criterion should provide approximate values.

It is of interest that the onset of circulation of liquid drops is associated with deformation of the spherical drop into an ellipsoid (R8, C6, G2). Deformation of the spherical drops was found to be associated with oscillations and with higher transfer rates (C6) even in highly viscous fluids where stagnant drop characteristics are generally assumed. Garner (G12), who studied the wake behind the deformed drops, concluded that the higher transfer rates were due to the onset of instability and oscillation of the wake at this relatively low Reynolds number (200) compared with 400 to 450 for solid spheres. However, no quantitative relationship is available.

Terjesen *et al.* (T3, B13) suggested that internal circulation in itself does

not account for the higher transfer coefficients of drops, compared with solid spheres. For pure fluids the higher transfer coefficients were accounted for by the higher velocities of circulating drops, rather than by the effect of circulation on the thickness of the external boundary layer. Drop velocity was found to be much more sensitive to the presence of surfactant than the transfer coefficients. "Solid-drop" velocities were reached at concentrations of surface active agent about 10 times lower than those required for the limiting reduction in the rate of mass transfer. Thus, if reduction in velocity represents reduction and eventual elimination of the internal circulation, they suggest that the higher mass-transfer rates realized are due to hydrodynamic causes such as formation of a vortex ring, rather than to internal circulation. This explanation is only partial, since the higher transfer rates measured with the noncirculating "slow" drops at low concentrations of the surfactants are related both to the area covered by the surfactant at the rear and to the turbulent wake characteristics.

The effect of the wake behavior and boundary layer separation on the rate of mass transfer was studied by Garner and Tayeban (G12). The volumes of the wakes behind highly viscous drops of about 300 cP viscosity, assumed stagnant, were found to be about twice those behind circulating drops of 6.5 cP viscosity. This corresponds to a large difference in the angle of boundary layer separation. Conkie and Savic (C5) suggest that the angle of separation for circulating spherical drops should be  $108^\circ$  (the same as for a solid sphere at higher Reynolds numbers). Garner showed that, for Reynolds numbers of 500, the angle for stagnant drops and for solid spheres is about  $105^\circ$ , whereas for circulating drops the value is  $140^\circ$ . Boundary layer separation was first observed at  $(N_{Re})_c = 60$  for circulating drops of water in benzyl alcohol, compared with about 20 for solid spheres and stagnant drops. For fully circulating drops, the separation point should shift to the rear stagnation point, and no boundary layer separation should occur. The transfer coefficients should then approach the values predicted by potential-flow theory; Levich (F5, L8) reports that at  $(N_{Re})_c = 300$  the turbulent wake of an uncontaminated gas occupies only an angle of  $2^\circ$  at the rear.

Thus, even for drops of low viscosity if not completely circulating, the interfacial velocity gradient is smaller and the contact area larger, resulting with higher transfer coefficients compared with stagnant "solid" spheres. For small drops, below 0.25 cm, the wake is nearly saturated, and steady transfer coefficients are obtained. The concentration in the wake decreases below the saturation value with increasing drop diameter and velocity, corresponding to higher Reynolds numbers and higher turbulence in the wake. Even with highly viscous drops, the onset of instability of the wake at  $(N_{Re})_c = 160$  resulted in transfer coefficients higher by some 30% (G12). Thus the toroidal vortex, setting in under boundary layer separation at

Reynolds numbers of about 20 (in stagnant drops), gains strength as the separation point shifts at higher Reynolds numbers. The increase in transfer coefficient in the continuous phase, even for drops not fully circulating, may thus be attributed to the combined effect of the increased disturbance intensity around the separation point and in the wake, to the forward movement of the separation point, and to higher velocities.

The relative importance of the rear part of the drops compared with solid spheres was noted by Garner and also by Terjesen (T3). Garner (G4, G11) and others (A1) showed that at moderate Reynolds numbers, up to 2500, most of the transfer takes place in the front part of the solid spheres ahead of the separation point. However, no frontal diffusion into liquid drops could be detected at high rates of fall (G2), whereas it was readily noticeable behind the drop. Thorsen and Terjesen (T3) concluded that the relative importance of the front and rear for drops and solid spheres is reversed, beginning with Reynolds numbers above 20. This hypothesis does not account for the extreme case where internal circulation is reversed (L17), probably due to higher transfer rates at the front and to the nonnegligible internal resistance to transfer.

Another aspect, usually overlooked, is the effect of natural convection inside the drop on the transfer coefficient. Transfer coefficients differing by about 25% were found (W12) when drops were heated or cooled in the continuous phase (see Section IV,B).

A decrease of the transfer coefficient of drops and bubbles with time, due to decay of circulation, has been noted in a number of studies. Deindoerfer and Humphrey (D8) showed that the transfer coefficients of one- to two-second-old oxygen bubbles rising in water were in agreement with those obtained from the Higbie (H15) penetration theory, whereas the coefficients of six-second-old bubbles were close to those predicted by the rigid-drop theories. High absorption rates during the first few seconds after drop formation were also measured (G7) for single liquid drops suspended in a gas stream. Garner and Lane (G7) attributed such high rates to a high initial rate of circulation within the drop due to oscillations arising in the breaking away of the drop from the forming nozzle. They found a direct relation between circulation (as based on the flow adjacent to the interface) and the internal resistance to mass transfer, but none between drop oscillation and mass transfer inside the drop. However, recent cinecamera studies of Marsh and Heideger (M1a) on mass transfer to falling drops showed no oscillations of the newly formed drops upon separation from the forming nozzle. The very high mass-transfer rates in the first second following formation were attributed to the presence of disordered internal motion caused by the high velocity of the liquid comprising the drop. An approximate mathematical

model predicting the decay of the transfer coefficient was applied with apparent success (M1a). The sharp decrease in the transfer coefficient may thus be understood in the light of the rapid decay of the internal motion after the detachment of the drop from the nozzle; after this brief time, the drop will be either stagnant or slowly circulating, depending on relative velocity, drop diameter, interfacial tension, and viscosity.

Calderbank and Lochiel (C1a) have recently substantiated Hammerton and Garner's findings (H4) that the rate of transfer does not vary as bubble ages from roughly 1–6 sec after bubble release, over a bubble diameter range of 0.5–2.65 cm. This is in some disagreement with the results of Deindorfer and Humphrey, obtained with bubbles smaller than 0.5 cm. However, about 45% of the decay of the transfer coefficient reported by the latter workers occurs between 0.5–1.0 sec, which is in general agreement with the more recent studies of Marsh and Heideger.

For suspended bubbles, rigid-drop values were obtained (G21) after some 40–60 sec. Gradual absorption of surface active agents would account for these facts.

The decay of circulation was also reported by Rumscheidt and Mason (R8), who studied internal and external streamlines associated with circulating drops. They showed that behavior inside the drop is highly sensitive to traces of surface active agents present in either fluid phase, and suggested that accumulation of the latter at the interface could render it viscoelastic. Thus the time of complete decay is dependent on the rate at which the surface active impurities are conveyed to the interface (L8, L17). With all surface active agents assumed to be inside the drop, the decay time was found (R8) directly proportional to the velocity gradient and inversely proportional to  $(\mu_d/\mu_c) + 1$ . However, circulation decay does appear in systems believed to be extremely pure, which is consistent with Henniker's ideas on the viscoelasticity of the interface (H14).

Aging of the transfer coefficients was also noticed by Baird and Davidson (B1) in experiments on absorption of very large  $\text{CO}_2$  bubbles in tap water. As suggested earlier by Garner (G12), the unsteady value of the transfer coefficient can probably be attributed to slow saturation of the turbulent wake under the spherical-cup bubble, where transfer is by eddy diffusion rather than by convection. With bubbles less than 2.5 cm diam, time-independent transfer coefficients were obtained. This was attributed (B1) to more rapid bubble circulation and renewal of the wake, which permit a steady state to set in faster behind the smaller bubbles; it is consistent both with the dependence of the steady-state time on the Peclet number (B6), which for spherical bubbles yields  $\Theta \propto R$ , and with the relationship  $\Theta \propto R^{2/3}$ , suggested by Levich (L8). However, due to the irregular hydrodynamic

behavior of the "large" spherical-cup bubbles in question, some other factors may be involved. A detailed discussion of some of these factors in relation to gas-liquid mass transfer is given by Calderbank (C1a).

The time dependence of the transfer coefficient is closely related to the observed decrease of the transfer coefficients per unit height with increasing column height (B11, E1, G12, P2), and undoubtedly introduces a significant error in the determination of end effects by the variable-column-height technique.

## 2. Transfer Coefficients Outside Circulating Drops

Internal circulation is generally assumed to cause thinning of the outside boundary layer, thus increasing appreciably the transfer rate between the drop and the ambient fluid (B12, G3). In other words, because of the mobility of the interface, a smaller velocity gradient exists near it that results in larger convective heat transfer. Rumscheidt and Mason (R8) proved the dependence of the streamlines outside and inside spherical drops undergoing laminar shear flow on the viscosity ratio of the fluids. As the exact velocity profiles for normal flow conditions are unknown, the solutions for the transfer rate that account for this effect are only approximate.

Johnson *et al.* (B12) followed Friedlander's (F2) solution based on the Stokes velocity profiles around solid particles, and numerically calculated the external coefficients for  $N_{Re} < 1$ . Only a slight difference in the Nusselt number was observed when the velocity profiles of Stokes and Hadamard were postulated. These calculations showed that the transfer coefficient ratio of drops and solids increases from 1 for  $(N_{Pe})_c = 1$  to 3 for  $(N_{Pe})_c = 10^4$ . In the absence of oscillation, similar results may be expected at moderately higher Reynolds numbers (C1, H3).

The solution for low Reynolds number (or "creeping" flow),  $(N_{Re})_c < 1$ , and high Prandtl numbers, i.e.,  $N_{Pe} \gg 1$ , was analytically derived by Levich (L8, p. 404). The approximate streamline is given as

$$\psi = u_s R(r - R) \sin^2 \phi \quad (16)$$

When  $u_s$ , the velocity at the drop's equator, is taken as  $u\mu_c/2(\mu_c + \mu_d)$ , the Nusselt number is

$$(N_{Nu})_c = 0.65(N_{Pe})_c^{0.5} \left( \frac{\mu_c}{\mu_c + \mu_d} \right)^{0.5}; \quad N_{Pe} \gg 1, \quad N_{Re} < 1 \quad (17)$$

A similar equation is suggested by Griffith (G21). Experimental confirmation of Eq. (17) is reported (L8). Some other proposed solutions are given in Table III and compared graphically in Fig. 7.

No exact analytical solution for heat transfer to drops at  $(N_{Re})_c > 1$  is possible at present. However, some approximate solutions are possible, depending on the degree of motion postulated for the fluid interface. For the Reynolds number range  $10 < N_{Re} < 30$  and  $N_{Pe} \gg 1$ , Hamielec and Johnson

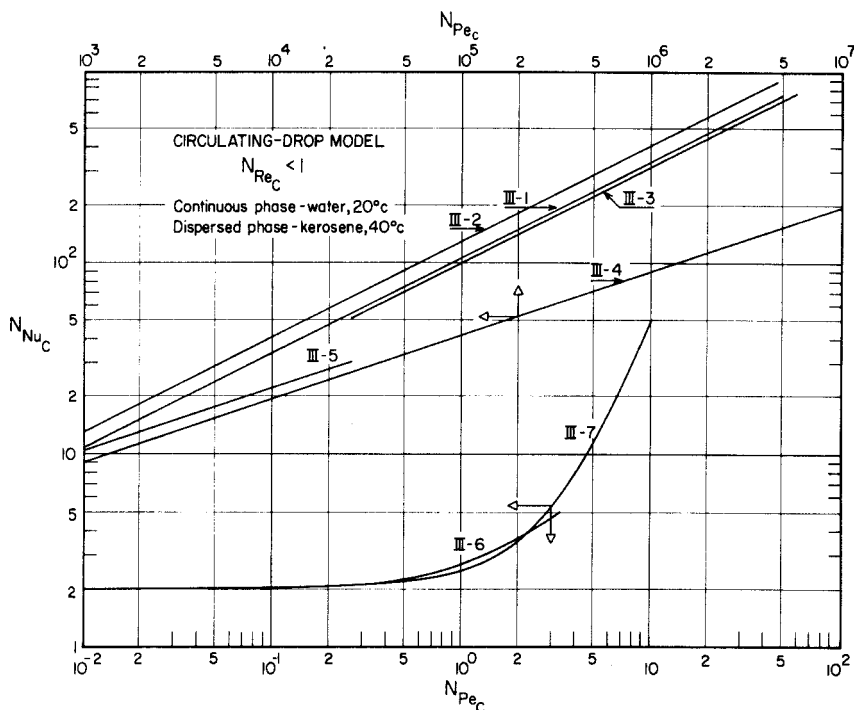


FIG. 7. Comparison of equations for outside Nusselt number (Table III).

(H3) obtained functional approximations for the velocity components by assuming a trial stream function in the Navier-Stokes equations and evaluating the undetermined coefficients from the boundary conditions using the method of residuals. Their relationship can be presented in the form of

$$(N_{Nu})_c = 1.13 f(N_{Pe})^{0.5} \quad (17a)$$

Recurrence formulas related the higher coefficients in the original stream function to their respective first coefficients, and these were given graphically as a function of the Reynolds numbers; up to 30. An extension of this solution to  $N_{Re} = 70$  was subsequently given (graphically) by Baird and Hamielec (B1a). Some of the other proposed solutions are summarized in Table III and compared in Fig. 8.

The theoretically simplest approach is to assume that no external boundary layer exists, thus obtaining the highest average values for the external transfer coefficients. Experience proves this assumption to hold for many important practical applications (D8, H8, H13, W3, and others), where the Reynolds number and viscosity ratio  $\mu_c/\mu_d$  are high. Boussinesq (B10) was the first to

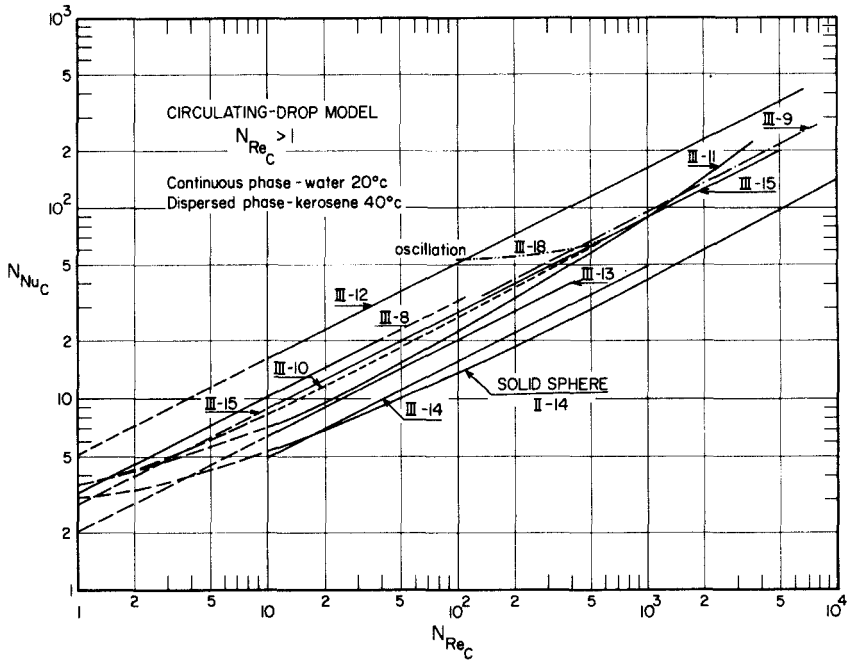


FIG. 8. Comparison of equations for outside Nusselt number (Table III).

apply potential flow in solving forced convection heat transfer and, recently, Ruckenstein (R7) applied it in determining heat-transfer coefficients at the interface of growing vapor bubbles. With certain simplifying assumptions, the well-known equation for steady-state heat transfer is obtained:

$$(N_{Nu})_c = 1.13(N_{Pe})_c^{0.5}; \quad N_{Pe} \gg 1 \quad (18)$$

By modifying Boussinesq's transformation to allow for unsteady state, the time-dependent temperature distribution in potential flow past a spherical bubble was recently obtained (B6) numerically. For low Peclet numbers ( $2 < (N_{Pe})_c < 100$ ), where the conduction contribution cannot be neglected, graphical integration of the steady-state temperature profiles yields approximately

$$(N_{Nu})_c \simeq 1.25(N_{Pe})_c^{0.5}; \quad 2 < N_{Pe} < 100 \quad (19)$$

We note that Higbie's penetration theory (H15), with contact time assumed as that required by the drop to traverse a distance of one diameter (W6), gives an expression identical with Eq. (18). Although potential-flow theory, unlike the penetration theory, takes interfacial acceleration into account, the two are actually physically identical, both being based on diffusion into an element of fluid sliding over the constant-temperature interface.

Conkie and Savic (C5) proposed a correction factor for the presence of a boundary layer by introducing a velocity factor  $K_v$  defined as the ratio of the true interfacial velocity and potential-theory velocity, and dependent on the Reynolds number and viscosity ratio (Fig. 9). In their view, the boundary

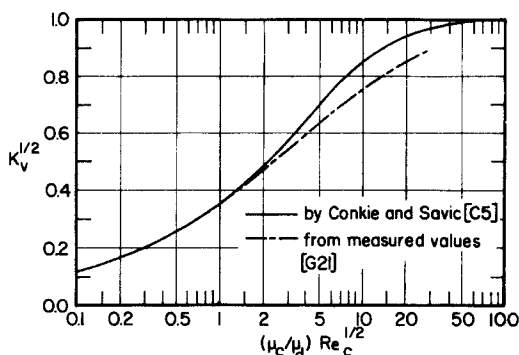


FIG. 9. The ratio  $K_v$  of the speed with which the interface between a drop and surrounding fluid moves to that speed with which the interface would move if the fluids were ideal (G21). (Courtesy of *Chemical Engineering Science*.)

layer velocity around the drop varies by a factor of  $(1 - K_v)^{0.5}$ , with  $K_v$  tending to zero at very low Reynolds numbers and to 1 at high Reynolds numbers. Griffith (G20, G21) extended this approach and incorporated the velocity factor in his equations for both slowly and rapidly circulating drops. The suggested equation for rapidly circulating drops is

$$N_{Nu} = 2 + 1.13(N_{Pe})_c \cdot K_v^{0.5}; \quad N_{Pe} \gg 1 \quad (20)$$

where the constant "2" was artificially introduced to allow for the lowest theoretical Nusselt number in a stagnant medium. With  $K_v = 0.53$ , one obtains Eq. (III-14). A basically similar relationship was obtained by Chao (C4a) who applied boundary layer theory to flow around circulating fluid spheres by considering viscous effects as a perturbation on potential flow. Comparison of his expression for the Nusselt number with Eq. (20) yields

$$K_v = 1 - 1.43(N_{Re})_c^{-1/2} \quad (20a)$$

applicable for  $100 < (N_{Re})_c < 1000$ . A more accurate expression, including



the viscosity ratio, is given by Lochiel and Calderbank (L18):

$$K_v = 1 - \frac{2 + 3\mu_d/\mu_c}{1 + (\rho_d\mu_d/\rho_c\mu_c)^{1/2}} 1.45(N_{Re})_c^{-1/2} \quad (20b)$$

Solutions for the transfer coefficients around axisymmetric bodies of revolution (oblate and prolate spheroids and bubbles with spherical caps shapes) in potential flow were also reported (L18) and related to experiment (C1a).

The maximum possible continuous-phase heat transfer coefficient obtainable for nonoscillating drops was suggested by Elzinga and Banchero (E2). Their equation is based on the maximum heat transfer to a solid sphere, calculated in the vicinity of the front stagnation point. Applying it to drops with internal circulation they obtained

$$(N_{Nu})_c = 1.96(N_{Pe})_c^{0.5} \quad (21)$$

As mentioned previously, Terjesen *et al.* (B13, T3) attribute the high transfer coefficients characterizing circulating drops, in contrast to non-circulating drops, to their relatively higher velocities. Thus circulation is associated with higher drop velocity, and accordingly with higher Reynolds numbers and higher transfer rates. They also showed that the effect of interfacial turbulence (or "interfacial agitation") is rather small compared with that of velocity. The higher coefficients are attributed to hydrodynamic disturbances in the unstable boundary layer and the vortex formed behind the moving drop. Thus, "in contrast to the solid spheres above a certain Reynolds number, most of the transfer takes place at the rear of the drop" where the boundary layer is unstable and undefined, and turbulence exists. Terjesen's data are in good agreement with Garner's equation (III-16) where the exponent of the Prandtl number is 0.42, as well as with his own (III-17) where the exponent is  $\frac{1}{3}$ ; this also indicates that drop viscosity (in the range 0.6–1.7 cP) has very little effect on the external transfer coefficient.

Drop oscillation was found to increase the rate of mass transfer by a factor of two (G9) to four (S13), unlike gas-liquid systems (C6), due probably to reduced external resistance (G12). Oscillation usually sets in at Reynolds numbers between 150 and 200, bringing about a higher power than  $\frac{1}{2}$  for the Reynolds number (G12, L13, C7), which is consistent with Eq. (6). Oscillation of the wake, setting in at about the same Reynolds number (200), was found to have a similar effect on the rate of transfer (G12). Oscillation effects are of importance in systems with a low-viscosity continuous phase, where Reynolds numbers higher than 200 are obtained. Oscillation is also stronger in systems with low interfacial tension and low viscosity of the dispersed phase (G12). For circulating and oscillating drops Garner suggests the

following empirical equation:

$$(N_{Nu})_c = 50 + 8.5 \times 10^{-3} (N_{Re})_c^1 (N_{Pr})^{0.7} \quad (22)$$

The maximum deviation of the experimental data in the range of  $150 < (N_{Re})_c < 700$  was reported as 12%

### 3. *Transfer Coefficients Inside Circulating Drops*

The equations of fluid motion inside and outside a circulating drop under viscous flow regime were solved by Hadamard (H2) and Rybczynski (R9) in 1911, and are quoted in hydrodynamics textbooks (L2). The complete derivation is also repeated by Levich (L8). Although Hadamard's stream functions are strictly applicable to the viscous region only, visual observations (G10, S18) indicated that the function approximates actual flows (E2, H3). Hadamard's stream function inside the drop, as given in polar coordinates with the origin at the center of the drop (K5), is

$$\psi = -\frac{g \Delta \rho R^2}{6(2\mu_c + 3\mu_d)} (1 - r^2) r^2 \sin^2 \phi \quad (23)$$

Kronig and Brink (K5) used the Fourier-Poisson equation to derive equations for the temperature distribution and heat transfer inside a drop with internal circulation described by Eq. (23). Assuming that diffusion is negligible along internal streamlines and that the isotherms at any particular moment coincide with the streamlines, and disregarding external film resistance, they obtained the following equation for the transfer efficiency:

$$E_m = 1 - \frac{3}{8} \sum_{n=1}^{\infty} A_n^2 \exp \left[ -\frac{\lambda_n 16 \alpha_d \Theta}{R^2} \right] \quad (24)$$

The constants  $A_n$  and eigenvalues  $\lambda_n$  were recalculated more recently by Elzinga and Banchemo (E2), who also determined them for various external film resistances. Their data are summarized in Tables A-II and A-III in the Appendix.

Danckwerts (D1) has pointed out that Eq. (24) is not as limited as originally implied; this is evident from many experiments (C1, Table I) with Reynolds numbers up to 2000 under oscillation-free conditions. A simpler empirical equation (Eq. IV-6, Table IV) in close agreement with Eq. (24) was suggested by Calderbank and Korchinski (C1). A graphical comparison of Eq. (24) with Eq. (IV-6) and Eqs. (8)–(10) is shown in Fig. 10. Kronig and Brink's solution gives heat-transfer coefficients about 1.5 times higher than the solid drop model, corresponding to an effective diffusivity 2.25 times larger than the molecular diffusivity. This is to be expected, as their model in effect implies reduction of the drop diameter (by about half) to a size charac-

teristic of the circulation pattern (H5). Since Kronig and Brink's stream lines are closed loops, the transfer rate calculated by Eq. (24) is independent of the circulation velocity.

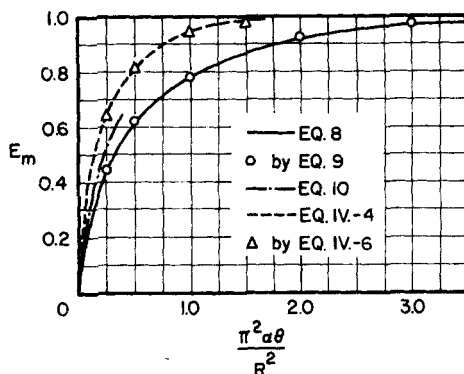


FIG. 10. Equations for diffusion into stagnant and circulating drops (C1).

Handlos and Baron (H5) proposed another model for the more practical range of Reynolds numbers (about 1000). They assumed that the tangential motion caused by circulation is combined with an assumed random radial motion caused by internal vibration, and determined the eddy diffusivity  $\alpha_e$  subsequently used in solving the appropriate Fourier-Poisson equations. They postulated radial stream lines, as shown in Fig. 11, rather than those

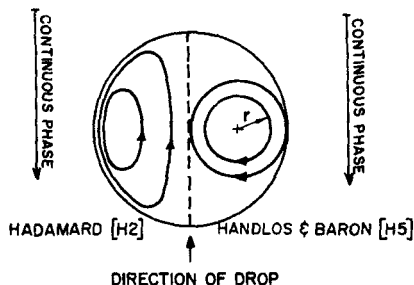


FIG. 11. Comparison of drop-circulating models.

derived by Hadamard. Using probability functions, Kronig and Brink's average circulation time, and Einstein's equation to correct the mean-square deviation for a given time to the effective diffusivity, they obtained

$$\alpha_e = \frac{(N_{Pe'})_d}{2048} (6\omega^2 + 8\omega + 3) \quad (25)$$

where

$$(N_{Pe'})_d = \frac{(N_{Pe})_d}{1 + \mu_d/\mu_c} \quad (26)$$

$\omega = 4r/D$ , and  $r$  is the radial distance from the center of the circulation torus. Using the first eigenvalue only, the transfer efficiency of Eq. (IV-7) is conveniently reduced to

$$E_m \simeq 1 - \exp\left[-5.62 \times 10^{-3}(N_{Pe'}) \frac{\alpha_d \Theta}{R^2}\right] \quad (27)$$

The internal Nusselt number is given (H5) by

$$(N_{Nu})_d = 0.00375(N_{Pe'})_d \quad (28)$$

Their experimental data are in agreement with the theoretical values within 20%. Extension of Handlos and Baron's model to include surface resistance was recently proposed by Welleck and Skelland (W4a).

If potential flow and constant surface temperature are assumed, an equation analogous to Eq. (18) is obtained for the internal Nusselt number. Note, however, that the reference velocity in the internal Peclet number is the drop velocity. Similar results will be obtained from the penetration theory, according to which the film is assumed infinite with respect to the depth of heat penetration during the short contact time of a fluid element "sliding" over the interface. Licht and Pansing (L13) report West's equation, based on the transient film concept, for the case of mass transfer through the combined film resistance. In terms of the overall heat-transfer resistance,  $1/U$  ( $= 1/h_d + 1/h_c$ ) and if the contact time is that required for the drop to traverse a distance equal to its diameter, West's equations yield

$$E_m = 1 - \exp\left[-3.39\left(\frac{\alpha_U \Theta}{R^2}\right)^{0.5}\right] \quad (29)$$

where

$$\alpha_U^{1/2} = \frac{(\alpha_c \alpha_d)^{1/2}}{\alpha_c^{1/2} + \alpha_d^{1/2}}$$

For negligible drop-side film resistance,  $U = h_c$ ,  $\alpha_c/\alpha_d \ll 1$ , and  $\alpha_U^{1/2}$  approaches  $\alpha_c^{1/2}$ . For negligible continuous side film resistance,  $U = h_d$ ,  $\alpha_c/\alpha_d \gg 1$ , and  $\alpha_U^{1/2}$  approaches  $\alpha_d^{1/2}$ .

An experimentally convenient technique for relating internal transfer coefficients is based on applying an experimental factor  $\bar{R}$ , the effective diffusivity factor, to the rigid-drop equations.  $\bar{R}$  is the ratio of effective and molecular diffusivity in a stagnant drop. Equation (IV-8), in effect, defines the  $\bar{R}$  factor.  $\bar{R}$  ranges from 1.6 to 3.3 circulating drops at moderate Reynolds

numbers and up to 70 for moderate and high Reynolds numbers, in the presence of drop oscillations (C1).

The experimental effective diffusivity factor should normally approach the value of 2.25 calculated by Kronig and Brink (K5) at low Reynolds numbers. For drops with "turbulent" circulation described by Handlos and Baron's model,  $\bar{R}$  is given (J2) by

$$\bar{R} = (N_{Pe})_d / 2048 \quad (30)$$

In practice, lower values than those calculated according to Eq. (30) are found for intermediate Reynolds numbers, only approaching them in the presence of oscillation. A compilation of experimental  $\bar{R}$  factors is available (C1). The experimental effective diffusivity in gas absorption with internal circulation has been plotted against the axial velocity representing the flow adjacent to the interface (G7), and shows a direct relation between circulation and internal resistance. Similar results are reported (C6) for other gas-liquid and liquid-liquid systems.

Constan and Calvert (C6) recently proposed a theoretical equation for the effective diffusivity, as a function of the transfer efficiency and of a pseudo-film-thickness dependent on circulation velocity. However, no correlation between the film thickness and the Reynolds number yet exists. Use of this theoretical equation necessitates measurement of the circulation velocity, which does not simplify matters.

The various equations derived for the transfer efficiency are summarized in Table IV. The equations for the rigid-drop model are included for comparison.

#### IV. Heat Transfer to Drops Moving in a Continuously Varying Temperature Field

##### A. SINGLE-DROP STUDIES

Compared with the large volume of work dealing with drops at constant temperature (or concentration), very little has been reported on single drops moving in a variable temperature (or concentration) medium. A variable temperature, with an approximately linear temperature gradient, was used by Wakeshima (W1, W2), to study the limit of superheat of pure liquid drops. However, since drop temperature could not be measured, his data cannot be used for determination of heat-transfer coefficients.

An interesting study on the effect of continuous longitudinal temperature gradient at the surface of a droplet on its flow characteristics is given by Young *et al.* (Y1). Under these conditions, droplets (and bubbles) were shown

to move in the direction of their warmer poles. "Small bubbles are attracted by hot objects."

The internal heat-transfer efficiency for a rigid drop with zero external film resistance, moving at a constant velocity in a fluid under linear temperature change along the drop path, can be shown (C4) to be

$$E_m = 1 - \frac{R^2}{\alpha\Theta} \left( \frac{1}{15} - \frac{6}{\pi^4} \sum_{n=1}^{\infty} \frac{1}{n^4} \exp \left[ -\frac{n^2 \pi^2 \alpha \Theta}{R^2} \right] \right) \quad (31)$$

For a rigid drop (with a finite external film resistance) moving in an arbitrary but continuous temperature field of the continuous phase, following Barbotteau's (B3) model, the internal heat-transfer efficiency (S8) was found to be

$$\bar{E}_m = \frac{T_0 - T_i}{T_{c0} - T_i} = -\frac{2}{3(B-1)} - 6 \sum_{n=1}^{\infty} C_n \exp[-\lambda_n^2 SZ/R] \quad (32)$$

where  $T_{c0}$  is the average temperature of the continuous phase at its outlet (or at the same cross section where  $T_i$ , the inlet drop temperature, is measured),  $Z$  the column height (or distance traversed by the drop), and

$$S = \frac{\alpha_d}{UR} = \frac{1}{(N_{pe})_d}, \quad B = (GC_{p\rho})_d / (GC_{p\rho})_c,$$

$$C_n = [(3B + E\lambda_n^2)^2 + \lambda_n^2(1 - E) - 9B]^{-1}$$

The eigenvalues  $\lambda_n$  may be calculated from

$$\tan \lambda_n = \frac{3B + E\lambda_n^2}{3B + (E-1)\lambda_n^2} \cdot \lambda_n$$

where

$$E = \frac{k_d}{h_c R} = \frac{1}{N_{Bi}}$$

The continuous-phase temperature  $T_{cz}$  at any cross section of the column may be determined from the following equation:

$$\frac{T_{cz} - T_{c0}}{T_{c0} - T_i} = 6B \sum_{n=1}^{\infty} C_n [1 - \exp(-\lambda_n^2 SZ/R)] \quad (33)$$

For gas oil dispersed in water, with the external film-transfer coefficient taken as 25 Btu/hr/ft<sup>2</sup>/°F, the first two eigenvalues are  $\lambda_1 = 2.07$  and  $\lambda_2 = 2.07 + \pi$  (B3).

In spite of the reported agreement of the derived equation with experimental data of a gas-oil-water spray column (B3), modification for actual spray columns is indicated. Actual velocities and contact areas per unit volume are functions of the dispersed phase holdup and should replace the

single-drop terminal velocity and contact area used in the above derivation. Also, Elgin's (B7, W4) rather than Hayworth's (H12) correlation for drop diameter seems advantageous (L5).

## B. COUNTERCURRENT SPRAY-COLUMN HEAT EXCHANGERS

High liquid throughputs, large contact area per unit equipment volume, and relatively inexpensive operation as well as relatively low equipment costs encourage the use of countercurrent spray columns as direct-contact heat exchangers. Spray columns are almost as efficient as packed columns, when one is working with systems of low interfacial tension, due to the small drops formed. For work with high-surface-tension systems, packed beds are considerably more efficient (S17), although their operation is usually more expensive compared with spray columns. A schematic diagram of a spray column is shown in Fig. 12.

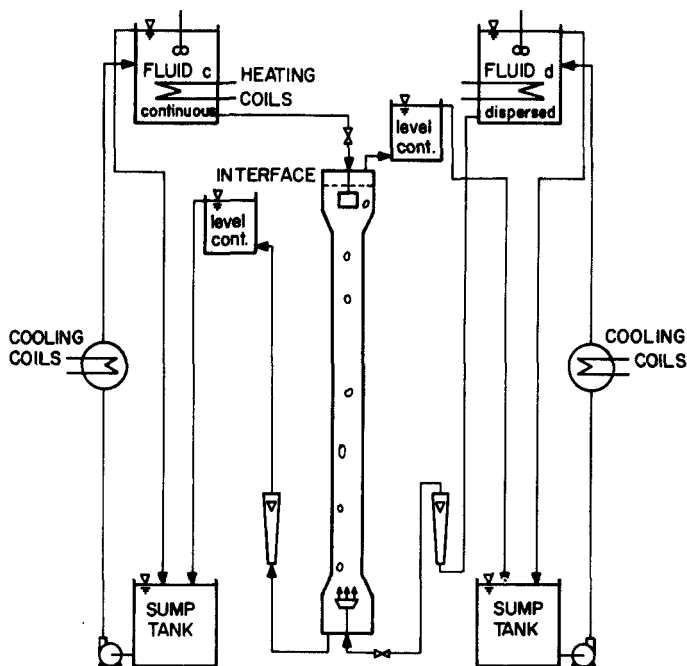


FIG. 12. Schematic diagram of spray column.

The numerous variables involved in spray-column exchangers have hitherto defied even approximate engineering correlation. Collation and adaptation of the information and experience accumulated in mass-transfer

and fluidization studies is highly desirable. Also, further basic experimental studies under closely controlled conditions are needed to determine interrelationships of the various factors affecting the flow characteristics as well as the heat-transfer phenomena. Nevertheless, in spite of certain reservations and contradictory evidence, some important general characteristics emerge to guide future applications of this promising mode of heat transfer.

Heat-transfer data are normally reported in terms of the volumetric heat-transfer coefficients, defined as

$$U_v = \frac{q}{V(\Delta T)_{\ln}} \quad (34)$$

where  $q$  is the amount of heat transferred between the phases in the column per unit time,  $V$  the total column volume, and  $(\Delta T)_{\ln}$  the log-mean average of the measured temperature differences between the two phases at the inlet and outlet. Some workers use the plate or transfer unit, HTU. For the continuous phase the relationship between the volumetric heat transfer coefficient and the apparent height of the transfer unit, based on the over-all resistance to transfer between the phases  $HTU_{0c}$ , is given by

$$HTU_{0c} = \frac{(GC_p \rho)_c}{U_v} = Z \left( \int_{T_{c1}}^{T_{c2}} \frac{dT_c}{T_c - T_d} \right)^{-1} \quad (35)$$

where  $G_c$  is the superficial velocity of the continuous phase.

For spherical drops, the total transfer area per unit column volume is given by

$$\frac{A}{V} = \frac{6F}{D}$$

where  $F$  is the holdup ratio, i.e., the ratio of the dispersed phase volume and the total volume of the column. Thus the obvious relation between the volumetric and the surface heat-transfer coefficients is

$$U_v = \frac{6F}{D} U \quad (36)$$

As is expected intuitively, the surface heat-transfer coefficient decreases with increasing dispersed-phase holdup (G13). This is probably due to the impeded flow characteristics, decreasing internal circulation and possible obstruction of the interfacial area by closely packed drops. Under normal operating conditions (up to the flooding point) the increase of  $A/V$  is appreciably larger than the decrease of  $U$  with  $F$ . Denser packing and therefore higher holdups yield higher volumetric heat-transfer coefficients.

Sakiadis and Johnson (S1) have proposed a general equation for flooding rates. With water as the continuous phase ( $\mu = 1$  cP) their equation for the



dispersed-phase superficial velocity reduces (T2) to

$$G_d \approx \frac{1.1(Dg \Delta\rho)^{1/2}}{1 + 3.6(\rho_d/\rho_c)^{1/4}(G_d/G_c)^{1/2} + 3.24(\rho_d/\rho_c)^{1/2}(G_d/G_c)} \quad (37)$$

where  $D$  is measured in feet and  $g = 4.17 \times 10^8$  ft/hr<sup>2</sup>.

The column should operate at maximum efficiency when the transfer coefficient is infinite, or else when the temperature gradient is the same for the two ends (or two phases). Thompson *et al.* (T2) suggested that the ratio  $(\Delta T)_d/(\Delta T)_c = 1$ ; hence, one should use

$$(G_d/G_c) = (C_p\rho)_c/(C_p\rho)_d \quad (38)$$

to obtain highest operating efficiency. They proposed an elaborate column design procedure which takes into account the change of heat capacity with temperature, in the column.

In general, at any given dispersed phase flow rate, the volumetric heat-transfer coefficient is only slightly affected by the continuous-phase flow rate. However, since holdup, flooding, and volumetric transfer coefficients are functions of the flow rate ratio  $(G_d/G_c)$ , different continuous-phase rates give different flooding conditions resulting in different values for the maximum volumetric coefficients. Once "optimal" ("near-flooding") conditions are reached, an increase of the dispersed-phase flow rate will cause larger drops to be formed and coalescence to set in, thus drastically reducing the transfer coefficients. It is therefore expected that the transfer coefficients should be some function of the flow ratio or the holdup, for any given system, and this indeed has been found experimentally.

The relationship between holdup and slip (relative) velocity between the two phases is, by definition,

$$V_s = \frac{G_c}{1 - F} + \frac{G_d}{F} \quad (39)$$

The slip velocity applies strictly when the two phases are in plug flow; higher slip velocities may be encountered, in practice, under nonideal flow conditions.

Relations between slip velocity, holdup, and drop diameter, from the data of Letan and Kehat (L5) for a 3-in. column (kerosene-water system), are illustrated in Fig. 13. The increase in drop diameter with increasing holdup and decreasing slip velocity has some effect on the transfer area per unit volume, which nevertheless increases with decreasing  $V_s$ . Volumetric transfer coefficients increase correspondingly.

It is evident from Fig. 13 that, as flooding (or rather "near flooding") is approached, the drop diameter for a given fluid system is then a function of flow rates, holdup, and temperature, rather than of the orifice diameter.<sup>3</sup>

<sup>3</sup> Holdup is independent of orifice diameter, but dependent on dispersed-phase flow rate [Q1].

This case is thus in agreement with the findings of Thompson *et al.* (T2), that for a given two-fluid system "heat transfer is practically independent of orifice diameter." This conclusion, though it may apply for the 0.04- to 0.064-in. nozzles tested by Thompson *et al.*, is subject to reservation for larger diameters. The extensive study of Minard and Johnson (M5) reveals a relatively small but appreciable effect of nozzle diameter over the range from 0.04 to 0.86 in.

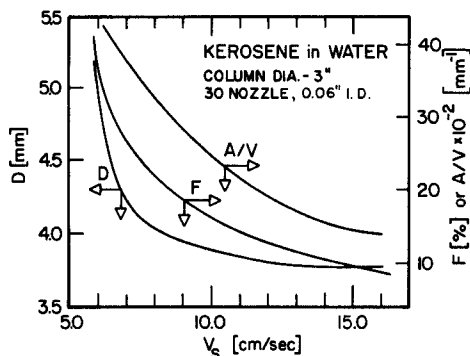


FIG. 13. Relationship between drop diameter, holdup, volumetric heat-transfer area, and slip velocity.

Spray-column heat exchange work is summarized in Table V. A brief review of these studies, with some general conclusions, follows. Some of the data for benzene, toluene, and water systems are compared in Fig. 14.

Garwin and Smith (G13) undertook an extensive study of a spray column with benzene dispersed in water, and determined overall heat-transfer coefficients as a function of holdup and phase velocity. Drop size was found to be independent of the water flow rate, and predictable by means of Hayworth and Treybal's equation (H12). However, this may not be true near the flooding point, where relatively few runs were made. The volumetric heat-transfer coefficient increased moderately with increasing water flow rate (except at the high benzene flow rates, where the observed increase was very high) and with benzene flow ratio and holdup. Statistical treatment of their results (T2) yields

$$U_v = 1.09 \times 10^4 F \quad (\text{hot water to benzene}) \quad (40)$$

$$U_v = 1.67 \times 10^4 F \quad (\text{hot benzene to water}) \quad (41)$$

where  $U_v$  is in Btu/hr/ft<sup>3</sup>/°F. The average drop diameter was 7.34 mm for hot-water runs, and 6.71 mm for hot-benzene runs; this difference accounts only partially for the difference in volumetric transfer coefficient, which is inversely proportional to the drop diameter (T2).

Rosenthal's earlier work (R5) with toluene dispersed in water is reported by Treybal (T6) as a plot of  $HTU_{0c}$  vs  $(G_d/G_c)$ , yielding, for thirteen nozzles each 0.281 in. i.d.,

$$HTU_{0c} = 6.2(G_c/G_d)^{1.04}; \quad \text{or} \quad U_v = 4.28G^{1.17}(G_d/G_c)^{1.13} \quad (42)$$

and for 71 nozzles each 0.120 in. i.d.,

$$HTU_{0c} = 4.4(G_c/G_d)^{1.15}; \quad \text{or} \quad U_v = 5.25G^{1.17}(G_d/G_c)^{1.13} \quad (43)$$

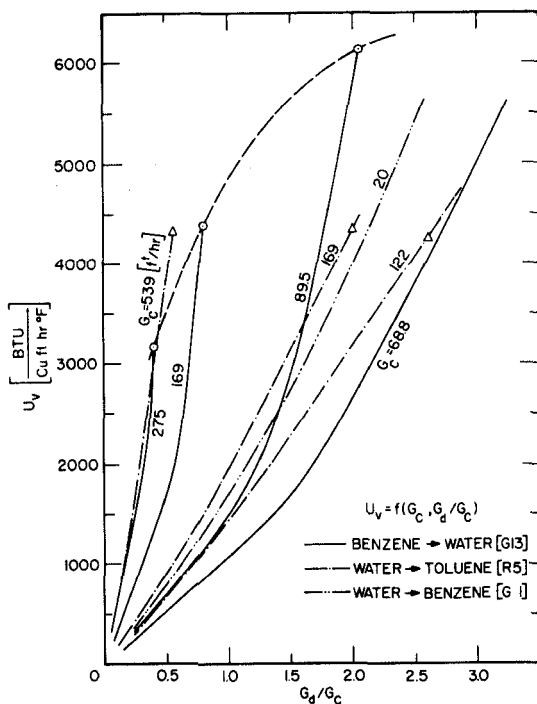


FIG. 14. Comparison of some spray-column heat-exchanger data.

The overall volumetric transfer coefficient is apparently independent of the continuous-phase flow rate over the range investigated.\* The ratio  $G_d/G_c = 2.87$  is recommended (T2) for maximum efficiency of this system.

Woodward (W12, T2) studied the operation of single, sectionalized, and double-column exchangers. Shell Fluid A and Shell Deodorized Spray Base were dispersed in water and in sea water. Data reported for the Fluid A–water system in a single column are summarized in Table V. From these, the dependence of the overall heat-transfer coefficient on dispersed-phase holdup

\* Similar results were recently reported for six perforated plate-column (S0) (In press).

is approximately

$$U_v \simeq 1.2 \times 10^4 F \quad (44)$$

for  $(G_d/G_c) = 2.5$ , the maximum efficiency ratio for the system.

No appreciable effect of column height (5 ft 4 in. to 8 ft 8 in.) on the transfer coefficient was noticed. Sea water and fresh water gave similar results. Contrary to Garwin's experience, the heat-transfer coefficients were found to be larger when the top of the column was hot than when the top was cold. With  $G_d/G_c = 2.58$  and  $F = 0.6$ , values of 8180 and 7030 Btu/ft<sup>3</sup>/hr/°F for hot and cold top, respectively, were obtained with spray base as the dispersed phase. The maximum values of the volumetric heat-transfer coefficient were 11,500 and 8500 Btu/ft<sup>3</sup>/hr/°F for the hot and cold top, respectively. These results probably reflect the natural convection currents in the column as well as with the very pronounced effect of fluidity of the oil on the volumetric heat-transfer coefficient (W12, Fig. 12). Since Garwin worked with benzene, it is likely that this fluidity effect would have been relatively less pronounced in his experiments.

The question of the effect of direction of heat flow between the phases on the transfer coefficients is intriguing. Evidently the results obtained are subject to at least three different effects, possibly mutually counteractive. These are internal natural convection, over-all natural convection currents in the column, and temperature effects on the properties affecting the local transfer coefficient. Johnson *et al.* (J3) worked with the heavy phase (carbon tetrachloride) as the dispersed phase, and found the heat-transfer coefficient to be higher when the dispersed phase was the hot one; this result is attributed by Johnson to the temperature effect on the boundary layer surrounding the drop. There is no contradiction, however, between Johnson's and Woodward's results, if the direction of heat flow in the towers, rather than between the phases, is considered. In both studies, higher transfer coefficients were found when the top of the column was hot, indicating a better transfer coefficient when the towers operate in their natural heat-flow direction. Reverse operation would most probably increase backmixing due to natural convection currents in the column. The larger differences in transfer coefficient for the two arrangements in Johnson's work, as compared with Woodward's, seem to indicate the existence of a small additional effect of the direction of heat flow as between the dispersed and continuous phase.

Because of his relatively larger differences in drop diameter, Garwin's results cannot be properly considered here. They conform with the concept that internal natural convection currents enhance the mobility of the interface which nevertheless fail in the light of Johnson's as well as Woodward's experimental results. The question is obviously open, and the need for controlled experiments under identical temperature and flow conditions is indicated. The theoretical study of Young *et al.* (Y1) on the motion of bubbles

TABLE V COMPARISON OF SO<sub>2</sub>

| No. | Dispersed phase, <i>d</i> | Continuous phase, <i>c</i> | Direction of transfer                  | Column   |                       | Nozzles         |               | $G_c$<br>(ft <sup>3</sup> /hr/ft) |
|-----|---------------------------|----------------------------|--|----------|-----------------------|-----------------|---------------|-----------------------------------|
|     |                           |                            |  | Diameter | Height                | No.             | i.d. (in.)    |                                   |
| 1   | Benzene                   | Water                      | $d \rightarrow c$<br>$c \rightarrow d$ | 2"       | 6'                    | 20 (?)          | 0.125         | 65-27                             |
| 2   | Toluene                   | Water                      | $c \rightarrow d$                      | 5.375"   | 10' 9"                | 13<br>71        | 0.281<br>0.12 | 147-59<br>122-53                  |
| 3   | CCl <sub>4</sub>          | Water                      | $c \rightarrow d$<br>$d \rightarrow c$ | 4"       | 8'                    | 21              | 0.228         | 93-64<br>93-61                    |
| 4   | Shell Oil A               | Water                      | $c \rightarrow d$                      | 4"       | 5' 8.5"               | 189             | 0.064         | 65-76                             |
|     | Shell Oil A <sup>a</sup>  | Water                      | $c \rightarrow d$                      | 4"       | 5' 4"-8' 8"           | 104-450         | 0.0625-0.04   | 40-86                             |
|     | Spray base                | Sea water                  | $d \rightarrow c$                      | 4"       |                       |                 |               |                                   |
|     | Spray base                | Water                      | $c \rightarrow d$<br>$d \rightarrow c$ | 4"       | 6'                    | 450<br>204      | 0.04<br>0.064 | 52<br>52                          |
| 5   | Gas-oil                   | Water                      | $d \rightarrow c$                      | 1' 3.7"  | 13' 1"                | 70              | 0.315         | 52-18                             |
| 6   | Kerosene                  | Water                      | $d \rightarrow c$                      | 3"       | 6' 11"                | 30              | 0.06          | 45-16                             |
| 7   | Mercury                   | Water                      | $d \rightarrow c$                      | 1"<br>2" | 1' 1.25"<br>1' 7.375" | 73-1<br>113-9   | 0.0225-0.189  | 295-88<br>148                     |
| 8   | Benzene                   | Water                      | $c \rightarrow d$                      | 2"       | $\frac{1' 6''^b}{8}$  | $62 \times 8^b$ | 0.127         | 20                                |

<sup>a</sup> Also Aeroshell Turbine Oil and AMSCO Odorless Solvent (T2).<sup>b</sup> 8 sieve-plates in column.

or droplets in a vertical temperature gradient due to surface stresses should also be considered in this connection.

The study of Pierce, Dwyer, and Martin (P3) on heat transfer and fluid dynamics in mercury-water spray columns serves to illustrate some of the factors which may greatly reduce the efficiency of spray-column operation. Backmixing was observed at the water inlet region, and water bypassed the stream of mercury drops in the column, resulting in two countercurrent streams of water flowing inside the column. This greatly increased the water temperature in the water-inlet region, and reduced the allowed temperature gradient in the column. The heat-transfer coefficients per unit area were thus found to be smaller than those calculated for stationary rigid spheres in a flowing constant-temperature medium. However, the differences between calculated and experimental values decrease with increasing Reynolds number from ten-to-one ratio (20/2) of the Nusselt number at  $(N_{Re})_c = 500$  to a 1.5 ratio (45/30) at  $(N_{Re})_c = 3000$ . Experiments were conducted at

## RAY-COLUMN HEAT-TRANSFER STUDIES

| $G_d$<br>ft <sup>3</sup> /hr/ft <sup>2</sup> ) | $F$<br>(Holdup)           | $U$<br>(Btu/ft <sup>3</sup> /hr/°F) | $U_v \times 10^{-3}$<br>(Btu/ft <sup>3</sup> /hr/°F) | $HTU_{0c}$<br>(ft) | Source  |
|--|---------------------------|-------------------------------------|--|--------------------|---|
| 45-185   | 0.08-0.74<br>0.04-0.36    | 40-70<br>30-50                      | 1-6.5<br>0.4-4                                       | —                  | Garvin and Smith<br>(G13)                     |
| 43-260<br>60-317                               | <0.275<<br>—              | —                                   | 1.3-5.6<br>1.2-6.3                                   | 2.5-70<br>1.5-40   | Rosenthal (R5, T6)                            |
| 32-250<br>32-250                               | Max                       | —                                   | 0.1-0.75<br>0.1-1.08                                 | —                  | Johnson <i>et al.</i> (J3)                    |
| 160-186<br>118-202                             | 0.20-0.56<br>0.48-0.72    | —                                   | 2.7-6.0<br>5.9-11.5<br>5.2-8.5                       | —                  | Woodward (W12)<br>Thompson <i>et al.</i> (T2) |
| 135<br>135                                     | 0.60<br>0.60              |                                     | 8.18<br>7.03   |                    |   |
| 52-204   | ?                         | 14-34                               | 0.26-1.26  | —                  | Barbouteau (B3)                               |
| 110-240  | 0.20-0.35                 | 20-50                               | 0.5-7.0  | —                  | Letan and Kehat (L5)                          |
| 140-355<br>64-100                              | 0.025-0.07<br>0.007-0.011 | 400-1170<br>520-760                 | 16-48<br>8.1-12.7                                    | —                  | Pierce (P3)                                   |
| 16-66  | 0.13-0.40                 | 30-60                               | 1.5-5.7  | 0.2-0.8            | Gardner (G1)                                  |

numerous combinations of column diameter and length, and number and diameter of nozzles, without yielding any general correlation. The effects of water flow rates, column diameter, height of top calming section, and mixing in the top section appear slight; variation of the volumetric heat-transfer coefficient with drop size were found to be less than expected due to increased mercury surface area. However, the transfer coefficients for a 19-in. column were found to be about 20% lower than those for a 13-in. column, demonstrating the peculiarity of the flow patterns in this experimental system.

Backmixing or longitudinal dispersion of either phase reduces the transfer efficiency in the column. A theoretical study involving a numerical solution with efficiency related to backmixing, was presented by Sleicher (S16). A comprehensive study of some general and specific cases of longitudinal dispersion was recently reported by Miyauchi and Vermeulen (M6). Analytical solutions and graphs are presented (M6) relating the various parameters affecting this phenomenon. In practice, backmixing is mainly associated with the continuous phase and increases with the decrease of the latter's flow rate. Backmixing is especially pronounced in the continuous-phase inlet region

and was found (G14) to be almost independent of continuous-phase inlet nozzle and column design. In general, the denser the packing of the dispersed phase and the higher the flow rates in the column, the lower the effect of backmixing and the higher the rates of heat transfer. Swirling motion of the dispersed phase at the inlet region of the latter was also noted (F1) when operating near the flooding point. For additional details see Section VI,A.

The operation of an industrial-size gas-oil-water spray column (13 ft high, 1.3 ft diam) was reported by Barbouteau (B3). The relatively low overall heat-transfer coefficients calculated from his data, up to 1250 Btu/ft<sup>3</sup>/hr/°F, seems to suggest operation at relatively low holdup. Umano (U1) studied spray column in the course of his work on direct-contact freezing units for water desalination.

Li (L10) and Gardner (G1) studied the effects of pulsation and of log-mean temperature gradient on heat transfer between benzene and water, in an eight-plate pulsed column. Their data do not reveal any advantage of a multiplate column over the conventional single-plate one. No effect of pulsation was noticed up to pulsating rates of 600 ft/hr, above which the transfer coefficients decreased appreciably. This contradicts the results obtained in mass-transfer studies, where better transfer coefficients are obtained through pulsation. It is of interest to note that a slight increase occurred in the surface transfer coefficients with increasing dispersed-phase flow rate; this may be attributed to increased agitation and oscillation of the drops in the multiplate column.

Dispersed-phase holdup, and hence the volumetric heat-transfer coefficient, is greatly affected by the presence of physical impurities. Recent experiments carried out in these laboratories (L5), with kerosene dispersed in water, elucidated the effect of dirt and scale which accumulate at the upper oil-water interface. This foreign matter greatly increases the rate of dispersed-phase coalescence at the dirty interface, and inhibits dense packing of droplets, thus greatly reducing the dispersed-phase holdup. With water flowing at a rate of 3.2 ft<sup>3</sup>/hr/ft<sup>2</sup> and kerosene at a rate of 7.0 ft<sup>3</sup>/hr/ft<sup>2</sup>, the volumetric transfer coefficients for clean and dirty interfaces were 4800 and 1800 Btu/ft<sup>3</sup>/hr/°F, respectively. The presence of scale may explain the relatively low transfer coefficients obtained by Barbouteau (B3), who used similar fluids in his large-scale experiments. Continuous removal of the sludge from the upper interface is required to eliminate this effect (T2).

### C. COCURRENT HEAT EXCHANGERS

The related studies on direct-contact cocurrent heat transfer are of practical interest. Grover and Knudsen (G25) determined the rate of heat transfer between a petroleum solvent and water, using a pipe of 8-ft length and 1.5-in. i.d. Three methods of solvent injection were compared; better dispersion

TABLE VI  
COCURRENT PIPE HEAT EXCHANGERS

| Dispersed phase   | Continuous phase | Pipe            |                   | $W_d$<br>(lb/hr) | $W_c$<br>(lb/hr) | $G_T' \times 10^{-6}$<br>(lb/hr/ft <sup>2</sup> ) | $U_v \times 10^{-3}$<br>(Btu/hr/ft <sup>2</sup> /°F) | Source                      |
|-------------------|------------------|-----------------|-------------------|------------------|------------------|---|--|-----------------------------|
|                   |                  | Length<br>(ft.) | Diameter<br>(in.) |                  |                  |   |  |                             |
| Petroleum solvent | Water            | 8               | 1.5               | 1470–3100        | 900–7300         | 0.2–0.8   | 5–50   | Grover and Knudsen<br>(G25) |
| Water             | Aroclor          | 15              | 3                 | —                | —                | 1.5–2   | 15–50  | Wilke <i>et al.</i> (W10)   |
| Water             | Oil <sup>a</sup> | 4.5–11.2        | 0.3–3             | —                | —                | 1.4–5.5   | 20–250   | Porter (P5)                 |

<sup>a</sup> 90 Neutral oil,



gave higher volumetric transfer coefficients, showing the latter to be a function of the total mass flow rate of the liquid. For a perforated injector, with flow rate ratios  $0.27 < G_d/G_c < 5$ , the relation is

$$U_v = 1.115 \times 10^{-3} G_T'^{1.26} \quad (45)$$

where  $G_T'$  is the total mass flow rate in lb/hr/ft<sup>2</sup>. Values ranging from 5000 to 50,000 Btu/hr/ft<sup>3</sup>/°F were obtained for total mass flow rates of  $0.2\text{--}0.8 \times 10^6$  lb/hr/ft<sup>2</sup> (2500–10,000 lb/hr). As one might expect, higher values were calculated for the mixing section only, which was about 3.74 ft long.

Similar experiments were reported by Wilke *et al.* (W10) who studied water injected into Aroclor in a 15-ft 3-in. pipe. Wilke's data also do not indicate any effect of temperature and physical properties on the volumetric transfer coefficients, and can be correlated in terms of the total mass flow rate, namely,

$$U_v = 2.38 \times 10^{-23} G_T'^{4.336} \quad (46)$$

Values in the range of 15,000–50,000 Btu/hr/ft<sup>3</sup>/°F were found for flow rates ranging from 1.5 to about  $2 \times 10^6$  lb/hr/ft<sup>2</sup> (73,000–90,000 lb/hr). However, more recent data for turbulent oil-water pipe flow (P5), is in general agreement with Grover and Knudsen's data for the mixing section. Temperatures of the two liquids in the pipe were obtained by monitoring the output of fine thermocouples on a very fast response recorder. Effects of volume fraction, velocity, pipe diameter, interfacial tension, and viscosity on  $U_v$  are reported (P6). General comparison of available data is given in Table VI.

Pipe exchangers seem to give higher volumetric transfer coefficients than spray columns, mainly because of better atomization of the dispersed phase, which yields appreciably higher transfer areas per unit equipment volume. Adaption of the cocurrent mixer-settler type contactor for heat transfer between immiscible liquids has recently been suggested (H5a). By using two such liquid-liquid contactors and a third immiscible fluid as the transfer agent, as shown in Fig. 15(a,b) heat can be similarly transferred between two miscible fluids, flowing countercurrently to each other. However, this mode of operation is associated with emulsion formation, contamination, and some losses, and large settling equipment may be required. In practice, economic consideration should guide the choice between parallel-flow and counter-current exchangers.

## V. Heat Transfer to Drops and Bubbles with Simultaneous Change of Phase

Work on direct-contact heat exchangers was stimulated in the last decade by the quest for economic water-desalination units. Multiphase exchange,

where latent heat is transferred between the immiscible fluids, has been effectively used in direct-contact freezing units in which a dispersed volatile fluid evaporates in the saline water with simultaneous freezing of part of the water. The leaving vapors are then brought in contact with the withdrawn ice in another unit where condensation and melting occurs simultaneously (Fig. 15c).

In addition to the advantages seen in the two-phase liquid-liquid exchangers, utilization of a secondary refrigerant as a transfer agent in the direct-contact multiphase exchangers permits (S12): (a) an economical closed refrigeration cycle; (b) smaller quantities and lower flow rates of the cooling liquid; (c) larger, more effective, heat transfer areas; (d) convenient separation of the fluids in contact; (e) higher (by an order of magnitude) heat-transfer coefficients; (f) lower corrosion due to lower working temperatures. Some technical as well as economical aspects regarding the utilization of these multiphase exchangers were reported by Umano (U2), Weigandt (W8, W9), and others (K1).

Unlike the multiphase exchangers where both the dispersed phase and the continuous fluid medium undergo change of phase, three-phase exchangers may be used for heat transfer at various temperature levels. The latter depends on the choice of the transfer fluid. Stagewise operation of three-phase exchangers in a closed evaporation and condensation cycle was recently proposed by Harriott and Weigandt (H10a) for simultaneous cooling and heating of sea water and desalinated water streams flowing countercurrently (Fig. 15d).

A variation of the closed refrigeration cycle was suggested by Wilke *et al.* (W10), who studied evaporation of water from sea water flowing in direct-contact cocurrent flow with hot Aroclor in an horizontal 3-in. pipe. The water vapors were then condensed by direct contact with cold Aroclor in a packed bed column. The reported volumetric heat-transfer coefficients for the boiling section were two to three times higher than those shown in Table VI for the nonboiling section.

A general scheme for utilizing flash evaporation of a secondary refrigerant in water conversion by liquid-liquid water extraction from saline water was outlined recently (C3).

A combination of flash evaporators, direct-contact condensers, and liquid-liquid exchangers has been described by Othmer (O1). In this process water vapors, produced in a multistage flash distillation of heated sea water at successively reducing pressures, are condensed by direct contact with a recycle steam of product water. The heat is from the hot product water and is recovered by an immiscible petroleum oil in one spray column and transferred to the incoming sea water feed in a second spray column.

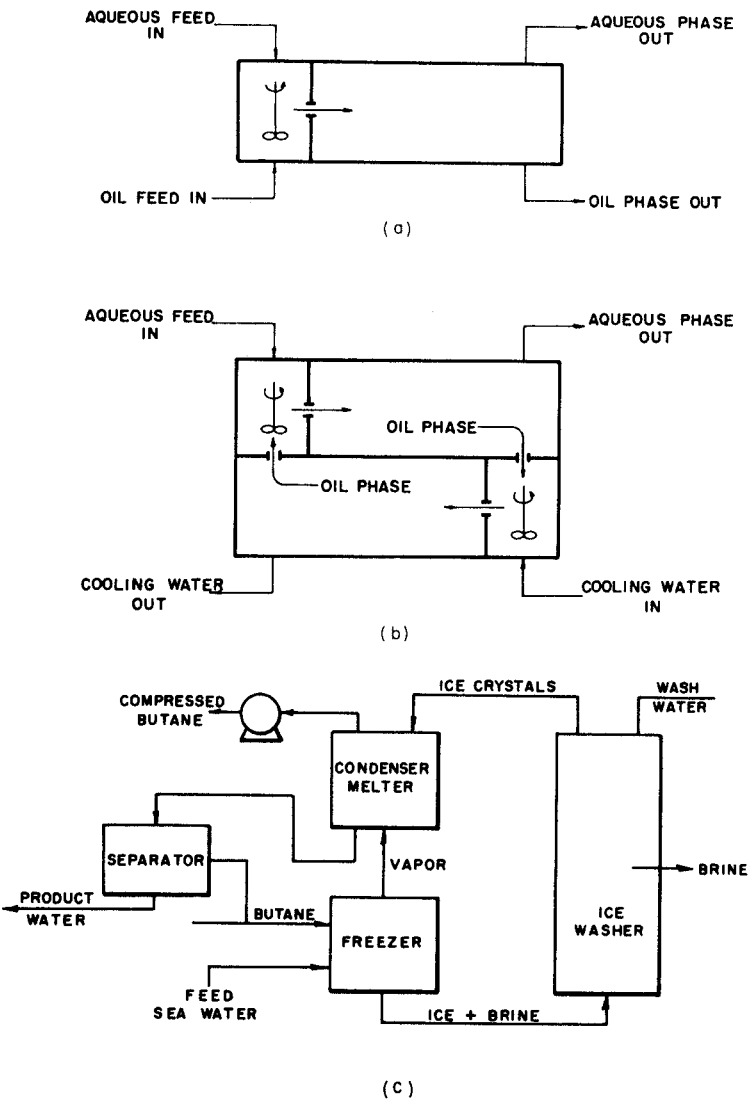
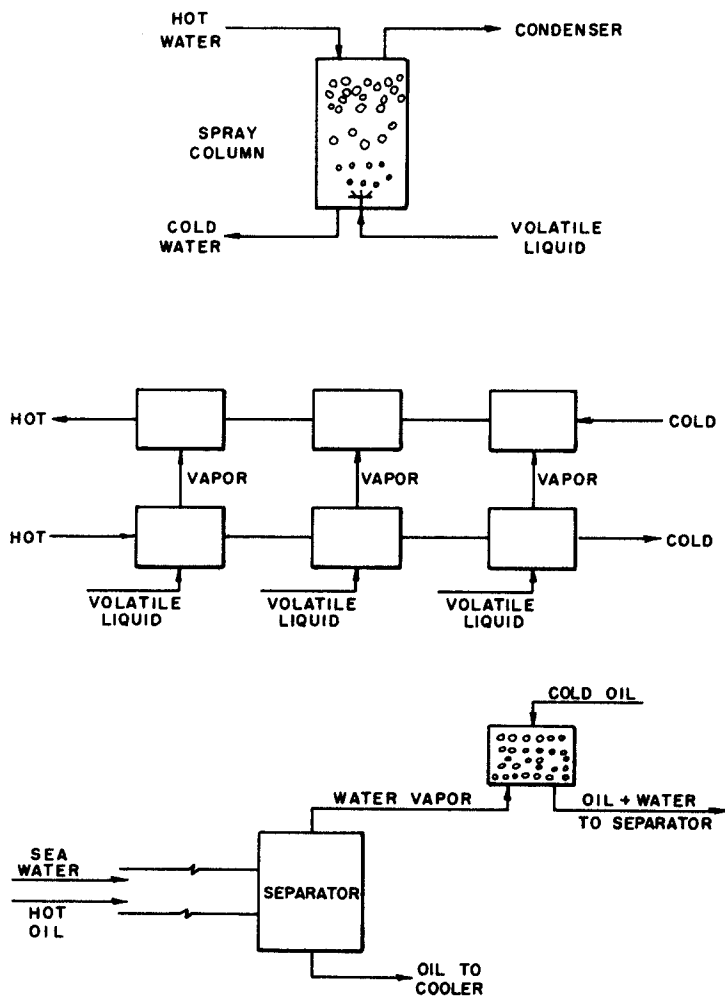


FIG. 15(a). Direct-contact heat exchangers using mixer-settler contactors for immiscible liquids, after (H5a). (b). Direct-contact heat exchangers using mixer-settler contactors for miscible liquids using a third immiscible liquid, after (H5a). (c). Schematic diagram



(d)

of multiphase exchangers in direct-contact freezing process. (d). Schematic diagrams of three-phase exchangers: top—single-stage countercurrent spray column; center—counter-current exchangers in stages; bottom—pipe evaporator and packed bed condenser.



FIG. 16. Pentane drop evaporating in water (S12).

#### A. EVAPORATION OF DROPS IN IMMISCIBLE LIQUID MEDIA

Although some general technical information on direct-contact heat transfer with change of phase is available, little is known regarding the basic mechanism and heat transfer coefficients encountered when a drop of a volatile fluid evaporates while moving in an immiscible liquid. By means of cinecamera studies of single butane and pentane drops evaporating in stagnant water, Sideman and Taitel (S12) have shown that the vapor concentrates at the upper part of the drop, while the remaining volatile liquid concentrates at the bottom part of the spheroid-like drop. Figure 16 shows a pentane drop evaporating in water at various evaporation ratios. Obviously,

the flow characteristics of the two-phase drop approaches that of a gas bubble as evaporation progresses. Assuming the two-phase drop to be a sphere of constant radius moving in a potential flow field and the volatile liquid at a constant (boiling) temperature, i.e., outside film controlling, the authors obtained an analytical solution for the steady-state heat transfer (S12). Local and average heat transfer coefficients were determined as a function of the opening angle of the vapor phase. The average Nusselt number was found to be

$$(N_{Nu})_c = \left( \frac{3 \cos \beta - \cos^3 \beta + 2}{\pi} \right)^{0.5} (N_{Pe})_c^{0.5} = C(N_{Pe})_c^{0.5} \quad (47)$$

where  $\beta$  is equivalent opening half-angle of the vapor phase in the two-phase "drop." Based on experimental data it is suggested that, for  $\beta = 135^\circ$ , or  $C = 0.27$ , the maximum average heat transfer coefficient per unit of overall drop area will be obtained. As is to be expected, the Nusselt number decreases with increasing  $\beta$ . For  $\beta = 0$ , Eq. (47) reduces to Eq. (18), the well-known equation of Boussinesq and Higbie for flow past a sphere.

The overall heat-transfer coefficient, related to the instantaneous total area of the rising two-phase drop, increases sharply with evaporation up to 3–10 wt-% vapor content, depending on the system and conditions, and then decreases quite moderately until evaporation is complete. Thus it indicates the decreasing effect of the internal resistance to heat transfer in the first stages of the evaporation process, and the moderate decrease in the relative transfer area in the subsequent stages of the process (S12). The instantaneous overall heat-transfer coefficients are 200–400 Btu/hr/ft<sup>2</sup>/°F for  $D^* = 3.5$  mm, and 500–700 Btu/hr/ft<sup>2</sup>/°F for  $D^* = 2.0$  mm.

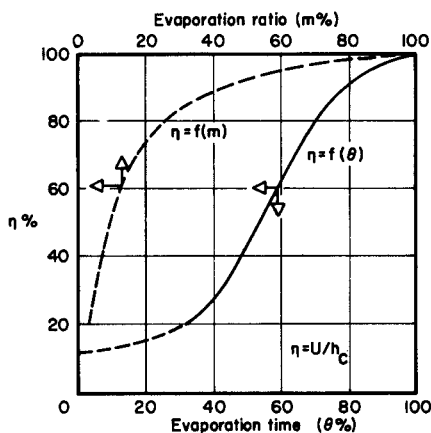


FIG. 17. External resistance controlling factor—pentane drop evaporating in water (S10).

Approximate calculations of the relative importance of the internal and external resistance to transfer in the evaporating drop (S10) show the external resistance to be controlling over more than 70% of the evaporation process, when expressed in terms of the vapor to total mass ratio. However, if the time dependence of the evaporation process is considered, the very beginning of the evaporation process, where internal resistance is controlling, is found to take up some 50% of the total evaporation time. Thus some exchanger volume may be saved if the volatile liquid is introduced in saturated state, preferably with some initial vapor content. The approximate predominance of the individual film coefficients as function of the evaporation ratio and time is shown in Fig. 17, where the external resistance controlling factor is defined as  $U/h_c$ . The approximate individual and over-all heat-transfer coefficients, calculated per unit of effective liquid-liquid contact area, are shown in Fig. 18. Detailed studies of the initial evaporation stages of single drops are presently underway (P4).

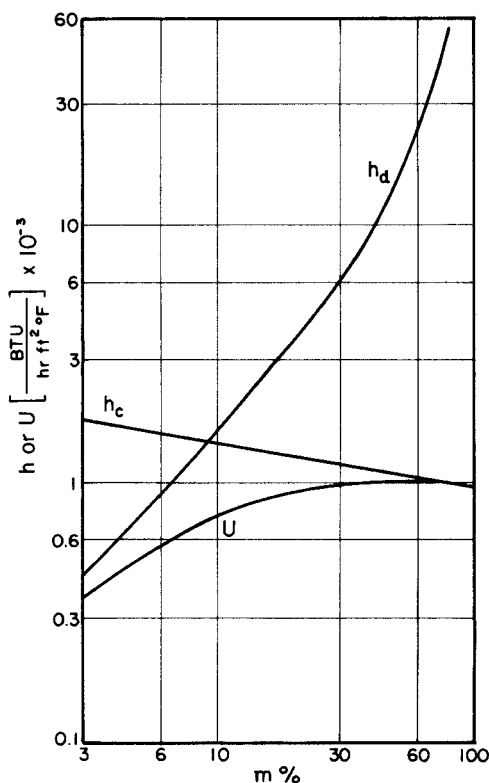


FIG. 18. Estimated individual and over-all heat-transfer coefficients—pentane drop (3.6 mm diam) evaporating in water (S10).

As the heat-transfer area varies during the evaporation process, the overall heat-transfer coefficient is best defined in relation to the initial drop area. By calculating the overall resistance to heat transfer directly from the temperature driving force, the total evaporation time and the total heat content of the drop, Sideman, Hirsch, and Gat (S11a) obtained a relationship between the average overall heat-transfer coefficient and the initial diameter. For single pentane drops evaporating in sea water,

$$\bar{U}^* = 1.05 \times 10^4 d^{*-0.64} \quad (48)$$

when  $\bar{U}^*$  is expressed in  $\text{Btu/hr/ft}^2/^\circ\text{F}$  and  $d^*$  is in millimeters. Direct plotting of the average experimental instantaneous heat-transfer coefficients (Fig. 19)

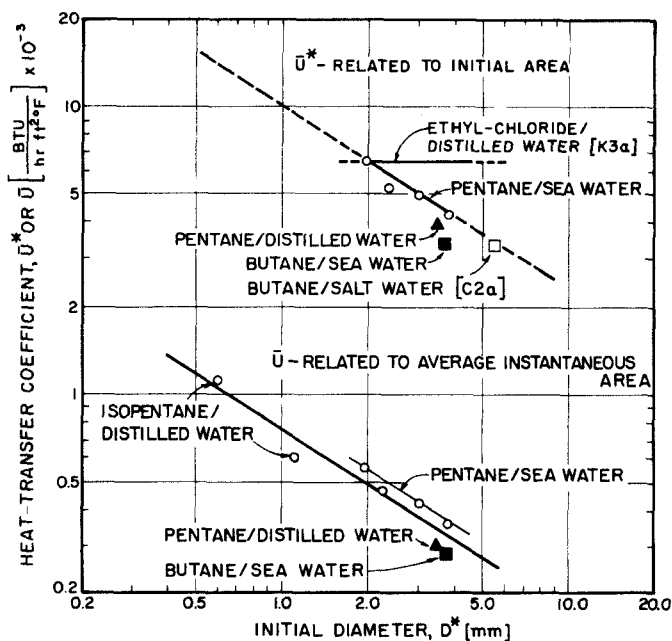


FIG. 19. Heat-transfer coefficients as a function of initial drop diameter (S11a).

for all the hydrocarbon-water systems tested (including condensation of isopentane in water), related to the total area of the rising two-phase drop, gives

$$\bar{U} = 0.76 \times 10^3 d^{*-0.64} \quad (49)$$

The constant for the pentane-sea-water system alone is  $0.882 \times 10^3$ .

The independence of  $\bar{U}^*$  on the initial drop diameter exhibited by Klipstein's (K3a) data in Fig. 19 is most probably due to the nucleation technique employed by him whereby a sharp electric power pulse was given



to each drop through a nichrome heating wire in contact with the drop (S11a). In contrast, all the other data reported here, including those for butane in 24% NaCl-water solution (C2a), were obtained by allowing the bubbles to nucleate naturally in unaerated systems.

Comparison of the above equations shows that the characteristic average of the total instantaneous transfer area is some 12 times larger than the initial area, or some 35% of the final area of the completely evaporated drop. This is in accord with the smaller evaporation rates in the beginning of the evaporation process shown in Figs. 17 and 18.

As seen from Fig. 19, the heat-transfer coefficient related to the initial drop area is about one order of magnitude larger than the one related to the "time average" of the instantaneous total area. However, if heat transfer is assumed to take place only between the volatile liquid at the bottom of the two-phase bubble and the continuous phase, then the liquid-liquid transfer coefficient can be approximated (S10) to be about 2.5 the value of  $\bar{U}$ . The corresponding coefficients for nonevaporating drops are about 60 Btu/ft<sup>2</sup>/hr/°F, which is at least one order of magnitude lower than that of the values realized with the evaporating drops.

Some degree of superheating is required before nucleation sets in in the drop, depending on drop size as well as the physical and chemical purity of the fluids. Similar phenomena have also been observed in countercurrent spray column studies (S9), where the temperature of the continuous phase can be lowered to the desired value only after some evaporation starts. As is to be expected, the time required for complete evaporation of the drop is inversely proportional to the temperature driving-force. A similar relationship exists for the length of the evaporation path of single drops. This, however, may not be directly extended to populations of drops, where the onset of nucleation is not simultaneous but rather depends on the dispersed phase flow rate, holdup, and degree of turbulence of the system.

As shown in Fig. 16, a droplet leaving the nozzle at the bottom evaporates and grows while rising in the column. Three operating zones were noticed in the spray column operating with a multiorifice plate: a free-rising zone at the bottom, a turbulent zone, and a foam zone at the top of the column. In the free-rising zone, equivalent to the "streamline" region noted in gas-liquid contacting columns at low gas flow rates and low holdups, the evaporating drops rise unhindered. As the superficial velocity increases with vapor generation, the growing drops lose their individual identity, and coalescence as well as turbulence is observed. This turbulent zone is analogous to the turbulent region noted in gas-liquid systems at superficial gas velocities above approximately 10 ft/min. Obviously, the interfacial area decreases with increased coalescence. The foam height, which varied with the operating conditions from 10 to 50 mm, was not considered (S9) to contribute much to the

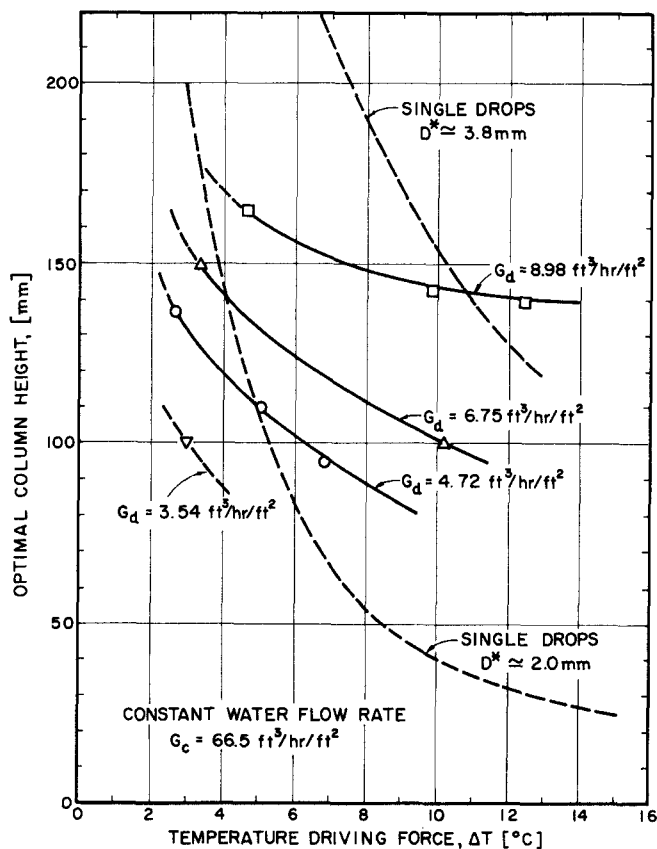


FIG. 20. Effect of temperature driving-force on optimal column height—pentane-water system (S9).

overall transfer area, but was included in the subsequent evaluation of the optimal column heights and the volumetric transfer coefficients.

In Fig. 20 the optimal column height (defined as the height in which evaporation is complete but no superheating of the vapors occurs) is plotted against the log-mean temperature driving-force at various dispersed-phase flow rates. It is noted that identical orifice velocities of pentane were used, and the initial diameter in all the runs shown was about 1.40 mm. Comparison with the single-drop data included in Fig. 20 allows some insight into the effect of drop interaction. Increasing the pentane flow rate at a constant temperature driving-force is equivalent to increasing the diameter of single drops. This is consistent with the observed increase in coalescence with increasing pentane flow rates. Also, the greater the coalescence, the smaller the effect of the temperature driving-force. Hence the effect of initial drop

diameter will decrease as the dispersed phase flow rate and the temperature driving-force are increased.

At a constant pentane flow rate ( $4.72 \text{ ft}^3/\text{hr}/\text{ft}^2$ ) the volumetric heat-transfer coefficient was found (S11a) to depend only slightly on the initial drop diameter. Approximately,

$$U_v \sim D^{*-0.1}$$

for  $G_c = 66.5 \text{ ft}^3/\text{hr}/\text{ft}^2$ . The effect of the continuous-phase flow rate is generally small. An exponent of 0.135 was found for  $G_c = 30.4 \text{ ft}^3/\text{hr}/\text{ft}^2$ . Evidently the effect of the initial drop diameter is mainly in the free-rise "streamline" zone in the lower part of the column. The upper "turbulent" zone is practically unaffected by the initial drop size, consistent with the independence of gas holdup and the specific interfacial transfer area relative to the orifice diameter at high gas flow rates that is observed in gas-liquid contacting systems.

The volumetric heat-transfer coefficients obtained in the countercurrent spray column are plotted against the mass flow-rate ratio in Fig. 21, allowing direct comparison with Fig. 14 where some of the analogous data for liquid-liquid spray columns are presented. For direct comparison with Table V, it is noted that the spray-column diameter was 2.75 in. with a total height of 33.5 in. Orifice diameter was 0.5 mm, and the number of orifices varied between 9 and 22 depending on the desired pentane flow rate. Holdup fraction varied from 0.12 to 0.22 at the range of flow rates indicated in Fig. 21, and the volumetric transfer coefficients varied from  $4.8 \times 10^3$  to  $12.1 \times 10^3 \text{ Btu}/\text{ft}^3/\text{hr}/^\circ\text{F}$ . These results clearly demonstrate the higher efficiency of the three-phase exchanger as compared with the liquid-liquid heat exchangers.

For comparison with other evaporation studies, it is noteworthy that the data presented in Fig. 21 was obtained with a temperature approach of  $1.7^\circ\text{C}$  at the continuous-phase outlet, and that the pentane feed entered the nozzles subcooled by some  $1.5^\circ\text{C}$ . A reduction in the free-rising stream line zone is feasible with superheated dispersed-phase feeds and closer approach temperatures. This would greatly increase the volumetric transfer coefficient which is inversely proportional to the temperature driving-force and the optimal column height.

Harriott and Wiegandt (H10a) studied an upflow cocurrent flash evaporator in which pentane or methylene chloride was mixed with the water before entering the 2-in. column. A sieve plate with  $\frac{1}{4}$ - or  $\frac{1}{8}$ -in. holes was placed 1 ft upstream to facilitate dispersion. The volumetric transfer coefficients were estimated to be about  $17 \times 10^4 \text{ Btu}/\text{hr}/\text{ft}^3/^\circ\text{F}$ , based on an approach exit temperature of  $0.5^\circ\text{C}$  and a 1-ft length of pipe. This result is similar to that reported by Wilke *et al.* (W10) for a cocurrent pipe evaporator, and is about one order of magnitude larger than that reported for the countercurrent spray

column. As in the case of liquid-liquid exchangers, this is probably due to better atomization of the dispersed phase and the closer temperature approaches measured in the cocurrent pipe-type exchangers.

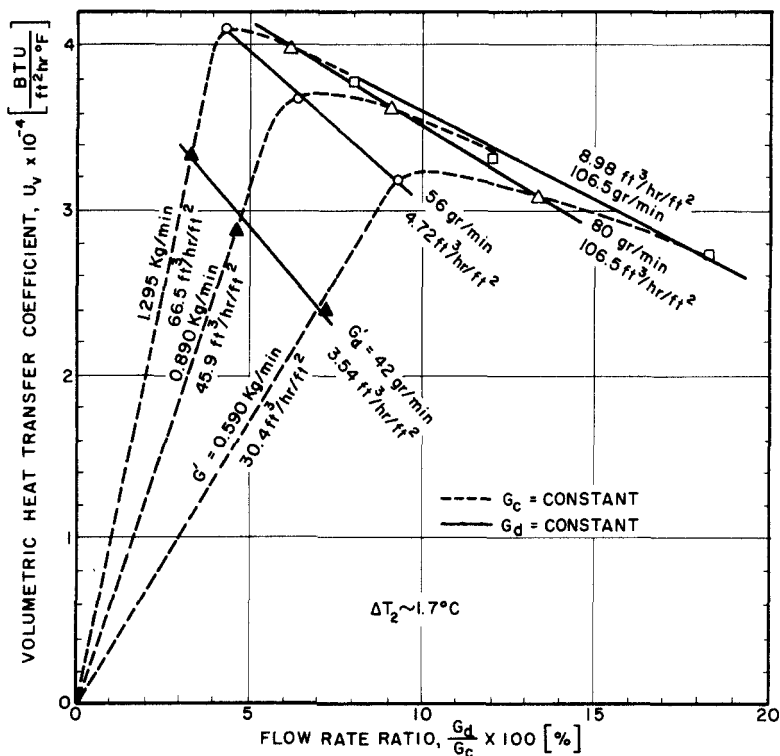


FIG. 21. Volumetric heat-transfer coefficient as a function of  $G_d/G_c$ ;  $\Delta T_2 = \text{constant}$ ; pentane-water.

Mechanical agitation increases the rate of evaporation. This is due to increase of interfacial area with drop breakup, heterogeneous nucleation, and higher turbulence. By combining the concept of local isotropy in turbulent agitation together with the particular characteristics of the volatile drops evaporating in immiscible media, Sideman and Barsky (S8a) related the specific heat flow rate (per unit volume) to the specific power input  $P_v$  of the agitator and the temperature driving-force. Using small-scale as well as pilot-plant data, they demonstrated that the general form of the derived relationships

$$q_v \sim P_v^x \Delta T^y \quad (50)$$

holds even for nonhomogeneous mixtures as well as for evaporation at liquid-

liquid interfaces, where local isotropy may not exist. The exponents  $x$  and  $y$  vary with operating conditions, the controlling mixing regimes (viscous, kinetic, or coalescence preventing), and mixing intensity. The exponents decrease with increased coalescence and decrease of the mixing intensity, as is evident from Fig. 22. For completely dispersed systems at high mixing

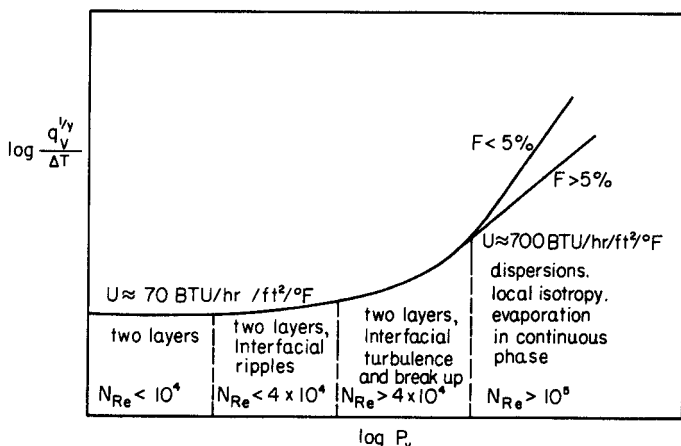


FIG. 22. A general presentation of the effect of specific power input and turbulence intensity on heat transfer between a nonvolatile liquid and an immiscible, volatile, evaporating liquid.  $N_{Re} = Nd^2\rho_c/\mu_c$  (S8a).

intensity,  $x = 8-12$  and  $y = 4-6$ , depending on the dispersed-phase holdup and the mixing regime. For the practical case of operating with some excess butane in sea water (H10a), where a butane layer floats above the continuously agitated fluid,  $x = 3.84$  and  $y = 1.54$ . Values of  $x = 0.08$  and  $y = 1.43$  were found for heat transfer between agitated water and pentane layers at  $(N_{Re})_{mixer}$  between 1 and  $4 \times 10^4$ . At lower mixer Reynolds numbers,  $x = 0$ . The contact area is well defined;  $q_A$ , the heat flow rate per unit area, may replace  $q_v$ , and Eq. (50) reduces to the well-known boiling correlation

$$q_A \sim \Delta T^y \quad (50a)$$

For the pentane-water system,  $y = 1.42$ , in good agreement with the exponent of 1.33 calculated for turbulent natural convection and commonly applied to surface boiling. For nucleate boiling of a single component, the value of the exponent in Eq. (50a) reported in the literature varies between approximately 2.5 and 5. Comparison with the exponents given above for the two-component three-phase system seems to indicate that, although the evaporation in the latter system is of the surface-evaporation type, the hydrodynamic

effects associated with high turbulence are responsible for the high heat-transfer coefficients realized in these systems.

Some elaboration on boiling heat transfer at liquid-liquid interfaces (without external mixing) is instructive. A comparison of all available interfacial boiling data is presented in Fig. 23. Note that the slope of the lines  $n$  is

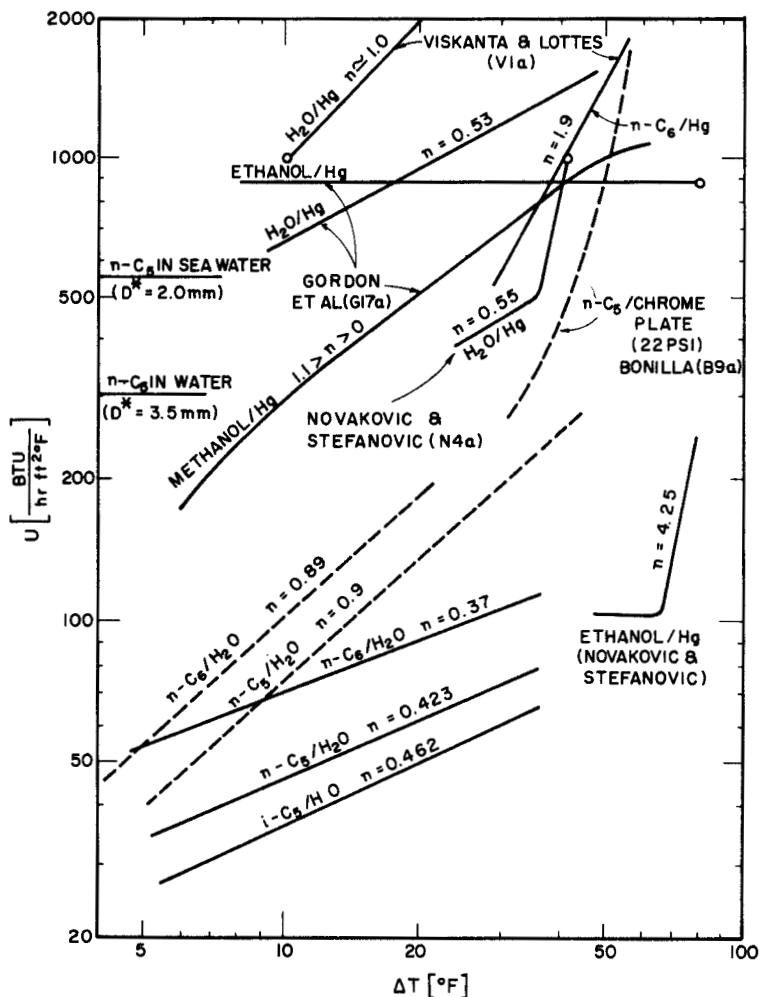


FIG. 23. Comparison of boiling data from liquid surfaces.

equal to  $\gamma - 1$  since, by definition,  $U = q_A \Delta T$ . The dotted lines for the  $n$ -pentane and  $n$ -hexane were obtained by seeding the water interface with artificial nuclei. The ensuing higher evaporation rates are seen by the larger

slopes of these lines as compared with those obtained with clean water interfaces. These results are consistent with Novakovic and Stefanovic's (N4a) observations on the effects of surface contamination and boiling from the walls of the vessel on the apparent transfer coefficients. The differences in the data of Novakovic, Gordon (G17a), and Viskanta (V1a) obtained in boiling from the mercury interface shown in Fig. 22 is thus readily explained: neither Gordon nor Viskanta used deaerated mercury; thus, "boiling usually started at lower superheats . . . because of the presence of contaminants and gases absorbed and adsorbed on the mercury surface" (V1a). Moreover, since thick mercury layers were used in these two studies, large oscillations and bouncing (G17a) of the mercury interface were evident at high heat fluxes. Whereas Novakovic's data, taken with thin mercury layers (3–6 mm) and with extreme precaution to avoid contamination and wall effects, indicate a transformation from surface to nucleate boiling, the data of Viskanta and Gordon (as well as ours with a seeded interface) represent some averages of these two basic boiling mechanisms.

Also included in Fig. 23 are Bonilla's data (B9a) for nucleate boiling of pentane from a chrome-plated heater, as well as the average over all heat-transfer coefficient, related to the instantaneous overall heat-transfer area, for pentane drops evaporating while rising in water. As noted earlier, the heat-transfer coefficient in the latter case was found to be practically independent of the temperature driving-force in the range studied (up to 15°C).

In conclusion, it is evident from Figs. 22 and 23 that the rate of heat-transfer increases with increasing interfacial turbulence, irrespective of whether this turbulence is induced by high heat fluxes (as in Gordon's mercury surface), induced boiling by artificial nucleation sites (gas or solid contaminants), or mechanical agitation at the liquid-liquid interface.

## B. CONDENSATION OF BUBBLES IN IMMISCIBLE LIQUID MEDIA

The related work of Bankoff and Mason (B2) on latent heat transfer from steam bubbles condensing in a turbulent subcooled water stream casts light on this interesting phenomenon. A train of steam bubbles was injected into a submerged jet of subcooled water. Depending on the steam flow rate, water temperature, and velocity, three distinct types of bubble behavior could be distinguished: (1) ellipsoid bubbles with smooth surface at low steam rates and high temperature gradients (90–130°F); (2) ellipsoid bubbles with irregular surface at increased steam flow rates and about 90°F temperature gradient; and (3) irregular bubbles which (unlike the first two groups) did not completely collapse at the lower temperature gradients (30–50°F).<sup>\*</sup> The surface heat-transfer coefficients for all three groups varied between 13,000 and

<sup>\*</sup> The relative significance of the effects of the liquid inertia and the heat transfer on the collapse rate was recently reported (F1a).

316,000 Btu/hr/ft<sup>2</sup>/°F, with Reynolds numbers varying from 172 to 14,000. The frequency of the bubbles varied between 200 to 2500 cps. Empirical equations for the Nusselt number as function of the Peclet and Strouhal numbers are given (B2) for the three different bubble groups.

The transfer coefficients reported by Bankoff compare favorably with those reported by Grassmann and Wyss (G19), who studied heat transfer between steam bubbles and water. With a bubble frequency of about 20/sec, they obtained water-side coefficients ranging from 14,000 to 20,000 Btu/hr/ft<sup>2</sup>/°F. Superheated vapor-side coefficients were 40–160 Btu/hr/ft<sup>2</sup>/°F. Bankoff's higher values are undoubtedly due to the highly turbulent nature of his system.

The analogous studies of direct-contact condensation involving immiscible fluids are rather meager. Sideman and Hirsch (S11) have recently reported some low-speed cinecamera studies of single isopentane bubbles condensing while rising in stagnant water. Two different nozzles of 3 and 6 mm i.d. were used in this work, resulting in initial bubble diameters of about 3.8 and 5.5 mm. The smaller bubbles usually appear as ellipsoids with relatively small fluctuations in shape. The larger bubbles deform appreciably, appearing in various shapes, such as disks, cones, saucers. A typical sequence of condensation of the larger size bubble is shown in Fig. 24. The greatest changes in the volume and area of the bubbles occur at the initial stages of the evaporation process. This so-called "turbulent" region of high deformation extends up to some 80–90 wt % of liquid content in the bubble. In the second "laminar" region, the transfer rate decreases appreciably as the internal resistance to heat transfer gradually dominates the rate of heat transfer.

The characteristics of the instantaneous heat-transfer coefficients are basically similar (but in reverse) to those found earlier in the complementary study of evaporating drops, leading to the conclusion that here too most of the heat transfer takes place at the liquid-liquid interface. Absolute comparison based on liquid or vapor fraction in the two-phase particle is difficult, since some condensation takes place during bubble formation; despite prior superheating of the bubble, the exact amount of liquid in the initial bubble is unknown. Also, in the range of small temperature driving-forces studied (up to 6°F), condensation was not spontaneous and not complete. Unlike the evaporation studies (Fig. 16), no distinction between the vapor and the volatile liquid in the bubble could be observed at these low temperature-differences. Condensation was complete only at higher temperature driving-forces, allowing clear distinction of the phases in the condensing bubbles similar to that shown in Fig. 16 for the initial evaporation stages.

The suggested similarity of the heat-transfer mechanism in evaporation and condensation in immiscible media is substantiated by the similar characteristics of the data when plotted as instantaneous Nusselt vs Reynolds



numbers, and the good agreement of the condensation data with the values predicted by Eq. (47) (S11). The general agreement of the average over-all condensation heat-transfer coefficients with those of evaporation is also evident in Fig. 19.

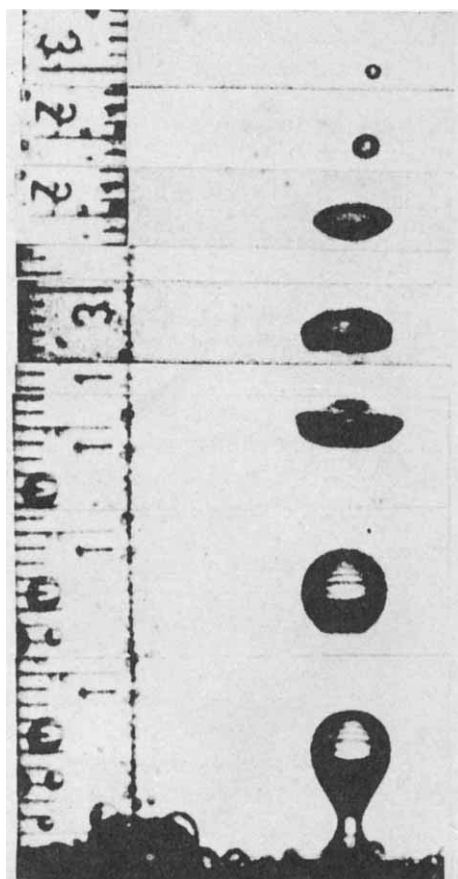


FIG. 24. Isopentane bubble condensing in water (S11).

It is interesting to note that the two phases in the bubble were distinct in the presence of air in the bubble. An analysis of the pictures of a condensing isopentane-air bubble indicated no effect of the presence of air on the condensation rate. However, more work is required before a final conclusion can be drawn, especially since all available information regarding condensation on solid surfaces as well as condensation of steam bubbles in water (G19)

indicates a decrease in the condensation rate in the presence of non-condensable gases. Similarly, the presence of an inert gas in  $\text{CO}_2$  bubbles in water reduced the absorption mass-transfer coefficient by some 20 to 40 percent (L4). It is not yet clear whether this latter effect is due to smaller radial motion of the contracting bubble, to internal surface resistance, or to formation of an insulating gas cap on top of the bubble; should the latter be the cause, this would hardly affect the over-all transfer coefficient for condensation, which is apparently mostly controlled by the external resistance to transfer at the liquid-liquid interface.

In agreement with the single-drop evaporation studies, no significant effects of the temperature difference on the heat-transfer coefficient were observed in the narrow temperature range studied. An attempt to isolate these effects is presently underway, especially since the temperature driving-force was found to affect the initial and final liquid content of the bubble (S11) as well as the volumetric coefficient (W9).

The overall transfer coefficients (related to the overall transfer area) obtained in this three-phase two-component condensation study were about 600 and 1100 Btu/hr/ft<sup>2</sup>/°F for the large and small bubbles, respectively. These compare favorably with the values reported for condensation of steam in water, which are, however, one order of magnitude larger. The difference is reasonable in view of the possibility for mass diffusion at the gas-liquid interface in the two-phase steam-water system, as well as the much higher turbulence encountered, especially in Bankoff's system (B2).

Wiegandt (W9) studied isobutane condensation in an ice-packed column, utilizing small temperature gradients. The experimental data reported indicate a decrease in the volumetric heat-transfer coefficients from 1000 to 660 Btu/hr°F/ft<sup>2</sup> (column cross section) with increasing temperature driving-force from 2 to 7°F. Although only small effects of the temperature gradient on the transfer coefficients in latent heat transport have been reported (S12, W9, W10), extrapolation of data of large  $\Delta T$  to small temperature gradients (to about 1°C, which is of practical interest for economic reasons) may be erroneous, mainly since hydrostatic-head effects on the normal boiling temperature are very pronounced at small  $\Delta T$ 's.

Condensation studies of butane in water-ice slurries in a 2-in. diam column were also reported (W9), indicating increasing condensation rates with increasing ice content of the slurry. With a butane feed rate of 1.24 lb/ft<sup>2</sup>/min and an average temperature gradient of 6°F, the overall heat transfer coefficient is reported to be 2000 Btu/hr/°F/ft<sup>2</sup> (column cross section).

Direct-contact condensation of steam in Aroclor, with a venturi as mixing device, was reported by Lackey (L1). Working with temperature gradients of about 10, 40, and 70°F between the two fluids, he observed a strong effect of the temperature gradients on the steam flow rate, the latter decreasing

strongly with decreasing temperature gradient. The apparent volumetric heat-transfer coefficients reported are in the range of 150,000–400,000 Btu/hr/ft<sup>3</sup>/°F.

The heat-transfer characteristics of condensing steam in Aroclor in a simulated cocurrent spray column were also reported (L1). The volumetric heat-transfer coefficient, in Btu/hr/ft<sup>3</sup>/°F, was assumed directly proportional to the steam flow rate  $W_d$ , and is given by

$$U_v = 9.2 \times 10^3 W_d \quad (51)$$

where  $W_d$  is measured in lb/hr.

Direct condensation of methylene chloride in a cocurrent downflow sieve-plate condenser in a 6-in. pipe was reported by Harriott and Wiegandt (H10a). Transfer coefficient, based on average condensation and exit liquid temperatures and the turbulent bubbling froth area only (0.09 ft<sup>2</sup>), were from 70,000 to 100,000 Btu/hr/ft<sup>2</sup>/°F, increasing with superficial gas velocity from about 1 to 2.2 ft/sec. The corresponding volumetric coefficients are up to 400,000 Btu/hr/ft<sup>3</sup>/°F, based on 3-in. froth height.

For condensation of methylene chloride in water, in cocurrent downflow 4-in. and 6-in. diam columns packed with  $\frac{1}{2}$ -in. Intalox saddles, the volumetric transfer coefficients reported (H10a) were less than half those obtained with the sieve-plate column. The difference may be due partially to the different definition of the temperature driving-force applied for these two columns. (The log-mean  $\Delta T$  was used for the packed bed, and a 2-in. transfer height was assumed.) The volumetric heat transfer coefficients "increased with the 0.4–0.6 power of the liquid rate" from 65,000 to 150,000 Btu/hr/ft<sup>3</sup>/°F with the liquid rate increasing from 1 to  $4 \times 10^4$  lb/hr/ft<sup>2</sup>. Contrary to the sieve-plate and spray-column studies, no effects of the vapor flow rate (from 1100 to 2500 lb/hr/ft<sup>2</sup>) on the heat-transfer coefficient were noted in the packed bed study.

Wilke *et al.* (W10) reported data on steam condensation in countercurrent flow with Aroclor in 2- and 3-feet-high 12-in. diam columns packed with 1-in. Raschig rings. The experimental  $HTU_L$  (liquid-resistance-controlling height of a transfer unit) varied from 0.8 to 1.5 ft for Aroclor flow rates of 1.5 to  $3 \times 10^4$  lb/hr/ft<sup>2</sup>, corresponding to over-all transfer coefficients of about 6000 Btu/hr/ft<sup>3</sup>/°F (H10a). The comparison between these two studies is difficult, as different condensation heights were used in evaluating the transfer coefficients. Smaller area with the 1-in. rings, the higher viscosity of Aroclor, and possible channeling in countercurrent flow may explain some of the difference.

It is noteworthy that spray-column exchangers are usually more efficient than packed beds for systems yielding small drops and consequent higher transfer area per unit column volume. However, because of pressure drop

through the liquid and backmixing in the column, packed beds may be preferred.

Some attempts to predict the volumetric heat-transfer coefficients were also reported. Hu (H19) suggested a design procedure for packed towers for use as direct-contact gasoline condensers. Hu's technique was later severely criticized by Lackey (L1), who presented a detailed procedure for determining the *HTU* by analogy to, and based on data of (S7), liquid-film controlling mass transfer in gas-liquid systems (W10). [An equation for calculating the *HTU* for the gas desuperheating section is also given (W10).] A somewhat different procedure to predict the volumetric heat-transfer coefficients in packed beds was suggested by Harriott and Wiegandt (H10a), who applied the penetration theory for the heat- and mass-transfer analogy. Application of the mass-transfer analogy (oxygen desorption data) to condensation in sieve plates (H10a) seems unsatisfactory.

In concluding this chapter on heat transfer with change of phase it is noted that, despite the advantages and effectiveness realized in utilizing latent heat transport, relatively little is known on the basic mechanism of this important phenomenon, and the various factors affecting it. It is probably instructive to note that the high heat-transfer coefficients obtained due to turbulence at the surface of these rapidly growing or contracting two-phase particles are comparable to those realized in nucleate boiling.

## VI. Miscellaneous Effects on Heat Transfer

### A. DROP AND COLUMN END EFFECTS

All equations and relationships reviewed in Sections III and IV and summarized in Tables I-III refer to the constant-velocity region of transfer. Drop end effects, associated with drop formation and coalescence, may sometimes affect the transfer to a considerable degree and should be taken into consideration. Numerous workers (G8, G12, G23, H13, L11, L13, S6, W6) have attempted to isolate the end effects. A relationship designed to distinguish between the overall and end transfer efficiencies was proposed by Johnson and Hamielec (J2).

The transfer efficiency in the drop-formation region varies approximately as the square root of the drop-formation time and inversely as the drop diameter. Since the drop acceleration interval is quite short, acceleration effects are normally combined with drop-formation effects. Heertjes (H13), basing his analysis on Higbie's penetration theory, suggested equations for the drop-formation and coalescence regions. For the drop-formation region,

$$E_{f1} = 10.3 \left( \frac{\alpha \Theta}{\pi R^2} \right)^{0.5} \quad (52)$$

where  $\Theta$  is the time of drop formation. Somewhat different relations were derived by Licht (L13) and by Groothuis and Kramers (G23) who applied different procedures to the same basic assumptions.

Assuming that coalescence time is equal to drop-formation time, and that the drop spreads at the interface of the two phases, exposing a fresh film of area  $\bar{A}$ , it can be shown (S8) that the ratio of transfer efficiencies in the drop-formation and coalescence regions can be approximated by

$$\frac{E_{f1}}{E_{f2}} \approx 1.75 \frac{A}{\bar{A}} \quad (53)$$

where  $A$  is the drop surface area. Assuming that a drop with a diameter of 1 mm spreads to 5–10 mm diam, the transfer efficiency in the coalescence region is 3–15 times that of the drop-formation region. This consideration applies only if the new drop forms a fresh surface at the contact area between the phases, which obviously is far from reality.

A simple relationship exists between the overall end-effect transfer efficiency  $E_F$ , the transfer efficiency in the constant velocity region  $E_m$ , and the over-all transfer efficiency  $E_T$ . Defining  $(1 - E)$  as the “complementary efficiency,” it can be shown that

$$1 - E_F = \frac{1 - E_T}{1 - E_m} \quad (54)$$

Experimental data can be used to determine  $E_F$ . As expected,  $E_F$  depends on the drop diameter as well as on the nozzle design. Experiments (J2) with 2.8-mm-diam cyclohexanol drops, falling in water out of a flat nozzle at 25°C, gave a complementary end effect,  $1 - E_F$ , of 0.81; whereas for a 4.3-mm drop from a sharp-edged nozzle (45°), the complementary value was only 0.78.

In spite of occasional pronounced drop end effects, they are commonly neglected in practice. This is especially justified in industrial units, where drop formation is rapid and the constant-velocity region is quite large, usually due to overdesign of the column. However, column end effects, associated with the longitudinal-dispersion and flow patterns in spray columns, strongly affect the transfer efficiency of the column.

Column end effects, though on a larger scale, are sometimes considered analogous to those associated with drop formation. The latter undoubtedly contributes to increase the former. However, no quantitative relationships between drop and column end effects are as yet known for countercurrent operation. As suggested by Vermeulen and others, the concentration (or temperature) of each incoming stream increases or decreases abruptly on entering the column. In contrast, the concentration pattern for each outgoing stream becomes flat as it approaches its outlet, and no discontinuity is

observed at this end (M6). As mentioned in connection with Pierce's spray-column studies (P3), the sharp drop in the driving force is especially pronounced in the continuous-phase inlet region, and was found to be almost independent of continuous-phase inlet nozzle and column design (G14). These phenomena are attributed to recirculation ("backmixing") of the continuous phase (P3), longitudinal dispersion (M6) or continuous phase envelopes (G15a) or wakes (L5a) carried with the dispersed phase.

Complete temperature profiles in the column, rather than external end values, are required for proper evaluation of the true transfer coefficients, the longitudinal-dispersion coefficient, and the column end effects. Geankoplis (G15) measured concentration profiles inside the column to determine the "true" transfer coefficients, and suggested a procedure for correlating tower and effects in terms of a fictitious height of column. Miyauchi and Vermeulen (M6) have provided a general theoretical treatment, which permits evaluation of the over-all behavior of two-phase countercurrent flow by considering the effect of longitudinal dispersion of both fluids. A trial-and-error procedure was suggested for determining inlet discontinuity as a measure of column performance on the basis of interior concentration data at the inlet and outlet ends. "Jump ratios" are available to facilitate trial-and-error calculation of the individual Peclet numbers from experimental data. (Peclet numbers here are defined in terms of the effective longitudinal-dispersion coefficient of each phase.) A method for calculating the maximum transfer efficiency by approximate determination of the "number of over-all dispersion units" is also presented (M6). The analytical solutions and graphs presented should allow for quantitative treatment of the data.

In a recent study of mixing in spray-column heat exchangers, Letan and Kehat (L5a) have shown that the temperature jump occurs only at the inlet of the continuous phase, i.e., water. This sharp discontinuity, a measure of the amount of mixing in the column, was found to be a function of the holdup fraction of the dispersed phase (kerosene) and the ratio of flow rates of the two phases. A hydrodynamic model based on the idea that considerable transfer to and from the drop occurs on the downstream side of the drops, to a toroidal vortex downstream of the drops, successfully explains the temperature profiles obtained by Letan and Kehat, as well as in other extraction studies. A high portion of the heat is transferred from the drops to the wakes at the bottom of the column, and a high portion of this heat is transferred to the continuous phase by the wakes shed in the middle of the column. This model can explain the flat temperature profiles at the bottom of the column, and the rise of the temperature of the continuous phase in the middle of the column. New material from the upstream side of the drop enters the circulating core of the wake through the boundary layer and is shed at a higher temperature some time later higher in the column. At the upper section of the

column the drop temperature becomes constant, and the rate of heat transfer diminishes to zero. At the top of the column, the holdup of the drops increases rapidly, and the detached wakes mix with the inlet water stream which immediately loses its original identity, similar to a liquid entering a highly mixed system. At the same holdup fraction, the total amount of water carried in the wakes up the column increases with increasing the flow ratio, resulting with greater mixing and higher jump ratios. At  $F = 0.24$ , the jump ratio rose from 0.1 to 0.55 when the flow rate ratio increased from 1 to 3.5.

At low holdups, longitudinal dispersion due to continuous-phase velocity profiles controls the amount of mixing in the countercurrent spray column; whereas at higher holdups the velocity profile flattens, and the shed-wake mechanism controls. Above holdups of 0.24, the temperature jump ratio is linearly proportional to the dispersed-to-continuous-phase flow ratio, and all mixing is caused by shed wakes into the bulk water and coalescence of drops. As column size decreases, it approaches the characteristics of a perfect mixer, and the jump ratio approaches unity (as compared with the value of zero for true countercurrent flow). It is interesting to note that changing the inlet temperature of dispersed phase by about 55°F hardly affected the jump ratio, probably due to the balancing effects of reduced viscosities and a decrease of drop diameter.

## B. TEMPERATURE AND TEMPERATURE-GRADIENT EFFECTS

Temperature obviously affects the physical properties of the fluids, thus indirectly affecting the transfer coefficients. As in the case of heat transfer in pipes, equations involving viscosity corrections for temperature differences between bulk and interface have been suggested (Eq. II-14, Table II) and are especially applicable for viscous continuous phases. No correction is needed for water, for instance, especially at  $(N_{Re})_c > 50$ . At lower  $(N_{Re})_c$ , natural convection is pronounced, especially in liquid systems with low kinematic viscosity. Since the transfer coefficient for natural convection is a function of the Grashof number, one may expect some effects of the temperature gradient. Steinberger and Treybal's equation (Eq. 6) allows for these effects.

As already mentioned, the viscosity of the dispersed phase affects the maximum obtainable transfer coefficients in spray-column operation; lower viscosities allow higher coefficients at lower operating temperature level. For the "hot-top" spray column, a linear dependence of the transfer coefficients and the fluidity of the dispersed phase was found (T2). This phenomenon may also be associated with reduction in surface tension. A decrease in drop diameter and increase in transfer area per unit volume of column may then be expected to increase the volumetric transfer coefficients.

The temperature gradient in heat exchangers is commonly expressed in

terms of the apparent log-mean temperature, which is computed from end temperatures of incoming and outgoing streams and is based on the assumption of a linear temperature gradient between top and bottom. This is evidently not the actual situation in countercurrent spray columns, due to backmixing and end effects associated with irregular flow patterns. True temperature profiles are required to obtain the true driving-force. Different inlet and outlet conditions correspond to the same externally apparent column performance, whereas a unique situation exists inside the column for any specific set of conditions. The difference and the relation of the transfer coefficients, derived from true, apparent (external ends), and measured interior temperature profiles in the column is demonstrated by Miyauchi and Vermeulen (M6) in their theoretical study of longitudinal dispersion in countercurrent two-phase operations.

The log-mean average is highly sensitive to the approach temperature at the columns ends, requiring highly accurate measurements of the true temperatures. Thus, the lower the approach temperature, the higher becomes the uncertainty of the calculated results. In these cases, recourse to the arithmetic-mean average should probably be advisable, to ensure more "conservative" design data. For a  $1^\circ$  approach temperature at one end and a  $5^\circ$  temperature difference at the other end, the ratio of the logarithmic- and arithmetic-mean temperature gradients is 1.25. For a given constant flow ratio of one of the fluid streams, the mean temperature is a function of the flow rate as well as of the absolute temperatures of the other streams. Li (L10) observed that a certain relationship exists between the apparent log-mean temperature, and the volumetric transfer coefficient. By manipulating the temperature at the ends of the column, Gardner (G1) obtained, for the specific case of  $G_c = 20$  ft/hr and  $(G_d/G_c) = 1$ ,

$$U_v = 2000(\Delta T)_{\ln}^{-0.146} \quad (55)$$

Contrary to suggestion (G1), Eq. 55 cannot be used for other flow conditions, because  $(\Delta T)_{\ln}$  is in itself a function of the flow-rate ratio.

Consider a special case of a spray column, where the temperature of one phase, say the dispersed phase, is constant throughout. This situation is ideally obtained when the dispersed phase is volatile and evaporates while rising in the column. Under ideal operating conditions (no subcooling or superheating), with constant mass flow rate of the dispersed phase,

$$(GC_p \rho \Delta T)_c = \text{const}, \quad \text{or} \quad \Delta T_c \propto 1/G_c \quad (56)$$

and the mean temperature gradient will vary accordingly. This case is similar, though not identical, to the special case of negligible concentration change



in one phase treated by Miyauchi and Vermeulen (M6), where

$$M = (GC_p\rho)_c / (GC_p\rho)_d = \Delta T_d / \Delta T_c$$

In that case,  $M \rightarrow 0$  since  $\Delta T_d \rightarrow 0$  and Colburn's equation (M6, Eq. 11), derived for piston flow (apparent external transfer coefficient), reduces to

$$U_v = \frac{q}{V (\Delta T)_{\ln}} = \frac{(GC_p\rho)_c}{Z} \ln \frac{T_{c2} - T_d}{T_{c1} - T_d} \quad (57)$$

The latter is obviously obtained independently (and for all  $M$ ) from the definition of the over-all volumetric transfer coefficient, based on apparent exterior temperatures. The obvious and common technique of studying column performance is to keep  $G_d$  and  $T_{c1}$  (in) constant and vary  $G_c$  until the desired minimum approach temperature is obtained, corresponding to  $(G_c)_{\min}$ , Fig. 25(a). Now, since  $T_{c2}$  (out) ideally approaches  $T_d$  only asymptotic-

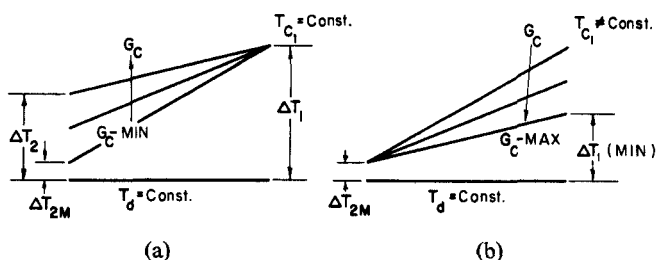


FIG. 25. Schematic presentation of column operation: (a) constant continuous-phase inlet temperature; (b) constant continuous-phase outlet temperature.

ally, a minimum practical approach-temperature gradient,  $\Delta T_{2M}$ , is set in practice. Obviously, for any  $G_c > (G_c)_{\min}$ , we get  $\Delta T_2 > \Delta T_{2M}$ . Since  $(\Delta T)_{\ln} > [(\Delta T)_{\ln}]_{\min}$ , hence,  $U_v < (U_v)_{\min}$ . This is demonstrated in Fig. 26, curve A, for the system pentane-water (S9), which shows that for a given dispersed-phase mass flow rate and a constant  $T_{c1}$  the transfer coefficient decreases with increasing continuous-phase flow rate. Similar, almost parallel, curves are obtained for different continuous-phase inlet temperature. As shown by curve B of Fig. 26, the opposite conclusion is also true, if the column is operated under the restrictions of constant  $\Delta T_{2M}$ . Under these conditions [Fig. 25(b)]  $G_c$  can theoretically increase to infinity, thus decreasing  $\Delta T_1$  and  $(\Delta T)_{\ln}$ . Practical limitations, such as flooding, holdup, etc., would however dictate  $(G_c)_{\max}$ . Thus, at any  $G_c < (G_c)_{\max}$ , we obtain  $\Delta T_1 > (\Delta T_1)_{\min}$ , hence,  $(\Delta T)_{\ln} > [(\Delta T)_{\ln}]_{\min}$  and  $U_v < (U_v)_{\max}$ . Thus, curve B of Fig. 26 is the locus of all points of optimum operating conditions, yielding  $(G_c)_{\min}$  and  $(U_v)_{\min}$  for any desired  $T_{c1}$ . Similar curves are obtained for other values of  $\Delta T_{2M}$ , as well as for different values of  $G_d$ , permitting determination of the optimum



in its presence the Prandtl exponent may be  $\frac{1}{2}$ . Garner *et al.* showed that internal circulation sets in at a Reynolds number of about 20. Terjesen *et al.* (T3) attributed the large increase in heat-transfer coefficient to an increase in velocity and vortex formation behind the drop above a Reynolds number of about 25. Since the higher transfer rates are certainly associated with the mobility of the drops' interface, we can leave aside the question as to whether circulation induces heat transfer directly or indirectly due to higher drop velocity and larger angle of separation. Experimental evidence of both schools indicates that transition from "small" to "large" drop behavior is governed by the Reynolds number, hence by velocity and fluid viscosity.

Calderbank and Moo-Young (C2) suggested two different correlations for the two drop-size ranges, substantiating it with an impressive amount of heat- and mass-transfer experimental data of various workers. Their equation for "small" drops or bubbles is

$$(N_{Nu})_c = 2 + 0.31(N_{Ra})^{1/3} \quad (58)$$

and for drops and bubbles larger than 2–3 mm,

$$(N_{Nu})_c = 0.42 \left( \frac{\Delta \rho g D^3 \rho_c}{\mu_c^2} \right)^{1/3} (N_{Pr})_c^{1/3} \quad (59)$$

Equations (58) and (59) indicate the transfer coefficient to be independent of the drop diameter. This conclusion, however, should be accepted with caution.

Beginning with the small drops, assumed to behave like solid spheres, the transfer coefficient can be plotted against drop diameter according to the classical Froessling equation or Eq. (5) originally derived for a solid sphere. Such a plot (H10) shows an almost straight line for diameters of 0.1–2.3 mm, as might have been expected. (In this size range the terminal drop velocity is approximately proportional to the diameter.) Below 50–200  $\mu$ , however, the transfer coefficient should increase with decreasing diameter, since the Nusselt number can never fall below 2, its limit for diffusion in a stagnant medium.

Experimental work with drops and bubbles of 2–7 mm diam indicates rather small changes in heat-transfer coefficient with changing drop diameter. Experiments (B1, B11, G26, H4, L13) with aqueous solutions showed very small decrease in the transfer coefficient with increasing diameter, as may be expected from Eq. (18). Only absorption experiments (H4) in glycol solutions showed a large increase in the transfer coefficient in the same size range. This, however, may be accounted for by the low Reynolds numbers involved.

Relatively little experimental evidence not favoring the practical independence of the transfer coefficients from drop diameter within the above size

ranges is available. Hammerton and Garner's (H4) experimental work on water absorption of  $\text{CO}_2$  and ethylene bubbles (2–3 mm diam) showed that the transfer coefficients, as well as bubble velocity, are directly proportional to the bubble diameter. Spence and Streeton (S19) reported similar relationship for extraction of uranyl nitrate from organic solvent (butex) to water drops, ranging in diameter from 0.5 to 5 mm. However, this relationship is heavily biased by a few values for the smallest and largest drops.

An hypothesis assigning Garner's results to a transition zone was recently refuted by new evidence. Leonard and Houghton (L4) substantiated Hammerton and Garner's observations in their work on water absorption of  $\text{CO}_2$  bubbles, 2–5 mm diam. The close relationship between bubble diameter and bubble velocity, as well as between bubble diameter and transfer coefficient, indicates that hydrodynamic relationships exist between the bubble velocity and the transfer coefficient. The higher velocities of immiscible bubbles (such as nitrogen and helium in water), compared with miscible ( $\text{CO}_2$ ) bubbles, raises questions as to the possible effect of transfer rates on bubble velocity (D3). Some dependence of rate of transfer and concentration on drop velocity is also indicated by Spence's data (S19); it is of interest to note that experiments have shown (L4) that immiscible bubble velocity decreases with increasing diameter up to 6 mm, whereas that of miscible bubbles increases in the same range.

Baird and Davidson (B1) derived an equation for the transfer coefficient of very large bubbles. Based on Davies and Taylor's model of potential flow past a spherical cap (D7), this relationship predicts a decrease in transfer with increasing bubble diameter, as does Eq. (18). For large bubbles or high Reynolds numbers, the transfer coefficient varies as the  $-\frac{1}{4}$ th power of the diameter. The experimental data with bubbles up to 20 mm diam are of the order of magnitude predicated by these equations, although a slight *increase* of the transfer coefficient with increasing diameter is observed. Bubbles larger than 25 mm exhibited unstable transfer rates (B1, L4). A detailed comparison between experimental gas absorption data and theoretical relationship between the transfer coefficient and the equivalent spherical diameter (up to 3 cm) is given by Calderbank and Lochiel (C1a).

As already stated, the high transfer coefficients exhibited by "large" drops and bubbles (above 2–3 mm diam) is closely related to the presence or absence of circulation. Therefore any outside factors affecting drop circulation, such as impurities and surface-active agents, will naturally affect the relationship between drop size and transfer coefficient. This is especially true in the transitional drop-size range of 1–3 mm, where the presence of surface-active agents affects the transfer coefficient by a factor of two to three, depending on whether the drop falls into the "small" or "large" category.

A workable criterion for the transitional drop radius is given (L8) by

$$R_{cr} \approx \left[ \frac{3}{g} \frac{\sigma - \sigma_s}{\rho_d - \rho_c} \right]^{1/2} \quad (60)$$

which is based on the maximum decrease in the interfacial tension  $\sigma$  of a pure system to  $\sigma_s$  observed in solutions of the given surface-active agents.

Experimental evidence (B13, T3) shows the effect of surface-active agents on transfer coefficients of noncirculating drops to be negligible, while quite significant in "large" drops near the transition zone. In the presence of surface-active agents, velocities of drops up to 4 mm diam were found (T3) almost identical with those of solid particles of the same diameter, and the coefficients were accordingly small. However, pure drops gave much higher coefficients with little dependence on drop diameter within the same size range. It may be concluded that the presence of surface-active impurities affects the behavior of a drop as "small" or "large," but has almost no effect in either "small" or "large" drops once the classification is made. Surface-active agents affect the boundary flow conditions by inducing viscous stresses. Hence the effect of surface-active agents decreases at higher ratios of the inertial to viscous forces, i.e., higher Reynolds numbers. For a given system, the larger the drops (or bubbles) and the higher their velocity, the smaller the effect of surface-active agents (B1, L8). Bubbles in the range of 4.5 to 10 mm indicated no effect of the presence of surface-active agents (L8), and neither did larger bubbles of up to 40 mm diam (B1).

The relationships between drop diameter, internal and external resistance to transfer, and overall transfer rates in agitated liquid-liquid systems are shown by Nagata and Yamaguchi (N1). As also found in solid-liquid agitated systems, the smaller the difference in density between the two phases, the smaller is the effect of increasing agitator speed (and decreasing drop diameter) on reducing the continuous-phase resistance. The drop-side transfer efficiency decreases with increased agitation. Large drops ( $\approx 1.0$  mm diam) at the lower agitation range (100–200 rpm) indicated high transfer efficiencies, comparable to the mixed-drop model. The transfer efficiency of small drops (0.1–0.05 mm) associated with higher agitation speeds ( $\approx 1000$  rpm) approached the theoretical molecular-diffusion values. However, as the values of the over-all transfer rate calculated by the mixed-drop and rigid-drop theories approach each other for small drops at high agitation speeds, the effect of agitation on the internal transfer efficiency becomes insignificant. In general, the effect of increasing agitation intensity is mainly to increase the interfacial transfer area, hence the volumetric transfer coefficient. An almost linear relationship between these is indicated. The obvious advantages of the higher residence

time, associated with agitated systems, on the transfer process is irrelevant to the problem at hand.

Coalescence, hence drop size, is sometimes strongly promoted by the transfer of solute from droplets to the ambient continuous phase. The recent experimental work of Groothuis and Zuiderweg (G24) showed that the addition of about 1.5 wt % of solute to the dispersed phase increased the average drop size by up to 80 %, while increasing coalescence rates about twenty-fold, which is equivalent to the effect of a forty-fold increase in power input. Larger drops were found at higher holdup ratios, which is consistent with the data obtained in these laboratories (Fig. 13) in spray-column heat-transfer studies.

In spray columns smaller drops have a lower terminal as well as slip velocity at the same holdup, and flooding points appear at lower ( $G_d/G_c$ ) ratios and lower holdups. As shown by Elgin's (W4) correlation, at a given slip velocity holdup decreases with decreasing drop diameter. However, the transfer area per unit column volume increases inversely with drop diameter and the transfer coefficient should increase accordingly. This, as well as the interrelationships between drop diameter, holdup, and slip velocity, explains the independence of spray-column performance, over a fairly wide range, of the nozzle diameter.

## VII. Related Works

A number of works closely related to the subject of heat transfer to a single drop were not incorporated in this chapter but should be borne in mind when dealing with this problem. These are works dealing with the mechanism of drop formation (B5, D4, H6, H11, H12, H21, N4, N6), the hydrodynamics of drops and bubbles, their drag and velocities (E3, G17, G18, H3, H7, K3, L7, M1, M4, N5, R3a, R4, S2, S5, W7, Z1, Z2), and interfacial agitation (D5, S21). In addition, certain important factors affecting transfer rates were not included or elucidated. Among these are oscillation (C6, G12, H9, H20, H21, L9, L12, S15), vortex formation behind a moving drop (G2, G10, G12, L6), natural convection (G4, G20, S20, T7), turbulence (C2, H5, H8, L8, N2), surface tension (G5, H1, H16, L8, L15, L17, S4, S15, W5), and interfacial resistance (S4) and drop frequencies (B11).

## ACKNOWLEDGMENTS

The author acknowledges with thanks the financial support of the Israel National Council for Research and Development, which enabled this work to be carried out. Thanks are due to Mr. E. Goldberg of the Technion, Israel Institute of Technology, for editorial advice.

## Nomenclature

|           |   |             |   |
|-----------|---|-------------|---|
| $A$       | Surface area of drops   | $q$         | heat flow, Btu/hr, Eq. (31)   |
| $\bar{A}$ | Surface area of spread drop in coalescence zone, Eq. (53)                       | $q_A$       | Heat-transfer rate, Btu/hr/ft <sup>2</sup>                                |
| $A_n$     | Constants   | $q_v$       | Specific heat flow rate, Btu/hr/ft <sup>3</sup>                           |
| $a$       | Constant, Eqs. (4)  | $\bar{R}$   | Factor, ratio of effective to molecular diffusivity                       |
| $B$       | Ratio of heat capacities of disperse to continuous phase, Eq. (32)              | $R$         | Drop radius   |
| $b$       | Constant, Eq. (4)   | $r$         | Radial distance   |
| $C_n$     | Constant, Eqs. (32), (33), (47)   | $S$         | Reciprocal of Peclet number, Eqs. (32), (33)                              |
| $C_p$     | Specific heat capacity  | $T$         | Temperature   |
| $D$       | Drop diameter   | $\Delta T$  | Temperature difference between phases                                     |
| $D^*$     | Initial drop diameter   | $U$         | Overall heat-transfer coefficient, Btu/hr/ft <sup>2</sup> /°F             |
| $\bar{D}$ | Column diameter   | $\bar{U}$   | Overall transfer coefficient, related to average of instantaneous area    |
| $d$       | Agitator diameter, Fig. 22  | $\bar{U}^*$ | Overall transfer coefficient, related to initial drop area                |
| $E$       | Reciprocal of Biot number, Eqs. (32), (33)                                      | $U_v$       | Volumetric over-all heat transfer coefficient, Btu/hr/ft <sup>3</sup> /°F |
| $E_{f1}$  | Transfer efficiency, drop-formation region                                      | $u$         | Drop velocity, relative   |
| $E_{f2}$  | Transfer efficiency, coalescence region   | $u_s$       | Velocity at drop equator, Eq. (16)  |
| $E_F$     | Transfer efficiency, end effects, overall ( $=E_{f1} + E_{f2} - E_{f1}E_{f2}$ ) | $V$         | Volume, of drop or column   |
| $E_m$     | Transfer efficiency, constant-velocity region                                   | $V_s$       | Slip velocity, Eq. (39)   |
| $E_T$     | Transfer efficiency, over-all   | $W$         | Mass-flow rate (lb/hr)  |
| $F$       | Holdup, fractional volume of dispersed phase in column                          | $x$         | Distance vector, parallel to drop interface, Eq. (15); exponent, Eq. (50) |
| $f$       | Coefficient, function of $(N_{re})_c$   | $y$         | Distance vector, normal to drop interface, Eq. (15); exponent, Eq. (50)   |
| $G$       | Superficial velocity, ft <sup>3</sup> /hr/ft <sup>2</sup>                       | $Z$         | Height of column  |
| $G'$      | Mass velocity, lb/hr/ft <sup>2</sup>  |             |   |
| $g$       | Acceleration; coefficient, viscosity-dependent                                  |             |   |
| $H$       | Rate of heat transfer, Btu/hr/ft <sup>2</sup>                                   |             |   |
| $h$       | Heat-transfer coefficient, Btu/hr/ft <sup>2</sup> /°F                           |             |   |
| $K$       | Log-mean average of distribution coefficients, Eq. (2)                          |             |   |
| $K_v$     | Ratio of true to potential-theory interfacial velocity                          |             |   |
| $k$       | Thermal conductivity, Btu/hr/ft/°F  |             |   |
| $L$       | Geometric factor $(D + \bar{D}/D)$ , Eq. (2)                                    |             |   |
| $M$       | $(GC_p\rho)_c/(GC_p\rho)_d = 1/B$   |             |   |
| $m$       | Exponent, Eq. (4); per cent vapor in two-phase drop                             |             |   |
| $N$       | Rate of agitator, rpm, Fig. 22  |             |   |
| $n$       | Exponent, Eq. (4); also $\gamma - 1$ , Fig. 23                                  |             |   |
| $P_v$     | Specific power input  |             |   |
| $Q$       | Total heat transferred, Btu, Eq. (12)   |             |   |

## GREEK LETTERS

|            |   |
|------------|---|
| $\alpha$   | Molecular diffusivity, ft <sup>2</sup> /hr  |
| $\alpha_e$ | Eddy diffusivity, ft <sup>2</sup> /hr   |
| $\beta$    | Coefficient of thermal expansion; opening half angle of vapor in evaporating drop |
| $\eta$     | External resistance controlling factor, $U/h_c$                                   |
| $\sigma$   | Surface tension   |
| $\sigma_s$ | Surface tension at high concentration of surface-active agent                     |
| $\Theta$   | Time  |
| $\lambda$  | Eigenvalue  |
| $\mu$      | Viscosity   |

|                      |   |                                       |  |
|----------------------|---|---------------------------------------|--|
| $\nu$                | Kinematic viscosity   | $N_{Ra}$                              | Rayleigh number, $[=D^3g\Delta\rho/\mu_c\alpha_c]$ |
| $\rho$               | Density   | $N_{Re}$                              | Reynolds number, $[=Du\rho/\mu]$                   |
| $\phi$               | Angle, Eq. (16)   | $N_{We}$                              | Weber number, $[=\rho u^2 D/\sigma]$               |
| $\psi$               | Stream function, Eq. (16)   |                                       |  |
| $\omega$             | Radius, dimensionless, Eq. (25)   |                                       |  |
| DIMENSIONLESS GROUPS |   |                                       |  |
| $N_{Bi}$             | Biot number, $[h_c R/k_d]$  |                                       |  |
| $N_{Fo}$             | Fourier number, $[=\alpha\Theta/D^2]$   |                                       |  |
| $N_{Gr}$             | Grashof number, $[=D^3g\rho_c\Delta\rho/\mu_c^2]$<br>or $[D^3g\beta\Delta T/\nu^2]$ |                                       |  |
| $K$                  | Log-mean average of partition coefficients, Eq. (2)                                 |                                       |  |
| $L$                  | Geometric factor, $[=(D+\bar{D})/\bar{D}]$ , Eq. (2)                                |                                       |  |
| $N_{Nu}$             | Nusselt number, $[=hD/k]$   |                                       |  |
| $N_{Pe}$             | Peclet number, $[=Du/\alpha]$   |                                       |  |
| $N_{Pe}'$            | Peclet number, modified, Eq. (26)   |                                       |  |
| $N_{Pr}$             | Prandtl number, $[=\mu C_p/k]$  |                                       |  |
| SUBSCRIPTS           |   |                                       |  |
|                      | 1   | Inlet, continuous phase               |  |
|                      | 2   | Outlet, continuous phase              |  |
|                      | 2M  | Outlet, minimum approach temperature  |  |
|                      | c   | Continuous phase                      |  |
|                      | co  | Continuous phase, outlet              |  |
|                      | cr  | Critical, radius, Eq. (60)            |  |
|                      | cz  | Continuous phase, at height z         |  |
|                      | d   | Dispersed phase, drop                 |  |
|                      | i   | Inlet                                 |  |
|                      | 0   | Outlet                                |  |
|                      | s   | Surface-active agent, slip (velocity) |  |
|                      | t   | Total                                 |  |
|                      | v   | Volumetric, overall                   |  |

TABLE AI  
VALUES FOR EQ. (11) (E2)

| $\frac{h_c D}{k_d}$ | $\lambda_1$ | $\lambda_2$ | $\lambda_3$ | $\lambda_4$ | $A_1$ | $A_2$   | $A_3$   | $A_4$   |
|---------------------|-------------|-------------|-------------|-------------|-------|---------|---------|---------|
| 4                   | 2.029       | 4.913       | 7.979       | 11.086      | 0.159 | 0.00634 | —       | —       |
| 6                   | 2.289       | 5.087       | 8.096       | 11.173      | 0.153 | 0.0109  | —       | —       |
| 8                   | 2.456       | 5.233       | 8.205       | 11.256      | —     | —       | —       | —       |
| 10                  | 2.570       | 5.354       | 8.303       | 11.335      | 0.142 | 0.0179  | 0.00408 | —       |
| 12                  | 2.654       | 5.454       | 8.391       | 11.409      | —     | —       | —       | —       |
| 14                  | 2.717       | 5.538       | 8.470       | 11.477      | 0.134 | 0.0220  | 0.00600 | —       |
| 16                  | 2.765       | 5.608       | 8.541       | 11.541      | —     | —       | —       | —       |
| 18                  | 2.804       | 5.667       | 8.603       | 11.599      | 0.129 | 0.0242  | 0.0119  | 0.00291 |
| 20                  | 2.836       | 5.717       | 8.659       | 11.653      | —     | —       | —       | —       |
| 22                  | 2.863       | 5.761       | 8.708       | 11.703      | 0.125 | 0.0255  | 0.00858 | 0.00359 |
| 32                  | 2.948       | —           | —           | —           | 0.118 | —       | —       | —       |
| 42                  | 2.993       | —           | —           | —           | —     | —       | —       | —       |
| 62                  | 3.041       | —           | —           | —           | 0.111 | —       | —       | —       |
| 82                  | 3.080       | —           | —           | —           | —     | —       | —       | —       |
| 102                 | 3.080       | —           | —           | —           | 0.107 | —       | —       | —       |
| 00                  | —           | —           | —           | —           | —     | —       | —       | —       |



TABLE AII  
VALUES FOR EQ. (IV-4) ( $h_c = \infty$ )

| $n$ | $\lambda_n$ | $A_n$ | Reference |
|-----|-------------|-------|-----------|
| 1   | 1.656       | 1.29  | (E2)      |
| 2   | 9.08        | 0.596 |           |
| 3   | 22.2        | 0.386 |           |
| 4   | 38.5        | 0.35  | (H13)     |
| 5   | 63.0        | 0.28  |           |
| 6   | 89.8        | 0.22  |           |
| 7   | 123.8       | 0.16  |           |

TABLE AIII  
VALUES FOR EQ. (IV-5) (E2)

| $\frac{h_c D}{k_d}$ | $\lambda_1$ | $\lambda_2$ | $\lambda_3$ | $A_1$ | $A_2$ | $A_3$ |
|---------------------|-------------|-------------|-------------|-------|-------|-------|
| 3.20                | 0.262       | 4.24        | —           | 1.49  | 0.107 | —     |
| 5.33                | 0.386       | —           | —           | —     | —     | —     |
| 8.00                | 0.534       | —           | —           | —     | —     | —     |
| 10.7                | 0.680       | 4.92        | —           | 1.49  | 0.300 | —     |
| 16.0                | 0.860       | 5.26        | —           | 1.48  | 0.382 | —     |
| 21.3                | 0.982       | 5.63        | —           | 1.47  | 0.428 | —     |
| 26.7                | 1.082       | 5.90        | 15.7        | 1.49  | 0.495 | 0.205 |
| 53.3                | 1.324       | 7.04        | 17.5        | 1.43  | 0.603 | 0.298 |
| 107                 | 1.484       | 7.88        | 19.5        | 1.39  | 0.603 | 0.384 |
| 213                 | 1.560       | 8.50        | 20.8        | 1.31  | 0.588 | 0.396 |
| 320                 | 1.600       | 8.62        | 21.3        | 1.31  | 0.583 | 0.391 |
| ∞                   | 1.656       | 9.08        | 22.2        | 1.29  | 0.596 | 0.386 |

#### REFERENCES

- A1. Akselrud, G. A., *Zh. Fiz. Khim.* **28**, 1446 (1953).  
 B1. Baird, M. H. I., and Davidson, J. F., *Chem. Eng. Sci.* **17**, 87 (1962).  
 B1a. Baird, M. H. I., and Hamielec, A. E., *Can. J. Chem. Eng.* **40**, 119 (1962).  
 B2. Bankoff, S. G., and Mason, J. P., *A.I.Ch.E. (Am. Inst. Chem. Engrs.) J.* **8**, 30 (1962).  
 B3. Barbouteau, I., *Rev. Inst. Franc. Pétrole Ann. Combust. Liquides* **11**, 358 (1956).  
 B4. Bartok, W., and Mason, S. G., *J. Colloid Sci.* **13**, 293 (1958); **14**, 13 (1959).  
 B5. Baston, J. B., M.S. thesis, Univ. Tennessee, Knoxville, Tennessee, 1951.  
 B6. Bentwich, M., Szwarcbaum, B., and Sideman, S., *8th Natl. Heat Transfer Conf., Los Angeles, Calif.*, 1965, ASME Paper 65-HT-38 (1965).

- B7. Beyaert, B. O., Lapidus, L., and Elgin, J. C., *A.I.Ch.E. (Am. Inst. Chem. Engrs.) J.* **7**, 46 (1961).
- B8. Bond, W. N., *Phil. Mag.* [7] **57**, 890 (1927).
- B9. Bond, W. N., and Newton, D. R., *Phil. Mag.* [7] **57**, 794 (1928).
- B9a. Bonilla, C. F., and Cichelle, M. T., *Trans. Am. Inst. Chem. Engrs.* **41**, 755 (1945).
- B10. Boussinesq, M., *J. Math. Pures Appl.* **1**, 285 (1905); *Ann. Chim. e Phys. (Paris)* **29**, 364 (1913).
- B11. Bowman, C. W., and Johnson, A. I., *Can. J. Chem. Eng.* **40**, 139 (1962).
- B12. Bowman, C. W., Ward, D. M., Johnson, A. I., and Trass, O., *Can. J. Chem. Eng.* **39**, 9 (1961).
- B13. Boye-Christensen, G., and Terjesen, S. G., *Chem. Eng. Sci.* **9**, 225 (1959).
- B14. Brenner, H., *Chem. Eng. Sci.* **18**, 109 (1963).
- B15. Brown, G., *ASME, Proc. Gen. Discussion Heat Transfer* 1951, p. 41.
- B16. Brown, W. S., Pitts, C. C., and Leppert, G., *Am. Soc. Mech. Engrs., Paper* **61-SA-26** (1961).
- C1. Calderbank, P. H., and Korchinski, I. J. O., *Chem. Eng. Sci.* **6**, 65 (1956).
- C1a. Calderbank, P. H., and Lochiel, A. C., *Chem. Eng. Sci.* **19**, 485 (1964).
- C2. Calderbank, P. H., and Moo-Young, M. B., *Chem. Eng. Sci.* **16**, 39 (1961).
- C2a. Canning, F. T., personal communication (1965).
- C3. Carr, B. B., *Chem. Eng. Progr.* **59**, 59 (1963).
- C4. Carslaw, H. S., and Jaeger, J. C., "Conduction of Heat in Solids," 2nd ed., p. 235, Oxford Univ. Press, London and New York, 1959.
- C4a. Chao, B. F., *Phys. Fluids* **5**, 69 (1962).
- C5. Conkie, W. R., and Savic, P., *Natl. Res. Council Can. Rept.* **MT-23** (1953).
- C6. Constan, G. L., and Calvert, S., *A.I.Ch.E. (Am. Inst. Chem. Engrs.) J.* **9**, 109 (1963).
- C7. Coulson, J. M., and Skinner, S. J., *Chem. Eng. Sci.* **1**, 197 (1952).
- D1. Danckwerts, P. V., *Trans. Faraday Soc.* **47**, 1014 (1951).
- D2. Danckwerts, P. V., *Ind. Eng. Chem.* **43**, 1460 (1951).
- D3. Datta, R. L., Napier, D. H., and Newitt, D. M., *Trans. Inst. Chem. Engrs. (London)* **28**, 14 (1950).
- D4. Davidson, J. F., and Schuler, B. O. G., *Trans. Inst. Chem. Engrs. (London)* **38**, 335 (1960).
- D5. Davies, J. T., and Rideal, E. K., "Interfacial Phenomena," Academic Press, New York, 1961.
- D6. Davies, J. T., *56th Ann. Meeting, A.I.Ch.E., Houston, Tex.*, Dec. 1963.
- D7. Davies, R. M., and Taylor, G. I., *Proc. Roy. Soc.* **A200**, 375 (1950).
- D8. Deindoerfer, F. H., and Humphrey, A. E., *Ind. Eng. Chem.* **53**, 755 (1961).
- E1. Eckenfelder, W. W., and Barnhart, E. L., *42nd Natl. Meeting A.I.Ch.E., Atlanta*, (1960).
- E2. Elzinga, E. R., and Banchero, J. T., *Chem. Eng. Progr., Symp. Ser.* **55**, 149 (1959).
- E3. Elzinga, E. R., and Banchero, J. T., *A.I.Ch.E. (Am. Inst. Chem. Engrs.) J.* **7**, 394 (1961).
- F1. Fleming, J. F., and Johnson, H. F., *Chem. Eng. Progr.* **49**, 497 (1953).
- F1a. Florschuetz, I. W., and Chao, B. F., *ASME J. Heat Transfer* **82**, 209 (1965).
- F2. Friedlander, S. K., *A.I.Ch.E. (Am. Inst. Chem. Engrs.) J.* **3**, 43 (1957).
- F3. Frisch, H. L., *J. Chem. Phys.* **22**, 123 (1954).
- F4. Frossling, N., *Beitr. Geophys.* **52**, 170 (1938).
- F5. Frumkin, A., and Levich, V. G., *Zh. Fiz. Khim.* **21**, 1183 (1947).
- G1. Gardner, R. P., *At. Energy. Comm. Contract* AT-(40-1)-1320 (1958); M.S. Thesis in Chem. Eng., North Carolina State College, Raleigh, North Carolina, 1958.
- G2. Garner, F. H., *Trans. Inst. Chem. Engrs. (London)* **28**, 88 (1950).

- G3. Garner, F. H., Foord, A., and Tayeban, M., *J. Appl. Chem.* **9**, 315 (1959).  
G4. Garner, F. H., and Grafton, R. W. *Proc. Roy. Soc.* **A224**, 64 (1954).  
G5. Garner, F. H., and Hale, A. R., *Chem. Eng. Sci.* **2**, 157 (1953).  
G6. Garner, F. H., and Hayock, P. J., *Proc. Roy. Soc.* **A252**, 457 (1957).  
G7. Garner, F. H., and Lane, J. J., *Trans. Inst. Chem. Engrs. (London)* **37**, 162 (1959).  
G8. Garner, F. H., and Skelland, A. H. P., *Trans. Inst. Chem. Engrs. (London)* **29**, 315 (1951).  
G9. Garner, F. H., and Skelland, A. H. P., *Ind. Eng. Chem.* **46**, 1255 (1954).  
G10. Garner, F. H., and Skelland, A. H. P., *Chem. Eng. Sci.* **4**, 149 (1955).  
G11. Garner, F. H., and Suckling, R. D., *A.I.Ch.E. (Am. Inst. Chem. Engrs.) J.* **4**, 114 (1958).  
G12. Garner, F. H., and Tayeban, M., *Anales Real Soc. Espan. Fis. Quim. (Madrid)* **(B56)**, 479 and 491 (1960).  
G13. Garwin, L., and Smith, B. D., *Chem. Eng. Progr.* **49**, 591 (1953).  
G14. Geankoplis, C. J., and Hixon, A. N., *Ind. Eng. Chem.* **42**, 1142 (1950).  
G15. Geankoplis, C. J., Wells, P. L., and Hawk, E. L., *Ind. Eng. Chem.* **43**, 1843 (1951).  
G15a. Geankoplis, C. J., *Ind. Eng. Chem.* **44**, 2458 (1952).  
G16. Geddes, A. P., *Trans. Am. Inst. Chem. Engrs.* **42**, 79 (1946).  
G17. Gibbons, J. H., Houghton, G., and Coull, J., *A.I.Ch.E. (Am. Inst. Chem. Engrs.) J.* **8**, 274 (1962).  
G17a. Gordon, K. F., Singh, T., and Weissman, E. Y., *Intern. J. Heat Mass Transfer* **3**, 90 (1961).  
G18. Grassmann, P., and Reinhardt, A., *Chem.-Ing.-Tech.* **33**, 348 (1961).  
G19. Grassmann, P., and Wyss, E., *Chem.-Ing.-Tech.* **34**, 755 (1963).  
G20. Griffith, R. M., Ph.D. thesis, Univ. Wisconsin, Madison, Wisconsin, 1958.  
G21. Griffith, R. M., *Chem. Eng. Sci.* **12**, 198 (1960).  
G22. Grober, H., *Z. Ver. Deut. Ing.* **69**, 705 (1925).  
G23. Groothuis, H., and Kramers, H., *Chem. Eng. Sci.* **4**, 17 (1955).  
G24. Groothuis, H., and Zuiderweg, F. J., *Chem. Eng. Sci.* **19**, 63 (1964).  
G25. Grover, S. S., and Knudsen, J. G., *Chem. Progr., Symp. Ser.* **51**, 71 (1955).  
G26. Guyer, A., and Pfister, X., *Helv. Chim. Acta* **29**, 1173 and 1400 (1946).  
H1. Haberman, W. L., and Morton, R. K., David Taylor Model Basin Rept. No. 802. U.S. Navy Dept., Washington, D.C., 1953.  
H2. Hadamard, J., *Compt. Rend.* **152**, 1735 (1911).  
H3. Hamielec, A. E., and Johnson, A. I., *Can. J. Chem. Eng.* **40**, 41 (1962).  
H4. Hammerton, D., and Garner, F. H., *Trans. Inst. Chem. Engrs. (London)* **32**, S18 (1954).  
H5. Handlos, A. E., and Baron, T., *A.I.Ch.E. (Am. Inst. Chem. Engrs.) J.* **3**, 127 (1957).  
H5a. Hanson, C., and Ingham, J., *Brit. Chem. Eng.* **10**, 391 (1965).  
H6. Harkins, W. D., and Brown, F. E., *J. Am. Chem. Soc.* **38**, 246 (1916); **41**, 499 (1919).  
H7. Harmathy, T. Z., *A.I.Ch.E. (Am. Inst. Chem. Engrs.) J.* **6**, 281 (1960).  
H8. Harriott, P., *Can. J. Chem. Eng.* **40**, 60 (1962).  
H9. Harriott, P., *Chem. Eng. Sci.* **17**, 149 (1962).  
H10. Harriott, P., *A.I.Ch.E. (Am. Inst. Chem. Engrs.) J.* **8**, 93 (1962).  
H10a. Harriott, P., and Wiegandt, H. F., *A.I.Ch.E. (Am. Inst. Chem. Engrs.) J.* **10**, 755 (1964).  
H11. Hayes, W., Hardy, B. W., and Holland, C. D., *A.I.Ch.E. (Am. Inst. Chem. Engrs.) J.* **5**, 318 (1959).  
H12. Hayworth, C. B., and Treybal, R. E., *Ind. Eng. Chem.* **42**, 1174 (1950).  
H13. Heertjes, P. M., Holve, W. A., and Talsma, H., *Chem. Eng. Sci.* **3**, 122 (1954).

- H14. Henniker, J. C., *Rev. Mod. Phys.* **21**, 322 (1949).
- H15. Higbie, R., *Trans. Am. Inst. Chem. Engrs.* **31**, 365 (1935).
- H16. Holm, P., and Terjesen, S. G., *Chem. Eng. Sci.* **3**, 265 (1954).
- H17. Hsu, N. T., and Sage, B. H., *A.I.Ch.E. (Am. Inst. Chem. Engrs.) J.* **3**, 405 (1957).
- H18. Hsu, N. T., Sato, K., and Sage, B. H., *Ind. Eng. Chem.* **46**, 870 (1954).
- H19. Hu, S., *Refining Engr. C-12*, 722 (1956).
- H20. Hu, S., and Kinter, R. C., *A.I.Ch.E. (Am. Inst. Chem. Engrs.) J.* **1**, 42 (1955).
- H21. Hughes, G. R. R., and Gilliland, E. R., *Chem. Eng. Progr.* **48**, 497 (1952).
- J1. Jakob, M., "Heat Transfer," Vol. 1. Wiley, New York, 1949.
- J2. Johnson, A. I., and Hamielec, A. E., *A.I.Ch.E. (Am. Inst. Chem. Engrs.) J.* **6**, 145 (1960).
- J3. Johnson, A. I., Minard, G. W., Huang, C. J., Hansuld, J. H., and McNamara, V. M., *A.I.Ch.E. (Am. Inst. Chem. Engrs.) J.* **3**, 101 (1957).
- J4. Johnstone, H. F., Pigford, R. L., and Chapin, J. H., *Trans. Am. Inst. Chem. Engrs.* **37**, 95 (1941).
- K1. Karnofsky, G., and Steinhoff, P. F., *U.S. Office Saline Water, Saline Water Res. Develop. Progr. Rept.* **40** 1960.
- K2. Kinzer, G. D., and Gunn, R., *J. Meteorol.* **8**, 71 (1951).
- K3. Klee, A. J., and Treybal, R. E., *A.I.Ch.E. (Am. Inst. Chem. Engrs.) J.* **2** 444 (1956).
- K3a. Klipstein, D. H., D.Sci. thesis, Mass. Inst. Technol., Cambridge, Massachusetts, 1963.
- K4. Kramers, H., *Physica* **12**, 61 (1946).
- K5. Kronig, R., and Brink, J. C., *Appl. Sci. Res.* **A2**, 142 (1950).
- K6. Kronig, R., and Bruijsten, J., *Appl. Sci. Res.* **A2**, 439 (1950).
- K7. Kusik, C. L., and Happel, J., *Ind. Eng. Chem., Fundamentals* **1**, 163 (1962).
- L1. Lackey, D. L., UCRL-10339, M.S. thesis, Univ. California, Berkeley, California, 1961.
- L2. Lamb, H., "Hydrodynamics," 6th ed., p. 200. Cambridge Univ. Press, London and New York, 1932.
- L3. Langmuir, I., *Phys. Rev.* **12**, 368 (1918).
- L4. Leonard, J. H., and Houghton, G., *Chem. Eng. Sci.* **18**, 133 (1963).
- L5. Letan, R., and Kehat, E., *Rept. Israel Natl. Council Res. Develop.*, 1963 (in Hebrew).
- L5a. Letan, R., and Kehat, E., *A.I.Ch.E. (Am. Inst. Chem. Engrs.) J.* **11**, 804 (1965).
- L6. Levich, V. G., *Zh. Obshch. Khim.* **19**, 18 (1949).
- L7. Levich, V. G., *Intern. Chem. Eng.* **2**, 78 (1962).
- L8. Levich, V. G., "Physiochemical Hydrodynamics," Prentice-Hall, Englewood Cliffs, New Jersey, International Series, 1962.
- L9. Lewis, J. B., and Pratt, H. R. C., *Nature* **171**, 1155 (1953).
- L10. Li, S. C., M.S. Thesis, North Carolina State College, Raleigh, North Carolina, 1957.
- L11. Licht, W., and Conway, C. J. B., *Ind. Eng. Chem.* **42**, 1151 (1950).
- L12. Licht, W., and Narasimhamurty, G. S. R., *A.I.Ch.E. (Am. Inst. Chem. Engrs.) J.* **1**, 366 (1955).
- L13. Licht, W., and Pansing, W. F., *Ind. Eng. Chem.* **45**, 1885 (1953).
- L14. Lileeva, A. K., and Smirnov, N., *J. Appl. Chem. USSR (English Transl.)* **34**, 1103 and 1295 (1961).
- L15. Lindland, K. P., and Terjesen, S. C., *Chem. Eng. Sci.* **5**, 1 (1956).
- L16. Linton, W. H., Jr., and Sherwood, T. K., *Chem. Eng. Progr.* **46**, 258 (1950).
- L17. Linton, M., and Sutherland, K. L., *Proc. 2nd Intern. Conf. Surface Activity*, Vol. 1, p. 494 (1957).

- L18. Lochiel, A. C., and Calderbank, P. H., *Chem. Eng. Sci.* **19**, 471 (1964).
- M1. Ma, S. T., *IBM J. Res. Develop.* **6**, 472 (1962).
- M1a. Marsh, B. D., and Heideger, W. J., *Ind. Eng. Chem., Fundamentals* **4**, 129 (1965).
- M2. McAdams, W. H., "Heat Transmission," 3rd ed. Mc-Graw Hill, New York, 1954.
- M3. McDowell, R. V., and Myers, J. E., *A.I.Ch.E. (Am. Inst. Chem. Engrs.) J.* **2**, 384 (1956).
- M4. Meksyn, D., *J. Aerospace Sci.* **25**, 631 and 664 (1958).
- M5. Minard, G. W., and Johnson, A. I., *Chem. Eng. Progr.* **48**, 62 (1952).
- M6. Miyauchi, T., and Vermeulen T., *Ind. Eng. Chem. Fundamentals* **2**, 113 (1963).
- N1. Nagata, S., and Yamaguchi, I., *Mem. Fac. Eng. Kyoto Univ.* **22**, 249 (1960).
- N2. Naisel, D. S., and Sherwood, T. K., *Chem. Eng. Progr.* **46**, 131 and 172 (1950).
- N3. Newman, A. B., *Trans. Am. Inst. Chem. Engrs.* **27**, 310 (1931).
- N4. Nordberg, S., *Dechema Monograph* **41** (1962).
- N4a. Novakovic, M., and Stefanovic, M., *Intern. J. Heat Mass Transfer* **7**, 801 (1964).
- N5. Novoselov, V. S., *A.R.S. J. (Suppl.)* **31**, 686 (1961).
- N6. Null, H. R., and Johnson, H. F., *A.I.Ch.E. (Am. Inst. Chem. Engrs.) J.* **4**, 273 (1958).
- O1. Othmer, D. F., Benenati, R. F., and Goulandris, G. C., *Chem. Eng. Progr.* **59**, 63 (1963).
- P1. Pasternak, I. S., and Gauvin, W. H., *Can. J. Chem. Eng.* **38**, 35 (1960).
- P2. Pattle, R. E., *Trans. Inst. Chem. Engrs. (London)* **28**, 32 (1950).
- P3. Pierce, R. D., Dwyer, O. E., and Martin, J. J., *A.I.Ch.E. (Am. Inst. Chem. Engrs.) J.* **5**, 257 (1959).
- P4. Pinder, K. L., Univ. British Columbia, personal communication 1965.
- P5. Porter, J. W., Ph. D. Thesis, Univ. of California, Berkeley, 1965.
- P6. Porter, J. W., Goren, S. L., and Wilke, C. R. (to be published).
- Q1. Quigley, C. J., Johnson, A. I., and Harris, B. L., *Chem. Eng. Progr., Symp. Ser.* **51**, 31 (1955).
- R1. Radusch, R., *Chem.-Ing.-Tech.* **28**, 275 (1956).
- R2. Ranz, W. E., *Chem. Eng. Progr.* **48**, 247 (1952).
- R3. Ranz, W. E., and Marshall, W. R., Jr., *Chem. Eng. Progr.* **48**, 141 (1952).
- R3a. Redfield, J. A., and Houghton, G., *Chem. Eng. Sci.* **20**, 131 (1965).
- R4. Rosenberg, B., David Taylor Model Basin Rept. No. 727 (1950).
- R5. Rosenthal, H., M.S. Thesis, New York University (1949).
- R6. Ruby, G. L., and Elgin, J. C., *Chem. Eng. Progr., Symp. Ser.* **51**, 17 (1955).
- R7. Ruckenstein, E., *Chem. Eng. Sci.* **10**, 22 (1959).
- R8. Rumscheidt, D., and Mason, S. G., *J. Colloid Sci.* **16**, 210 (1961).
- R9. Rybozynski, W., *Bull. Intern. Acad. Polon. Sci.* **A40** (1911).
- S0. Sagar, D. V., Ramanujam, T. K., Krishnamurty, V. V. G., and Rao, C. V., *Indian J. Tech.* **3**, 79 (1965).
- S1. Sakiadis, B. C., and Johnson, A. J., *Ind. Eng. Chem.* **46**, 1229 (1954).
- S2. Satapathy, R., and Smith, W., *J. Fluid Mech.* **10**, 561 (1961).
- S3. Savic, P., *Natl. Res. Council Can. Rept.* **MT-22** (1953).
- S4. Schechter, R. S., and Farley, R. W., *Brit. Chem. Eng.* **18**, 1 (1963).
- S5. Schlichting, H., "Boundary Layer Theory," p. 403. Pergamon Press. Oxford, 1955.
- S6. Sherwood, T. K., Evans, J. E., and Longcor, J. V. A., *Ind. Eng. Chem.* **31**, 1146 (1939).
- S7. Sherwood, T. K., and Holloway, C., *Trans. Am. Inst. Chem. Engrs.* **36**, 39 (1940).
- S8. Sideman, S., and Shabtai, H., *Can. J. Chem. Eng.* **42**, 107 and 238 (1964).
- S8a. Sideman, S., and Barsky, Z., *A.I.Ch.E. (Am. Inst. Chem. Engrs.) J.* **11**, 539 (1965).

- S9. Sideman, S., and Gat, Y., *57th Natl. Meeting A.I.Ch.E., Minneapolis, 1965 A.I.Ch.E. (Am. Inst. Chem. Engrs.) J.* **12**, No. 2 (1966).
- S10. Sideman, S., and Hirsch, G., *Israel J. Technol.* **2**, 234 (1964).
- S11. Sideman, S., and Hirsch, G., *A.I.Ch.E. (Am. Inst. Chem. Engrs.) J.* **11**, 1019 (1965).
- S11a. Sideman, S., Hirsch, G., and Gat, Y., *A.I.Ch.E. (Am. Inst. Chem. Engrs.) J.* **11**, 1081 (1965).
- S12. Sideman, S., and Taitel, Y., *Intern. J. Heat Mass Transfer* **7**, 1273 (1964).
- S13. Siemes, W., and Franke, M., *Chem.-Ing.-Tech.* **30**, 165 (1958).
- S14. Skelland, A. H. P., and Cornish, A. R. H., *A.I.Ch.E. (Am. Inst. Chem. Engrs.) J.* **9**, 73 (1963).
- S15. Skelland, A. H. P., and Welleck, R. M., *A.I.Ch.E. (Am. Inst. Chem. Engrs.) J.* **10**, 491 (1964).
- S16. Sleicher, C. A., Jr., *A.I.Ch.E. (Am. Inst. Chem. Engrs.) J.* **5**, 145 (1959).
- S17. Smith, G. C., and Beckman, R. B., *A.I.Ch.E. (Am. Inst. Chem. Engrs.) J.* **4**, 180 (1958).
- S18. Spelles, K. E., *Proc. Phys. Soc. (London)* **B65**, 541 (1952).
- S19. Spence, R., and Streeton, R. J. W., *Chem.-Process. Eng.* **44**, 597 (1963).
- S20. Steinberger, R. L., and Treybal, R. E., *A.I.Ch.E. (Am. Inst. Chem. Engrs.) J.* **6**, 227 (1963).
- S21. Sternling, C. V., and Scriven, L. E., *A.I.Ch.E. (Am. Inst. Chem. Engrs.) J.* **5**, 514 (1959).
- T1. Tang, Y. S., Duncan, J. M., and Schweyer, H. E., *Natl. Advisory Comm. Aeron., Tech. Note* **2867** (1953).
- T2. Thompson, W. S., Woodward, T., Shrode, W. A., Baird, E. D., and Oliver, D. A., *U.S. Office Saline Water, Saline Water Res. Develop. Progr. Rept.* **63** (1962).
- T3. Thorsen, G., and Terjesen, S. G., *Chem. Eng. Sci.* **17**, 137 (1962).
- T4. Timson, W. J., and Dunn, C. G., *Ind. Eng. Chem.* **52**, 799 (1960).
- T5. Toor, H. L., and Marchello, J. M., *A.I.Ch.E. (Am. Inst. Chem. Engrs.) J.* **4**, 97 (1958).
- T6. Treybal, R. E., "Liquid Extration," 1st ed, p. 328. McGraw-Hill, New York, 1951.
- T7. Tsubouchi, T., and Sato, S., *Chem. Eng. Progr. Symp. Ser.* **56**, 285 (1960).
- U1. Umamo, S., *Japan. Govt. Chem. Ind. Res. Inst.* **54**, 9 (1959) (in Japanese).
- U2. Umamo, S., *Japan. Govt. Chem. Ind. Res. Inst.* **61**, 5 (1959) (in Japanese).
- V1. Vermeulen, T., *Ind. Eng. Chem.* **45**, 1664 (1953).
- V1a. Viskanta, R., and Lottes, P. A., *Proc. Heat Transfer Fluid Mech. Inst.* p. 171, 1962,
- V2. Vliet, G. C., and Lepper, G., *Heat Transfer Conf., Buffalo., Buffalo, N.Y.*, ASME publication 60-HT-5 (1960).
- W1. Wakeshima, H., and Takata, K., *J. Phys. Soc. Japan* **13**, 1398 (1958).
- W2. Wakeshima, H., and Takata, K., Superheat of Droplets in mercury. Private communication (1962).
- W3. Ward, D. M., Trass, O., and Johnson, A. I., *Can. J. Chem. Eng.* **40**, 164 (1962).
- W4. Weaver, R. E. C., Lapidus, L., and Elgin, J. C., *A.I.Ch.E. (Am. Inst. Chem. Engrs.) J.* **5**, 533 (1959).
- W4a. Welleck, R. M., and Skelland, A. H. F., *A.I.Ch.E. (Am. Inst. Chem. Engrs.) J.* **11**, 557 (1965).
- W5. West, F. B., Herman, A. J., and Chong, A. T., *Ind. Eng. Chem.* **44**, 625 (1952).
- W6. West, F. B., Robinson, P. A., Morgenthales, A. C., Beck, T. R., and McGregor, D. K., *Ind. Eng. Chem.* **43**, 234 (1951).
- W7. White, E. T., and Beardmore, R. H., *Chem. Eng. Sci.* **17**, 351 (1962).
- W8. Wiegandt, H. F., *Natl. Acad. Sci. Publication* 568, 377 (1958).

- W9. Wiegandt, H. F., *U.S. Office Saline Water, Saline Water Res. Develop. Progr. Rept.* **41** (1960).
- W10. Wilke, C. R., Cheng, C. T., Ledesma, V. L., and Porter, J. W., *Chem. Eng. Progr.* **59**, 69 (1963).
- W11. Williams, G. C., Sc.D. thesis in Chem. Eng., Mass. Inst. Techn., Cambridge, Massachusetts, 1942.
- W12. Woodward, T., *Chem. Eng. Progr.* **57**, 52 (1961).
- Y1. Young, N. O., Goldstein, J. S., and Block, M. J., *J. Fluid Mech.* **6**, 350 (1959).
- Z1. Zwick, S. A., *J. Math. Phys.* **37**, 246 (1958).
- Z2. Zwick, S. A., and Plesset, M. S., *J. Math. Phys.* **23**, 308 (1955).

# HYDRODYNAMIC RESISTANCE OF PARTICLES AT SMALL REYNOLDS NUMBERS

Howard Brenner\*

Department of Chemical Engineering  
New York University, Bronx, New York

|  |     |
|--|-----|
| I. Introduction.....   | 287 |
| II. Stokes Flows.....  | 289 |
| A. Introduction.....   | 289 |
| B. Equations of Motion.....  | 289 |
| C. Single Particles.....   | 290 |
| D. Multiparticle Systems.....  | 341 |
| III. Flow at Small, Nonzero Reynolds Numbers.....                        | 356 |
| A. Introduction.....   | 356 |
| B. Regular Perturbation Methods.....                                     | 359 |
| C. Singular Perturbation Methods.....                                    | 360 |
| D. Experimental Data in the "Transition" Region.....                     | 374 |
| E. Lateral Migration in Tubes.....                                       | 377 |
| IV. Heat- and Mass-Transfer Analogies, Brownian Motion, and Summary..... | 403 |
| A. Heat- and Mass-Transfer Analogs.....                                  | 403 |
| B. Brownian Motion.....  | 408 |
| C. Summary and Commentary.....   | 421 |
| Nomenclature.....  | 423 |
| References.....  | 429 |

## I. Introduction

The forces acting on a volume element in a fluid continuum are essentially of three types: (i) viscous forces, expressing resistance to change of shape; (ii) inertial forces, expressing resistance to changes in speed and direction; (iii) external volume forces—typically gravitational or electrodynamic in origin. The subject matter of the present review is concerned with situations where inertial forces are small compared with viscous forces, at least in a

\* Present address: Department of Chemical Engineering, Carnegie Institute of Technology, Pittsburgh, Pennsylvania.



global sense. In short, we deal with low Reynolds number flows—more specifically with the hydrodynamic resistance of particles in the Stokes and Oseen regimes. The distinguishing feature of such flows is the linearity<sup>1</sup> or quasi-linearity of the underlying equations of motion. This is in marked contrast to laminar boundary layer flows, which lie at the opposite extreme of the Reynolds number spectrum.

In order to keep the size of the review within moderate bounds while, at the same time, furnishing sufficient detail to make this summary intelligible to the nonspecialist, we have—somewhat arbitrarily—eliminated a number of important topics which would ordinarily have found a place here. Active areas of contemporary research pertaining directly to Stokes and Oseen flows around particles that are *not* systematically discussed here include the following: two-dimensional flows; unsteady flows; deformable particles, including liquid drops; non-Newtonian flows; magnetohydrodynamic flows; compressible flows; numerical and variational mathematical methods in low Reynolds number flows; and heat and mass transfer from particles. Brief comments on some of these topics are, however, offered where pertinent to the main discussion. This partial listing furnishes some indication of the remarkable growth of the field during recent years. Readers interested in a broader and more systematic survey of the general area of low Reynolds number flows are directed to the following recent monographs and review articles: B4, F13, H9, H11, I1, L1, L4, L4a, L9, M8. The classical treatises of Oseen (O4), Villat (V4), and Lamb (L5), though somewhat dated, are still serviceable. Landau and Lifshitz's text (L6, Chapter II) provides a concise, but illuminating, summary from an elementary viewpoint.

The recent development of tensorial schemes for characterizing the intrinsic hydrodynamic resistance of particles of arbitrary shape, and the application of singular perturbation techniques to obtain asymptotic solutions of the Navier–Stokes equations at small Reynolds numbers constitute significant contributions to our understanding of “slow” viscous flow around bodies. It is with these topics that this review is primarily concerned. In presenting this material we have elected to use Gibbs' polyadics in preference to conventional tensor notation. For in our view, the former symbolism—dealing as it does with *direction* as a primitive concept—is more closely related to the physical world in which we live than is the latter notation.

<sup>1</sup> Not all such flows, however, are linear—as, for example, in the case of *non-Newtonian* creeping flows around spherical particles (B4a, B4b, C1, D3, F9, F10, G5, L8, L10, R1, S2, S10, T4, T7, W2, W3, W3a, W3b, W4, W5, W6, Z1). Similarly, owing to the unknown shape of the interface at the outset, free-boundary problems involving liquid droplets in nonuniform flows (Section II, C, 2, *b*) are intrinsically nonlinear despite the possible linearity of the equations of motion (and boundary conditions) inside and outside of the droplet.

Moreover, polyadic symbols, being free from extraneous indices which detract from the invariant significance of the *single* entities they represent, are more suggestive and possess greater aesthetic appeal than do their tensor counterparts. Our polyadic notation is essentially equivalent to that employed in Milne's book (M16). Other useful discussions of this notation will be found in References B6, D6, G3, M15.

## II. Stokes Flows

### A. INTRODUCTION

A nonspherical particle is generally anisotropic with respect to its hydrodynamic resistance; that is, its resistance depends upon its orientation relative to its direction of motion through the fluid. A complete investigation of particle resistance would therefore seem to require experimental data or theoretical analysis for each of the infinitely many relative orientations possible. It turns out, however, at least at small Reynolds numbers, that particle resistance has a tensorial character and, hence, that the resistance of a solid particle of any shape can be represented for all orientations by a few tensors. And the components of these tensors can be determined from either theoretical or experimental knowledge of the resistance of the particle for a *finite* number of relative orientations. The tensors themselves are intrinsic geometric properties of the particle alone, depending only on its size and shape. These observations and various generalizations thereof furnish most, but not all, of the subject matter of this section.

### B. EQUATIONS OF MOTION

The Navier-Stokes and continuity equations for an incompressible, nonpolar (D1, D2), Newtonian fluid are

$$\rho \left( \frac{\partial \mathbf{v}}{\partial t} + \mathbf{v} \cdot \nabla \mathbf{v} \right) = -\nabla p + \mu \nabla^2 \mathbf{v} \quad (1)$$

$$\nabla \cdot \mathbf{v} = 0 \quad (2)$$

where  $\rho$  and  $\mu$  are the fluid density and viscosity (both assumed constant),  $\mathbf{v}$  and  $p$  are the local fluid velocity and pressure, and  $t$  is the time. The stress dyadic for an incompressible Newtonian fluid is

$$\pi = -\mathbf{I}p + \mu[\nabla \mathbf{v} + (\nabla \mathbf{v})^\dagger] \quad (3)$$

In Eq. (1) it is assumed that the only external body forces acting on the fluid are either due to gravity or are otherwise derivable from a potential. As such, these forces have been absorbed into the pressure term.

Let  $a$ ,  $V$ , and  $\tau$  be, respectively, a representative particle length, speed, and time, and let  $R = aV\rho/\mu$  be the particle Reynolds number. By introducing the dimensionless variables

$$\begin{aligned}\underline{\mathbf{v}} &= \frac{\mathbf{v}}{V} & \underline{p} &= \frac{pa}{\mu V} & \underline{t} &= \frac{t}{\tau}, \\ \underline{\mathbf{r}} &= \frac{\mathbf{r}}{a} & \underline{\nabla} &= a\nabla\end{aligned}\tag{4}$$

where  $\mathbf{r}$  is the position vector, Eqs. (1) and (2) may be written in the dimensionless forms

$$R\left(\frac{a}{\tau V}\frac{\partial \underline{\mathbf{v}}}{\partial \underline{t}} + \underline{\mathbf{v}} \cdot \underline{\nabla} \underline{\mathbf{v}}\right) = -\underline{\nabla} \underline{p} + \underline{\nabla}^2 \underline{\mathbf{v}}\tag{5}$$

$$\underline{\nabla} \cdot \underline{\mathbf{v}} = 0\tag{6}$$

If the motion is steady when viewed from an inertial reference frame, the term  $\partial \mathbf{v}/\partial t$  vanishes identically. Providing that the remaining nondimensional terms remain finite as  $R \rightarrow 0$ , these then reduce to Stokes equations at sufficiently small Reynolds numbers. In dimensional form, Stokes equations are

$$\nabla^2 \mathbf{v} = \frac{1}{\mu} \nabla p\tag{7}$$

$$\nabla \cdot \mathbf{v} = 0\tag{8}$$

These also result even if the motion is unsteady, providing that  $a/\tau V$  and the other dimensionless terms remain finite in the limit  $R = 0$ .<sup>2</sup> Equations (7) and (8) are then referred to as the *quasi-static* or *quasi-steady* Stokes equations. In this case the time variable enters the equations of motion only in an implicit form. The precise relationship between the solutions of Eqs. (7) and (8) and the asymptotic solutions of the Navier-Stokes equations at small Reynolds numbers is discussed in Section III.

### C. SINGLE PARTICLES

#### 1. *Quiescent Fluids*

In this section we treat the steady and quasi-steady motions of rigid, three-dimensional particles in a fluid at rest at infinity on the basis of Stokes

<sup>2</sup> See, for example, the discussions (I2, K2) of unsteady low Reynolds number flows based on singular perturbation methods.

A general discussion of the circumstances in which it is permissible to adopt the quasi-static approximation is provided by Happel and Brenner (H9, pp. 52-55).

equations (B18, B19, B22). Since the fluid adheres to the surface of the solid particle the appropriate boundary conditions are

$$\mathbf{v} = \mathbf{U}_O + \boldsymbol{\omega} \times \mathbf{r}_O \quad \text{on the body } B \quad (9)$$

$$\mathbf{v} \rightarrow \mathbf{0} \quad \text{at infinity} \quad (10)$$

where  $O$  may be any point permanently affixed to the particle.  $\mathbf{U}_O$  is the instantaneous translational velocity of point  $O$  and  $\boldsymbol{\omega}$  is the instantaneous angular velocity of the particle. The instantaneous axis of rotation need *not* pass through  $O$ . The position vector  $\mathbf{r}_O$  is drawn from an origin at  $O$ .

Because of linearity, the translational and rotational motions may be separately treated. Thus, one may define a translational Stokes flow  $\mathbf{v}_O^{(t)}, p_O^{(t)}$  satisfying Eqs. (7) and (8) and the boundary conditions

$$\mathbf{v}_O^{(t)} = \mathbf{U}_O \quad \text{on } B \quad (11)$$

$$\mathbf{v}_O^{(t)} \rightarrow \mathbf{0} \quad \text{at infinity} \quad (12)$$

The subscript  $O$  indicates that the field depends on the choice of origin. Similarly, one may define a rotational Stokes field satisfying the boundary conditions

$$\mathbf{v}_O^{(r)} = \boldsymbol{\omega} \times \mathbf{r}_O \quad \text{on } B \quad (13)$$

$$\mathbf{v}_O^{(r)} \rightarrow \mathbf{0} \quad \text{at infinity} \quad (14)$$

The general field satisfying (9) and (10) is then

$$\mathbf{v} = \mathbf{v}_O^{(t)} + \mathbf{v}_O^{(r)} \quad (15)$$

$$p = p_O^{(t)} + p_O^{(r)} \quad (16)$$

Both the translational and rotational fields depend upon the viscosity of the fluid and the magnitude and orientation of the vectors  $\mathbf{U}_O$  and  $\boldsymbol{\omega}$  relative to axes fixed in the body. By virtue of linearity, however, it is possible to define dyadic "velocity" fields and vector "pressure" fields which are wholly independent of these parameters. Thus, one may define a translational

dyadic velocity field  $\overset{(t)}{\mathbf{V}}$  and its associated vector pressure field  $\overset{(t)}{\mathbf{P}}$  by the differential equations (B22)

$$\nabla^2 \overset{(t)}{\mathbf{V}} - \nabla \overset{(t)}{\mathbf{P}} = \mathbf{0} \quad (17)$$

$$\nabla \cdot \overset{(t)}{\mathbf{V}} = \mathbf{0} \quad (18)$$

and boundary conditions

$$\overset{(t)}{\mathbf{V}} = \mathbf{I} \quad \text{on } B \quad (19)$$

$$\overset{(t)}{\mathbf{V}} \rightarrow \mathbf{0} \quad \text{at infinity} \quad (20)$$

where  $\mathbf{I}$  is the dyadic idemfactor. The ordinary translational velocity and pressure fields are then expressible in terms of these higher-order fields via the relations

$$\overset{(t)}{\mathbf{v}}_O = \overset{(t)}{\mathbf{V}} \cdot \overset{(t)}{\mathbf{U}}_O \quad (21)$$

$$p_O = \mu \overset{(t)}{\mathbf{P}} \cdot \overset{(t)}{\mathbf{U}}_O \quad (22)$$

for all values of  $\mu$ ,  $\overset{(t)}{\mathbf{U}}_O$ , and all choices of origin  $O$ . The fields  $\overset{(t)}{\mathbf{V}}$  and  $\overset{(t)}{\mathbf{P}}$  are themselves independent of these parameters. By means of Eqs. (21) and (22),  $\overset{(t)}{\mathbf{V}}$  and  $\overset{(t)}{\mathbf{P}}$  may be determined from knowledge of  $\overset{(t)}{\mathbf{v}}_O$  and  $p_O$  for any three noncoplanar values of  $\overset{(t)}{\mathbf{U}}_O$ . Alternatively, they can be obtained directly by solving the dyadic equations of motion, (17) to (20).

A similar analysis applies to the rotational motion. In particular (B22)

$$\overset{(r)}{\mathbf{v}}_O = \overset{(r)}{\mathbf{V}}_O \cdot \boldsymbol{\omega} \quad (23)$$

$$p_O = \mu \overset{(r)}{\mathbf{P}}_O \cdot \boldsymbol{\omega} \quad (24)$$

where the rotational dyadic velocity field  $\overset{(r)}{\mathbf{V}}_O$  and vector pressure field  $\overset{(r)}{\mathbf{P}}_O$  are the solutions of the equations

$$\nabla^2 \overset{(r)}{\mathbf{V}}_O - \nabla \overset{(r)}{\mathbf{P}}_O = \mathbf{0} \quad (25)$$

$$\nabla \cdot \overset{(r)}{\mathbf{V}}_O = \mathbf{0} \quad (26)$$

$$\overset{(r)}{\mathbf{V}}_O = \boldsymbol{\varepsilon} \cdot \mathbf{r}_O \quad \text{on } B \quad (27)$$

$$\overset{(r)}{\mathbf{V}}_O \rightarrow \mathbf{0} \quad \text{at infinity} \quad (28)$$

in which  $\mathbf{\varepsilon}$  is the unit isotropic triadic.<sup>3</sup> These polyadic fields, though independent of  $\mu$  and  $\omega$ , do depend upon the location of  $O$ , as required by the right-hand member of Eq. (27).

As examples of these intrinsic translational and rotational velocity fields we note that one can express Stokes' original solution for a translating sphere of radius  $a$  (L5, p. 597) in the form

$$\mathbf{V}^{(t)} = \frac{3}{4} \frac{a}{r} \left( \mathbf{I} + \frac{\mathbf{r}\mathbf{r}}{r^2} \right) + \frac{1}{4} \left( \frac{a}{r} \right)^3 \left( \mathbf{I} - 3 \frac{\mathbf{r}\mathbf{r}}{r^2} \right) \quad (29)$$

$$\mathbf{P}^{(t)} = \frac{3a}{2} \frac{\mathbf{r}}{r^3} \quad (30)$$

Similarly, if  $O$  is chosen at the sphere center, the solution for a rotating sphere (L5, p. 588) may be written as

$$\mathbf{V}_O^{(r)} = (a/r)^3 \mathbf{\varepsilon} \cdot \mathbf{r} \quad (31)$$

$$\mathbf{P}_O^{(r)} = \mathbf{0} \quad (32)$$

where  $\mathbf{r}$  is measured from  $O$ .

Equation (3) for the stress dyadic, applied to the translational motion, gives

$$\pi_O^{(t)} = -\mathbf{I} p_O + \mu \left[ \nabla \mathbf{V}_O^{(t)} + \left( \nabla \mathbf{V}_O^{(t)} \right)^\dagger \right] \quad (33)$$

<sup>3</sup> In terms of any right-handed triad of mutually perpendicular unit vectors ( $\mathbf{i}_1, \mathbf{i}_2, \mathbf{i}_3$ ) the unit isotropic triadic may be written as (M16)

$$\mathbf{\varepsilon} = \mathbf{i}_j \mathbf{i}_k \mathbf{i}_l \varepsilon_{jkl} \quad (\text{summation convention})$$

where  $\varepsilon_{jkl}$  is the permutation symbol

$$\varepsilon_{jkl} = \begin{cases} 0, & \text{if any two of } j, k, l \text{ are the same;} \\ 1, & \text{if } jkl, \text{ in that order, is an even permutation of } 1, 2, 3; \\ -1, & \text{if } jkl, \text{ in that order, is an odd permutation of } 1, 2, 3 \end{cases}$$

Thus

$$\mathbf{\varepsilon} = \mathbf{i}_1 \mathbf{i}_2 \mathbf{i}_3 - \mathbf{i}_1 \mathbf{i}_3 \mathbf{i}_2 + \mathbf{i}_2 \mathbf{i}_3 \mathbf{i}_1 - \mathbf{i}_2 \mathbf{i}_1 \mathbf{i}_3 + \mathbf{i}_3 \mathbf{i}_1 \mathbf{i}_2 - \mathbf{i}_3 \mathbf{i}_2 \mathbf{i}_1$$

This invariant can be shown to be equivalent to

$$\mathbf{\varepsilon} = -\mathbf{I} \times \mathbf{I}$$

It thus follows from Eqs. (21) and (22) that there exists an intrinsic translational triadic "stress" field<sup>4</sup>

$$\overset{(t)}{\Pi} = -\overset{(t)}{\mathbf{I}}\overset{(t)}{\mathbf{P}} + \overset{(t)}{\mathbf{V}}\overset{(t)}{\mathbf{V}} + \overset{(t)}{\mathbf{V}}\overset{(t)}{\mathbf{V}}^\dagger \quad (34)$$

which is independent of the choice of  $\mu$ ,  $\mathbf{U}_O$ , and  $O$ , such that

$$\pi_O = \mu \overset{(t)}{\Pi} \cdot \mathbf{U}_O \quad (35)$$

Analogously, for the rotational motion one has

$$\overset{(r)}{\pi}_O = \mu \overset{(r)}{\Pi}_O \cdot \boldsymbol{\omega} \quad (36)$$

where

$$\overset{(r)}{\Pi}_O = -\overset{(r)}{\mathbf{I}}\overset{(r)}{\mathbf{P}}_O + \overset{(r)}{\mathbf{V}}\overset{(r)}{\mathbf{V}}_O + \overset{(r)}{\mathbf{V}}\overset{(r)}{\mathbf{V}}_O^\dagger \quad (37)$$

These intrinsic stress fields play fundamental roles in the theory of the hydrodynamic resistance of particles in the Stokes regime.

The hydrodynamic force  $\mathbf{F}$  and torque about  $O$ ,  $\mathbf{T}_O$ , exerted by the fluid on the particle (exclusive of buoyant forces and torques) are linear vector functions of the velocity and spin of the particle. In particular (B22)

$$\mathbf{F} = -\mu \left( \overset{(t)}{\mathbf{K}} \cdot \mathbf{U}_O + \overset{(c)}{\mathbf{K}}_O^\dagger \cdot \boldsymbol{\omega} \right) \quad (38)$$

$$\mathbf{T}_O = -\mu \left( \overset{(c)}{\mathbf{K}}_O \cdot \mathbf{U}_O + \overset{(r)}{\mathbf{K}}_O \cdot \boldsymbol{\omega} \right) \quad (39)$$

where  $\overset{(t)}{\mathbf{K}}$  is the translation dyadic and  $\overset{(c)}{\mathbf{K}}_O$  and  $\overset{(r)}{\mathbf{K}}_O$  are, respectively, the coupling and rotation dyadics at  $O$ . These intrinsic hydrodynamic resistance coefficients are constant relative to axes fixed in the particle. They depend only upon the external geometric configuration of the particle wetted by the fluid; that is, on its size and shape. The two "direct" dyadics are related to the intrinsic stress fields via the expressions (B22)

$$\overset{(t)}{\mathbf{K}} = -\int_B d\mathbf{S} \cdot \overset{(t)}{\Pi} \quad (40)$$

$$\overset{(r)}{\mathbf{K}}_O = -\int_B \mathbf{r}_O \times \left( d\mathbf{S} \cdot \overset{(r)}{\Pi}_O \right) \quad (41)$$

<sup>4</sup> With regard to transposes of polyads and polyadics, we adopt the convention that the transposition operator ( $\dagger$ ) has the following properties:

$$(\cdots \mathbf{abcd})^\dagger = \cdots \mathbf{abdc}$$

and

$$\dagger(\mathbf{abcd} \cdots) = \mathbf{bacd} \cdots$$

where  $\mathbf{a}$ ,  $\mathbf{b}$ ,  $\mathbf{c}$ ,  $\mathbf{d}$ ,  $\dots$ , are any vectors. The former represents a *post*transposition, while the latter represents a *pre*transposition. For dyads and dyadics these operations are equivalent.

The "indirect," cross-term may be computed from either of the following formulas:

$$\mathbf{K}_O^{(c)} = - \int_B \mathbf{r}_O \times (d\mathbf{S} \cdot \mathbf{\Pi}^{(t)}) \quad (42a)$$

or

$$\mathbf{K}_O^{(c)} = - \int_B d\mathbf{S} \cdot \mathbf{\Pi}_O^{(r)\dagger} \quad (42b)$$

the result being the same in either case. Here,  $d\mathbf{S}$  is a directed element of surface area pointing into the fluid. Integration is over the wetted surface  $B$  of the body.

The dimensions of the translation, coupling, and rotation dyadics are, respectively,  $L$ ,  $L^2$ , and  $L^3$  ( $L$  = length). Thus, if  $a$  be some characteristic length of the body, one may write Eqs. (38) and (39) in the forms

$$\begin{aligned} \mathbf{F} &= -\mu \left( a \mathbf{K}^{(t)} \cdot \mathbf{U}_O + a^2 \mathbf{K}_O^{(c)\dagger} \cdot \boldsymbol{\omega} \right) \\ \mathbf{T}_O &= -\mu \left( a^2 \mathbf{K}_O^{(c)} \cdot \mathbf{U}_O + a^3 \mathbf{K}_O^{(r)} \cdot \boldsymbol{\omega} \right) \end{aligned}$$

The dimensionless  $\mathbf{K}$  dyadics are *intensive* properties of the body. They might aptly be called *specific* resistance dyadics, for they are independent of the *size* of the body—depending only upon its *shape*.

The direct dyadics are symmetric,

$$\mathbf{K}^{(t)} = \mathbf{K}^{(t)\dagger} \quad (43a)$$

$$\mathbf{K}_O^{(r)} = \mathbf{K}_O^{(r)\dagger} \quad (43b)$$

the latter relation holding at all origins  $O$ . Proof of these symmetry relations is based upon a *macroscopic* reciprocity theorem (B18, B22). This macroscopic proof is in marked contrast to the usual *microscopic* proof of the symmetry of the various transport coefficients via Onsager's reciprocal relations (cf. D4a). The symmetry of these coefficients indicates that no dissipationless (gyrostatic) forces or torques act on the particle (B22). In consequence of the nonnegative nature of the time rate of mechanical energy dissipation, these dyadics are necessarily positive-definite forms. The three eigenvalues of  $\mathbf{K}$ , say  $K_j$  ( $j = 1, 2, 3$ ), corresponding to the three real roots of the cubic equation

$$\det \|\mathbf{K} - \mathbf{IK}\| = 0$$

are thus essentially positive for each of the direct dyadics. Furthermore, in consequence of the symmetry properties noted in Eq. (43), the normalized eigenvectors,  $\mathbf{e}_j$  ( $j = 1, 2, 3$ ), of  $\mathbf{K}$ , corresponding to the nontrivial solutions of the vector equation

$$\mathbf{K} \cdot \mathbf{e} = K \mathbf{e}$$



are thus mutually perpendicular. The direct dyadics may therefore be written in the canonical forms

$$\mathbf{K} = \mathbf{e}_1 \mathbf{e}_1 K_1 + \mathbf{e}_2 \mathbf{e}_2 K_2 + \mathbf{e}_3 \mathbf{e}_3 K_3 \quad (44)$$

and

$$\mathbf{K}_O = \mathbf{e}_1^{(r)}(O) \mathbf{e}_1^{(r)}(O) K_1^{(r)}(O) + \mathbf{e}_2^{(r)}(O) \mathbf{e}_2^{(r)}(O) K_2^{(r)}(O) + \mathbf{e}_3^{(r)}(O) \mathbf{e}_3^{(r)}(O) K_3^{(r)}(O) \quad (45)$$

where  $|\mathbf{e}_j| = 1$ ,  $\mathbf{e}_j \cdot \mathbf{e}_k = \delta_{jk}$ , and  $K_j > 0$ , in which  $\delta_{jk}$  is the Kronecker delta. The two triads of orthonormal vectors lie parallel to the principal axes of translation and to the principal axes of rotation at  $O$ , respectively.

Equations (38)–(39) are surprising in two respects. First, they show that the translational and rotational motions of a particle are generally coupled, in the sense that a rotary motion may give rise to a force, while a translatory motion may give rise to a torque. Second, what is equally surprising is the fact that the *same* coupling coefficient appears in both expressions. That this should be the case is by no means obvious; rather, demonstration of this fact requires use of the same macroscopic reciprocity principle (B18, B22) employed in the proof of Eqs. (43a, b). The identity of the cross coefficients in Eqs. (38)–(39), in conjunction with the symmetry relations (43), leads one to regard the former equations as Onsager relations. We emphasize, however, that this conclusion does not require the invocation of Onsager's reciprocity relations, but follows directly from conventional mechanical principles.

The fundamental resistance equations, (38) and (39), may be written as a single matrix equation (B22). Let  $\mathbf{i}_1, \mathbf{i}_2, \mathbf{i}_3$  be any triad of mutually perpendicular unit vectors, and consider the column matrices

$$\|\mathbf{F}\| = \begin{Bmatrix} F_1 \\ F_2 \\ F_3 \end{Bmatrix}, \quad \|\mathbf{U}_O\| = \begin{Bmatrix} U_1(O) \\ U_2(O) \\ U_3(O) \end{Bmatrix}, \text{ etc.}$$

and the  $3 \times 3$  square matrices

$$\|\mathbf{K}_O\| = \begin{Bmatrix} K_{11}^{(r)}(O) & K_{12}^{(r)}(O) & K_{13}^{(r)}(O) \\ K_{21}^{(r)}(O) & K_{22}^{(r)}(O) & K_{23}^{(r)}(O) \\ K_{31}^{(r)}(O) & K_{32}^{(r)}(O) & K_{33}^{(r)}(O) \end{Bmatrix}, \text{ etc.}$$

Further, define the  $6 \times 1$  partitioned *wrench* matrix

$$\|\mathcal{F}_O\| = \begin{Bmatrix} \|\mathbf{F}\| \\ \|\mathbf{T}_O\| \end{Bmatrix} \quad (46)$$

the  $6 \times 1$  partitioned *screw-velocity* matrix

$$\|\mathcal{U}_O\| = \left\| \begin{array}{c} \|\mathbf{U}_O\| \\ \|\boldsymbol{\omega}\| \end{array} \right\| \quad (47)$$

and the  $6 \times 6$  partitioned *resistance* matrix

$$\|\mathcal{K}_O\| = \left\| \begin{array}{cc} \left\| \begin{array}{c} {}^{(t)}\mathbf{K} \\ {}^{(c)}\mathbf{K}_O \end{array} \right\| & \left\| \begin{array}{c} {}^{(c)}\mathbf{K}_O \\ {}^{(r)}\mathbf{K}_O \end{array} \right\|^\dagger \\ \left\| \begin{array}{c} {}^{(c)}\mathbf{K}_O \\ {}^{(r)}\mathbf{K}_O \end{array} \right\| & \left\| \begin{array}{c} {}^{(r)}\mathbf{K}_O \\ {}^{(c)}\mathbf{K}_O \end{array} \right\| \end{array} \right\| \quad (48)$$

In terms of these we find

$$\|\mathcal{F}_O\| = -\mu \|\mathcal{K}_O\| \|\mathcal{U}_O\| \quad (49)$$

In a Stokes flow occurring within a fluid at rest at infinity, the rate of mechanical energy dissipation is equal to the rate at which the stresses acting over the particle surface are doing work; namely,  $-\|\mathcal{U}_O\|^\dagger \|\mathcal{F}_O\|$ . The dissipation rate in the entire fluid is thus  $\mu \|\mathcal{U}_O\|^\dagger \|\mathcal{K}_O\| \|\mathcal{U}_O\|$ . As the dissipation rate is essentially positive, and since the velocity  $\|\mathcal{U}_O\|$  is arbitrary, this requires that the resistance matrix be positive-definite. Furthermore, in view of the symmetry of the translation and rotation submatrices, the resistance matrix is itself symmetric. According to a theorem of Frobenius (cf. M18) a symmetric (hermitian) matrix is positive-definite if and only if all the determinants of its principal minors are positive. This theorem ultimately gives rise to  $2^6 - 1$  inequalities involving the scalar elements of the resistance matrix, though not all such inequalities are independent. The most important of these are (for  $j \neq k$ ),

$$\begin{aligned} {}^{(t)}K_{jj} > 0, \quad {}^{(t)}K_{jj} {}^{(t)}K_{kk} &> \left({}^{(t)}K_{jk}\right)^2, \quad \det \left\| \begin{array}{c} {}^{(t)}\mathbf{K} \end{array} \right\| > 0, \\ {}^{(r)}K_{jj}(O) > 0, \quad {}^{(r)}K_{jj}(O) {}^{(r)}K_{kk}(O) &> \left({}^{(r)}K_{jk}(O)\right)^2, \quad \det \left\| \begin{array}{c} {}^{(r)}\mathbf{K}_O \end{array} \right\| > 0, \\ {}^{(t)}K_{jj} {}^{(r)}K_{kk}(O) &> \left({}^{(c)}K_{kj}(O)\right)^2, \quad \det \|\mathcal{K}_O\| > 0 \end{aligned} \quad (50)$$

(no summation on the indices).

All the preceding equations are valid for any choice of origin. If the coupling and rotation dyadics are known at any point  $O$  they may be computed at any other point  $P$  by means of the *origin displacement theorems* (B22)

$${}^{(c)}\mathbf{K}_P = {}^{(c)}\mathbf{K}_O - \mathbf{r}_{OP} \times {}^{(t)}\mathbf{K} \quad (51)$$

and

$${}^{(r)}\mathbf{K}_P = {}^{(r)}\mathbf{K}_O - \mathbf{r}_{OP} \times {}^{(t)}\mathbf{K} \times \mathbf{r}_{OP} + {}^{(c)}\mathbf{K}_O \times \mathbf{r}_{OP} - \mathbf{r}_{OP} \times {}^{(c)}\mathbf{K}_O^\dagger \quad (52)$$

where  $\mathbf{r}_{OP}$  is the vector drawn from  $O$  to  $P$ . The translation dyadic is independent of the choice of origin. These formulas derive from the fact that the hydrodynamic force on the particle must be independent of the choice of origin, whereas the torque will vary with choice of origin according to the relation  $\mathbf{T}_P = \mathbf{T}_O - \mathbf{r}_{OP} \times \mathbf{F}$ —the translational velocities at the two points being connected by the expression  $\mathbf{U}_P = \mathbf{U}_O + \boldsymbol{\omega} \times \mathbf{r}_{OP}$ .

For centrally symmetric bodies such as spheres, ellipsoids, and the like, it is intuitively obvious that the rotation and coupling dyadics will adopt their simplest and most symmetrical forms when expressed in terms of an origin at the center of symmetry. It is natural, therefore, to inquire as to the existence of a corresponding point for a body of arbitrary shape. Such an inquiry, based on Eqs. (51) and (52), discloses the fact (B22) that every body possesses a unique point, termed its *center of reaction* ( $R$ ), at which the coupling dyadic is symmetric, i.e.,

$$\overset{(c)}{\mathbf{K}}_R = \overset{(c)}{\mathbf{K}}_R^\dagger \quad (53)$$

It is at this point that the dyadics assume their most physically significant forms. In general, this point does not coincide with the centroid of the body, though it does for centrally symmetric bodies. If the coupling dyadic is known at any point  $O$  the location of the center of reaction can be determined from the expression<sup>5</sup>

$$\mathbf{r}_{OR} = \left[ \left( \overset{(t)}{\mathbf{I}} : \overset{(t)}{\mathbf{K}} \right) \overset{(t)}{\mathbf{I}} - \overset{(t)}{\mathbf{K}} \right]^{-1} \cdot \boldsymbol{\varepsilon} : \overset{(c)}{\mathbf{K}}_O \quad (54)$$

The symmetric dyadic  $\overset{(c)}{\mathbf{K}}_R$  is identically zero for a large class of symmetrical particles, including spheres and ellipsoids. For such bodies Eqs. (38) and (39) adopt the simple forms

$$\mathbf{F} = -\mu \overset{(t)}{\mathbf{K}} \cdot \mathbf{U}_R \quad (55a)$$

$$\mathbf{T}_R = -\mu \overset{(r)}{\mathbf{K}}_R \cdot \boldsymbol{\omega} \quad (55b)$$

so that the translational and rotational motions become uncoupled. A non-zero value of  $\overset{(c)}{\mathbf{K}}_R$  is therefore associated with propeller-like properties of the

<sup>5</sup> The superscript  $-1$  denotes an inverse dyadic. With regard to multiple operations such as the indicated double-dot multiplications, we employ the "nesting convention" of Chapman and Cowling (C6). It is only in this one respect that we depart from the original convention of Gibbs (G3). According to the nesting convention the ordering of the operations is as follows: operations are performed from bottom to top; pairings of vectors are from the inside out; arrangement of products is from left to right. For example,

$$abc \overset{\times}{\times} defg = (c \times d)(b \times e)(a \cdot f) \mathbf{g} (= \text{a triad})$$

where  $\mathbf{a}$ ,  $\mathbf{b}$ , ...,  $\mathbf{g}$  are any vectors.

body; that is, in the absence of external torques about  $R$ , a translational motion of the body generally causes the particle to spin—while, in the absence of external forces, a rotational motion of the particle generally causes it to translate. One should bear in mind that the source of such propeller-like behavior is not to be found in the inertia of the fluid, which ordinarily accounts for such action at large Reynolds numbers. Rather, the effect derives exclusively from the viscous stresses. It is important to note that only at the center of reaction does a nonzero value of the coupling dyadic imply propeller-like properties: for, in accordance with Eq. (51), even a sphere will give rise to a nonzero value of the coupling dyadic at any point other than its centroid. This merely reflects the fact that a sphere rotating about a noncentral axis will experience a net hydrodynamic force, while a translating sphere will experience a hydrodynamic torque about any point other than its geometric center (B18).

Two mirror-image (*enantiomorphic*) forms necessarily possess identical  $\overset{(t)}{\mathbf{K}}$  and  $\overset{(r)}{\mathbf{K}}_R$  values, and differ only in the algebraic sign of  $\overset{(c)}{\mathbf{K}}_R$ .

The values of the various resistance dyadics for a spherical particle of radius  $a$  are

$$\overset{(t)}{\mathbf{K}} = \mathbf{I}6\pi a, \quad \overset{(r)}{\mathbf{K}}_R = \mathbf{I}8\pi a^3, \quad \overset{(c)}{\mathbf{K}}_R = \mathbf{0} \quad (56)$$

$R$  coincides with the sphere center. These dyadics are isotropic, as clearly they must be.

For the ellipsoidal particle

$$\frac{x_1^2}{a_1^2} + \frac{x_2^2}{a_2^2} + \frac{x_3^2}{a_3^2} = 1 \quad (57)$$

the three dyadics are (B23)

$$\overset{(t)}{\mathbf{K}} = 16\pi \left( \mathbf{e}_1 \mathbf{e}_1 \frac{1}{\chi + a_1^2 \alpha_1} + \mathbf{e}_2 \mathbf{e}_2 \frac{1}{\chi + a_2^2 \alpha_2} + \mathbf{e}_3 \mathbf{e}_3 \frac{1}{\chi + a_3^2 \alpha_3} \right) \quad (58)$$

$$\overset{(r)}{\mathbf{K}}_R = \frac{16\pi}{3} \left( \mathbf{e}_1 \mathbf{e}_1 \frac{a_2^2 + a_3^2}{a_2^2 \alpha_2 + a_3^2 \alpha_3} + \mathbf{e}_2 \mathbf{e}_2 \frac{a_3^2 + a_1^2}{a_3^2 \alpha_3 + a_1^2 \alpha_1} + \mathbf{e}_3 \mathbf{e}_3 \frac{a_1^2 + a_2^2}{a_1^2 \alpha_1 + a_2^2 \alpha_2} \right) \quad (59)$$

$$\overset{(c)}{\mathbf{K}}_R = \mathbf{0} \quad (60)$$

where  $R$  lies at the center of the ellipsoid and  $\mathbf{e}_j$  is a unit vector parallel to  $Rx_j$ . In these expressions

$$\alpha_j = \int_0^\infty \frac{d\lambda}{(a_j^2 + \lambda) \Delta(\lambda)} \quad (j = 1, 2, 3) \quad (61)$$

$$\chi = \int_0^\infty \frac{d\lambda}{\Delta(\lambda)} \quad (62)$$

where

$$\Delta(\lambda) = [(a_1^2 + \lambda)(a_2^2 + \lambda)(a_3^2 + \lambda)]^{1/2} \quad (63)$$

For the slightly deformed sphere (A2, B21)

$$r = a \left[ 1 + \varepsilon \sum_{k=0}^{\infty} f_k(\theta, \phi) \right] \quad (64)$$

the three resistance dyadics are (B21)

$$\stackrel{(i)}{\mathbf{K}} = 6\pi a [\mathbf{I} + \varepsilon \{ \mathbf{I}f_0 - \frac{1}{10} \nabla \nabla (r^2 f_2) \} + O(\varepsilon^2)] \quad (65)$$

$$\stackrel{(r)}{\mathbf{K}}_R = 8\pi a^3 [\mathbf{I} + 3\varepsilon \{ \mathbf{I}f_0 - \frac{1}{10} \nabla \nabla (r^2 f_2) \} + O(\varepsilon^2)] \quad (66)$$

$$\stackrel{(c)}{\mathbf{K}}_R = o(\varepsilon) \quad (67)$$

where  $\varepsilon$  is a small disposable constant;  $(r, \theta, \phi)$  are spherical coordinates having their origin either at the center  $O$  of the undeformed sphere or at the center of reaction of the deformed sphere;  $f_k(\theta, \phi)$  is a surface spherical harmonic of degree  $k$ . The position of  $R$  relative to  $O$  is

$$\mathbf{r}_{OR} = \varepsilon a \nabla (r f_1) + O(\varepsilon^2) \quad (68)$$

To the first order in  $\varepsilon$  the center of reaction coincides with the centroid of the deformed sphere.

As an example of the application of these relations, consider the slightly deformed sphere obtained by setting

$$a_1 = a(1 + \varepsilon_1), \quad a_2 = a(1 + \varepsilon_2), \quad a_3 = a(1 + \varepsilon_3)$$

in Eq. (57), it being assumed that  $|\varepsilon_1|, |\varepsilon_2|, |\varepsilon_3| \ll 1$ . Upon putting  $x_1 = r \cos \theta$ ,  $x_2 = r \sin \theta \cos \phi$ , and  $x_3 = r \sin \theta \sin \phi$ , and defining  $\delta = \frac{1}{3}(\varepsilon_1 + \varepsilon_2 + \varepsilon_3)$ , the equation of the ellipsoid (57) in polar form is found to be

$$r = a[1 + \varepsilon(f_0 + f_2)] + O(\varepsilon^2)$$

in which  $\varepsilon f_0 = \delta P_0(\cos \theta) = \delta$  and

$$\varepsilon f_2 = (\varepsilon_1 - \delta)P_2(\cos \theta) + \frac{1}{6}(\varepsilon_2 - \varepsilon_3)P_2^2(\cos \theta) \cos 2\phi$$

The quantities  $P_n$  and  $P_n^m$  are, respectively, Legendre and associated Legendre functions. It follows that

$$\varepsilon r^2 f_2 = (\varepsilon_1 - \delta)x_1^2 + (\varepsilon_2 - \delta)x_2^2 + (\varepsilon_3 - \delta)x_3^2$$

From Eqs. (65) and (66) the translation and rotation dyadics are found to be

$$\stackrel{(i)}{\mathbf{K}} = 6\pi a [\mathbf{I}(1 + \frac{6}{5}\delta) - \frac{1}{5}(\mathbf{e}_1 \mathbf{e}_1 \varepsilon_1 + \mathbf{e}_2 \mathbf{e}_2 \varepsilon_2 + \mathbf{e}_3 \mathbf{e}_3 \varepsilon_3)] + O(\varepsilon^2)$$

and

$$\mathbf{K}_R^{(r)} = 8\pi a^3 \left[ \mathbf{I} \left( 1 + \frac{18}{5} \delta \right) - \frac{3}{5} (\mathbf{e}_1 \mathbf{e}_1 \varepsilon_1 + \mathbf{e}_2 \mathbf{e}_2 \varepsilon_2 + \mathbf{e}_3 \mathbf{e}_3 \varepsilon_3) \right] + O(\varepsilon^2)$$

The value  $\delta = 0$  corresponds to the case where the volume of the ellipsoid is the same as that of a sphere of radius  $a$ , correctly to terms of  $O(\varepsilon)$ . These results may be confirmed by direct expansion of Eqs. (58) and (59) for small departures from the spherical shape.

From an operational point of view, equations of the form (65) and (66) are not entirely satisfactory, for they are not written in a truly *invariant* form. Given an irregular particle, where is the "axis"  $|\cos \theta| = 1$ , and how is the radius  $a$  of the "undeformed sphere" to be defined? The difficulty stems, of course, from the description of the surface of the particle in terms of the surface spherical harmonic expansion (64). From an operational viewpoint it is more consistent with the nature of the requisite physical measurements to express the size and shape of the body in terms of an expansion involving its volumetric moments. The  $k$ th such moment is

$$\int_V \overbrace{\mathbf{r} \mathbf{r} \cdots \mathbf{r} \mathbf{r}}^{k \text{ times}} dV$$

where  $\mathbf{r}$  is measured from the centroid. Even more simply, one may resort to an expansion in terms of surface moments, the  $k$ th moment being

$$\int_S \overbrace{\mathbf{r} \mathbf{r} \cdots \mathbf{r} \mathbf{r}}^{k \text{ times}} \cdot d\mathbf{S}$$

In such terms, Eqs. (65) and (66) adopt the invariant forms (B21)

$$\mathbf{K}^{(r)} = 6\pi \left( \frac{V}{3S} \right) \left[ \mathbf{I} + \left\{ \frac{1}{10} \mathbf{I} - \frac{1}{8\pi} \left( \frac{3S}{V} \right)^5 \int_S d\mathbf{S} \cdot \mathbf{r} \mathbf{r} \mathbf{r} \right\} + O(\varepsilon^2) \right] \quad (69)$$

and

$$\mathbf{K}_R^{(r)} = 8\pi \left( \frac{V}{3S} \right)^3 \left[ \mathbf{I} + 3 \left\{ \frac{1}{10} \mathbf{I} - \frac{1}{8\pi} \left( \frac{3S}{V} \right)^5 \int_S d\mathbf{S} \cdot \mathbf{r} \mathbf{r} \mathbf{r} \right\} + O(\varepsilon^2) \right] \quad (70)$$

where  $V$  and  $S$  are, respectively, the volume of space occupied by the particle and its wetted surface area.

There are no other simple particle shapes for which the three resistance dyadics are wholly known, though some artificial bodies have been devised (B18, B22) to demonstrate that: (i) the center of reaction is not generally the same as the centroid; and (ii) bodies exist for which  $\mathbf{K}_R^{(c)} \neq 0$ .

Complete characterization of the hydrodynamic resistance of a solid particle in quasi-steady Stokes motion generally requires knowledge of 21

independent scalar resistance coefficients—six for the translation dyadic, six for the rotation dyadic, and nine for the coupling dyadic.<sup>6</sup> The number of such nonzero coefficients is reduced by virtue of any geometric symmetry that the particle may possess. Such a priori knowledge is useful in designing laboratory experiments to measure these phenomenological coefficients when they cannot be computed theoretically. The geometric symmetry investigation outlined by Brenner (B22) depends upon the fact that the direct resistance dyadics, regarded as tensors, transform under rotation and reflection as true (polar) second-rank tensors, whereas the coupling dyadic transforms as a second-rank pseudotensor<sup>7</sup> (axial tensor). In the following paragraphs some of the more significant results of the symmetry analysis are summarized.

If a body possesses three mutually perpendicular planes of reflection symmetry, its center of reaction lies at the point of intersection of these planes. The coupling dyadic is zero at this point, whereas the translation dyadic and rotation dyadic at  $R$  adopt the forms shown in Eqs. (44) and (45), in which the principal axes of translation and rotation (at  $R$ ) coincide and lie normal to the three symmetry planes. An ellipsoid is an example of such a body [see Eqs. (58)–(60)].

If the shape of the particle is similarly related to each of the three mutually perpendicular planes, the resistance dyadics adopt the isotropic forms

$$\stackrel{(t)}{\mathbf{K}} = \mathbf{I}K_t \quad (71a)$$

$$\stackrel{(r)}{\mathbf{K}}_R = \mathbf{I}K_r \quad (71b)$$

$$\stackrel{(c)}{\mathbf{K}}_R = \mathbf{0} \quad (71c)$$

Such bodies are said to be *spherically isotropic*. Examples are spheres and the five regular polyhedrons—the tetrahedron, hexahedron (cube), octahedron,

<sup>6</sup> Only six coefficients are required to characterize the coupling dyadic at the center of reaction. But then an additional three scalars are required to specify the location of this point, so that the total number of independent scalars required for a complete characterization is still nine. Similarly, three scalars suffice for the translation dyadic if we refer them to the principal axes of translation [see Eq. (44)], but then three additional scalars (e.g., an appropriate set of Eulerian angles) are required to specify the orientations of these axes. So it comes down to the same thing—namely, that six scalars are required. The same is true of the rotation dyadic at any point, and of the coupling dyadic at the center of reaction.

<sup>7</sup> The components of a Cartesian pseudotensor satisfy the same transformation law as do those of a true Cartesian tensor of the same rank, except when the transformation alters the right- or left-handedness of the axes (an “improper” rotation), as for the case of reflection in a plane (*inversion*). In this case the two transformation laws differ by an algebraic sign.

dodecahedron, and icosahedron. It is remarkable that the latter have the same character as the sphere.

If the particle is a solid of revolution its center of reaction lies along the axis (say the  $Rx_1$  axis). At this point the coupling dyadic vanishes, while both the translation and rotation dyadics at any point along the axis each adopt the general form

$$\mathbf{K} = \mathbf{I}K_{\parallel} + (\mathbf{I} - \mathbf{e}_1\mathbf{e}_1)K_{\perp} \quad (72)$$

where  $\mathbf{e}_1$  is a unit vector along the symmetry axis, in either direction. The position of the center of reaction along the axis cannot be determined by inspection unless the body possesses fore-aft symmetry, i.e., a plane of reflection symmetry normal to the axis of revolution.

A particle possesses an axis of helicoidal symmetry if it is identical to itself when turned about that axis through the same angle  $\nu$  in *either* direction (excluding the values  $\nu = 0, \pi/2, \pi$ ). In such a case the center of reaction lies along this axis (say, the  $Rx_1$  axis), while the translation, rotation, and coupling dyadics at  $R$  each have the form indicated in Eq. (72).

If a body possesses two distinct axes of helicoidal symmetry they must intersect. The point of intersection is then the center of reaction of the body. The three resistance dyadics are then isotropic at  $R$ :

$$\stackrel{(t)}{\mathbf{K}} = \mathbf{I}K_t \quad (73a)$$

$$\stackrel{(r)}{\mathbf{K}}_R = \mathbf{I}K_r \quad (73b)$$

$$\stackrel{(c)}{\mathbf{K}}_R = \mathbf{I}K_c \quad (73c)$$

Such bodies are termed *helicoidally isotropic*. Their resistance is characterized by the two scalars  $K_t$ ,  $K_r$ , and the pseudoscalar<sup>8</sup>  $K_c$ . Examples of isotropic helicoids are described by Brenner (B22). Spherical isotropy is clearly a special case of this more general type. On account of the inequalities set forth in Eq. (50), the various scalars satisfy the relations

$$K_t > 0 \quad (74a)$$

$$K_r > 0 \quad (74b)$$

$$K_t K_r > K_c^2 \quad (74c)$$

$K_c$  is negative for "right-handed" (*dextral*) bodies. Conversely, it is positive

<sup>8</sup> A pseudoscalar is a pseudotensor of rank zero. This entity changes sign on reflection of the coordinates in a plane.



for "left-handed" (*sinistral*) bodies.<sup>9</sup> Enantiomorphic isotropic helicoids possess the same  $K_t$  and  $K_r$  values, differing only in the algebraic sign of  $K_c$ . The existence of such sense-dependent isotropic bodies is remarkable, though such behavior has long been known in another context (L7, pp. 337–343).

There exist a variety of three-dimensional bodies whose resistance dyadics are known only in part. Foremost among these are axially symmetric bodies for which the coefficients  $K_{||}^{(r)}$  and  $K_{\perp}^{(r)}$  appearing in Eq. (72) are known. In the translational case, formulas are available for toroids (P2, R4), lens-shaped bodies, including hemispheres and spherical caps (C16, P1), two-spheres (S20), and spindles (P3). Departing from the axisymmetric case, Roscoe (R6) and Gupta (G12) have developed electrostatic analogies which permit one to obtain the forces on flat disks of various cross sections undergoing translational motion perpendicular to the plane of the disk. Approximate methods have been proposed (B36, B37, T3, T8) for calculating the forces on finite circular cylinders. [See the pertinent discussion of Shi (S9a) bearing on the validity of such approximations.] Hill and Power (H13) have developed a pair of extremum principles which permit one to obtain upper and lower bounds for the drag on a body of arbitrary shape.

With regard to the rotation of axially symmetric bodies about their symmetry axes in the Stokes regime, explicit formulas for  $K_{||}^{(r)}$  are available for the following bodies: toroids (K1, R3), spherical caps (C15), lens-shaped bodies<sup>10</sup> (K1), two-spheres (J3, W1), and spindles (M3). A formula for  $K_{||}^{(r)}$  for a dumbbell consisting of two touching spheres, each of radius  $a$ , may be obtained as a limiting result from Jeffery's (J3) solution for the rotation of two equal spheres with equal angular velocities about their line of centers. This may be done by resorting to expansions of the type utilized in deriving Eq. (133a) from Eq. (130). The result ultimately obtained is

$$K_{||}^{(r)} = 12\pi\zeta(3)a^3$$

where  $\zeta(3) = 1.20206\dots$  is the Riemann zeta function of argument 3. Since, for a single sphere,  $K_{||}^{(r)} = 8\pi a^3$ , it follows from the fact that  $12\pi\zeta(3)/(2 \times 8\pi) = 0.90154\dots$  that the torque on the dumbbell is slightly *less* than on two

<sup>9</sup> A helicoidally isotropic body is said to be right-handed if, when it translates through the fluid,  $\omega$  is parallel to  $\mathbf{U}_R$  (in the absence of an external torque about the center of reaction). Conversely, it is left-handed if  $\omega$  is antiparallel to  $\mathbf{U}_R$  under these circumstances.

<sup>10</sup> Professor Kanwal has asked me to point out the following omission in his paper (K1): His Eq. (40) for the torque on a hemisphere should read (in our notation)

$$|T| = [8(135 - 59\sqrt{3})/81] \pi\mu a^3\omega + \frac{8}{3} \pi\mu a^3\omega = 18.56\pi\mu a^3\omega$$

where  $a$  is the radius.

spheres rotating separately. Kearsley (K7) gives a formula for obtaining an upper bound to the torque on a rotating body which holds for *all* angular Reynolds numbers, providing that the resulting motion is steady. This bound contains the Reynolds number as a parameter.

Collins (C14) points out a simple analogy for obtaining the Stokesian velocity field due to the rotation of an axisymmetric body about its axis, from a knowledge of the corresponding axially symmetric, *streaming, potential* flow of an incompressible ideal fluid past the body. When combined with Kanwal's (K1) formula, expressing the Stokes torque in terms of the asymptotic expansion of the velocity field at great distances from the rotating body, it yields a potent method for determining the torque on bodies whose surfaces are not members of any particular system of curvilinear coordinates. Thus, for example, airship forms and Rankine solids of a variety of shapes (M17) can be generated by an appropriate combination of point and line sources and sinks, doublets, etc., lying entirely within the body, providing that the total intake of the sinks equals the output of the sources. The combined Collins-Kanwal formula for the Stokes torque  $T$  about any point on the axis of the body rotating with angular speed  $\omega$  in a fluid of viscosity  $\mu$  is

$$|T| = 16\pi\mu\omega \lim_{r \rightarrow \infty} \frac{r^3\psi}{\varpi^2} \quad (75)$$

where  $\psi$  is the stream function for potential flow around the body with unit stream velocity, and  $r$  and  $\varpi$  are spherical and cylindrical coordinates, respectively, measured from any point on the axis. For example, for a prolate spheroid, Lamb (L5, p. 141) gives as the stream function for potential flow past this body

$$\psi = \frac{1}{2}\varpi^2 \frac{g(\zeta)}{g(\zeta_0)}$$

where

$$g(\zeta) = \frac{\zeta}{\zeta^2 - 1} - \frac{1}{2} \ln \frac{\zeta + 1}{\zeta - 1}$$

The spheroid dimensions are related to the spheroidal coordinate  $\zeta_0$  as follows:

$$a = c\zeta_0, \quad b = c(\zeta_0^2 - 1)^{1/2}$$

where  $a$  and  $b$  are the polar and equatorial radii and  $c = (a^2 - b^2)^{1/2}$  is half the distance between the focii of the spheroid. The couple is thus

$$|T| = \frac{8\pi\mu\omega}{g(\zeta_0)} \lim_{r \rightarrow \infty} r^3 g(\zeta)$$

As  $\zeta \rightarrow \infty$ ,  $r \rightarrow c\zeta$ . Moreover

$$\ln \frac{\zeta + 1}{\zeta - 1} = \ln \frac{1 + 1/\zeta}{1 - 1/\zeta} = 2 \left( \frac{1}{\zeta} + \frac{1}{3\zeta^3} + \frac{1}{5\zeta^5} + \dots \right)$$

and

$$\frac{\zeta}{\zeta^2 - 1} = \frac{1}{\zeta} \left( \frac{1}{1 - 1/\zeta^2} \right) = \frac{1}{\zeta} \left( 1 + \frac{1}{\zeta^2} + \frac{1}{\zeta^4} + \cdots \right)$$

An easy calculation then yields

$$\lim_{\zeta \rightarrow \infty} r^3 g(\zeta) = \frac{2}{3} c^3$$

whence

$$|T| = \frac{(16\pi/3)\mu\omega c^3}{(ac/b^2) - \frac{1}{2} \ln[(a+c)/(a-c)]}$$

in agreement with Jeffery's (J3) result for the prolate ellipsoid of revolution.

Accurate experimental data of recent vintage are available (C10, J1, J2a, H12, K11, M4, M11, P6) for the translational resistances of a large variety of simple, well-defined geometric shapes in the Stokes regime. (Earlier data are reviewed by these investigators.) These data are based on measurements of terminal settling velocities. Typical of the bodies studied were regular tetrahedrons, cubes, cube-octahedrons, rectangular prisms and finite cylinders of various aspect ratios, and square flat disks—to name a few. Many of these were studied for more than one orientation. These bodies, when homogeneous, are neutrally stable and can fall stably in any orientation, contrary to their usual behavior at higher Reynolds numbers. In most of these cases, sufficient experimental data are therefore available to permit evaluation of the complete translation dyadics. Jones and Knudsen (J6) measured the translational resistances of a number of bodies by towing them through a viscous oil, measuring, by means of a spring balance, the force required to impart a given velocity to the body. Their data show a large scatter owing partly to the inherent difficulties of the technique and partly to the question of how to correct for the resistance of the tow-wire itself.

Much of the data cited above originally included significant wall-effects, which the investigators attempted to correct for in various ways. Theoretically sound ways of making such corrections are discussed in Section II,C,3.

Experiments aimed at measuring the rotational resistances of simple bodies in infinite media appear nonexistent. Also lacking are experiments on screw- and propeller-like bodies (which rotate as they settle), as are quantitative experiments on the nonvertical fall of anisotropic bodies.<sup>11</sup>

<sup>11</sup> Experiments of this type are currently being pursued by N. Ganiaris (New York University) employing a nonvertically mounted column, inclined so as to be parallel to the direction of fall of the particle. In this way the particle always falls along the tube axis, never striking the wall.

Experimental data on the inclined fall of circular rods are presented by Mohr and Blumberg (M19). Their results, covering the complete range of possible orientations of the rod axis relative to the gravity field, agree with theoretical predictions.

Theoretical computation of the trajectory and ultimate state of motion of a solid particle of arbitrary shape falling under the influence of gravity in the Stokes regime is partially discussed by Brenner (B22). Such calculations involve a complex interplay between the three resistance dyadics, the moment of inertia dyadic, the relative positions of the centers of reaction, mass, and buoyancy, the mass and volume of the particle, the density and viscosity of the fluid, the gravity field vector, and the initial orientation, velocity, and spin of the particle. The difficulty implicit in such calculations stems from the fact that the nonscalar particle properties are constant only when referred to axes fixed in the particle, whereas the gravity vector is constant relative to axes fixed in space. As yet, no completely general theory of the "terminal" state of motion of a particle exists. Lacking are suitable criteria of the stability of such motions. However, in a few simple situations one is able to make definite assertions about the terminal motion (B22). Among the more interesting results are the following: (i) A homogeneous anisotropic particle such as an ellipsoid attains a neutrally stable terminal motion in which it settles without rotation. In general, it does not fall vertically but drifts horizontally as it settles, in a manner dependent upon the initial conditions of release; and (ii) A body such as an isotropic helicoid attains a neutrally stable terminal state in which it falls vertically and rotates about a vertical axis. The sense of the direction of rotation depends upon whether the helicoid is right or left handed.

The lack of suitable general stability criteria alluded to in the preceding paragraph has recently been partially overcome by Goldman, Cox, and Brenner (G5c).

Repeated sedimentation experiments performed on a randomly oriented, nonskew, neutrally stable, anisotropic particle (e.g., an ellipsoid) will, in general, display a spread in terminal settling velocities, owing to the dependence of settling velocity on orientation. Equivalently, a dilute suspension of identical, randomly oriented bodies will display a range of settling velocities. In these experiments the (gravity) force on each particle is the same. If all orientations are equally probable the average velocity  $\bar{\mathbf{U}}$  will lie parallel to  $\mathbf{F}$ , so that the average translational resistance  $\bar{\mathbf{K}}_t$  in the formula  $\bar{\mathbf{U}} = -\mu^{-1}(\bar{\mathbf{K}}_t)^{-1}\mathbf{F}$  is the *scalar* (B18)

$$(\bar{\mathbf{K}}_t)^{-1} = \frac{1}{3} \text{trace} \left\| \overset{(t)}{\mathbf{K}} \right\|^{-1} = \frac{1}{3} \left( \overset{(t)}{K}_1^{-1} + \overset{(t)}{K}_2^{-1} + \overset{(t)}{K}_3^{-1} \right)$$

where  $\overset{(t)}{K}_j^{-1} = 1/\overset{(t)}{K}_j$ , in which the  $\overset{(t)}{K}_j$  ( $j = 1, 2, 3$ ) are the eigenvalues of the translation dyadic. On the other hand, for streaming flow past a randomly oriented collection of identical particles, the stream velocity vector  $\mathbf{U}$  will be the same for each particle and the average force  $\bar{\mathbf{F}}$  will lie parallel to  $\mathbf{U}$ . The

average resistance  $\bar{K}_t$  in the formula  $\bar{\mathbf{F}} = \mu \bar{K}_t \mathbf{U}$  is therefore, once again, a scalar, but it is now given by the formula

$$\bar{K}_t = \frac{1}{3} \text{trace} \left\| \overset{(t)}{\mathbf{K}} \right\| = \frac{1}{3} \left( \overset{(t)}{K}_1 + \overset{(t)}{K}_2 + \overset{(t)}{K}_3 \right)$$

These two average resistances are not the same, though the difference is not likely to be large. [For example, for a circular disk of radius  $a$  ( $\overset{(t)}{K}_1 = \overset{(t)}{K}_2 = \frac{3}{2}a$ ,  $\overset{(t)}{K}_3 = 16a$ ) the two average resistances are  $12a$  and  $12\frac{4}{9}a$ , respectively.] Nevertheless, the calculation does reveal the need for caution when utilizing *average* results in the form  $\mathbf{F} = -\mu \bar{K}_t \mathbf{U}$ .

In a somewhat similar vein, a clear distinction must be made between the true translational resistance dyadic  $\overset{(t)}{\mathbf{K}}$  of a skewed particle and the *apparent* value thereof that would be directly observed in a settling velocity experiment. If, in Eq. (39),  $O$  is the point about which the net gravitational plus buoyant torques on a freely settling particle vanish, we find upon setting  $\mathbf{T}_O = \mathbf{0}$  and eliminating  $\boldsymbol{\omega}$  between Eqs. (38) and (39) that

$$\mathbf{F} = -\mu \left[ \overset{(t)}{\mathbf{K}} - \overset{(c)}{\mathbf{K}}_O^\dagger \cdot \overset{(r)}{\mathbf{K}}_O^{-1} \cdot \overset{(c)}{\mathbf{K}}_O \right] \cdot \mathbf{U}_O$$

The dyadic coefficient of proportionality between the force and translational velocity in this expression is, therefore, not the same as the true translational resistance dyadic in the formula  $\mathbf{F} = \mu \overset{(t)}{\mathbf{K}} \cdot \mathbf{U}$ , applicable to the case of, say, streaming flow past the *immobilized* particle (with stream velocity  $\mathbf{U}$ ). A homogeneous, isotropic helicoid furnishes a simple, but definite example of this distinction; for if  $O$  refers to its center, the outcome of the settling velocity experiment corresponds to the formula [see Eq. (71)]

$$\mathbf{F} = -\mu \left[ K_t - \frac{K_c^2}{K_r} \right] \mathbf{U}_O$$

In accordance with Eq. (74) the apparent translational resistance of this particle is positive-definite.

## 2. Shear and Higher-Order Flows

*a. Solid Particles.* In this section we discuss the quasi-static Stokes resistance of a solid particle of any shape immersed in a fluid which is in a state of net motion at infinity (B23, B24, B26). The fluid motion is thus governed by the quasi-steady Stokes equations, the continuity equation for incompressible fluids, and the boundary conditions

$$\mathbf{v} = \mathbf{U} + \boldsymbol{\omega} \times \mathbf{r} \quad \text{on } B \quad (76)$$

$$\mathbf{v} \rightarrow \mathbf{u} \quad \text{at infinity} \quad (77)$$

where  $\mathbf{U}$  is the velocity of an arbitrary point  $O$  affixed to the particle and  $\mathbf{r}$  is measured from  $O$ . The arbitrary field  $\mathbf{u} = \mathbf{u}(\mathbf{r})$  at infinity must itself satisfy the equations of motion—otherwise the system of equations and boundary conditions are incompatible. Examples of such compatible flows at infinity are shear and Poiseuille (parabolic) flows, for these satisfy Stokes equations identically.

Rather remarkably, the forces and torques experienced by particles in such arbitrary flows can be obtained solely from knowledge of the corresponding translational and rotational solutions of Stokes equations *for the case where the fluid is at rest at infinity*. Explicitly, if  $\overset{(t)}{\Pi}$  and  $\overset{(r)}{\Pi}_O$  are the intrinsic translational and rotational triadic stress fields for the particle in question, defined in Eqs. (35) and (36), the force and torque experienced by the body in an arbitrary flow are (B24, B26)

$$\mathbf{F} = \mu \int_B d\mathbf{S} \cdot \overset{(t)}{\Pi}^\dagger \cdot (\mathbf{v} - \mathbf{u}) \quad (78)$$

$$\mathbf{T}_O = \mu \int_B d\mathbf{S} \cdot \overset{(r)}{\Pi}_O^\dagger \cdot (\mathbf{v} - \mathbf{u}) \quad (79)$$

where  $\mathbf{u}(\mathbf{r})$  is the arbitrarily prescribed Stokes flow field at infinity and  $\mathbf{v}$  refers to the velocity field at the surface  $B$  of the particle. These relations do not actually require that the particle be solid, but rather apply for any arbitrary field  $\mathbf{v}$  at the particle surface. By expressing the intrinsic stress triadics in trinomial form in an arbitrary system of Cartesian coordinates  $(x_1, x_2, x_3)$ ,

$$\overset{(\cdot)}{\Pi} = \frac{1}{\mu} \left[ \overset{(\cdot)}{\pi}_1 \mathbf{i}_1 + \overset{(\cdot)}{\pi}_2 \mathbf{i}_2 + \overset{(\cdot)}{\pi}_3 \mathbf{i}_3 \right]$$

Eqs. (78) and (79) may be written alternatively in terms of their Cartesian components,

$$F_j = \int_B d\mathbf{S} \cdot \overset{(t)}{\pi}^{[j]} \cdot (\mathbf{v} - \mathbf{u}) \quad (j = 1, 2, 3)$$

$$(T_O)_j = \int_B d\mathbf{S} \cdot \overset{(r)}{\pi}_O^{[j]} \cdot (\mathbf{v} - \mathbf{u}) \quad (j = 1, 2, 3)$$

where  $\mathbf{i}_1, \mathbf{i}_2, \mathbf{i}_3$  are unit vectors parallel to the coordinate axes. Here,  $\overset{(t)}{\pi}^{[j]}$  is the conventional stress dyadic [cf. Eq. (3)] for translational motion of the particle with *unit* velocity in the  $x_j$  direction in a fluid at rest at infinity, and  $\overset{(r)}{\pi}_O^{[j]}$  is the stress dyadic for rotation of the particle about an axis through  $O$  with *unit* angular velocity, parallel to the  $x_j$  axis, in a fluid at rest at infinity. In these expressions  $F_j = \mathbf{i}_j \cdot \mathbf{F}$ , with a similar expression for the torque.

If the particle is solid,  $\mathbf{v}$  is given on  $B$  by Eq. (76). It is convenient to expand  $\mathbf{u}$  in a *symbolic* Taylor series<sup>12</sup>

$$\mathbf{u}(\mathbf{r}) = \exp(\mathbf{r} \cdot \nabla_O) \mathbf{u}(\mathbf{r}_O) \quad (80)$$

where  $O$ , once again, refers to the arbitrary point moving with the particle. We then find from Eqs. (78) and (79) that (B26)

$$\mathbf{F} = -\mu \mathfrak{F} \cdot (\mathbf{U} + \boldsymbol{\omega} \times \mathbf{r} - \mathbf{u}) \quad (81)$$

$$\mathbf{T}_O = -\mu \mathfrak{T}_O \cdot (\mathbf{U} + \boldsymbol{\omega} \times \mathbf{r} - \mathbf{u}) \quad (82)$$

where the dyadic entities

$$\mathfrak{F} = - \int_B d\mathbf{S} \cdot \mathbf{\Pi}^{(t)} \exp(\mathbf{r} \cdot \nabla_O) \quad (83)$$

and

$$\mathfrak{T}_O = - \int_B d\mathbf{S} \cdot \mathbf{\Pi}_O^{(r)} \exp(\mathbf{r} \cdot \nabla_O) \quad (84)$$

are *symbolic operators*. The nabla operator  $\nabla_O$  is to be regarded as a constant in the  $\mathbf{r}$ -space integration. These intrinsic force and torque operators depend only on the exterior shape and size of the particle, though the latter operator also depends upon the location of  $O$ . These dyadic differential operators operate on the "slip velocity" between particle and fluid,  $\mathbf{U} + \boldsymbol{\omega} \times \mathbf{r} - \mathbf{u}$ . In a broader sense, Eqs. (81) and (82) express the fact that the force and torque are *linear vector functionals* of the difference between the particle and fluid velocities. An alternative form of these relations is

$$\mathbf{F} = -\mu \left( \mathbf{K} \cdot \mathbf{U}_O + \mathbf{K}_O^{(c)} \cdot \boldsymbol{\omega} - \mathfrak{F} \cdot \mathbf{u} \right) \quad (85)$$

$$\mathbf{T}_O = -\mu \left( \mathbf{K}_O^{(c)} \cdot \mathbf{U}_O + \mathbf{K}_O^{(r)} \cdot \boldsymbol{\omega} - \mathfrak{T}_O \cdot \mathbf{u} \right) \quad (86)$$

<sup>12</sup> That is,

$$\mathbf{u}(x, y, z) = \left[ \exp \left( x \frac{\partial}{\partial x_O} + y \frac{\partial}{\partial y_O} + z \frac{\partial}{\partial z_O} \right) \right] \mathbf{u}(x_O, y_O, z_O)$$

Symbolic methods are useful not only for representing resistance formulas but also for obtaining detailed solutions of the equations of motion for arbitrary boundary conditions. The general methods have much in common with the use of Green's functions (F12, L5a, M20) to represent the solution for arbitrary boundary conditions. However, in contrast with Green's functions, which express the solution in the form of an *integral operator* operating on the boundary conditions, the solution appears here in the form of a *symbolic differential operator* operating on the boundary conditions. The connection between the two methods lies in the fact that when the boundary data are sufficiently smooth the Green's function integrals can be evaluated by resorting to symbolic expansions of the type given by Eq. (80).

Since the translational and rotational Stokes problems are completely solved for the sphere and the ellipsoid, one can evaluate these symbolic operators for such bodies. For the sphere (B26)

$$\mathfrak{F} = 16\pi a \frac{\sinh(a\nabla_R)}{a\nabla_R} \quad (87)$$

and

$$\mathfrak{T}_R = -\frac{12\pi a^3}{(a\nabla_R)^2} \left[ \cosh(a\nabla_R) - \frac{\sinh(a\nabla_R)}{a\nabla_R} \right] \boldsymbol{\varepsilon} \cdot \nabla_R \quad (88)$$

where  $R$  is the sphere center. Here,  $\nabla = (\nabla^2)^{1/2}$ , where  $\nabla^2$  is the ordinary Laplace operator. Note carefully the distinction between the scalar operator  $\nabla$  and the ordinary vector nabla operator  $\nabla$ . The symbolic operators appearing above may be interpreted by employing the infinite series expansions

$$\sinh x = x + \frac{x^3}{3!} + \frac{x^5}{5!} + \frac{x^7}{7!} + \cdots$$

$$\cosh x = 1 + \frac{x^2}{2!} + \frac{x^4}{4!} + \frac{x^6}{6!} + \cdots$$

Substitution into (81) and (82) eventually yields

$$\mathbf{F} = -6\pi\mu a \left[ (\mathbf{U}_R - \mathbf{u}_R) - \frac{a^2}{6} (\nabla^2 \mathbf{u})_R \right] \quad (89a)$$

$$\mathbf{T}_R = -8\pi\mu a^3 [\boldsymbol{\omega} - \tfrac{1}{2}(\nabla \times \mathbf{u})_R] \quad (89b)$$

where the affix  $R$  implies evaluation at the sphere center. In obtaining these it has been noted that  $(\boldsymbol{\varepsilon} \cdot \nabla) \cdot \mathbf{u} = -\nabla \times \mathbf{u}$ . We have also utilized the fact that since  $\mathbf{u}$  satisfies Stokes equations, then  $\nabla^4 \mathbf{u} = \mathbf{0}$  and  $\nabla^2(\nabla \times \mathbf{u}) = \mathbf{0}$ , whereupon all the higher-order terms in the original infinite series expansions vanish. Equations (89) are Faxén's laws (F2, P4). They directly furnish the force and torque on a solid spherical particle translating and spinning within a fluid in an arbitrary state of Stokes flow at infinity. The last term in Eq. (89a) may be expressed in alternative form by noting that  $\nabla^2 \mathbf{u} = \mu^{-1} \nabla p^0$ , where  $p^0$  is the unperturbed pressure field.

The symbolic operators (87)–(88) for the sphere possess a greater degree of generality than do Faxén's laws. In particular, if we consider any Stokes flow  $\mathbf{v}(r, \mathbf{r}/r)$  vanishing at infinity and satisfying the arbitrary boundary condition  $\mathbf{v} = \mathbf{f}(\mathbf{r}/r) \equiv \mathbf{f}(\theta, \phi)$  at  $r = a$ , then the force on the sphere may be obtained directly from the prescribed velocity boundary condition via the expression

$$\mathbf{F} = -6\pi\mu a \frac{\sinh(a\nabla_R)}{a\nabla_R} \mathbf{f}\left(\frac{\mathbf{r}_R}{a}\right)$$



or, what is equivalent,

$$\mathbf{F} = -6\pi\mu a \left[ \frac{\sinh \nabla}{\nabla} \mathbf{f}(\mathbf{r}) \right]_R \quad (90a)$$

The function  $\mathbf{f}(\mathbf{r})$  need not satisfy Stokes equations, nor indeed any conditions other than that of analyticity at the origin. Similarly, for the torque we have

$$\mathbf{T}_R = -12\pi\mu a^2 \left[ \frac{1}{\nabla^2} \left( \cosh \nabla - \frac{\sinh \nabla}{\nabla} \right) \nabla \times \mathbf{f}(\mathbf{r}) \right]_R \quad (90b)$$

Suppose, for example, that the prescribed boundary condition is

$$\mathbf{v} = \mathbf{i}_1(A + B \sin^2 \theta + C \sin \theta \sin \phi) \quad \text{at } r = a$$

where  $A, B, C$  are constants and  $(r, \theta, \phi)$  are spherical coordinates related to the Cartesian system  $(x_1, x_2, x_3)$  as in the example following Eq. (68). This makes

$$\mathbf{f}(\mathbf{r}) = \mathbf{i}_1[A + B(x_2^2 + x_3^2) + Cx_3]$$

which ultimately yields

$$\mathbf{F} = -\mathbf{i}_1 6\pi\mu a(A + \frac{2}{3}B)$$

$$\mathbf{T}_R = -\mathbf{i}_2 4\pi\mu a^2 C$$

in agreement with results cited by Brenner and Happel (B28). Formulas of the type (90) are inapplicable unless  $\mathbf{f}(\mathbf{r})$  is infinitely differentiable at the origin, in which case one must revert to the original integral formulas (78)–(79). For the sphere these reduce to (B24)

$$\mathbf{F} = -\frac{3}{2}\mu a \int_{S_1} \mathbf{f} \left( \frac{\mathbf{r}}{r} \right) d\Omega \quad (91a)$$

$$\mathbf{T}_R = -3\mu a^2 \int_{S_1} \frac{\mathbf{r}}{r} \times \mathbf{f} \left( \frac{\mathbf{r}}{r} \right) d\Omega \quad (91b)$$

where  $d\Omega = \sin \theta d\theta d\phi$  is an element of surface area on a unit sphere,  $S_1$ . The relationship between the integral forms (91) and the differential forms (90) is readily grasped by considering the equivalent one-dimensional relation

$$\int_{-a}^a f(x) dx = 2 \frac{\sinh\{a(d/dx_o)\}}{(d/dx_o)} f(x_o)$$

for any  $f(x)$ . That symbolic methods have attained no systematic degree of popularity appears to be due in large measure to the preoccupation of mathematicians with pathological functions for which such integration formulas are invalid. Where applicable, such methods are very potent, for they replace integration by differentiation.

The symbolic operators for the ellipsoid, Eq. (57), are (B26)

$$\mathfrak{F} = \mathbf{K} \frac{^{(t)} \sinh D_R}{D_R} \quad (92a)$$

and

$$\mathfrak{I}_R = -3 \left\{ \frac{1}{D_R} \frac{d}{dD_R} \left( \frac{\sinh D_R}{D_R} \right) \right\} \mathbf{Q} \cdot \boldsymbol{\varepsilon} \cdot \square_R \quad (92b)$$

where  $R$  refers to the center of the ellipsoid, i.e., its center of reaction;  $\mathbf{K}$  is the translation dyadic for the ellipsoid, given in Eq. (58);  $D = (D^2)^{1/2}$  is a scalar operator in which

$$D^2 = a_1^2 \frac{\partial^2}{\partial x_1^2} + a_2^2 \frac{\partial^2}{\partial x_2^2} + a_3^2 \frac{\partial^2}{\partial x_3^2} \quad (93)$$

is a sort of distorted Laplace operator;  $\mathbf{Q}$  is the constant dyadic

$$\mathbf{Q} = \frac{16\pi}{3} \left[ \frac{\mathbf{e}_1 \mathbf{e}_1}{a_2^2 \alpha_2 + a_3^2 \alpha_3} + \frac{\mathbf{e}_2 \mathbf{e}_2}{a_3^2 \alpha_3 + a_1^2 \alpha_1} + \frac{\mathbf{e}_3 \mathbf{e}_3}{a_1^2 \alpha_1 + a_2^2 \alpha_2} \right] \quad (94)$$

in which  $\mathbf{e}_j$  ( $j = 1, 2, 3$ ) is a unit vector drawn parallel to a principal axis  $Rx_j$  of the ellipsoid, and  $\alpha_j$  is defined in Eq. (61). Lastly,  $\square$  is the vector differential operator

$$\square = \mathbf{e}_1 a_1^2 \frac{\partial}{\partial x_1} + \mathbf{e}_2 a_2^2 \frac{\partial}{\partial x_2} + \mathbf{e}_3 a_3^2 \frac{\partial}{\partial x_3} \quad (95)$$

Substitution into Eqs. (81)–(82) or (85)–(86) yields

$$\mathbf{F} = -\mu \mathbf{K} \cdot \left[ \mathbf{U} - \left( \frac{\sinh D}{D} \right) \mathbf{u} \right]_R \quad (96)$$

and

$$\mathbf{T}_R = -\mu \mathbf{K}_R \cdot \left[ \boldsymbol{\omega} - 3\mathbf{A} \cdot \left\{ \frac{1}{D} \frac{d}{dD} \left( \frac{\sinh D}{D} \right) \right\} \square \times \mathbf{u} \right]_R \quad (97)$$

$\mathbf{K}_R$  is given in Eq. (59);  $\mathbf{A}$  is the constant dyadic

$$\mathbf{A} = \frac{\mathbf{e}_1 \mathbf{e}_1}{a_2^2 + a_3^2} + \frac{\mathbf{e}_2 \mathbf{e}_2}{a_3^2 + a_1^2} + \frac{\mathbf{e}_3 \mathbf{e}_3}{a_1^2 + a_2^2}$$

When the operators appearing in (96) and (97) are expanded via their infinite series representations the resulting expansions do not terminate after a finite number of terms, as do Faxén's laws for the sphere, Eqs. (89).

To illustrate the applicability of these relations consider the case of an ellipsoid in a uniform shear field [see Eq. (106), where  $O$  is taken at the center

of the ellipsoid]. From Eqs. (81)–(82), (92), and (106) one finds, upon expanding the hyperbolic functions, that

$$\mathbf{F} = -\mu \mathbf{K} \cdot \left[ \left( 1 + \frac{D^2}{6} + \frac{D^4}{120} + \cdots \right) \{ \mathbf{U} - \mathbf{u} + (\boldsymbol{\omega} - \boldsymbol{\omega}_f) \times \mathbf{r} - \mathbf{S} \cdot \mathbf{r} \} \right]_R$$

and

$$\mathbf{T}_R = -\mu \mathbf{Q} \cdot \left[ \left( 1 + \frac{D^2}{10} + \frac{D^4}{280} + \cdots \right) \square \times \{ (\boldsymbol{\omega} - \boldsymbol{\omega}_f) \times \mathbf{r} - \mathbf{S} \cdot \mathbf{r} \} \right]_R$$

where it has been noted that  $\square \times (\mathbf{U}_R - \mathbf{u}_R) = \mathbf{0}$ , as follows from the constancy of the vectors  $\mathbf{U}_R$  and  $\mathbf{u}_R$ . Since  $D^2 \mathbf{r} = \mathbf{0}$  everywhere, and since  $\mathbf{r} = \mathbf{0}$  at the center of the ellipsoid, these reduce to

$$\mathbf{F} = -\mu \mathbf{K} \cdot (\mathbf{U}_R - \mathbf{u}_R)$$

and

$$\mathbf{T}_R = -\mu \mathbf{Q} \cdot [\square \times \{ (\boldsymbol{\omega} - \boldsymbol{\omega}_f) \times \mathbf{r} - \mathbf{S} \cdot \mathbf{r} \}]$$

If the sphere is neutrally buoyant the former relation requires that  $\mathbf{U}_R = \mathbf{u}_R$ , so that the center of the ellipsoid is carried along with the fluid. We note the identities  $\square \times \{ (\boldsymbol{\omega} - \boldsymbol{\omega}_f) \times \mathbf{r} \} = (\boldsymbol{\omega} - \boldsymbol{\omega}_f) \cdot (\mathbf{I} \square \cdot \mathbf{r} - \square \mathbf{r})$  and  $\square \times (\mathbf{S} \cdot \mathbf{r}) = -\mathbf{S}^\dagger \times \square \cdot \mathbf{r}$ . Thus, in terms of a system of Cartesian coordinates instantaneously coinciding with the principal axes of the ellipsoid, the following expressions are obtained for the components of the couple about the center of the ellipsoid:

$$T_1 = \frac{16\pi\mu}{3(a_2^2\alpha_2 + a_3^2\alpha_3)} \{ (a_2^2 - a_3^2)S_{23} + (a_2^2 + a_3^2)(\omega_1^f - \omega_1) \}$$

$$T_2 = \frac{16\pi\mu}{3(a_3^2\alpha_3 + a_1^2\alpha_1)} \{ (a_3^2 - a_1^2)S_{31} + (a_3^2 + a_1^2)(\omega_2^f - \omega_2) \}$$

$$T_3 = \frac{16\pi\mu}{3(a_1^2\alpha_1 + a_2^2\alpha_2)} \{ (a_1^2 - a_2^2)S_{12} + (a_1^2 + a_2^2)(\omega_3^f - \omega_3) \}$$

in which  $S_{ij} = \mathbf{e}_j \mathbf{e}_i : \mathbf{S}$ . The validity of the preceding relations depends upon the symmetry of  $\mathbf{S}$ . These results agree identically with those originally given by Jeffery (J4). Jeffery, however, obtained his formulas by actually solving the boundary-value problem appropriate to an ellipsoid at incidence in a shear field.

For the slightly deformed sphere described by Eq. (64) Ripps and Brenner (R5a) give the following expression for the symbolic dyadic force operator:

$$\begin{aligned} \mathfrak{F} = 6\pi a \left[ \mathbf{I} \frac{\sinh(a\nabla_R)}{a\nabla_R} + \varepsilon \sum_{n=0}^{\infty} \left\{ \left( 2n+1 + a\nabla_R \frac{d}{d(a\nabla_R)} \right) \mathbf{I} \Omega_n^{(0)}(a\nabla_R) \right. \right. \\ \left. \left. - \frac{(2n+1)}{(n+2)(2n+5)} \mathfrak{P}_n^{(2)}(a\nabla_R) \right\} \left\{ \frac{1}{a\nabla_R} \frac{d}{d(a\nabla_R)} \right\}^n \frac{\sinh(a\nabla_R)}{a\nabla_R} \right] + O(\varepsilon^2) \quad (98) \end{aligned}$$

in which

$$\mathfrak{L}_n^{(0)}(a\nabla_R) = \frac{1}{n!} \mathbf{C}_n \boxed{n} (a\nabla_R)^n$$

and

$$\mathfrak{L}_n^{(2)}(a\nabla_R) = \frac{1}{n!} \mathbf{C}_{n+2} \boxed{n} (a\nabla_R)^n$$

are, respectively, scalar and dyadic operators of argument  $a\nabla_R$ . Here

$$\mathbf{C}_k = \overbrace{\nabla\nabla \cdots \nabla\nabla}^{k \text{ times}} (r^k f_k)$$

is a (dimensionless) *constant*  $k$ -adic and

$$(a\nabla_R)^n = a^n \overbrace{\nabla_R \nabla_R \cdots \nabla_R \nabla_R}^{n \text{ times}}$$

is a (dimensionless)  $n$ -adic differential operator in “ $R$ -space.” The symbol  $\boxed{n}$  denotes  $n$  successive polydot multiplications. The two  $\mathfrak{L}$ -operators may also be written, respectively, in the following scalar and dyadic forms:

$$\mathfrak{L}_n^{(0)}(a\nabla_R) = \frac{a^n}{n!} (\nabla \cdot \nabla_R)^n (r^n f_n)$$

$$\mathfrak{L}_n^{(2)}(a\nabla_R) = \frac{a^n}{n!} \nabla\nabla (\nabla \cdot \nabla_R)^n (r^{n+2} f_{n+2})$$

where

$$\nabla \cdot \nabla_R \equiv \frac{\partial}{\partial x} \frac{\partial}{\partial x_R} + \frac{\partial}{\partial y} \frac{\partial}{\partial y_R} + \frac{\partial}{\partial z} \frac{\partial}{\partial z_R}$$

bearing in mind that the  $R$ -space differentiations do not operate on the physical space variables  $(r, \theta, \phi)$  or  $(x, y, z)$ . The force operator may be interpreted via the expansion

$$\begin{aligned} \left( \frac{1}{\xi} \frac{d}{d\xi} \right)^n \frac{\sinh \xi}{\xi} &= \frac{1}{\xi^n} \left( \frac{\pi}{2\xi} \right)^{1/2} I_{n+1/2}(\xi) \\ &= \frac{2^n n!}{(2n+1)!} \left[ 1 + \frac{\xi^2}{2(2n+3)} + \frac{\xi^4}{2 \cdot 4(2n+3)(2n+5)} + \cdots \right] \end{aligned}$$

where  $I_{n+1/2}$  is the modified Bessel function of the first kind of order  $n + \frac{1}{2}$ . The comparable expression for the symbolic dyadic torque operator for the slightly deformed sphere is also available (R5a).

A systematic investigation of the number and nature of the nonzero coefficients of the symbolic force dyadic and torque pseudodyadic operators may be made for bodies possessing various types of geometric symmetry.

In certain applications it is physically more enlightening to express the operator equations (81) and (82) in terms of polyadic resistance coefficients (B23, B24), rather than leaving them in their present symbolic forms. This may be achieved by utilizing the expansion

$$\begin{aligned}\exp(\mathbf{r} \cdot \nabla_O) &= 1 + \frac{1}{1!} \mathbf{r} \cdot \nabla_O + \frac{1}{2!} \mathbf{r} \mathbf{r} : \nabla_O \nabla_O + \dots \\ &= \sum_{n=0}^{\infty} \frac{1}{n!} \mathbf{r}^{\overline{n}} \nabla_O^n\end{aligned}\quad (99)$$

where  $\mathbf{r}^{\overline{n}}$  is the  $n$ -adic

$$\mathbf{r}^{\overline{n}} = \overbrace{\mathbf{r} \mathbf{r} \cdots \mathbf{r}}^{n \text{ times}}$$

in which  $\mathbf{r}$  is measured from  $O$ ;  $\nabla_O^n$  is the  $n$ -adic differential operator

$$\nabla_O^n = \overbrace{\nabla_O \nabla_O \cdots \nabla_O}^{n \text{ times}}$$

$\overline{n}$  denotes  $n$  successive polydot multiplications. In this notation the symbolic force and torque operators defined in (83) and (84) may be written as

$$\mathfrak{F} = \sum_{n=0}^{\infty} {}_{n+2} \mathfrak{F}_O^{(F)} \overline{n} \nabla_O^n \quad (100)$$

and

$$\mathfrak{T}_O = \sum_{n=0}^{\infty} {}_{n+2} \mathfrak{T}_O^{(T)} \overline{n} \nabla_O^n \quad (101)$$

in which

$${}_{n+2} \mathfrak{F}_O^{(F)} = -\frac{1}{n!} \int_B d\mathbf{S} \cdot \Pi^{\dagger} \mathbf{r}^{\overline{n}} \quad (102)$$

is a constant  $(n+2)$ -adic intrinsic force resistance coefficient, and

$${}_{n+2} \mathfrak{T}_O^{(T)} = -\frac{1}{n!} \int_B d\mathbf{S} \cdot \Pi_O^{(r)} \mathbf{r}^{\overline{n}} \quad (103)$$

is a constant, pseudo $(n+2)$ -adic intrinsic torque resistance coefficient (B24). Thus, from (100) and (101)

$$\mathfrak{F} \cdot \mathbf{u} = \sum_{n=0}^{\infty} {}_{n+2} \mathfrak{F}_O^{(F)} \overline{n+1} (\nabla^n \mathbf{u})_O \quad (104)$$

$$\mathfrak{T}_O \cdot \mathbf{u} = \sum_{n=0}^{\infty} {}_{n+2} \mathfrak{T}_O^{(T)} \overline{n+1} (\nabla^n \mathbf{u})_O \quad (105)$$

Substitution into (85) and (86) yields expressions for the force and torque in terms of these polyadic resistance coefficients.

For a sphere of radius  $a$  these polyadic resistance coefficients are, upon choosing the origin  $O$  at the sphere center (B24),

$$\begin{aligned} {}^{(F)}_{n+2}\mathfrak{R}_O &= \begin{cases} 6\pi a \mathbf{I} & \text{for } n = 0 \\ \pi a^3 \mathbf{II} & \text{for } n = 2 \\ \mathbf{0} & \text{for all other } n \end{cases} \\ {}^{(T)}_{n+2}\mathfrak{R}_O &= \begin{cases} -4\pi a^3 \boldsymbol{\varepsilon} & \text{for } n = 1 \\ \mathbf{0} & \text{for all other } n \end{cases} \end{aligned}$$

The corresponding results for the ellipsoid, Eq. (57), relative to an origin at its center, are (B24)

$$\begin{aligned} {}^{(F)}_{n+2}\mathfrak{R}_O &= \begin{cases} \frac{1}{n!(n+1)!} {}^{(t)}\mathbf{K}(D^2)^{n/2} \mathbf{r}^n & \text{for } n \text{ even} \\ \mathbf{0} & \text{for } n \text{ odd} \end{cases} \\ {}^{(T)}_{n+2}\mathfrak{R}_O &= \begin{cases} -\frac{3}{n!(n+2)!} \mathbf{Q} \cdot \boldsymbol{\varepsilon} \cdot (D^2)^{(n+1)/2} \mathbf{r}^{n+1} & \text{for } n \text{ odd} \\ \mathbf{0} & \text{for } n \text{ even} \end{cases} \end{aligned}$$

where the constant dyadics  $\mathbf{K}$  and  $\mathbf{Q}$  are defined in Eqs. (58) and (94), respectively. The differential operator  $D^2$  is defined in Eq. (93), and  $\mathbf{r} = \mathbf{e}_1 x_1 + \mathbf{e}_2 x_2 + \mathbf{e}_3 x_3$ . Note that the  $n$ -adic  $(D^2)^{n/2} \mathbf{r}^n$  and  $(n+1)$ -adic  $(D^2)^{(n+1)/2} \mathbf{r}^{n+1}$  are *constant* polyadics. The force polyadic for the slightly deformed sphere, Eq. (64), is (R5a)

$$\begin{aligned} {}^{(F)}_{n+2}\mathfrak{R}_O &= \delta_{n2} \pi a^3 \mathbf{II} + \varepsilon \frac{2^n 6\pi a^{n+1}}{(2n)!} \left[ \frac{1}{2} n(n-1)(2n-1) \mathbf{I} \mathbf{C}_{n-2} \mathbf{I} \right. \\ &\quad \left. + \mathbf{I} \mathbf{C}_n - \frac{(n-1)(2n-3)}{2(2n+1)} \mathbf{C}_n \mathbf{I} - \frac{1}{(n+2)(2n+5)} \mathbf{C}_{n+2} \right] + O(\varepsilon^2) \end{aligned}$$

valid for  $n' \geq 1$ . Here  $\delta_{ij}$  is the Kronecker delta and  $\mathbf{C}_m = \mathbf{V}^m(r^m f_m)$  is a constant  $m$ -adic. For the special case  $n = 0$ ,  ${}^{(F)}_2\mathfrak{R}_O$  is identical to  $\mathbf{K}$  in Eq. (65). The origin  $O$  refers to the center of the undeformed sphere. By deleting the  $f_1$ -term the preceding formula may also be applied at the center of reaction of the slightly deformed sphere. A comparable formula is also available for the torque polyadic  ${}^{(T)}_{n+2}\mathfrak{R}_O$  to the first order in  $\varepsilon$  (R5a).

It should be clearly understood that the formulas tabulated in the preceding paragraph apply only to the case where  $\mathbf{u}$  is a Stokes flow.

For simple flow fields the polyadic resistance formulation normally provides more insight into the physical phenomena which arise than does the equivalent symbolic operator method. In the case of a general linear shear field the undisturbed flow at infinity may be written in the form (B23)

$$\mathbf{u} = \mathbf{u}_O + \boldsymbol{\omega}_f \times \mathbf{r} + \mathbf{S} \cdot \mathbf{r} \quad (106)$$

where  $O$  is an arbitrary point affixed to the particle;  $\mathbf{u}_O$  is the approach velocity at  $O$ ;  $\mathbf{r}$  is measured from  $O$ ;

$$\boldsymbol{\omega}_f = \frac{1}{2} \nabla \times \mathbf{u} \quad (107)$$

is the angular velocity of a fluid particle, and

$$\mathbf{S} = \frac{1}{2} [\nabla \mathbf{u} + (\nabla \mathbf{u})^\dagger] \quad (108)$$

is the rate of shear dyadic for the incompressible flow;  $\boldsymbol{\omega}_f$  and  $\mathbf{S}$  are constants, independent of choice of origin. The hydrodynamic force and torque about  $O$  are then

$$\mathbf{F} = -\mu \left[ \overset{(t)}{\mathbf{K}} \cdot (\mathbf{U}_O - \mathbf{u}_O) + \overset{(c)}{\mathbf{K}}_O^\dagger \cdot (\boldsymbol{\omega} - \boldsymbol{\omega}_f) + \overset{(F)}{\boldsymbol{\mathfrak{S}}}_O : \mathbf{S} \right] \quad (109)$$

$$\mathbf{T}_O = -\mu \left[ \overset{(c)}{\mathbf{K}}_O \cdot (\mathbf{U}_O - \mathbf{u}_O) + \overset{(r)}{\mathbf{K}}_O \cdot (\boldsymbol{\omega} - \boldsymbol{\omega}_f) + \overset{(T)}{\boldsymbol{\mathfrak{S}}}_O : \mathbf{S} \right] \quad (110)$$

where the constant triadic  $\overset{(F)}{\boldsymbol{\mathfrak{S}}}_O$  and the pseudotriadic  $\overset{(T)}{\boldsymbol{\mathfrak{S}}}_O$  are, respectively, the intrinsic *shear-force* and *shear-torque* resistance triadics at  $O$  (B23). They are related to the previous resistance polyadics by the expressions

$$\overset{(F)}{\boldsymbol{\mathfrak{S}}}_O = -\overset{(F)}{3}\boldsymbol{\mathfrak{R}}_O - \frac{1}{2} \overset{(c)}{\mathbf{K}}_O^\dagger \cdot \boldsymbol{\varepsilon} \quad (111)$$

$$\overset{(T)}{\boldsymbol{\mathfrak{S}}}_O = -\overset{(T)}{3}\boldsymbol{\mathfrak{R}}_O - \frac{1}{2} \overset{(r)}{\mathbf{K}}_O \cdot \boldsymbol{\varepsilon} \quad (112)$$

Equations (109)–(110) show that the force and torque on the particle are *linear* vector functions of the translational slip velocity  $\mathbf{U}_O - \mathbf{u}_O$ , the angular slip velocity  $\boldsymbol{\omega} - \boldsymbol{\omega}_f$ , and the shear rate  $\mathbf{S}$ .

For an ellipsoidal particle the two shear triadics take the following forms at its center (B23):

$$\overset{(F)}{\boldsymbol{\mathfrak{S}}}_R = \mathbf{0} \quad (113)$$

and

$$\begin{aligned} \overset{(T)}{\boldsymbol{\mathfrak{S}}}_R = \frac{8\pi}{3} & \left[ (\mathbf{e}_1 \mathbf{e}_2 \mathbf{e}_3 + \mathbf{e}_1 \mathbf{e}_3 \mathbf{e}_2) \frac{a_3^2 - a_2^2}{a_3^2 \alpha_3 + a_2^2 \alpha_2} \right. \\ & + (\mathbf{e}_2 \mathbf{e}_3 \mathbf{e}_1 + \mathbf{e}_2 \mathbf{e}_1 \mathbf{e}_3) \frac{a_1^2 - a_3^2}{a_1^2 \alpha_1 + a_3^2 \alpha_3} \\ & \left. + (\mathbf{e}_3 \mathbf{e}_1 \mathbf{e}_2 + \mathbf{e}_3 \mathbf{e}_2 \mathbf{e}_1) \frac{a_2^2 - a_1^2}{a_2^2 \alpha_2 + a_1^2 \alpha_1} \right] \quad (114) \end{aligned}$$

These may also be derived from Eqs. (96) and (97).

The corresponding formulas for the slightly deformed sphere, Eq. (64), are (B23)

$$\mathfrak{S}_R^{(F)} = \varepsilon \frac{2\pi}{7} a^2 \nabla \nabla \nabla (r^3 f_3) + O(\varepsilon^2) \quad (115)$$

and

$$\mathfrak{S}_R^{(T)} = \varepsilon 2\pi a^3 [\boldsymbol{\varepsilon} \cdot \nabla \nabla (r^2 f_2) + \{\boldsymbol{\varepsilon} \cdot \nabla \nabla (r^2 f_2)\}^\dagger] + O(\varepsilon^2) \quad (116)$$

Alternatively, in invariant form,

$$\mathfrak{S}_R^{(F)} = \frac{15}{8} \left( \frac{3S}{V} \right)^2 \int_S d\mathbf{S} \cdot \mathbf{r} \mathbf{r} \mathbf{r} \mathbf{r} + O(\varepsilon^2) \quad (117)$$

$$\mathfrak{S}_R^{(T)} = \frac{5}{2} \left( \frac{3S}{V} \right)^2 \left[ \boldsymbol{\varepsilon} \cdot \int_S \mathbf{r} \mathbf{r} \mathbf{r} \cdot d\mathbf{S} + \left( \boldsymbol{\varepsilon} \cdot \int_S \mathbf{r} \mathbf{r} \mathbf{r} \cdot d\mathbf{S} \right)^\dagger \right] + O(\varepsilon^2) \quad (118)$$

where  $\mathbf{r}$  is measured from the centroid.

To illustrate the application of these relations, consider the force experienced by the ovoid body of revolution

$$r = a[1 + \varepsilon P_3(\cos \theta)]$$

when immersed in a uniform simple shearing flow with streamlines instantaneously parallel to its symmetry axis, the velocity being zero at its centroid (see Fig. 1). Here,

$$P_3(\cos \theta) = \frac{1}{2}(5 \cos^3 \theta - 3 \cos \theta)$$

is the Legendre polynomial of order 3. This body lacks fore-aft symmetry. As stated following Eq. (68), the center of reaction of any slightly deformed sphere coincides with its centroid to at least  $O(\varepsilon)$  (B21). Let the positive  $Rx_1$  axis point from the blunted pole of the ovoid to its pointed end, as in Fig. 1, and set  $\cos \theta = x_1/r$ , where  $\mathbf{r} = \mathbf{e}_1 x_1 + \mathbf{e}_2 x_2 + \mathbf{e}_3 x_3$  is measured from  $R$ . This makes  $\varepsilon \geq 0$ . The uniform simple shearing flow is taken to be

$$\mathbf{u} = \mathbf{e}_1 x_3 S$$

with  $S \geq 0$ . The orthogonal triad of unit vectors  $\mathbf{e}_1, \mathbf{e}_2, \mathbf{e}_3$  are to be right handed in their natural order and of such a nature that the positive  $Rx_2$  axis points in the direction of the vorticity vector,  $\nabla \times \mathbf{u}$ . In the present case we have that  $\mathbf{U}_R - \mathbf{u}_R = \mathbf{0}$  and, from Eq. (67),  $\mathbf{K}_R^{(e)} = O(\varepsilon^2)$ . Thus, according to Eq. (109), the body experiences a force

$$\mathbf{F} = -\mu \mathfrak{S}_R^{(F)} : \mathbf{S} + O(\varepsilon^2)$$

But

$$r^3 f_3 = r^3 P_3 = \frac{1}{2}(5x_1^3 - 3r^2 x_1)$$



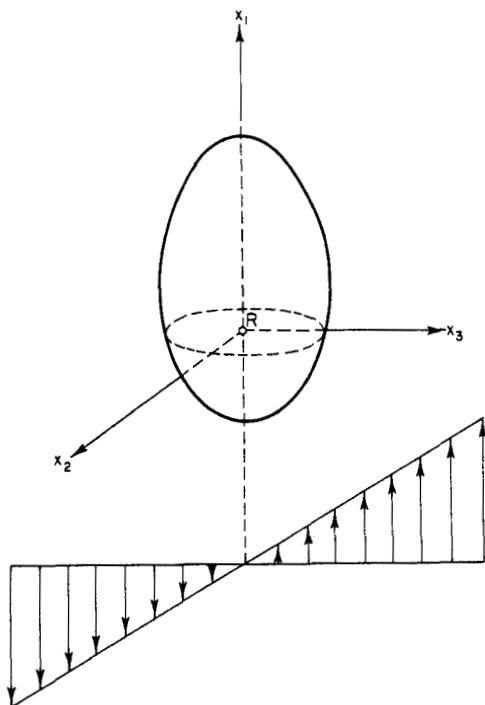


FIG. 1. Simple shear flow parallel to the axis of an ovoid body of revolution.

Hence, from Eq. (115),

$$\mathfrak{G}_R^{(F)} = \varepsilon \frac{6\pi}{7} a^2 [5\mathbf{e}_1\mathbf{e}_1\mathbf{e}_1 - \{\mathbf{I}\mathbf{e}_1 + (\mathbf{I}\mathbf{e}_1)^\dagger + \mathbf{e}_1\mathbf{I}\}] + O(\varepsilon^2)$$

Furthermore, from Eq. (108),

$$\mathbf{S} = \frac{1}{2}S(\mathbf{e}_3\mathbf{e}_1 + \mathbf{e}_1\mathbf{e}_3)$$

The body thus experiences a lift force

$$\mathbf{F} = \mathbf{i}_3 \frac{6\pi}{7} \varepsilon \mu a^2 S + O(\varepsilon^2)$$

at right angles to both the streamlines and vortex lines, in the sense shown in Fig. 1. This calculation agrees with a result of Bretherton (B30), obtained from a detailed solution of the equations of motion for the ovoid body.

A systematic investigation of the reduction in the number and type of independent components of the shear-force and torque triadics is presented by Brenner (B23) for particles possessing some common types of geometric

symmetry. These properties might have been more simply obtained directly from the symmetry properties of the original symbolic force and torque operators. It is found, for example, that a body of revolution (about the  $Rx_1$  axis, say) possessing fore-aft symmetry is characterized by a *single* scalar coefficient, in accordance with the relations  $\overset{(F)}{\mathfrak{S}}_R = 0$  and

$$\overset{(T)}{\mathfrak{S}}_R = [\boldsymbol{\varepsilon} \cdot \mathbf{e}_1 \mathbf{e}_1 + (\boldsymbol{\varepsilon} \cdot \mathbf{e}_1 \mathbf{e}_1)^\dagger] \mathfrak{S} \quad (119)$$

where  $\mathbf{e}_1$  is a unit vector parallel to the axis of revolution and  $\mathfrak{S}$  is a scalar.

The contrast in behavior between the force and torque triadics depends on the fact that the former is a true tensor whereas the latter is a pseudotensor. If the particle under consideration is either spherically or helicoidally isotropic then  $\overset{(\cdot)}{\mathfrak{S}}_R$  must be a scalar or pseudoscalar multiple of the alternator  $\boldsymbol{\varepsilon}$ , for the latter is the only isotropic third-rank tensor (A5). But, since  $\mathbf{S}$  is a symmetric dyadic,  $\boldsymbol{\varepsilon} : \mathbf{S}$  vanishes identically. Hence, neither the shear-force nor shear-torque triadics can contribute to the force or torque on the particle. Both may therefore be taken to be identically zero, in agreement with a more formal analysis (B23).

Though relations of the form (109) and (110) are merely special cases of the more general symbolic operator relations (81) and (82), they may also be regarded as phenomenological equations in their own right. The polyadic resistance coefficients appearing therein can, at least in principle, be determined experimentally from appropriate measurements of the hydrodynamic forces and torques for an appropriate number of orientations of the particle relative to the principal axes of dilatation of the fluid motion.

The hydrodynamic force and torque on a homogeneous, neutrally buoyant body vanish, providing that the motion is sufficiently slow. Equations (109) and (110) then yield for the translational and angular slip velocities (B23)

$$\mathbf{U}_O - \mathbf{u}_O = - \left[ \left( \overset{(t)}{\mathbf{K}} - \overset{(c)}{\mathbf{K}}_O^\dagger \cdot \overset{(r)}{\mathbf{K}}_O^{-1} \cdot \overset{(c)}{\mathbf{K}}_O \right)^{-1} \cdot \left( \overset{(F)}{\mathfrak{S}}_O - \overset{(c)}{\mathbf{K}}_O^\dagger \cdot \overset{(r)}{\mathbf{K}}_O^{-1} \cdot \overset{(T)}{\mathfrak{S}}_O \right) \right] : \mathbf{S} \quad (120)$$

$$\boldsymbol{\omega} - \boldsymbol{\omega}_f = - \left[ \left( \overset{(r)}{\mathbf{K}}_O - \overset{(c)}{\mathbf{K}}_O \cdot \overset{(t)}{\mathbf{K}}^{-1} \cdot \overset{(c)}{\mathbf{K}}_O^\dagger \right)^{-1} \cdot \left( \overset{(T)}{\mathfrak{S}}_O - \overset{(c)}{\mathbf{K}}_O \cdot \overset{(t)}{\mathbf{K}}^{-1} \cdot \overset{(F)}{\mathfrak{S}}_O \right) \right] : \mathbf{S} \quad (121)$$

The constant triadic and pseudotriadic in square brackets are intrinsic resistance coefficients. Furthermore, the latter is independent of choice of origin, as can be seen from the fact that  $\boldsymbol{\omega} - \boldsymbol{\omega}_f$  and  $\mathbf{S}$  are. These relations show that an anisotropic, neutrally buoyant particle immersed in a shear flow is, in general, unable to follow the local fluid motion. Rather, linear and angular slip must obtain.

It follows, upon substituting Eqs. (60) and (113) into (120), that a neutrally buoyant ellipsoidal particle is carried along with the flow; that is,  $\mathbf{U}_R = \mathbf{u}_R$ . Furthermore, as shown by Jeffery (J4), and as follows from integration of (121), a homogeneous ellipsoid of revolution in a uniform, simple shear flow moves in a closed, periodic orbit relative to an observer translating with the particle. Jeffery's theoretical calculation of the orbit is accurately confirmed by the experimental work of Mason and co-workers (F7, G8, M5) using spheres, circular disks, fused spherical doublets, and circular rods, though for long rods it was found necessary to introduce an "equivalent length" to account for the fact that the experimental period of rotation was only one-half to three-quarters that predicted by Jeffery's relationships. Bretherton (B30) has pointed out that the latter two bodies behave like ellipsoids of revolution with respect to their motion in a Couette flow. Based essentially on Eqs. (120) and (121), Bretherton (B30) has also shown that there exist exceptional shapes, including bodies of revolution of large aspect ratio, which behave very differently in such flows. They do not undergo periodic motion, but rather directly take up one of two opposite stable orientations and, remaining in that orientation, migrate across the streamlines towards the walls of the apparatus or to the center of the flow. Questions of permanent orientations of this type are utilized by Ericksen (E2) in connection with models of the non-Newtonian behavior displayed by "anisotropic fluids." Application of Eq. (121) to other models of non-Newtonian behavior is discussed by Giesekus (G4, G5a).

*b. Liquid Droplets.* The behavior of *deformable* bodies in shear and related flows is very different from that of rigid bodies. In particular, the shape of a neutrally buoyant immiscible liquid droplet immersed in a continuous liquid undergoing shear is not governed solely by the bulk and interfacial properties of the two phases, but depends also upon the rate of shear. Accordingly, the shape of the boundary must be determined simultaneously along with the detailed solution for the inner and outer fluid motions. Thus, despite the linearity of Stokes equations, the problem is intrinsically nonlinear. Upon expressing the equations of motion and boundary conditions in terms of non-dimensional variables, it is readily shown that the surface of the droplet is expressible in the following general form:

$$\mathbf{r}/a = \text{function}(\mu a \mathbf{S}/\gamma, \eta)$$

where  $\mathbf{r}$  is the position vector of a point on the surface of the droplet (relative to, say, an origin at the centroid of the deformed drop),  $a$  is the radius of a sphere having the same volume as the deformed droplet,  $\gamma$  is the equilibrium interfacial tension,  $\mu$  is the continuous-phase viscosity, and  $\eta$  is the ratio of droplet to continuous-phase viscosity. Because of the nonlinearity, the preceding functional relationship has never been established in its full generality.

Taylor (T1b, T2) has, however, obtained first-order perturbation solutions valid for two limiting cases.

For the case where the interfacial forces dominate those due to viscosity, Taylor (T2) found that the surface of the droplet is described by the equation of the slightly deformed sphere<sup>13</sup>

$$\frac{1}{a^2} \left( \mathbf{I} - \frac{4\mu a}{\gamma} \frac{19\eta + 16}{16\eta + 16} \mathbf{S} \right) : \mathbf{r}\mathbf{r} + o(\varepsilon) = 1 \quad (122a)$$

for sufficiently small values of the deformation parameter  $\varepsilon = \mu a \bar{S} / \gamma$ . Here,  $\bar{S} = (\mathbf{S} : \mathbf{S})^{1/2}$  is the intensity of the shear. To the first order in the deformation the droplet is therefore ellipsoidal, its principal axes coinciding with the principal axes of dilatation, i.e., of  $\mathbf{S}$ . To this approximation the departure from the spherical shape is proportional to the rate of strain. Equation (122a) applies to any incompressible flow, provided that  $\mathbf{S}$  is interpreted as the *local* rate of strain of the unperturbed flow (C2, C3); that is, the shear need not be uniform. For a simple uniform shear flow the principal axes of dilatation are inclined at an angle of  $45^\circ$  with respect to the streamlines; hence, the principal axes of the droplet are equally inclined relative to the streamlines. Equation (122a) was experimentally confirmed for Couette and hyperbolic shear flows by Taylor (T2) and, more accurately, by Rumscheidt and Mason (R9) for  $\eta < 10$  (approx.), and by Goldsmith and Mason (G9) for Poiseuille flows. For values of the deformation parameter  $\varepsilon$  greater than about 0.2, significant departure from the linear relation (122a) was observed in most cases. The droplets burst at about  $\varepsilon = 0.5$ , in good agreement with Taylor's (T1b) qualitative prediction, this being approximately the point at which the viscous forces tending to stretch the drop exceed the interfacial forces tending to maintain its integrity. Beyond the effective linear range the drop shape depends nonlinearly on the shear  $\mathbf{S}$ . The shape of the drop just prior to bursting is therefore different for different nonuniform shear flows (and, of course, for different viscosity ratios). Rumscheidt and Mason (G9) noted a large variety of differently shaped drops prior to bursting.

Taylor (T2) also treated the other extreme case where  $\varepsilon \rightarrow \infty$ , but only for the special case of the "very viscous drop"—that is,  $\eta^{-1} \rightarrow 0$ . When  $\varepsilon$  is large the viscous forces greatly exceed the interfacial forces, and Taylor ignores the latter as a first approximation. The shape of the droplet is then only a function of the viscosity ratio. For a simple uniform shear, Taylor finds, on

<sup>13</sup> In polar form the equation of this slightly deformed sphere is

$$r = a \left[ 1 + \frac{2\mu a}{\gamma} \frac{19\eta + 16}{16\eta + 16} \frac{\mathbf{S} : \mathbf{r}\mathbf{r}}{r^2} + o\left(\frac{\mu a \bar{S}}{\gamma}\right) \right]$$

the assumption that the droplet departs but little from the spherical shape, that the droplet is ellipsoidal—its major axis being parallel to the streamlines of the unperturbed flow. The equation of the droplet surface projected onto the plane containing the shear is

$$r/a = 1 + \frac{5}{4}\eta^{-1} \cos 2\phi + o(\eta^{-1}) \quad (122b)$$

where the angle  $\phi = 0^\circ$  lies parallel to the direction of the streamlines. The experiments of Taylor (T2) and Rumscheidt and Mason (R9) only approximately confirmed this result at the larger  $\eta$  values [ $\eta > 5$  (approx.)] in the linear range. Above this range the droplets did not burst, but rather were elongated into long filaments in the Couette apparatus. These droplets did, however, burst in the “four-roller” apparatus, where the shear was hyperbolic rather than uniform.

Though agreement with experiment seems rather good, further theoretical analysis is obviously required to fix the ranges of validity of Eqs. (122a) and (122b). This is especially true in the very viscous droplet problem. One is dealing here with a two-parameter problem; and as is true for all such problems, the range of applicability is not fixed merely by requiring that the two parameters  $\varepsilon^{-1}$  and  $\eta^{-1}$  each be small. For the quantity  $\varepsilon^{-1}/\eta^{-1}$  (or some variation thereof) may then be either small or large, depending upon experimental circumstances; and it seems highly unlikely that one formula could correctly describe all possible limiting cases. It thus appears that Taylor's analysis applies only to the case where  $\varepsilon^{-1} \ll \eta^{-1} \ll 1$ .

### 3. Wall-Effects

Though wall-effects are rarely important in industrial-size equipment they are important in small-scale laboratory apparatus. Indeed, because of the relatively large wall-effects in Stokes flows it is difficult to perform experiments which are free of such effects. A sphere falling along the axis of circular tube whose cross sectional area is 100 times that of the sphere settles at less than 75 percent of the velocity it would achieve in an unbounded fluid. Even with a 10,000 : 1 cross sectional area ratio the settling velocity is decreased by more than 2 percent. As a consequence, wall-effects have been extensively studied in the Stokes regime. In this section we shall examine some general principles and results pertaining to such effects. Attention is again restricted to quasi-static motions.

Consider a solid particle of arbitrary shape settling in a container of any shape which partially or completely bounds the fluid externally. If it does not wholly bound the fluid, it is assumed in the subsequent discussion either that the fluid extends to an effectively infinite distance from the particle (e.g., an

infinite or semi-infinite circular cylinder) or else that a planar free surface exists at a finite distance from the body. In short, the general theory depends upon the condition that no work is done by the fluid stresses at the apparatus boundaries. Under these circumstances Eqs. (38) and (39) continue to describe the instantaneous hydrodynamic force and torque on a particle moving through an otherwise quiescent fluid (B22). The three resistance dyadics remain independent of  $\mu$ ,  $U_0$ , and  $\omega$ . However, they are no longer intrinsic properties of the particle alone, but now also depend upon the geometrical configuration of the boundary wetted by the fluid, as well as upon the instantaneous orientation and position of the particle relative to these boundaries. They are, nevertheless, purely geometric parameters. With this reservation the entire general theory outlined in Section II,C,1 up to and including Eq. (55), remains valid, providing that we supplement the definition of the intrinsic translational and rotational fields with the additional boundary conditions appropriate to the fluid at the container boundaries. In the presence of boundaries, the point at which the coupling dyadic is symmetric does not generally coincide with the center of reaction of the particle in an unbounded fluid.

There exist few particle-boundary combinations for which the *particle-boundary resistance dyadics* in Eqs. (38) and (39) are known for all physically possible particle-to-wall dimensions. They are known, for example, for the trivial case of a spherical particle at the center of a concentric spherical boundary, the space between them being filled with fluid.<sup>14</sup> The translation and rotation dyadics for this case are clearly isotropic, while the coupling dyadic obviously vanishes at this common center.

Fortunately, in most practical investigations, such complete information is unnecessary. Rather, it usually suffices to know only certain components of these dyadics, and then only in limiting cases. If  $a/l$  represents a characteristic particle-to-wall dimension ratio, these limiting cases correspond to the extreme cases where  $a/l$  is either very small or very near unity. In the former case the method of "reflections" (cf. H9) provides a useful technique for obtaining the wall correction. In the latter case, corresponding to the situation where the particle is extremely close to the wall, lubrication-theory type approximations (B7, B29, C11, D7, G5d, H15, K8, M9, M10, S8) normally suffice to obtain the required correction. Intermediate cases are rarely of interest.

As a case in point consider a spherical particle of radius  $a$  at the axis of an infinitely long circular cylinder of radius  $l$ . If we choose the origin ( $R$ ) at the sphere center and let  $\mathbf{e}_1$  be a unit vector parallel to the cylinder axis,

<sup>14</sup> The force on the inner sphere for the translational case is given independently by Cunningham (C21), Haberman and Sayre (H3), and Williams (W8), though the first-mentioned reference contains a typographical error. The torque on the inner sphere for the rotational case is given by Lamb (L5, p. 589).

it is clear on symmetry grounds that

$$\mathbf{K}^{(t)} = \mathbf{e}_1 \mathbf{e}_1 K_{\parallel}^{(t)} + (\mathbf{I} - \mathbf{e}_1 \mathbf{e}_1) K_{\perp}^{(t)} \quad (123)$$

$$\mathbf{K}_R^{(r)} = \mathbf{e}_1 \mathbf{e}_1 K_{\parallel}^{(r)} + (\mathbf{I} - \mathbf{e}_1 \mathbf{e}_1) K_{\perp}^{(r)} \quad (124)$$

$$\mathbf{K}_R^{(c)} = \mathbf{0} \quad (125)$$

The components of primary interest are the parallel components,  $K_{\parallel}^{(t)}$  and  $K_{\parallel}^{(r)}$ , for these give the force and torque on the sphere when it translates along the axis and rotates about this axis, respectively.

In the translational case the method of reflection yields (see B8, H3, and references to earlier papers given therein), to the lowest degree of approximation,

$$K_{\parallel}^{(t)} = \frac{6\pi a}{1 - 2.10444(a/l) + O(a/l)^3} \quad (126)$$

for small  $a/l$ . For  $a/l$  near unity an elementary lubrication-theory treatment yields (M10)

$$K_{\parallel}^{(t)} = 6\pi a \frac{3\pi\sqrt{2}/8}{(1 - a/l)^{5/2}} \quad (127)$$

The former of these results agrees quite accurately with the "exact" solution (B8, H3) and with experimental data up to  $a/l \approx 0.2$  (cf. H3). Equation (127) also agrees well with experiment for  $a/l > 0.95$  (M10).

Similarly, in the rotational case, we have in the two extreme limits (B29, H1)

$$K_{\parallel}^{(r)} = \frac{8\pi a^3}{1 - 0.79682417(a/l)^3 + O(a/l)^{10}} \quad (128)$$

and, as  $a/l \rightarrow 1$  (B29),<sup>15</sup>

$$K_{\parallel}^{(r)} = 8\pi a^3 \frac{\pi}{2(a/l)^2} \left[ \frac{1}{\{1 - (a/l)^2\}^{1/2}} - 1 \right] \quad (129)$$

These both agree remarkably well with the "exact" solution (B29), as can be

<sup>15</sup> This is an even better approximation than the one derived in the original paper (B29). It is obtained by utilizing the velocity field generated by the relative rotation of two coaxial circular cylinders of radii  $a$  and  $l$ , rather than utilizing the velocity field generated by the shearing motion of two parallel planes separated by a distance  $l - a$ , as was done originally. D. L. Ripps pointed out this improvement to me.

seen from Table I, in which is tabulated the ratio of the torque  $T$  on the sphere to the torque  $T_\infty$  in the unbounded fluid under otherwise identical conditions.

TABLE I  
WALL-EFFECT FOR THE TORQUE ON A SPHERE ROTATING ABOUT THE AXIS OF A  
CIRCULAR CYLINDER<sup>a</sup>

| $a/l$ | $T/T_\infty$                  |   |   |
|-------|-------------------------------|---|---|
|       | Exact solution,<br>Ref. (B29) | First reflection<br>approximation,<br>Eq. (128) | Lubrication theory<br>approximation,<br>Eq. (129) |
| 0     | 1                             | 1   | —   |
| 0.1   | 1.0007975                     | 1.0007975                                       | —   |
| 0.2   | 1.0064155                     | 1.0064154                                       | —   |
| 0.3   | 1.0219877                     | 1.0219872                                       | —   |
| 0.4   | 1.0537442                     | 1.053737  | —   |
| 0.5   | 1.1106942                     | 1.11062   | —   |
| 0.6   | 1.2084380                     | 1.2078  | —   |
| 0.7   | 1.3795032                     | 1.376   | —   |
| 0.8   | 1.7101933                     | 1.69  | —   |
| 0.85  | 2.0145515                     | 1.96  | —   |
| 0.9   | 2.5567226                     | —   | 2.51  |
| 0.95  | 3.8610279                     | —   | 3.83  |
| 0.975 | 5.7962397                     | —   | 5.784   |
| 0.99  | 9.75569                       | —   | 9.758   |
| 0.995 | 14.288                        | —   | 14.299  |
| 0.999 | 33.5                          | —   | 33.63   |
| 1     | $\infty$                      | —   | $\infty$  |

$$^a |T_\infty| = 8\pi\mu a^3\omega.$$

Similar agreement exists for the quasi-steady approach of a sphere towards a rigid plane wall. If  $F$  is the force on the sphere of radius  $a$ , and  $h$  is the distance from the sphere center to the wall, the exact solution, valid for all  $a/h$ , is (B14, M6)

$$\frac{|F|}{6\pi\mu aU} = \sigma = \frac{4}{3} \sinh \alpha \sum_{n=1}^{\infty} \frac{n(n+1)}{(2n-1)(2n+3)} \times \left[ \frac{2 \sinh(2n+1)\alpha + (2n+1) \sinh 2\alpha}{4 \sinh^2(n+\frac{1}{2})\alpha - (2n+1)^2 \sinh^2 \alpha} - 1 \right] \quad (130)$$

where the parameter  $\alpha$  is defined as

$$\cosh \alpha = h/a \quad (131)$$



In the limit  $a/h \rightarrow 0$ , a straightforward expansion of the hyperbolic functions for large values of  $\alpha$  yields

$$\sigma = \frac{1}{1 - (9/8)(a/h) + O(a/h)^3} \quad (132)$$

This accords with the original result of Lorentz (L11), obtained by employing a first reflection.<sup>16</sup> In the opposite case, where the sphere is very near the wall, i.e.,  $a/H \rightarrow \infty$  (where  $H = h - a$ ), one finds from (131) that  $\alpha^2 \rightarrow 2H/a$ . Upon expansion of all the hyperbolic functions in (130) for small  $\alpha$ , one obtains

$$\sigma \rightarrow \frac{64}{\alpha^2} \sum_{n=1}^{\infty} \frac{n(n+1)}{(2n-1)^2(2n+1)(2n+3)^2}$$

The sum over  $n$  may be performed by the following artifice. By identity

$$\begin{aligned} \frac{n(n+1)}{(2n-1)^2(2n+1)(2n+3)^2} &= \frac{1}{64} \left[ \frac{1}{(2n-1)(2n+1)} - \frac{1}{(2n+1)(2n+3)} \right] \\ &\quad + \frac{3}{128} \left[ \frac{1}{(2n-1)^2} - \frac{1}{(2n+3)^2} \right] \end{aligned}$$

But

$$\begin{aligned} \sum_{n=1}^{\infty} \frac{1}{(2n-1)(2n+1)} - \sum_{n=1}^{\infty} \frac{1}{(2n+1)(2n+3)} &= \left( \frac{1}{1 \cdot 3} + \frac{1}{3 \cdot 5} + \frac{1}{5 \cdot 7} + \cdots \right) \\ &\quad - \left( \frac{1}{3 \cdot 5} + \frac{1}{5 \cdot 7} + \cdots \right) = \frac{1}{1 \cdot 3} \end{aligned}$$

and

$$\begin{aligned} \sum_{n=1}^{\infty} \frac{1}{(2n-1)^2} - \sum_{n=1}^{\infty} \frac{1}{(2n+3)^2} &= \left( \frac{1}{1^2} + \frac{1}{3^2} + \frac{1}{5^2} + \frac{1}{7^2} + \cdots \right) \\ &\quad - \left( \frac{1}{5^2} + \frac{1}{7^2} + \cdots \right) = \frac{1}{1^2} + \frac{1}{3^2} \end{aligned}$$

Hence, when the sphere is very near the wall

$$\sigma \rightarrow a/H \quad (133a)$$

This result is identical to that obtained from a conventional lubrication-theory approximation (M1), based on the flow field generated when two parallel plane approach one another (L6). The general formula (130) is in excellent agreement, over the entire  $a/h$  range, with the experimental results of MacKay *et al.* (M1, M2).

<sup>16</sup> Lorentz's general scheme for solving boundary-value problems involving plane walls has been rederived by Maude (M7), apparently unaware of the original work.

Conventional lubrication-theory methods may be regarded as furnishing only the leading term in an asymptotic expansion of the exact solution of the problem. Progress has recently been made (C19) in the formulation of a general theory leading to higher-order terms in the expansion. Singular perturbation methods requiring the formation of inner and outer expansions (cf. Section III,C) are involved, the inner expansion being valid near the point of contact between the particle and wall. The results take the form of an asymptotic expansion in a small, nondimensional clearance parameter. For example, for a sphere approaching a plane wall, Eq. (133a) is replaced by

$$\sigma = \left(\frac{H}{a}\right)^{-1} \left[ 1 - \frac{1}{5} \frac{H}{a} \ln \frac{H}{a} + O\left(\frac{H}{a}\right) \right] \quad (133b)$$

if the quasi-static Stokes equations are regarded as the governing equations of motion. This equation is asymptotically valid as  $H/a \rightarrow 0$ . Small inertial effects may also be incorporated into the singular perturbation analysis (C19), in which case the solution takes the form of a double expansion in two small parameters—a dimensionless gap width and an appropriate Reynolds number based on gap width. Thus, when the complete Navier–Stokes equations (including *unsteady-state* terms) are applied to the motion of a sphere towards a plane wall, Eq. (133b) is replaced by

$$\sigma = \left(\frac{H}{a}\right)^{-1} \left[ 1 - \left( \frac{1}{5} \frac{H}{a} + \frac{19}{5} R \right) \ln \frac{H}{a} + \dots \right] \quad (133c)$$

where  $R = HU\rho/\mu$ . The above expansion is valid for  $H/a \ll 1$  and  $R \ll 1$ , it further being supposed that  $R(H/a)^{-1} = aU\rho/\mu$  is of order unity with respect to the parameter  $H/a$ ; that is, the solution is asymptotically valid in the limit as  $H/a \rightarrow 0$  with  $aU\rho/\mu$  fixed.

The validity of Eq. (133b) [including an explicit calculation of the coefficient ( $= 0.804597$ ) of the term of  $O(H/a)$  within the brackets] was independently confirmed (C19) by including higher-order terms in the expansion of Eq. (130) leading to Eq. (133a). The resulting sum over  $n$  is itself highly singular, and requires the formation of “inner” and “outer” portions; for no matter how small  $\alpha$  may be,  $n\alpha$  will not be small for sufficiently large  $n$ .

When  $a/l$  is small it is possible to obtain a general expression for the effect of boundaries on the quasi-static force and torque experienced by a translating-rotating particle of arbitrary shape in a fluid which is otherwise at rest (B16, B20, C20). This relation takes the form

$$\begin{pmatrix} \mathbf{F} \\ \mathbf{T}_o \end{pmatrix} = \begin{pmatrix} \mathbf{F}^\infty \\ \mathbf{T}_o^\infty \end{pmatrix} + \begin{pmatrix} {}^{(t)}\mathbf{K}^\infty \\ {}^{(c)}\mathbf{K}_o^\infty \end{pmatrix} \cdot \mathbf{W}_o \cdot \mathbf{F}^\infty + O\left(\frac{a}{l}\right)^2 \quad (134a)$$

$$(134b)$$

Here,  $\mathbf{F}^\infty$  and  $\mathbf{T}_O^\infty$  refer to the force and torque (about the arbitrary point  $O$ ) experienced by the particle in the *unbounded* fluid when it translates and rotates with the same velocities  $\mathbf{U}_O$  and  $\boldsymbol{\omega}$  as in the bounded fluid, the orientation of the particle being the same for the two cases. The quantities  $\overset{(t)}{\mathbf{K}}^\infty$  and  $\overset{(c)}{\mathbf{K}}_O^\infty$  are the translation and coupling dyadics for the particle in the unbounded fluid. Also,  $\mathbf{W}_O$  is the wall-effect dyadic (B20, C20) evaluated at the point in the fluid presently occupied by  $O$ . In general,  $\mathbf{W}_O$  is a constant, *symmetric* dyadic which depends only upon the size and shape of the boundaries and upon the location of  $O$  relative to the bounding walls. In particular,  $\mathbf{W}_O$  is independent of  $\mu$ ,  $\mathbf{U}_O$ ,  $\boldsymbol{\omega}$ , of the size and shape of the particle, and of the orientation of the particle relative to the boundaries. At each point  $O$  in space it is, therefore, an intrinsic geometric property of the container boundaries alone. Inasmuch as  $\overset{(t)}{\mathbf{K}}^\infty = O(a)$ ,  $\overset{(c)}{\mathbf{K}}_O^\infty = O(a^2)$ ,  $\mathbf{W}_O = O(l^{-1})$  and  $\mathbf{T}_O^\infty = O(aF^\infty)$ , Eq. (134) furnishes an expression for the wall-effect correctly to terms of  $O(a/l)$ . Thus, the significance of Eq. (134) lies in the fact that to this order the wall correction factor is divided into *separate* contributions from the particle and boundary. Equations (134a)–(134b) are equivalent to the three relations

$$\begin{aligned}\overset{(t)}{\mathbf{K}} &= \overset{(t)}{\mathbf{K}}^\infty + \overset{(t)}{\mathbf{K}}^\infty \cdot \mathbf{W}_O \cdot \overset{(t)}{\mathbf{K}}^\infty + O(a/l)^2 \\ \overset{(r)}{\mathbf{K}}_O &= \overset{(r)}{\mathbf{K}}_O^\infty + \overset{(c)}{\mathbf{K}}_O^\infty \cdot \mathbf{W}_O \cdot \overset{(c)}{\mathbf{K}}_O^{\infty\dagger} + O(a/l)^2 \\ \overset{(c)}{\mathbf{K}}_O &= \overset{(c)}{\mathbf{K}}_O^\infty + \overset{(c)}{\mathbf{K}}_O^\infty \cdot \mathbf{W}_O \cdot \overset{(t)}{\mathbf{K}}^\infty + O(a/l)^2\end{aligned}\quad (134c)$$

where the  $\mathbf{K}$ 's without the superscript  $\infty$  refer to the values in the bounded fluid. Note that  $\overset{(t)}{\mathbf{K}}$  and  $\overset{(r)}{\mathbf{K}}_O$  are symmetric, as they should be.

For some commonly occurring types of geometric symmetry, Eq. (134a) applied to a body translating without rotation can be expressed in the more accurate form

$$\mathbf{F} = \left[ \mathbf{I} - \overset{(t)}{\mathbf{K}}^\infty \cdot \mathbf{W}_O \right]^{-1} \cdot \mathbf{F}^\infty + O(a/l)^3 \quad (134d)$$

which is equivalent to the relation

$$\overset{(t)}{\mathbf{K}} = \left[ \mathbf{I} - \overset{(t)}{\mathbf{K}}^\infty \cdot \mathbf{W}_O \right]^{-1} \cdot \overset{(t)}{\mathbf{K}}^\infty + O(a/l)^3 \quad (134e)$$

These more accurate formulas apply irrespective of the shape of the particle if, for example, the boundary possesses three mutually perpendicular symmetry planes intersecting at  $O$ . This occurs if the (point  $O$  fixed in the) particle translates along the axis of a circular cylinder or midway between two parallel planes (W8a). The more accurate formulas are also applicable to completely

asymmetric boundaries if, for example, the particle possesses three mutually planes of reflection symmetry intersecting at  $O$ , e.g., a sphere or ellipsoid with center at  $O$  (W8a).

By way of example, the wall-effect dyadic for a solid plane wall bounding a semi-infinite fluid domain is (B20)

$$\mathbf{W}_o = [\mathbf{e}_1 \mathbf{e}_1 2 + (\mathbf{I} - \mathbf{e}_1 \mathbf{e}_1)] \frac{9}{16l}$$

where  $\mathbf{e}_1$  is a unit vector normal to the wall and  $l$  is the perpendicular distance from the wall to the point  $O$  fixed in the particle. The comparable expression for a planar *free surface* is (B20)

$$\mathbf{W}_o = [\mathbf{e}_1 \mathbf{e}_1 2 - (\mathbf{I} - \mathbf{e}_1 \mathbf{e}_1)] \frac{3}{8l}$$

The utility of (134a) is most simply seen by considering the highly symmetrical case where one of the principal axes of translation of the particle lies parallel to a principal axis of the wall dyadic. In this case (134a) is equivalent to the scalar relation (B16)

$$\frac{F}{F_\infty} = \frac{1}{1 - \underline{W}_o \frac{|F_\infty|}{6\pi\mu U l} + o\left(\frac{a}{l}\right)} \quad (135)$$

where  $F$  is the hydrodynamic force on the particle in the bounded medium when it moves with speed  $U$ , and  $F_\infty$  is the force on the particle when it moves with the same speed and orientation (relative to  $\mathbf{U}$ ) in the unbounded medium. The nondimensional scalar  $\underline{W}_o$  is one of the *specific*, normalized eigenvalues of  $\mathbf{W}_o$ . This scalar has been made into an intensive property, independent of the *size* of the boundaries, by setting  $\underline{W}_o = lW_o$ . The wall dimension  $l$  may be chosen arbitrarily. The extraneous factor of  $6\pi$  is included merely to give the equation a simple form for spherical particles. In the important case of a particle translating along the axis of a long circular cylinder of radius  $l$ ,  $\underline{W}_o = 2.10444$ , as follows from Eq. (126) by observing that  $|F_\infty|/6\pi\mu U = a$  for a spherical particle of radius  $a$ . An independent proof for this case is given by Chang (C4).

In general, the error term in Eq. (135) will be  $O(a/l)^2$ . However, if the prevailing symmetry is such that Eq. (134d) applies, the error will only be  $O(a/l)^3$ .

Values of  $\underline{W}_o$  for other boundaries and various particle orientations relative to these boundaries are tabulated by Brenner (B16). In particular, for a particle falling at a fractional distance  $\beta = b/l$  ( $b$  = distance from center

of reaction of particle to cylinder axis) from the axis of a long circular cylinder,  $\underline{W}_0 = f(\beta)$  (B28).<sup>17</sup> For  $\beta \rightarrow 0$

$$f(\beta) = 2.10444 - 0.6977\beta^2 + O(\beta^4) \quad (136)$$

and for  $\beta \rightarrow 1$  (F1)

$$f(\beta) \rightarrow \frac{9}{16(1-\beta)} \quad (137)$$

provided that  $a/l$  and  $(1-\beta)^{-1}a/l$  are both small compared with unity. The coefficient  $9/16$  arises from Lorentz's (L11) formula for the fall of a sphere parallel to a *plane* wall when the sphere is small compared with its distance from the wall. Famularo (F1) has evaluated  $f(\beta)$  for intermediate values of  $\beta$  with results shown in Table II. Rather remarkably,  $f(\beta)$  does not change monotonically with  $\beta$  but possesses a minimum at  $\beta \approx 0.40$ . This then is the point at which a sufficiently small particle would settle with its greatest speed.

TABLE II  
DRAG ON AN ECCENTRICALLY POSITIONED PARTICLE IN A CIRCULAR CYLINDER;  
TABULATION OF  $f(\beta)$  VS  $\beta$

| $\beta$ | $f(\beta)$ | $\beta$ | $f(\beta)$ |
|---------|------------|---------|------------|
| 0       | 2.10444    | 0.40    | 2.04401    |
| 0.01    | 2.10436    | 0.41    | 2.04407    |
| 0.03    | 2.10381    | 0.43    | 2.04530    |
| 0.05    | 2.10270    | 0.45    | 2.04825    |
| 0.10    | 2.09763    | 0.50    | 2.06566    |
| 0.20    | 2.07942    | 0.60    | 2.16965    |
| 0.30    | 2.05691    | 0.70    | 2.45963    |
| 0.35    | 2.04805    | 0.80    | 3.2316     |
| 0.37    | 2.04567    | 0.90    | 5.905      |
| 0.39    | 2.04426    | 1       | $\infty$   |

In connection with terminal settling velocity experiments at the axis of a long circular cylinder, Eq. (135) may be written in the equivalent form

$$\frac{U_\infty}{U} = 1 + 2.10444 \frac{|F|}{6\pi\mu U l} + o\left(\frac{a}{l}\right) \quad (138)$$

where  $U_\infty$  and  $U$  are, respectively, the terminal settling speeds of the particle in the unbounded and bounded fluids for the same force  $F$ . Usually, one can

<sup>17</sup> Though Brenner and Happel (B28) did not consider the case where the particle rotated as it fell, the contribution of such rotation to the drag on the particle can be shown to be of smaller order than  $O(a/l)$  (B20); hence, it is negligible to the present degree of approximation.

measure directly the weight  $|F|$  of the particle corrected for the buoyancy of the fluid. From a *single* measurement of the settling velocity  $U$  in the cylinder one can therefore calculate what speed the same particle would have attained in the *unbounded* fluid, the orientation of the body relative to the direction of the gravitational field being the same in both cases. Equation (138) is in excellent agreement with a large body of experimental data (B16), and holds quite accurately even for  $a/l$  as large as 0.2,  $a$  being one-half the maximum linear dimension of the particle.

A formula comparable to Eq. (135) holds for the wall-effect experienced by rotating bodies (B16, B20). In the case of an axially symmetric body rotating symmetrically about the axis of a circular cylinder of radius  $l$ , the general formula reduces to

$$\frac{T}{T_\infty} = \frac{1}{1 - 0.79682417 \frac{|T_\infty|}{8\pi\mu\omega l^3} + o\left(\frac{a}{l}\right)^3} \quad (139)$$

where  $T$  and  $T_\infty$  are the respective torques in the bounded and unbounded fluids for the same angular speed  $\omega$ . [Compare with (128) for a spherical particle, bearing in mind that  $T_\infty = -8\pi\mu a^3\omega$ .] Since  $T_\infty = O(\mu\omega a^3)$  it follows that for small  $a/l$  the wall-effect is of  $O(a/l)^3$ . This is much less than for translating particles, where Eq. (135) shows the effect to be of  $O(a/l)$ . In general, Eq. (139) holds quite well, even for  $a/l$  as large as 0.5 (B29, B25).

Formulas of the type (135) apply even when more than one type of surface bounds the fluid. For a particle at the axis of a semi-infinitely long circular cylinder bounded below by the planar container bottom, Tanner (T1a) gives values of  $\underline{W}_0$  as a function of  $h_1/l$  ( $h_1$  = distance from particle to container bottom) based on an approximate, numerical solution of Stokes equations. In a similar context, an exact solution, obtained by the method of reflections, is available for the axially symmetric rotation of a small particle in a circular cylinder bounded below by the rigid container bottom and above by the planar free surface of the liquid (B25). The torque correction is presented in the form of Eq. (139) with the coefficient 0.7968 replaced by a more general rotational wall coefficient, *function*( $h_1/l, h_2/l$ ),  $h_1$  and  $h_2$  being measured from the center of the particle to the container bottom and free surface, respectively. Results are tabulated for the complete ranges  $0 < h_1/l < \infty$ ,  $0 < h_2/l < \infty$ . The techniques employed in solving this rotational wall-effect problem have recently been applied by Sonshine, Cox, and Brenner (S16) to the case of a nonskew particle *translating* parallel to a principal axis of translation along the axis of a circular cylinder of finite length possessing both a rigid bottom and a free surface. In addition to generalizing the results of

Tanner (T1a) the treatment is analytical rather than numerical. The results having important applications in falling-ball viscometry.

An extensive discussion and bibliography of further references to conventional wall-effects will be found in Happel and Brenner (H9). To this list should be added the theoretical study by Dean and O'Neill (D4) of the rotation of a sphere about an axis parallel to a nearby plane wall in an otherwise unbounded fluid, and a companion study by O'Neill (O2a) of the translation of a sphere parallel to a plane wall. Bipolar coordinates were employed to obtain exact solutions of the Stokes equations. These studies are particularly interesting in view of the fact that, due to the asymmetry of the flow, the rotating sphere experiences a force parallel to the wall whereas the translating sphere experiences a torque about the sphere center parallel to the wall. According to the remarks made in the second paragraph of Section II,C,3, these *cross effects* may be expressed in terms of the coupling dyadic in Eqs. (38) and (39) (where  $O$  refers to the sphere center). The Dean-O'Neill investigation permits computation of  $\overset{(c)}{\mathbf{K}}_O$  from Eq. (38), whereas the O'Neill study permits a comparable computation via Eq. (39). Though these independent methods should have yielded the same value for the coupling dyadic, they did not. This discrepancy prompted a detailed check (G5d) of their calculations, which revealed a numerical error in the Dean-O'Neill (D4) paper. After rectifying the error it was found that the two independent computations of  $\overset{(c)}{\mathbf{K}}_O$  did indeed agree.

The sphere-plane wall configuration represents one of the few nontrivial cases for which the particle-boundary resistance dyadics in Eqs. (38) and (39) are completely known. If  $\mathbf{e}_1$  is a unit vector normal to the plane then the translation and rotation dyadics are given by equations of the form (123) and (124), provided that  $R$  is replaced by  $O$ —the sphere center;  $\overset{(t)}{K}_\parallel$  is given as a function of  $a/h$  [see Eqs. (130)–(131)] by Brenner (B14) and Maude (M6);  $\overset{(t)}{K}_\perp$  by O'Neill (O2a);  $\overset{(r)}{K}_\parallel$  by Jeffery (J3); and  $\overset{(r)}{K}_\perp$  by Goldman, Cox, and Brenner (G5d) based on their corrected version of the Dean-O'Neill (D4) treatment. The comparable expression for the coupling dyadic at the sphere center is

$$\overset{(c)}{\mathbf{K}}_O = \boldsymbol{\varepsilon} \cdot \mathbf{e}_1 \overset{(c)}{K}$$

where  $\boldsymbol{\varepsilon}$  is the isotropic triadic. The scalar  $\overset{(c)}{K}$  is given as a function of  $a/h$  by O'Neill (O2a) and by Goldman, Cox, and Brenner (G5d).

With regard to wall effects in fluids undergoing net flow, Goldman, Cox, and Brenner (G5e), using bipolar coordinates, obtained an exact solution to the problem of a neutrally buoyant sphere near a single plane wall in a semi-infinite fluid undergoing simple shear. In an unbounded fluid the translational

velocity of the sphere center and angular velocity of the sphere are  $U_0 = Sh$  and  $\omega = \frac{1}{2}S$ , respectively, where  $S$  is the shear rate and  $h$  the distance from the wall to the sphere center. Corrections to these results due to the wall are given in terms of  $a/h$ . The method of solution is of interest in that the calculations of the force and torque were performed without having to solve the corresponding boundary-value problem. Rather, Eqs. (78)–(79) were employed, utilizing the rotational stress triadic  $\Pi_O^{(r)}$  gleaned from the bipolar coordinate solutions of Dean and O'Neill (D4; see the corrections to the latter given in Ref. G5d) and Jeffery (J3) for the rotation of a sphere near a plane wall in a quiescent fluid, and the translational stress triadic  $\Pi^{(t)}$  obtained from the comparable translational solutions given by O'Neill (O2a), and by Brenner (B14) and Maude (M6). The limiting case where the sphere approaches the wall ( $a/h \rightarrow 1$ ) is independently treated via a lubrication-theory analysis.

Calculation of wall-effects when the fluid undergoes net flow, as in Poiseuille flow through a long tube open at both ends and containing a suspended particle, may be carried out by utilizing Eqs. (81) and (82). These symbolic operator equations continue to be valid, even in the presence of rigid bounding walls (see the remarks in the second paragraph of the present subsection—which are pertinent here too), providing that the quasi-static Stokes approximation is applicable. For a nonscrew-like body (i.e.,  $\mathbf{K}_R^{(c)\infty} = \mathbf{0}$ ), or one which is not rotating, the hydrodynamic force on any solid particle is (B20)

$$\mathbf{F} = -\mu \mathbf{K}^{(t)} \cdot (\mathbf{U}_R - \mathbf{u}_R) + o(a/l) \quad (140)$$

where  $\mathbf{K}^{(t)}$  is given to the first order in  $a/l$  by Eq. (134c);  $\mathbf{u}_R$  refers to the value of the unperturbed flow field (e.g., the Poiseuille field) at the center of reaction of the particle. When sufficient particle-boundary symmetry is involved, this reduces to the same form as (135), the only modification required being the replacement of  $F_\infty$  in the left-hand side by  $F_\infty'$ , the infinite-medium force based on the *approach velocity*  $\mathbf{u}_R$  (B16); i.e., if  $U \neq 0$ ,

$$F_\infty' = F_\infty \left[ 1 - \frac{\mathbf{u}_R \cdot \mathbf{U}}{U^2} + o(a/l) \right] \quad (141)$$

In the case of Poiseuille flow in a circular tube,  $\mathbf{u}_R = 2\mathbf{V}_m(1 - \beta^2)$ . The vector  $\mathbf{V}_m$  is equal in magnitude to the superficial velocity and points in the direction of net flow.

In the special case of a spherical particle moving parallel to the axis of a circular tube the force on the particle is (B28)

$$\mathbf{F} = -6\pi\mu a \left[ \frac{\mathbf{U}_R - 2\mathbf{V}_m(1 - \beta^2) + (4/3)\mathbf{V}_m(a/l)^2}{1 - f(\beta)(a/l)} + O(a/l)^3 \right] \quad (142)$$



which is a higher-order approximation then is furnished by (140). The numerator arises from Faxén's law, Eq. (89a), where the unperturbed flow  $\mathbf{u}$  corresponds to Poiseuille flow in the tube. Equation (142) is applicable only when the sphere is not too near to wall; that is, when

$$1 \gg \frac{a}{l-b} = \frac{a}{l} \left( \frac{1}{1-\beta} \right)$$

This condition will always be met for sufficiently small  $a/l$ , irrespective of how near  $\beta$  is to unity. Equation (142) applies even if the sphere is rotating, for the additional wall-effect arising from the rotation is smaller than  $O(a/l)^2$ . Equation (142) is in excellent agreement with the experimental data of Fayon and Happel (F4) for Poiseuille flow past rigidly supported spherical particles in a long tube.

There exists a rather remarkable type of wall-effect which, rather than vanishing, approaches a finite limit as  $a/l \rightarrow 0$ —that is, as the fluid becomes “unbounded” relative to the particle. When a particle settles in an otherwise quiescent fluid confined within a vertical duct of constant cross section, a dynamic pressure difference  $\Delta P^+$  is set up, the pressure being greatest on that end of the duct towards which the particle is moving. The vector  $\Delta P^+$  points in the direction of diminishing pressure. It is natural to expect that when  $a/l \rightarrow 0$  the vertical container walls can play no role. In this event, elementary momentum principles require that the external pressure-drop force,  $\Delta P^+ A$ , exerted on the fluid be exactly equal to  $\mathbf{F}$ , where  $A$  is the cross sectional area of the duct and  $\mathbf{F}$  is the hydrodynamic force on the particle (equal and opposite to the net gravity force on the latter). Detailed theoretical analysis (B13, B17, B28) reveals that such is not the case. Rather, in this limit, one obtains for a particle of any shape in a duct of any cross section (B17)

$$\Delta P^+ A = \frac{u_R}{V_m} \mathbf{F} \quad (143)$$

Here,  $u$  is the local fluid velocity which would ensue if fluid flowed through the duct at mean velocity  $V_m$  in the absence of the particle. For example, in a circular duct the Poiseuille velocity distribution gives  $u_R/V_m = 2(1 - \beta^2)$ , where  $\beta$  is the fractional distance of the center of reaction of the particle from the cylinder axis. Also, if the particle is spherical,  $\mathbf{F} = -6\pi\mu a \mathbf{U}_R$ , providing we neglect conventional wall-effects. For a particle at the centerline of a symmetrical duct, the coefficient  $u_R/V_m$  in Eq. (143) is 2 for a circular duct, 20/9 for an equilateral triangular duct, and 2.093 for a square duct, these values being based on the known velocity distributions for one-dimensional flow through conduits of these cross sections (B4, pp. 67ff.) In none of these cases is the coefficient unity, as would normally be expected for an “unbounded” fluid.

The origin of the paradoxical result (143) can be seen by observing that, since the sum of all external forces acting on the fluid in the duct is zero, there must exist a shearing force  $F_w$  exerted by the fluid on the duct walls, such that (B17)

$$F_w = \left( \frac{u_R}{V_m} - 1 \right) F \quad (144)$$

The existence of this force derives from the fact that fluid is dragged along by the settling particle. In order to maintain the condition of no net flow through any horizontal plane, a compensating reverse flow must occur near the walls. Since the fluid adheres to the duct walls this flow produces the shearing force  $F_w$ . These facts are not surprising. What is surprising, however, is the fact that the force does not tend to zero as  $a/l \rightarrow 0$ . For in this limit the fluid in the proximity of the walls, being infinitely distant from the disturbance, must be *at rest*. And if the fluid is at rest, how can it produce a shearing force? The resolution of the paradox lies in the fact that even though the shearing motion and, hence, the stresses near the wall are only infinitesimal, they act over an area which is infinitely large in comparison with that of the particle. These infinitesimal stresses acting over an infinite area are thereby able to produce a finite force.

It is clear from the preceding discussion that the apparent paradox is intimately bound up with the no-slip condition at the duct walls. Were the fluid free to glide effortlessly over the walls, the homogeneous flow  $u$  would simply be a plug flow, for which  $u/V_m = 1$  everywhere. In this event Eqs. (143) and (144) would adopt their originally anticipated forms.

Since  $u/V_m$  has its maximum value ( $> 1$ ) at the duct centerline, decreasing to zero at the walls, the force on the wall changes in both magnitude and *direction* as the radial position of the particle is altered. The force is zero at a fractional eccentricity of  $\beta = 0.707$  in the case of a circular cylinder.

Equations (143) and (144) apply also to the important case where the fluid itself may be in a state of net motion relative to the walls (B17), e.g., in a Poiseuillian flow through a tube containing a suspended particle. Here, however,  $\Delta P^+$  and  $F_w$  must be interpreted as the *additional* pressure drop and force, above and beyond that which would be observed in the absence of the particle with fluid flowing at the same mean velocity  $V_m$ . Furthermore,  $F$  is the force on the particle due to both its own motion and that of the fluid, e.g.,  $F = -6\pi\mu a(U_R - u_R)$  for a spherical particle in the absence of conventional wall-effects.

Equation (143) and, hence, indirectly (144) have been experimentally confirmed for both a settling particle in a stationary fluid (P9) and a stationary particle in a moving fluid (B17), the latter using the data of Fayon (F3).

Equation (143) may be applied to dilute multiparticle systems by simply

summing the pressure drops for each of the separate particles (B12, H8). When a large body is immersed in a suspension of much smaller particles, customary practice is to calculate the "buoyant force" on the larger body by employing Archimedes' law in conjunction with the *mean density*,  $\rho_m$ , of the suspension. This assumes, in effect, that a pressure gradient exists within the "homogeneous" suspension which may be calculated by the hydrostatic formula

$$\nabla p = -\rho_m \mathbf{g} \quad (145)$$

where  $\mathbf{g}$  is the local acceleration of gravity vector, directed vertically downward. This static viewpoint is obviously erroneous, since the particles are continuously settling—even if at imperceptibly small rates in the case of very fine particles or very viscous fluids. Nevertheless, one could prove that the result is valid were it permissible to assume that the fluid is laterally unbounded. For in this case there is no possibility of wall forces; whence the pressure-drop force must balance the drag forces on the particles. But according to Eqs. (143) and (144) this assumption is unwarranted, and so the usual "proof" of the validity of Archimedes' law for suspensions cannot be correct. Rather fortuitously, however, we find upon integrating (143) over the duct cross section that for *homogeneous* suspensions (B12)

$$A \sum_i \Delta P_i^+ = \sum_i \mathbf{F}_i$$

( $i = i$ th particle). This relation depends entirely on the fact that, by definition,

$$\frac{1}{AV_m} \int_A u \, dA = 1$$

where  $dA$  is an element of cross sectional duct area. Now

$$\mathbf{F}_i + (\rho_p - \rho)v_i \mathbf{g} = 0$$

where  $\rho_p$  is the particle density,  $\rho$  the homogeneous fluid density, and  $v_i$  the volume of the  $i$ th particle. If  $L$  is the length of duct containing the suspended particles and  $\Delta P^+ = \sum_i \Delta P_i^+$  is the total additional pressure drop, then

$$\Delta P^+/L = -(\rho_p - \rho)\phi \mathbf{g}$$

where  $\phi = \sum_i v_i/AL$  is the fractional concentration of solid particles. Since, by the definition of mean density,  $(\rho_p - \rho)\phi = \rho_m - \rho$ , we find that the additional pressure gradient,  $\nabla p^+ = \Delta P^+/L$ , due to the presence of the particles is

$$\nabla p^+ = -(\rho_m - \rho)\mathbf{g}$$

This is the pressure gradient above and beyond that due to the homogeneous fluid alone, the latter being

$$\nabla p^* = -\rho \mathbf{g}$$

The total pressure is  $p = p^* + p^+$ . Upon adding the last two equations one arrives at Eq. (145).

Archimedes' law is thus, in fact, valid for suspensions—but not for the reasons usually stated. Similar remarks apply to the usual “proof” that the pressure drop in a fluidized bed is equal to the net weight of the bed divided by the cross sectional area (B12, H8). Based on this analysis it seems likely that dilute, laterally inhomogeneous suspensions would display deviations from Archimedes' law.

The pressure drop formula given by Eq. (143) can be explicitly corrected for conventional wall-effects as follows. By a slight generalization of Eqs. (31)–(34) of Brenner (B17), one has for a spherical particle of radius  $a$  that<sup>18</sup>

$$\Delta P^+ \cdot \mathbf{V}_m A = \left[ \mathbf{u}_R + \frac{a^2}{6\mu} (\nabla p^0)_R \right] \cdot \mathbf{F} + \boldsymbol{\omega}_R^f \cdot \mathbf{T}_R + \frac{5}{2} v (2\mu \mathbf{S}_R : \mathbf{S}_R) + O(a/l)^3 \quad (146)$$

where  $p^0$  is the pressure arising from the unperturbed, unidirectional flow  $\mathbf{u}$  through the duct;  $\boldsymbol{\omega}^f = \frac{1}{2}(\nabla \times \mathbf{u})$  is the angular velocity of a fluid particle;  $v = 4\pi a^3/3$  is the volume of the sphere;  $\mathbf{S} = \frac{1}{2}[\nabla \mathbf{u} + (\nabla \mathbf{u})^T]$  is the rate of strain dyadic. As usual, the subscript  $R$  refers to evaluation at the center of the space presently occupied by the sphere. The force and torque on the sphere are, respectively, of the forms

$$\mathbf{F} = -6\pi\mu a \left[ \frac{\mathbf{U}_R - \mathbf{u}_R - (a^2/6\mu)(\nabla p^0)_R}{1 - \underline{W}_R(a/l)} + O(a/l)^3 \right]$$

$$\mathbf{T}_R = -8\pi\mu a^3(\boldsymbol{\omega} - \boldsymbol{\omega}_R^f) + O(a/l)^3$$

where  $\underline{W}_R$  is the nondimensional, wall-effect factor for motion of the sphere parallel to the axis of the cylinder; e.g.,  $\underline{W}_R = f(\beta)$  for a circular cylinder. In

<sup>18</sup> Only the term  $\nabla p^0$  does not appear in the original reference (B17). It arises by including second derivatives in the Taylor series expansion of the unperturbed Stokes flow about  $R$ ,

$$\mathbf{u} = \mathbf{u}_R + \boldsymbol{\omega}_R^f \times \mathbf{r} + \mathbf{S}_R \cdot \mathbf{r} + \mathbf{rr} : (\nabla \nabla \mathbf{u})_R + \dots$$

by observing that  $\nabla \cdot \mathbf{u} = 0$  and  $\mathbf{I} : \nabla \nabla \mathbf{u} = \nabla^2 \mathbf{u} = \mu^{-1} \nabla p^0$ . Note the close relationship to Faxén's law, Eq. (89).

the case of a circular cylinder of radius  $l$  we have

$$\begin{aligned}\mathbf{u}_R &= 2\mathbf{V}_m(1 - \beta^2) \\ \nabla p^0 &= -8\mu\mathbf{V}_m/l^2 \\ \boldsymbol{\omega}_R^f &= 2\mathbf{V}_m \times \mathbf{b}/l^2 \\ \mathbf{S}_R : \mathbf{S}_R &= 8\mathbf{V}_m \cdot \mathbf{V}_m b^2/l^4\end{aligned}$$

where  $\mathbf{b}$  is the position vector of the sphere center relative to the tube axis. These make

$$\Delta P^+(\pi l^2) = 2 \left[ (1 - \beta^2) - \frac{2}{3} \left( \frac{a}{l} \right)^2 \right] \mathbf{F} + \frac{2\mathbf{b}}{l^2} \times \mathbf{T}_R + \frac{160}{3} \pi \mu a^3 \beta^2 \mathbf{V}_m + O\left(\frac{a}{l}\right)^3 \quad (147a)$$

in which  $\mathbf{F}$  is given by Eq. (142), and

$$\mathbf{T}_R = -8\pi\mu a^3 \left( \boldsymbol{\omega} - 2\mathbf{V}_m \times \frac{\mathbf{b}}{l^2} \right) + O\left(\frac{a}{l}\right)^3$$

This expression for the pressure drop agrees in all particulars with a comparable formula obtained via a detailed solution of Stokes equations for the motion of a sphere in a circular cylinder (B28; unpublished calculations).

The couple on the sphere vanishes unless it is restrained from rotating. If the sphere is also neutrally buoyant then  $\mathbf{F} = \mathbf{0}$ , and only the last term in Eq. (147a) survives. By noting that the local rate of mechanical energy dissipation in the unperturbed flow is  $2\mu\mathbf{S}_R : \mathbf{S}_R$ , this ultimately leads to a simple proof of Einstein's law of suspension viscosity (E1a) for flow through cylinders (B17), provided that the spheres are randomly distributed over the duct cross section.

For a sphere settling under the influence of gravity in a quiescent fluid ( $\mathbf{V}_m = \mathbf{0}$ ), Eq. (147a) reduces to

$$\Delta P^+ A = 2 \left[ (1 - \beta^2) - \frac{2}{3} \left( \frac{a}{l} \right)^2 \right] \mathbf{F} + O\left(\frac{a}{l}\right)^3 \quad (147b)$$

where

$$\mathbf{F} = -\frac{6\pi\mu a \mathbf{U}_R}{1 - f(\beta)(a/l)} + O\left(\frac{a}{l}\right)^3$$

This result [or more generally, Eq. (147a)] constitutes the extension of Eq. (143) to situations where conventional wall effects are not negligible. It is interesting to note that Archimedes' law is now no longer strictly valid; rather, in place of Eq. (145) we now obtain

$$\nabla p = -\rho_m \mathbf{g} \left[ 1 - \frac{4}{3} \left( \frac{a}{l} \right)^2 \left( 1 - \frac{\rho}{\rho_m} \right) + O\left(\frac{a}{l}\right)^3 \right]$$

for a dilute, homogeneous suspension of equisized spheres in a circular cylinder. The comparable result for spherical particles in a cylinder of any cross section is obtained by replacing the factor  $\frac{4}{3}(a/l)^2$  by  $a^2|\nabla p^0|/6\mu V_m$ . For example, from the known solution for laminar flow in an elliptical duct (B4, p. 69) of semiaxes  $b$  and  $c$  one obtains  $2a^2(b^2 + c^2)/3b^2c^2$  as the appropriate wall-correction factor.

Closely related to the preceding is the problem of calculating the pressure drop due to Stokes flow through a cylinder of arbitrary (but constant) cross section for *arbitrary* boundary conditions on the surfaces bounding the cylinder. A simple application of the Reciprocal theorem (B18) permits one to express this pressure drop *directly* in terms of the prescribed velocity field on the cylinder walls, top, and bottom. If  $(\mathbf{v}, \boldsymbol{\pi})$  and  $(\mathbf{v}^{(0)}, \boldsymbol{\pi}^{(0)})$  denote the velocity and dyadic stress fields associated with any two solutions of Stokes equations, one may write

$$\oint_{S_w + S_t + S_b} d\mathbf{S} \cdot \boldsymbol{\pi} \cdot \mathbf{v}^{(0)} = \oint_{S_w + S_t + S_b} d\mathbf{S} \cdot \boldsymbol{\pi}^{(0)} \cdot \mathbf{v}$$

where  $S_w$ ,  $S_t$  and  $S_b$  refer, respectively, to the cylinder walls, top, and bottom. Choose  $\mathbf{v}^{(0)}$  to be the classical, no-slip, unidirectional laminar flow through the cylinder corresponding to a *unit* mean velocity of flow (e.g., for a circular cylinder,  $\mathbf{v}^{(0)} = ku$ , where  $u = 2[1 - (R/l)^2]$ ). Now  $\mathbf{v}^{(0)}$  vanishes on  $S_w$ ; furthermore,  $d\mathbf{S} \cdot \boldsymbol{\pi} \cdot \mathbf{v}^{(0)} = \pm p u dA$  on  $S_t$  and  $S_b$ , where  $p$  is necessarily constant for the class of problems to which the present method of calculation is applicable (otherwise the definition of pressure drop is ambiguous). Since  $\int u dA = A$  over both  $S_t$  and  $S_b$ , the left-hand integral of the preceding displayed equation is simply  $\Delta P A$ . Hence,

$$\Delta P = \frac{1}{A} \oint_{S_w + S_t + S_b} d\mathbf{S} \cdot \boldsymbol{\pi}^{(0)} \cdot \mathbf{v}$$

Calculation of the pressure drop from the prescribed field  $\mathbf{v}$  on  $S_w$ ,  $S_t$ , and  $S_b$  is thus reduced to a quadrature whenever the classical solution for laminar flow through the cylinder is already known. A relationship comparable to the above was previously given for the special case of a circular cylinder by Brenner (B13) along with an example of its utility in applications.

## D. MULTIPARTICLE SYSTEMS

### 1. Finite Particle Systems

*a. Quiescent Fluids.* In this section we consider situations where a *finite* number of solid particles, each of any shape, in any relative positions and orientations, move through a fluid. Initially, attention is confined to the case

where the fluid is unbounded and at rest at infinity. Let  $O_i$  be any origin fixed, once and for all, in the  $i$ th particle. The hydrodynamic force  $\mathbf{F}_i$  and torque  $\mathbf{T}_i$  (about  $O_i$ ) exerted by the fluid on the  $i$ th particle are then linear vector functions of the translational velocities  $\mathbf{U}_j$  (origin  $O_j$ ) and angular velocities  $\boldsymbol{\omega}_j$  of *all* the particles. In particular, we have (B22)

$$\mathbf{F}_i = -\mu \sum_{j=1}^n \left[ \mathbf{K}_{ij}^{(t)} \cdot \mathbf{U}_j + \mathbf{K}_{ji}^{(c)} \cdot \boldsymbol{\omega}_j \right] \quad (148)$$

$$\mathbf{T}_i = -\mu \sum_{j=1}^n \left[ \mathbf{K}_{ij}^{(c)} \cdot \mathbf{U}_j + \mathbf{K}_{ij}^{(r)} \cdot \boldsymbol{\omega}_j \right] \quad (149)$$

where  $i = 1, 2, 3, \dots, n$ , the latter being the total number of particles in the system.

Each constant  $\mathbf{K}_{ij}$  resistance dyadic is an intrinsic geometric property of the instantaneous configuration of the entire particle system, dependent upon the sizes, shapes, mode of arrangement, and relative orientations of all the particles.  $\mathbf{K}_{ij}^{(r)}$  depends on the choice of  $O_i$  and  $O_j$ , whereas  $\mathbf{K}_{ij}^{(c)}$  depends only on the choice of  $O_i$ . The translation dyadics,  $\mathbf{K}_{ij}^{(t)}$ , are origin-independent. The various resistance dyadics are independent of the fluid viscosity and of the velocities and spins of all the particles. It should be noted that the two indices associated with each dyadic refer not to tensor indices, but rather to numbers used in identifying the individual particles. For example,  $\mathbf{K}_{ij}^{(r)}$  is associated with the torque on the  $i$ th particle due to the rotation of the  $j$ th particle while all other particles are at rest. These dyadics satisfy the symmetry relations (B22)

$$\mathbf{K}_{ij}^{(t)} = \mathbf{K}_{ji}^{(t)\dagger} \quad (150a)$$

$$\mathbf{K}_{ij}^{(r)} = \mathbf{K}_{ji}^{(r)\dagger} \quad (150b)$$

When the two indices of these "direct" dyadics are equal, the resulting dyadics are symmetric and positive-definite.

The dyadic resistance coefficients derive from the quasi-steady Stokes equations as follows: Let  $(\mathbf{V}_j, \mathbf{P}_j)$  be the intrinsic solutions of the dyadic Stokes equations [cf. Eqs. (17) and (18)] associated with the motion of the  $j$ th particle while all other particles are at rest. Explicitly, let the translational solutions satisfy the dyadic boundary conditions

$$\mathbf{V}_j^{(t)} = \begin{cases} \mathbf{I} & \text{on } S_j \\ \mathbf{0} & \text{on } S_k \quad (k \neq j) \quad (k = 1, 2, 3, \dots, n) \\ \mathbf{0} & \text{at infinity} \end{cases} \quad (151)$$

and let the rotational solutions satisfy

$$\mathbf{V}_j^{(r)} = \begin{cases} \boldsymbol{\varepsilon} \cdot \mathbf{r}_j & \text{on } S_j \\ \mathbf{0} & \text{on } S_k \quad (k \neq j) \\ \mathbf{0} & \text{at infinity} \end{cases} \quad (k = 1, 2, 3, \dots, n) \quad (152)$$

where  $S_i$  denotes the surface of the  $i$ th particle, and  $\mathbf{r}_i$  is measured from  $O_i$ . If the intrinsic triadic stress fields deriving from these solutions [cf. Eqs. (34) and (37)] are denoted by  $\mathbf{\Pi}_j$ , then the direct resistance coefficients may be calculated from the relations

$$\mathbf{K}_{ij}^{(t)} = - \int_{S_i} d\mathbf{S} \cdot \mathbf{\Pi}_j^{(t)} \quad (153)$$

$$\mathbf{K}_{ij}^{(r)} = - \int_{S_i} \mathbf{r}_i \times (d\mathbf{S} \cdot \mathbf{\Pi}_j^{(r)}) \quad (154)$$

while the cross-coefficients may be obtained either from the relation

$$\mathbf{K}_{ij}^{(c)} = - \int_{S_i} \mathbf{r}_i \times (d\mathbf{S} \cdot \mathbf{\Pi}_j^{(t)}) \quad (155a)$$

or from the equivalent relation

$$\mathbf{K}_{ij}^{(c)} = - \int_{S_j} d\mathbf{S} \cdot \mathbf{\Pi}_i^{(r)\dagger} \quad (155b)$$

The unity of this mode of representing the intrinsic resistance of finite multiparticle systems is best shown by resorting to a matrix representation of Eqs. (148) and (149). Define the four, partitioned  $3n \times 1$  column matrices  $\|F\|$ ,  $\|T\|$ ,  $\|U\|$ ,  $\|\omega\|$  by expressions of the general form

$$\|F\| = \begin{Bmatrix} \|\mathbf{F}_1\| \\ \|\mathbf{F}_2\| \\ \vdots \\ \|\mathbf{F}_n\| \end{Bmatrix}, \quad \text{etc.} \quad (156)$$

in which

$$\|\mathbf{F}_i\| = \begin{Bmatrix} F_i^{(1)} \\ F_i^{(2)} \\ F_i^{(3)} \end{Bmatrix} \quad (157)$$

is a  $3 \times 1$  column matrix whose three scalar elements,  $F_i^{(1)}$ ,  $F_i^{(2)}$ ,  $F_i^{(3)}$ , are the components of the vector force  $\mathbf{F}_i$  in any convenient Cartesian system.



Also define the  $3n \times 3n$  square, partitioned matrices  $\|K\|^{(t)}$ ,  $\|K\|^{(r)}$ ,  $\|K\|^{(c)}$  by expressions of the general form

$$\|K\|^{(t)} = \begin{pmatrix} \|K_{11}\|^{(t)} & \|K_{12}\|^{(t)} & \cdots & \|K_{1n}\|^{(t)} \\ \|K_{21}\|^{(t)} & \|K_{22}\|^{(t)} & \cdots & \|K_{2n}\|^{(t)} \\ \vdots & \vdots & \ddots & \vdots \\ \|K_{n1}\|^{(t)} & \|K_{n2}\|^{(t)} & \cdots & \|K_{nn}\|^{(t)} \end{pmatrix}, \quad \text{etc.} \quad (158)$$

in which

$$\|K_{ij}\|^{(t)} = \begin{pmatrix} K_{ij}^{(11)} & K_{ij}^{(12)} & K_{ij}^{(13)} \\ K_{ij}^{(21)} & K_{ij}^{(22)} & K_{ij}^{(23)} \\ K_{ij}^{(31)} & K_{ij}^{(32)} & K_{ij}^{(33)} \end{pmatrix} \quad (159)$$

is a  $3 \times 3$  matrix whose nine scalar elements are the components of the dyadic

$\|K_{ij}\|^{(t)}$  in the same Cartesian system as used for the column matrices.

If we now define the  $6n \times 1$  partitioned column matrices

$$\|\mathcal{F}\| = \begin{pmatrix} \|F\| \\ \|T\| \end{pmatrix}, \quad \|\mathcal{U}\| = \begin{pmatrix} \|U\| \\ \|\omega\| \end{pmatrix} \quad (160)$$

and the  $6n \times 6n$  square, partitioned matrix

$$\|\mathcal{K}\| = \begin{pmatrix} \|K\|^{(t)} & \|K\|^{(c)\dagger} \\ \|K\|^{(c)} & \|K\|^{(r)} \end{pmatrix} \quad (161)$$

then Eqs. (148) and (149) are equivalent to the single matrix equation (B22)

$$\|\mathcal{F}\| = -\mu \|\mathcal{K}\| \|\mathcal{U}\| \quad (162)$$

[cf. Eq. (49) for a *single* particle.]

Incorporated into the  $\|\mathcal{K}\|$  matrix is the intrinsic resistance of the entire particle system. It is called the *grand resistance matrix*. In view of the symmetry relations

$$\|K\|^{(t)} = \|\|K\|^{(t)}\|^\dagger, \quad \|K\|^{(r)} = \|\|K\|^{(r)}\|^\dagger \quad (163)$$

the grand resistance matrix is symmetric:

$$\|\mathcal{K}\| = \|\mathcal{K}\|^\dagger \quad (164)$$

Furthermore, the latter is positive-definite, as are the direct submatrices  $\|K^{(t)}\|$  and  $\|K^{(r)}\|$  too. The scalar elements of these matrices must therefore satisfy a host of inequalities [see the paragraph containing Eq. (50)].

Insight into the internal structure of the multiparticle resistance dyadics may be obtained from the two-sphere example discussed by Brenner (B22). Let  $a_1$  and  $a_2$  be the radii of the spheres;  $\mathbf{e}_{12}$  is a unit vector drawn from the center  $O_1$  of sphere 1 to the center  $O_2$  of sphere 2, and  $2h$  is the center-to-center distance. The resistance dyadics are then, to terms of the lowest orders in  $a_i/h$ ,

$$\mathbf{K}_{11}^{(t)} = 6\pi a_1 \left[ \mathbf{I} + \frac{9}{64} \left( \frac{a_1}{h} \right) \left( \frac{a_2}{h} \right) (\mathbf{I} + 3\mathbf{e}_{12}\mathbf{e}_{12}) + o\left(\frac{a_i}{h}\right)^2 \right] \quad (165a)$$

$$\mathbf{K}_{11}^{(r)} = 8\pi a_1^3 \left[ \mathbf{I} + \frac{3}{64} \left( \frac{a_2}{h} \right) \left( \frac{a_1}{h} \right)^3 (\mathbf{I} - 3\mathbf{e}_{12}\mathbf{e}_{12}) + o\left(\frac{a_i}{h}\right)^4 \right] \quad (165b)$$

$$\mathbf{K}_{11}^{(c)} = -\frac{9}{16} \pi a_1 a_2 \left[ \left( \frac{a_1}{h} \right)^3 \boldsymbol{\varepsilon} \cdot \mathbf{e}_{12} + o\left(\frac{a_i}{h}\right)^3 \right] \quad (165c)$$

$$\mathbf{K}_{12}^{(t)} = -\frac{9}{4} \pi a_1 \left[ \left( \frac{a_2}{h} \right) (\mathbf{I} + \mathbf{e}_{12}\mathbf{e}_{12}) + o\left(\frac{a_i}{h}\right) \right] \quad (165d)$$

$$\mathbf{K}_{12}^{(r)} = \frac{1}{2} \pi a_1^3 \left[ \left( \frac{a_2}{h} \right)^3 (\mathbf{I} - 3\mathbf{e}_{12}\mathbf{e}_{12}) + o\left(\frac{a_i}{h}\right)^3 \right] \quad (165e)$$

$$\mathbf{K}_{12}^{(c)} = \frac{3}{2} \pi a_1 a_2 \left[ \left( \frac{a_1}{h} \right)^2 \boldsymbol{\varepsilon} \cdot \mathbf{e}_{12} + o\left(\frac{a_i}{h}\right)^2 \right] \quad (165f)$$

The  $\mathbf{K}_{22}$  and  $\mathbf{K}_{21}$  coefficients may be obtained from these by interchanging the indices, bearing in mind that  $\mathbf{e}_{21} = -\mathbf{e}_{12}$ . Note that Eqs. (165) correctly satisfy the symmetry relations cited in Eq. (150).

A much more complete discussion of recent work on the interaction of two and more spherical particles, including a detailed comparison with experimental data, will be found in Happel and Brenner (H9). To the list of references given there should be added the experimental work of Bammi [(B1); summarized by McNown (M8)], Timbrell (T5), Andersson (A3), Eveson (E3), Gasparian (G2), and Jayaweera *et al.* (J2). Andersson (A4) presents data on the sedimentation of two rods. In addition there are recent theoretical analyses by Kaufman (K6) on the axisymmetric motion of two equal spheres, and Hocking (H14) on the motion of clusters of identical spheres. Pshenai-Severin (P12, P13) and Hocking (H13a) theoretically treat the case where the spheres are of unequal size. Berker (B4, p. 247) presents some interesting general theorems pertaining to the motion of two equal spheres. More recently, Goldman, Cox, and Brenner (G5b), using bipolar

coordinates, solved *exactly* the problem of two identical spheres for the general case where their line of centers is arbitrarily inclined relative to the direction of gravity. Their treatment includes the case where the spheres fall without rotation (i.e., like a rigid dumbbell), as well as the case where the individual spheres rotate freely about their own centers in response to the hydrodynamic couple caused by the translational motion. Their two-sphere results, which apply for all values of  $a/h$ —including the limiting case where the spheres touch, supercede the approximate results discussed in Chapter 6 of Happel and Brenner (H9).

With regard to systems consisting of more than two spherical particles settling in an unbounded, quiescent fluid, Srimathi and Bhat (S17) present experimental data on drag interaction effects when a number of identical spheres rigidly joined together in a line by a thin rod are allowed to settle.

The multiple-sphere experiments of Jayaweera *et al.* (J2) point up a truly remarkable ordering phenomenon. Three to six equal spheres released as a compact cluster in a viscous fluid eventually arrange themselves in the same horizontal plane at the vertices of the corresponding regular polygon, provided that the Reynolds number is sufficiently small ( $R = 0.06$  to  $7.0$  in the experiments, these being based on sphere radius and settling velocity). The polygon dimensions continuously expand during its fall, but at an ever-decreasing rate. If the number of spheres exceeds six, or if  $R > 7$ , the cluster exhibits no tendency to form a regular polygon, but rather separates into two or more groups. On the basis of Stokes equations, Hocking (H14) furnished a partial theoretical analysis of these phenomena by investigating the stability of a configuration of  $n$  equal spheres at the vertices of a regular horizontal polygon. The distance between adjacent spheres was assumed sufficiently large compared with the sphere radii to permit the use of only first-order hydrodynamic interactions. Hocking showed that the configuration was neutrally stable to small perturbations for  $n = 3$  to  $6$ , but unstable for  $n \geq 7$ —thus explaining why no regular polygonal array was observed for more than six spheres. However, he was unable to explain the increasing size of the polygon, or to prove positive stability for  $n = 3$  to  $6$  on the basis of the Stokes equations; rather, the small oscillations of the spheres were of constant amplitude. Bretherton (B31) completed the analysis by allowing for the existence of small, nonzero inertial effects in the equations of motion. Thereby he demonstrated, among other things, that the observed increase in the size of the array and the damping of the oscillations for  $3 \leq n \leq 6$  were due to the inertia of the fluid.

First-order interactions between two particles of any shape translating and rotating in an unbounded fluid at rest at infinity can be directly expressed in terms of the fundamental resistance dyadics of the individual particles themselves. Denote by  $\overset{(\cdot)}{\mathbf{K}}_1$  and  $\overset{(\cdot)}{\mathbf{K}}_2$  the appropriate resistance dyadics for

particles 1 and 2, respectively, when each is alone in the unbounded fluid. The origins  $O_1$  and  $O_2$  to which the rotation and coupling dyadics are referred may be any points fixed in each of the particles. Let  $\mathbf{e}$  be a unit vector drawn along the line from  $O_1$  and  $O_2$  or vice versa; since  $\mathbf{e}$  always occurs as the dyad  $\mathbf{ee}$  it is immaterial which of the two possible directions is selected. The multi-particle resistance dyadics are then expressible in the form (B20, B22, C20)

$$\mathbf{K}_{11}^{(t)} = \mathbf{K}_1^{(t)} + (16\pi h)^{-2} \mathbf{K}_1^{(t)} \cdot (\mathbf{I} + \mathbf{ee}) \cdot \mathbf{K}_2^{(t)} \cdot (\mathbf{I} + \mathbf{ee}) \cdot \mathbf{K}_1^{(t)} + O(a/h)^3 \quad (166a)$$

$$\mathbf{K}_{11}^{(r)} = \mathbf{K}_1^{(r)} + (16\pi h)^{-2} \mathbf{K}_1^{(c)} \cdot (\mathbf{I} + \mathbf{ee}) \cdot \mathbf{K}_2^{(t)} \cdot (\mathbf{I} + \mathbf{ee}) \cdot \mathbf{K}_1^{(c)\dagger} + O(a/h)^3 \quad (166b)$$

$$\mathbf{K}_{11}^{(c)} = \mathbf{K}_1^{(c)} + (16\pi h)^{-2} \mathbf{K}_1^{(c)} \cdot (\mathbf{I} + \mathbf{ee}) \cdot \mathbf{K}_2^{(t)} \cdot (\mathbf{I} + \mathbf{ee}) \cdot \mathbf{K}_1^{(t)} + O(a/h)^3 \quad (166c)$$

$$\mathbf{K}_{12}^{(t)} = -(16\pi h)^{-1} \mathbf{K}_1^{(t)} \cdot (\mathbf{I} + \mathbf{ee}) \cdot \mathbf{K}_2^{(t)} + O(a/h)^2 \quad (166d)$$

$$\mathbf{K}_{12}^{(r)} = -(16\pi h)^{-1} \mathbf{K}_1^{(c)} \cdot (\mathbf{I} + \mathbf{ee}) \cdot \mathbf{K}_2^{(c)\dagger} + O(a/h)^2 \quad (166e)$$

$$\mathbf{K}_{12}^{(c)} = -(16\pi h)^{-1} \mathbf{K}_1^{(c)} \cdot (\mathbf{I} + \mathbf{ee}) \cdot \mathbf{K}_2^{(t)} + O(a/h)^2 \quad (166f)$$

where  $a$  is a characteristic particle dimension and  $2h$  is the "center-to-center" distance  $\overrightarrow{O_1 O_2}$ . The remaining dyadics,  $\mathbf{K}_{22}^{(t)}$  and  $\mathbf{K}_{21}^{(t)}$ , may be obtained by permuting the indices. Observe that these coefficients correctly satisfy the symmetry conditions set forth in Eq. (150). Under relatively mild symmetry conditions imposed upon the shapes of the two particles, Eqs. (166a) and (166d) can be expressed in the considerably more accurate forms (C20)

$$\mathbf{K}_{11}^{(t)} = \mathbf{K}_1^{(t)} \cdot \left[ \mathbf{I} - (16\pi h)^{-2} (\mathbf{I} + \mathbf{ee}) \cdot \mathbf{K}_2^{(t)} \cdot (\mathbf{I} + \mathbf{ee}) \cdot \mathbf{K}_1^{(t)} \right]^{-1} + O(a/h)^3$$

$$\mathbf{K}_{12}^{(t)} = -(16\pi h)^{-1} \mathbf{K}_{11}^{(t)} \cdot (\mathbf{I} + \mathbf{ee}) \cdot \mathbf{K}_2^{(t)} + O(a/h)^3$$

with comparable expressions for  $\mathbf{K}_{22}^{(t)}$  and  $\mathbf{K}_{21}^{(t)}$  obtained by permuting the indices.

Equations of the form (148)–(149), as well as their matrix counterparts, continue to be applicable even if the fluid is partly or wholly bounded by non-deformable boundaries on which no work can be done by the stresses, i.e., solid boundaries and nondeformable free surfaces. The only modification required in the analysis is that the boundary conditions (151) and (152) must be supplemented by the additional boundary conditions appropriate to these external boundaries—for example,  $\mathbf{V}_j^{(t)} = \mathbf{0}$  and  $\mathbf{V}_j^{(r)} = \mathbf{0}$  on  $S_w$  if the surface  $S_w$  of the boundary is solid.

*b. Shear and Higher-Order Flows.* If the fluid is in a state of net Stokes flow with velocity  $\mathbf{u} = \mathbf{u}(\mathbf{r})$  at infinity, the force and torque (about  $O_i$ ) on the  $i$ th particle in a multiparticle system are given by (B26)

$$\mathbf{F}_i = -\mu \sum_{j=1}^n \mathfrak{F}_{ij} \cdot (\mathbf{U}_j + \boldsymbol{\omega}_j \times \mathbf{r}_j - \mathbf{u}) \quad (167)$$

$$\mathbf{T}_i = -\mu \sum_{j=1}^n \mathfrak{T}_{ij} \cdot (\mathbf{U}_j + \boldsymbol{\omega}_j \times \mathbf{r}_j - \mathbf{u}) \quad (168)$$

The dyadics  $\mathfrak{F}_{ij}$  and  $\mathfrak{T}_{ij}$  are two-index, symbolic operators termed the multiparticle force and torque operators. They are defined by the relations

$$\mathfrak{F}_{ij} = \int_{S_j} d\mathbf{S} \cdot \boldsymbol{\Pi}_i^{(r)\dagger} \exp(\mathbf{r}_j \cdot \nabla_j) \quad (169)$$

and

$$\mathfrak{T}_{ij} = \int_{S_j} d\mathbf{S} \cdot \boldsymbol{\Pi}_i^{(r)\dagger} \exp(\mathbf{r}_j \cdot \nabla_j) \quad (170)$$

These operators are intrinsic properties of the geometrical configuration of the multiparticle system.

Equations (167) and (168) express the fact that the force and torque on each particle are linear vector functionals of the "slip velocities" of *all* the particles. It should be clearly noted that these operators are calculable solely from a knowledge of the intrinsic translational and rotational solutions of Stokes equations resulting from motion of the  $j$ th particle when *all the other particles, as well as the fluid at infinity, are at rest*. In the case where  $\mathbf{u} = \mathbf{0}$ , Eqs. (167) and (168) reduce to (148) and (149), respectively. As yet, there exists no system for which these operators are known.

The interaction of two rigid spherical particles in a shear field have been experimentally investigated by Mason and co-workers. Their results are summarized by Mason and Bartok (M5) and by Goldsmith and Mason (G9d), where references to earlier work will be found.

*c. Wall-Effects.* Equations of the form (167) and (168) continue to be applicable even when the fluid is partially bounded externally by rigid walls or nondeformable free surfaces on which the stresses do no work. Equations (151) and (152), from which the intrinsic stress triadics in (169) and (170) derive, must, of course, be supplemented by the appropriate boundary conditions at the bounding surfaces. With this further generalization, Eqs. (167) and (168) summarize completely *all* the prior general force and torque formulas.

By superposing solutions for the Stokes flow resulting from the action of isolated point forces directed along the axis of a circular cylinder, Sonshine and Brenner (S15) have computed the wall-effect on the motion of a number of

identical, equally-spaced particles settling in a single column along the axis of an infinitely long circular cylinder. With  $a$  a characteristic particle dimension,  $2h$  the distance between adjacent particles, and  $l$  the cylinder radius, the analysis requires  $a/h \ll 1$  and  $a/l \ll 1$ , but applies for all values of  $h/l$  in the range  $0 \leq h/l < \infty$ . Calculations are presented for  $n = 1, 2, 3, \dots, \infty$  particles. When  $n$  is finite, the drag force on each of the particles remains finite as the wall recedes to infinity ( $h/l \rightarrow 0$  and  $a/l \rightarrow 0$ ). [See also the experimental data of Srimathi and Bhat (S17).] On the other hand, as the number of particles is increased indefinitely, the drag force on each particle becomes infinite when the walls are removed, despite the fact that it remains finite when walls are present. This divergence in unbounded media accords with previous calculations of Burgers (B38) on the related problem of three-dimensional periodic arrays (H10). The contrasting behavior of the bounded vs unbounded cases stems from the fact that the motion generated by the action of a single point force decays exponentially with axial distance in the former case, but only inversely with distance in the latter case (see also footnote 48). The fundamental role played by an encircling boundary in determining the settling velocity of a dilute suspension of particles has already been recognized by Famularo and Happel (F1). It appears that their analysis could be greatly simplified by applying the point force summation techniques of Sonshine and Brenner (S15) to the case where the particles are free to occupy any position within the circular cylinder (B28).

## 2. Infinite Particle Systems

The topic of flow through an effectively infinite system of particles belongs to the more general domain of flow through porous media (C12, C13, P10, R5, S3, S4). In the absence of physicochemical interaction between the particles and fluid, the slow quasi-static Newtonian flow of incompressible fluids through such media is governed by Darcy's law. This linear phenomenological law has the form

$$\mathbf{q} = -(\mathbf{k}/\mu) \cdot \nabla p \quad (171)$$

to which is appended the condition of incompressibility,

$$\nabla \cdot \mathbf{q} = 0 \quad (172)$$

$\mathbf{q}$  is the local volumetric flow rate per unit of superficial cross sectional area (*filter velocity*) at a "point" in the medium,  $p$  is the average local dynamic pressure, and  $\mathbf{k}$  is the local permeability dyadic. The latter is an intrinsic geometric property of the porous medium itself. For isotropic media,  $\mathbf{k} = Ik$ , where  $k$  is a scalar; hence,

$$\mathbf{q} = -(k/\mu)\nabla p \quad (173)$$

Darcy's law is an empirical relation derived by induction from experimental data. Though many attempts have been made to "derive" this law directly from the Navier-Stokes equations—especially from the linearized form of the latter—the legitimacy and generality of these "proofs" remain open questions (S4, p. 661). A primary aim of these treatments is to establish the relationship between the permeability coefficient and the geometrical structure of the porous medium. An even broader goal is the elucidation of the structure of the "subcontinuum" velocity field  $\mathbf{v}$  in the proximity of the individual particles, from which  $\mathbf{q}$  ultimately derives by appropriate averaging. Only through such more detailed knowledge can one calculate from first principles such quantities as heat- and mass-transfer coefficients, and the degree of macroscopic dispersion ("mixing") in such media. In this connection, simple cell models of the types proposed by Happel (H4, H5, H7) and Kuwabara (K12) display significant engineering promise (H6, H9, P7, P8, R8).

Hasimoto's (H10) treatment of flow through *periodic* arrays of identical particles offers a variety of opportunities towards achieving these objectives. When the particles are arrayed in an infinite periodic lattice, the subcontinuum flow field itself becomes periodic, at least in so far as the Stokes approximation is concerned. The filter velocity and *macroscopic* pressure gradient, however, remain constant—as had previously been pointed out (B11, U1) in prior, less potent, attempts to treat the periodic flow problem. [The Stokes flow problem for flow through a cubic periodic array of touching spheres has recently been solved by Snyder and Stewart (S14) using a Galerkin approximation scheme. Their results furnish the detailed *local* velocity and pressure fields as well as the drag on the particles. Their calculated friction factors agree to within 5 per cent with the experimental values for the two configurations studied by them.] Thus, the concept of cell models with fluid boundaries is already implicit in the concept of periodic assemblages—but in a much less arbitrary, albeit complex, fashion than in Happel's treatment. In principle, Hasimoto's technique permits one to relate the gross properties of the porous medium directly to the geometric structure and arrangement of the individual particles comprising it. Though the original analysis (H10) of three-dimensional systems is limited to spherical particles, we have in mind its extension to anisotropic media consisting, say, of identical anisotropic particles, similarly oriented, in periodic array. It is already intuitively obvious, for example, that a periodic assemblage consisting of finite circular cylinders with axes parallel and with centers at the nodal points of a simple cubic lattice gives rise to an anisotropic porous medium in which the permeability dyadic is *symmetric*. The principal axes of  $\mathbf{k}$  clearly lie parallel to those of the individual cylinders. In a more general context, Ripps and Brenner (R5b) have shown that *any* infinite collection of identical, similarly oriented particles

in periodic array gives rise to a symmetric permeability tensor—irrespective of the shape of the particles comprising the array. The symmetry of this tensor is thus a consequence of the periodicity of the array alone, and does not further require that the particles themselves be symmetric. Moreover, it is shown (R5b) that if the individual particles possess screw symmetry the fluid will exert a torque on each particle. Such periodic models, coupled with the broader ideas of Dahler and Scriven (D2) on the general theory of *structured continua*, offer promise in advancing our understanding of flow through porous media.

In connection with the relationship between the macro- and microstructure of porous media, we wish to put forward some frankly speculative thoughts on what appears to be a fundamental limitation on the generality of Darcy's law in its presently accepted form. Consider two artificial porous media composed of identical particles differing only in their *screw-sense*; that is, suppose one medium is entirely composed of right-handed particles, and the other of the same species of left-handed particles. Since  $\mathbf{q}$ ,  $\mathbf{k}$ , and  $\mu$  are usually regarded as *true* tensors, Eqs. (171)-(172) predict that flows through these two media would be macroscopically indistinguishable. Only through the intervention of *pseudo*-tensors can a sense-difference be manifested. In view of our findings for isolated particles, and of our knowledge of other sense-dependent physical phenomena, e.g., magnetism, optical rotation, and the like, it seems unlikely that the screw-sense of the individual particles is somehow lost in the averaging process, as implied by Darcy's law. Rather, it is more likely that the law is incomplete—a defect we shall attempt to remedy. In what follows we follow in broad outline the general theory of structured continua advanced by Dahler and Scriven (D2).

The most likely manifestation of this screw-sense lies in the existence of a torque exerted by the fluid on the particles comprising the porous medium and vice versa. The vector  $-\nabla\mu\,dV$  gives the force exerted by the surroundings on the contents of a small volume element  $dV$ . Hence, the external moment of the forces acting on a volume  $V$  of the medium, about some arbitrary origin, is

$$\mathbf{M}_{\text{ext}} = - \int_V \mathbf{r} \times \nabla\mu\,dV$$

We now assume the existence of a local torque density pseudovector  $\mathbf{t}$  such that  $\mathbf{t}\,dV$  gives the torque exerted on the contents of  $dV$  by its immediate surroundings. There is thus an internal moment, which is independent of the choice of origin, such that

$$\mathbf{M}_{\text{int}} = \int_V \mathbf{t}\,dV$$



The total first moment about the origin is, therefore,

$$\mathbf{M} = - \int_V \mathbf{r} \times \nabla \mu dV + \int_V \mathbf{t} dV$$

The internal moment may be replaced by an *equivalent* macroscopic distribution by utilizing the identity

$$\mathbf{t} = \frac{1}{2} \mathbf{r} \times (\nabla \times \mathbf{t}) + \frac{1}{2} \nabla \cdot [(\mathbf{I} \times \mathbf{t}) \times \mathbf{r}]$$

whence, by the divergence theorem,

$$\int_V \mathbf{t} dV = \frac{1}{2} \int_V \mathbf{r} \times (\nabla \times \mathbf{t}) dV + \frac{1}{2} \oint_S (d\mathbf{S} \times \mathbf{t}) \times \mathbf{r}$$

where  $S$  is the closed surface bounding  $V$ .

Following Landau and Lifshitz (L7, pp. 37 and 114) and Dahler and Scriven (D2) we choose  $S$  *outside* of the isolated volume  $V$  of the body. Since  $\mathbf{t} = \mathbf{0}$  outside the body, the surface integral vanishes. The total first moment is thus

$$\mathbf{M} = - \int_V \mathbf{r} \times (\nabla \mu - \frac{1}{2} \nabla \times \mathbf{t}) dV$$

Upon comparison with the expression for the external moment of the force (per unit volume) distribution we see that the internal moment is indeed represented by an equivalent macroscopic distribution, the *proper* (D2) pressure gradient being

$$\nabla \mu^* = \nabla \mu - \frac{1}{2} \nabla \times \mathbf{t} \quad (174)$$

It appears on the basis of our analysis that the proper pressure gradient is a more fundamental entity than is the conventional pressure gradient  $\nabla \mu$ .

In order to complete the analysis we require constitutive equations relating both the pressure gradient and the torque density to the local velocity field  $\mathbf{q}$ . Assuming these relations to be linear, the least restrictive assumption we can make is to suppose that these vectors possess a Taylor series expansion. Thus

$$\nabla \mu = -\mu(\mathbf{K}_r \cdot \mathbf{q} - \frac{1}{2} \mathbf{K}_c' : \nabla \mathbf{q})$$

$$\mathbf{t} = \mu(\mathbf{K}_c'' \cdot \mathbf{q} - \frac{1}{2} \mathbf{K}_r : \nabla \mathbf{q})$$

in which it has been assumed that higher-order terms in the expansion may be neglected. The dyadic  $\mathbf{K}_r$ , pseudodyadic  $\mathbf{K}_c''$ , triadic  $\mathbf{K}_c'$ , and pseudotriadic  $\mathbf{K}_r$  are assumed to depend only on the geometrical properties of the porous medium. We restrict ourselves further to helicoidally isotropic porous media.

(The usual spherical isotropy is a special case of this.) This requires that we set

$$\mathbf{K}_t = \mathbf{I}K_t, \quad \mathbf{K}_c' = \varepsilon K_c'$$

$$\mathbf{K}_c'' = \mathbf{I}K_c'', \quad \mathbf{K}_r = \varepsilon K_r$$

where  $K_t$  and  $K_r$  are true scalars and  $K_c'$  and  $K_c''$  are pseudoscalars. Though it is not strictly essential, we shall also *assume* that

$$K_c' = K_c'' = K_c, \quad \text{say}$$

This reduces from four to three the number of independent phenomenological coefficients required to describe the intrinsic resistance of the porous medium. Inasmuch as  $\varepsilon : \nabla \mathbf{q} = -\nabla \times \mathbf{q}$ , the constitutive equations thus become

$$\nabla \mu = -\mu(K_t \mathbf{q} + K_c \tfrac{1}{2} \nabla \times \mathbf{q}) \quad (175a)$$

$$\mathbf{t} = \mu(K_c \mathbf{q} + K_r \tfrac{1}{2} \nabla \times \mathbf{q}) \quad (175b)$$

In a certain sense these equations are the analogs of the fundamental single particle equations (38)–(39), at least in the isotropic case. [See also Eqs. (109)–(110) for the case where the particle neither translates nor rotates, bearing in mind that  $\boldsymbol{\omega}_f = \tfrac{1}{2} \nabla \times \mathbf{u}$ , and that the shear-force and shear-torque triadics vanish for isotropic particles.] It is on the basis of this analogy that we have assumed the symmetry relation  $K_c' = K_c''$ .

To the order of the approximation, the local energy dissipation rate (per unit time per unit volume) is

$$E = -\nabla \mu \cdot \mathbf{q} + \mathbf{t} \cdot \tfrac{1}{2} \nabla \times \mathbf{q}$$

which from (175) is

$$E = \mu[K_t \mathbf{q}^2 + 2K_c \mathbf{q} \cdot (\tfrac{1}{2} \nabla \times \mathbf{q}) + K_r (\tfrac{1}{2} \nabla \times \mathbf{q})^2]$$

Since the energy dissipation is positive-definite this requires that

$$\det \begin{vmatrix} K_t & K_c \\ K_c & K_r \end{vmatrix} > 0$$

and, hence,

$$K_t > 0 \quad (176a)$$

$$K_r > 0 \quad (176b)$$

$$K_t K_r > K_c^2 \quad (176c)$$

The scalar coefficient  $K_t$  is, of course, the reciprocal of the ordinary permeability  $k$ . Two porous media which are statistically equivalent in all

respects except screw-sense ought to possess the same  $K_t$ ,  $K_r$ , and  $|K_c|$  values, differing only in the algebraic sign of the pseudoscalar  $K_c$ . For porous media devoid of screw-like particles (or paths) or consisting of homogeneous racemic mixtures of screw-like particles it is natural to suppose that  $K_c = 0$ .

In accordance with Eqs. (174) and (175) the equation of motion is

$$\nabla \mu^* = -\mu(K_t \mathbf{q} + \frac{1}{2} K_c \nabla \times \mathbf{q} - \frac{1}{4} K_r \nabla^2 \mathbf{q}) \quad (177)$$

which is to be considered simultaneously with the continuity relation

$$\nabla \cdot \mathbf{q} = 0 \quad (178)$$

The coefficients  $K_t$ ,  $K_c$ , and  $K_r$  are dimensionally of orders  $a^{-2}$ ,  $a^{-1}$ , and  $a^0$ , respectively, where  $a$  is a characteristic particle dimension (or average spacing between adjacent particles). If we conceive of the porous medium as a discrete collection of touching particles we may then write

$$K_t = a^{-2} \underline{K}_t \quad (179a)$$

$$K_c = a^{-1} \underline{K}_c \quad (179b)$$

$$K_r = \underline{K}_r \quad (179c)$$

where the dimensionless coefficients  $\underline{K}_t$ ,  $\underline{K}_c$ , and  $\underline{K}_r$  depend only on the structure of the porous medium, but not on the size of the particles of which it is comprised. Consider an experiment performed with a porous medium confined within some apparatus of characteristic dimension  $l$  (e.g., a circular cylinder of radius  $l$ ). Equations (177) and (178) may then be expressed in nondimensional form by introducing the substitutions

$$\nabla = l^{-1} \underline{\nabla}$$

$$\mathbf{q} = V_m \underline{\mathbf{q}}$$

$$\mu^* = \mu V_m l^{-1} \underline{\mu}^*$$

where the underlined quantities are dimensionless, and  $V_m$  is a characteristic fluid speed. Upon introducing these and Eq. (179) into Eq. (177), we obtain

$$\underline{\nabla} \underline{\mu}^* = - \left[ \underline{K}_t \left( \frac{l}{a} \right)^2 \underline{\mathbf{q}} + \frac{1}{2} \underline{K}_c \left( \frac{l}{a} \right) \underline{\nabla} \times \underline{\mathbf{q}} - \frac{1}{4} \underline{K}_r \underline{\nabla}^2 \underline{\mathbf{q}} \right]$$

In the limit as  $a/l \rightarrow 0$  the last two terms on the right become negligibly small compared with the first. In this limit we thus recover the conventional form of Darcy's law. Darcy's law therefore applies strictly only to very finely divided media ( $a \rightarrow 0$ ) or to unbounded media ( $l \rightarrow \infty$ ). These same

dimensional arguments justify retention of only the leading terms in the Taylor expansions (175).<sup>19</sup>

In the absence of screw-like properties ( $K_c = 0$ ), and for the case  $a/l \neq 0$ , a number of prior investigators (B32, B33, B34, B35, D4c) have proposed an empirical modification of Darcy's law having a form substantially identical to Eq. (177). [See the discussion of these modifications by Hermans (H12a) and Scheidegger (S3, 1st ed., pp. 111–113).] This is done by heuristic arguments beginning with Stokes equations in the presence of a continuous distribution of external volume forces:

$$\nabla^2 \mathbf{v} - \frac{1}{\mu} \nabla p = -\mathbf{f} \quad (180a)$$

$$\nabla \cdot \mathbf{v} = 0 \quad (180b)$$

where  $\mathbf{f}$  denotes the external force per unit volume exerted by the surroundings at a point of the fluid. By invoking Darcy's law in the form

$$\mathbf{f} = -K_t \mathbf{v} \quad (K_t > 0) \quad (181)$$

they are thus led to the relation

$$\nabla p = -\mu(K_t \mathbf{v} - \nabla^2 \mathbf{v}) \quad (182)$$

which bears an unmistakable resemblance to Eq. (177) (including the algebraic sign of the coefficients) in the absence of screw-like behavior.<sup>20</sup> Depending upon the magnitude of the dimensionless ratio  $K_t l^2 = \underline{K}_t (l/a)^2$ , Eq. (182) yields Stokes-like flows when  $l/a$  is small. Conversely, when  $l/a$  is large,

<sup>19</sup> A relationship of the same functional form as Eq. (177) is obtained by assuming that  $\nabla/\ell^*$  possesses a Taylor series expansion of the general form

$$\nabla/\ell^* = -\mu(\mathbf{K}^{(2)} \cdot \mathbf{q} + \mathbf{K}^{(c)} : \nabla \mathbf{q} + \mathbf{K}^{(r)} : \nabla \nabla \mathbf{q} + \dots)$$

The unit isotropic Cartesian tensors of ranks two and three are  $\delta_{ij}$  and  $\varepsilon_{ijk}$ , respectively, whereas the three unit isotropic tensors of rank four are, respectively,  $\delta_{ij} \delta_{kl}$ ,  $\delta_{ik} \delta_{jl} + \delta_{il} \delta_{jk}$ , and  $\delta_{ik} \delta_{jl} - \delta_{il} \delta_{jk}$ . These, in conjunction with the condition of incompressibility,  $\nabla \cdot \mathbf{q} = 0$ , thereby lead to following expression for an isotropic porous medium:

$$\nabla/\ell^* = -\mu(K^{(r)} \mathbf{q} + K^{(c)} \nabla \times \mathbf{q} + K^{(r)} \nabla^2 \mathbf{q} + \dots)$$

Though such an analysis leads to a relationship formally identical to Eq. (177) it furnishes no insight into the algebraic signs of the coefficients, nor does it suggest that the origin of these additional terms is due in part to the action of local couples within the porous medium.

<sup>20</sup> In the presence of screw-like properties it seems natural to extend Eq. (181) by writing

$$\mathbf{f} = -(K_t \mathbf{v} + K_c \frac{1}{2} \nabla \times \mathbf{v})$$

in which case the analogy with Eq. (177) is even more perfect.

Darcy-like flows obtain except in a thin boundary layer near solid walls, where Darcy's equation is unable to satisfy the no-slip boundary condition [cf. Brinkman's treatment (B35) of flow through a porous medium bounded externally by a circular cylinder with solid walls].

Solutions of Eqs. (177)–(178) appear relatively easy to obtain since they require that

$$\nabla^2 \mu^* = 0$$

It seems reasonable to demand satisfaction of the no-slip boundary condition  $\mathbf{q} = \mathbf{0}$  at solid boundaries. For the practical case where  $l/a$  is large ( $K_t l/K_c$  and  $K_t l^2/K_c$  large), ordinary Darcy flow will prevail except in a thin boundary layer near solid surfaces. Only in this region will the last two terms on the right side of Eq. (177) be of the same order as the leading term.

### III. Flow at Small, Nonzero Reynolds Numbers

#### A. INTRODUCTION

Section II dealt in its entirety with Stokes flows. The velocity fields, forces, torques, and the like associated with such flows are independent of the Reynolds number,  $R = aV\rho/\mu$ . As such, these flows may be regarded as the leading term [i.e., the term of  $O(R^0)$ ] in an asymptotic solution of the Navier–Stokes equations for small Reynolds numbers. In this section we deal with various perturbation schemes for obtaining asymptotic solutions to terms of higher order in  $R$ . The schemes are essentially of two kinds—regular and singular perturbations (V1). In the former case, typified by the rotation of a sphere about its axis in an infinite fluid, the Stokes solution provides a uniformly valid zero-order approximation to the solution of the Navier–Stokes equations throughout the *entire* fluid domain. Higher-order terms may then be obtained by conventional perturbation methods, with  $R$  as the small perturbation parameter. In the latter case, typified by streaming flow past a sphere in an unbounded fluid, the Stokes solution is no longer a uniformly valid zero-order approximation to the solution of the Navier–Stokes equations throughout the entire flow field. Rather, as Oseen first showed, the approximation becomes invalid at dimensionless distances  $\underline{r}$  from the sphere such that  $\underline{R}\underline{r} = O(1)$ . In such cases recourse may be had to *singular* perturbation schemes. Van Dyke's book (V1) discusses the application of such “matched asymptotic expansion” techniques to a wide variety of fluid dynamical problems.

With dimensionless variables defined as in Eq. (4), the steady-state Navier–Stokes and continuity equations may be written in the nondimensional forms

$$\underline{\nabla} p - \underline{\nabla}^2 \underline{\mathbf{v}} + R \underline{\mathbf{v}} \cdot \underline{\nabla} \underline{\mathbf{v}} = \mathbf{0} \quad (183)$$

and

$$\underline{\nabla} \cdot \underline{y} = 0 \quad (184)$$

The dimensionless boundary conditions for streaming flow past a sphere are

$$\underline{y} \rightarrow \underline{U} \quad \text{as } \underline{r} \rightarrow \infty \quad (185a)$$

$$\underline{y} = \underline{0} \quad \text{at } \underline{r} = 1 \quad (185b)$$

The corresponding conditions for the rotating sphere are

$$\underline{y} \rightarrow \underline{0} \quad \text{as } \underline{r} \rightarrow \infty \quad (186a)$$

$$\underline{y} = \underline{\omega} \times \underline{r} \quad \text{at } \underline{r} = 1 \quad (186b)$$

where we have put  $V = a\omega$  in Eq. (4).

Assume a perturbation solution of the form

$$\underline{y}(\underline{r}; R) = \underline{y}_0(\underline{r}) + R\underline{y}_1(\underline{r}) + o(R) \quad (187)$$

with a similar expansion for the pressure field. Upon substituting these into the equations of motion and boundary conditions, one finds upon equating terms of order  $R^0$  that the zero-order fields satisfy Stokes equations,

$$\begin{aligned} \underline{\nabla} p_0 - \underline{\nabla}^2 \underline{y}_0 &= \underline{0} \\ \underline{\nabla} \cdot \underline{y}_0 &= 0 \end{aligned} \quad (188)$$

Furthermore, the zero-order boundary conditions require that

$$\begin{aligned} \underline{y}_0 &\rightarrow \underline{U} \quad \text{as } \underline{r} \rightarrow \infty \\ \underline{y}_0 &= \underline{0} \quad \text{at } \underline{r} = 1 \end{aligned} \quad (189)$$

in the case of streaming flow past the sphere, and

$$\begin{aligned} \underline{y}_0 &\rightarrow \underline{0} \quad \text{as } \underline{r} \rightarrow \infty \\ \underline{y}_0 &= \underline{\omega} \times \underline{r} \quad \text{at } \underline{r} = 1 \end{aligned} \quad (190)$$

for rotary motion of the sphere. Hence, the zero-order solutions are merely the appropriate Stokes solutions.

Upon equating terms of order  $R^1$  it is found that the first-order fields satisfy the differential equations

$$\begin{aligned} \underline{\nabla}^2 \underline{y}_1 - \underline{\nabla} p_1 &= \underline{y}_0 \cdot \underline{\nabla} \underline{y}_0 \\ \underline{\nabla} \cdot \underline{y}_1 &= 0 \end{aligned} \quad (191)$$

and boundary conditions

$$\underline{y}_1 = \underline{0} \quad \text{at both } \underline{r} = 1 \quad \text{and } \underline{r} = \infty \quad (192)$$

Since the zero-order fields are known, these perturbation equations are linear, *inhomogeneous*, Stokes-type equations. Particular integrals are very easy to obtain. To do so we note that Eq. (191) is formally equivalent to Stokes equations in the presence of nonconservative external volume forces. If  $\underline{\mathbf{f}} = \mathbf{f}a^2/\mu V$  denotes the dimensionless force per unit volume exerted by the surroundings at a point in the fluid, Stokes equations in nondimensional form become

$$\begin{aligned}\nabla^2 \underline{\mathbf{v}} - \nabla p &= -\underline{\mathbf{f}} \\ \nabla \cdot \underline{\mathbf{v}} &= 0\end{aligned}\quad (193)$$

But the fundamental solution of these equations for an isolated point force of strength  $\underline{\mathbf{F}} = \mathbf{F}/\mu aV$  at the point  $\underline{\mathbf{R}} = \mathbf{0}$  [i.e.,  $\underline{\mathbf{f}} = \underline{\mathbf{F}}\delta(\underline{\mathbf{R}})$ , where  $\delta$  is the Dirac delta function] is (L1, p. 48; L5, p. 605)

$$\begin{aligned}\underline{\mathbf{v}}(\underline{\mathbf{R}}) &= \frac{1}{8\pi|\underline{\mathbf{R}}|}\left(\mathbf{I} + \frac{\underline{\mathbf{R}}\underline{\mathbf{R}}}{|\underline{\mathbf{R}}|^2}\right) \cdot \underline{\mathbf{F}} \\ \underline{p}(\underline{\mathbf{R}}) &= \frac{\underline{\mathbf{R}}}{4\pi|\underline{\mathbf{R}}|^3} \cdot \underline{\mathbf{F}}\end{aligned}\quad (194)$$

Hence, the particular integral of (193) which vanishes when external forces are absent is

$$\underline{\mathbf{v}}(\underline{\mathbf{r}}) = \frac{1}{8\pi} \int \frac{1}{|\underline{\mathbf{r}} - \underline{\mathbf{r}}_0|} \left( \mathbf{I} + \frac{(\underline{\mathbf{r}} - \underline{\mathbf{r}}_0)(\underline{\mathbf{r}} - \underline{\mathbf{r}}_0)}{|\underline{\mathbf{r}} - \underline{\mathbf{r}}_0|^2} \right) \cdot \underline{\mathbf{f}}(\underline{\mathbf{r}}) dV_0 \quad (195a)$$

$$\underline{p}(\underline{\mathbf{r}}) = \frac{1}{4\pi} \int \frac{(\underline{\mathbf{r}} - \underline{\mathbf{r}}_0)}{|\underline{\mathbf{r}} - \underline{\mathbf{r}}_0|^3} \cdot \underline{\mathbf{f}}(\underline{\mathbf{r}}_0) dV_0 \quad (195b)$$

where  $dV_0 = d\underline{x}_0 d\underline{y}_0 d\underline{z}_0$ . Integration is over all of  $\underline{\mathbf{r}}_0$  space. By setting  $\underline{\mathbf{f}} = -\underline{\mathbf{v}}_0 \cdot \nabla \underline{\mathbf{v}}_0$  we obtain a particular integral of Eqs. (191).

In order to satisfy the boundary conditions (192) one may add to this particular integral the general solution of the homogeneous Stokes equations [cf. Brenner (B21), where general methods are developed for solving Stokes equations for spherical bodies]. This complementary function together with the particular integral furnish the solution of the perturbation equations (191) and (192).

As Whitehead (W7) showed long ago, no solution of the perturbation equations exists for streaming flow past a sphere or, in fact, for flow past any particle. The source of the difficulty is easily traced. At great distances from the sphere

$$\underline{\mathbf{v}}_0 = \underline{\mathbf{U}} + O(\underline{r}^{-1}) \quad (196)$$

so that  $\underline{\mathbf{v}}_0 \cdot \nabla \underline{\mathbf{v}}_0 = O(\underline{r}^{-2})$ . This immediately leads to a particular integral of (191) such that  $\underline{\mathbf{v}}_1 = O(\underline{r}^0)$ . But the term of  $O(\underline{r}^0)$  is not a constant vector—

for if it were it would satisfy the homogeneous, rather than inhomogeneous, Stokes equations. In order to satisfy the boundary condition (192) at infinity we must add to this particular integral a solution of the homogeneous Stokes equations, i.e., the complementary solution. But the only solution of the latter which is of  $O(r^0)$  at infinity is a *constant* vector. And this cannot cancel the *variable* vector of  $O(r^0)$  arising from the inhomogeneous equations. The nonexistence of solutions of the perturbation equations for streaming flows is known as Whitehead's paradox.

In the case of a rotating sphere the zero-order Stokes solution is (L5, p. 588)  $\underline{v}_0 = \underline{\omega} \times \underline{r}/r^3$ , and so<sup>21</sup>

$$\underline{v}_0 = O(r^{-2}) \quad (197)$$

This makes  $\underline{v}_0 \cdot \nabla \underline{v}_0 = O(r^{-5})$ , which obviously gives rise to a particular integral of the perturbation equations of the form  $\underline{v}_1 = O(r^{-3})$ . There is now no difficulty in finding a complementary function to permit satisfying the boundary conditions (192). Whitehead's paradox does not therefore extend to such rotary motions. These may be handled by the conventional perturbation scheme proposed by Whitehead.

## B. REGULAR PERTURBATION METHODS

Investigations of the perturbation equations for the rotating sphere have been carried out more or less independently by a number of individuals. The first of these appears to be due to Bickley (B5), who obtained a solution correct to the first order in  $R$ . His solution indicates an inflow of fluid towards the poles and a corresponding outflow around the equator. Rather interestingly, to this order in  $R$  the torque itself is unaffected and continues to be given by the Stokes formula

$$\mathbf{T} = -8\pi\mu a^3\omega[1 + o(R)]$$

In an important paper, Collins (C14) extended the above analysis to higher powers in  $R$ . Here, the series (187) proceeds in integral powers of  $R = a^2\omega\rho/\mu$ . Collins showed that the torque may be written as an infinite power series involving only *even* powers of  $R$ , the first three terms of which are

$$\mathbf{T} = -8\pi\mu a^3\omega \left[ 1 + \frac{1}{1200} R^2 - 7.542 \times 10^{-7} R^4 + O(R^6) \right] \quad (198)$$

<sup>21</sup> This rapid rate of attenuation of the velocity field is characteristic of all bodies for which the coupling dyadic vanishes at the center of reaction, providing that the body rotates about an axis through this point. However, it is only for axially symmetric bodies rotating about their symmetry axes that such motions may be stable.



Ovseenko (O5), apparently unaware of Collin's prior work, made a similar analysis and obtained exactly the same  $R^2$  torque correction term. Similar investigations of the rotation of a sphere in an unbounded fluid are given by DiFrancia (D5), Goldshtik (G6), and Khamrui (K9). In a subsequent paper (K10) the latter also investigated the rotation of an ellipsoid of revolution of small ellipticity about its symmetry axis.

Comparable investigations of the rotation of a sphere bounded externally by an outer, concentric sphere are presented by Bratukhin (B9), Haberman (H2), Langlois (L9), and Ovseenko (O6).

As a special case of some results due to Cox (C17), discussed at length in Section III,C, it appears that the torque on *any* body of revolution is unaffected by Reynolds number to the first order in  $R$  when it rotates about its symmetry axis. Rather, the torque is affected only in the  $O(R^2)$  approximation. Cox also finds that when the body lacks fore-aft symmetry it experiences a *force* of  $O(R)$  parallel to the symmetry axis [see Eq. (236)]. No such force appears in the Stokes approximation.

The remarkably small effect of Reynolds number indicated by Eq. (198) is well borne out experimentally. The torque on rotating bodies has been extensively studied in connection with power requirements for mixers, agitators, and similar devices. In the so-called "laminar" regime, logarithmic plots of the dimensionless Power number

$$N_{Po} = \frac{T}{\mu d^3 \omega} (N_{Re})^{-1}$$

vs the impeller Reynolds number  $N_{Re} = d^2 \omega \rho / \mu$  ( $d$  = impeller diameter) are usually linear up to about  $N_{Re} = 10$  (P5), roughly in agreement with the effective linear range indicated by Eq. (198). It should be pointed out, however, that these data pertain to propellers, turbine blades, and paddles, rather than spheres. This writer is not aware of any data on spherical particles with which (198) may be more quantitatively compared.

Conventional perturbation schemes have also found application in the problem of flow through a wavy pipe with corrugated walls (B3). A comparable two-dimensional problem involving shearing flow past a sinusoidal wall was solved long ago by Rayleigh (R2).

### C. SINGULAR PERTURBATION METHODS

Whitehead's paradox was resolved by Oseen (O3, O4), who pointed out a fundamental inconsistency in connection with Stokes-type approximations of the streaming flow problem. This lack of internal consistency is evident if we compute the ratio of inertial to viscous terms from Stokes solution (196).

Since  $\underline{\mathbf{v}} = O(\underline{r}^{-1})$  this ratio is

$$\frac{R|\underline{\mathbf{v}}_0 \cdot \underline{\nabla} \underline{\mathbf{v}}_0|}{|\underline{\nabla}^2 \underline{\mathbf{v}}_0|} = \frac{RO(\underline{r}^{-2})}{O(\underline{r}^{-3})} = O(R\underline{r})$$

when  $\underline{r}$  is large. Thus, no matter how small  $R$  may be, the assumption that the inertial terms are negligible compared with the viscous terms becomes invalid for sufficiently large  $\underline{r}$ . In particular, the assumption breaks down when  $R\underline{r} = O(1)$ <sup>22</sup>. Evidently, the *global* criterion that  $R$  be small is a necessary but insufficient condition for the success of Stokes-type approximations.

When  $R$  is small, Stokes solution is inconsistent only for large  $\underline{r}$ . But at these large distances the flow is virtually a uniform stream,  $\underline{\mathbf{U}}$ . Oseen therefore suggested replacing the nonlinear inertial term  $\underline{\mathbf{v}} \cdot \underline{\nabla} \underline{\mathbf{v}}$  in the Navier-Stokes equations (183) by the linearized approximation  $\underline{\mathbf{U}} \cdot \underline{\nabla} \underline{\mathbf{v}}$ . The resulting linear equations,

$$\begin{aligned} \underline{\nabla} p - \underline{\nabla}^2 \underline{\mathbf{v}} + R \underline{\mathbf{U}} \cdot \underline{\nabla} \underline{\mathbf{v}} &= \mathbf{0} \\ \underline{\nabla} \cdot \underline{\mathbf{v}} &= 0 \end{aligned} \quad (199)$$

are known as Oseen's equations (O4) (for steady flows). Oseen himself obtained a first-order solution, satisfying the differential equations and boundary condition  $\underline{\mathbf{v}} = \underline{\mathbf{U}}$  at  $\underline{r} = \infty$  exactly, and the boundary condition  $\underline{\mathbf{v}} = \mathbf{0}$  on the sphere  $\underline{r} = 1$  correctly to  $O(R)$ . As is well known, he found the force on the sphere to be given correctly to the zeroth order in  $R$  by Stokes law,  $\mathbf{F} = 6\pi\mu a \mathbf{U}$ .

By removing the inconsistency, Oseen thus placed Stokes result on a firmer mathematical footing. In effect, Oseen's solution provides a uniformly valid zero-order approximation to the solution of the Navier-Stokes equations throughout all space. Unfortunately, a stronger interpretation than this was ascribed to Oseen's solution. Prevailing opinion at the time, and indeed for many years after, held that Oseen's solution was, in fact, an asymptotically valid solution of the Navier-Stokes equations to  $O(R)$ . This led to the well-known Oseen correction of Stokes law,<sup>23</sup>

$$\mathbf{F} = 6\pi\mu a \mathbf{U} [1 + \frac{3}{8}R + o(R)] \quad (200)$$

and occasioned a vast body of literature dealing with the solution of Oseen's equations for a variety of physical situations.

<sup>22</sup> Note from Eq. (197) for a *rotating* sphere that the ratio of inertial to viscous terms is of  $O(R\underline{r}^{-2})$ . Thus, Stokes assumption is consistent for all  $\underline{r}$  when  $R \rightarrow 0$ . In essence, this is the reason why regular perturbation schemes work for the rotating sphere, but are invalid for streaming flow.

<sup>23</sup> Goldstein's (G10) extension of Oseen's solution to  $O(R^5)$  was found by Shanks (S9) to be in error in the last term.

Though inconsistencies were discovered in this interpretation,<sup>24</sup> it was not until the work of Lagerstrom, Cole, and Kaplun (K3, K4, L2, L3) and of Proudman and Pearson (P11) that this long-standing issue was resolved by the introduction of singular perturbation techniques. Their work showed that Oseen's analysis was not, in fact, correct to  $O(R)$ —but only to  $O(R^0)$ . In its application to low Reynolds number streaming flows the underlying theme of the technique is as follows: One abandons, at least temporarily, attempts to obtain a single, *uniformly valid* expansion of the exact Navier–Stokes equations in orders of  $R$ . Instead, one attempts to find *two* expansions of the exact solution, each one of which is only *locally valid* in a different region of the fluid.

The “inner” expansion, valid only in the neighborhood of the particle, is essentially of the type envisioned by Whitehead (W7):

$$\underline{\mathbf{v}}(R; \underline{\mathbf{r}}) = \underline{\mathbf{v}}_0(\underline{\mathbf{r}}) + R\underline{\mathbf{v}}_1(\underline{\mathbf{r}}) + o(R) \quad (201a)$$

$$\underline{p}(R; \underline{\mathbf{r}}) = \underline{p}_0(\underline{\mathbf{r}}) + R\underline{p}_1(\underline{\mathbf{r}}) + o(R) \quad (201b)$$

When these are substituted into the exact Navier–Stokes equations (183)–(184), and into the “inner” boundary condition (185b), and terms of the same order in  $R$  equated, one finds that the first few terms in the expansion satisfy the relations

$$\begin{aligned} \underline{\nabla}^2 \underline{\mathbf{v}}_0 - \underline{\nabla} \underline{p}_0 &= \mathbf{0} \\ \underline{\nabla} \cdot \underline{\mathbf{v}}_0 &= 0 \\ \underline{\mathbf{v}}_0 &= \mathbf{0} \quad \text{at} \quad \underline{r} = 1 \end{aligned} \quad (202)$$

and

$$\begin{aligned} \underline{\nabla}^2 \underline{\mathbf{v}}_1 - \underline{\nabla} \underline{p}_1 &= \underline{\mathbf{v}}_0 \cdot \underline{\nabla} \underline{\mathbf{v}}_0 \\ \underline{\nabla} \cdot \underline{\mathbf{v}}_1 &= 0 \\ \underline{\mathbf{v}}_1 &= \mathbf{0} \quad \text{at} \quad \underline{r} = 1 \end{aligned} \quad (203)$$

Observe that these equations are linear. Since it is not expected that the inner expansion will be valid at great distances from the sphere, these fields are not required to satisfy the physical boundary conditions at infinity. In the absence of some additional “outer” boundary condition these fields are not unique. The additional boundary condition required for uniqueness is furnished by the “matching” requirement with the outer expansion.

The “outer” expansion, valid only at great distances from the sphere, is

<sup>24</sup> See, for example, the paradox uncovered by Garstang (G1a) and subsequently resolved by Rubinow and Keller (R7).

of a very different character. We first stretch the coordinates by defining the outer coordinates

$$\underline{\tilde{\mathbf{r}}} = R\underline{\mathbf{r}} \quad (204)$$

and scale the independent variables by introducing the outer variables

$$\begin{aligned} \underline{\tilde{\mathbf{v}}}(R; \underline{\tilde{\mathbf{r}}}) &= \underline{\mathbf{v}}\left(R; \underline{\mathbf{r}} = \frac{\underline{\tilde{\mathbf{r}}}}{R}\right) \\ \underline{\tilde{p}}(R; \underline{\tilde{\mathbf{r}}}) &= \frac{1}{R} \underline{p}\left(R; \underline{\mathbf{r}} = \frac{\underline{\tilde{\mathbf{r}}}}{R}\right) \end{aligned} \quad (205)$$

In terms of these new quantities the exact Navier-Stokes equations and boundary conditions become

$$\begin{aligned} \underline{\tilde{\nabla}}^2 \underline{\tilde{\mathbf{v}}} - \underline{\tilde{\nabla}} \underline{\tilde{p}} - \underline{\tilde{\mathbf{v}}} \cdot \underline{\tilde{\nabla}} \underline{\tilde{\mathbf{v}}} &= \mathbf{0} \\ \underline{\tilde{\nabla}} \cdot \underline{\tilde{\mathbf{v}}} &= 0 \\ \underline{\tilde{\mathbf{v}}} &= \underline{\mathbf{U}} \quad \text{at } \underline{\tilde{r}} = \infty \\ \underline{\tilde{\mathbf{v}}} &= \mathbf{0} \quad \text{at } \underline{\tilde{r}} = R \end{aligned} \quad (206)$$

These transformations have explicitly removed the Reynolds number from the differential equations of motion, thus making the viscous and inertial terms of comparable order. It was, in fact, to accomplish this (at least in the limiting case  $R \rightarrow 0$ ) that the various transformations were originally introduced.

The outer expansion is assumed to be of the form

$$\underline{\tilde{\mathbf{v}}}(R; \underline{\tilde{\mathbf{r}}}) = \underline{\tilde{\mathbf{v}}}_0(\underline{\tilde{\mathbf{r}}}) + R\underline{\tilde{\mathbf{v}}}_1(\underline{\tilde{\mathbf{r}}}) + o(R) \quad (207a)$$

$$\underline{\tilde{p}}(R; \underline{\tilde{\mathbf{r}}}) = \underline{\tilde{p}}_0(\underline{\tilde{\mathbf{r}}}) + R\underline{\tilde{p}}_1(\underline{\tilde{\mathbf{r}}}) + o(R) \quad (207b)$$

Upon substituting these into the equations of motion and outer boundary condition in (206), one finds upon equating terms of equal order in  $R$  that the first few terms in the expansion satisfy the relations

$$\begin{aligned} \underline{\tilde{\nabla}}^2 \underline{\tilde{\mathbf{v}}}_0 - \underline{\tilde{\nabla}} \underline{\tilde{p}}_0 - \underline{\tilde{\mathbf{v}}}_0 \cdot \underline{\tilde{\nabla}} \underline{\tilde{\mathbf{v}}}_0 &= \mathbf{0} \\ \underline{\tilde{\nabla}} \cdot \underline{\tilde{\mathbf{v}}}_0 &= 0 \\ \underline{\tilde{\mathbf{v}}}_0 &= \underline{\mathbf{U}} \quad \text{at } \underline{\tilde{r}} = \infty \end{aligned} \quad (208)$$

and

$$\begin{aligned} \underline{\tilde{\nabla}}^2 \underline{\tilde{\mathbf{v}}}_1 - \underline{\tilde{\nabla}} \underline{\tilde{p}}_1 - (\underline{\tilde{\mathbf{v}}}_1 \cdot \underline{\tilde{\nabla}} \underline{\tilde{\mathbf{v}}}_0 + \underline{\tilde{\mathbf{v}}}_0 \cdot \underline{\tilde{\nabla}} \underline{\tilde{\mathbf{v}}}_1) &= \mathbf{0} \\ \underline{\tilde{\nabla}} \cdot \underline{\tilde{\mathbf{v}}}_1 &= 0 \\ \underline{\tilde{\mathbf{v}}}_1 &= \mathbf{0} \quad \text{at } \underline{\tilde{r}} = \infty \end{aligned} \quad (209)$$

Both sets of equations are linear. Since it is not expected that the outer expansion is valid near the body, these fields are not required to satisfy the inner boundary conditions on the body. Accordingly, Eqs. (208) and (209) are not unique without the specification of some "inner" boundary condition. This additional condition is furnished by the "matching" requirement with the inner expansion.

As they presently stand, neither the inner nor outer fields are uniquely defined. The inner fields lack an outer boundary condition for large  $\underline{r}$ , whereas the outer fields lack an inner boundary condition for small  $\underline{\tilde{r}}$ . Both sets of conditions are simultaneously furnished by the *matching principle*. According to this principle, two asymptotic solutions of the same differential equations and boundary conditions must be asymptotically equal in their common domain of validity (if such an overlap region exists). The principle is based on the observation that the inner and outer expansions are merely two alternative asymptotic expansions (for small  $R$ ) of the one *exact* solution of the problem, one being the "Stokes expansion,"  $R \downarrow 0$  with  $\underline{r}$  fixed, and the other being the "Oseen expansion,"  $R \downarrow 0$  with  $R\underline{r}$  fixed. On the basis of earlier observations it is to be expected that the overlap domain in which both solutions are equally valid occurs when  $R\underline{r} = O(1)$ . This dimensionless distance from the sphere is small in terms of the stretched coordinate  $\underline{\tilde{r}} = R\underline{r}$ , but it is very large in terms of the unstretched inner coordinate  $\underline{r}$ . Thus, roughly speaking, the matching condition requires that, when expressed in one common set of coordinates and variables—either inner or outer—

$$\underline{\tilde{v}}(R; \underline{\tilde{r}} \rightarrow 0) \equiv \underline{v}(R; \underline{r} \rightarrow \infty) \quad (210)$$

to any order in  $R$ .

Matching to the zeroth order in  $R$  requires that

$$\underline{\tilde{v}}_0(\underline{\tilde{r}} \rightarrow 0) \equiv \underline{v}_0(\underline{r} \rightarrow \infty)$$

In conjunction with Eqs. (202) and (207) it is found that the zero-order term in the outer expansion is simply

$$\underline{\tilde{v}}_0 = \underline{U} \quad (211)$$

with  $\underline{\tilde{p}}_0 = 0$ , while the zero-order term,  $(\underline{v}_0, \underline{p}_0)$ , in the inner expansion is, as would be expected, Stokes solution for streaming flow past the sphere.

Substitution of (211) into (209) shows that the first-order term in the outer expansion satisfies Oseen's equations (199). The first-order term in the inner expansion, defined by Eq. (203), obviously corresponds to a Whitehead-type term, except that the original difficulty (W7) encountered in attempting to satisfy the actual boundary condition at infinity no longer exists. Final expressions for these fields satisfying the matching conditions to  $O(R)$  are given in the original reference (P11). With regard to the force on the sphere,

Proudman and Pearson obtained Oseen's result, Eq. (200). That they obtained the same result as did Oseen is, however, fortuitous. For Oseen's original velocity field does not agree to  $O(R)$  with the correct asymptotic solution of the Navier-Stokes equations. Rather it is correct only to  $O(R^0)$ .

Continuing their approximation, Proudman and Pearson (P11) find

$$\mathbf{F} = 6\pi\mu a\mathbf{U}\left[1 + \frac{3}{8}R + \frac{9}{40}R^2 \ln R + O(R^2)\right] \quad (212)$$

The appearance of transcendental terms in  $R$  is in marked contrast to Goldstein's (G10) formula for the force on a sphere to  $O(R^5)$  (see footnote 23) when the Oseen, rather than Navier-Stokes, equations are taken as the basic equations of motion. Equation (212) represents an asymptotic expansion having the general form

$$\mathbf{F} = 6\pi\mu a\mathbf{U}[f_0(R) + f_1(R) + f_2(R) + \dots]$$

where  $f_0(R) = 1$  and, for  $n = 0, 1, 2, \dots$ ,

$$f_{n+1}(R)/f_n(R) \rightarrow 0 \quad \text{as } R \rightarrow 0$$

An expression of the same general structure as (212) was obtained by Breach (B10) for axially symmetric streaming flow past prolate and oblate spheroids. In a significant extension of Breach's analysis, Shi (S9a) treats the problem of streaming flow past a prolate spheroid of large aspect ratio for the case where the axis of revolution of the ellipsoid is perpendicular, rather than parallel, to the uniform stream at infinity. The observation is made that such an ellipsoidal "needle" possesses *two* characteristic lengths (the major and minor semi-axes), each of which gives rise to its own distinct Reynolds number. In contrast with Breach's treatment, where it is implicitly assumed that both of these Reynolds numbers are small compared with unity, Shi analyzes the case where the minor-axis Reynolds number tends to zero for a *fixed* value of the major-axis Reynolds number. The latter need not be small. Though the ellipsoidal needle is a strictly three-dimensional particle, the drag per unit length is found to be the same as for two-dimensional streaming flow past a circular cylinder (K3, K4, P11), at least to terms of lowest order in the minor-axis Reynolds number. As such, the asymptotic expansion formula for the drag proceeds in inverse powers of the logarithm of the minor-axis Reynolds number, in marked contrast with formulas of the type (212). The coefficients of these logarithmic terms explicitly involve the major-axis Reynolds number. Shi's analysis clarifies the relationship between Oberbeck's classical solution for Stokes flow past an ellipsoid [see Eq. (58)] of large aspect ratio and two-dimensional "Oseen" flow past a circular cylinder.

Using these asymptotic matching techniques, Rubinow and Keller (R7) calculated, to  $O(R)$ , the force and torque on a translating sphere simultaneously spinning about any axis through its center in a fluid at rest at infinity.

They found for the force

$$\mathbf{F} = -6\pi\mu a \mathbf{U}(1 + \frac{3}{8}R) + R \frac{\pi\mu a^2}{U} \boldsymbol{\omega} \times \mathbf{U} + \mu a U o(R) \quad (213)$$

and, for the torque about the sphere center,

$$\mathbf{T} = -8\pi\mu a^3 \boldsymbol{\omega}[1 + O(R)] \quad (214)$$

The hydrodynamic force thus consists of a drag force,

$$\mathbf{F}_D = -6\pi\mu a \mathbf{U}[1 + \frac{3}{8}R + o(R)] \quad (215)$$

antiparallel to the direction of motion of the sphere, and a lift force,

$$\mathbf{F}_L = \pi a^3 \rho \boldsymbol{\omega} \times \mathbf{U}[1 + O(R)] \quad (216)$$

at right angles to this direction. Rather remarkably, this sidewise force is independent of viscosity for small values of  $R$ . This force is comparable to the well-known Magnus force (G11), arising at very high Reynolds numbers, usually invoked to explain such phenomena as the curving of a pitched baseball.

The solution of the Rubinow-Keller problem had previously been attempted by Garstang (G1a) on the basis of the Oseen equations. His result for the lift force is larger than (216) by a factor of  $4/3$ . But as Garstang himself pointed out, his result was not unequivocal. Rather, different results were obtained according as the integration of the momentum flux was carried out at the surface of the sphere or at infinity. Garstang's "paradox" is clearly due to the fact that the term  $\mathbf{U} \cdot \nabla \mathbf{v}$  does not represent a uniformly valid approximation of the inertial term  $\mathbf{v} \cdot \nabla \mathbf{v}$  throughout all portions of the fluid, at least not to the first order in  $R$ .

To terms of  $O(R)$ , Brenner (B15) and Chester (C7) independently<sup>25</sup> extended the Proudman and Pearson analysis (P11) to streaming flow past the general class of bodies possessing sufficient symmetry to cause the hydrodynamic vector force on the body to be reversed when the direction of the stream velocity at infinity is reversed without change of magnitude, e.g., an ellipsoid at an arbitrary angle of incidence. A simple algebraic expression was found relating this force directly to the Stokes translation dyadic for the body. (This general formula, as well as those discussed in subsequent paragraphs, is applicable only to the case where the Reynolds number based upon the *maximum* linear dimension of the particle is small compared with unity.)

These results were further generalized by Brenner and Cox (B27) to rigid bodies of arbitrary shape, devoid of any symmetry whatsoever, and extended

<sup>25</sup> These results to  $O(R)$  were also obtained independently by O'Brien (O1) in the special case of axially symmetric flow past a body of revolution possessing fore-aft symmetry.

by them to terms of  $O(R^2 \ln R)$ . Finally, to this same order in  $R$ , Cox (C17) generalized the latter analysis to the case where the body in question may also rotate as it translates. In particular, general expressions were obtained for the force and torque, to  $O(R^2 \ln R)$ , experienced by a rigid translating-rotating body of arbitrary shape in steady or quasi-steady motion through a fluid at rest at infinity. The results are expressed explicitly in terms of the intrinsic translational and rotational *Stokes* dyadic velocity fields (see Section II,C,1). Thus, detailed knowledge of the translational and rotational flow fields to  $O(R^0)$  permits an immediate computation of the force and torque on the body in question to  $O(R^2 \ln R)$ . The calculation itself involves only a straightforward, though perhaps tedious, quadrature. Moreover, if the body possesses certain geometric symmetries, one need not even know the detailed Stokes velocity fields for the body. Rather, the forces and torques to  $O(R^2 \ln R)$  may be computed, without quadrature, solely from knowledge of the Stokes translation, rotation, and coupling dyadics for the body in question. And these are purely phenomenological coefficients which, at least in principle, may be obtained from purely macroscopic experiments on the body in the Stokes regime. One by-product of this investigation (B27, C17) is that Oseen's equation, though furnishing the correct vector force to  $O(R)$  on bodies possessing a high degree of symmetry, e.g., spheres and ellipsoids, generally leads to an incorrect result to  $O(R)$  for less symmetrical bodies.

As the Brenner-Cox (B27, C17) relations are not readily susceptible to further generalization it is appropriate to summarize them in some detail here. A nondimensional form is most convenient. As usual, let  $\mathbf{U}$  be the velocity of any point  $O$  affixed to the body and  $\boldsymbol{\omega}$  the angular velocity of the body. Further, let  $a$  be any characteristic particle dimension and  $\mathcal{V}$  be any characteristic speed, e.g.,  $|\mathbf{U}|$  or  $a|\boldsymbol{\omega}|$ . The ultimate results are independent of the choice of these characteristic parameters.  $R = a\mathcal{V}\rho/\mu$  denotes the particle Reynolds number. A dimensionless hydrodynamic force and torque about  $O$  are defined as follows:

$$\begin{aligned}\underline{\mathbf{F}} &= \mathbf{F}/6\pi\mu a\mathcal{V} \\ \underline{\mathbf{T}} &= \mathbf{T}/6\pi\mu a^2\mathcal{V}\end{aligned}\tag{217}$$

Introduction of the extraneous factor of  $6\pi$  has the advantage of rendering many of the subsequent coefficients unity for translating spherical particles. The vectors

$$\underline{\mathbf{U}} = \mathbf{U}/\mathcal{V}, \quad \underline{\boldsymbol{\omega}} = \boldsymbol{\omega}a/\mathcal{V}\tag{218}$$

denote the dimensionless particle velocity and spin. Note carefully that these are not unit vectors in general, though either one could be made so by an



appropriate choice of  $\mathcal{V}$ . Furthermore, let

$$\begin{aligned}\underline{\mathbf{K}}^{(t)} &= \mathbf{K}/6\pi a \\ \underline{\mathbf{K}}^{(c)} &= \mathbf{K}/6\pi a^2 \\ \underline{\mathbf{K}}^{(r)} &= \mathbf{K}/6\pi a^3\end{aligned}\quad (219)$$

represent the dimensionless Stokes translation, coupling, and rotation dyadics at  $O$ . Finally, set

$$\underline{\mathbf{V}}^{(t)} = \mathbf{V}, \quad \underline{\mathbf{V}}^{(r)} = \mathbf{V}/a \quad (220)$$

where  $\mathbf{V}^{(t)}$  and  $\mathbf{V}^{(r)}$  are the (dimensional) intrinsic Stokes translational and rotational dyadic "velocity" fields defined in Section II,C,1. The corresponding dimensionless rate-of-strain triadic fields are denoted by

$$\underline{\mathbf{E}}^{(c)} = \frac{1}{2} [\underline{\mathbf{V}}\underline{\mathbf{V}} + {}^t(\underline{\mathbf{V}}\underline{\mathbf{V}})] \quad (221)$$

in which  $\underline{\mathbf{V}} = a\nabla$ .

The principal results are as follows:

(i) The force and torque on a solid body of arbitrary shape moving with steady or quasi-steady<sup>26</sup> motion through an incompressible fluid at rest at infinity are given to  $O(R^2 \ln R)$  by the expressions

$$\begin{pmatrix} \underline{\mathbf{F}} \\ \underline{\mathbf{T}} \end{pmatrix} = \begin{pmatrix} {}^1\underline{\mathbf{F}} \\ {}^1\underline{\mathbf{T}} \end{pmatrix} + \begin{pmatrix} {}^2\underline{\mathbf{F}} \\ {}^2\underline{\mathbf{T}} \end{pmatrix} + O(R^2) \quad (222a)$$

Here,

$$\begin{aligned}\begin{pmatrix} {}^1\underline{\mathbf{F}} \\ {}^1\underline{\mathbf{T}} \end{pmatrix} &= \begin{pmatrix} \underline{\mathbf{F}}_0 \\ \underline{\mathbf{T}}_0 \end{pmatrix} - \begin{pmatrix} {}^{(t)}\underline{\mathbf{K}} \\ {}^{(c)}\underline{\mathbf{K}} \end{pmatrix} \cdot \left[ \frac{3}{16} R \frac{1}{|\underline{\mathbf{U}}|} (3\underline{\mathbf{F}}_0 \underline{\mathbf{U}} \cdot \underline{\mathbf{U}} - \underline{\mathbf{F}}_0 \cdot \underline{\mathbf{U}}\underline{\mathbf{U}}) \right. \\ &\quad \left. + \frac{3}{320} (R^2 \ln R) (31 \underline{\mathbf{F}}_0 \underline{\mathbf{F}}_0 \cdot \underline{\mathbf{U}} - 7 \underline{\mathbf{U}} \underline{\mathbf{F}}_0 \cdot \underline{\mathbf{F}}_0) \right] \end{aligned} \quad (223a)$$

$$(223b)$$

in which

$$\begin{pmatrix} \underline{\mathbf{F}}_0 \\ \underline{\mathbf{T}}_0 \end{pmatrix} = - \begin{pmatrix} {}^{(t)}\underline{\mathbf{K}} \\ {}^{(c)}\underline{\mathbf{K}} \end{pmatrix} \cdot \underline{\mathbf{U}} - \begin{pmatrix} {}^{(c)}\underline{\mathbf{K}}^\dagger \\ {}^{(r)}\underline{\mathbf{K}} \end{pmatrix} \cdot \underline{\boldsymbol{\omega}} \quad (224)$$

$$(225)$$

are, respectively, the Stokes force and torque on the body.

<sup>26</sup> By quasi-steady motion here, we mean an unsteady motion for which the time-dependent terms in the equations of motion and boundary conditions are of higher order in  $R$  than  $O(R^2 \ln R)$ .

The remaining terms are given by the expressions

$$\begin{pmatrix} 2\mathbf{F} \\ 2\mathbf{T} \end{pmatrix} = \frac{R}{6\pi} \left[ \begin{pmatrix} (t) \\ (r) \end{pmatrix} \mathcal{K}^{[tt]} : \mathbf{U}\mathbf{U} + 2 \begin{pmatrix} (t) \\ (r) \end{pmatrix} \mathcal{K}^{[rt]} : \mathbf{U}\boldsymbol{\omega} + \begin{pmatrix} (t) \\ (r) \end{pmatrix} \mathcal{K}^{[rr]} : \boldsymbol{\omega}\boldsymbol{\omega} \right] \quad (226a)$$

$$\quad (226b)$$

in which the  $\mathcal{K}$ 's are intrinsic, constant, dimensionless, inertial resistance triadics, dependent solely upon the external shape of the body. Written in Cartesian tensor form<sup>27</sup> they may be expressed in terms of the detailed translational and rotational Stokes fields for the body in question by means of the relations

$$\mathcal{K}_{jkl}^{(t)} = \int_{\Gamma} \underline{E}_{mnj}^{(t)} \underline{V}_{mk}^{(r)} \underline{V}_{nl}^{(r)} d\Gamma \quad (227a)$$

$$\mathcal{K}_{jkl}^{(r)} = \int_{\Gamma} \underline{E}_{mnj}^{(r)} \underline{V}_{mk}^{(t)} (\underline{V}_{nl}^{(t)} - \delta_{nl}) d\Gamma \quad (227b)$$

$$\begin{aligned} \mathcal{K}_{jkl}^{(tt)} = & -\frac{1}{2} \left[ \int_{\underline{S}_L} -{}_2\underline{V}_{kj} d\underline{S}_l + \int_{\underline{S}_L} -{}_2\underline{V}_{lj} d\underline{S}_k \right] \\ & + \int_{\Gamma} \underline{E}_{mnj}^{(t)} (\underline{V}_{mk}^{(t)} - \delta_{mk}) (\underline{V}_{nl}^{(t)} - \delta_{nl}) d\Gamma \end{aligned} \quad (227c)$$

which holds for  $(\ ) \equiv (t)$  or  $(r)$ . In these expressions  $\Gamma$  is the volume of space external to the particle,  $\underline{S}_L$  is a spherical surface of indefinitely large radius containing the particle at its center, and  ${}_2\underline{V}$  is that term in  $\underline{V}$  which is homogeneous in  $\underline{r}^{-2}$  in the asymptotic expansion of  $\underline{V}$  for large  $\underline{r}$ . The distance  $\underline{r}$ , surface  $\underline{S}_L$ , and volume  $\Gamma$  have been made dimensionless with the particle dimension  $a$ .

We note from Eq. (221) that

$$\underline{E}_{mnj}^{(\ )} = \frac{1}{2} (\underline{V}_{nj,m}^{(\ )} + \underline{V}_{mj,n}^{(\ )})$$

(ii) The tensors  $\mathcal{K}_{ijk}^{[tt]}$ ,  $\mathcal{K}_{ijk}^{[rr]}$ , and  $\mathcal{K}_{ijk}^{[rt]}$  are *true* (polar) third-order tensors.

<sup>27</sup> That is, if  $\mathbf{i}_1, \mathbf{i}_2, \mathbf{i}_3$  are any triad of orthonormal vectors, constant throughout space, then

$$\mathbf{d} = \mathbf{i}_j \mathbf{i}_k d_{jk} \quad (\text{summation convention})$$

$$\mathbf{t} = \mathbf{i}_j \mathbf{i}_k \mathbf{i}_l t_{jkl} \quad (\text{summation convention})$$

where  $\mathbf{d}$  is any dyadic and  $\mathbf{t}$  any triadic.

The two “translational” ( $t$ )-tensors satisfy the trivial symmetry conditions

$$\underline{\mathcal{K}}_{ijk}^{[tt]} = \underline{\mathcal{K}}_{ikj}^{[tt]} \quad (228a)$$

$$\underline{\mathcal{K}}_{ijk}^{[rr]} = \underline{\mathcal{K}}_{ikj}^{[rr]} \quad (228b)$$

The tensors  $\underline{\mathcal{K}}_{ijk}^{[rr]}$ ,  $\underline{\mathcal{K}}_{ijk}^{[rt]}$ , and  $\underline{\mathcal{K}}_{ijk}^{[rt]}$  are *pseudo* (axial) third-order tensors. The two “rotational” ( $r$ )-tensors satisfy the trivial symmetry conditions

$$\underline{\mathcal{K}}_{ijk}^{[rr]} = \underline{\mathcal{K}}_{ikj}^{[rr]} \quad (229a)$$

$$\underline{\mathcal{K}}_{ijk}^{[rt]} = \underline{\mathcal{K}}_{ikj}^{[rt]} \quad (229b)$$

The dependence of these six inertial resistance triadics on choice of origin may be obtained by application of the general methods described in the paragraph immediately following Eq. (50). [See also the similar calculations in Section 3 of Brenner (B23).]

(iii) The  ${}^1\mathbf{F}$  and  ${}^1\mathbf{T}$  terms in Eq. (222) can be computed solely from knowledge of the three phenomenological Stokes resistance dyadics. The  ${}^2\mathbf{F}$  and  ${}^2\mathbf{T}$  terms require detailed knowledge of the Stokes velocity fields themselves.<sup>28</sup> In dimensional form the  ${}^2\mathbf{F}$  and  ${}^2\mathbf{T}$  terms are independent of viscosity, and are directly proportional to the fluid density.

The results given here apply to the case where the particle translates (and rotates) in a fluid at rest at infinity. To convert them to the case of streaming flow past the body with stream velocity  $\underline{\mathbf{U}}$ , as in Brenner and Cox (B27), replace  $\underline{\mathbf{U}}$  in the preceding equations by  $-\underline{\mathbf{U}}$ , and  $\underline{\mathbf{V}}$  by  $\underline{\mathbf{I}} - \underline{\mathbf{V}}$ . Note that the latter substitution requires that  $\underline{\mathbf{E}}$  be replaced by  $-\underline{\mathbf{E}}$ .

(iv) If the vectors  $\underline{\mathbf{U}}$  and  $\underline{\boldsymbol{\omega}}$  are *both* reversed, then  ${}^1\mathbf{F}$  and  ${}^1\mathbf{T}$  are reversed, whereas  ${}^2\mathbf{F}$  and  ${}^2\mathbf{T}$  remain unaltered.

(v) If  $\{\underline{\mathbf{U}}, \underline{\boldsymbol{\omega}}\} \neq \mathbf{0}$ , the {force, torque},  $\{{}^2\mathbf{F}, {}^2\mathbf{T}\}$ , may be written as the sum of a *lift* term

$$\begin{pmatrix} {}^2\mathbf{F}_L \\ {}^2\mathbf{T}_L \end{pmatrix} = \frac{R}{6\pi} \begin{pmatrix} (\underline{\mathbf{I}} - \underline{\mathbf{U}}\underline{\mathbf{U}}/|\underline{\mathbf{U}}|^2) \\ (\underline{\mathbf{I}} - \underline{\boldsymbol{\omega}}\underline{\boldsymbol{\omega}}/|\underline{\boldsymbol{\omega}}|^2) \end{pmatrix} \cdot \left[ \begin{pmatrix} \underline{\mathcal{K}}^{[tt]} \\ \underline{\mathcal{K}}^{[rt]} \end{pmatrix} : \underline{\mathbf{U}}\underline{\mathbf{U}} \right. \quad (230a)$$

$$\left. + 2 \begin{pmatrix} \underline{\mathcal{K}}^{[rt]} \\ \underline{\mathcal{K}}^{[rr]} \end{pmatrix} : \underline{\mathbf{U}}\underline{\boldsymbol{\omega}} + \begin{pmatrix} \underline{\mathcal{K}}^{[rr]} \\ \underline{\mathcal{K}}^{[rr]} \end{pmatrix} : \underline{\boldsymbol{\omega}}\underline{\boldsymbol{\omega}} \right] \quad (230b)$$

<sup>28</sup> One could, of course, alternatively regard the  $\mathcal{K}$  coefficients as intrinsic phenomenological parameters to be determined from macroscopic experiments on the particle at small, but nonzero Reynolds numbers.

and a *drag* term

$$\begin{aligned} \begin{pmatrix} {}^2\mathbf{F}_D \\ {}^2\mathbf{T}_D \end{pmatrix} = -\frac{R}{6\pi} \begin{pmatrix} \mathbf{U}\boldsymbol{\omega}/|\mathbf{U}|^2 \\ \boldsymbol{\omega}\mathbf{U}/|\boldsymbol{\omega}|^2 \end{pmatrix} \cdot \left[ \begin{pmatrix} {}^{(r)}\mathcal{K}^{[tr]} \\ {}^{(t)}\mathcal{K}^{[tr]} \end{pmatrix} : \mathbf{U}\mathbf{U} \right. \\ \left. + 2 \begin{pmatrix} {}^{(r)}\mathcal{K}^{[rt]} \\ {}^{(t)}\mathcal{K}^{[rt]} \end{pmatrix} : \mathbf{U}\boldsymbol{\omega} + \begin{pmatrix} {}^{(r)}\mathcal{K}^{[rr]} \\ {}^{(t)}\mathcal{K}^{[rr]} \end{pmatrix} : \boldsymbol{\omega}\boldsymbol{\omega} \right] \end{aligned} \quad (231a)$$

$$\begin{aligned} & + 2 \begin{pmatrix} {}^{(r)}\mathcal{K}^{[rt]} \\ {}^{(t)}\mathcal{K}^{[rt]} \end{pmatrix} : \mathbf{U}\boldsymbol{\omega} + \begin{pmatrix} {}^{(r)}\mathcal{K}^{[rr]} \\ {}^{(t)}\mathcal{K}^{[rr]} \end{pmatrix} : \boldsymbol{\omega}\boldsymbol{\omega} \end{aligned} \quad (231b)$$

the lift term being perpendicular to  $\{\mathbf{U}, \boldsymbol{\omega}\}$ , and the drag term parallel to  $\{\mathbf{U}, \boldsymbol{\omega}\}$ .

(vi) For nonrotating bodies  ${}^2\mathbf{F}_D$  vanishes, so that  ${}^2\mathbf{F}$  is purely a *lift* force. It follows that the *drag* on a body of arbitrary shape is thus given to  $O(R^2 \ln R)$  by that component of  ${}^1\mathbf{F}$  lying parallel to  $\mathbf{U}$ . This drag is reversed by a reversal of  $\mathbf{U}$ , and is expressible entirely in terms of the Stokes force  $\mathbf{F}_0$  on the body. The dimensional drag formula can be expressed in elementary form by setting  $\mathcal{V} = |\mathbf{U}|$  and  $\mathbf{U} = \boldsymbol{\alpha}U$ , where  $\boldsymbol{\alpha}$  is a unit vector parallel to the direction of motion. This yields for the drag on any translating body<sup>29</sup>

$$\begin{aligned} |F_\alpha| = |(F_0)_\alpha| + \frac{3}{16}R \frac{[3(F_0)^2 - \{(F_0)_\alpha\}^2]}{6\pi\mu aU} \\ + \frac{9}{40}(R^2 \ln R) \frac{|(F_0)_\alpha|(F_0)^2}{(6\pi\mu aU)^2} + \mu aUO(R^2) \end{aligned} \quad (232)$$

where the subscript  $\alpha$  refers to the  $\alpha$  component of the corresponding vector force, i.e.,  $F_\alpha = \mathbf{F} \cdot \boldsymbol{\alpha}$ .

If, in addition, the orientation of the body is parallel to a Stokes principal axis of translation, the particle experiences no lift force in Stokes flow, whence  $(F_0)_\alpha = F_0$ . Hence, the drag on the particle is

$$\frac{F_\alpha}{F_0} = 1 + \frac{3}{8} \left( \frac{|F_0|}{6\pi\mu aU} \right) R + \frac{9}{40} \left( \frac{F_0}{6\pi\mu aU} \right)^2 R^2 \ln R + O(R^2) \quad (233)$$

As indicated by the notation, the *vector* force on the particle at higher Reynolds numbers need not be parallel to the direction of motion, even though

<sup>29</sup> Actually, one obtains

$$F_\alpha = (F_0)_\alpha - \frac{3}{16}R \frac{[3(F_0)^2 - \{(F_0)_\alpha\}^2]}{6\pi\mu aU} + \frac{9}{40}(R^2 \ln R) \frac{(F_0)_\alpha(F_0)^2}{(6\pi\mu aU)^2} + \mu aUO(R^2)$$

But since the  $F$ 's (i.e., the components of the corresponding vector forces  $\mathbf{F}$ ) are *negative* quantities, the alternative form in Eq. (232) is less misleading.

it is in Stokes flow for the assumed circumstances. By setting  $F_0 = -6\pi\mu aU$ , Eq. (233) reproduces Proudman and Pearson's (P11) result for the sphere, Eq. (212).

Upon putting  $R = aU\rho/\mu$  in (233) it adopts the form<sup>30</sup>

$$\frac{F_a}{F_0} = 1 + \frac{|F_0|\rho}{16\pi\mu^2} + \frac{8}{5} \left( \frac{F_0\rho}{16\pi\mu^2} \right)^2 \ln \left( \frac{aU\rho}{\mu} \right) + O(R^2) \quad (234)$$

In this form it is somewhat more obvious that the term of  $O(R)$  here, and in the more general result, is indeed independent of the choice of the characteristic parameters,  $a$  and  $\mathcal{V}$ . On the other hand, the term of  $O(R^2 \ln R)$  does depend weakly on the explicit definition of these parameters. This shows that the terms of  $O(R^2 \ln R)$  and  $O(R^2)$  are, in a sense, inseparable.

(vii) The inertial resistance triadics  $\mathcal{K}$  may be regarded as purely phenomenological coefficients to be determined from macroscopic experiments. For bodies possessing various types of geometric symmetry, the number and nature of independent tensor components of each of these resistance tensors is appropriately decreased. Systematic calculations of such symmetry reductions, based on the properties set forth in Paragraph (ii), are tabulated for some common types of symmetry in Refs. (B27), (C17), and (B23), though the latter investigation was originally made in a very different context.

Some of the more important examples of these symmetry restrictions and applications thereof are set forth in the following paragraphs.

(viii) If, for a nonrotating particle, body symmetry demands that a certain component of the vector force be reversed to all orders in  $R$  for a reversal of  $\underline{U}$ , then this component is given to  $O(R^2 \ln R)$  by the corresponding component of  ${}^1\underline{F}$  in Eq. (223a). An ellipsoidal particle at an arbitrary angle of incidence is an example of such a body. In this case Eq. (223a) gives the *complete* vector force on the ellipsoid.

(ix) A nonrotating particle for which the coupling dyadic vanishes at the center of reaction experiences a couple about this point given by<sup>31</sup>

$$\underline{T} = R \frac{1}{6\pi} \mathcal{K}^{(r)[iii]} : \underline{U}\underline{U} + O(R^2) \quad (235)$$

<sup>30</sup> The coefficient  $8/5$  may be written as  $1/(1 - 3/8)$ . Because of the frequent occurrence of the  $3/8$  coefficient at various places in the theory, e.g., in Eq. (233), this is thought to be more than coincidental.

<sup>31</sup> In dimensional form,

$$\underline{T} = \rho \mathcal{K}^{(r)[iii]} : \underline{U}\underline{U} + \mu a^2 U O(R^2)$$

where  $\mathcal{K}^{(r)[iii]} = a^3 \underline{\mathcal{K}}^{(r)[iii]}$ .

A translating ellipsoid, for example, thus experiences a couple of  $O(R)$  unless it moves normal to one of its three symmetry planes, in which case no couple acts to any order in  $R$ . By evaluating a key component of  $\underline{\mathcal{K}}^{(r)[rr]}$  for the slightly deformed spheroid of revolution

$$\underline{r} = 1 + \varepsilon P_2(\cos \theta) + O(\varepsilon^2)$$

Cox (C17) solved the pertinent equations describing the terminal motion of the spheroid. Cox's calculation reveals that a homogeneous ellipsoid of revolution, albeit of small eccentricity, if allowed to fall freely through the fluid ultimately takes up a stable orientation such that its axis is horizontal if prolate ( $\varepsilon < 0$ ) and vertical if oblate ( $\varepsilon > 0$ ). Thus, the terminal orientation is such as to make the resistance to motion a maximum and, consequently, the settling velocity a minimum. This conclusion is well supported by experimental data in the "transition" range of Reynolds numbers (H12, K11, M4, P6), as is the converse theoretical conclusion (B18, B22) that, in the absence of inertial effects, a homogeneous body possessing three orthogonal planes of reflection symmetry is neutrally stable in *any* orientation.

(x) If a nontranslating body of revolution rotates about its symmetry axis (the  $Ox_1$  axis, say) with angular speed  $\underline{\omega}_1$  the components of the force and couple are<sup>32</sup>

$$\underline{F}_1 = R \frac{1}{6\pi} \underline{\mathcal{K}}_{111}^{(r)[rr]} \underline{\omega}_1^2 + O(R^2) \quad (236)$$

$$\underline{T}_1 = -\underline{K}_{11}^{(r)} \underline{\omega}_1 + O(R^2) \quad (237)$$

The other components are zero to all orders in  $R$ . That the lowest-order correction to the Stokes couple is of  $O(R^2)$  is in agreement with Collins (C14) formula for the rotating sphere, cited in Eq. (198). Equation (236) shows that the rotating body experiences a force directed along the symmetry axis, and that this force is unaltered by a reversal of the angular velocity vector. If the body also possesses fore-aft symmetry, then  $\underline{\mathcal{K}}_{111}^{(r)[rr]} = 0$ , whence no force results. In the absence of such symmetry the force clearly arises from an unequal influx of fluid towards the poles of the body.

In accordance with the discussion of Section III,B it seems likely that Eqs. (236) and (237) could, perhaps, be more simply obtained by regular, rather than singular, perturbation procedures. That the former technique

<sup>32</sup> In dimensional form the force is

$$F_1 = \rho \underline{\mathcal{K}}_{111}^{(r)[rr]} \omega_1^2 + \mu a^2 \omega_1 O(R^2)$$

where  $\underline{\mathcal{K}}_{111}^{(r)[rr]} = a^4 \underline{\mathcal{K}}_{111}^{(r)[rr]}$  and  $R = a^2 \omega_1 \rho / \mu$ .

should work despite the force experienced by the body can be seen by the following reasoning: If the fluid is at rest at infinity, but the body experiences a force, the Stokes velocity field at great distances is of  $O(\underline{r}^{-1})$  (C17). Thus, as  $\underline{r} \rightarrow \infty$ ,

$$\frac{R|\underline{v}_0 \cdot \underline{\nabla} \underline{v}_0|}{|\underline{\nabla}^2 \underline{v}_0|} = \frac{RO(\underline{r}^{-3})}{O(\underline{r}^{-3})} = O(R)$$

which is uniformly small.

(xi) Consider an *isotropic* particle moving through the fluid. Though the forms of the six resistance triadics in Eq. (226) can be established by formal symmetry arguments (B23, B27, C17) it is instructive to proceed by less rigorous invariance arguments. Since the particle is isotropic so must be the triadics. But the only isotropic tensor of third order is the alternating triadic  $\underline{\varepsilon}$  (A5). The six resistance triadics must therefore be scalar or pseudoscalar multiples of  $\underline{\varepsilon}$ . Since  $\underline{\varepsilon} : \underline{U}\underline{U} = -\underline{U} \times \underline{U} = \underline{0}$  (with a similar identity for  $\underline{\omega}$ ), one may conclude that the four "direct" triadics in (226) cannot contribute to the final results and, hence, may be taken to be identically zero. Only the "cross" triadics remain. Consequently, at the center of reaction,

$$\underline{^2F} = R \frac{1}{3\pi} \underline{\mathcal{K}}^{(i)[rt]} \underline{U} \times \underline{\omega} \quad (238)$$

$$\underline{^2T} = R \frac{1}{3\pi} \underline{\mathcal{K}}^{(r)[rt]} \underline{U} \times \underline{\omega} \quad (239)$$

where  $\underline{\mathcal{K}}^{(i)[rt]}$  is a true scalar and  $\underline{\mathcal{K}}^{(r)[rt]}$  is a pseudoscalar.<sup>33</sup> Thus, if the particle is *spherically isotropic* we require that  $\underline{\mathcal{K}}^{(r)[rt]} = 0$ , and the body experiences only a Magnus-type lift force of the form found by Rubinow and Keller (R7) for the sphere.<sup>34</sup> On the other hand, if the body is *helicoidally isotropic* the pseudoscalar coefficient need not vanish. In this case the body also experiences a "lifting" couple at right angles to  $\underline{U}$  and  $\underline{\omega}$ , the sense of the couple depending upon whether the isotropic helicoid is right- or left-handed.

#### D. EXPERIMENTAL DATA IN THE "TRANSITION" REGION

##### 1. Unbounded Fluids

In addition to the existence of accurate data for spherical particles (M7b), a modest amount of recent experimental data are available for the resistance

<sup>33</sup> These properties follow from the fact that  $\underline{F}$  and  $\underline{U}$  are true vectors, whereas  $\underline{T}$  and  $\underline{\omega}$  are pseudovectors. And the entities appearing on opposite sides of an equality sign must be of the same tensorial type, either pseudo or true.

<sup>34</sup> The value  $\underline{\mathcal{K}}^{(i)[rt]} = -\frac{1}{2}\pi$ , found by Rubinow and Keller [see Eq. (216)] for a sphere of radius  $a$ , has been confirmed by Cox (C17) by direct integration of Eq. (227b).

to translational motion of nonspherical bodies of various shapes in the so-called "transition" regime<sup>35</sup> (B2, C10, J2a, M4, M11, P6, W9). This region lies between the Stokes regime, where the drag coefficient  $C_D$  is asymptotically proportional to  $R^{-1}$ , and the Newton's law regime, where  $C_D$  is essentially independent of  $R$ . Based on the Brenner-Chester-Cox theory, Chow and Brenner (C8, C9) have proposed a theoretically sound method for the correlation of experimental data on nonspherical particles in the transition region. According to Eq. (234) the drag force  $F$  on symmetrical bodies at small, nonzero Reynolds numbers is related to the Stokes force  $F_0$  by the general expression

$$F/F_0 = \text{function}(R^*) \quad (240)$$

where

$$R^* = \frac{|F_0|\rho}{6\pi\mu^2} \quad (241)$$

is a generalized Reynolds number.  $F_0$  refers to the hypothetical Stokes drag force which the body would experience if it moved with the same speed  $U$  and orientation in a fluid of equal viscosity but zero density. The superfluous factor of  $6\pi$  is introduced to make  $R^*$  identical with the actual particle Reynolds number,  $aU\rho/\mu$ , for a spherical particle of radius  $a$ .

The function appearing in (240) is a *universal* function, applicable to all particles possessing sufficient symmetry. Rather than employing the expression for this function given in Eq. (234), the functional relationship was established (C8, C9) by drawing a single, average curve through the experimental data of Malaika (M4, M11) for a wide variety of particle shapes setting in their stable orientations. The result is shown in Fig. 2.<sup>36</sup> For any particular orientation the Stokes force is necessarily of the form

$$|F_0|/6\pi\mu aU = C \quad (242)$$

where  $a$  is any representative particle length and  $C$  is a nondimensional constant, dependent only on particle shape and orientation. Since  $C$  is, in principle, determinable from a *single* terminal settling velocity experiment in

<sup>35</sup> In much of the engineering literature this is referred to as the "laminar" regime. Such terminology is inappropriate, since it incorrectly excludes the possibility that flow in the higher Reynolds number regime may also be laminar.

<sup>36</sup> A more sensitive test of the general theory would be furnished by a log-log plot of  $(F/F_0) - 1$  vs  $R^*$ ; however, the accuracy of existing data do not warrant such a critical test. [See the comments of Maxworthy (M7b) with regard to the accuracy of such a plot for spherical particles.]



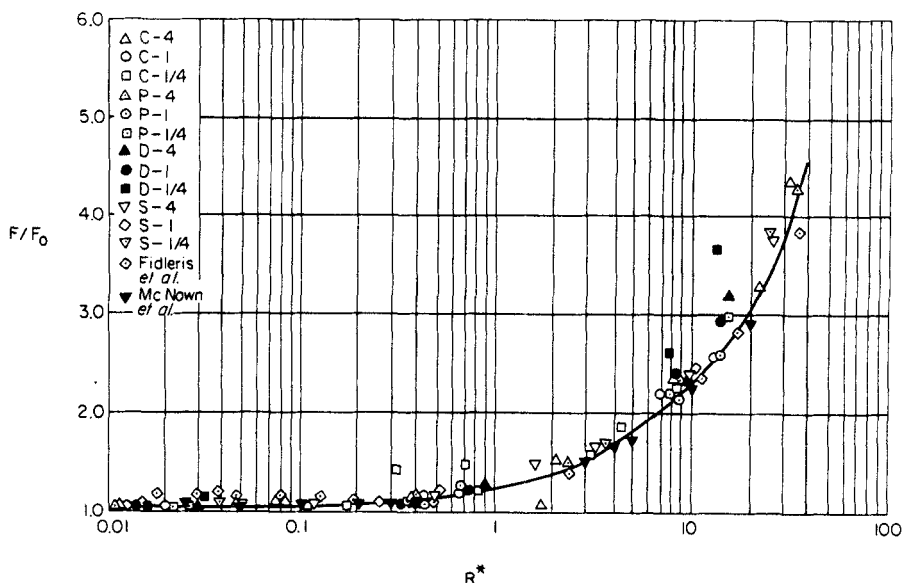


FIG. 2. Generalized drag coefficient vs generalized Reynolds number.

either the Stokes or transition regimes,<sup>37</sup> the plot, in essence, empirically characterizes the resistance of the body for a given orientation by means of a single parameter.

## 2. Wall-Effects

All other things being equal, wall-effects diminish with increasing particle Reynolds numbers (F6, M12, M13). Based on the analyses of Brenner (B15) and O'Brien (O1), Chow and Brenner (C8, C9) have suggested a universal plot encompassing both wall and inertial effects, providing that both effects are each not too large. For a symmetrical particle falling, say, along the axis of a circular cylinder of radius  $l$ , the dimensionless parameter

$$\xi^* = \frac{|F_0|}{6\pi\mu Ul} \quad (243)$$

plays the role of a generalized particle-to-cylinder radius ratio (e.g., for a

<sup>37</sup> The  $C$  value can be derived from experimental data obtained in the transition region by cross-plotting Eq. (240) in the form

$$\frac{F}{F_0} = \text{function} \left( \frac{|F|\rho}{6\pi\mu^2} \right)$$

$|F|$  is then merely the weight of the settling particle corrected for the buoyancy of the fluid.

sphere of radius  $a$ ,  $\xi^* = a/l$ ). According to the underlying theory<sup>38</sup>(B15, O1),

$$F/F_0 = \text{function}(R^*, \xi^*) \quad (244)$$

where the function appearing above is universally applicable to all sufficiently symmetrical particles.  $F_0$  is, again, the hypothetical Stokes force on the particle in an unbounded fluid. For  $R^* = 0$ , Eq. (244) is equivalent to (135), with appropriate changes in notation. The *spherical* particle data of Fidleris and Whitmore (F5, F6) and McNown *et al.* (M10, M14) were used (C8) to prepare the required plot of Eq. (244). It seems likely that the theory is applicable for  $R^* < 20$  and  $\xi^* < 0.2$ , but insufficient data are available to provide a truly satisfactory test.

## E. LATERAL MIGRATION IN TUBES

### 1. Introduction

Segré and Silberberg (S5, S6) observed that a single, rigid, neutrally buoyant, spherical particle suspended in a low Reynolds number Poiseuille flow migrates across the streamlines, its center ultimately attaining a stable equilibrium position at about 0.6 tube radius distant from the axis. This position is reached independently of the initial lateral location of the sphere relative to the tube axis; a neutrally buoyant sphere introduced near the wall migrates inward, whereas it migrates outward when introduced near the axis. This lateral migration effect was subsequently confirmed by others (G9a, J5, K5, K5b, O2, R4a, R4b) and found to be relatively insensitive to tube Reynolds number and sphere-cylinder diameter ratio. The observations of Segré and Silberberg spawned a remarkable number and variety of related lateral migration experiments. Especially important was the extension to non-neutrally buoyant spherical particles (D4b, E1, J5, R4a, R4b, T3a). Lateral forces were observed here too, but now—with the sole exception of the closely related two-dimensional Poiseuille flow experiments performed by Repetti and Leonard (R4a, R4b)—the particles no longer attained a fractionally eccentric equilibrium position. Rather, they migrated permanently to either the wall or the tube axis, depending essentially upon whether they were denser or lighter than the fluid and upon whether the Poiseuille flow was up or down the tube. No sidewise (lift) forces can arise under comparable circumstances in the Stokes regime (B28, B30, S1). Such effects are therefore necessarily inertial in origin.

<sup>38</sup> The theory is most likely to be useful in the cross-plotted form

$$\frac{F}{F_0} = \text{function}\left(\frac{|F|\rho}{6\pi\mu^2}, \frac{|F|}{6\pi\mu Ul}\right)$$

Radial migration phenomena are of obvious importance in the flow of suspensions through tubes, especially in dilute systems where they are not overshadowed by hydrodynamic interactions among particles. Thus, in the case of a dilute suspension of neutrally buoyant particles, the experiments of Segré and Silberberg (S5, S6) revealed a so-called "tubular pinch effect" in which the particles were observed to accumulate in a narrow annular portion of the tube centered at a distance of about 0.6 tube radius from the axis. At steady-state the particles are therefore nonuniformly distributed over the tube cross section, an effect previously noted by Tollert (T6) and implied in the work of others (M5a, M7a, S18, S19). Such anomalous behavior is important, for example, in interpreting suspension viscosity measurements obtained in capillary tubes (S7); for when the shear is nonuniform, as is true for Poiseuille flow, the contribution of each particle to the additional energy dissipation depends upon its radial position in the tube (B12). This results in an apparent non-Newtonian behavior (S7). Recognition of nonuniformities in radial distribution is also important in applying Archimedes' law to suspensions [see Eq. (145)] and in related applications dealing with the pressure drop through liquid fluidized beds and with the power requirements for pumping dilute slurries (H8). Experiments have shown (F8) that when deformable wood-pulp fibers suspended in water are pumped through a pipe a clear layer exists adjacent to the tube wall, though this manifestation of radial forces is as likely due to particle deformation as to fluid inertia (G9).

Unless the contrary is explicitly stated, the following discussion of experimental and theoretical results is restricted to single, rigid, spherical particles freely suspended in a Poiseuille flow within a circular tube of effectively infinite length. Notation is as follows:  $a$  = sphere radius;  $R_o$  = tube radius ( $l$  was used previously for this quantity);  $b$  = radial distance from tube axis to sphere center;  $\beta = b/R_o$  = fractional distance from axis;  $b^*$  = stable equilibrium distance of sphere from tube axis;  $\beta^* = b^*/R_o$ ;  $\rho$  = fluid density;  $\rho_p$  = particle density;  $\mu$  = viscosity;  $\nu = \mu/\rho$  = kinematic viscosity. All velocities defined below are measured relative to the fixed cylinder walls;  $\mathbf{V}_m$  = mean velocity of flow vector (equal in magnitude to the superficial velocity and pointing parallel to tube axis in the direction of net flow);  $\mathbf{U}$  = particle velocity vector—that is, the velocity of the sphere center;  $\omega$  = angular velocity of the sphere. The local velocity in the unperturbed Poiseuille flow is

$$\mathbf{u} = 2\mathbf{V}_m[1 - (R/R_o)^2] \quad (245)$$

where  $R$  is the distance from the axis to a general point in the fluid.

In resolving the various vector velocities into components it is convenient to define a right-handed system of Cartesian coordinates  $Ox_1, Ox_2, Ox_3$  with origin  $O$  at the tube axis, as in Fig. 3.  $Ox_1$  lies along the tube axis in the direction of net flow;  $Ox_3$  lies parallel to the vector drawn perpendicularly from

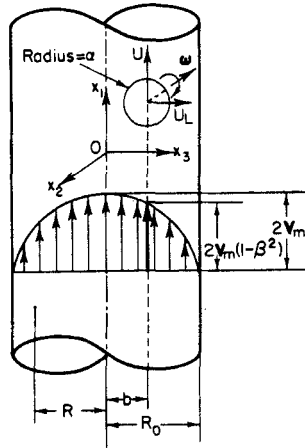


FIG. 3. Sphere in a Poiseuille flow.

the cylinder axis which passes through the sphere center. Corresponding unit vectors are denoted by  $\mathbf{i}_1, \mathbf{i}_2, \mathbf{i}_3$ . By definition we thus have  $\mathbf{V}_m = \mathbf{i}_1 V_m$  where the scalar  $V_m \geq 0$ . The particle velocity may be expressed in the component form  $\mathbf{U} = \mathbf{i}_1 U + \mathbf{i}_3 U_L$ , where the axial velocity<sup>39</sup>  $U$  and radial velocity  $U_L$  may be positive or negative scalars.  $U_L > 0$  implies migration toward the wall, whereas  $U_L < 0$  implies migration towards the axis. Similarly, the hydrodynamic force exerted by the fluid on the particle may be expressed as  $\mathbf{F} = \mathbf{i}_1 F_D + \mathbf{i}_3 F_L$ . The "drag" force  $F_D$  and "lift" force  $F_L$  may also be positive or negative scalars.

Another quantity of importance is the axial slip velocity of the particle,

$$u_p = U - 2V_m(1 - \beta^2) \quad (246)$$

which represents the particle velocity relative to the surrounding fluid. When the particle is neutrally buoyant and the Reynolds number small, the slip velocity may be obtained by setting  $\mathbf{F} = \mathbf{0}$  in Eq. (142), yielding

$$u_p = -\frac{4}{3}V_m\left(\frac{a}{R_0}\right)^2 + O\left(\frac{a}{R_0}\right)^3 \quad (247)$$

The negative sign is a consequence of the fact that the particle lags the fluid. When the particle is not neutrally buoyant it proves useful to introduce the settling velocity vector  $\mathbf{U}_\infty$  of the particle in the *unbounded fluid at rest*. Of

<sup>39</sup> It would be more consistent with our general vector notation to reserve the symbol  $U$  for the magnitude of the vector  $\mathbf{U}$ . But since the lateral velocity is such a small fraction of the total velocity, the discrepancy between the magnitude of this vector and the absolute value of the axial velocity  $U$  is negligible.

particular interest is the axial component  $U_\infty = \mathbf{i}_1 \cdot \mathbf{U}_\infty$  of this vector. At sufficiently small Reynolds numbers it is given by Stokes law,

$$U_\infty = \frac{2a^2(\rho_p - \rho)\mathbf{i}_1 \cdot \mathbf{g}}{9\mu} \quad (248)$$

and may be either positive or negative;  $\mathbf{g}$  is the local acceleration of gravity vector, directed towards the center of Earth. If wall-effects are neglected in Eq. (142) the axial slip velocity is then simply

$$\mathcal{U}_p = U_\infty + O(a/R_o) \quad (249)$$

which is obtained by noting that  $\mathbf{F} = -6\pi\mu a\mathbf{U}_\infty$  in Eq. (142). When wall-effects are not negligible one finds for a vertical tube that

$$\mathcal{U}_p = U_\infty \left[ 1 - f(\beta) \frac{a}{R_o} \right] - \frac{4}{3} V_m \left( \frac{a}{R_o} \right)^2 + O\left( \frac{a}{R_o} \right)^3 \quad (250)$$

The relative importance of inertial to viscous effects depends upon the following two Reynolds numbers (based on *diameter*):

$$\text{Re}_t = 2R_o V_m / \nu = \text{tube Reynolds number} \quad (251)$$

$$\text{Re}_p = 2a|\mathcal{U}_p|/\nu = \text{particle Reynolds number based on axial slip velocity} \quad (252)$$

The Reynolds number based upon the angular velocity of the particle is not an independent parameter for a freely supported particle; rather according to Eq. (89b) a homogeneous spherical particle will, in the absence of wall and particle inertia effects, rotate with the local angular velocity of the undisturbed flow at its center—at least at sufficiently small Reynolds numbers. This velocity is

$$\boldsymbol{\omega} = -\mathbf{i}_2 \omega \quad (253a)$$

in which

$$\omega = 2bV_m/R_o^2 \quad (253b)$$

is the angular speed.

Most experimental data obtained to date have been interpreted on the basis of the Rubinow-Keller equation (216) for the lift force on a spinning, translating sphere in an unbounded fluid at rest (or in uniform flow) at infinity. The spin is assumed to be given by Eq. (253), whereas the velocity  $\mathbf{U}$  appearing in Eq. (216) has usually been interpreted as the axial slip velocity  $\mathbf{i}_1 \mathcal{U}_p$ . This gives rise to a lift force

$$F_L = \pi a^3 \rho \omega \mathcal{U}_p [1 + O(\text{Re}_p)] \quad (254)$$

[where  $\omega$  is given by Eq. (253b)] and hence, by Stokes law,

$$F_L = 6\pi\mu a U_L [1 + O(\text{Re}_p)] \quad (255)$$

to a radial migration velocity

$$\frac{U_L}{V_m} = \frac{1}{6} \left( \frac{2a\mathscr{U}_p}{v} \right) \left( \frac{a}{R_o} \right) \beta [1 + O(\text{Re}_p)] \quad (256)$$

Before discussing the credibility of this theory we shall summarize pertinent experimental data bearing on the phenomenon of radial migration at small Reynolds numbers. The range of variables encompassed by these experiments is tabulated in Table III. Unless otherwise stated, the experiments to be described were conducted in vertical tubes.

## 2. Experimental Data

*a. Segré and Silberberg (S6).* These experiments were performed with dilute suspensions of neutrally buoyant spheres, rather than with single particles. However, it appears that the suspensions were sufficiently dilute (0.33–4 particles/cm<sup>3</sup>) to insure negligible hydrodynamic interactions among the particles. Particles were observed to attain stable equilibrium positions at about  $\beta^* = 0.63$ . Based primarily on observations made in the vicinity of the tube axis they correlated their measured radial migration velocities by means of the empirical relation

$$U_L/V_m = 0.34 \text{Re}_t(a/R_o)^{2.84} \beta(\beta^* - \beta) \quad (257)$$

Further experiments were also conducted at tube Reynolds numbers up to 650, but the data scattered too much to conclusively determine whether or not the particles ultimately attained a stable equilibrium position.

*b. Karnis, Goldsmith, and Mason (G7, G9, K5, K5b).* An initial set of experiments by Goldsmith and Mason (G7, G9) was performed with essentially neutrally buoyant spheres for  $\text{Re}_p \approx 10^{-6}$ . No lateral migration was observed as the particle moved axially through distances as large as 3,500 cm. Very precise measurements were also made of the axial and angular velocities. For  $a/R_o < 0.04$  they verified the theoretical relationships  $U = 2V_m(1 - \beta^2)$  and  $\omega = 2bV_m/R_o^2$  to within 1 percent. For  $a/R_o = 0.1$  to 0.5, where wall-effects are not negligible, they observed significant departures from the no-slip axial velocity condition. According to Eqs. (246) and (247) one should have

$$\frac{2V_m(1 - \beta^2) - U}{2V_m(1 - \beta^2)} \frac{3}{2(a/R_o)^2} = \frac{1}{1 - \beta^2} \quad (258)$$

provided that  $(a/R_o)(1 - \beta)^{-1} \ll 1$ . Their data agree very well with this

TABLE III SUMMARY OF EXPERIMENTAL CONDITIONS FOR THE LATERAL

| Observer                             | Fluid-particle density difference  | Duct diameter, $2R_o$ (cm)  | Sphere-to-cylinder radius, $a/R_o$                                     |
|--------------------------------------|--|---|--|
| Segré and Silberberg (S6)            | Dilute suspension of neutrally buoyant spheres   | 1.12  | 0.028–0.153  |
| Goldsmith and Mason (G9)             | Neutrally buoyant sphere   | 0.800   | 0.123–0.135  |
| Karnis, Goldsmith, and Mason (K5)    | Neutrally buoyant sphere   | 0.400   | 0.250  |
| Oliver (O2)                          | Neutrally buoyant sphere (see also discussion for other cases)                             | 0.940   | 0.245–0.361  |
| Small and Eichhorn (E1)              | More dense sphere in upflow in an inclined tube  | 1.07  | 0.146–0.301  |
| Theodore and Brenner (T3a)           | Immobile sphere in a horizontal tube   | 14.0  | 0.046–0.136  |
| Denson, Christiansen, and Salt (D4b) | Less dense sphere in downflow  | 2.58  | 0.120–0.190  |
| Day and Genetti (D3a)                | More dense sphere in upflow  | See Denson<br>See Denson  | See Denson<br>See Denson   |
| Repetti and Leonard (R4a)            | Neutrally buoyant sphere<br>Less dense sphere in downflow<br>More dense sphere in downflow | Rectangular duct<br>$2.54 \times 10.16$ cm<br>( $R_o \equiv 1.27$ cm) | $\left\{ \begin{array}{l} 0.187 \\ 0.187 \\ 0.187 \end{array} \right.$ |
| Jeffrey and Pearson (J5)             | Neutrally buoyant sphere<br>More dense sphere in downflow<br>More dense sphere in upflow   | 3.25<br>3.25<br>3.25  | 0.046–0.089<br>0.046–0.089<br>0.046–0.089                              |

<sup>a</sup>  $\mathcal{U}_p$  was obtained from Eq. (246) using the experimentally measured values of  $U$  and  $V_m$ ; when  $\mathcal{U}_p$  was too small to be accurately determined from these experimental values, or when it was not experimentally determined, it was estimated from Eq. (250) using an average value of  $f(\beta) = 2.1$  (see Table II), the latter number being quite accurate over the  $\beta$  range of all investigators.

<sup>b</sup> The  $U_\infty$  values required in this calculation were determined from the experimental particle radii, density differences, and viscosities by assuming the applicability of Stokes law,

$$|U_\infty| = \frac{2a^2|\Delta\rho|g}{9\mu}$$

Strictly speaking this is accurate only for  $Re_\infty < 0.5$ . Thus, for those experiments for which  $Re_\infty > 0.5$  the  $U_\infty$  values represent hypothetical values, rather than the values that would be observed experimentally.

## MIGRATION OF RIGID SPHERICAL PARTICLES IN POISEUILLE FLOWS

| Tube<br>Reynolds<br>number,<br>$Re_t = \frac{2R_o V_m \rho}{\mu}$ | Particle<br>Reynolds<br>number <sup>a</sup> ,<br>$Re_p = \frac{2a \mathcal{U}_p \rho}{\mu}$ | Particle Reynolds<br>number in an<br>unbounded<br>stationary fluid <sup>b</sup> ,<br>$Re_\infty = \frac{2a U_\infty \rho}{\mu}$ | Settling<br>velocity-mean<br>fluid velocity<br>ratio <sup>b</sup> ,<br>$ U_\infty /V_m$ | Eccentric<br>equilibrium<br>position of<br>sphere center,<br>$\beta^* = b^*/R_o$ |
|---|---|---|---|--|
| 2-30  | < 0.01  | ?   | 0.0(?)  | 0.63   |
| $0.80-1.6 \times 10^{-3}$   | $2.2-5.3 \times 10^{-6c}$   | $6.2-8.3 \times 10^{-7}$  | 0.0032-0.0077   | No radial<br>migration   |
| $\approx 0.01$  | $0.09-1.9 \times 10^{-2c}$  | ?   | 0.0 (?)   | 0.5  |
| 100-500   | 1.0-13.0  | ?   | 0.0(?)  | 0.47-0.63  |
| 860-2400  | 80-247 <sup>d</sup>   | 306-1900 <sup>e</sup>   | 1.7-21.8 <sup>e</sup>   | } Lift force directed<br>towards axis at all<br>eccentric locations              |
| 2.3-42.8  | 0.13-8.1 <sup>d</sup>   | —   | —   |  |
| 208-890   | 6.0-120 <sup>f</sup>  | 17-340  | 0.22-5.5  | Axis   |
| See Denson<br>See Denson  | < 120 <sup>f</sup><br>550 <sup>f</sup>  | See Denson<br>See Denson  | See Denson<br>See Denson  | Axis<br>Undamped radial<br>oscillation   |
| 500 (estimated)   | ?   | 0.0(?)  | 0.0(?)  | ?  |
| 500 (estimated)   | 27 (estimated)  | 35 (estimated)  | 0.38 (estimated)  | Axis   |
| 500 (estimated)   | 10 (estimated)  | 24 (estimated)  | 0.26 (estimated)  | Wall   |
| 11.2-76.8   | 0.010-0.11  | 0.0091-0.040  | 0.0025-0.040  | 0.68   |
| 22.7-116  | 0.37-1.3  | 0.28-1.7  | 0.028-0.43  | Wall   |
| 22.0-180  | 0.28-1.6  | 0.28-1.7  | 0.029-0.42  | Axis   |

<sup>c</sup> Because the direction of net flow oscillated periodically between upflow and downflow, the algebraic sign of  $U_\infty$  (relative to  $V_m$ ) underwent similar changes. Accordingly,  $\mathcal{U}_p$  was calculated from Eq. (247) rather than Eq. (250).

<sup>d</sup> Note that, since the sphere center did not move relative to the tube wall in these experiments,  $U = 0$  and hence  $\mathcal{U}_p = -2V_m(1 - \beta^2)$ .

<sup>e</sup> Note that the  $U_\infty$  values required in this calculation were obtained as outlined in footnote *b* to this table. No account was taken of the fact that  $i_1 \cdot g$  in Eq. (248) is not the same as  $g = 981 \text{ cm/sec}^2$ , due to the inclination of the tube.

<sup>f</sup> These particle Reynolds numbers are based on the *total* (axial plus radial) "slip velocity," defined by Denson (D4b) as

$$|\mathcal{U}_p| = \left[ U_L^2 + \left\{ U - 2V_m(1 - \beta^2) + \frac{4}{3} V_m \left( \frac{a}{R_o} \right)^2 \right\}^2 \right]^{1/2}$$



relationship for  $\beta < 0.3$ . Their failure to confirm Eq. (258) at the larger values of  $\beta$  is due to the fact that the condition  $(a/R_o)(1 - \beta)^{-1} \ll 1$  was violated, owing to the relatively large values of  $a/R_o$  employed. Measurements of the angular velocity of the sphere when its center lay within one diameter of the tube wall confirmed Vand's (V2, V3) theoretical relationship for the wall-effect due to a sphere rotating near a plane wall in Couette flow. This observed agreement should, however, be scrutinized more closely since Vand's analysis fails to satisfy the zero tangential-slip boundary condition at the wall. An exact solution of Vand's problem is given by Goldman, Cox, and Brenner (G5e). It is with this more rigorous result that the angular velocity data of Karnis *et al.* should be compared.

In a subsequent investigation in the range  $Re_p = 10^{-3}$  to  $10^{-2}$ , Karnis, Goldsmith, and Mason (K5, K5b) observed both inward and outward radial migration, the equilibrium position occurring at approximately  $\beta^* = 0.5$ . Further experiments by Goldsmith and Mason (G9a, Fig. 15) confirmed these results.

That no radial migration was observed in the first set of experiments was undoubtedly due to the minuteness of the particle Reynolds numbers and, concomitantly, of the fact that despite the relatively enormous axial distances over which the radial position was observed, they were nevertheless insufficient to reveal the phenomenon. No matter how small the Reynolds number, inertial effects are present to some extent in all real flows. These effects, though practically infinitesimal at very small Reynolds numbers, are cumulative and would almost certainly have been observed had greater axial distances been involved. Commenting on this point, Rubinow (R6a) estimates that 4 to  $8 \times 10^3$  cm would have been required in the original series of experiments. Goldsmith and Mason reply to Rubinow's remarks in Reference G9c.

*c. Oliver (O2).* Both inward migration from the wall and outward migration from the axis were observed for neutrally buoyant spheres. Equilibrium was attained at  $\beta^* = 0.47$ – $0.63$  (average =  $0.55$ ). Wall-effects were larger in these experiments than in those of other investigators, since the final positions of the sphere centers were within one diameter of the tube walls. Experiments were also conducted with neutrally buoyant spheres whose centers of mass were eccentrically located to prevent rotation. Here, again, both inward and outward migration were observed, though the final equilibrium position was much nearer the tube axis ( $\beta^* = 0.07$ – $0.42$ ; average =  $0.26$ ) than in the previous case.

In a few experiments conducted with nonneutrally buoyant spheres which were free to rotate, a sphere slightly more dense than the fluid in downflow attained equilibrium somewhat closer to the wall than previously. A less dense sphere in a downwardly flowing fluid drifted away from the wall.

*d. Small and Eichhorn (E1, S13).* In an ingeniously simple experiment, these authors indirectly measured both the drag and lift forces (as well as the angular velocity) for single, hydrodynamically supported spheres at various nonaxial positions. This was accomplished by suspending the particles in a less dense fluid flowing upward through an inclined tube. In this manner both the drag and lift forces were balanced by the corresponding components of the net gravitational force in the sphere. The radial force was directed inward, towards the tube axis, in all cases. They correlated their data on the lift force via the empirical equation

$$F_L = -4.4 \times 10^5 \rho v^2 (a/R_o)^4 (\beta/1 - \beta^2)^2 \quad (259)$$

but remark that only a tentative recommendation can be made for the formula. In this we concur, since it predicts a velocity-independent radial force. For comparison purposes this relation may be converted into an equivalent radial velocity by means of Eq. (255), though the use of Stokes law at their conditions of operation may not be warranted.

Equally tentative correlations are presented by them for the drag force and angular velocity.

*e. Theodore and Brenner (T3a).* Direct measurements were made of the lift force on a nonrotating sphere by means of a static-head opening drilled through the wall of a horizontally mounted pipe. This opening permitted a steel sphere to be connected via a thin vertical wire to an analytical balance, thereby furnishing a direct measurement of the lift. This force was always in towards the axis. Data were empirically correlated via the relation

$$F_L = -2.8 \times 10^2 \rho a^2 V_m^2 (a/R_o) [1 - 6.0(a/R_o)] \beta (1 - \beta^2) \quad (260)$$

Here again, by applying Eq. (255) this may be converted into an equivalent radial velocity.

A few additional experiments were conducted in which the sphere was allowed to rotate. Though not wholly conclusive, no statistically significant effect of particle rotation on lift was found.

*f. Denson, Christiansen, and Salt (D4b).* Experiments were performed with nonneutrally buoyant particles less dense than the entraining fluid. Density differences ranged from 3.3 to 10.4 percent of that of the fluid. Flow was vertically downward in all cases. An electromagnetic device was employed to release the particles into the fully developed portion of the flow, in contrast to the prior work of Segré and Silberberg (S6) where the particles entered with the entraining fluid. Data were obtained for the instantaneous radial, axial, and angular velocities of the spheres.

Particles always migrated permanently to the tube axis. At the lower particle Reynolds numbers (6.0–10.0) the approach to the axis was monotonic.

However, at the larger values (15.0–120) the sphere oscillated across the tube axis one or more times before the migration ceased—the frequency of the oscillation increasing with increasing  $Re_p$  and flow rate; that is, the radial motion was such that while remaining in the same vertical meridian plane the particle crossed the axis, continued to the other side of the tube (but not all the way to the wall), turned, and moved back towards the centerline, etc. The two distinct modes of motion observed in the different  $Re_p$  ranges are termed “overdamped” and “damped” by Denson.

Denson provides a quantitative theoretical analysis which adequately accounts for these phenomena. Agreement is quite good, especially in the range  $Re_p < 40$ . No adjustable parameters appear in the treatment. The unsteady-state analysis depends critically upon the applicability of the Rubinow–Keller theory to the *instantaneous* particle motion, and the observed agreement is construed by Denson as evidence of its applicability for  $Re_p < 40$ . (See, however, the remarks in the last paragraph of Section III,E,3.)

*g. Day and Genetti (D3a).* Denson (D4b) refers in his thesis to the related experimental work of Day and Genetti (D3a) conducted in collaboration with him at the University of Utah. Their studies revealed that a sphere, more dense than the entraining fluid, migrated to the tube axis when the fluid flowed vertically upward. These observations were made over the same range of particle and tube Reynolds numbers covered in Denson’s investigation. At particle Reynolds numbers near 550, Day and Genetti found, however, that the oscillatory radial motion observed by Denson at the lower values of  $Re_p$  (up to 120) was no longer damped. Rather, the sphere oscillated across the tube axis with constant amplitude and frequency, in a manner similar to that of an undamped harmonic oscillator. They attributed this phenomenon to periodic shedding of vortices from the sphere, but Denson states that further studies would be required to substantiate this hypothesis.

*h. Repetti and Leonard (R4a, R4b).* These experiments, performed in a *rectangular* duct, revealed phenomena analogous to those observed in circular tubes. By using a gap width small in comparison with the breadth, an essentially two-dimensional Poiseuille flow was achieved. Drift was examined between the narrowly separated walls and was confined to the mid-plane between the other walls. A sphere more dense than the downflowing fluid migrated to the nearer duct wall. Less dense spheres in downflow migrated to the axis. When the fluid-particle density differences were very small (0.04 percent for the more dense sphere and 0.06 percent for the less dense one) the migration apparently ceased before the sphere reached its extreme position at the axis or wall.<sup>40</sup> This suggests, as pointed out by Repetti and

<sup>40</sup> The summary reported here is based upon only a preliminary account (R4a) of their work. A presumably more detailed account is now available (R4b).

Leonard, that the stable equilibrium position will depend upon the density difference.

*i. Jeffrey and Pearson (J5).* These represent perhaps the most complete and systematic radial migration experiments performed to date. Single spheres were introduced at various radial positions, ranging from the axis to the wall, in the fully developed portion of the flow. Their angular, axial, and radial velocities were measured by cinematographic techniques. Results were obtained for neutrally buoyant particles as well as for particles denser than the fluid in both upflow and downflow.

*Neutrally buoyant particles.* In the range  $\beta = 0.0$ – $0.85$  investigated, measured angular<sup>41</sup> and axial velocities were found to be only a few percent smaller than their theoretical values,  $\omega = 2bV_m/R_o^2$  and  $U = 2V_m(1 - \beta^2)$ , respectively, the discrepancies being attributable to slight wall-effects. The effect of the lateral migration was to move the particles away from both the tube axis and wall, a particle eventually taking up a stable position at approximately  $\beta^* = 0.68$ . The empirical relationship selected to represent the radial migration velocity was<sup>42</sup>

$$U_L/V_m = 0.70(\text{Re}_t)^{1/2}(a/R_o)^2\beta(\beta^* - \beta) \quad (261)$$

although Jeffrey points out that changing the coefficient to 0.10 and the exponent of  $a/R_o$  to 1.5 would have resulted in an equally satisfactory correlation of the data.

*More dense particle in downflow.* Density differences varied from 0.9 to 2.3 percent. In the range  $\beta = 0.0$ – $0.85$  investigated, the angular velocities agreed quite closely with Eq. (253). Axial velocity data were very well correlated by the empirical relation

$$U = (U_\infty + 2V_m)(1 - \beta^2) \quad (262)$$

This formula, however, is at odds with the theoretical formula

$$U = U_\infty + 2V_m(1 - \beta^2) \quad (263)$$

<sup>41</sup> Jeffrey remarks that Kohlman (K10a) also confirmed the correctness of Eq. (253) for  $\text{Re}_t(a/R_o)^2 < 0.25$ . (This is a particle Reynolds number based on sphere radius and mean shear rate,  $2V_m/R_o$ , in the tube.)

<sup>42</sup> Jeffrey also reworked the original data of Segré and Silberberg (S6) and showed that their data could equally well be represented by the equation

$$U_L/V_m = 0.186(\text{Re}_t)^{1/2}(a/R_o)^2\beta(\beta^* - \beta)$$

with roughly the same degree of precision as the original correlation, Eq. (257). The above relation differs by a factor of about 4 from Jeffrey's.

and is clearly in error in the limiting case  $V_m = 0$ . However, in the  $U_\infty/V_m$  and  $\beta$  ranges investigated, the discrepancy is not too serious, particularly in view of the fact that Jeffrey did not explicitly take account of wall-effects [cf. Eqs. (246) and (250)]. When wall-effects are considered, the correct relation in Stokes flow is

$$U = U_\infty \left[ 1 - f(\beta) \frac{a}{R_o} \right] + 2V_m(1 - \beta^2) - \frac{4}{3}V_m \left( \frac{a}{R_o} \right)^2 + O\left( \frac{a}{R_o} \right)^3 \quad (264)$$

The particles migrated permanently to the tube wall with a radial velocity given by

$$U_L/V_m = 0.044(\text{Re}_\infty)^{1/2}\beta(1 - \beta^2) \quad (265)$$

where

$$\text{Re}_\infty = \frac{2a|U_\infty|}{\nu} \quad (266)$$

is the particle Reynolds number based on free-fall velocity in the unbounded fluid at rest.

*More dense particle in upflow.* Density differences varied from 0.9 to 2.3 percent;  $\beta$  values varied from 0.0 to 0.7. Measured angular velocities again agreed quite closely with the theoretical formula, Eq. (253). Axial particle velocity data scattered more than in the comparable downflow case, and Jeffrey was unable to decide between Eqs. (262) and (263). They both agree moderately well with the data though Jeffrey favors the latter in order to avoid the unacceptable inference that  $U \rightarrow 0$  as  $\beta \rightarrow 1$ .

Particles migrated permanently to the tube axis with a radial velocity given by

$$U_L/V_m = -0.10(|U_\infty|/V_m)^{1/2}(\text{Re}_\infty)^{3/4}\beta \quad (267)$$

Upon comparing Eqs. (265) and (267) with Eqs. (254)–(255) using the experimentally measured angular and axial slip velocities, Jeffrey concludes that the radial velocities predicted by the Rubinow–Keller theory are too small by an order of magnitude, except at the larger values of  $|U_\infty|$ , where their theory yields results too small by a factor of only about 1.5–3.

Jeffrey observed a curious “regimentation” phenomenon when a dilute suspension of particles more dense than the fluid flowed downward: “. . . The particles in the suspension migrated rapidly to the tube wall and there aligned themselves into regular vertical columns. Similarly, adjacent columns exerted an influence upon each other such that the columns moved parallel to one another in a vertical direction without disturbing the regimentation within a column until the centroids of any two adjacent particles in one column formed

an equilateral triangle with the centroid of the nearest particle in the adjacent column. . . .” Regimentation phenomena of this type seem also to have been observed by Segré and Silberberg (S6, S4a). Jeffrey goes on to state that “The obvious physical explanation of this is that, under these conditions of flow, the wake of a particle considerably influences the motion of any particle close to it. It would therefore seem probable that the motion of a particle in a suspension would be different [from] that of the motion of an individual particle.”

### 3. Theoretical Interpretation

As observed repeatedly, most investigators concerned with the radial migration problem have attempted to analyze their data on the basis of a rather broad interpretation of the Rubinow–Keller equation. In the neutrally buoyant case, i.e.,  $|U_\infty|/V_m \rightarrow 0$ , this interpretation predicts [cf. Eqs. (256) and (247)] a radial velocity

$$U_L/V_m = -\frac{2}{9}\text{Re}_t(a/R_o)^4\beta$$

which acts to move the particle inward, all the way to the tube axis. As recognized by Rubinow and Keller (R7) themselves, this conclusion is at odds with the experimental fact that the actual stable equilibrium position occurs at  $\beta^* \approx 0.5\text{--}0.68$ . Rubinow and Keller empirically suggest multiplying the above by the factor  $-(\beta^* - \beta)/\beta^*$  to bring it at least into qualitative agreement with experiment, but this suggestion has little rational basis to commend it.

In the limiting case of a nonneutrally buoyant particle, where  $|U_\infty|/V_m \rightarrow \infty$ , (but  $V_m \neq 0$ ), the slip velocity is given approximately by Eq. (249), so that Eq. (256) predicts

$$\frac{U_L}{V_m} = \frac{1}{6} \left( \frac{2aU_\infty}{v} \right) \left( \frac{a}{R_o} \right) \beta \quad (268)$$

According to this relation the particle migrates permanently to either the tube axis or wall, according as  $U_\infty$  is negative or positive. Stated in more general terms, the particle will attain a stable equilibrium position at the axis if the scalar  $(\rho_p - \rho)\mathbf{V}_m \cdot \mathbf{g}$  is negative, and, conversely, will attain a stable equilibrium position at the wall if this scalar is positive. Thus, if flow is down the tube ( $\mathbf{V}_m \cdot \mathbf{g} > 0$ ) the particle migrates to the axis if it is lighter than the fluid [cf. Denson (D4b), Oliver (O2), and Repetti and Leonard (R4a)], and to the wall if it is denser than the fluid [cf. Jeffrey (J5), Oliver (O2), and Repetti and Leonard (R4a)]. Similarly, in upflow ( $\mathbf{V}_m \cdot \mathbf{g} < 0$ ) migration to the tube axis occurs if the particle is denser than the fluid [cf. Jeffrey (J5) and Day and Genetti (D3a)], and to the tube wall if it is lighter than the fluid. The

experiments of Eichhorn and Small (E1) conducted with upflow in an inclined tube correspond to the former case ( $\mathbf{V}_m \cdot \mathbf{g} < 0$ ;  $\rho_p - \rho > 0$ ). Their observation that the lift force is directed inward towards the axis thus accords with the general criterion. Without exception, the data of every investigator of nonneutrally buoyant particles is therefore consistent with the conclusion that when the sphere lags the fluid it ends up at the axis, and when it leads the fluid it ends up at the wall—provided that the ratio  $|U_\infty|/V_m$  is not too near zero. Though the Rubinow–Keller theory predicts this behavior, such agreement does not necessarily imply the applicability of their theory to the nonneutrally buoyant case.

In an attempt to explain their observed dependence of  $\beta^*$  on small density differences, Repetti and Leonard (R4a) employ the Rubinow–Keller relation (256). However, the required axial slip velocity is not obtained from Eq. (250), but rather from an empirical modification of it derived, in part, from the experimental axial slip velocity data of Goldsmith and Mason (G9). The equation they propose contains an adjustable parameter, which they evaluate by a heuristic argument. Though their theory yields a value of  $\beta^* = 0.53$  for a neutrally buoyant particle and “explains” at least qualitatively the various modes of behavior observed for nonneutrally buoyant particles—including the extreme cases of migration to the wall or axis for large density differences, and the dependence of  $\beta^*$  on small density differences for *almost* neutrally buoyant particles—their proposal cannot be quantitatively correct; for it ignores the fact that for small  $a/R_o$  the slip velocity is correctly given by Eq. (250). And the term involving  $f(\beta)(a/R_o)$ , ignored by them, is an order of magnitude larger than the term of  $O(a/R_o)^2$  which they retain, at least when  $|U_\infty|$  and  $V_m$  are comparable in magnitude. But even apart from this, the Rubinow–Keller theory itself is not applicable to tube flow, as shown from different points of view by Saffman (S1a) and Cox and Brenner (C18). Their theories are discussed later. In particular, the latter advance an alternative, theoretically sound explanation of the phenomena observed by Repetti and Leonard.

The data of Theodore (T3a) for the lift force on a nonrotating sphere in a Poiseuille flow, and, to a lesser extent, the comparable data of Oliver (O2), show that lateral forces arise at small Reynolds numbers even in the absence of particle rotation. Thus, inertial lift forces can arise from “slip-shear” as well as from “slip-spin.” That the character of these two forces is very different is shown clearly by the theoretical analysis of Saffman (S1a).

Saffman (S1a) analyzes the motion of a rigid spherical particle relative to an unbounded, uniform, simple shear flow, the translational velocity of the sphere center lying parallel to the streamlines of the undisturbed motion. Particle Reynolds numbers are assumed to be small, leading to a first-order

analysis of inertial effects.<sup>43</sup> Let  $O'$  be an origin at the sphere center and denote by  $x_1', x_2', x_3'$  a right-handed system of Cartesian coordinates measured relative to  $O'$ . Referred to axes translating with the sphere, the boundary conditions considered by Saffman are

$$\mathbf{v}' = -\mathbf{i}_1(Sx_3' + \mathcal{U}_p) \quad \text{at infinity} \quad (269a)$$

$$\mathbf{v}' = -(\mathbf{i}_2\omega) \times \mathbf{r}' \quad \text{at } r = a \quad (269b)$$

where  $\mathbf{r}' = \mathbf{i}_1x_1' + \mathbf{i}_2x_2' + \mathbf{i}_3x_3'$ . The translational velocity  $\mathcal{U}_p$  of the sphere center relative to the surrounding fluid may be either positive or negative.  $\mathcal{U}_p < 0$  signifies that the particle lags the fluid whereas  $\mathcal{U}_p > 0$  indicates that it leads the fluid. No loss in generality results from taking the constant "velocity gradient"  $S \geq 0$ . The angular velocity of the sphere,  $\omega = -\mathbf{i}_2\omega$ , may be arbitrarily specified.<sup>44</sup>

<sup>43</sup> The problem is solved via singular perturbation techniques requiring the formation of inner and outer expansions of the flow field. Using a Fourier transform in the manner originally suggested by Childress (C7a) in the solution of a similar problem, Saffman is able to avoid the very tedious computation of the outer flow field; rather, the calculation is brought to fruition solely from a knowledge of its Fourier transform. This general technique almost certainly has important computational advantages in a variety of related problems.

<sup>44</sup> Insofar as possible we have chosen the notation here to coincide with that of the tube flow problem. In the latter case, when the sphere is restrained to move parallel to the tube axis, the boundary conditions at infinity and on the sphere, measured relative to an origin which translates with the sphere, are: at infinity,

$$\begin{aligned} \mathbf{v}' &= \mathbf{v} - \mathbf{U} = \mathbf{i}_1 2V_m(1 - R^2/R_o^2) - \mathbf{i}_1 U \\ &= -\mathbf{i}_1[2V_m(R^2 - b^2)/R_o^2 + \mathcal{U}_p] \end{aligned}$$

and, on the sphere [see Eq. (253)],

$$\mathbf{v}' = -(\mathbf{i}_2\omega) \times \mathbf{r}'$$

Here,  $\mathcal{U}_p$  is defined by Eq. (246) in the tube flow case. Compare these with Eqs. (269a) and (269b), respectively. Observe that as we move in the positive 3-direction (increasing  $R$  in the tube flow case and increasing  $x_3'$  in the shear flow case) the undisturbed velocity  $\mathbf{v}'$  at infinity decreases algebraically in both cases. The quantities

$$Sx_3' \quad \text{and} \quad 2V_m(R^2 - b^2)/R_o^2$$

are comparable. They both vanish at the sphere center ( $x_3' = 0$  and  $R = b$ , respectively). In comparing these terms, one should bear in mind that  $x_3 = x_3' + b$  and  $x_2 = x_2'$ , where  $x_2, x_3$  are measured from the cylinder axis. Furthermore, since  $R^2 = x_2^2 + x_3^2$ , we have the identity

$$2V_m \left( \frac{R^2 - b^2}{R_o^2} \right) = 2V_m \frac{(x_2')^2 + (x_3')^2 + 2bx_3'}{R_o^2}$$

In the vicinity of the sphere,  $x_2' \rightarrow 0$  and  $x_3' \rightarrow 0$ , this approaches  $4V_m bx_3'/R_o^2$ . Comparison with the comparable term  $Sx_3'$  shows that the "equivalent" local shear rate for tube flow is

$$S = 4V_m b/R_o^2$$



Three independent Reynolds numbers arise when the equations of motion and boundary conditions are cast in nondimensional form: the particle Reynolds number based on slip velocity,  $Re_p = 2a|U_p|/\nu$ ; a shear Reynolds number,  $Re_s = (2a)^2 S/\nu$ ; and a rotational Reynolds number,  $Re_\omega = (2a)^2 |\omega|/\nu$ . It is assumed that

$$Re_p, Re_s, Re_\omega \ll 1 \quad (270)$$

Employing singular perturbation methods to solve the Navier-Stokes equations, Saffman obtains, for the drag, torque about the sphere center, and lift force,

$$F_D = -i_1 6\pi\mu a U_p + O\{\mu a^2 U_p (S/\nu)^{1/2}\} \quad (271)$$

$$T = -i_2 8\pi\mu a^3 (\tfrac{1}{2}S - \omega) + o(\mu) \quad (272)$$

$$F_L = i_3 81.2 \mu a^2 U_p (S/\nu)^{1/2} + o(\nu^{-1/2}) \quad (273)^{45}$$

These expressions are only valid when

$$Re_s \gg (Re_p)^2 \quad (274)$$

it also apparently being assumed that  $Re_\omega$  is of the same or smaller order than  $Re_s$ .

To a first approximation the lateral migration velocity may be obtained by adding to Eq. (273) the Stokes law hydrodynamic force,  $-i_3 6\pi\mu a U_L$ , and equating the total lift force to zero. This yields a lateral velocity

$$U_L = \frac{81.2}{6\pi} U_p \left( \frac{a^2 S}{\nu} \right)^{1/2} \quad (275)$$

Since the couple vanishes for an unrestrained particle, one finds that  $\omega = \tfrac{1}{2}S$  to terms of lowest order. To this order the sphere therefore spins with the

<sup>45</sup> This result may be compared with that found by Bretherton (B29a, Eq. 10) for the lift force per unit length experienced by a circular cylinder of radius  $a$  for the comparable two-dimensional problem:

$$\text{lift force/length} = i_3 74.5 \mu U_p \left( \ln \frac{Sa^2}{\nu} \right)^{-2} + O \left( \ln \frac{Sa^2}{\nu} \right)^{-3}$$

This force acts in the same direction as that found for the sphere. Note that there is a misprint in Bretherton's equation (10), a minus sign having been omitted before the second term.

Zierep (Z2), using the Euler equations, obtained the following approximate solution of Saffman's problem for an *inviscid* fluid:

$$F_L = i_3 \frac{16\pi}{3} \rho a^3 U_p S$$

Rotation of the sphere was, however, not considered.

angular velocity of the unperturbed flow. For these same circumstances, the corresponding prediction of the Rubinow-Keller theory, obtained from Eqs. (254) and (255) by setting  $\omega = \frac{1}{2}S$ , is

$$U_L = \frac{1}{12} \mathcal{U}_p \left( \frac{a^2 S}{\nu} \right) \quad (276)$$

This differs radically from Eq. (275) although it does predict the correct direction of the lateral motion in the two possible cases,  $\mathcal{U}_p > 0$  and  $\mathcal{U}_p < 0$ . Even apart from this formal difference is the fact that, to terms of lowest order, the lift force predicted by Saffman is independent of the angular velocity of the particle<sup>46</sup>; that is, the lift force would be the same even if the particle were prevented from rotating. On the other hand, the Rubinow-Keller lift force depends critically upon the particle rotation.

When the conditions required by the inequality (274) are met, the slip-shear Saffman lift force is larger, by an order of magnitude, than the slip-spin Rubinow-Keller lift force; for from Eqs. (275) and (276) we find

$$\frac{(U_L)_{\text{Saffman}}}{(U_L)_{\text{Rubinow-Keller}}} = O\left\{ \frac{1}{(\text{Re}_s)^{1/2}} \right\}$$

This ratio clearly becomes infinite in the limit  $\text{Re}_s \rightarrow 0$ . Saffman demonstrates that terms of the Rubinow-Keller type, among others, will appear in the next higher-order approximation to Eq. (273).

Saffman's decision to analyze only the case for which the inequality (274) is satisfied rests entirely on the enormous analytical difficulties posed by the other possible limiting cases,  $\text{Re}_s \ll (\text{Re}_p)^2$  and  $\text{Re}_s = O(\text{Re}_p)^2$ —the various Reynolds numbers still being supposed small compared with unity. Only in Saffman's case do single inner and outer expansions suffice; the other cases appear to require three or more distinct regions of expansion [cf. Chang (C5) and Shi (S9a) for examples of this in other contexts]. Thus, in a sense, the a priori restriction to the range encompassed by Eq. (274) rigs the problem at the outset to one in which the slip-shear force dominates that due to slip-spin. Consideration of the opposite case,  $(\text{Re}_p)^2 \gg \text{Re}_s$ , might have reversed the conclusion or, more likely, made the two lift forces of comparable order. Therefore, though Saffman's calculation unequivocally demonstrates the lack of universal applicability of the Rubinow-Keller theory to the lateral migration problem, it does not, without further argument, demonstrate their theory to be substantially in error in any plausible physical situation. Such arguments are, however, furnished by the following line of reasoning: In the case of tube flow the local shear rate  $S$  is of the order  $4V_m b/R_o^2$ . Hence, in the

<sup>46</sup> Note that in the derivation of Eq. (273) no use has been made of the relation  $\omega = \frac{1}{2}S$ ; rather, the angular velocity was carried along as an arbitrary parameter.

neutrally buoyant case, where  $\mathcal{U}_p$  is of the order  $(4/3)V_m(a/R_o)^2$  [cf. Eq. (247)], one finds that  $Re_s/Re_p = O(\beta)$ , which is of order unity. This makes

$$Re_s/(Re_p)^2 = O(1/Re_p)$$

As  $Re_p \rightarrow 0$  this ratio becomes infinite, showing that the restriction required by Eq. (274) is indeed met. Thus, at least in the neutrally buoyant case, the Rubinow-Keller theory is wholly inapplicable to Poiseuille flows. It should not be surmised, however, that Saffman's results themselves have any direct application to such flows; for Saffman's calculations take no account of either the nonconstancy of the local shear rate or of the presence of boundaries constraining the flow. And either of these effects may result in the appearance of contributions to the lift force more dominant than Saffman's, at least for some ranges of the many independent variables.

Saffman attempts to make plausible the applicability of his relationship to tube flows under certain conditions. Even granting the correctness of these arguments, the possible range of applicability is very limited indeed. To its credit, however, is the fact that it predicts certain qualitative features which agree with experiment. Thus, it furnishes the correct direction of the lift force observed by Theodore (T3a) for an immobile, nonrotating sphere in a Poiseuille flow. Furthermore, it indicates that the force on the sphere ought not to be significantly affected by allowing it to freely rotate. This too agrees with Théodôre's observations. Despite this agreement as regards gross behavior, Eq. (273) with  $S = 4V_m b/R_o^2$  and  $\mathcal{U}_p = -2V_m(1 - \beta^2)$  fails to agree with Theodore's experimental results for the lift force, Eq. (260). The qualitative agreement may therefore be fortuitous.

In a direct attack upon the radial migration problem in essentially its full generality, Cox and Brenner (C18) succeeded in obtaining a first-order solution of the Navier-Stokes and continuity equations for the motion of a rigid spherical particle immersed in a Poiseuille flow within a circular tube of finite radius.<sup>47</sup> No couple acts on the particle, so it is free to rotate. It is presumed in the analysis that the sphere center moves parallel to the tube axis. The lateral force required to maintain the sphere at a fixed distance from the axis is computed and converted into an equivalent radial migration velocity by application of Stokes law to this sidewise motion.

When the equations of motion and boundary conditions are expressed in nondimensional form, the following functional relationship ultimately emerges:

$$\frac{U_L}{V_m} = \text{function}\left(Re_t, \frac{a}{R_o}, \frac{U_\infty}{V_m}, \beta\right) \quad (277)$$

<sup>47</sup> Their solution actually applies to particles and ducts of more general shape, but only the results for the sphere and circular tube are cited here. They also give results for the case where the sphere is prevented from rotating.

The angular velocity of the particle is not an independent parameter. In fact, to the order of the approximation, the particle spins with the local angular velocity of the undisturbed fluid. The analysis assumes that

$$\text{Re}_t \ll 1 \quad (278a)$$

$$a/R_o \ll 1 \quad (278b)$$

Using singular perturbation methods<sup>48</sup> a solution is obtained in the form of a double expansion in the two parameters  $\text{Re}_t$  and  $a/R_o$ . No restriction is placed on the parameter  $\beta$  except that the particle not be too near the wall; i.e.,  $a/(R_o - b) \ll 1$ , or, what is equivalent,

$$\frac{a}{R_o} \left( \frac{1}{1 - \beta} \right) \ll 1 \quad (279)$$

This constitutes a very mild restriction. The parameter  $|U_\infty|/V_m$  may be large or small.

As might be expected on the basis of prior observations, the form of the solution depends, at least in part, on the order of  $|U_\infty|/V_m$  relative to that of  $a/R_o$ . Five separate cases arise, ranging from that for a neutrally buoyant particle to that for a particle settling in an otherwise quiescent (but bounded) fluid. The results are tabulated below.

- (i) Neutrally buoyant sphere:  $|U_\infty|/V_m \ll (a/R_o)^2$ ;

$$U_L/V_m = \text{Re}_t(a/R_o)^3 F_I(\beta) \quad (280)$$

- (ii) Intermediate case between a neutrally buoyant and nonneutrally buoyant sphere:  $|U_\infty|/V_m = O(a/R_o)^2$ ;

$$U_L/V_m = \text{Re}_t(a/R_o)[(a/R_o)^2 F_I(\beta) + (U_\infty/V_m) F_{II}(\beta)] \quad (281)$$

- (iii) Nonneutrally buoyant sphere:  $(a/R_o)^2 \ll |U_\infty|/V_m \ll 1$ ;

$$U_L/V_m = \text{Re}_t(a/R_o)(U_\infty/V_m) F_{II}(\beta) \quad (282)$$

<sup>48</sup> In a sense, the case where the flow is bounded is conceptually easier to treat than is the comparable unbounded flow; for when the flow is bounded the disturbance created by the sphere dies away exponentially with axial distance (T1a, S16) rather than inversely with some power of the distance, as is true for the unbounded case. For this reason, the outer boundary conditions satisfied by the lower-order terms of the inner expansion can be determined without having to apply the "matching principle" except in a trivial sense; that is, the outer boundary conditions satisfied by the lower-order terms of the inner expansion are identical to the physical outer boundary conditions. Since the force and torque on the sphere can be determined from the inner expansion alone, it is therefore not necessary to compute *any* terms in the outer expansion in order to obtain the leading terms in the force and torque. Thus, the analysis differs greatly from those of Rubinow and Keller (R7) and Saffman (S1a).

- (iv) Intermediate case between a nonneutrally buoyant sphere and no net flow in the tube:  $|U_\infty|/V_m = O(1)$ ;

$$U_L/V_m = \text{Re}_t(a/R_o)(U_\infty/V_m)[F_{II}(\beta) + (U_\infty/V_m)F_{III}(\beta)] \quad (283)$$

- (v) No net flow in tube:  $1 \ll |U_\infty|/V_m$ ;

$$U_L/U_\infty = (2aU_\infty/\nu)F_{III}(\beta) \quad (284)$$

provided that the following additional restriction,

$$\text{Re}_\infty = \text{Re}_t(a/R_o)|U_\infty|/V_m = 2a|U_\infty|/\nu \ll 1$$

is met in Case (v).

Note that Case (ii) is merely a composite of Cases (i) and (iii), while Case (iv) is a composite of Cases (iii) and (v).

The three nondimensional functions of  $\beta$  appearing in these expressions are defined in terms of integrals involving the fundamental solution (L1) of Stokes equations for an eccentrically located vector point force of arbitrary orientation in an infinitely long circular cylinder for the case where the fluid is at rest at infinity. This fundamental solution is defined explicitly in the following way. All distances appearing in the following are made *dimensionless* with the cylinder radius. Let  $\underline{\mathbf{r}}$  denote the nondimensional position vector of the singular point force relative to an arbitrary origin and let  $\underline{\mathbf{r}}$  be the nondimensional position vector of any other point in the fluid relative to this same origin. The fundamental solution required is the dyadic "velocity" field,  $\mathbf{V} = \mathbf{V}(\underline{\mathbf{r}}, \underline{\mathbf{r}})$ , and vector "pressure" field,  $\mathbf{P} = \mathbf{P}(\underline{\mathbf{r}}, \underline{\mathbf{r}})$ , satisfying the inhomogeneous<sup>49</sup> Stokes equations

$$\bar{\nabla}^2 \mathbf{V} - \bar{\nabla} \mathbf{P} = -\mathbf{I} \delta(\underline{\mathbf{r}} - \underline{\mathbf{r}}) \quad (285a)$$

$$\bar{\nabla} \cdot \mathbf{V} = 0 \quad (285b)$$

and boundary conditions

$$\mathbf{V} = 0 \quad \text{on the cylinder wall} \quad (286)$$

and

$$\mathbf{V} \rightarrow 0 \quad \text{at infinite axial distances on either side of the singularity} \quad (287)$$

<sup>49</sup> Alternatively, by adding the supplementary condition

$$\mathbf{V} \rightarrow \frac{1}{8\pi|\underline{\mathbf{r}} - \underline{\mathbf{r}}|} \left\{ \mathbf{I} + \frac{(\underline{\mathbf{r}} - \underline{\mathbf{r}})(\underline{\mathbf{r}} - \underline{\mathbf{r}})}{|\underline{\mathbf{r}} - \underline{\mathbf{r}}|^3} \right\} \quad \text{as } (\underline{\mathbf{r}} - \underline{\mathbf{r}}) \rightarrow 0$$

one may solve instead the corresponding *homogeneous* Stokes equations.

Note that though  $\mathbf{V}$  and  $\mathbf{P}$  defined by Eqs. (285)–(287) are dimensionless, in order to keep the notation concise they have not been underlined, despite our usual practice for such entities.

Here,  $\delta$  denotes the Dirac delta function, and  $\mathbf{I}$  the idemfactor [cf. Eqs. (193)–(194)]. Physically, the Cartesian tensor equivalent of  $\mathbf{V}$ , namely,  $V_{ij}$ , represents the  $i$ th component of the Stokes velocity field at  $\underline{\mathbf{r}}$  due to a unit point force exerted on the fluid at  $\underline{\mathbf{r}}$  in the  $j$ th direction.

In order to express the various  $F(\beta)$  in terms of  $\mathbf{V}$ , let  $\underline{\mathbf{r}} \equiv (\underline{x}_1, \underline{x}_2, \underline{x}_3)$  be Cartesian coordinates having the sense previously assigned to the 1, 2, and 3 directions (see Fig. 3). (It is not essential, however, that the origin lie along the cylinder axis.) Furthermore, let  $\underline{R}$  and  $\underline{\bar{R}}$  be radial cylindrical distances measured from the axis to the points  $\underline{\mathbf{r}}$  and  $\underline{\bar{\mathbf{r}}}$ , respectively. The functions in question are then given by the expressions

$$F_I(\underline{R}) = \frac{40\pi}{3} \underline{R} \sum_{k=1}^3 \int_{\underline{\Gamma}} \left[ (\underline{R}^2 - \underline{\bar{R}}^2) V_{k3} \frac{\partial}{\partial \underline{\bar{x}}_1} \left( \frac{\partial V_{k1}}{\partial \underline{x}_3} + \frac{\partial V_{k3}}{\partial \underline{x}_1} \right) + \left\{ \frac{\partial}{\partial \underline{\bar{x}}_k} (\underline{R}^2 - \underline{\bar{R}}^2) \right\} V_{13} \left( \frac{\partial V_{k1}}{\partial \underline{x}_3} + \frac{\partial V_{k3}}{\partial \underline{x}_1} \right) \right] d\underline{\Gamma} \quad (288)$$

$$F_{II}(\underline{R}) = 6\pi \sum_{k=1}^3 \int_{\underline{\Gamma}} \left[ (\underline{R}^2 - \underline{\bar{R}}^2) V_{k3} \frac{\partial V_{k1}}{\partial \underline{\bar{x}}_1} + \left\{ \frac{\partial}{\partial \underline{\bar{x}}_k} (\underline{R}^2 - \underline{\bar{R}}^2) \right\} V_{13} V_{k1} \right] d\underline{\Gamma} \quad (289)$$

$$F_{III}(\underline{R}) = -3\pi \sum_{k=1}^3 \int_{\underline{\Gamma}} V_{k3} \frac{\partial V_{k1}}{\partial \underline{\bar{x}}_1} d\underline{\Gamma} \quad (290)$$

in which  $d\underline{\Gamma} \equiv d\underline{\bar{x}}_1 d\underline{\bar{x}}_2 d\underline{\bar{x}}_3$  is a volume element, and  $\underline{\Gamma}$  denotes integration over the entire space (including the singularity) lying within the cylinder.

Calculation of the Lorentz dyadic  $\mathbf{V}$  can be performed by an obvious generalization of the work of Brenner and Happel (B28). Though straightforward in principle, the algebraic effort required is prodigious, and the work is as yet incomplete. At this stage we are therefore unable to describe any general features of the  $F(\beta)$ . In order to explain existing experimental data these functions would have to possess at least the following properties:

$$F_I(\beta) = \begin{cases} 0 & \text{at } \beta = 0 \\ >0 & \text{for } 0 < \beta < \beta^* \\ 0 & \text{for } \beta = \beta^* \approx 0.6 \\ <0 & \text{for } \beta^* < \beta < 1 \end{cases} \quad (291)$$

and

$$F_{II}(\beta) = \begin{cases} 0 & \text{at } \beta = 0 \\ >0 & \text{for } 0 < \beta < 1 \end{cases} \quad (292)$$

and

$$F_{III}(\beta) = \begin{cases} 0 & \text{for } \beta = 0 \\ < 0 & \text{for } 0 < \beta < 1 \end{cases} \quad (293)^{50}$$

Though quantitative comparisons with experimental data are denied us as yet, various qualitative comparisons are possible. Thus, except for a slight difference in the exponent of  $a/R_o$ , the functional form of Eq. (280) agrees with that observed by Segré and Silberberg, Eq. (257). According to Eq. (280) the equilibrium position attained by the sphere corresponds to  $F_I(\beta^*) = 0$ . This implies that the equilibrium position of a neutrally buoyant sphere should be independent of  $Re_t$  and  $a/R_o$ , at least when these are sufficiently small. The experiments of Segré and Silberberg (S6), Oliver (O2), Karnis *et al.* (K5, K5b), and Jeffrey (J5), covering a rather large range of these variables, tends to bear this out. Equation (282) indicates that the direction of lateral migration depends upon the algebraic sign of  $U_\infty/V_m$  in the nonneutrally buoyant case. This conclusion too is borne out by the experiments of all investigators.

In practical problems one is unlikely to encounter particles which are precisely neutrally buoyant. For this reason, Case (ii) is likely to be of greater interest in applications than is Case (i). According to Eq. (281) the stable equilibrium position depends upon the dimensionless ratio

$$\Lambda = \frac{U_\infty/V_m}{(a/R_o)^2} \quad (294)$$

which may be either positive or negative. According to the general properties noted in Eqs. (291) and (292), the equilibrium position  $\beta^*$  will lie nearer to the axis than 0.6 when the particle lags the fluid ( $\Lambda < 0$ ) and nearer to the wall than 0.6 when the particle leads the fluid ( $\Lambda > 0$ ). These phenomenon appear to have been observed by Repetti and Leonard (R4a) in a *two-dimensional* Poiseuille flow, but they do not report sufficient data in their initial communication to settle the matter unequivocally. Failure of previous investigators to observe this phenomenon in circular tubes is not surprising, since the range of density differences required to prevent migration of the particle all the way

<sup>50</sup> Oliver (O2) observed that a sphere settling slowly near the wall of a tube in an otherwise stagnant fluid moved inwardly, towards the tube axis. Karnis (K4a, K5b), in a series of more detailed measurements, made similar observations and followed the motion of the sphere all the way to the tube axis. It is on the basis of these observations that  $F_{III}(\beta)$  is concluded to be negative. This conclusion accords with Oseen's (O4) theoretical finding [also summarized in Berker (B4, p. 328)] that, when small inertial effects are considered, a sphere moving parallel to a plane wall in a semi-infinite fluid experiences a *repulsive* hydrodynamic force, due to the source-like behavior of the flow at points distant from the sphere not lying within the wake [cf. Lamb (L5, p. 613)].

to the tube axis or wall is remarkably narrow. Thus, Repetti and Leonard find that, starting with neutrally buoyant particles, small density differences resulting from temperature changes of the order of  $\pm 5^\circ\text{C}$  (corresponding to density differences of the order of  $\pm 0.05$  percent) are quite sufficient to radically alter the ultimate equilibrium position.

An order of magnitude estimate of the density differences required to observe the Repetti-Leonard phenomenon in a tube may be obtained by arbitrarily considering the  $\Lambda$  range,  $|\Lambda| = (0.1-10.0)(4/3)$  [see Eq. (250) for the  $4/3$  factor]. Assuming the validity of Stokes law,  $|U_\infty| = 2a^2|\Delta\rho|g/9\mu$ , this requires that the fluid-particle density difference lie in the range

$$\frac{|\Delta\rho|gR_o^2}{\mu V_m} = 0.6-60 \quad (295)$$

or, in terms of the tube Reynolds number,

$$\frac{|\Delta\rho|}{\rho} = (0.3-30) \frac{\text{Re}_t v^2}{gR_o^3} \quad (296)$$

For example, for water ( $v \approx 10^{-5}$  ft<sup>2</sup>/sec), taking  $\text{Re}_t = 1$  and  $R_o = 1$  in., this yields  $100 \times |\Delta\rho|/\rho \approx 10^{-7}-10^{-5}$  percent!!! Thus, the effect is never likely to be observed in water. On the other hand, at the same tube Reynolds number, increasing the viscosity by 100-fold and decreasing the radius by one-half multiplies the above percentages by a factor of about  $10^5$ . Hence, observation of the phenomenon should not be too difficult with a sufficiently viscous fluid.

As mentioned previously, Repetti and Leonard (R4a) attempted an explanation of this phenomenon on the basis of a questionable modification of the Rubinow-Keller theory. It is now clear, however, that their proposal cannot be correct.

Since the equilibrium position for Case (ii) is independent of particle size and depends only on the parameter  $\Delta\rho gR_o^2/\mu V_m$ , a novel separation technique suggests itself. Particles of different density will accumulate in different streamlines, irrespective of particle size. By choosing the operating conditions carefully, it appears possible to separate particles whose densities differ only infinitesimally from one another.

Granting the correctness of the inequalities set forth in Eqs. (292) and (293), it appears from the results of Case (iv) that there may exist fractionally eccentric equilibrium positions originating from circumstances very different from those already investigated to date under the general domain of Cases (i) and (ii).

With regard to the interpretation of available experimental data, the only outstanding point seemingly in need of further discussion is the observation by Denson (D4b) that the Rubinow-Keller theory agrees well with his



data. Equation (282) may be rewritten as

$$\frac{U_L}{V_m} = \frac{2aU_\infty}{v} F_{II}(\beta) \quad (297)$$

Comparison with Eq. (268), bearing in mind that Denson's data only covers a limited range of  $a/R_0$  values, suggests that this agreement might be fortuitous if  $F_{II}(\beta)$  were approximately equal to  $(0.12-0.19)\beta/6$ . Whether or not this is indeed the case awaits the numerical evaluation of the function in question.

#### 4. Radial Migration Under More General Circumstances

The preceding discussion of experimental and theoretical studies pertaining to lateral migration applies only to the case of a rigid spherical particle suspended in a fully-developed, laminar, Newtonian flow within a circular tube. As discussed in subsequent paragraphs, related experimental and theoretical work on radial migration has also been conducted for a variety of situations in which one or more of these restrictions is relaxed.

Lateral migration is possible even in the absence of inertial effects if the particle is not spherical. Thus, on the basis of Stokes equations, Bretherton (B30) demonstrated theoretically that a rigid, neutrally buoyant, anisotropic particle lacking a center of symmetry can undergo lateral migration in Couette and Poiseuille flows. Similarly, Goldsmith and Mason (G7, G9) experimentally observed radial migration of *flexible* rods and disks to the axis of a Poiseuille flow. This occurred at values of  $Re_p < 10^{-6}$  and  $Re_t < 2 \times 10^{-2}$ , where no discernible lateral motion was detected for rigid spheres (or for rigid rods or disks, either<sup>51</sup>).

Also in the context of Stokes flow, a neutrally buoyant *liquid droplet* immersed in a Poiseuille or other nonuniform shear flow deforms in response to the local shear and migrates across the streamlines, provided that the viscosity ratio,  $\eta = \text{droplet viscosity}/\text{continuous phase viscosity}$ , is not too large. When the latter condition is met, the droplet acquires the ellipsoidal shape described by Eq. (122a). In a Poiseuille flow this leads to the conclusion that the principal axes of a nonaxially situated droplet are *permanently* inclined at definite angles to the tube axis (though the extent of the deformation decreases as it approaches the tube axis), leading to an asymmetry of the flow and, hence, to the existence of radial forces arising from the nonuniformity of the shear. [In connection with this observation it should be noted that in contrast to the behavior of ellipsoid-like liquid droplets, *rigid* disks and rods do not maintain a fixed orientation relative to the tube walls, but rather undergo a periodic rotation (G9) of the type predicted by Jeffery (J4). Thus,

<sup>51</sup> At larger particle Reynolds numbers ( $Re_p \approx 10^{-3}$ ), where inertial effects are more significant, rigid, neutrally buoyant rods and disks behave in essentially the same manner as do rigid spheres. They migrate inward if introduced near the wall and outward if introduced near the axis, attaining a stable terminal position at about  $\beta^* = 0.5$  (K5, K5b).

averaging over one period, any radial forces associated with the asymmetric orientation of a *rigid* centrally symmetric particle relative to the streamlines will tend to cancel.] Such droplets always migrated rapidly to the tube axis (G9), at least for  $\eta < 10$  (K5). This phenomenon was observed at conditions ( $Re_p < 10^{-6}$ ) where comparable experiments with *rigid*, neutrally buoyant particles (including disks and rods) yielded no detectable radial motion. No radial motion was observed under similar conditions when the viscosity ratio was large, i.e.,  $\eta = 50$  (K5, T1). This anomalous behavior appears to be connected with the fact that, according to Eq. (122b), the droplet behaves like a rigid sphere for such large viscosity ratios, its deformation being nil. Moreover, at somewhat larger values of  $Re_p$  ( $> 10^{-3}$ ), these highly viscous droplets attained stable equilibrium positions at about  $\beta^* = 0.63$  (T1), in a manner identical to that observed for rigid spheres.

If the droplet is not neutrally buoyant it may migrate either to the axis or to the wall, depending, at least in part, upon the algebraic sign of the density difference and the direction of net flow relative to the gravity field. Thus, Jeffrey (J5) performed a few qualitative experiments with liquid droplets whose density was greater than that of the entraining liquid flowing in Poiseuille flow. The Reynolds number range was similar to that previously described in connection with his experiments on rigid spheres. With flow up the tube the droplets migrated permanently to the axis; with flow down the tube they migrated to the wall. Purely visual observations indicated radial migration velocities to be of the same order of magnitude as those observed for rigid spherical particles. The droplet migrations observed by Jeffrey were thus probably due, in large measure, to inertial effects. It should be noted, however, that these effects, including the observed sense of the radial motion, would be expected even in the Stokes regime; for, as has been pointed out, the droplet acquires the shape of an ellipsoid whose axes are permanently inclined relative to those of the tube. And even a *rigid* ellipsoid with its axes obliquely inclined to the direction of gravity will drift laterally as it settles in a quiescent fluid—the sense of the drift depending upon whether the particle is denser or lighter than the fluid.<sup>52</sup>

<sup>52</sup> A theoretical analysis of the Stokes flow problem for a nonneutrally buoyant droplet is clearly called for. Germane to this problem is the theoretical analysis of Haberman (H3), dealing with axially symmetric Stokes flow relative to a liquid droplet at the axis of a circular tube, and Taylor and Acrivos' (T2c) extension of the classical Hadamard-Rybczyński liquid droplet problem to the case of nonzero Reynolds numbers. In particular, Haberman shows that the assumption of a spherical shape for the droplet in a tube is incompatible with the differential equations and boundary conditions. Taylor and Acrivos (T2c) point out that, though Hadamard (H3a) and Rybczyński (R10) were able to solve the Stokes flow problem by assuming a spherical shape for a liquid droplet, irrespective of the magnitude of the interfacial tension, the correctness of their a priori assumption was, to some extent, fortuitous. These remarks are undoubtedly pertinent to the resolution of Haberman's "paradox" and, ultimately, to the solution of the nonaxially symmetric droplet problem.

The radial migration of a neutrally buoyant liquid droplet with its center lying in the mid-plane between two equal counter-rotating disks was theoretically studied by Chaffey, Brenner, and Mason (C2) on the basis of Stokes equations. This constitutes a simple example of a nonuniform shear field, the rate of shear increasing outwardly from the axis of rotation. The unperturbed velocity in the mid-plane between these disks is zero, so that radial motion arises entirely from the nonuniformity of the shear over the droplet surface. The sense of the migration is found to depend upon the ratio  $\eta$  of drop viscosity to continuous phase viscosity. For  $\eta > 0.139$  the droplet migrates inwardly, towards the axis of rotation of the disks. For  $\eta < 0.139$  the migration is outward. When  $\eta = 0.139$  no migration occurs. In another paper (C3), these same authors also considered the lateral motion of a deformable liquid droplet near a plane wall when suspended in another liquid undergoing Couette flow. Migration away from the wall is predicted on the basis of Stokes equations.

Karnis, Goldsmith, and Mason (K5, K5d) performed experiments on the radial migration of rigid spheres suspended in a *viscoelastic* fluid flowing through a circular tube. Migration towards the axis was observed under conditions where inertial effects would normally be expected to be nil. The observed radial motion is thus apparently attributable to the non-Newtonian properties of the fluid. The unperturbed velocity profile is very flat over the central portion of the tube. Particles placed in this region neither rotated nor moved radially. Experiments are also reported for rods and disks (G9b, K5d).

In regard to *nonsteady* tube flows, Mason *et al.* have observed both inward and outward radial migration of rigid, neutrally buoyant spheres in oscillatory (S9b, G9b) and pulsatile (T1) flows in circular tubes at frequencies up to 3 cps, at which frequencies inertial effects are likely to be important.<sup>53</sup> We refer here to inertial effects arising from the *local* acceleration terms in the Navier-Stokes equations, rather than from the *convective* acceleration terms. In the oscillatory case the spheres ( $a/R_0 \approx 0.10$ ) attained equilibrium positions at about  $\beta^* = 0.85$ . Important Reynolds numbers here are those based upon mean tube velocity for one-half cycle and upon frequency. Nonneutrally buoyant spheres in oscillatory flow migrate permanently to the tube axis, irrespective of whether they are denser or lighter than the fluid (K4a).

Convective radial velocities arise during the entrance of a fluid into a tube. The particles in an initially uniform suspension will therefore be redistributed upon entering the tube, giving rise to anomalous effects (K5c, M5a, M7a, S18, S19).

Again, in relation to end effects, a statistical type of "tubular pinch effect"

<sup>53</sup> An oscillatory flow is one in which there is no *net* flow. A pulsatile flow is an oscillatory flow superposed on a steady net flow. The latter is important in blood flow phenomena, the pulsations arising from the periodic action of the heart.

is possible in batch, liquid-fluidized beds when the densities of particles and fluid are not matched (H8). This occurs even in the Stokes regime and has a simple explanation. The phenomenon is well known experimentally, and manifests itself by the existence of a very high concentration of particles near the tube walls.

Radial particle motions also arise during the initial filling of an empty tube with a suspension of neutrally buoyant particles. This "meniscus effect" (K5c) is most pronounced near the interface between the free surface of the liquid and the atmosphere. This type of end effect occurs even in the absence of inertial effects, i.e., in the Stokes regime.

Many of the single-particle radial migration experiments described above are currently being extended to concentrated suspensions of particles by Goldsmith, Mason, and their co-workers (K5a). This work is likely to prove of great significance to chemical engineers and others. The bulk of their work to date on all aspects of fluid-particle dynamics is critically surveyed in their review chapter on "The Microrheology of Dispersions" (G9d).

#### IV. Heat- and Mass-Transfer Analogies, Brownian Motion, and Summary

##### A. HEAT- AND MASS-TRANSFER ANALOGS

In view of the many analogies between momentum-transport and heat- and mass-transport, it is not surprising to find applications of much of the preceding hydrodynamic theory in the latter areas of scalar transport. It is not our intention here to systematically survey the general field of heat- and mass-transfer at small Reynolds numbers. Rather, we shall restrict ourselves exclusively to situations in which the Péclet number is *small*. For it is here that the analogies are strongest. Since the Péclet number is a global measure of the ratio of convective to molecular energy (or mass) transport it plays the same role in heat- and mass-transfer as does the Reynolds number in momentum transfer. Techniques for treating low Reynolds number heat- and mass-transfer at *large* Péclet numbers are admirably discussed in Levich's book (L10a).

With appropriate simplifying assumptions, the energy equation for steady-state forced-convection heat-transfer may be written as

$$\mathbf{v} \cdot \nabla T = \alpha \nabla^2 T \quad (298)$$

where  $T$  is the temperature and  $\alpha$  the thermal diffusivity. Attention is confined to the case where  $\mathbf{v}$  refers to a Stokes flow past the body. In this case the Nusselt number is a function only of the Péclet number, since the Reynolds number is no longer a parameter. The velocity may be made dimensionless with a characteristic speed  $U$ , the position vector with a characteristic particle

“radius”  $a$ , and the temperature with some characteristic temperature. By these means the energy equation may be written in the nondimensional form

$$\nabla^2 T - \text{Pé}^* \mathbf{y} \cdot \nabla T = 0 \quad (299)$$

where

$$\text{Pé}^* = aU/\alpha \quad (300)$$

is the Péclet number based on “radius.”

### 1. Zero Péclet Number

Assuming that the various dimensionless quantities remain finite in the limit as  $\text{Pé}^* \rightarrow 0$ , Eq. (299) reduces to Laplace’s equation. Thus, in dimensional form,

$$\nabla^2 T = 0 \quad (301)$$

This relation may be regarded as the counterpart of Stokes equations, Eqs. (7)–(8). Roughly speaking, Eq. (301) bears the same relationship to Eq. (299) at very small Péclet (and Reynolds) numbers as do Stokes equations to the complete Navier–Stokes equations at very small Reynolds numbers. Hence, many of the results of Section II pertaining to the solutions of Stokes equations have analogs in the theory of heat- (and mass-) transfer at asymptotically small Péclet numbers. It will suffice, therefore, to illustrate these analogs by a few salient examples.

Consider the case of heat transfer in the infinite space external to some body  $B$ . Suppose that the body is maintained at a constant uniform temperature  $T_B$ , and that the unperturbed temperature field at infinity is some arbitrarily prescribed solution of Laplace’s equation,  $T_\infty(\mathbf{r})$ . Thus, one is to solve Eq. (301) so as to satisfy these boundary conditions. A conventional heat-transfer coefficient cannot be defined for this situation because of the spatially-variable nature of  $T_\infty$ . However, by resorting to *symbolic* methods the rate of heat transfer per unit time from the body to the surrounding medium may be written in the symbolic form

$$Q = hA(T_B - T_\infty) \quad (302)$$

in which  $A$  is the external surface area of the body and the “heat-transfer coefficient”  $h$  is a *scalar, symbolic, differential operator*. This relation is the analog of the comparable momentum-transfer relations (81)–(82). In particular, for a spherical particle of radius  $a$  embedded in a medium of thermal conductivity  $k$ , the symbolic Nusselt number (based on radius) is

$$\frac{ha}{k} = \frac{\sinh(a\nabla_0)}{a\nabla_0} \quad (303)$$

in which  $O$  refers to the sphere center and  $\nabla = (\nabla^2)^{1/2}$ . This should be compared with Eqs. (87)–(88). By resorting to the infinite series expansion for the hyperbolic sine, and noting that  $\nabla^2 T_\infty = 0$  everywhere, and that  $A = 4\pi a^2$ , one thus obtains

$$Q = 4\pi k a \{T_B - (T_\infty)_O\} \quad (304)$$

where the subscript  $O$  implies evaluation at the sphere center. This relation is the analog of Faxén's laws, Eqs. (89a)–(89b). As the series expansion (304) terminates after a finite number of terms, the sphere does not provide a convincing example of the significant advantages afforded by the use of a symbolic heat-transfer coefficient. Rather, the comparable expression for the ellipsoid [see also Eqs. (92a)–(92b)],

$$\hbar A = \frac{8\pi k \sinh D_O}{\chi} \frac{D_O}{D_O} \quad (305)$$

illustrates the technique to better advantage. Here,  $\chi$  and  $D$  are defined in Eqs. (62) and (93), respectively. The subscript  $O$  refers to evaluation at the center of the ellipsoid.

Equation (302) originates from the relation

$$Q = -k \int_B (T - T_\infty) \nabla \tau \cdot d\mathbf{S} \quad (306)$$

where the scalar field  $\tau$  satisfies the following differential equation and boundary conditions:

$$\begin{aligned} \nabla^2 \tau &= 0 \\ \tau &= 1 \quad \text{on } B \\ \tau &\rightarrow 0 \quad \text{at infinity} \end{aligned} \quad (307)$$

These relations are the precursors of Eqs. (303) and (305). Equation (306) is the counterpart of Eqs. (78)–(79), whereas the field  $\tau$  defined by Eq. (307) is comparable to the intrinsic fields defined in Eqs. (17)–(20) and (25)–(28). The derivation of Eq. (306) depends upon the use of a reciprocal theorem, in the form of Green's second identity (L5a), in much the same way as the derivation of Eqs. (78)–(79) devolves upon the use of a comparable reciprocal theorem (B18). Fourier's law,  $\mathbf{q} = -k\nabla T$ , for the heat-flux vector plays a role comparable to Newton's law of viscosity, Eq. (3), in the former derivation.

The representation of the macroscopic properties of bodies by symbolic operators may be applied in other contexts. In electrostatics, for example, if we interpret  $Q$  as the charge on a conducting body, and  $T$  as the electric potential, then  $\hbar A$  in Eq. (302) may be interpreted as the symbolic capacitance of the body, viewed as a condenser;  $k$  then plays the role of the dielectric constant (capacitivity) of the medium external to the body, this medium being assumed homogeneous and isotropic.

## 2. Small, Nonzero Péclet Numbers

The preceding development furnishes formulas for the rate of heat transfer in Stokes flow correctly to the zeroth order in the Péclet number. As Acrivos and Taylor (A1a) have so convincingly demonstrated in the case of streaming flows, higher-order terms in the Nusselt number-Péclet number expansion cannot be obtained by conventional perturbation schemes. Rather, such attempts encounter the same fundamental difficulty as is met in attempts to obtain higher-order terms, beyond Stokes law, in the drag coefficient-Reynolds number expansion, as discussed in Section III,A. In particular, no matter how small the Péclet number, the leading term in the expansion, that is to say, the solution of Eq. (301), does not furnish a uniformly valid solution of the energy equation (299). This leads to a Whitehead-type "paradox" analogous to that discussed in a hydrodynamic context in Section III,A. Again, the difficulty may be resolved by resorting to singular perturbation methods (Section III,C), utilizing separate, locally valid, inner and outer expansions of the temperature field, and asymptotically "matching" them in their common domain of validity, i.e., where  $Pé^* \underline{r} = O(1) - \underline{r}$  being the dimensionless distance from the body.

By this technique Acrivos and Taylor obtained the following result<sup>54</sup> for streaming Stokes flow past a spherical particle of radius  $a$  maintained at uniform temperature in a fluid whose temperature is uniform at infinity:

$$Nu = 2 + \frac{1}{2} Pé + \frac{1}{4} Pé^2 \ln Pé + 0.03404 Pé^2 + \frac{1}{16} Pé^3 \ln Pé + O(Pé^3) \quad (308)$$

in which

$$Nu = 2ha/k \quad (309)$$

is the average Nusselt number based on sphere diameter ( $h$  being the conventional heat-transfer coefficient), and

$$Pé = 2aU/\alpha \quad (310)$$

is the Péclet number based on sphere diameter ( $U$  being the speed of the stream at infinity). Each successive term,  $f_n(Pé)$ , in Eq. (308) has the property that

$$\lim_{Pé \rightarrow 0} f_{n+1}(Pé)/f_n(Pé) = 0$$

Equation (308) is the analog of Proudman and Pearson's (P11) result for the drag on a sphere at small, nonzero Reynolds numbers, quoted in Eq. (212).

<sup>54</sup> The leading term in the comparable asymptotic expansion for *large* Péclet numbers, i.e.,  $Pé \rightarrow \infty$ , obtained by thermal boundary layer arguments (L10a, F11, A1a), is

$$Nu = 0.991(Pé)^{1/3} + O(Pé^0)$$

Higher-order terms in this expansion are given explicitly by Acrivos and Goddard (A1).

The appearance of transcendental terms in these expansions is characteristic of the spatially nonuniform properties of the individual perturbation terms.

Equation (308) was generalized by Brenner (B18a) to particles of arbitrary shape (not necessarily *solid* particles), resulting in the following expansion:

$$\text{Nu} = \text{Nu}_0 + \frac{1}{8} \text{Nu}_0^2 \text{Pé} + \frac{1}{16} \text{Nu}_0^2 f_{0\alpha} \text{Pé}^2 \ln \text{Pé} + O(\text{Pé}^2) \quad (311)$$

where

$$\text{Nu} = \frac{hA}{2\pi ka} \quad (312a)$$

$$\text{Nu}_0 = \frac{h_0 A}{2\pi ka} \quad (312b)$$

is a generalized Nusselt number based on the characteristic particle "diameter"  $2a$  ( $A$  being the wetted area of the particle), and  $\text{Pé}$  is as defined in Eq. (310) with  $U$  the speed of the stream at infinity. The subscript "0" on the Nusselt number in Eq. (312b) refers to its value for a *stagnant fluid* i.e., for  $\text{Pé} = 0$ . Furthermore,

$$f_{0\alpha} = |(F_0)_\alpha|/6\pi\mu aU \quad (313)$$

is the dimensionless Stokes drag on the particle,  $(F_0)_\alpha$  being the dimensional drag on the body—that is, the component of the (Stokes) vector force on the particle in the direction of the stream velocity vector  $\mathbf{U} = \alpha U$ . For a solid sphere of radius  $a$  ( $\text{Nu}_0 = 2$ ,  $f_{0\alpha} = 1$ ), this correctly reproduces the first three terms of Eq. (308). The terms of  $O(\text{Pé}^2)$  and higher in Eq. (311) depend explicitly on the geometry of the particle and on the fluid-dynamical boundary conditions at its surface.

Equation (311) is the heat-transfer analog of the corresponding hydrodynamic formula, Eq. (232), expressing the drag on a particle of arbitrary shape in terms of the Stokes force. The utility of Eq. (311) lies in the fact that it permits one to predict the heat-transfer coefficient  $h$  for streaming flow past the body solely from a knowledge of the comparable coefficient  $h_0$  for molecular conduction, and from a knowledge of the Stokes drag on the body. Inasmuch as the drag necessarily depends upon the orientation of the body relative to the free-stream velocity, Eq. (311) provides an explicit illustration of the fact that the heat-transfer coefficient varies with the orientation of the body.

The overall rate of heat transfer, from bodies of any shape past which fluid streams in Stokes flow, has the remarkable property of being invariant to reversal of the direction of the streaming flow at infinity (B26b); that is, for a particle of uniform surface temperature immersed in a fluid of different uniform temperature at infinity, the average Nusselt number is the same for



flow past the particle in any specified direction, as for flow at the same speed in the opposite direction. What makes this result surprising is that the local temperature field, defined by Eq. (298), does not itself generally display such invariance. This theorem applies irrespectively of the magnitude of the Péclet number ( $0 \leq \text{Pé} < \infty$ ) – even in the thermal boundary-layer regime,  $\text{Pé} \rightarrow \infty$ . As such, it contradicts intuition; for the detailed structure of the thermal boundary-layer for flow past nonspherical particles (lacking fore-aft symmetry relative to the direction of streaming) depends markedly upon the direction of flow. Equation (311), valid at small  $\text{Pé}$ , is concordant with this flow-reversal theorem. In fact, it was the prior existence of this result that originally suggested the general theorem. Inasmuch as proof of the theorem depends only upon the fact that, except for the algebraic sign, the local velocity field  $\mathbf{v}$  is invariant to flow reversal, and requires only that the *normal* velocity component vanish at the particle surface, the general result also applies to other classes of “reversible” flows, e.g., streaming potential flow past the particle.

O'Brien (O1a) applied the Acrivos–Taylor analysis to the case where the Reynolds number, though small, is not identically zero as in the Stokes flow case. The analysis is vastly more complicated because, to any order in the Reynolds number, the velocity field  $\mathbf{v}$  appearing in Eq. (298) is now expressed in terms of *two*, locally valid expansions [the inner and outer expansions of  $\mathbf{v}$  given by the Proudman–Pearson analysis (P11)], rather than the single Stokes velocity field. For a solid spherical particle she obtains for small  $\text{Pé}$  and  $\text{Re}$

$$\text{Nu} = 2 + \frac{1}{2} \text{Pé} \left(1 - \frac{1}{64} \text{Re}\right) + \cdots \quad (314)$$

where  $\text{Re} = 2aU/v$  is the Reynolds number based on sphere diameter,  $v$  being the kinematic viscosity. This result apparently applies to the case where

$$\text{Re} \ll \text{Pé} \ll 1 \quad (315a)$$

Alternatively, since  $\text{Pé} = \text{Pr Re}$ , where  $\text{Pr} = \nu/\alpha$  is the Prandtl number, the range of applicability is

$$1 \ll \text{Pr} \ll (\text{Re})^{-1} \quad (315b)$$

An extension of the Acrivos–Taylor (A1a) heat transfer analysis to slip flow past the sphere is given by Taylor (T2a). Hartunian and Liu (H9a) and Taylor (T2b) include the effect of surface chemical reactions in their singular perturbation treatment of Stokes-flow mass transfer from spheres at small Péclet numbers.

## B. BROWNIAN MOTION

In this subsection we present a general theory of the translational and rotational Brownian motions of rigid particles of arbitrary shape.

One of the important applications of Stokes law occurs in the theory of Brownian motion. According to Einstein (E1a) the translational and rotary diffusion coefficients for a spherical particle of radius  $a$  diffusing in a medium of viscosity  $\mu$  are, respectively,

$$D_t = \frac{kT}{6\pi\mu a} \quad (316a)$$

$$D_r = \frac{kT}{8\pi\mu a^3} \quad (316b)$$

where  $k$  is Boltzmann's constant (the gas constant per molecule) and  $T$  is the absolute temperature. These relations presuppose that the diffusing solute particle is large compared with the mean-free path of the solvent molecules. Thus, from the point of view of the diffusing particle, the surrounding solvent medium may be regarded as continuous, and the conventional principles of continuum fluid mechanics applied. The minute dimensions of the solute particles insure that the pertinent translational and rotational Reynolds numbers will, on the average, be small, thereby bringing the phenomenon within the domain of a Stokes flow. The denominators  $6\pi\mu a$  and  $8\pi\mu a^3$  appearing above are the proportionality coefficients between the hydrodynamic force and translational velocity, and hydrodynamic torque and angular velocity, respectively.

In addition to Eqs. (316), Einstein also deduced the fundamental laws describing the mean-square linear and angular displacements of a free particle in a small time interval  $\Delta t$ , these being

$$\overline{(\Delta x)^2} = 2D_t\Delta t \quad (317a)$$

$$\overline{(\Delta \phi)^2} = 2D_r\Delta t \quad (317b)$$

Because of the symmetry of the sphere, no coupling occurs between the translational and rotational Brownian movements, leading to the further relation

$$\overline{(\Delta x)(\Delta \phi)} = 0 \quad (317c)$$

This subsection is concerned with the generalization of Eqs. (316) and (317) to particles of arbitrary shape, and with certain fundamental analogies relating the general theory of Brownian motion to the corresponding general theory of hydrodynamic resistance at small Reynolds numbers. For the most part, what follows is a brief summary and commentary on results reported by Brenner (B25a, B26a).

In the presence of a nonuniformity in concentration a diffusive flux occurs, resulting in the creation of entropy. The rate of irreversible entropy production is, in general, a homogeneous quadratic function of the gradients of

concentration in both physical and orientation space, the proportionality coefficient being an appropriately generalized diffusion tensor. From another point of view, the (mean) ensuing motion (both translational and rotational) of the macroscopic solute particles relative to the solvent results in the dissipation of mechanical energy. The rate of such dissipation is a homogeneous quadratic function of the velocities, the coefficient of proportionality being, apart from the viscosity, the hydrodynamic resistance tensor. Because of the intimate connection between entropy production and dissipation rate,<sup>55</sup> and of the interrelation between diffusion currents and particle velocities, there exists an almost perfect analogy between the macroscopic theory of diffusion in fluids and of the hydrodynamic resistance of particles. The analogy is deeper than is implied by quantitative relationships of the Stokes-Einstein type, Eq. (316). Rather, the analogy extends to the underlying structure of the fundamental equations governing both phenomena. The remarkable similarities are best brought out by considering the diffusion of particles of arbitrary shape. For it is here, in the most general case, that the analogies are most striking.

Consider a large number of identical rigid particles of arbitrary shape distributed throughout a fluid. Specification of the instantaneous "configuration" of each particle requires knowledge of an appropriate set of six independent parameters ( $q^1, q^2, \dots, q^6$ ). These constitute the generalized curvilinear coordinates of the particle in the six-dimensional "configuration space." Three of these, say ( $q^1, q^2, q^3$ ), are required to specify the position of the particle in "physical space" (e.g., the Cartesian coordinates of some arbitrary origin  $O$  fixed in the particle, relative to an origin fixed in the fluid). The remaining three ( $q^4, q^5, q^6$ ) are required to specify the orientation of the particle in "orientation space" (e.g., the Eulerian angles of a set of Cartesian axes fixed in the particle, relative to a set of Cartesian axes fixed in the fluid).

The geometrical properties of the configuration space are entirely determined by its metric tensor. If  $ds$  is the distance between two adjacent points in the space, then

$$ds^2 = g_{ij} dq^i dq^j \quad (318)$$

where the  $g_{ij} = g_{ji}$  are the covariant components of the metric tensor, the latter being a positive-definite form. Unless the contrary is explicitly stated, we utilize the Einstein summation convention on a repeated index when it

<sup>55</sup> The relation is, in fact (L5b, pp. 382-387),

$$\dot{S} = \frac{1}{T} \dot{\Phi}$$

where  $\dot{S}$  is the time rate of irreversible entropy production,  $\dot{\Phi}$  the rate of mechanical energy dissipation, and  $T$  the absolute temperature of the system.

appears as both a covariant and contravariant index. Latin indices range over the integers from 1 to 6. At a given instant of time  $t$  the number of particles whose coordinates lie within the volume element between  $q^1$  and  $q^1 + dq^1$ ,  $q^2$  and  $q^2 + dq^2$ , ...,  $q^6$  and  $q^6 + dq^6$  is denoted by  $\sigma(q^1, q^2, \dots, q^6; t) dV$ , where the volume element is given by  $dV = \sqrt{g} dq^1 dq^2 \dots dq^6$  in which  $g = \det \|g_{ij}\|$ ;  $\sigma$  is thus the local density of particles in the configuration space; that is, the number of particles per unit volume of physical space per unit volume of orientation space. Integration over all orientations yields the ordinary number density  $\rho$ —the number of solute particles per unit volume of physical space.

The physical laws ultimately derived are necessarily independent of the particular  $q$ -parametrization selected. No conceptual difficulties arise in an invariant treatment of the "translation group" in physical space, and conventional vector methods suffice. However, an invariant treatment of the "rotation group" (G2a) in orientation space demands a somewhat more sophisticated knowledge of group-theoretic methods. Accordingly, it is convenient to formulate the general theory in terms of a particular parametrization which allows application of ordinary Cartesian vector methods to the latter as well. Choose an arbitrary origin  $O$  fixed in the body and select any set of right-handed Cartesian axes,  $Ox^1, Ox^2, Ox^3$ , fixed in the particle, with their origin at  $O$ . As a result of Brownian motion and/or convective transport the particle will, in some small time interval  $dt$ , be displaced from its original position and orientation. The infinitesimal change in the position of point  $O$  in physical space may be represented by the vector

$$d\mathbf{r} = \mathbf{i}_1 dx^1 + \mathbf{i}_2 dx^2 + \mathbf{i}_3 dx^3 \quad (319)$$

where  $dx^1, dx^2, dx^3$  denote the projections of the displacement vector onto the body axes, and  $\mathbf{i}_1, \mathbf{i}_2, \mathbf{i}_3$  are unit vectors parallel to these axes. Similarly, the change of orientation may be represented by the infinitesimal rotation vector  $d\phi$  defined in the following manner: The magnitude of this vector is the angle  $|d\phi|$  through which the body must be rotated from its original orientation to produce its final orientation. The direction of this vector is along the instantaneous axis of rotation in a right-handed sense (L7a, p. 18). If  $d\phi^1, d\phi^2, d\phi^3$  denote the projections of this vector onto the body axes, then

$$d\phi = \mathbf{i}_1 d\phi^1 + \mathbf{i}_2 d\phi^2 + \mathbf{i}_3 d\phi^3 \quad (320)$$

The quantity  $d\phi$  is a vector only for infinitesimal rotations, but not for finite rotations (G9e).

In terms of this representation we have

$$ds^2 = (dx^1)^2 + (dx^2)^2 + (dx^3)^2 + (d\phi^1)^2 + (d\phi^2)^2 + (d\phi^3)^2 \quad (321)$$

so that for the body coordinates,  $g_{ij} = \delta_{ij}$ . It is convenient to set

$$\|dq^1, dq^2, dq^3\| = \|dx^1, dx^2, dx^3\| \equiv d\mathbf{r} \quad (322)$$

$$\|dq^4, dq^5, dq^6\| = \|d\phi^1, d\phi^2, d\phi^3\| \equiv d\phi \quad (323)$$

As finite rotations cannot be represented by this vector method, there exist no quantities  $\phi^1, \phi^2, \phi^3$  for which  $d\phi^1, d\phi^2, d\phi^3$  are the differentials; that is to say, the latter are inexact differentials. Hence, the curvilinear coordinates  $q^4, q^5, q^6$  are defined only in a *local* sense, and any operations performed with them should be regarded as purely symbolic (L7a, p. 109; L5b, pp. 138, 149).

The translational flux vector,  $\mathbf{J}_O^{(t)}$ , is defined in the usual way in terms of the number of points  $O$  crossing a unit area of physical space per unit time, irrespective of the orientations of the individual particles. Analogously, the rotary flux vector,  $\mathbf{J}^{(r)}$ , is defined in terms of the number of particles crossing a unit area of orientation space per unit time, irrespective of the positions of the particles in physical space. The former flux depends upon the choice of origin  $O$ , whereas the latter does not—hence the difference in subscript notation. Each of the two fluxes consists of two parts: (i) a convective contribution arising either from macroscopic motion of the fluid (translational or rotational) or from the action of external forces or torques on the individual particles, and (ii) a diffusional contribution arising from the thermal agitation of the particles. Thus

$$\mathbf{J}_O^{(t)} = {}_c\mathbf{J}_O^{(t)} + {}_d\mathbf{J}_O^{(t)} \quad (324a)$$

$$\mathbf{J}^{(r)} = {}_c\mathbf{J}^{(r)} + {}_d\mathbf{J}^{(r)} \quad (324b)$$

The convective fluxes are<sup>56</sup>

$${}_c\mathbf{J}_O^{(t)} = \sigma \mathbf{U}_O \quad (325a)$$

$${}_c\mathbf{J}^{(r)} = \sigma \boldsymbol{\omega} \quad (325b)$$

<sup>56</sup> If the fluid is macroscopically at rest, convective fluxes can arise only from the action of external forces and torques on the particles. The particle velocities can then be obtained from the given forces and torques by solving Eqs. (38) and (39) for  $\mathbf{U}_O$  and  $\boldsymbol{\omega}$ , bearing in mind that the hydrodynamic and external forces acting on a particle are in equilibrium. Equivalently, these velocities may be obtained by inverting the matrix equation (49),

$$\|\mathcal{U}_O\| = -\frac{1}{\mu} \|\mathcal{K}_O\|^{-1} \|\mathcal{F}_O\|$$

If the fluid is not macroscopically at rest, but is, rather, undergoing some net motion, say a shearing flow, then  $\mathbf{U}_O$  and  $\boldsymbol{\omega}$  may be obtained from Eqs. (109)–(110). If no external forces and torques act in the latter case the particle velocities are then given by Eqs. (120) and (121).

in which

$$\mathbf{U}_O = \mathbf{i}_1 \dot{x}^1 + \mathbf{i}_2 \dot{x}^2 + \mathbf{i}_3 \dot{x}^3 \quad (326a)$$

and

$$\boldsymbol{\omega} = \mathbf{i}_1 \dot{\phi}^1 + \mathbf{i}_2 \dot{\phi}^2 + \mathbf{i}_3 \dot{\phi}^3 \quad (326b)$$

are, respectively, the translational velocity of point  $O$  and the angular velocity of the particle. The overdot denotes a derivative with respect to time.

The translational and rotational diffusion fluxes can be shown to be linear functions of the gradients, the general relation being of the form (B26a):

$${}_a \mathbf{J}_O^{(t)} = -\mathbf{D}_O^{(t)} \cdot \frac{\partial \sigma}{\partial \mathbf{r}} - \mathbf{D}_O^{(c)\dagger} \cdot \frac{\partial \sigma}{\partial \boldsymbol{\phi}_O} \quad (327)$$

$${}_a \mathbf{J}^{(r)} = -\mathbf{D}_O^{(c)} \cdot \frac{\partial \sigma}{\partial \mathbf{r}} - \mathbf{D}^{(r)} \cdot \frac{\partial \sigma}{\partial \boldsymbol{\phi}_O} \quad (328)$$

where  $\mathbf{D}_O^{(t)}$  is the translational diffusivity dyadic at  $O$ ,  $\mathbf{D}^{(r)}$  is the rotational diffusivity dyadic, and  $\mathbf{D}_O^{(c)}$  is the coupling diffusivity dyadic at  $O$ .<sup>57</sup> As usual, the subscript  $O$  indicates that the quantity to which it is affixed depends upon the choice of origin,  $O$ . The dyadic diffusivities (second-rank tensor diffusion coefficients) appearing in Eqs. (327) and (328) are constant relative to body axes. These diffusion dyadics are intrinsic entities, being independent of the particular choice of body axes. The “direct” dyadics,  $\mathbf{D}_O^{(t)}$  and  $\mathbf{D}^{(r)}$ , are symmetric, positive-definite, true tensors, whereas the “cross” dyadic,  $\mathbf{D}_O^{(c)}$ , is a pseudotensor. The latter is associated with any screw-like geometric properties of the diffusing particle, and vanishes for bodies lacking such properties, e.g., ellipsoidal particles, providing that the origin is properly chosen. The coupling diffusivity dyadic is a measure of the degree of interaction between the translational and rotational Brownian motions.

Equations (327)–(328) are the complete analogs of the hydrodynamic

<sup>57</sup> Here,

$$\begin{aligned} \frac{\partial}{\partial \mathbf{r}} &= \mathbf{i}_1 \frac{\partial}{\partial x^1} + \mathbf{i}_2 \frac{\partial}{\partial x^2} + \mathbf{i}_3 \frac{\partial}{\partial x^3} \\ \frac{\partial}{\partial \boldsymbol{\phi}} &= \mathbf{i}_1 \frac{\partial}{\partial \phi^1} + \mathbf{i}_2 \frac{\partial}{\partial \phi^2} + \mathbf{i}_3 \frac{\partial}{\partial \phi^3} \end{aligned}$$

the former derivative being equivalent to the ordinary  $\nabla$ -operator.

equations (38)–(39). Accordingly, as in the case of Eq. (49), one may resort to the matrix forms

$$\|_c \mathcal{J}_O\| = \sigma \| \mathcal{U}_O \| \quad (329)$$

in which

$$\| \mathcal{U}_O \| = \begin{Bmatrix} \dot{x}^1 \\ \dot{x}^2 \\ \dot{x}^3 \\ \dot{\phi}^1 \\ \dot{\phi}^2 \\ \dot{\phi}^3 \end{Bmatrix} \quad (330)$$

and

$$\|_d \mathcal{J}_O\| = - \| \mathcal{D}_O \| \| \text{grad}_O \sigma \| \quad (331)$$

where

$$\| \mathcal{J}_O \| = \begin{Bmatrix} {}^{(t)}J^1(O) \\ {}^{(t)}J^2(O) \\ {}^{(t)}J^3(O) \\ {}^{(r)}J^1 \\ {}^{(r)}J^2 \\ {}^{(r)}J^3 \end{Bmatrix}, \quad \| \text{grad}_O \sigma \| = \begin{Bmatrix} \partial \sigma / \partial x^1 \\ \partial \sigma / \partial x^2 \\ \partial \sigma / \partial x^3 \\ \partial \sigma / \partial \phi_o^1 \\ \partial \sigma / \partial \phi_o^2 \\ \partial \sigma / \partial \phi_o^3 \end{Bmatrix} \quad (332a,b)$$

and  $\| \mathcal{D}_O \|$  is the  $6 \times 6$  partitioned diffusivity matrix

$$\| \mathcal{D}_O \| = \begin{Bmatrix} \| {}^{(t)}\mathbf{D}_O \| & \| {}^{(c)}\mathbf{D}_O \|^\dagger \\ \| {}^{(c)}\mathbf{D}_O \| & \| {}^{(r)}\mathbf{D} \| \end{Bmatrix} \quad (333)$$

in which

$$\| {}^{(t)}\mathbf{D}_O \| = \begin{Bmatrix} D^{11}(O) & D^{12}(O) & D^{13}(O) \\ D^{21}(O) & D^{22}(O) & D^{23}(O) \\ D^{31}(O) & D^{32}(O) & D^{33}(O) \end{Bmatrix}, \quad \text{etc.} \quad (334)$$

In certain applications it is more convenient to express these relations in the general tensor form

$$J^i = {}_c J^i + {}_d J^i \quad (335)$$

in which the  $J^i$  ( $i = 1, 2, \dots, 6$ ) are the contravariant components of the flux vector in configuration space. For simplicity we have suppressed the  $O$ -indices. In this form the convective flux is

$${}_c J^i = \sigma q^i \quad (336)$$

whereas the diffusion flux is

$${}_d J^i = -D^{ij} \frac{\partial \sigma}{\partial q^j} \quad (337)$$

in which the  $D^{ij}$  are the contravariant components of the diffusivity tensor. These tensor relations hold in any system of coordinates as, indeed, do the corresponding dyadic and matrix relations when properly interpreted. It should be clearly understood, however, that the various diffusion dyadics, matrices, and tensors are constant only when referred to body axes.

Equations (327)–(328) or, equivalently, their matrix and tensor counterparts, constitute the generalization of Fick's law of diffusion to the six-dimensional configuration space. The derivation of this generalization (B25a, B26a) proceeds along lines originally set forth by Einstein (E1a). In the absence of sources or sinks, conservation of probability density in configuration space leads to the following continuity relation (B25a):

$$\frac{\partial \sigma}{\partial t} + \frac{1}{\sqrt{g}} \frac{\partial}{\partial q^i} (\sqrt{g} J^i) = 0 \quad (338)$$

the second term being the expression for the divergence (of the flux vector) in general tensor form. Equations (335)–(338) lead to a partial differential equation for the density  $\sigma$ . The resulting equation, expressed in a convenient system of space axes, rather than body axes, is given by Brenner (B26a). Space axes are the more useful of the two systems in the actual solution of initial- and boundary-value problems.

The degree of completeness of the analogies between Eqs. (331) and (49) is quite remarkable;  $\|\mathcal{D}_O\|$  and  $\|\mathcal{K}_O\|$  are each symmetric, positive-definite forms, as are their direct submatrices too. The positive-definiteness of  $\|\mathcal{D}_O\|$  stems from the positivity of the rate of irreversible entropy production. In contrast to the proof of the symmetry of the hydrodynamic resistance matrix (B22),<sup>58</sup> the corresponding proof of the symmetry of the diffusion matrix is trivial. The latter may be taken to be symmetric by *definition* since its antisymmetric part gives rise to no observable macroscopic physical consequence.

<sup>58</sup> In their volume on "Mechanics," Landau and Lifshitz (L7a, p. 76) state, in effect, that symmetry of the resistance matrix cannot be demonstrated by purely macroscopic mechanical arguments. Their statement is, however, refuted by the macroscopic symmetry proof offered by Brenner (B22).



As implied by the subscript notation in Eqs. (327)–(328), the translational and coupling diffusivity dyadics vary with choice of origin. This dependence can be quantitatively established. By invoking appropriate kinematic arguments, it can be shown (B26a) that, whereas  $\mathbf{J}^{(r)}$  and  $\partial\sigma/\partial\mathbf{r}$  are independent of choice of origin,

$$\mathbf{J}_P = \mathbf{J}_O - \mathbf{r}_{OP} \times \mathbf{J}^{(r)}$$

$$\frac{\partial\sigma}{\partial\boldsymbol{\phi}_P} = \frac{\partial\sigma}{\partial\boldsymbol{\phi}_O} + \frac{\partial\sigma}{\partial\mathbf{r}} \times \mathbf{r}_{OP}$$

in which  $O$  and  $P$  are any arbitrary points fixed in the particle, and  $\mathbf{r}_{OP}$  is the vector drawn from  $O$  to  $P$ . These relations are the analogs of those given in the sentence following Eq. (52). By these means one arrives at the following expressions for the origin-dependence of the various diffusivity dyadics:

$$\mathbf{D}_P^{(c)} = \mathbf{D}_O^{(c)} + \mathbf{D}^{(r)} \times \mathbf{r}_{OP} \quad (339)$$

$$\mathbf{D}_P^{(t)} = \mathbf{D}_O^{(t)} - \mathbf{r}_{OP} \times \mathbf{D}^{(r)} \times \mathbf{r}_{OP} + \mathbf{D}_O^{(c)\dagger} \times \mathbf{r}_{OP} - \mathbf{r}_{OP} \times \mathbf{D}_O^{(c)} \quad (340)$$

The rotational diffusivity dyadic is origin-independent. These origin-displacement theorems are the counterparts of the comparable hydrodynamic relations set forth in Eqs. (51) and (52).

As in the hydrodynamic case, there exists a unique origin, say  $R$ , at which the coupling diffusivity dyadic is symmetric; that is,

$$\mathbf{D}_R^{(c)} = \mathbf{D}_R^{(c)\dagger} \quad (341)$$

If the value of the coupling diffusivity dyadic is known at some point  $O$ , and if the value of the rotational diffusivity dyadic is also known, the location of  $R$  (relative to  $O$ ) may be determined from the relation

$$\mathbf{r}_{OR} = - \left[ \left( \mathbf{I} : \mathbf{D}^{(r)} \right) \mathbf{I} - \mathbf{D}^{(r)} \right]^{-1} \cdot \boldsymbol{\varepsilon} : \mathbf{D}_O^{(c)} \quad (342)$$

which is the analog of Eq. (54). In general, if Eq. (350) applies, the hydrodynamic center of reaction is identical to the diffusive center of reaction (B26a). In any event, the two points can be shown to be the same for particles possessing various types of geometric symmetries, even if Eq. (350) is not applicable.

The symmetric dyadic  $\mathbf{D}_R^{(c)}$  is identically zero for a large class of symmetrical particles, including spheres and ellipsoids. For such bodies there is no

coupling between the translational and rotary Brownian motions, and Eqs. (327) and (328) adopt the simple, "uncoupled" forms

$${}^{(t)}_a \mathbf{J}_R = -\mathbf{D}_R^{(t)} \cdot \frac{\partial \sigma}{\partial \mathbf{r}} \quad (343a)$$

$${}^{(r)}_a \mathbf{J} = -\mathbf{D}^{(r)} \cdot \frac{\partial \sigma}{\partial \phi_R} \quad (343b)$$

analogous to Eqs. (55a, b), *et seq.* With regard to various types of geometric symmetry that particles may possess, it is obvious that the symmetry properties of the diffusion dyadics  $\mathbf{D}_R^{(t)}$  and  $\mathbf{D}^{(r)}$  are analogous to those of the resistance dyadics  $\mathbf{K}^{(t)}$  and  $\mathbf{K}_R^{(r)}$ , respectively; whereas  $\mathbf{D}_R^{(c)}$  and  $\mathbf{K}_R^{(c)}$  are comparable as regards their symmetry properties. Accordingly, one is led *inter alia* to the conclusion that in regard to their diffusive properties, there exist helicoidally isotropic particles (B25a):

$$\mathbf{D}_R^{(t)} = \mathbf{I} D_t \quad (344a)$$

$$\mathbf{D}_R^{(r)} = \mathbf{I} D_r \quad (344b)$$

$$\mathbf{D}_R^{(c)} = \mathbf{I} D_c \quad (344c)$$

as well as spherically isotropic particles, characterized by setting  $D_c = 0$  in the above. The scalar diffusivities  $D_t$  and  $D_r$ , and pseudoscalar diffusivity  $D_c$  satisfy the inequalities

$$D_t > 0 \quad (345a)$$

$$D_r > 0 \quad (345b)$$

$$D_t D_r > D_c^2 \quad (345c)$$

$D_c$  being positive for right-handed bodies, and conversely. These relations are comparable to those given in Eq. (74). The existence of a coupling diffusivity term, relating to the screw-like geometric properties of particles, seems to have escaped notice before now.

Correlations between the linear displacement (of the origin  $O$ ) and angular displacement in a given time interval due to Brownian motion may be expressed in terms of a generalized form of Eq. (317). It is found that (B26a)

$$\begin{aligned} \overline{\Delta \mathbf{r}_O \Delta \mathbf{r}_O} &= 2 \mathbf{D}_O^{(t)} \Delta t, & \overline{\Delta \mathbf{r}_O \Delta \phi} &= 2 \mathbf{D}_O^{(c) \dagger} \Delta t \\ \overline{\Delta \phi \Delta \mathbf{r}_O} &= 2 \mathbf{D}_O^{(c)} \Delta t, & \overline{\Delta \phi \Delta \phi} &= 2 \mathbf{D}^{(r)} \Delta t \end{aligned} \quad (346)$$

provided that  $|\Delta\phi| \ll \pi$ . The average displacements themselves are identically zero:

$$\overline{\Delta\mathbf{r}_O} = \mathbf{0}, \quad \overline{\Delta\phi} = 0$$

Equivalently, Eq. (346) may also be expressed as the single matrix equation

$$\overline{\|\Delta\mathcal{Q}_O\|^\dagger \|\Delta\mathcal{Q}_O\|} = 2\|\mathcal{Q}_O\|\Delta t \quad (347)$$

where  $\|\Delta\mathcal{Q}_O\|$  is the row matrix

$$\|\Delta\mathcal{Q}_O\| = \|\Delta x^1(O), \Delta x^2(O), \Delta x^3(O), \Delta\phi^1, \Delta\phi^2, \Delta\phi^3\| \quad (348)$$

and its transpose,  $\|\Delta\mathcal{Q}_O\|^\dagger$ , is the corresponding column matrix.

The preceding relations apply to rigid particles of any shape. If the origin is chosen at the center of reaction, cross-correlations between the linear and angular displacements will vanish whenever the symmetry of the particle is such that  $\overset{(c)}{\mathbf{D}_R} = \mathbf{0}$ . This occurs, for example, in the case of ellipsoidal particles. In the interesting case where the particles are helicoidally isotropic, the correlation relations take the highly symmetric form

$$\overline{\Delta x^\alpha \Delta x^\beta} = 2D_i \Delta t \quad (349a)$$

$$\overline{\Delta\phi^\alpha \Delta\phi^\beta} = 2D_\phi \Delta t \quad (349b)$$

$$\overline{\Delta x^\alpha \Delta\phi^\beta} = 2D_c \Delta t \quad (349c)$$

where  $\alpha, \beta = 1, 2, 3$ . When the particle is spherically isotropic  $D_c = 0$ , leading to relations of the type given in Eq. (317), originally obtained by Einstein for spherical particles.

The general theory of Brownian motion set forth thus far is a self-contained, purely phenomenological theory which does not depend upon any special hydrodynamic assumptions. If, however, following Einstein, it is further assumed that, on the average, the diffusing particle experiences a hydrodynamic force governed by Stokes equations, the diffusion matrix is then found to be (B26a)

$$\|\mathcal{Q}_O\| = \frac{kT}{\mu} \|\mathcal{K}_O\|^{-1} \quad (350)^{59}$$

<sup>59</sup> The general form of this relationship agrees with the well-known Nernst-Planck-Einstein formula, according to which the diffusion coefficient is given by the relation

$$\text{Diffusion Coefficient} = kT (\text{Mobility})$$

where the mobility is the velocity imparted to the particle by a unit external force; for, as is clear from Eq. (49), the generalized mobility is  $\mu^{-1} \|\mathcal{K}_O\|^{-1}$ .

This constitutes the generalization of the Stokes-Einstein formulas (316). It applies for any choice of origin. The positive-definite character of the resistance matrix assures the existence of its inverse, as required by the preceding relation.

Equation (350) furnishes a wholly independent proof of the symmetry and positive-definiteness of the diffusivity matrix, for these characteristics now follow from the comparable properties of the hydrodynamic resistance matrix.

Expressed in terms of the individual resistance and diffusion dyadics, Eq. (350) may be written as

$$\mathbf{D}_O^{(t)} = \frac{kT}{\mu} \left( \mathbf{K} - \mathbf{K}_O^\dagger \cdot \mathbf{K}_O^{-1} \cdot \mathbf{K}_O \right)^{-1} \quad (351a)$$

$$\mathbf{D}^{(r)} = \frac{kT}{\mu} \left( \mathbf{K}_O - \mathbf{K}_O \cdot \mathbf{K}_O^{-1} \cdot \mathbf{K}_O^\dagger \right)^{-1} \quad (351b)$$

$$\mathbf{D}_O^{(c)} = -\frac{kT}{\mu} \mathbf{K}_O^{-1} \cdot \mathbf{K}_O \cdot \left( \mathbf{K} - \mathbf{K}_O^\dagger \cdot \mathbf{K}_O^{-1} \cdot \mathbf{K}_O \right)^{-1} \quad (351c)$$

In the case of a particle for which no coupling occurs at the center of reaction, these reduce to

$$\mathbf{D}_R^{(t)} = \frac{kT}{\mu} \mathbf{K}^{-1} \quad (352a)$$

$$\mathbf{D}^{(r)} = \frac{kT}{\mu} \mathbf{K}_R^{-1} \quad (352b)$$

$$\mathbf{D}_R^{(c)} = \mathbf{0} \quad (352c)$$

For example, in the case of an ellipsoidal particle, one easily finds from Eqs. (58)–(59) that

$$\mathbf{D}_R^{(t)} = \frac{kT}{16\pi\mu} [\mathbf{e}_1 \mathbf{e}_1 (\chi + a_1^2 \alpha_1) + \mathbf{e}_2 \mathbf{e}_2 (\chi + a_2^2 \alpha_2) + \mathbf{e}_3 \mathbf{e}_3 (\chi + a_3^2 \alpha_3)] \quad (353a)$$

and

$$\mathbf{D}^{(r)} = \frac{3kT}{16\pi\mu} \left( \mathbf{e}_1 \mathbf{e}_1 \frac{a_2^2 \alpha_2 + a_3^2 \alpha_3}{a_2^2 + a_3^2} + \mathbf{e}_2 \mathbf{e}_2 \frac{a_3^2 \alpha_3 + a_1^2 \alpha_1}{a_3^2 + a_1^2} + \mathbf{e}_3 \mathbf{e}_3 \frac{a_1^2 \alpha_1 + a_2^2 \alpha_2}{a_1^2 + a_2^2} \right) \quad (353b)$$

In the case of helicoidally isotropic particles it follows from Eqs. (73), (344), and (351) that

$$D_t = \frac{kT}{\mu} \frac{K_r}{K_t K_r - K_c^2} \quad (354a)$$

$$D_r = \frac{kT}{\mu} \frac{K_t}{K_t K_r - K_c^2} \quad (354b)$$

$$D_c = -\frac{kT}{\mu} \frac{K_c}{K_t K_r - K_c^2} \quad (354c)$$

In accordance with Eq. (74) the above denominators are essentially positive. It is also clear that the inequalities set forth in Eq. (345) are satisfied.

When the particles are spherically isotropic these reduce to the forms  $D_c = 0$  and

$$D_t = \frac{kT}{\mu K_t} \quad (355a)$$

$$D_r = \frac{kT}{\mu K_r} \quad (355b)$$

of which the original Stokes-Einstein formulas (316) are special cases.

If all particle orientations are assumed equally probable, one finds upon integrating over orientation space that the usual form of Fick's law in physical space applies:

$$\frac{\partial \rho}{\partial t} = \bar{D}_t \nabla^2 \rho \quad (356)$$

where

$$\rho = \int \int \int \sigma d\phi^1 d\phi^2 d\phi^3 \quad (357)$$

is the number density of particles in physical space. For nonskew particles the mean diffusivity is the scalar (P4a)

$$\bar{D}_t = \frac{1}{3} \text{trace} \left\| \mathbf{D}_R^{(t)} \right\|$$

whence, from Eq. (352a),

$$\bar{D}_t = \frac{1}{3} \frac{kT}{\mu} \text{trace} \left\| \mathbf{K}^{(t)} \right\|^{-1} \quad (358)$$

This should be compared with the comparable formula for the average resistance of a nonskew particle near the end of Section II,C,1. For helicoidally isotropic particles the mean diffusivity is identical to  $D_t$  given in Eq. (354a) (B25a).

### C. SUMMARY AND COMMENTARY

An attempt has been made in this article to critically survey the field of low Reynolds number flows, with particular regard to the hydrodynamic resistance of particles in this regime. A remarkable burgeoning of interest in such problems has occurred within the past decade. Significant advances have been recorded on both the theoretical and experimental sides, with the former gains far outdistancing the latter in scope. Problems which would have been impossible to solve rigorously before the advent of singular perturbation techniques are now being regularly solved, though hardly in a routine fashion; insight, intuition, inspiration, and ingenuity are still the order of the day.

For those interested in direct engineering applications of the material covered by this review, the perspective from which many of the more general results set forth here should be viewed is, perhaps, best illustrated by an example: The resistance of any solid particle to translational and rotational motions in Stokes flow may be completely calculated from knowledge of a set of 21 scalar coefficients (Section II,C,1). While it seems highly improbable to expect that all these coefficients could be experimentally measured in practice, except perhaps in the trivial case of highly symmetrical bodies for which many of the coefficients vanish identically, this does not detract from the conceptual advantages of knowing exactly how much one does not know. Having an ideal goal against which the extent of present knowledge can be gaged permits a rational decision as to how to optimize one's investment of time, effort, and money in the pursuit of additional data. Furthermore, with the development of high-speed digital computers it may soon be possible to *calculate* all these coefficients for any given body (O1b). The general theory provides a rigorous framework into which such knowledge may be embedded.

Use of symbolic "drag coefficients" (Section II,C,2) and symbolic heat- and mass-transfer "coefficients" (Section IV,A) furnishes a unique method for describing the intrinsic, interphase transport properties of particles for a wide variety of boundary conditions. Here, the particle resistance is characterized by a partial differential operator that represents its intrinsic resistance to vector or scalar transfer, independently of the physical properties of the fluid, the state of motion of the particle, or of the unperturbed velocity or temperature fields at infinity. Though restricted as yet in applicability, the general ideas underlying the existence of these operators appear capable of extension in a variety of ways.

A recurrent theme arising throughout the analysis pertains to the screw-like properties of particles and of their intrinsic right- and left-handedness (Sections II,C,1; II,C,2; III,C and IV,B). Such properties reflect an inseparable coupling between the translational and rotational motions of the particle.

Helicoidally isotropic particles furnish the simplest examples of bodies manifesting screw-like behavior. These particles are isotropic, in that their properties are the same in all directions. Yet they possess a sense, and spin as they settle in a fluid. These ideas are likely to be of interest to microbiologists, biophysicists, geneticists, and others in the life sciences for whom handedness and life are intimately intertwined. The microscopic dimensions of the objects of interest to them insures *ipso facto* that the motion takes place at very small Reynolds numbers. Readers interested in an elementary but broad survey of sense in the physical and biological sciences are referred to Gardner's delightful book "The Ambidextrous Universe" (G1).

First-order corrections to the Stokes force on a particle, arising from wall- or inertial-effects, can be directly expressed in terms of the Stokes force on the body in the absence of such effects. Thus, with regard to wall-effects in the Stokes regime, Eq. (135) expresses the force experienced by a particle falling in, say, a circular cylinder, in terms of the comparable force experienced by the particle when falling with the same velocity and orientation in the unbounded fluid. Equation (139) expresses a similar relationship for the torque on a rotating particle in a circular cylinder, as does Eq. (166) for the first-order interaction between two particles in an unbounded fluid in terms of the properties of the individual particles. Analogously, Eq. (234) expresses the inertial correction to the Stokes drag force in terms of the Stokes force itself. A comparable relationship exists (Section IV,A) between the heat-transfer coefficient at small, nonzero Péclet numbers and the heat-transfer coefficient at zero Péclet number—that is, the coefficient for conduction heat transfer. Finally, Eqs. (78)–(79) (or their symbolic operator counterparts) permit direct calculation of the Stokes force and torque experienced by a particle in an arbitrary field of flow solely from knowledge of the elementary solutions of Stokes equations for translation and rotation of the particle in a fluid at rest at infinity. The utility of already available knowledge is thus greatly extended by the existence of such relations. It permits one whose interests lie entirely in the macroscopic manifestation of the motion, e.g., the force and torque on the body, to bypass the oftentimes difficult problem of obtaining a detailed solution of the equations of motion, and to proceed directly to the computation of the force and torque on the body from the prescribed boundary conditions alone. The calculation is thereby reduced to a quadrature.

The contents of this review may be read simultaneously from two different points of view. First and foremost it may be regarded as a compendium of recent advances in low Reynolds number flows. Secondly, from a pedagogic viewpoint it may be profitably used to illustrate the direct application of invariant techniques, that is, vector-polyadic and tensor methods, to a class of physical problems. Because of the relative simplicity and rich variety of

physical problems associated with low Reynolds number motions, intuitive arguments may be employed to gain insight into the nature of polyadics and tensors; the role played by the concept of direction as a primitive entity is brought out here to a degree not usually found in standard works on tensor analysis.

## ACKNOWLEDGMENTS

The author is grateful to Dr. S. G. Mason and the Pulp and Paper Research Institute of Canada for their encouragement and continued interest in this work. Part of the writing of this chapter was supported by a grant from the National Science Foundation (Grant No. NSF GK-56), to whom the author wishes to express his thanks. A debt of gratitude is also due Dr. Raymond G. Cox for his many stimulating and penetrating comments. During the all-too-brief tenure of his postdoctoral fellowship in the Chemical Engineering Department at New York University, he was a constant source of inspiration and fresh insight.

Nomenclature<sup>60,61</sup>

## ROMAN LETTERS

|                 |   |           |   |
|-----------------|---|-----------|---|
| $a$             | Representative particle length (4); radius of sphere (29); polar radius of prolate spheroid (75)–(76)     | $C$       | Dimensionless Stokes force (242)                          |
| $a_1, a_2, a_3$ | Lengths of semiaxes of an ellipsoid (57)  | $C_k$     | Constant $k$ -adic (98)–(99)                              |
| $A$             | Cross sectional area (143); external surface area (302)   | $d$       | Particle diameter (198)–(199)                             |
| $A, B, C$       | Constants (90b)–(91)  | $ds$      | Distance element in configuration space (318)             |
| $A$             | Constant dyadic (97)  | $dS$      | Directed element of surface area pointing into fluid (40) |
| $b$             | Equatorial radius of prolate spheroid (75)–(76); distance from cylinder axis to sphere center (135)–(136) | $dV$      | Volume element in configuration space (318)–(319)         |
| $B$             | Refers to surface of body (11)  | $d\phi^i$ | Cartesian component of vector $d\phi$ (320)               |
| (c)             | Over symbol denoting coupling (38)  | $d\phi$   | Differential angular displacement vector (320)            |
| $c$             | One-half the distance between foci of a prolate spheroid (75)–(76)  | $d\Omega$ | Element of surface area on a unit sphere (91b)–(92)       |
|                 |   | $D$       | Symbolic operator = $(D^2)^{1/2}$ (92a)                   |
|                 |   | $D^2$     | Ellipsoidal differential operator (93)                    |

<sup>60</sup> Numbers in parentheses refer to the equation number in which the symbol first appears or is first defined. When the first appearance of the symbol occurs within the text, rather than in a displayed equation, this is so indicated by giving the equation numbers lying on either side of that portion of the text. For example, (75)–(76) indicates that the first appearance of the symbol occurs somewhere between Eqs. (75) and (76).

<sup>61</sup> An underlined symbol is nondimensional. It has the same meaning as its dimensional, nonunderlined counterpart.



- $D_c, D_r, D_t$  Coupling, rotation, and translational diffusion coefficients for an isotropic body (316), (344)  
 $D^{ij}$  Contravariant component of diffusion tensor (337)  
 $^{(c)} D, ^{(r)} D, ^{(t)} D$  Coupling, rotational, and translational diffusivity dyadics (327), (328)  
 $e$  Normalized eigenvector of  $\mathbf{K}$  (43)–(44); unit vector (166)  
 $e_1, e_2, e_3$  Normalized eigenvectors of  $\mathbf{K}$  (44); unit vectors parallel to principal axes of ellipsoid (58)  
 $e_1$  Unit vector along symmetry axis of body of revolution (72)  
 $e_{12}$  Unit vector from center of particle 1 to center of particle 2 (165)  
 $E_{ijk}$  Cartesian component of  $\mathbf{E}$  (227)  
 $\mathbf{E}$  Intrinsic rate of strain triadic (221)  
 $f(x)$  Analytic function of  $x$  (91b)–(92)  
 $f(\beta)$  Wall-correction factor for nonaxial particle (136)  
 $f_k(\theta, \phi)$  Surface spherical harmonic of degree  $k$  (64)  
 $f_n(\text{Pé})$  Function of Péclet number (310)–(311)  
 $f_n(R)$  Function of Reynolds number (212)–(213)  
 $f_{0\alpha}$  Dimensionless Stokes drag in the  $\alpha$  direction (313)  
 $\mathbf{f}$  External force per unit volume (180)  
 $\mathbf{f}(\mathbf{r})$  Analytic function of position (90a)  
 $(F)$  Over symbol denoting force (100)  
 $F$  Component of hydrodynamic force (130)  
 $F_D$  Drag force in axial direction (245)–(246)  
 $F_L$  Lift force in radial direction (245)–(246)  
 $(F_0)_\alpha$  Stokes drag in  $\alpha$  direction (232)  
 $F_\infty'$  Infinite medium force based on approach velocity (141)  
 $F_I(\beta), F_{II}(\beta), F_{III}(\beta)$  Functions of  $\beta$  (288), (289), (290)  
 $\mathbf{F}$  Vector hydrodynamic force exerted by fluid on particle (38)  
 $\mathbf{F}_D$  Drag force vector (215)  
 $\mathbf{F}_L$  Lift force vector (216)  
 $\mathbf{F}_w$  Force exerted by fluid on duct walls (144)  
 $g$  Magnitude of local acceleration of gravity vector  $\mathbf{g}$  (295); determinant of fundamental tensor  $g_{ij}$  (318)–(319)  
 $g(\zeta)$  Function of  $\zeta$  (75)–(76)  
 $g_{ij}$  Covariant component of metric tensor (318)  
 $\|\text{grad}\|$  Matrix of generalized vector gradient  $\partial/\partial q^i$  in configuration space (332b)  
 $\mathbf{g}$  Local acceleration of gravity vector (145)  
 $h$  Distance from particle center to plane (131); center-to-center distance (165); heat-transfer coefficient (309)  
 $H$  Gap width (132)–(133)  
 $\mathbf{i}_1, \mathbf{i}_2, \mathbf{i}_3$  Right-handed triad of mutually perpendicular unit vectors (footnote 3)  
 $I_{n+1/2}$  Modified Bessel function of the first kind (98)–(99)  
 $\mathbf{I}$  Dyadic idemfactor (3)  
 $\mathbf{J}^i$  Tensor component of flux vector  $\mathbf{J}$  (335)  
 $^{(r)} \mathbf{J}, ^{(t)} \mathbf{J}$  Rotational and translational flux vectors (323)–(324)  
 $^c \mathbf{J}, ^d \mathbf{J}$  Convective and diffusive flux vectors (325), (327)  
 $k$  Permeability of isotropic porous medium (173); thermal conductivity (303); Boltzmann constant (316)  
 $\mathbf{k}$  Dyadic permeability coefficient (171)  
 $K$  Eigenvalue of  $\mathbf{K}$  (43)–(44)  
 $K_1, K_2, K_3$  Eigenvalues of  $\mathbf{K}$  (44)

- $K_c, K_r, K_t$  Coupling, rotation, and translational resistances for an isotropic body (71)
- $K^{(r)} K^{(t)}, K^{(c)}$  Scalar and pseudoscalar resistance coefficients for a porous medium (footnote 19)
- $K_{\parallel}, K_{\perp}$  Respective components of  $\mathbf{K}$  parallel and perpendicular to symmetry axis (72)
- $K_{ij}$  Cartesian tensor component of  $\mathbf{K}$  (45)–(46)
- $K_{ij}^{(kl)}$  ( $k, l$ ) Cartesian tensor component of the dyadic  $\mathbf{K}_{ij}$  (159)
- $\mathbf{K}$  Generic symbol for a resistance dyadic (43)–(44)
- $\overset{(c)}{\mathbf{K}}, \overset{(r)}{\mathbf{K}}, \overset{(t)}{\mathbf{K}}$  Coupling, rotation, and translation dyadics (38), (39)
- $\mathbf{K}^{(t)}, \mathbf{K}^{(c)}, \mathbf{K}^{(r)}$  Dyadic, triadic and tetradic, resistance coefficients, respectively, for a porous medium (footnote 19)
- $\mathbf{K}_t, \mathbf{K}_c''$  Dyadic resistance coefficients for a porous medium (174)–(175)
- $\mathbf{K}_c', \mathbf{K}_t$  Triadic resistance coefficients for a porous medium (174)–(175)
- $\mathbf{K}_{\infty}$  Resistance dyadic in an unbounded fluid (134)
- $\mathbf{K}_1, \mathbf{K}_2$  Resistance dyadics for particles 1 and 2, respectively, in an unbounded fluid (166)
- $\mathbf{K}_{ij}$  Resistance dyadic in a multi-particle system (148), (149)
- $l$  Characteristic distance of particle from boundary (122)–(123); radius of circular cylinder (126); characteristic apparatus dimension (179)–(180)
- $L$  Length of duct (145)–(146)
- $\mathbf{M}$  Vector moment of forces (173)–(174)
- $\boxed{n}$  Polydot multiplication symbol (98)–(99)
- $N_{Po}$  Dimensionless power number (198)–(199)
- $N_{Re}$  Reynolds number (198)–(199)
- $Nu$  Average Nusselt number (309)
- $O$  Arbitrary origin affixed to particle (9)
- $(O)$  Refers to evaluation at origin  $O$  (45)
- $p$  Pressure (1)
- $p^0$  Unperturbed pressure field (89)–(90)
- $p^+$  Additional pressure field (145)–(146)
- $p^*$  Static pressure field (145)–(146)
- $P_k(\cos \theta)$  Legendre polynomial of degree  $k$  and argument  $\cos \theta$  (235)–(236)
- $P_n, P_n^m$  Legendre functions (68)–(69)
- $Pé$  Péclet number based on "diameter" (310)
- $Pé^*$  Péclet number based on "radius" (300)
- $Pr$  Prandtl number (315a)–(315b)
- $\mathbf{P}$  Vector "pressure" field (17), (25), or (285a)
- $\Delta P^+$  Additional pressure drop vector (142)–(143)
- $q^i$  Generalized coordinate in configuration space (317)–(318)
- $\dot{q}^i$  Generalized contravariant velocity component in configuration space (336)
- $\frac{\partial}{\partial q^i}$  Generalized vector gradient in configuration space (337)
- $\mathbf{q}$  Superficial velocity vector in a porous medium (171); heat-flux vector (307)–(308)
- $Q$  Rate of heat transfer (302)
- $\mathbf{Q}$  Constant dyadic (94)
- $(r)$  Over symbol denoting rotation (13)
- $r$  Spherical coordinate (29); distance  $|\mathbf{r}|$  from some origin (29)
- $\mathbf{r}$  Position vector of a point (4)
- $\mathbf{r}^n$  Polyadic (99)
- $\mathbf{r}_{OP}$  Vector drawn from  $O$  to  $P$  (51)
- $\frac{\partial}{\partial \mathbf{r}}$  Symbolic representation for vector gradient in physical space (footnote 57)

- $\Delta \mathbf{r}$  Linear displacement vector in physical space (346)  
 $R$  Particle Reynolds number (5); cylindrical coordinate (245)  
 $R^*$  Generalized particle Reynolds number (241)  
 $R_o$  Cylinder radius (245)  
 $Re$  Reynolds number based on sphere diameter (314)  
 $Re_p$   $2a|\mathcal{U}_p|/\nu$ ; particle Reynolds number based on axial slip velocity (252)  
 $Re_s$   $(2a)^2 S/\nu$ ; shear Reynolds number (269)–(270)  
 $Re_t$   $2R_o V_m/\nu$ ; tube Reynolds number (251)  
 $Re_\omega$   $(2a)^2 |\omega|/\nu$ ; rotational Reynolds number (269)–(270)  
 $Re_\infty$   $2a|U_\infty|/\nu$ ; Reynolds number based on free-fall velocity in an unbounded fluid at rest (266)  
 $\mathbf{R}$  Relative position vector of two points (194)  
 $S$  Wetted surface area of particle (70); velocity gradient (269a)  
 $\dot{S}$  Time rate of irreversible entropy production (footnote 55)  
 $\mathcal{S}$  Intensity of shear (122)  
 $S_1$  Unit sphere (91b)–(92)  
 $S_{ij}$  Cartesian tensor component of dyadic  $\mathbf{S}$  (97)–(98)  
 $\mathbf{S}$  Rate of shear dyadic (108)  
 $(t)$  Over symbol denoting translation (11)  
 $t$  Time (1)  
 $\Delta t$  Small interval of time (317)  
 $\mathbf{t}$  Torque per unit volume (173)–(174)  
 $(T)$  Over symbol denoting torque (101)  
 $T$  Component of vector torque  $\mathbf{T}$  (75); temperature (298); absolute temperature (316)  
 $T_B$  Temperature at surface of body (302)  
 $T_i$  Component of vector torque  $\mathbf{T}$  parallel to principal axis of ellipsoid (97)–(98)  
 $T_\infty$  Undisturbed temperature field at infinity (302)  
 $\mathbf{T}$  Vector hydrodynamic torque exerted by fluid on particle (39)  
 $u$  Component of vector  $\mathbf{u}$  (143)  
 $\mathbf{u}$  Unperturbed vector flow field (77)  
 $U$  Particle speed; component of  $\mathbf{U}$  (135); axial component of sphere velocity in direction of net flow (245)–(246)  
 $U_L$  Radial (lift) velocity component (245)–(246)  
 $U_\infty$  Terminal settling speed in an unbounded fluid (138); component of settling velocity vector  $\mathbf{U}_\infty$  parallel to direction of net flow (247)–(248)  
 $\mathbf{U}$  Particle velocity vector (9); stream velocity vector (199)  
 $\mathbf{U}_\infty$  Settling velocity vector in an unbounded fluid at rest (247)–(248)  
 $v$  Particle volume (145)–(146)  
 $\mathbf{v}$  Local fluid velocity vector (1)  
 $\mathbf{v}'$  Local fluid velocity vector measured relative to an observer translating with particle (269a)  
 $V$  Representative particle speed (4); volume (318)–(319)  
 $V_m$  Mean velocity of flow (143)  
 $V_{ij}$  Cartesian tensor component of dyadic  $\mathbf{V}$  (227)  
 $\mathbf{V}$  Dyadic “velocity” field, (17), (25), or (285a)  
 $\mathbf{V}_m$  Mean velocity of flow vector (141)–(142)  
 $W$  An eigenvalue of  $\mathbf{W}$  (135)  
 $\mathbf{W}$  Wall-effect dyadic (134)  
 $x_1, x_2, x_3$  Cartesian coordinates measured parallel to principal axes (57)  
 $x_1', x_2', x_3'$  Cartesian coordinates measured relative to sphere center (268)–(269)  
 $\underline{x}_1, \underline{x}_2, \underline{x}_3$  Cartesian coordinates made dimensionless with cylinder radius (287)–(288)

|                                   |   |              |  |
|-----------------------------------|---|--------------|--|
| $\bar{x}_1, \bar{x}_2, \bar{x}_3$ | Nondimensional Cartesian coordinates measured relative to a variable origin (287)–(288) | $x^i$        | Cartesian velocity component (326)                             |
| $x^1, x^2, x^3$                   | Cartesian coordinates (318)–(319)   | $\Delta x^i$ | Cartesian component of vector $\Delta \mathbf{r}$ (317), (349) |
|                                   |   | $x, y, z$    | Cartesian coordinates (195)–(196)                              |

## SCRIPT ROMAN LETTERS

|  |  |                          |  |
|--|--|--------------------------|--|
| $\ \mathcal{D}\ $                        | $6 \times 6$ Diffusion matrix (333)  | $\mathcal{K}$            | Inertial resistance triadic (226)                                    |
| $\ \mathcal{F}\ $                        | Wrench matrix (46), (160a)   | $\bar{p}$                | Mean pressure in Darcy's law (171)                                   |
| $h$                                      | Symbolic heat transfer coefficient (302)                                   | $\bar{p}^*$              | "Proper" pressure in Darcy's law (174)                               |
| $\ \mathcal{J}\ $                        | Flux matrix in configuration space (332a)                                  | $\ \Delta \mathcal{Q}\ $ | 6-dimensional matrix of generalized displacements $\Delta q^i$ (348) |
| $\ _c \mathcal{J}\ , \ _d \mathcal{J}\ $ | Convective and diffusive flux matrices in configuration space (329), (331) | $\mathcal{U}_p$          | Axial component of particle slip velocity (246)                      |
| $\ \mathcal{K}\ $                        | Resistance matrix (48); grand resistance matrix (161)                      | $\ \mathcal{U}\ $        | Screw-velocity matrix (47), (160b)                                   |
| $\mathcal{K}_{i,j,k}$                    | Cartesian tensor component of $\mathcal{K}$ (227)                          | $\mathcal{V}$            | Characteristic speed (217)   |

## GREEK LETTERS

|                                |   |               |   |
|--------------------------------|---|---------------|---|
| $\alpha$                       | Thermal diffusivity (298)   | $\eta$        | Viscosity ratio (122)   |
| $\alpha_1, \alpha_2, \alpha_3$ | Functions of $a_1, a_2, a_3$ (61)   | $\theta$      | Polar angle in spherical coordinates (64)   |
| $\alpha$                       | Unit vector parallel to $\mathbf{U}$ (231)–(232)  | $\lambda$     | Dummy variable of integration (61)  |
| $\beta$                        | $b/l$ or $b/R_0$ ; fractional distance from cylinder axis to particle center (136)                | $\Lambda$     | Dimensionless ratio (294)   |
| $\beta^*$                      | Stable equilibrium value of $\beta$ (244)–(245)   | $\mu$         | Viscosity (1)   |
| $\gamma$                       | Interfacial tension (122a)  | $\nu$         | Angle defined in connection with helicoidal symmetry (72)–(73); kinematic viscosity (244)–(245) |
| $\Gamma$                       | Volume of space external to particle (227); entire volume of space within circular cylinder (288) | $\xi^*$       | Generalized ratio of representative particle-to-boundary dimensions (243)                       |
| $\delta$                       | Dirac delta function (193)–(194); small parameter (68)–(69)                                       | $\pi$         | Stress dyadic (3)   |
| $\delta_{jk}$                  | Kronecker delta (45)–(46)   | $\Pi$         | Intrinsic "stress" triadic (34), (37)   |
| $\Delta(\lambda)$              | Function of $\lambda$ (63)  | $\rho$        | Fluid density (1)   |
| $\epsilon$                     | Small dimensionless deformation parameter (64)  | $\rho_p$      | Particle density (244)–(245)  |
| $\epsilon_{jkl}$               | Permutation symbol (footnote 3)   | $\rho_m$      | Mean density of a suspension (145)  |
| $\epsilon$                     | Isotropic triadic (footnote 3)  | $\Delta \rho$ | Fluid-particle density difference (295)   |
| $\zeta$                        | Prolate spheroidal coordinate (75)–(76)   | $\sigma$      | Wall-correction factor (130); density of particles in configuration space (318)–(319)           |

- $\tau$  Characteristic time (4); fundamental temperature field (307)
- $\phi$  Azimuthal angle in spherical coordinates (64); fractional volume of solid particles in a suspension (145)–(146)
- $\phi^i$  Cartesian component of angular velocity (326b)
- $\Delta\phi^i$  Cartesian component of vector  $\Delta\phi$  (317), (349)
- $\Delta\phi$  Angular displacement vector in orientation space (346)
- $\frac{\partial}{\partial\phi}$  Symbolic representation for vector gradient in orientation space (footnote 57)
- $\Phi$  Rate of mechanical energy dissipation (footnote 55)
- $\chi$  Function of  $a_1, a_2, a_3$  (62)
- $\psi$  Stream function (75)
- $\omega$  Angular speed; component of  $\omega$  (75)
- $\omega_i^f$  Component of angular velocity vector  $\omega_f$  parallel to principal axis of ellipsoid (97)–(98)
- $\varpi$  Cylindrical coordinate (75)
- $\omega$  Angular velocity vector (9)
- $\omega_f$  Angular velocity of fluid particle (107)

## GERMAN LETTERS

- $\mathfrak{F}$  Symbolic dyadic force operator (83)
- ${}_{n+2}\mathfrak{R}$  Constant resistance polyadic (102), (103)
- $\mathfrak{Q}_n^{(0)}, \mathfrak{Q}_n^{(2)}$  Symbolic scalar and dyadic operators, respectively (98)
- $\mathfrak{C}$  Cartesian component of  $\mathfrak{C}$  (119)
- $\mathfrak{S}$  Constant shear resistance triadic (111), (112)
- $\mathfrak{T}$  Symbolic dyadic torque operator (84)

## OTHER SYMBOLS

- $\nabla$  Symbolic scalar operator  $= (\nabla^2)^{1/2}$  (87)
- $\nabla^2$  Laplace operator (1)
- $\nabla$  Vector nabla operator (1)
- $\nabla^n$  Polyadic differential operator (98)–(99)
- $\square$  Vector differential operator (92b)
- $\parallel$  Matrix brackets (45)–(46)
- Under symbol denoting dimensionless quantity (4); over symbol denoting mean value (75)–(76), (317)
- $\cdot$  Over symbol denoting derivative with respect to time (326)
- $\cdot$  Dot product (1)
- $:$  Double-dot product (54)
- $\times$  Cross product (9)
- $\sim$  Over symbol denoting “stretched” variable (204)

## SUBSCRIPTS

- $B$  Body
- $c$  Coupling
- $c$  Presubscript denoting convective
- $d$  Presubscript denoting diffusive
- $D$  Drag
- ext External
- $f$  Fluid
- int Internal
- $i, j, k, l, m, n$  Summation or tensor indices
- $L$  Lift force
- $m$  Mean value
- $n+2$  Presubscript denoting degree of a polyadic
- $O$  Arbitrary origin
- $p$  Particle
- $P$  Any point
- $r$  Rotation
- $R$  Center of reaction

|          |   |             |  |
|----------|---|-------------|--|
| $s$      | Shear                                     | $\parallel$ | Parallel   |
| $t$      | Translation, or tube                      | $\perp$     | Perpendicular  |
| $w$      | Wall                                      | $\infty$    | Infinite medium                                      |
| $\alpha$ | Component of vector in $\alpha$ direction | 0           | Stokes field   |
| $\omega$ | Angular spin                              | -2          | Presubscript denoting a term homogeneous in $r^{-2}$ |

## SUPERSCRIPTS

|                        |   |           |  |
|------------------------|---|-----------|--|
| $f$                    | Fluid                                   | 1, 2      | Presuperscript denoting vectors which are reversed and invariant, respectively, to a reversal of direction of motion |
| $i, j, k, l, \dots$    | Tensor indices                          | $\dagger$ | Transposition operator   |
| $\alpha, \beta, \dots$ | Tensor indices in 3-space               | $\infty$  | Unbounded fluid  |
| 0                      | Unperturbed flow                        | +         | Additional value, above and beyond value in the unperturbed flow   |
| -1                     | Inverse (reciprocal) dyadic             | •         | Static fluid   |
| (1), (2), (3)          | Cartesian tensor components of a vector |           |  |
| (11), (12), ..., (33)  | Cartesian tensor components of a dyadic |           |  |

## REFERENCES

- A1. Acrivos, A., and Goddard, J. D., *J. Fluid Mech.* **23**, 273 (1965).  
A1a. Acrivos, A., and Taylor, T. D., *Phys. Fluids* **5**, 387 (1962).  
A2. Acrivos, A., and Taylor, T. D., *Chem. Eng. Sci.* **19**, 445 (1964).  
A3. Andersson, O., *Svensk Papperstid.* **59**, 540 (1956); **60**, 153 (1957).  
A4. Andersson, O., *Svensk Papperstid.* **60**, 341 (1957).  
A5. Aris, R., "Vectors, Tensors and the Basic Equations of Fluid Mechanics," p. 30. Prentice-Hall, Englewood Cliffs, New Jersey, 1962.  
B1. Bammi, J. R., Mutual influence of two freely falling spherical particles and the effects of a plane vertical boundary on a single spherical particle. M.S. Dissertation, Univ. Iowa, Iowa City, 1950.  
B2. Becker, H. A., *Can. J. Chem. Eng.* **37**, 85 (1959).  
B3. Belinfante, D. C., *Proc. Cambridge Phil. Soc.* **58**, 405 (1962).  
B4. Berker, R., in "Encyclopedia of Physics: Fluid Dynamics II" (S. Flügge and C. Truesdell, eds.), Vol. 8, Part 2, p. 200. Springer, Berlin, 1963.  
B4a. Bhatnagar, P. L., and Rajeswari, G. K., *Compt. Rend.* **256**, 3823 (1963).  
B4b. Bhatnagar, R. K., *Proc. Indian Acad. Sci.* **A60**, 99 (1964).  
B5. Bickley, W. G., *Phil. Mag.* [7] **25**, 746 (1938).  
B6. Block, H. D., "Introduction to Tensor Analysis." Merrill, Columbus, Ohio, 1962.  
B7. Block, R. B., *J. Appl. Phys.* **11**, 635 (1940).  
B8. Bohlin, T., *Trans. Roy. Inst. Technol., Stockholm* **155**, 1 (1960); see comments by Faxén, H., *Kolloid-Z.* **167**, 146 (1959).  
B9. Bratukhin, Iu. K., *J. Appl. Math. Mech.* (English Transl. of *Prikl. Mat. Mekh.*), **25**, 1286 (1961).  
B10. Breach, D. R., *J. Fluid Mech.* **10**, 306 (1961).  
B11. Brenner, H., A theoretical study of slow viscous flow through assemblages of spherical particles. Eng. Sc.D. Dissertation, New York University, New York, 1957.  
B12. Brenner, H., *Phys. Fluids* **1**, 338 (1958).

- B13. Brenner, H., *J. Fluid Mech.* **6**, 542 (1959).
- B14. Brenner, H., *Chem. Eng. Sci.* **16**, 242 (1961).
- B15. Brenner, H., *J. Fluid Mech.* **11**, 604 (1961).
- B16. Brenner, H., *J. Fluid Mech.*, **12**, 35 (1962).
- B17. Brenner, H., *Chem. Eng. Sci.* **17**, 435 (1962).
- B18. Brenner, H., *Chem. Eng. Sci.* **18**, 1 (1963).
- B18a. Brenner, H., *Chem. Eng. Sci.* **18**, 109 (1963).
- B19. Brenner, H., *Chem. Eng. Sci.* **18**, 557 (1963).
- B20. Brenner, H., *J. Fluid Mech.* **18**, 144 (1964).
- B21. Brenner, H., *Chem. Eng. Sci.* **19**, 519 (1964).
- B22. Brenner, H., *Chem. Eng. Sci.* **19**, 599 (1964).
- B23. Brenner, H., *Chem. Eng. Sci.* **19**, 631 (1964).
- B24. Brenner, H., *Chem. Eng. Sci.* **19**, 703 (1964).
- B25. Brenner, H., *Appl. Sci. Res.* **A13**, 81 (1964).
- B25a. Brenner, H., *J. Colloid Sci.* **20**, 104 (1965).
- B26. Brenner, H., *Chem. Eng. Sci.* **21**, 97 (1966).
- B26a. Brenner, H., Coupling between the translational and rotational Brownian motions of rigid particles of arbitrary shape: II. General theory. *J. Coll. Interface Sci.* (in press).
- B26b. Brenner, H., On the invariance of the heat-transfer coefficient to flow reversal in Stokes flow past arbitrary particles (to be published).
- B27. Brenner, H., and Cox, R. G., *J. Fluid Mech.* **17**, 561 (1963).
- B28. Brenner, H., and Happel, J., *J. Fluid Mech.* **4**, 195 (1958).
- B29. Brenner, H., and Sonshine, R. M., *Quart. J. Mech. Appl. Math.* **17**, 55 (1964).
- B29a. Bretherton, F. P., *J. Fluid Mech.* **12**, 591 (1962).
- B30. Bretherton, F. P., *J. Fluid Mech.* **14**, 284 (1962).
- B31. Bretherton, F. P., *J. Fluid Mech.* **20**, 401 (1964).
- B32. Brinkman, H. C., *Verhandel. Koninkl. Ned. Akad. Wetenschap.*, **50**, 618, 860 (1947).
- B33. Brinkman, H. C., *Physica* **13**, 447 (1947).
- B34. Brinkman, H. C., *Appl. Sci. Res.* **A1**, 27 (1947); **A1**, 81 (1948).
- B35. Brinkman, H. C., *Research* (London) **2**, 190 (1949).
- B36. Broersma, S., *J. Chem. Phys.* **32**, 1632 (1960).
- B37. Burgers, J. M., *Verhandel. Koninkl. Ned. Akad. Wetenschap., Afdel. Natuurk., Sect. I* (Chapter 3) **16**, 113 (1938).
- B38. Burgers, J. M., *Verhandel. Koninkl. Ned. Akad. Wetenschap.* **44**, 1045, 1177 (1941); **45**, 9, 126 (1942).
- C1. Caswell, B., and Schwarz, W. H., *J. Fluid Mech.* **13**, 417 (1962).
- C2. Chaffey, C. E., Brenner, H., and Mason, S. G., *Rheol. Acta* **4**, 56 (1965).
- C3. Chaffey, C. E., Brenner, H., and Mason, S. G., *Rheol. Acta* **4**, 64 (1965).
- C4. Chang, I-Dee, *J. Appl. Math. Phys. (ZAMP)*, **12**, 56 (1961).
- C5. Chang, I-Dee, *J. Appl. Math. Phys. (ZAMP)*, **14**, 134 (1963).
- C6. Chapman, S., and Cowling, T. G., "The Mathematical Theory of Non-Uniform Gases." Cambridge Univ. Press, London and New York, 1961.
- C7. Chester, W., *J. Fluid Mech.* **13**, 557 (1962).
- C7a. Childress, S., *J. Fluid Mech.* **20**, 305 (1964).
- C8. Chow, P. S.-H., A generalized drag coefficient-Reynolds number plot for non-spherical particles. M.S. Dissertation, Univ. Minnesota, Minneapolis, Minnesota, 1964.
- C9. Chow, P. S.-H., and Brenner, H., A generalized drag coefficient-Reynolds number plot for non-spherical particles (to be published).

- C10. Chowdhury, K. C. R., and Fritz, W., *Chem. Eng. Sci.* **11**, 92 (1959).
- C11. Christopherson, D. G., and Dowson, D., *Proc. Roy. Soc.* **A251**, 550 (1959).
- C12. Collins, R. E., "Flow of Fluids through Porous Media." Reinhold, New York, 1961.
- C13. Collins, R. E., in "Modern Chemical Engineering" (A. Acrivos, ed.), Vol. 1, p. 307. Reinhold, New York, 1963.
- C14. Collins, W. D., *Mathematika* **2**, 42 (1955).
- C15. Collins, W. D., *Quart. J. Mech. Appl. Math.* **12**, 232 (1959).
- C16. Collins, W. D., *Mathematika* **10**, 72 (1963).
- C17. Cox, R. G., *J. Fluid Mech.* **23**, 273 (1965).
- C18. Cox, R. G., and Brenner, H., The lateral migration of solid particles in Poiseuille flows (to be published).
- C19. Cox, R. G., and Brenner, H., The motion of a sphere near a plane wall at small Reynolds numbers (to be published).
- C20. Cox, R. G., and Brenner, H., Effect of finite boundaries on the Stokes resistance of an arbitrary particle: Part III. Translation and rotation (to be published).
- C21. Cunningham, E., *Proc. Roy. Soc.* **A83**, 357 (1910).
- D1. Dahler, J. S., and Scriven, L. E., *Nature* **192**, 36 (1961).
- D2. Dahler, J. S., and Scriven, L. E., *Proc. Roy. Soc.* **A275**, 504 (1963).
- D3. Datta, S. K., *Appl. Sci. Res.* **A11**, 47 (1962).
- D3a. Day, J. T., and Genetti, W. E., Motion of spinning particles in shear fields. B.S. thesis, Univ. Utah, Salt Lake City, Utah, 1964.
- D4. Dean, W. R., and O'Neill, M. E., *Mathematika* **10**, 13 (1963).
- D4a. deGroot, S. R., and Mazur, P., "Non-Equilibrium Thermodynamics." North-Holland Publ., Amsterdam, 1962.
- D4b. Denson, C. D., Particle migration in shear fields. Ph.D. thesis, Univ. Utah, Salt Lake City, Utah, 1965; see also Denson, C. D., Christiansen, E. B., and Salt, D. L., *A.I.Ch.E. (Am. Inst. Chem. Engrs.) J.* **12**, 589 (1966).
- D4c. Debye, P., and Bueche, A. M., *J. Chem. Phys.* **16**, 573 (1948).
- D5. DiFrancia, G. T., *Boll. Unione Mat. Ital.* [3] **5**, 273 (1950).
- D6. Drew, T. B., "Handbook of Vector and Polyadic Analysis." Reinhold, New York, 1961.
- D7. Duffing, G., *Z. angew. Math. Mech. (ZAMM)* **13**, 366 (1933).
- E1. Eichhorn, R., and Small, S., *J. Fluid Mech.* **20**, 513 (1964).
- E1a. Einstein, A., "Investigations on the Theory of the Brownian Movement," (R. Fürth, ed.). Dover, New York, 1956.
- E2. Ericksen, J. L., *Trans. Soc. Rheol.* **4**, 29 (1960).
- E3. Eveson, G. F., *Brit. J. Appl. Phys.* **11**, 88 (1960).
- F1. Famularo, J., Theoretical study of sedimentation of dilute suspensions in creeping motion. Eng. Sc.D. Dissertation, New York University, New York, 1962; see also Famularo, J., and Happel, J., *A.I.Ch.E. (Am. Inst. Chem. Engrs.) J.* **11**, 981 (1965).
- F2. Faxén, H., *Arkiv Mat. Astron. Fysik* **18**, 1 (1924).
- F3. Fayon, A. M., Effect of a cylindrical boundary on rigid spheres suspended in a moving viscous liquid. Eng. Sc.D. Dissertation, New York University, New York, 1959.
- F4. Fayon, A. M., and Happel, J., *A.I.Ch.E. (Am. Inst. Chem. Engrs.) J.* **6**, 55 (1960).
- F5. Fidleris, V., Determination of wall-effect for spheres falling axially in cylindrical vessels. Ph.D. Dissertation, Univ. Nottingham, Nottingham, England, 1958.
- F6. Fidleris, V., and Whitmore, R. L., *Brit. J. Appl. Phys.* **12**, 490 (1961).



- F7. Forgacs, O. L., and Mason, S. G., *J. Colloid Sci.* **14**, 457 (1959).
- F8. Forgacs, O. L., Robertson, A. A., and Mason, S. G. "Fundamentals of Papermaking Fibres," p. 447. British Paper and Board Makers' Assoc., Kenley, Surrey, England, 1958.
- F9. Foster, R. D., and Slattery, J. D., *Appl. Sci. Res.* **A12**, 213 (1963).
- F10. Frater, K. R., *J. Fluid Mech.* **20**, 369 (1964).
- F11. Friedlander, S. K., *A.I.Ch.E. (Am. Inst. Chem. Engrs.) J.* **3**, 43 (1957).
- F12. Friedman, B., "Principles and Techniques of Applied Mathematics." Wiley, New York, 1956.
- F13. Fuchs, N. A. "The Mechanics of Aerosols." Pergamon Press, New York, 1964.
- G1. Gardner, M., "The Ambidextrous Universe: Left, Right, and the Fall of Parity." Basic Books, New York, 1964.
- G1a. Garstang, T. E., *Proc. Roy. Soc.* **A142**, 491 (1933).
- G2. Gasparian, A. M., and Zaminian, A. A., *Aikakan SSR Gritertionneri Akad. Zeikaitner* **26**, 39 (1958).
- G2a. Gel'fand, I. M., Minlos, R. A., and Shapiro, Z. Ya., "Representations of the Rotation and Lorentz Groups and Their Applications." Macmillan, New York, 1963.
- G3. Gibbs, J. W., and Wilson, E. B., "Vector Analysis." Dover, New York, 1960.
- G4. Giesekus, H., *Rheol. Acta* **2**, 101 (1962).
- G5. Giesekus, H., *Rheol. Acta* **3**, 59 (1963).
- G5a. Giesekus, H., *Proc. Intern. Symp. Second-order Effects Elasticity, Plasticity, Fluid Dynamics, Haifa, 1962*, pp. 533-584. MacMillan (Pergamon) Press, New York, 1964.
- G5b. Goldman, A. J., Cox, R. G., and Brenner, H., Slow viscous motion of two identical arbitrarily oriented spheres through a viscous fluid. *Chem. Eng. Sci.* (in press); see also Goldman, A. J., Investigations in low Reynolds number fluid-particle dynamics. Ph.D. Dissertation, New York University, New York, 1966.
- G5c. Goldman, A. J., Cox, R. G., and Brenner, H., The Stokes resistance of an arbitrary particle—Part VI: Terminal motion of a settling particle (to be published); see also Goldman, A. J., Investigations in low Reynolds number fluid-particle dynamics. Ph.D. Dissertation, New York University, New York, 1966.
- G5d. Goldman, A. J., Cox, R. G., and Brenner, H., Slow viscous motion of a sphere parallel to a plane wall—I. Motion through a quiescent fluid. *J. Fluid Mech.* (in press); see also Goldman, A. J., Investigations in low Reynolds number fluid-particle dynamics. Ph.D. Dissertation, New York University, New York, 1966.
- G5e. Goldman, A. J., Cox, R. G., and Brenner, H., Slow viscous motion of a sphere parallel to a plane wall—II. Motion in a Couette flow. *J. Fluid Mech.* (in press); see also Goldman, A. J., Investigations in low Reynolds number fluid-particle dynamics. Ph.D. Dissertation, New York University, New York, 1966.
- G6. Goldshtik, M. A., *Inzh.-Fiz. Zh. Akad. Nauk Belorussk SSR* **3**, 79 (1960).
- G7. Goldsmith, H. L., and Mason, S. G., *Nature* **190**, 1095 (1961).
- G8. Goldsmith, H. L., and Mason, S. G., *J. Fluid Mech.* **12**, 88 (1962).
- G9. Goldsmith, H. L., and Mason, S. G., *J. Colloid Sci.* **17**, 448 (1962).
- G9a. Goldsmith, H. L., and Mason, S. G., *Bibliotheca Anat.* **4**, 462 (1964).
- G9b. Goldsmith, H. L., and Mason, S. G., *Bibliotheca Anat.* (in press).
- G9c. Goldsmith, H. L., and Mason, S. G., *Biorheology* **3**, 33 (1965).
- G9d. Goldsmith, H. L., and Mason, S. G., in "Rheology: Theory and Applications" (F. R. Eirich, ed.), Vol. IV. Academic Press, New York, 1966.

- G9e. Goldstein, H., "Classical Mechanics," pp. 124-132. Addison-Wesley, Reading, Massachusetts, 1950.
- G10. Goldstein, S., *Proc. Roy. Soc. A* **123**, 225 (1929).
- G11. Goldstein, S., ed., "Modern Developments in Fluid Dynamics," Vol. 1, p. 83. Oxford Univ. Press, London and New York, 1938.
- G12. Gupta, S. C., *J. Appl. Math. Phys. (ZAMP)* **8**, 257 (1957).
- H1. Haberman, W. L., Flow about a sphere rotating in a viscous liquid inside a coaxially rotating cylinder. David W. Taylor Model Basin Rept. No. 1578. U.S. Navy Dept., Washington, D.C., 1961.
- H2. Haberman, W. L., *Phys. Fluids* **5**, 625, 1136 (1962).
- H3. Haberman, W. L., and Sayre, R. M., Motion of rigid and fluid spheres in stationary and moving liquids inside cylindrical tubes. David W. Taylor Model Basin Rept. No. 1143. U.S. Navy Dept., Washington, D.C., 1958.
- H3a. Hadamard, J. S., *Compt. Rend.* **152**, 1735 (1911); **154**, 109 (1912).
- H4. Happel, J., *J. Appl. Phys.* **28**, 1288 (1957).
- H5. Happel, J., *A.I.Ch.E. (Am. Inst. Chem. Engrs.) J.* **4**, 197 (1958).
- H6. Happel, J., *Trans. N.Y. Acad. Sci.* [2] **20**, 404 (1958).
- H7. Happel, J., *A.I.Ch.E. (Am. Inst. Chem. Engrs.) J.* **5**, 174 (1959).
- H8. Happel, J., and Brenner, H., *A.I.Ch.E. (Am. Inst. Chem. Engrs.) J.* **3**, 506 (1957).
- H9. Happel, J., and Brenner, H., "Low Reynolds Number Hydrodynamics." Prentice-Hall, Englewood Cliffs, New Jersey, 1965.
- H9a. Hartunian, R. A., and Liu, S. W., *Phys. Fluids* **6**, 349 (1963).
- H10. Hasimoto, H., *J. Fluid Mech.* **5**, 317 (1959).
- H11. Hawksley, P. G. W., *Brit. Coal Util. Res. Assoc. Monthly Bull.* **15**, 105 (1951).
- H12. Heiss, J. F., and Coull, J., *Chem. Eng. Progr.* **48**, 133 (1952).
- H12a. Hermans, J. J., in "Flow Properties of Disperse Systems" (J. J. Hermans, ed.), pp. 226-233. Wiley (Interscience), New York, 1953.
- H13. Hill, R., and Power, G., *Quart J. Mech. Appl. Math.* **9**, 313 (1956).
- H13a. Hocking, L. M., in "Aerodynamic Capture of Particles" (E. G. Richardson, ed.), pp. 154-159. Pergamon, New York, 1960.
- H14. Hocking, L. M., *J. Fluid Mech.* **20**, 129 (1964).
- H15. Hubbard, R. M., and Brown, G. G., *Ind. Eng. Chem. (Anal. Edition)* **15**, 212 (1943).
- I1. Illingsworth, C. R., in "Laminar Boundary Layers" (L. Rosenhead, ed.), p. 163. Oxford Univ. Press, London and New York, 1963.
- I2. Illingsworth, C. R., *J. Appl. Math. Phys. (ZAMP)* **14**, 681 (1963).
- J1. Janke, N. C., Effect of shape upon the settling velocity of regular geometric particles. Ph.D. Dissertation, Univ. California, Los Angeles, California, 1963.
- J2. Jayaweera, K. O. L. F., Mason, B. J., and Slack, G. W., *J. Fluid Mech.* **20**, 121 (1964).
- J2a. Jayaweera, K. O. L. F., and Mason, B. J., *J. Fluid Mech.* **22**, 709 (1965).
- J3. Jeffery, G. B., *Proc. London Math. Soc.* [2] **14**, 327 (1915).
- J4. Jeffery, G. B., *Proc. Roy. Soc. A* **102**, 161 (1922).
- J5. Jeffrey, R. C., Particle motion in Poiseuille flow. Ph.D. Dissertation, Cambridge Univ., Cambridge, England, 1964; see also Jeffrey, R. C., and Pearson, J. R. A., *J. Fluid Mech.* **22**, 721 (1965).
- J6. Jones, A. M., and Knudsen, J. G., *A.I.Ch.E. (Am. Inst. Chem. Engrs.) J.* **7**, 20 (1961).
- K1. Kanwal, R. P., *J. Fluid Mech.* **10**, 17 (1961).
- K2. Kanwal, R. P., *J. Fluid Mech.* **19**, 631 (1964).
- K3. Kaplun, S., *J. Math. Mech.* **6**, 595 (1957).
- K4. Kaplun, S., and Lagerstrom, P. A., *J. Math. Mech.* **6**, 585 (1957).

- K4a. Karnis, A., The flow of suspensions through tubes. Ph.D. Dissertation, McGill University, Montreal, Canada, 1966.
- K5. Karnis, A., Goldsmith, H. L., and Mason, S. G., *Nature* **200**, 159 (1963).
- K5a. Karnis, A., Goldsmith, H. L., and Mason, S. G., The kinetics of flowing dispersions: I. Concentrated suspensions of rigid particles. *J. Coll. Interface Sci.* (in press).
- K5b. Karnis, A., Goldsmith, H. L., and Mason, S. G., The flow of suspensions through tubes: V. Inertial effects. *Can. J. Chem. Eng.* (in press).
- K5c. Karnis, A., and Mason, S. G., The flow of suspensions through tubes: VI. Meniscus effects. *J. Coll. Interface Sci.* (in press).
- K5d. Karnis, A., and Mason, S. G., Particle motions in sheared suspensions: XIX. Viscoelastic media (to be published).
- K6. Kaufman, R. N., *J. Appl. Math. Mech. (English Transl.)* **27**, 262 (1963); see *Prikl. Mat. Mekh.* **27**, 179 (1963).
- K7. Kearsley, E. A., *Arch. Rat. Mech. Anal.* **5**, 347 (1960).
- K8. Keller, J. B., *J. Fluid Mech.* **18**, 94 (1964).
- K9. Khamrui, S. R., *Bull. Calcutta Math. Soc.* **48**, 159 (1956).
- K10. Khamrui, S. R., *Bull. Calcutta Math. Soc.* **52**, 63 (1960).
- K10a. Kohlman, D. L., *Mass. Inst. Technol., Fluid Dynamics Res. Lab. Rept.* **63/1** (1963).
- K11. Kunkel, W. B., *J. Appl. Phys.* **19**, 1056 (1948).
- K12. Kuwabara, S., *J. Phys. Soc. Japan* **14**, 527 (1959).
- L1. Ladyzhenskaya, O. A., "The Mathematical Theory of Viscous Incompressible Flow," Gordon & Breach, New York, 1963.
- L2. Lagerstrom, P. A., and Cole, J. D., *J. Rat. Mech. Anal.* **4**, 817 (1955).
- L3. Lagerstrom, P. A., *J. Math. Mech.* **6**, 605 (1957).
- L4. Lagerstrom, P. A., in "Theory of Laminar Flows" (F. K. Moore, ed.). Princeton Univ. Press, Princeton, New Jersey, 1964.
- L4a. Lagerstrom, P. A., and Chang, I-Dee, in "Handbook of Engineering Mechanics" (W. Flügge, ed.), Chapter 81. McGraw-Hill, New York, 1962.
- L5. Lamb, H., "Hydrodynamics," 6th ed. Dover, New York, 1945.
- L5a. Lanczos, C., "Linear Differential Operators." Van Nostrand, Princeton, New Jersey, 1961.
- L5b. Landau, L. D., and Lifshitz, E. M., "Statistical Physics." Addison-Wesley, Reading, Massachusetts, 1958.
- L6. Landau, L. D., and Lifshitz, E. M., "Fluid Mechanics," pp. 70-71. Addison-Wesley, Reading, Massachusetts, 1959.
- L7. Landau, L. D., and Lifshitz, E. M., "Electrodynamics of Continuous Media," pp. 337-343. Addison-Wesley, Reading, Massachusetts, 1960.
- L7a. Landau, L. D., and Lifshitz, E. M., "Mechanics." Addison-Wesley, Reading, Massachusetts, 1960.
- L8. Langlois, W. E., *Quart. Appl. Math.* **21**, 61 (1963).
- L9. Langlois, W. E., "Slow Viscous Flow." Macmillan, New York, 1964.
- L10. Leslie, F. M. (with an appendix by R. I. Tanner), *Quart. J. Mech. Appl. Math.* **14**, 36 (1961).
- L10a. Levich, V. G., "Physicochemical Hydrodynamics." Prentice-Hall, Englewood Cliffs, New Jersey, 1962.
- L11. Lorentz, H. A., *Koninkl. Ned. Akad. Wetenschap., Verslag.* **5**, 168 (1896); "Collected Papers," Vol. 4, pp. 7-14. Martinus Nijhoff, The Hague, Holland, 1937.
- M1. Mackay, G. D. M., and Mason, S. G., *J. Colloid Sci.* **16**, 632 (1961).
- M2. Mackay, G. D. M., Suzuki, M., and Mason, S. G., *J. Colloid Sci.* **18**, 103 (1963).
- M3. Majumder, S. R., *Indian J. Theoret. Phys.* **8**, 39 (1960).

- M4. Malaika, J., Effect of shape of particles on their settling velocity. Ph.D. Dissertation, State Univ. of Iowa, Iowa City, 1949.
- M5. Mason, S. G., and Bartok, W., in "Rheology of Disperse Systems" (C. C. Mill, ed.), Chapter 2. Pergamon Press, Oxford, 1959.
- M5a. Maude, A. D., *Brit. J. Appl. Phys.* **10**, 371 (1959).
- M6. Maude, A. D., *Brit. J. Appl. Phys.* **12**, 293 (1961).
- M7. Maude, A. D., *Brit. J. Appl. Phys.* **14**, 894 (1963).
- M7a. Maude, A. D., and Whitmore, R. L., *Brit. J. Appl. Phys.* **7**, 98 (1956).
- M7b. Maxworthy, T., *J. Fluid Mech.* **23**, 369, 373 (1965).
- M8. McNown, J. S., *Houille Blanche* **6**, 701 (1951).
- M9. McNown, J. S., Analysis of the rolling ball viscometer. Mich. Eng. Coll. Ind. Program, Brochure IP-160. Univ. of Michigan, Ann Arbor, Michigan, 1956.
- M10. McNown, J. S., Lee, N. M., McPherson, M.B., and Engez, S. M., *Proc. 7th Intern. Congr. Appl. Mech., London, 1948*, Vol. 2, Part I, p. 17 (1948). (Reprinted as State University of Iowa, Reprints in Engineering, Reprint 81).
- M11. McNown, J. S., and Malaika, J., *Trans. Am. Geophys. Union* **31**, 74 (1950).
- M12. McNown, J. S., Malaika, J., and Pramanik, H. R., *Trans. 4th Meeting Intern. Assoc. Hydraulic Res. Bombay, India*, p. 511 (1951).
- M13. McNown, J. S., and Newlin, J. T., *Proc. 1st Natl. Congr. Appl. Mech., 1951*, p. 801. J. W. Edwards, Ann Arbor, Michigan, 1952.
- M14. McPherson, M. B., Boundary influence on the fall velocity of spheres at Reynolds numbers beyond the Stokes range. M.S. Dissertation, State Univ. of Iowa, Iowa City, 1947.
- M15. Menzel, D. H., "Mathematical Physics," pp. 86-141. Dover, New York, 1961.
- M16. Milne, E. A., "Vectorial Mechanics." Methuen, London, 1948.
- M17. Milne-Thomson, L. M., "Theoretical Hydrodynamics," 4th ed., pp. 458-62. Macmillan, New York, 1960.
- M18. Mirsky, L., "An Introduction to Linear Algebra." Oxford Univ. Press, London and New York, 1955.
- M19. Mohr, C. M., and Blumberg, P. N., "Effect of orientation on the settling characteristics of cylindrical particles" (to be published).
- M20. Morse, P. M., and Feshbach, H., "Methods of Theoretical Physics," Vols. I and II. McGraw-Hill, New York, 1953.
- O1. O'Brien, V., Axi-symmetric viscous flows correct to the first-order in the Reynolds number. Appl. Phys. Lab. Rept. No. CM-1003. Johns Hopkins Univ., Silver Spring, Maryland, 1961.
- O1a. O'Brien, V., *Phys. Fluids* **6**, 1356 (1963).
- O1b. O'Brien, V., Deformed spheroids in Stokes flow. Appl. Phys. Lab. Tech. Memo TG-716. Johns Hopkins Univ., Silver Spring, Maryland, 1965; see also *A.P.L. Technical Digest* **4**, 11 (1965).
- O2. Oliver, D. R., *Nature* **194**, 1269 (1962).
- O2a. O'Neill, M. E., *Mathematika* **11**, 67 (1964).
- O3. Oseen, C. W., *Arkiv Mat. Astron. Fysik* **6**, No. 29 (1910).
- O4. Oseen, C. W., "Neuere Methoden und Ergebnisse in der Hydrodynamik." Akademische Verlags., Leipzig, 1927.
- O5. Ovseenko, Yu. G., *Tr. Novocherk. Politekhn. Inst.* **109**, 51 (1960).
- O6. Ovseenko, Yu. G., *Izv. Vysshikh Uchebn. Zavedenii, Matematika* **35**, 129 (1963).
- P1. Payne, L. E., and Pell, W. H., *J. Fluid Mech.* **7**, 529 (1960).
- P2. Pell, W. H., and Payne, L. E., *Mathematika* **7**, 78 (1960).
- P3. Pell, W. H., and Payne, L. E., *Quart. Appl. Math.* **18**, 257 (1960).

- P4. Pèrès, J., *Compt. Rend.* **188**, 310, 440 (1929).
- P4a. Perrin, F., *J. Phys. Radium* **7**, 1 (1936).
- P5. Perry, J. H., ed., "Chemical Engineers' Handbook," 4th ed., Sect. 19, p. 15. McGraw-Hill, New York, 1963.
- P6. Pettyjohn, E. S., and Christiansen, E. B., *Chem. Eng. Progr.* **44**, 157 (1948).
- P7. Pfeffer, R., *Ind. Eng. Chem., Fundamentals* **3**, 380 (1964).
- P8. Pfeffer, R., and Happel, J., *A.I.Ch.E. (Am. Inst. Chem. Engrs.) J.* **10**, 605 (1964).
- P9. Pliskin, I., and Brenner, H., *J. Fluid Mech.* **17**, 89 (1963).
- P10. Polubarinova-Kochina, P. Ya., "Theory of Ground-Water Movement." Princeton Univ. Press, Princeton, New Jersey, 1962.
- P11. Proudman, I., and Pearson, J. R. A., *J. Fluid Mech.* **2**, 237 (1957).
- P12. Pshenai-Severin, S., *Izv. Akad. nauk SSSR, ser. geofiz.*, 1045 (1957).
- P13. Pshenai-Severin, S., *Izv. Akad. nauk SSSR, ser. geofiz.*, 1254 (1958).
- R1. Rathna, S. L., *Quart. J. Mech. Appl. Math.* **15**, 427 (1962).
- R2. Rayleigh, Lord, *Phil. Mag.* [5] **36**, 354 (1893).
- R3. Relton, F. E., *Phil. Mag.* [7] **11**, 129 (1931).
- R4. Relton, F. E., *Proc. Roy. Soc. A* **134**, 47 (1931-1932).
- R4a. Repetti, R. V., and Leonard, E. F., *Nature* **203**, 1346 (1964).
- R4b. Repetti, R. V., and Leonard, E. F., Physical basis for the axial accumulation of red cells. Paper No. 32b presented at 56th National A.I.Ch.E. Meeting, San Francisco, California, 1965.
- R5. Richardson, J. G., in "Handbook of Fluid Dynamics" (V. L. Streeter, ed.), Chapter 16. McGraw-Hill, New York, 1961.
- R5a. Ripps, D. L., and Brenner, H., The Stokes resistance of a slightly deformed sphere: II. Intrinsic resistance operators for an arbitrary initial flow (to be published); see also Ripps, D. L., Invariant differential operators for slow viscous flow past a particle. Ph.D. Dissertation, New York University, New York, 1966.
- R5b. Ripps, D. L., and Brenner, H., Slow viscous flow through an infinite periodic lattice of identical solid particles of arbitrary shape (to be published).
- R6. Roscoe, R., *Phil. Mag.* [7] **40**, 338 (1949).
- R6a. Rubinow, S. I., *Biorheology* **2**, 117 (1964).
- R7. Rubinow, S. I., and Keller, J. B., *J. Fluid Mech.* **11**, 447 (1961).
- R8. Ruckenstein, E., *Chem. Eng. Sci.* **19**, 131 (1964).
- R9. Rumscheidt, F. D., and Mason, S. G., *J. Colloid Sci.* **16**, 238 (1961).
- R10. Rybczyński, W., *Bull. Acad. Sci. Cracovie, Ser. A*, pp. 40-46 (1911).
- S1. Saffman, P. G., *J. Fluid Mech.* **1**, 540 (1956).
- S1a. Saffman, P. G., *J. Fluid Mech.* **22**, 385 (1965).
- S2. Sakadi, Z., *Mem. Fac. Eng., Nagoya Univ.* **10**, 42 (1958).
- S3. Scheidegger, A. E., "The Physics of Flow Through Porous Media," 2nd ed. Univ. of Toronto Press, Toronto, 1960.
- S4. Scheidegger, A. E., in "Encyclopedia of Physics: Fluid Dynamics II" (S. Flügge and C. Truesdell, eds.), Vol. 8, Part 2, p. 625. Springer, Berlin, 1963.
- S4a. Segré, S., *Trans. 4th Intern. Congr. Rheology, 1963* (A. L. Copley, ed.), Part 4, p. 103. Wiley (Interscience), London and New York, 1965.
- S5. Segré, G., and Silberberg, A., *Nature* **189**, 209 (1961).
- S6. Segré, G., and Silberberg, A., *J. Fluid Mech.* **14**, 115, 136 (1962).
- S7. Segré, G., and Silberberg, A., *J. Colloid Sci.* **18**, 312 (1963).
- S8. Selby, T. W., and Hunstad, N. A., The forced-ball viscometer and its application to the characterization of mineral oil systems. Presented at "Symposium on Non-Newtonian Viscometry," sponsored jointly by Research Division III on Flow

- Properties, Committee D-2 (ASTM) and Committee on Petroleum Products (A.P.I.), Washington, D.C., 1960.
- S9. Shanks, D., *J. Appl. Math. Phys. (ZAMP)* **34**, 1 (1955).
- S9a. Shi, Y. Y., *J. Fluid Mech.* **23**, 657 (1965).
- S9b. Shizgal, B., Goldsmith, H. L., and Mason, S. G., *Can. J. Chem. Eng.* **43**, 97 (1965).
- S10. Slattery, J. C., *Appl. Sci. Res.* **A10**, 286 (1961).
- S11. Slattery, J. C., *A.I.Ch.E. (Am. Inst. Chem. Engrs.) J.* **8**, 663 (1962).
- S12. Slattery, J. C., and Bird, R. B., *Chem. Eng. Sci.* **16**, 231 (1961).
- S13. Small S., Experiments on the lift and drag of spheres suspended in a low Reynolds number Poiseuille flow. Mech. Eng. Dept., Rept. FLD No. 11. Princeton Univ., Princeton, New Jersey, 1963.
- S14. Snyder, L. J., and Stewart, W. E., *A.I.Ch.E. (Am. Inst. Chem. Engrs.) J.* **12**, 167 (1966).
- S15. Sonshine, R. M., and Brenner, H., The Stokes translation of two or more particles along the axis of an infinitely long circular cylinder. *Appl. Sci. Res., Ser. A* (in press); see also Sonshine, R. M., The Stokes settling of one or more particles along the axis of finite and infinitely long circular cylinders. Ph.D. Dissertation, New York University, New York, 1966.
- S16. Sonshine, R. M., Cox, R. G., and Brenner, H., The Stokes translation of a particle of arbitrary shape along the axis of a circular cylinder filled to a finite depth with viscous liquid: I and II. *Appl. Sci. Res., Ser. A* (in press); see also Sonshine, R. M., The Stokes settling of one or more particles along the axis of finite and infinitely long circular cylinders. Ph.D. Dissertation, New York University, New York, 1966.
- S17. Srimathi, C. R., and Bhat, G. N., *Brit. J. Appl. Phys.* **16**, 551 (1965).
- S18. Starkey, T. V., *Brit. J. Appl. Phys.* **7**, 52 (1956).
- S19. Starkey, T. V., Hewlett, V. A., Roberts, J. H. A., and James, R. E., *Brit. J. Appl. Phys.* **12**, 545 (1961).
- S20. Stimson, M., and Jeffery, G. B., *Proc. Roy. Soc.* **A111**, 110 (1926).
- T1. Takano, M., and Mason, S. G. (to be published).
- T1a. Tanner, R. I., *J. Fluid Mech.* **17**, 161 (1963).
- T1b. Taylor, G. I., *Proc. Roy. Soc.* **A138**, 41 (1932).
- T2. Taylor, G. I., *Proc. Roy. Soc.* **A146**, 501 (1934).
- T2a. Taylor, T. D., *Phys. Fluids* **6**, 987 (1963).
- T2b. Taylor, T. D., *Intern. J. Heat Mass Transfer* **6**, 993 (1963).
- T2c. Taylor, T. D., and Acrivos, A., *J. Fluid Mech.* **18**, 466 (1964).
- T3. Tchen, C. M., *J. Appl. Phys.* **25**, 463 (1954).
- T3a. Theodore, L., Sidewise force exerted on a spherical particle in a Poiseuillian flow field. Eng. Sc.D. Dissertation, New York University, New York, 1964.
- T4. Thomas, R. H., and Walters, K., *Quart. J. Mech. Appl. Math.* **17**, 39. (1964).
- T5. Timbrell, V., *Brit. J. Appl. Phys.* **5**, Suppl. 3, S12 (1954).
- T6. Tollert, H., *Chem.-Ing.-Tech.* **26**, 141 (1954).
- T7. Tomita, Y., *Bull. JSME (Japan. Soc. Mech. Engrs.)* **2**, 469 (1959).
- T8. Tuck, E. O., *J. Fluid Mech.* **18**, 619 (1964).
- U1. Uchida, S., *Rept. Inst. Sci. Technol., Univ. Tokyo*, **3**, 97 (1949); abstracted in *Ind. Eng. Chem.* **46**, 1194 (1954).
- V1. van Dyke, M., "Perturbation Methods in Fluid Mechanics." Academic Press, New York, 1964.
- V2. Vand, V., *J. Phys. & Colloid Chem.* **52**, 277 (1948).
- V3. Vand, V., *J. Phys. & Colloid Chem.* **52**, 300 (1948).
- V4. Villat, H., "Leçons sur les Fluides Visqueux." Gauthier-Villars, Paris, 1943.

- W1. Wadhwa, Y. D., *J. Sci. Eng. Res., Indian Inst. Technol., Kharagpur* **2**, 245 (1958).
- W2. Wallick, G. C., Savins, J. G., and Arterburn, D. R., *Phys. Fluids* **5**, 367 (1962).
- W3. Walters, K., The rotating-sphere elastoviscometer. Presented at 35th Annual Meeting of the Society of Rheology, Mellon Institute, Pittsburgh, Pa., 1964.
- W3a. Walters, K., and Water, D., *Rheol. Acta* **3**, 312 (1963–1964).
- W3b. Walters, K., and Water, D., *Brit. J. Appl. Phys.* **15**, 989 (1964).
- W4. Walters, K., and Waters, N. D., *Brit. J. Appl. Phys.* **14**, 667 (1963).
- W5. Wasserman, M. L., and Slattery, J. C., *A.I.Ch.E. (Am. Inst. Chem. Engrs.) J.* **10**, 383 (1964).
- W6. Waters, N. D., *Brit. J. Appl. Phys.* **15**, 500 (1964).
- W7. Whitehead, A. N., *Quart. J. Math.* **23**, 78, 143 (1889).
- W8. Williams, W. E., *Phil. Mag.* [6] **29**, 526 (1915).
- W8a. Williams, W. E., *J. Fluid Mech.* **24**, 285 (1966).
- W9. Willmarth, W. W., Hawk, N. E., and Harvey, R. L., *Phys. Fluids* **7**, 197 (1964).
- Z1. Ziegenhagen, A. J., Bird, R. B., and Johnson, M. W., Jr., *Trans. Soc. Rheol.* **5**, 47 (1961).
- Z2. Zierep, J., *Zeit. Flugwiss.* **3**, 22 (1955).

## AUTHOR INDEX

Numbers in parentheses are reference numbers and indicate that an author's work is referred to although his name is not cited in the text. Numbers in *italic* show the page on which the complete reference is listed.

- Abbo, F. E., 186, 188, 203  
 Acrivos, A., 104, 121, 300 (A2), 401, 406 (A1a), 408, 429  
 Adamson, A. W., 64 (A1), 121  
 Adolph, E. F., 197, 203  
 Aksebrud, H. A., 212 (A1), 214 (A1), 226 (A1), 280  
 Alexander, M., 198, 205  
 Amundson, N. R., 135, 203  
 Andersson, O., 345, 429  
 Aris, R., 135, 203, 321 (A5), 374 (A5), 429  
 Arnold, W., 169 (E2), 204  
 Arterburn, D. R., 288 (W2), 438  
 Avsec, D., 66 (A4), 68 (A4), 70 (A4), 72 (A4), 95, 106 (A4), 108, 109 (A4), 111, 115 (A4), 121  
 Bailey, N. T. J., 127, 203  
 Baird, E. D., 240 (T2), 241 (T2), 242 (T2), 246 (T2), 270 (T2), 274 (B1), 275, 276 (B1), 285  
 Baird, M. H. I., 227, 229, 280  
 Bammi, J. R., 345, 429  
 Banchemo, J. T., 215 (E2), 217 (E2), 222 (E2), 231, 233, 277 (E2), 279 (E2), 280 (E2), 281  
 Bankoff, S. G., 1 (B8), 3 (B23), 4 (S13a), 7, 8 (B8), 9 (B7), 15 (B10), 17, 18 (B7), 19 (B8), 23 (B6, B9), 24, 26 (S12), 34 (S13), 35 (S12), 36, 38, 43 (B11), 45 (B11), 46 (B11), 47, 48, 49 (S12), 50 (B1, B2, B3, B4, B13), 52, 56, 59, 262, 265 (B2), 280  
 Barboubeau, I., 237, 244, 246, 263 (B2), 280  
 Barlow, E. J., 3 (B14), 17, 56  
 Barnhart, E. L., 228 (E1), 281  
 Baron, T., 136, 203, 210 (H5), 217 (H5), 222 (H5), 234, 235 (H5), 277 (H5), 282  
 Barsky, Z., 259, 260 (S8a), 284  
 Bartok, W., 222 (B4), 280, 322 (M5), 348, 435  
 Bartz, D. R., 52, 56  
 Baston, J. B., 277 (B5), 280  
 Batchelor, G. K., 98, 121  
 Battin, R. H., 194, 204  
 Bayne-Jones, S., 197, 203  
 Beardmore, R. H., 277 (W7), 285  
 Beck, T. R., 231 (W6), 267 (W6), 285  
 Becker, H. A., 375 (B2), 429  
 Beckman, R. B., 238 (S17), 285  
 Behar, M., 52 (B15, 16), 56  
 Behnken, D. W., 184, 192, 193, 203  
 Belinfante, D. C., 360 (B3), 429  
 Bell, S. H., 71 (B3), 72 (B3), 97, 103 (B3), 106, 121  
 Beliman, R. E., 142 (B5), 203  
 Bénard, H., 66, 67, 68, 69 (B4), 71 (B4, B7, B10, B11), 108 (B6), 109, 118, 121  
 Benenati, R. F., 251 (O1), 284  
 Benjamin, J. E., 36, 56  
 Bentwich, M., 215 (B6), 226 (B6), 230 (B6), 280  
 Berg, J. C., 78, 97, 101, 104, 111, 112 (B12), 113 (B12), 121



- Berker, R., 288 (B4), 336 (B4), 341 (B4), 345, 398, 429
- Beyaert, B. O., 238 (B7), 281
- Bharucha-Reid, A. T., 127, 128 (B1), 203
- Bhat, G. N., 346, 349, 437
- Bhatnagar, P. L., 288 (B4a), 429
- Bhatnagar, R. K., 288 (B4b), 429
- Bickley, W. G., 359, 429
- Bilous, O., 135, 203
- Bird, R. B., 288 (Z1), 437, 438
- Birkhoff, G., 8, 9, 17, 25, 56
- Block, H. D., 289 (B6), 429
- Block, M. J., 96, 102, 121, 236 (Y1), 245 (Y1), 286
- Block, R. B., 325, 429
- Blumberg, P. N., 306, 435
- Bohlin, T., 326 (B8), 429
- Boley, B. A., 19, 56
- Boltzmann, L., 8, 56
- Bond, W. N., 223, 281
- Bonilla, C. F., 17, 57, 262, 281
- Bosnjakovic, F., 10, 56
- Boussinesq, M., 215 (B10), 222 (B10), 230, 281
- Bowman, C. W., 212 (B12), 216 (B12), 222 (B12), 228 (B11, 12), 274 (B11), 277 (B11), 281
- Boye-Christensen, H., 222 (B13), 224 (B13), 232 (B13), 276 (B13), 281
- Boys, C. B., 64 (B15), 121
- Brandstaetter, F., 42, 56
- Bratukhin, Iu. K., 360, 429
- Breach, D. R., 365, 429
- Brenner, H., 212 (B14), 215 (B14), 281, 288 (H9), 290, 291 (B18, B19, B22), 292 (B22), 294 (B22), 295 (B18, B22), 296 (B18, B22), 297 (B22), 298 (B22), 299 (B18, B23), 300 (B21, 301 (B18, B21, B22), 302, 303, 307 (B18, G5c), 308 (B23, B24, B26), 309 (B24, B26), 310 (B26), 311 (B26), 312 (B24, B28), 313 (B26), 314, 315 (R52), 316 (B23, B24), 317 (B24, R5a), 318 (B23), 319 (B21, B23), 320, 321 (B23), 323 (C2, C3), 325 (B22, B29, G5d, H9), 326 (B29), 327 (B14, B29), 329 (B16, B20, C19, C20), 330 (B20, C20), 331 (B16, B20), 332 (B20), 333 (B16, B20, B25, B29), 334, 335 (B16, B20, B28, G5d), 336 (B13, B17, B28), 337 (B17, P9), 338 (B12, H8), 339 (B12, H8), 340 (B17), 341 (B18), 342 (B22), 344 (B22), 345, 346, 347 (B20, B22, C20), 348 (B26), 349 (B28), 350 (B11, H9), 351 (R5b), 358, 366, 367, 370, 372 (B23, B27), 373 (B18, B22), 374 (B23, B27), 375 (C9), 376, 377 (B28), 378 (B12, H8), 382, 384, 390, 394, 395 (S16), 397, 402 (C3), 403 (H8), 407 (B26b), 409, 413 (B26a), 415 (B25a), 416 (B26a), 417 (B25a, B26a), 418 (B26a), 420 (B25a), 429, 430, 431, 432, 433, 436, 437
- Bretherton, F. P., 320, 322, 346, 377 (B30), 392, 400, 430
- Brink, J. C., 217 (K5), 222 (K5), 233, 236, 283
- Brinkman, H. C., 355 (B32, B33, B34, B35), 356 (B35), 430
- Broersma, S., 304 (B36), 430
- Brown, A. H., 169 (F5, M9), 204, 205
- Brown, F. E., 277 (H6), 282
- Brown, G., 209 (B15), 220, 281
- Brown, G. G., 325 (H15), 433
- Brown, H. T., 169 (B9), 203
- Brown, S. C., 62 (B16), 121
- Brown, W. S., 211 (B16), 281
- Bruijn, P. J., 35, 56
- Bruijsten, J., 212 (K6), 222 (K6), 283
- Brunt, 96
- Brunt, D., 71, 92, 121, 122
- Buchanan, R. E., 126, 142 (B10), 203
- Bueche, A. M., 355 (D4c), 431
- Buehl, W. M., 38, 57
- Bumpus, C., 3 (B26), 56
- Burgers, J. M., 304 (B37), 349, 430
- Burns, V. W., 186, 203
- Cahn, J. W., 53, 58
- Calderbank, P. H., 211 (L18), 214 (C1), 218 (C1), 221, 222 (C1), 227, 228 (C1), 231 (C1a), 233, 234 (C1), 236 (C1), 273, 274, 275, 277 (C2), 281, 284
- Calvert, S., 224 (C6), 231 (C6), 236, 277 (C6), 281
- Canning, F. T., 256 (C2a), 281
- Carr, B. B., 251 (C3), 281
- Carslaw, H. S., 237 (C4), 281
- Caswell, B., 288 (C1), 430
- Chaffey, C. E., 323 (C2, C3), 402 (C3)
- Chaffey, I. Dee, 331 (C4), 430
- Chandra, K., 72 (C1), 73 (C1), 95, 121
- Chandrasekhar, S., 71 (C2), 83, 84, 94, 117, 121
- Chang, I-Dee, 393, 430, 434

- Chao, B. T., 52, 57, 231, 281  
 Chapin, J. H., 211 (J4), 283  
 Chapman, S., 298, 430  
 Cheng, C. T., 247 (W10), 248 (W10), 251 (W10), 258 (W10), 265 (W10), 266 (W10), 267 (W10), 285  
 Chester, W., 366, 430  
 Childress, S., 391, 430  
 Chong, A. T., 277 (W5), 285  
 Chow, P. S.-H., 375, 376, 377, 430  
 Chowdhury, K. C. R., 306 (C10), 375 (C10), 431  
 Christensen, H. N., 196, 203  
 Christiansen, E. B., 306 (P6), 373 (P6), 375 (P6), 382, 436  
 Christopherson, D. H., 117, 121, 325 (C11), 431  
 Cichelli, M. T., 17, 57, 262 (B9a), 281  
 Clark, H. B., 50 (C3), 57  
 Clark, J. A., 52, 58, 60  
 Cohen, G. N., 196, 203  
 Colahan, W. J., Jr., 52, 56  
 Cole, J. D., 362 (L2), 434  
 Cole, R., 51, 52, 57  
 Collins, R. E., 349 (C12, C13), 431  
 Collins, W. D., 304 (C15, C16), 305 (C14), 359, 373, 431  
 Conkie, W. R., 215 (C5), 225 (C5), 231, 281  
 Constan, G. L., 224, 236, 277 (C6), 281  
 Conway, C. J. B., 223 (L11), 267 (L11), 283  
 Cornish, A. R. H., 219 (S14), 285  
 Corty, C., 50 (C5), 57  
 Coull, J., 277 (G17), 282, 306 (H12), 373 (H12), 433  
 Coulson, J. M., 231 (C6, C7), 281  
 Cowling, T. G., 298, 430  
 Cox, R. G., 307 (G5c), 325 (G5d), 329 (C19, C20), 330 (C20), 333, 334, 335 (G5d), 345, 347 (C20), 360, 366, 367, 370, 372 (B27, C17), 373, 374 (B27), 384, 390, 394, 395 (S16), 430, 431, 432, 437  
 Cox, R. T., 199 (C3), 203  
 Crow, E. L., 194, 203  
 Cunningham, E., 325, 431  
 Dahler, J. S., 289 (D1, D2), 351, 352, 431  
 Danckwerts, P. V., 219 (D2), 233, 281  
 Darby, R., 37, 57  
 Datta, S. K., 288 (D3), 431  
 Datta, R. L., 275 (D3), 281  
 Dauzere, C., 81, 103, 107 (D3, D4, D5), 108, 121  
 Davidson, J. F., 227, 274 (B1), 277 (D4), 280, 281  
 Davies, J. T., 222 (D6), 223 (D6), 224, 277 (D5), 281  
 Davies, R. M., 222 (D7), 275, 281  
 Davis, F. A., 194 (C4), 203  
 Davis, H. T., 135, 136, 139, 203  
 Day, J. T., 382, 386, 389, 431  
 Dean, W. R., 334, 431  
 Debye, P., 355 (D4c), 431  
 de Groot, S. R., 431  
 Deindoerfer, F. H., 222 (D8), 226, 230 (D8), 281  
 Denson, C. D., 377 (D4b), 382, 383, 385, 386, 389, 399, 431  
 Dergarabedian, P., 7, 14, 15 (D2, D3), 16 (D2, D3), 35, 57  
 Derjagin, B., 52, 57  
 Di Francia, G. T., 360, 431  
 Doremus, R. H., 42, 57  
 Dougherty, D. E., 30, 57  
 Dowson, D., 325 (C11), 431  
 Drew, T. B., 289 (D6), 431  
 Duffing, G., 325 (D7), 431  
 Duncan, J. M., 214 (T1), 285  
 Dunn, C. G., 222 (T4), 285  
 Dwyer, O. E., 245, 269 (P3), 284  
 Eakman, J. M., 189, 192 (E1), 204  
 Eckenfelder, W. W., 228 (E1), 281  
 Eichhorn, R., 340 (E1a), 377 (E1a), 382, 385, 390, 431  
 Einstein, A., 409, 415, 431  
 Eisenberg, P., 51 (E1), 57  
 Elgin, J. C., 222 (R6), 238 (B7, W4), 277 (W4), 281, 284, 285  
 Ellion, M. E., 23, 45, 48, 57  
 Elsworth, R., 136 (H10), 164 (H10), 165 (H10), 204  
 Elzinga, E. R., 215 (E2), 217 (E2), 222 (E2), 231, 233, 277 (E2), 279 (E2), 280 (E2), 281  
 Emerson, R., 169 (E2), 204  
 Emerson, S., 197, 198, 204  
 Ende, W., 48, 57  
 Engez, S. M., 325 (M10), 377 (M10), 435  
 Epstein, P. E., 34, 35, 57  
 Erdélyi, A., 186 (E4), 204  
 Ericksen, J. L., 322, 431

- Escombe, F., 169 (B9), 203  
 Evans, J. E., 223 (S6), 267 (S6), 284  
 Eveson, G. F., 345, 431  
 Ewing, G., 81, 121
- Fabic, S., 51 (J1), 58  
 Famularo, J., 332, 349, 431  
 Faneuff, C. E., 51, 57  
 Farley, R. W., 223 (S4), 224 (S4), 277 (S4), 284  
 Faxén, H., 311, 431  
 Fayon, A. M., 336, 337, 431  
 Feller, W., 129 (F1), 194, 204  
 Fesbach, H., 310 (M20), 435  
 Feshbach, H., 19 (M8), 58  
 Fidleris, V., 376 (F6), 377, 431, 432  
 Finn, R. K., 135, 204  
 Finney, D. J., 182 (F3), 204  
 Firkel, C., 72, 78, 122  
 Fisher, J. C., 3 (F2), 49 (F2), 57  
 Fishenden, M., 80, 122  
 Flatt, H. P., 35, 57  
 Fleming, J. F., 246 (F1), 281  
 Foord, A., 222 (G3), 228 (G3), 282  
 Forgacs, O. L., 322 (F7), 378 (F8), 432  
 Forster, H. K., 10, 19, 20, 57  
 Forster, K. E., 49, 57  
 Foster, R. D., 288 (F9), 432  
 Foust, A. S., 50 (C5), 57  
 Franke, M., 231 (S13), 285  
 Frater, K. R., 288 (F10), 432  
 Fredrickson, A. G., 169 (M9), 170 (H3), 172 (H3), 174 (H3), 179, 184, 204, 205  
 Frenkel, J., 49 (F7), 57  
 Fricke, R., 34, 57  
 Friedlander, S. K., 211 (F2), 212 (F2), 228, 281, 406 (F11), 432  
 Friedman, B., 310 (F12), 432  
 Frisch, H. L., 212 (F3), 281  
 Fritz, W., 48, 57, 306 (C10), 375 (C10), 431  
 Frossling, N., 211 (F4), 214 (F4), 281  
 Frumkin, A., 222 (F5), 225 (F5), 281  
 Fuchs, N. A., 288 (F13), 432  
 Fulmer, E. I., 126, 142 (B10), 203
- Gaertner, R. F., 50 (G1, G2), 57  
 Gaffney, R. F., 42, 57  
 Gamble, D. P., 50 (H5), 58  
 Gardner, M., 422, 432  
 Gardner, R. P., 244, 246, 271, 281  
 Garner, F. H., 214 (G4, G11, G12), 215 (G2, G12), 219 (G12), 222 (G3, G5, G6, G8, G12, H4), 223 (G5, G8, G10), 224 (G2), 225, 226 (G2), 227, 228 (G3, G12), 231 (G9, G12), 233 (G10), 235 (G7), 267 (G8, G12), 274 (H14), 275, 277 (G2, G4, G5, G10, G12), 281, 282  
 Garstang, T. E., 362, 366, 432  
 Garwin, L., 239 (G13), 241, 244, 282  
 Gasparian, A. M., 345, 432  
 Gat, Y., 255, 256 (S9, S11a), 257 (S9), 258 (S11a), 271 (S9), 284, 285  
 Gauvin, W. H., 219 (P1), 284  
 Geankoplis, C. J., 246 (G14), 269 (G14, G15a), 282  
 Geddes, A. P., 220, 282  
 Gel'fand, I. M., 411 (G2a), 432  
 Genetti, W. E., 382, 386, 389, 431  
 Gibbons, J. H., 277 (G17), 282  
 Gibbs, J. W., 64 (G1), 119, 121, 289 (G3), 298, 432  
 Giese, A. C., 175 (G1), 204  
 Giesekus, H., 288 (G5), 322, 432  
 Gilbert, C. S., 49 (K1), 58  
 Gilliland, E. R., 277 (H21), 283  
 Glas, J. P., 38, 39 (G3), 40, 41 (G3), 42, 57  
 Glaser, D. A., 49 (G4, G5), 57  
 Goddard, J. D., 406, 429  
 Goldman, A. J., 307 (G5c), 325 (G5d), 334, 335 (G5d), 345, 384, 432  
 Goldshtik, M. A., 360, 432  
 Goldsmith, H. L., 322 (G8), 323, 324 (G9), 348, 377 (G9a, K5, K5b), 378 (G9), 381, 382, 384, 390, 398 (K5, K5b), 400 (K5, K5b), 401 (G9, K5), 402 (G9b, S9b), 403 (G9d, K5a, K5c), 432, 434, 437  
 Goldstein, H., 411 (G9e), 433  
 Goldstein, J. S., 236 (Y1), 245 (Y1), 286  
 Goldstein, R. J., 93 (S11), 94, 96 (S11), 123  
 Goldstein, S., 361, 365, 366 (G11), 433  
 Golovin, V. S., 52 (L3), 58  
 Gordon, K. F., 262, 282  
 Gor'kov, L. P., 119, 122  
 Gosnell, J. W., 22, 23 (S2), 49 (S2), 59  
 Goulandris, G. C., 251 (O1), 284  
 Grafton, R. W., 214 (G4), 226 (G4), 277 (G4), 282  
 Graham, A., 120, 122  
 Graham, J. R., 173, 205  
 Grassmann, P., 52 (M4), 58, 263, 264 (G19), 277 (G18), 282  
 Greene, C. H., 42, 57

- Griffith, P., 21, 23, 30, 31, 49 (G7), 50 (G8, H2), 57
- Griffith, R. M., 214 (G21), 215 (G21), 218 (G21), 222 (G20), 223 (G21), 224 (G21), 227 (G21), 228, 231, 277 (G20), 282
- Grober, H., 217 (G22), 221, 282
- Groothius, H., 267 (G23), 268, 277, 282
- Grover, S. S., 246, 247, 282
- Gunn, R., 214 (K2), 283
- Gunther, F. C., 43 (G10), 44 (G10), 45, 46, 57
- Gupta, S. C., 304, 433
- Guyer, A., 274 (G26), 282
- Haberman, W. L., 277 (H1), 282, 325, 326 (H3), 350 (H1), 360, 401, 433
- Hadamard, J., 19 (H1), 57, 222 (H2), 233, 282, 57
- Hadamard, J. S., 401, 433
- Hahn, W., 135, 204
- Hajjar, A. J., 50 (B13), 56
- Hale, A. R., 222 (G5), 223 (G5), 277 (G5), 282
- Halverson, H. O., 131, 206
- Halvorson, H. O., 204
- Hamielec, A. E., 217 (J2), 224, 228 (H3), 229, 233 (H3), 236 (J2), 267, 268 (J2), 277 (H3), 280, 282, 283
- Hammerton, D., 222 (H4), 227, 274 (H4), 275, 282
- Han, C. Y., 31, 50 (H2), 57
- Handlos, A. E., 210 (H5), 217 (H5), 222 (H5), 234, 235 (H5), 277 (H5), 282
- Hanson, C., 248 (H5a), 249 (H5a), 282
- Hanson, D. T. S., 170 (H3), 172, 174, 204
- Hansuld, J. H., 244 (J3), 283
- Happel, J., 211 (K7), 283, 288 (H9), 290, 312 (B28), 325 (H9), 332, 334, 335 (B28), 336 (B28), 338 (H8), 339 (H8), 345, 346, 349 (B28), 350 (P8), 377 (B28), 378 (H8), 397, 403 (H8), 430, 431, 433, 436
- Hardy, B. W., 277 (H11), 282
- Harkins, W. D., 277 (H6), 282
- Harmathy, T. Z., 277 (H7), 282
- Harriott, P., 208, 230 (H8), 251, 258, 260 (H10a), 266 (H10a), 267, 274 (H10), 277 (H8, H9), 282
- Harris, B. L., 240 (Q1), 284
- Harris, D. L., 94, 117, 122
- Harris, T. E., 179, 204
- Hartunian, R. A., 408, 433
- Harvey, E. N., 51 (H3), 58
- Harvey, R. L., 375 (W9), 438
- Harvey, R. T., 168, 205
- Hase, E., 169 (T1), 170 (T1), 173 (T1), 206
- Hasimoto, H., 326 (H10), 349 (H10), 350, 433
- Hawk, E. L., 269 (G15), 282
- Hawk, N. E., 375 (W9), 438
- Hawker, L. E., 198 (H5), 204
- Hawksley, P. G. W., 288 (H11), 433
- Hayes, W., 277 (H11), 282
- Hayock, P. J., 222 (G6), 282
- Hayworth, C. B., 238, 241, 277 (H12), 282
- Hedén, C., 142, 174, 204
- Heertjes, P. M., 215 (H13), 220 (H13), 230 (H13), 267, 280 (H13), 282
- Heideger, W. J., 226, 227 (M1a), 284
- Heiss, J. F., 306 (H12), 373 (H12), 433
- Hendricks, R. C., 52, 53 (H4), 58
- Henniker, J. C., 227 (H14), 283
- Henrici, A. T., 142, 174, 175, 204
- Herbert, D., 136, 164, 165, 166, 167, 168, 173, 175, 204
- Herman, A. J., 277 (W5), 285
- Hermans, J. J., 355, 433
- Hershey, A. V., 113, 122
- Hetrick, D. L., 50 (H5), 58
- Hewlett, V. A., 378 (S19), 402 (S19), 437
- Hickman, K. C. D., 80, 122
- Higbie, R., 219 (H15), 222 (H15), 226, 231, 283
- Hill, R., 304, 433
- Hirsch, G., 253 (S10), 254 (S10), 255, 256 (S10, S11a), 258 (S11a), 263, 264 (S11), 265 (S11), 284, 285
- Hixon, A. N., 246 (G14), 269 (G14), 282
- Hocking, L. M., 345, 346, 433
- Holder, D. W., 76, 81, 122
- Holland, C. D., 277 (H11), 282
- Holloway, C., 267 (S7), 284
- Holm, P., 277 (H16), 283
- Holve, W. A., 215 (H13), 220 (H13), 230 (H13), 267 (H13), 280 (H13), 282
- Hommelen, J., 65 (H5), 122
- Hood, J. R., Jr., 197 (S1), 205
- Horning, W. A., 8, 9, 17, 25 (B19), 38 (B19), 56
- Horowitz, J., 184 (B4), 192 (B4), 193 (B4), 203
- Horvay, G., 53, 58

- Houghton, G., 35, 42, 52, 56, 58, 265 (L4), 275, 277 (G17, R4), 282, 283, 284
- Hsieh, D., 52, 58, 59
- Hsu, N. T., 211 (H17), 214 (H18), 218 (H17), 283
- Hsu, Y. Y., 40, 50 (H10), 58
- Hu, S., 267, 277 (H20), 283
- Huang, C. J., 244 (J3), 283
- Hubbard, R. M., 325 (H15), 433
- Hughes, G. R. R., 277 (H21), 283
- Humphrey, A. E., 222 (D8), 226, 230 (D8), 281
- Hunstad, N. A., 325 (S8), 437
- Illingsworth, C. R., 288 (I1), 290 (I2), 433
- Ingham, J., 248 (H5a), 249 (H5a), 282
- Ivantsov, G. P., 53, 58
- Iwamura, T., 169 (T1), 170 (T1), 173 (T1), 206
- Jaeger, J. C., 237 (C4), 281
- Jakob, M., 221, 283
- James, R. E., 378 (S19), 402 (S19), 437
- Janke, N. C., 306 (J1), 433
- Jarvis, N. L., 72, 81, 93, 97, 122
- Jayaweera, K. O. L. F., 306 (J2a), 345, 346, 375 (J2a), 433
- Jaynes, E. T., 199 (J1), 204
- Jeffery, G. B., 304 (S20), 314, 322, 334, 335, 400, 433, 437
- Jeffrey, R. C., 377 (J5), 382, 387, 389, 398, 401, 433
- Jeffreys, H., 92, 97, 102 (J5), 115, 199 (J1), 200, 122
- Jenkins, F. A., 75 (J6), 122
- Johnson, A. I., 212 (B12, W3), 215 (W3), 216 (B12), 217 (J2), 222 (B12), 224, 228 (B11, H3), 229, 230 (W3), 233 (H3), 236 (J2), 240 (Q1), 244, 267, 268 (J2), 274 (B11), 277 (B11, H3), 281, 282, 283, 284, 285
- Johnson, A. J., 239, 241, 284
- Johnson, H. A., 51 (J1, 2, T1), 58, 59
- Johnson, H. F., 246 (F1), 277 (N6), 281, 284
- Johnstone, H. F., 211 (J4), 283
- Johnson, M. W., Jr., 288 (Z1), 438
- Jones, A. M., 306 (J6), 433
- Jonsson, V. K., 93 (S11), 94, 96 (S11), 123
- Kamiya, N., 198, 204
- Kanwal, R. P., 290 (K2), 304 (K1), 305, 434
- Kaplun, S., 362, 365 (K3, K4), 434
- Karnis, A., 377 (K5, K5b), 381, 382, 384, 398, 400 (K5, K5b), 401 (K5), 402 (K4a), 403 (K5a, K5c), 434
- Karnofsky, G., 251 (K1), 283
- Katz, S., 184 (B4), 192 (B4), 193 (B4), 203
- Kaufman, R. N., 345, 434
- Kavanau, J. L., 140, 206
- Kearsley, E. A., 305, 434
- Kehat, E., 238 (L5), 240, 244 (L5), 246 (L5), 269 (L5a), 283
- Keller, J. B., 325 (K8), 362, 365, 374, 389, 395, 434, 436
- Kendall, D. G., 181, 204
- Kenrick, F. B., 49 (K1), 58
- Keshock, E. G., 52 (K2, S9), 58, 59
- Khamrui, S. R., 360, 434
- Kinter, R. C., 277 (H20), 283
- Kirby, D. B., 52 (K3), 58
- Kirkaldy, J. J., 7, 8, 9, 34, 58
- Kinzer, G. D., 214 (K2), 283
- Klee, A. J., 277 (K3), 283
- Klipstein, D. H., 255, 283
- Knacke, O., 62 (K1), 122
- Knudsen, J. G., 246, 247, 282, 306 (J6), 433
- Koch, A. L., 190, 194, 196, 197 (S1), 204, 205
- Kohlman, D. L., 387, 434
- Kok, B., 169 (K4), 204
- Kol'chugin, B. A., 52 (L3), 58
- Kolodner, I., 19, 58
- Korchinski, I. J. O., 214 (C1), 217 (C1), 228 (C1), 233, 234 (C1), 236 (C1), 281
- Kramers, H., 211 (K4), 214 (K4), 267 (G23), 268, 282, 283
- Kreith, F., 43 (G10), 44 (G10), 45, 46, 57
- Kronig, R., 212 (K6), 217 (K5), 222 (K5, K6), 233, 236, 283
- Kubitschek, H. E., 182, 194, 204
- Kunkel, W. B., 306 (K11), 373 (K11), 434
- Kuo, H. L., 119, 122
- Kurihara, H. M., 52 (K6), 58
- Kusik, C. L., 211 (K7), 283
- Kuwabara, S., 350, 434
- Labuntsov, D. A., 52 (L1, L2, L3), 58
- Lackey, D. L., 265 (L1), 266 (L1), 267, 283
- Ladyzhenskaya, O. A., 288 (L1), 358 (L1), 396 (L1), 434
- Lagerstrom, P. A., 288 (L4, L4a), 362, 365 (K4), 434
- Laidler, K. J., 140 (L1), 204

- Lamb, H., 5 (L4), 45 (L4), 58, 233 (L2), 283, 288, 293 (L5), 305, 325, 358 (L5), 359 (L5), 398, 434
- Lanczos, C., 310 (L5a), 405 (L5a), 434
- Landau, L. D., 288, 304 (L7), 328 (L6), 410 (L5b), 411 (L7a), 412 (L5b, L7a), 415, 434
- Lane, J. J., 226, 236 (G7), 282
- Langlois, W. E., 3 (B14), 7, 17, 56, 58, 288 (L8, 9), 360, 434
- Langmuir, D. B., 103, 109, 122
- Langmuir, I., 103, 109, 122, 218 (L3), 283
- Laning, J. H., Jr., 194, 204
- Lapidus, L., 238 (B7, W4), 277 (W4), 281, 285
- Ledesma, V. L., 247 (W10), 248 (W10), 251 (W10), 258 (W10), 265 (W10), 266 (W10), 267 (W10), 285
- Lee, N. M., 325 (M10), 377 (M10), 435
- Leonard, E. F., 377, 382, 386, 389, 390, 398, 399, 436
- Leonard, J. H., 265 (L4), 275, 283
- Lepper, G., 214 (V2), 285
- Leppert, G., 211 (B16), 281
- Leslie, F. M., 288 (L10), 434
- Letan, R., 238 (L5), 240, 244 (L5), 246 (L5), 269 (L5a), 283
- Levengood, W. C., 72 (L2), 80 (L2), 122
- Levich, V. G., 208, 211 (L8), 215 (L8), 222 (F5, L6, L7, L8), 224, 225 (F5), 227, 228, 233, 276 (L8), 277 (L6, L7, L8), 281, 283, 403, 406 (L10a), 434
- Lewis, J. B., 277 (L9), 283
- Li, S. C., 246, 271, 283
- Liapunov, A., 204
- Licht, W., 211 (L13), 223 (L11), 231 (L13), 235, 267 (L11), 274 (L13), 277 (L12), 283
- Liebermann, L., 35, 42, 58
- Lienhard, J. H., 7, 51 (J2, L7), 58
- Lifshitz, E. M., 288, 304 (L7), 328 (L6), 410 (L5b), 411 (L7a), 412 (L5b, L7a), 415, 434
- Lileeva, A. K., 210, 283
- Lin, C. C., 83, 122
- Linde, H., 72, 78, 122
- Lindland, K. P., 222 (L15), 277 (L15), 283
- Linton, M., 222 (L17), 223 (L17), 224 (L17), 226 (L17), 227 (L17), 277 (L17), 283
- Linton, W. H., Jr., 214 (L16), 283
- Lipkis, R. P., 51, 58
- Liu, C., 51, 58
- Liu, S. W., 408, 433
- Lochiel, A. C., 211 (L18), 227, 228 (C1a), 231 (C1a), 275, 281, 284
- Loewenthal, M., 98, 122
- Longcor, J. V. A., 223 (S6), 267 (S6), 284
- Lorentz, H. A., 328, 332, 435
- Lotka, A. J., 139, 204
- Lottes, P. A., 50, 59, 262 (V1a), 285
- Low, 96
- Low, A. R., 71, 92, 93, 96, 97 (L7), 103, 122
- Lumry, R., 169 (R4), 205
- Luntz, M., 98, 122
- Maaløe, O., 186, 204
- Ma, J. T., 7, 58, 277 (M1), 284
- McAdams, W. H., 211 (M2), 214 (M2), 221, 284
- McAllister, E. D., 81, 121
- McDowell, R. V., 211 (M3), 222 (M3), 284
- McElroy, W. D., 51 (H3), 58
- McFadden, P. W., 52 (M4), 58
- McGlothlin, B. B., Jr., 50 (B13), 56
- McGregor, D. K., 231 (W6), 267 (W6), 285
- Mache, M., 42, 58
- Mackay, G. D. M., 328 (M1, M2), 435
- McLean, E. A., 51, 57
- McNamara, V. M., 244 (J3), 283
- McNown, J. S., 288 (M8), 306 (M11), 325 (M9, M10), 345, 375 (M11), 376 (M12, M13), 377, 435
- McPherson, M. B., 325 (M10), 377 (M10, M14), 435
- Majumder, S. R., 304 (M3), 435
- Màlaika, J., 306 (M4, M11), 373 (M4), 375, 376 (M12), 435
- Málek, I., 132 (M2), 204
- Malkus, W. V. R., 119, 122
- Malmgren, B., 142, 174, 204
- Manley, D. M. J. P., 35, 42, 58
- Mansion, H. D., 80, 122
- Marangoni, C., 65 (M2, M3), 122
- Marchello, J. M., 285
- Margulies, R. S., 8, 9, 17, 25 (B19), 38 (B19), 56
- Marr, A. G. 168, 205
- Marsh, B. D., 226, 227 (M1a), 284
- Marshall, K. C., 198, 205
- Marshall, W. R., Jr., 214 (R3), 284
- Martin, J. J., 245, 269 (P3), 284
- Martin, L., 182 (F3), 204
- Maruyama, Y., 186, 205

- Mason, B. J., 306 (J2a), 345 (J2), 346 (J2), 375 (J2a), 433
- Mason, J. P., 23 (B9), 47, 56, 262, 265 (B2), 280
- Mason, S. G., 222 (B4, R8), 224 (R8), 227 (R8), 228, 280, 284, 322 (F7, G8, M5), 323, 324 (G9), 328 (M1, M2), 348, 377 (G9a, K5, 5b), 378 (F8), 378 (G9), 381, 382, 384, 390, 398 (K5, K5b), 400 (K5, K5b), 401 (G9, K5, T1), 402 (C3, G9b, K5c, d, S9b, T1), 403 (G9d), K5, 5c 430, 432, 434, 435, 436, 437
- Maude, A. D., 327 (M6), 328, 334, 335, 378 (M5a, M7a), 402 (M5a, M7a), 435
- Maxfield, M. W., 194 (C4), 203
- Maxon, W. D., 136, 205
- Maxworthy, T., 374 (M7b), 375, 435
- Mazur, P., 431
- Meksyn, D., 277 (M4), 284
- Menten, M. L., 137, 205
- Menzel, D. H., 289 (M15), 435
- Merte, H., Jr., 52, 58
- Mesler, R. B., 42, 52, 53 (M7, R1), 58, 59
- Michaelis, L., 137, 205
- Mikesell, R. D., 15, 23, 36, 43 (B11), 45 (B11), 46 (B11), 47, 48, 56
- Miller, R. A., 204
- Miller, R. L., 169 (F5), 205
- Milne, E. A., 289 (M16), 293 (M16), 435
- Milner, H. W., 172 (M10), 205
- Milne-Thomson, L. M., 51 (M6), 58, 305 (M17), 435
- Milverton, S. W., 80, 81, 95, 123
- Minard, G. W., 241, 244 (J3), 283, 284
- Minceva, L. A., 142, 205
- Miner, R. W., 71 (M4), 122
- Minlos, R. A., 411 (G2a), 432
- Mirsky, L., 297 (M18), 435
- Mituya, A., 169 (T1), 170 (T1), 173 (T1), 206
- Miyauchi, T., 245, 269 (M6), 271, 273 (M6), 284
- M'Kendrick, A. G., 136, 137, 205
- Mohr, C. M., 306, 435
- Monod, J., 136, 137, 196, 203, 205
- Moore, F. D., 42, 52, 53 (M7), 58
- Moo-Young, M. B., 273, 274, 277 (C2), 281
- Morgenthales, A. C., 231 (W6), 267 (W6), 285
- Morse, P. M., 19 (M8), 58, 310 (M20), 435
- Morton, R. K., 277 (H1), 282
- Moser, H., 139, 205
- Myers, J., 170 (M15), 173, 205
- Myers, J. E., 52 (K6, R2), 58, 59, 211 (M3), 222 (M3), 284
- Mysels, K. J., 81, 122
- Nagata, S., 276, 284
- Naisel, D. S., 277 (N2), 284
- Napier, D. H., 275 (D3), 281
- Narasimhamurty, G. S. R., 277 (L12), 283
- Newitt, D. M., 275 (D3), 281
- Newlin, J. T., 376 (M13), 435
- Newman, A. B., 217 (N3), 220, 284
- Newton, D. R., 223 (B9), 281
- Nickelson, R. L., 50 (N1), 58
- Nield, D. A., 103, 122
- Nihei, T., 169 (T1), 170 (T1), 173 (T1), 206
- Nordberg, S., 277 (N4), 284
- Norman, A., 3 (B26), 50 (N2), 57, 58
- North, R. J., 81, 122
- Novick, A., 136, 205
- Novakovic, M., 262, 284
- Novoselov, V. S., 277 (N5), 284
- Null, H. R., 277 (N6), 284
- O'Brien, V., 366, 376, 408, 435
- Oliver, D. A., 240 (T2), 241 (T2), 242 (T2), 246 (T2), 270 (T2), 285
- Oliver, D. R., 377 (O2), 382, 384, 389, 390, 398, 435
- O'Neill, M. E., 334, 335, 431, 435
- Oparin, A. I., 126 (O1), 205
- Orchard, S. E., 114, 122
- Orell, A., 36, 37, 78, 59, 122
- Oseen, C. W., 288, 360, 361, 398, 435, 436
- Othmer, D. F., 251, 284
- Otterman, B., 50 (O1), 59
- Ovseenko, Yu. G., 360, 436
- Pai, M. K., 136, 137, 205
- Palm, E., 120, 122
- Pansing, W. F., 211 (L13), 231 (L13), 235, 267 (L13), 268 (L13), 274 (L13), 283
- Pardee, A. B., 186, 188, 203
- Pasternak, I. S., 219 (P1), 284
- Patten, T. D., 36, 59
- Pattle, R. E., 228 (P2), 284
- Payne, L. E., 304 (P1, P2, P3), 436
- Pearl, R., 134, 205
- Pearson, J. R. A., 62 (P2), 98, 101 (P2), 122, 362, 364 (P11), 365 (P11), 366, 372, 382, 406, 408, 433, 436

- Pell, W. H., 304 (P1, P2, P3), 436  
 Pellew, A., 84 (P3), 85, 93, 94 (P3), 115, 117 (P3), 122  
 Pérès, J., 311 (P4), 436  
 Perkins, A. S., 52 (P2), 59  
 Perrin, F., 420 (P4a), 436  
 Perry, J. H., 436  
 Pettyjohn, E. S., 306 (P6), 373 (P6), 375 (P6), 436  
 Pfaff, S., 72, 78, 122  
 Pfeffer, R., 350 (P7, P8), 436  
 Pfister, X., 274 (G26), 282  
 Pierce, R. D., 244 (P3), 245, 269 (P3), 284  
 Pigford, R. L., 211 (J4), 283  
 Pillow, A. F., 119, 122  
 Pinder, K. L., 254 (P4), 284  
 Pitts, C. C., 211 (B16), 281  
 Plesset, M. S., 4 (P6, P7), 5, 6 (P7), 9, 10, 11, 13 (26), 15 (P7), 17, 34, 35, 52, 57, 58, 59, 60, 277 (22), 286  
 Pliskin, I., 337 (P9), 436  
 Plomley, N. J. B., 197, 198, 205  
 Polubarinova-Kochina, P. Ya., 349 (P10), 436  
 Poritsky, H., 19, 59  
 Porter, J. W., 247 (W10), 248 (W10), 251 (W10), 258 (W10), 265 (W10), 266 (W10), 267 (W10), 285  
 Powell, E. O., 179, 181, 182, 189, 205  
 Power, G., 304, 433  
 Pramanik, H. R., 376 (M12), 435  
 Pratt, H. R. C., 277 (L9), 283  
 Preckshot, G. W., 50 (N1, W1), 58, 60  
 Prescott, D. M., 197, 205  
 Proudman, I., 362, 364 (P11), 365 (P11), 366, 372, 406, 408, 436  
 Pshenai-Severin, S., 345, 436  
 Quigley, C. J., 240 (Q1), 284  
 Rabotnova, I. L., 142, 205  
 Radusch, R., 284  
 Rahn, O., 181, 205  
 Rajeswari, G. K., 288 (B4a), 429  
 Ramkrishna, D., 139, 140, 142, 175, 176, 194, 205  
 Ranz, W. E., 214 (R2, R4), 284  
 Rathna, S. L., 288 (R1), 436  
 Rayleigh, Lord, 82, 115, 122, 360, 436  
 Redfield, J. A., 277 (R3a), 284  
 Reid, W. H., 94, 117, 122  
 Reinhardt, A., 277 (G18), 282  
 Relton, F. E., 304 (R3, R4), 436  
 Repetti, R. V., 377, 382, 386, 389, 390, 398, 399, 436  
 Richardson, J. G., 349 (R5), 436  
 Rideal, E. K., 277 (D5), 281  
 Rieske, J. S., 169, 205  
 Ripps, D. L., 314 317 (R5a) 350, 351 (R5b), 436  
 Ritchie, P. D., 35, 42, 56, 58  
 Roberts, J. H. A., 378 (S19), 402 (S19), 437  
 Robertson, A. A., 378 (F8), 432  
 Robinson, P. A., 231 (W6), 267 (W6), 285  
 Rogers, T. F., 53 (R1), 59  
 Roll, J. B., 52 (R2), 59  
 Roscoe, R., 314, 315 (R5a), 436  
 Rosenberg, B., 277 (R4), 284  
 Rosenthal, H., 242, 244, 284  
 Rosztoczy, Z. R., 51 (J2), 58  
 Rowland, W. R., 81, 97, 109, 123  
 Rubin, H. H., 30, 57  
 Rubinow, S. I., 362, 365, 374, 384, 389, 395, 436  
 Ruby, G. L., 222 (R6), 284  
 Ruckenstein, E., 52, 59, 230, 284, 350 (R8), 436  
 Rumford, Count, 66, 93, 122  
 Rumscheidt, D., 222 (R8), 224 (R8), 227 (R8), 228, 284  
 Rumscheidt, F. D., 323, 436  
 Rybozynski, W., 222 (R9), 233, 284, 401, 436  
 Saffman P. G., 377 (S1), 390, 395, 436  
 Sage, B. H., 211 (H17), 214 (H18), 218 (H17), 283  
 Sakiadis, B. C., 239, 284  
 Sakadi, Z., 288 (S2), 436  
 Salt, D. L., 382, 431  
 Sartory, G., 122  
 Sasa, T., 169 (T1), 170 (T1), 173 (T1), 206  
 Satapathy, R., 277 (S2), 284  
 Sato, K., 214 (H18), 283  
 Sato, S., 277 (T7), 285  
 Saunders, D. A., 80, 81, 95, 122, 123  
 Savic, P., 8, 22, 23 (S2), 49 (S2), 59, 215 (C5), 222 (S3), 224, 225, 231, 281, 284  
 Savins, J. G., 288 (W2), 438  
 Sayre, R. M., 325, 326 (H3), 433  
 Schaechter, M., 190, 194, 196, 197, 204, 205  
 Schardin, H., 76, 123



- Schechter, R. S., 223 (S4), 224 (S4), 277 (S4), 284  
 Scheidegger, A. E., 349 (S3, S4), 350 (S4), 355, 436, 437  
 Scherrer, V. E., 51, 57  
 Schlichting, H., 211 (S5), 277 (S5), 284  
 Schmidt, R. J., 80, 81, 95, 123  
 Schrock, V. E., 51 (J1, J2, T1), 58, 59  
 Schrödinger, E., 179, 205  
 Schuler, B. O. G., 277 (D4), 281  
 Schwarz, W. H., 288 (C1), 430  
 Schwyer, H. E., 214 (T1), 285  
 Scriven, L. E., 4 (S3, S4), 6 (S3), 8, 25, 33, 38, 71 (S6), 72 (S7), 102, 59, 123, 277 (S21), 285, 288 (D1, D2), 351, 352, 431  
 Segré, G., 377, 378 (S7), 381, 382, 385, 387, 389, 398, 437  
 Segré, S., 389, 437  
 Seitz, P., 50 (S5), 59  
 Selby, T. W., 325 (S8), 437  
 Sellin, R. H. J., 78, 123  
 Selph, F. B., 51 (J1, J2), 58  
 Semeria, R., 52 (B16, S7, S8), 56, 59  
 Semeria, R. L., 52 (S6), 59  
 Shabtai, H., 209 (S8), 222 (S8), 237 (S8), 268 (S8), 284  
 Shapiro, Z. Ya., 411 (62a), 432  
 Shanks, D., 361, 437  
 Sharp, R. R., 52, 53 (H4), 58  
 Sherwood, T. K., 214 (L16), 223 (S6), 267 (S6, S7), 277 (N2), 283, 284  
 Shi, Y. Y., 304, 365, 393, 437  
 Shibata, K., 169 (T1), 170 (T1), 173 (T1), 206  
 Shizgal, B., 402 (S9b), 437  
 Shrode, W. A., 240 (T2), 241 (T2), 242 (T2), 243 (T2), 244 (T2), 246 (T2), 270 (T2), 285  
 Sideman, S., 209 (S8), 215 (B6), 222 (S8), 227 (B6), 230 (B6), 237 (S8), 251 (S12), 252, 253 (S10, S12), 254 (S10), 255, 256 (S9, S10, S11a), 257 (S9), 258 (S11a), 259, 260 (S8a), 263, 264 (S11), 265 (S11, S12), 268 (S8), 272 (S9), 280, 284, 285  
 Siegel, R., 52 (K2, S9, S10, U1), 58, 59  
 Siemes, W., 231 (S13), 285  
 Silberberg, A., 377, 378 (S7), 381, 382, 385, 387, 389, 398, 437  
 Silveston, P. L., 123  
 Singh, T., 262 (G17a), 282  
 Skelland, A. H. P., 219 (S14), 222 (G8), 223 (G8, G10), 231 (G9), 233 (G10), 235, 267 (G8, G12), 277 (G10, S15), 282, 285  
 Skinner, L. A., 4 (S11, S13a), 17, 23, 24, 26 (S11, S12), 29 (S11), 30 (S11), 31, 34 (S13), 35 (S12), 49 (S12), 59  
 Skinner, S. J., 231 (C7), 281  
 Slack, G. W., 345 (J2), 346 (J2), 433  
 Slattery, J. C., 288 (S10, W5), 437, 438  
 Slattery, J. D., 288 (F9), 432  
 Sleicher, C. A., Jr., 245, 285  
 Small, S., 377 (E1), 382, 385, 390, 431, 437  
 Smirnov, N., 210, 283  
 Smith, B. D., 239 (G13), 241, 244, 282  
 Smith, G. C., 238 (S17), 285  
 Smith, J. H., 197, 205  
 Smith, W., 277 (S2), 284  
 Snyder, L. J., 350, 437  
 Sonshine, R. M., 325 (B29), 326 (B29), 327 (B29), 333 (B29), 348, 349, 395 (S16), 430, 437  
 Southwell, R. V., 84 (P3), 85, 94 (P3), 117 (P3), 122  
 Spangenberg, W. B., 78, 81, 97, 109, 123  
 Sparrow, E. M., 93, 94, 96, 123  
 Spelles, K. E., 222 (S18), 233 (S18), 285  
 Spence, R., 275, 285  
 Spicer, C. C., 135, 205  
 Spiegler, P., 3 (B26), 50 (N2), 57, 58  
 Spikes, J. D., 169 (R4), 205  
 Srimathi, C. R., 346 (S17), 349, 437  
 Stadler, D. R., 197, 205  
 Staniszeuski, B. E., 59  
 Starkey, T. V., 378 (S18, S19), 402 (S18, S19), 437  
 Stefanovic, M., 262, 284  
 Steinberger, R. L., 214 (S20), 218 (S20), 219 (S20), 277 (S20), 285  
 Steinhoff, P. F., 251 (K1), 283  
 Sternling, C. V., 71 (S6), 72 (S7), 102, 123, 277 (S21), 285  
 Stewart, W. E., 350, 437  
 Stimson, M., 304 (S20), 437  
 Strasberg, M., 51 (S15), 59  
 Stranski, I. N., 62 (K1), 122  
 Streeton, R. J. W., 275, 285  
 Streng, P. H., 36, 37, 59  
 Streng, P. S., 50 (C3), 57  
 Stuart, J. T., 119, 120, 123  
 Suckling, R. D., 214 (G11), 226 (G11), 282  
 Sutherland, K. L., 222 (L17), 223 (L17), 224 (L17), 226 (L17), 227 (L17), 277 (L17), 283  
 Sutton, O. G., 72 (S13), 73 (S13), 95, 123

- Suzuki, M., 328 (M2), 435  
 Szilard, L., 136, 205  
 Swzarchbaum, B., 215 (B6), 227 (B6), 230 (B6), 280  
 Taitel, Y., 251 (S12), 252, 253 (S12), 265 (S12), 285  
 Takano, M., 401 (T1), 402 (T1)  
 Takata, K., 236 (W1, W2), 285  
 Talsma, H., 215 (H13), 220 (H13), 230 (H13), 267 (H13), 280 (H13), 282  
 Tamiya, H., 169, 170, 173, 206  
 Tang, Y. S., 214 (T1), 285  
 Tanner, R. I., 333, 334, 395 (T1a), 437  
 Tayeban, M., 214 (G12), 215 (G12), 219 (G12), 222 (G3, G12), 224 (G12), 225, 227 (G12), 228 (G3, G12), 231 (G12), 267 (G12), 277 (G12), 282  
 Taylor, G. I., 92, 123, 222 (D7), 275, 281, 323, 324, 437  
 Taylor, T. D., 300 (A2), 401, 406 (A1a), 408, 429, 437  
 Tchen, C. M., 304 (T3), 437  
 Telling, R. C., 136 (H10), 164 (H10), 165 (H10), 204  
 Terada, T., 109, 123  
 Terjesen, S. C., 222 (L15), 277 (L15), 283  
 Terjesen, S. G., 215 (T3), 222 (B13, T3), 224 (B13), 226, 231 (B13), 273, 274, 276 (B13, S19), 277 (H16), 281, 283, 285  
 Theodore, L., 377 (T3a), 382, 385, 390, 394, 437  
 Thomas, R. H., 288 (T4), 438  
 Thomson, J. A., 35, 42, 56, 58  
 Thompson, J. J., 62, 63 (T3), 64, 65, 109, 123  
 Thompson, W. S., 240 (T2), 241, 242 (T2), 243, 244, 246 (T2), 270 (T2), 285  
 Thorsen, G., 215 (T3), 222 (T3), 224 (T3), 226, 231 (T3), 273, 274 (T3), 276 (T3), 285  
 Tien, C. L., 51 (T1), 59  
 Timbrell, V., 345, 438  
 Timson, W. J., 222 (T4), 285  
 Timmons, C. O., 81, 97, 122  
 Tollert, H., 378, 438  
 Tomita, Y., 288 (T7), 438  
 Tomlinson, C., 65, 123  
 Toor, H. L., 209, 285  
 Trass, O., 212 (B12, W3), 215 (W3), 230 (W3), 281, 285  
 Treybal, R. E., 214 (S20), 218 (S20), 219 (S20), 238 (H12), 241, 242, 244 (T6), 277 (H12, K3, S20), 282, 283, 285  
 Tsubouchi, T., 277 (T7), 285  
 Tsuchiya, H. M., 169 (F5, M9), 170 (H3), 172 (H3), 174 (H3), 179, 184, 204, 205  
 Tuck, E. O., 304 (T3), 438  
 Tulin, M. P., 51 (E1), 57  
 Uchida, S., 350 (U1), 438  
 Umano, S., 246, 251, 285  
 Usiskin, C. M., 52 (S10, U1), 59  
 Valentas, K. J., 192, 206  
 van Dyke, M., 356 (V1), 438  
 Vand, V., 384, 438  
 van Heerden, C., 135, 204  
 Van Stralen, S. J. D., 33 (V3), 36, 59, 60  
 Van Wijk, W. R., 20, 33, 36, 59  
 Varley, C., 62, 65, 123  
 Vermeulen, T., 217 (V1), 220, 245, 262, 269 (M6), 271, 273 (M6), 284, 285  
 Vernotte, P., 96, 123  
 Veronis, G., 119, 122  
 Villat, H., 288, 438  
 Viskanta, R., 50, 59, 262 (V1a), 285  
 Vladimirova, L. N., 52 (L3), 58  
 Vliet, G. C., 214 (V2), 285  
 Volkovisky, 118  
 Volkovisky, V., 66, 72, 96, 98, 109, 123  
 Volterra, V., 139, 206  
 von Bertalanffy, L., 195, 203  
 Vos, A. S., 33 (V3), 36, 59, 60  
 Wadhua, Y. D., 304 (W1), 438  
 Wakeshima, H., 236, 285  
 Wallick, G. C., 288 (W2), 438  
 Wallis, J. D., 50 (G8), 57  
 Walters, K., 288 (T4, W3, 3a, 3b, 4), 438  
 Wang, P. K., 7, 58  
 Ward, D. M., 212 (B12, W3), 215 (W3), 216 (B12), 222 (B12), 228 (B12), 230 (W3), 281, 285  
 Wasserman, M. L., 288 (W5), 438  
 Water, D., 288 (W3a, W3b), 438  
 Waters, N. D., 288 (W4, W6), 438  
 Weaver, R. E. C., 238 (W4), 277 (W4), 285  
 Wei, C. C., 50 (W1), 60  
 Weiss, P., 140, 206  
 Weissman, E. Y., 262 (G17a), 282

- Welleck, R. M., 235, 277 (S15), 285  
 Wells, P. L., 269 (G15), 282  
 West, F. B., 231 (W6), 267 (W6), 277 (W5), 285  
 Westerheide, D. E., 37, 38 (W2), 60  
 Westwater, J. W., 36, 37, 38 (W2), 39 (G2), 40, 41 (G3), 42, 50 (G3, G2), 52 (K3, P2), 78, 56, 57, 58, 59, 60, 122  
 White, E. T., 277 (W7), 285  
 White, H. E., 75 (J6), 122  
 Whitehead, A. N., 358, 362, 364 (W7), 438  
 Whiteley, A. H., 51 (H3), 58  
 Whitmore, R. L., 376 (F6), 377, 378 (M7a), 402 (M7a), 432, 435  
 Whittaker, E. T., 134, 139, 206  
 Wiegandt, H. F., 251 (W8, W9), 258, 260 (H10a), 265 (W9), 266 (H10a), 267, 282, 285  
 Wilke, C. R., 247, 248, 251, 258, 265 (W10), 266, 267 (W10), 285  
 Williams, G. C., 214 (W11), 286  
 Williams, W. E., 325 (W8), 330 (W8a), 331 (W8a), 438  
 Williamson, J. P., 197 (S1), 205  
 Willmarth, W. W., 375 (W9), 438  
 Wilson, E. B., 289 (G3), 432  
 Wilson, R. E., 135, 204  
 Wismer, K. L., 49 (K1), 58  
 Woodward, T., 226 (W12), 240 (T2), 241 (T2), 242 (T2), 243 (T2, W12), 244 (T2, W12), 246 (T2), 270 (T2), 285, 286  
 Woronetz, C., 118, 123  
 Wright, R. W., 50 (Z2), 60  
 Wyllie, G., 5 (W4), 60  
 Wyss, E., 263, 264 (G19), 282  
 Yamaguchi, I., 276, 284  
 Yanagita, T., 186, 205  
 Yang, W., 60  
 Yeh, G. C. K., 50 (Z2), 60  
 Young, N. O., 236, 245, 286  
 Zakharova, E. A., 52 (L3), 58  
 Zalokar, M., 197, 198, 206  
 Zaminian, A. A., 345 (G2), 432  
 Zavoiskii, V. K., 52, 60  
 Ziegenhagen, A. I., 288 (Z1), 438  
 Ziegler, N. R., 131, 204, 206  
 Zierep, J., 392, 438  
 Zisman, W. A., 81, 97, 122  
 Zivi, S. M., 50 (Z2), 60  
 Zmola, P. C., 36, 48, 60  
 Zuber, N., 10, 19, 42, 48, 51, 57, 58, 60  
 Zuiderweg, F. J., 277, 282  
 Zwick, S. A., 4 (P6, P7), 5, 6 (P7), 9, 10, 11, 13 (Z6), 15 (P7), 17, 51, 52, 59, 60, 277 (Z1, Z2), 286

## SUBJECT INDEX

- A**
- Abbau, 194  
 Age model, 175–193  
 Aging, microbials, 125  
 Algae, unicellular, 168–170  
   irradiance curves, 173  
 Archimede's law, 339  
 Aroclar, 250, 264  
 Aufbau, 194
- B**
- Beer's law, 169  
 Bénard cells, 107  
 Bionics, 124–125  
 Birth process, 126–130  
 Boiling, surface, 42–49  
   subcooled, 42–47  
 Bottleneck model, 141–163  
 Boussinesq  
   equations, 118–119  
   transformations, 229  
 Brownian motion, 408–420  
 Bubble  
   condensation, 261–266  
   dynamics, 2  
   electrolytic current density, 38  
   gas, 34–35, 37–42  
   growth  
     analytical solutions, 22–33  
     approximate solutions, 10–20  
     asymptotic, 7–20  
     Barlow-Langlois solution, 17–20  
     diffusion controlled, i–60  
     Dougherty and Rubin, 30–33  
     exponential thermal boundary, 29  
     heat balance, 48  
     nonuniform initial conditions, 20–33  
     numerical solutions, 21–22  
     rapid heating, 51–52  
     Savic and Gosnell, 22–23  
     self-similar solutions, 7–20  
     simplified models, 32  
     Skinner and Bankoff, 23–30  
     superheated liquid, 26  
     two-component liquids, 33–34  
   kinetic energy, 47  
   radius, 13–14  
   spherically symmetric, 3–35  
   vapor, 35–37  
   wall  
     heat balance, 6  
     velocity, 5  
 Buckingham II theorem, 209  
 Buoyancy, 63–64, 66  
   -driven convection, 82–83  
   Rayleigh theory, 98, 100–101  
   -surface tension, 102–103
- C**
- Cartesian coordinates, 87  
 Cavitation bubbles, 43  
 Cauchy principal values, 19  
 Cell  
   population, microbial, 124–205  
   models, 126–141, 162–194  
   structure, 174–175  
   and age, 175–176  
   life span, 193  
   mass, 189–194  
   single, 194–197  
   theory, 125  
   growth, 126  
   reproduction, 125–126  
 Chemostat, 131

- Chlorella ellipsoidea*, 169–171  
 Circulation, drop, 221–235  
   decay, 226  
 Coalescence, 276  
 Column end effects, 266–269  
 Condensation, 261–266  
 Condenser, 265–266  
 Convection  
   buoyancy driven, 66, 82–83  
   evaporative, 61–123  
     cell size, 112, 114–118  
     hydrodynamic stability, 82–105  
     in pure liquids, 111  
     Schlieren photographs, 110  
   experiments, 71–82  
   Grashof number, 217  
   heat flux, 71  
   Henri Bénard experiments, 66–71  
   morphology of, 105–120  
   steady cellular, 68  
   surface tension, 65  
   thermal, 66, 81–82  
 Culture  
   continuous, 169  
   life cycle, 162–163  
   steady-state, 178–179  
   synchronized, 185–188
- D**
- Darcy's law, 349–356  
 Diffusion  
   into drops, 233  
   effective, 233–234  
   mass, equation, 5–6  
 Direct-shadow optics, 78–81  
 Drag  
   coefficients, 421  
   hydrodynamically supported spheres, 385  
 Drop  
   circulation  
     equation, 230  
     internal, 221–235  
     models, 233  
   coalescence, 207  
   column end effects, 266–269  
   diameter, 272–276  
   evaporating in water, 251–261  
   formation and acceleration, 207  
   mixed, model, 220–221  
   rigid-, model, 210–220  
     -single, 235–237  
     temperature, constant, 210–235  
     velocity, constant, 207  
 Droplets, liquid, 322–324  
   buoyant, 400–403  
   surface, 323  
 Dyadics  
   coupling and rotation, 297–299, 302–303  
   diffusion, 417  
   direct, 295–296  
   Lorentz, V, 397–398  
   resistance, 299–302  
     coefficients, 342–345  
     particle boundary, 325  
   rotational diffusivity, 416  
   translation and rotation, 300–302  
 Dynamics, cell population, 124–205
- E**
- Economic theory, 141  
 Energy equation, 5  
   forced convection, 403–404  
 Euler equation, 31  
 Evaporation, 251–261  
 Evaporator  
   cocurrent pipe-type, 258  
   flash, 257–258  
 Exchange, multiphase, 247  
 Exchangers, heat, 237–245  
   cocurrent, 245–247  
   transfer coefficients, 247
- F**
- Faxen's laws, 311–313, 316  
 Fickian diffusion, 195  
 Fick's law, 415–420  
 Film, two-, theory, 220  
 Fission, cell, 175–176, 185  
   probability, 177  
 Flow  
   Darcy-like, 356  
   nonsteady, 402  
   shear and higher order, 308–324, 348  
   at small, nonzero Reynolds numbers, 356–403  
 Fluid(s)  
   mechanics  
     buoyancy, 63–64, 66  
     surface tension, 62–63

Fluid(s) (*continued*)  
 quiescent, 290–308, 341–347  
 unbounded, 374–376

#### Force

lift, 309

Saffman, 393–394

Stokes, 422

Forster's model, 49

Forster-Zuber

expression, 36

moving source solution, 19–20

Fouier-Poisson equation, 232–233

Frobenius, theorem of, 297

Froessling equation, 273

#### G

##### Gas

bubble, 37–42

growth, 34–35

inert, 7

##### Growth

batch, 131, 136–137, 140

logistic law, 133–134

optional, 146–149

phase, 155–161

lag, 141–163

rate expressions, 132–139

specific form, 150–154

stability, 134–139

#### H

Heat transfer, direct constant, 206–285

boiling, 260–261

coefficients, 251–261

aging, 226–227

circulating drops, 227–235

decrease with time, 225

rigid drops, 210–220

dimensionless similarity, 208–209

to drops, 210–247

and bubbles, 247–266

column end effects, 266–269

diameter effect, 272–275

efficiency equations, 216, 219, 232

in drop formation, 266–267

single drop, 236

liquid-liquid, 207

mass transfer analogs, 403–408

temperature effects, 269–272

Higbie penetration theory, 221, 230

Hydrocarbon-water systems, 254

Hydrogen, bubbles, 38–41

#### I

Interferometers, 73–76, 80

Isotropy

local, 258–259

spherical, 302–304

Iteration-perturbation method, 14–17

#### J

Jakob number, 8–9

#### L

Laplace equation, 34

Liapunov's theory, 138

Light, 168

Liquid (s)

immiscible, 206–285

-liquid interface, 50–51

two-component, 33–34

Lubrication-theory, 329

#### M

Macroscopic reciprocity, 295

Malthus law, 133–134

growth process, 130

Markov process, 127

Mass transfer, 403–408

Methylene chloride, 265

Migration

experiments, 381–403

conditions, 382

theory, 389–403

lateral, 377–403

radial, 378, 400–403

Morphology

natural convection, 105–120

pattern, 94

Monod

equations, 192, 195

growth model, 137, 163

aerobacter aerogenes, 167

aerobacter cloacae, 163–165

nonphotosynthetic organisms, 169–

171

results, 163–174

## Motion

- equation of, 289–290, 354
  - bubble growth, 2, 7–10
  - bubble wall, 4–5
  - flow stability, 83
  - nondimensional form, 392–395
- particle, 296
- quasi-steady, 301–302

## N

- Navier-Stokes equations, 289–290, 356–358
- Nucleation, 49–51, 254–255
- Nusselt number, 208, 227, 403, 406
  - and circulation, 272–273
  - drop models
    - circulating, 215
    - rigid, 211, 213
  - equation, for bubble groups, 262
  - internal, 234
  - outside, equations, 228–229

## O

- Oscillation, wake, 218, 223–224, 231
- Oseen's equations, 361–367

## P

## Particle

- dense, in upflow, 388–389
- drag, 332
- finite, systems, 341–349
- free, displacements, 409
- helicoidally isotropic, 420–422
- hydrodynamic force, 418–419
- infinite systems, 349–356
- multi-, systems, 341–356
- neutrally buoyant, 387–388
  - ellipsoidal, 322
- noneutrally buoyant, 385–386, 389–390
- nonspherical, 289
- resistance, 287–345
- rigid, spherical, 394
- single, 290–341
- solid, 308–322
- spherically isotropic, 302–303
- suspended, 71–73
  - aluminum, 72
- trajectory, 307
- Pearson's theory, 98–102

- Peclet numbers, 229, 262, 403
  - internal, 234
  - small, nonzero, 406–408
  - zero, 404–405

## Pentane

- iso-, bubbles, 262–264
- water systems, 251–261, 272
  - column height, 256–257

## Perturbation methods

- regular, 359–360
- singular, 360–374

## Plesset Zwick

- perturbation solution, 11–19, 24
- theory, 20

## Poiseuille flow, 335–336, 377, 390, 394, 400

- sphere in a, 379
  - nonrotating, 390
- two-dimensional, 398–399

## Polyhedrons, 302–303

## Population

- synchronized, 185–188
- transient behavior, 181

## Prandtl number, 227, 272–273

## Probability theory, 127, 176, 182, 198–200

## Propagation

- batch, 163
- continuous, 164–166
- steady-state, 167, 175–181

## Propagator, continuous, 131–134

## Protoplasm, 139

## R

- Rahn's hypothesis, 180–181, 184–185
- Rankine solids, 305
- Rankrishna's models, 139–141
- Rayleigh equation, 5, 43, 48
- Reactor, KEWB, 3
- Reynold's number, 222, 228, 273, 275
  - circulation onset, 227
  - low, 227
  - oscillation, 231–232
  - particle resistance, 287–345
  - small, nonzero, 356–403
- Repitti-Leonard phenomenon, 399
- Resistance
  - equations, 296–297
  - hydrodynamic, 287–345
  - polyadic, coefficients, 316–318
  - solid particle, 301–302
  - Stokes, quasi-static, 308–322

- Rubinow-Keller  
  equation, 380, 389-390  
  theory, 393-394, 399-400
- S**
- Schlieren optics, 76-78, 80  
Spermaceti, 70  
Spheres, 302-303  
  hydrodynamically supported, 385  
  multiple, 346  
  neutrally buoyant, 381  
Spray-columns  
  countercurrent, 237-245  
    backmixing, 243-245  
    column height, 242-243  
  liquid-liquid, 257  
  operation, 269-272  
Stability theory  
  linear, 114-118  
  nonlinear, 118-120  
Stokes  
  equations, 289-293  
    quasi-steady, 342-343  
  flows, 289-356  
Strouhal number, 262  
Superheating, 255  
Surface  
  active agents, 103  
  deformations, 113-114  
Surfactants, 104-105
- Suspensions, 339-341  
Synchronization, cell, 185-188
- T**
- Taylor  
  expansions, 147  
  number, 92  
Temperature-gradient effects, 269-272  
Thompson number, 101-102  
Torula utilis, 165-166  
Transfer, mass, 231-232  
Transition region, 374-377
- V**
- Vapor bubbles, 35-37  
Vaporization, microlayer, 52  
Velocity  
  at drop equator, 227  
  Stokesian, 305  
Viscosity, 269  
  Newtonian model, 4
- W**
- Wave effects, 324-341, 348-349  
  for torque, 327  
  transition region, 376-377  
Water, desalination, 247  
Wave number, 115
- Z**
- Zuber's model, 47-49